

Characterization and Identification of Per- and Polyfluoroalkyl
Substances (PFAS) in the Environment and Consumer Products
via High-Resolution Mass Spectrometry and Oxidative
Conversion

Dissertation
der Mathematisch-Naturwissenschaftlichen Fakultät
der Eberhard Karls Universität Tübingen
zur Erlangung des Grades eines
Doktors der Naturwissenschaften
(Dr. rer. nat.)

vorgelegt von
M.Sc. Jonathan Zweigle
aus Filderstadt

Tübingen
2023

Gedruckt mit Genehmigung der Mathematisch-Naturwissenschaftlichen Fakultät der Eberhard Karls Universität Tübingen.

Tag der mündlichen Qualifikation:

04.06.2024

Dekan:

Prof. Dr. Thilo Stehle

1. Berichterstatter:

Prof. Dr. Christian Zwiener

2. Berichterstatter:

Prof. Dr. Peter Grathwohl

3. Berichterstatter:

Prof. Dr. Torsten Schmidt

Contents

Contents.....	V
List of Abbreviations.....	VIII
Abstract.....	X
Zusammenfassung.....	XII
Acknowledgements.....	XV
List of Publications.....	XVI
Oral and Poster presentations.....	XVIII
1. Introduction.....	1
1.1. Per- and polyfluoroalkyl substances (PFAS).....	1
1.2. PFAS in the environment.....	3
1.3. Analytical chemistry of PFAS.....	5
2. Aim of the thesis.....	9
3. Methods.....	11
3.1. Non-target screening (NTS).....	11
3.1.1. PFAS extraction and HRMS measurements.....	11
3.1.2. NTS data evaluation.....	12
3.1.3. Theoretical evaluation of the MD/C-m/C approach.....	13
3.1.4. Fragment mass differences.....	14
3.1.5. NTS application to contaminated soil from NRW.....	14
3.1.6. Open-source PFAS NTS tool development.....	15
3.1.7. PFAS NTS review.....	16
3.2. PFAS characterization via oxidation and hydrolysis.....	16
3.2.1. PhotoTOP development.....	16
3.2.2. SFP characterization in functional textiles.....	16
4. Results and Discussion.....	19
4.1. Theoretical evaluation of the MD/C-m/C approach.....	19
4.2. Fragment mass differences to prioritize MS ² spectra.....	21
4.3. PFAS NTS in soil from NRW.....	22
4.4. Combination of workflows into a NTS tool.....	25
4.5. PFAS HRMS review.....	28
4.6. Precursor oxidation via UV/TiO ₂	29
4.7. Characterization of SFPs in textiles.....	31
5. Conclusions and outlook.....	35
6. References.....	39
7. Appendix Publication 1.....	53
8. Appendix Publication 2.....	74
9. Appendix Publication 3.....	105
10. Appendix Publication 4.....	135
11. Appendix Publication 5.....	161
12. Appendix Publication 6.....	173
13. Appendix Publication 7.....	203



List of Abbreviations

APCI	atmospheric pressure chemical ionization
CE	collision energy
DDA	data-dependent acquisition
EOF	extractable organic fluorine
ESI	electrospray ionization
F/C	fluorine to carbon ratio
GC	gas chromatography
HPLC	high-performance liquid chromatography
HRMS	high-resolution mass spectrometry
KMD	Kendrick mass defect
m/C	mass per carbon atom
m/z	mass to charge ratio
MD	mass defect
MD/C	mass defect per carbon atom
MRM	multiple reaction monitoring
MS	mass spectrometry
MS/MS	tandem mass spectrometry
NOM	natural organic matter
NTS	nontarget screening
PFAAs	perfluoroalkyl acids
PFCAs	perfluorocarboxylic acids
PFAS	per- and polyfluoroalkyl substances
QqQ	triple-quadrupole
QTOF	quadrupole time-of-flight
SFPs	side-chain fluorinated polymers
TF	total fluorine
THP	total hydrolysable precursors
TiO ₂	titanium dioxide
TOP	total oxidizable precursors
TP	transformation product
UV	ultraviolet
[•] OH	hydroxyl radical
Δ	mass difference



Abstract

Per- and polyfluoroalkyl substances (PFAS) are a large group of anthropogenic organic chemicals that are characterized by their carbon fluorine bonds. Due to their unique characteristics that include high stability, oil- and water-repellent properties and more, they are used in countless consumer products and industrial processes. While in perfluorinated compounds every C-H bond is substituted by a C-F bond, polyfluorinated compounds are only partially fluorinated and consist also of a hydrocarbon part. The fully fluorinated moieties of PFAS, usually perfluoroalkyl or perfluoroether chains, are extremely persistent in the environment. As a result of this persistence combined with the extensive use, PFAS can be detected everywhere in the environment as well as in humans. While some polyfluorinated compounds are partially transformed in the environment, they eventually form persistent end products such as perfluoroalkyl acids (PFAAs) which is why they are also referred to as precursors. The sheer number of individual PFAS makes their analytical detection very challenging. Since PFAS are industrial chemicals, the availability of reference standards is limited. Therefore, chromatographic techniques coupled to high-resolution mass spectrometry (HRMS) are necessary for a more comprehensive characterization of the PFAS in the environment.

In the first part of this dissertation, methods for a prioritization and subsequent identification of PFAS in both environmental and consumer product samples were developed and validated in selected case studies. Since during so-called non-target screening (NTS), large datasets are acquired, an efficient prioritization is crucial to isolate the analytes of interest from background signals and other detected compounds. In case of PFAS, their intrinsic properties were used to separate them from other organic compounds in the HRMS datasets. The novel MD/C-m/C approach that uses the chemical mass defect (MD) and the mass (m) normalized to the carbon number (C) was theoretically evaluated with ~490,000 chemical formulas from online database to show that a wide range of PFAS can efficiently be separated from non-PFAS in the presence of other substances. PFAS with at least 55 mass percent of fluorine, a F/C ratio > 0.8 , or a H/F ratio < 0.8 were separable from other compound classes showing the great potential to remove unwanted compounds from HRMS datasets. To also prioritize PFAS fragmentation spectra, important fragment mass difference (or neutral losses) of common PFAS were determined,

evaluated, and used to detect MS/MS spectra and identify PFAS in both extracts of coated papers and soils. This approach, combined with other NTS techniques was used to identify and semi-quantify several novel PFAS in a highly contaminated agricultural soil from north-western Germany where over 70 PFAS were detected that were previously unknown on this site. The total concentration was estimated to be > 30 mg/kg total identified PFAS. Furthermore, the contamination was almost entirely dominated by perfluorinated compounds including SF₅-perfluoroalkyl sulfonic acids which indicated a unique source of contamination.

Eventually, several existing and here developed NTS techniques were combined into PFAScreen, an open-source Python-based NTS tool for a vendor-independent prioritization and partial annotation of PFAS in HRMS raw data. The functionality of PFAScreen was demonstrated by its application to four contaminated soils from south-western Germany where over 80 PFAS were identified including novel transformation products.

In the second part, a photocatalytic oxidation method (PhotoTOP) was developed that allows the quantitative conversion of unknown precursors to their terminal end products perfluoroalkyl carboxylic acids (PFCAs). The PhotoTOP uses the production of hydroxyl radicals from irradiation of TiO₂ (UV/TiO₂) for the conversion of precursors in different samples and is complementary to the total oxidizable precursor (TOP) assay. Known precursors could be quantitatively oxidized to PFCAs and the PhotoTOP was shown to be able to almost completely conserve the perfluoroalkyl chain lengths of the oxidized precursors. This allows the prediction of chain-lengths of unknown precursors and was demonstrated by oxidation of pre-characterized PFAS-coated paper samples. A second promising advantage of the PhotoTOP is the absence of salts which simplified subsequent sample preparation and makes further direct injection with electrospray ionization MS possible.

To this end, the PhotoTOP was compared with the performance of complementary methods such as the direct TOP assay, hydrolysis (total hydrolysable precursors) and fluorine sum parameters (extractable organic fluorine and total fluorine; measured by the Federal Institute for Materials Research and Testing (BAM)) to characterize non-extractable side-chain fluorinated polymers (SFPs) in functional textiles. It was shown that several textiles contained high concentrations of short and long-chain perfluoroalkyl side chains that are not extractable and therefore not amenable to mass spectrometry without prior chemical conversion.

Zusammenfassung

Per- und polyfluorierte Alkylverbindungen (PFAS) bilden eine große Klasse von anthropogenen organischen Chemikalien und sind durch ihre Kohlenstoff-Fluor Bindungen gekennzeichnet. Aufgrund ihrer einzigartigen Eigenschaften wie beispielsweise hoher chemischer Stabilität und die Fähigkeit Öl und Wasser abzuweisen werden sie in zahllosen Konsumprodukten sowie in industriellen Prozessen verwendet. Während in einer perfluorierten Verbindung alle C-H Bindungen durch C-F Bindungen ersetzt sind, sind polyfluorierte Substanzen nur teilweise fluoriert und weisen noch ein Kohlenwasserstoffanteil auf. Die perfluorierten Gruppen von PFAS, in der Regel Perfluoralkyl- oder Perfluoretherketten, sind in der Umwelt extrem persistent. Infolge dieser Persistenz in Kombination mit der umfangreichen Anwendung können PFAS überall in der Umwelt und auch im Menschen nachgewiesen werden. Während einige polyfluorierte Verbindungen in der Umwelt teilweise transformiert werden, bilden diese letztendlich persistente Endprodukte wie Perfluoralkylsäuren (PFAA). Daher werden diese Verbindungen auch Vorläufer oder Präkursoren genannt. Die schiere Anzahl an PFAS Einzelverbindungen macht ihren analytischen Nachweis zu einer großen Herausforderung. Da es sich bei PFAS um Industriechemikalien handelt ist die Verfügbarkeit von analytischen Referenzstandards nur sehr begrenzt. Deshalb ist für eine umfassendere Charakterisierung von PFAS in der Umwelt die Kopplung von chromatographische Techniken mit hochauflösender Massenspektrometrie (HRMS) erforderlich.

Im ersten Teil dieser Dissertation wurden Methoden für eine Priorisierung und anschließende Identifizierung von PFAS in Umwelt- und Konsumproduktproben entwickelt und in ausgewählten Fallstudien validiert und angewandt. Da während des Non-Target-Screenings (NTS) große Datensätze generiert werden, ist eine effiziente Priorisierung notwendig um die zu untersuchenden Analyten von Hintergrundsignalen und anderen Substanzen zu isolieren. Im Falle von PFAS wurden deren intrinsische Eigenschaften genutzt, um sie von anderen Verbindungen in den HRMS-Datensätzen zu trennen. Der neuartige MD/C-m/C-Ansatz, der den chemischen Massendefekt (MD) und die Masse (m) auf die Kohlenstoffzahl (C) normiert, wurde mit ~490.000 chemischen Formeln aus einer Online-Datenbank evaluiert, um zu zeigen, dass eine breite Palette von PFAS in Gegenwart anderer Substanzen effizient von Nicht-PFAS getrennt werden kann. PFAS mit mindestens 55 Massenprozent Fluor, einem F/C-Verhältnis $> 0,8$ oder einem H/F-Verhältnis $< 0,8$ waren von anderen Verbindungsklassen trennbar, was das große Potenzial zur Entfernung ungewollter Verbindungen aus HRMS-Datensätzen zeigt. Um auch PFAS-

Fragmentierungsspektren priorisieren zu können, wurden wichtige Fragmentmassendifferenzen (oder Neutralverluste) von häufigen PFAS bestimmt und zur Erkennung von MS/MS-Spektren und der finalen Identifizierung von PFAS in Extrakten von beschichteten Papieren und Böden verwendet. Dieser Ansatz wurde in Kombination mit anderen NTS-Techniken zur Identifizierung und Semi-Quantifizierung mehrerer neuartiger PFAS in einem hochgradig kontaminierten Boden aus Nordrhein-Westfalen verwendet, in dem über 70 PFAS nachgewiesen wurden, die zuvor auf diesem speziellen landwirtschaftlichen Standort unbekannt waren. Die Gesamtkonzentration der identifizierten PFAS wurde auf > 30 mg/kg geschätzt. Die Kontamination war fast vollständig von perfluorierten Verbindungen einschließlich von SF₅-Perfluoralkylsulfonsäuren dominiert, was auf eine spezielle Kontaminationsquelle hindeutet.

Abschließend wurden mehrere bestehende und hier entwickelte NTS-Techniken in einem Open-Source-Python-basierten NTS-Tool (PFAScreen) kombiniert um eine herstellerunabhängige Priorisierung und tentative Identifizierung von PFAS in HRMS-Rohdaten zu ermöglichen. Die Funktionalität von PFAScreen wurde mittels der Anwendung auf vier kontaminierte Böden aus Südwestdeutschland demonstriert, in denen über 80 PFAS einschließlich neuartiger Transformationsprodukte identifiziert wurden.

Im zweiten Teil wurde eine photokatalytische Oxidationsmethode (PhotoTOP) entwickelt, die eine quantitative Umwandlung unbekannter Vorläufer zu ihren Endprodukten Perfluoralkylcarbonsäuren (PFCA) ermöglicht. Der PhotoTOP nutzt die Erzeugung von Hydroxylradikalen durch Bestrahlung von TiO₂ (UV/TiO₂) für die Umwandlung von Vorläufern in verschiedenen Proben und ist komplementär zum TOP-Assay (Total Oxidizable Precursors). Bekannte Vorläufer konnten quantitativ zu PFCA oxidiert werden und es war möglich die Perfluoralkylkettenlängen der oxidierten Vorläufer fast vollständig zu erhalten. Dies ermöglicht die Vorhersage der Kettenlängen unbekannter Vorläufer und wurde mittels Oxidation bereits charakterisierter PFAS-beschichteter Papierproben demonstriert. Ein zweiter vielversprechender Vorteil des PhotoTOP ist die Abwesenheit jeglichen Salzgehalts, was die anschließende Probenvorbereitung vereinfacht und insbesondere die Direktinjektion mit Elektrosprayionisation ermöglicht.

Abschließend wurde der PhotoTOP mit komplementären Methoden wie dem direkten TOP-Assay, der Hydrolyse (Total Hydrolysable Precursors) sowie Fluorsummenparametern (Extrahierbares organisches Fluor und Gesamtfluor; gemessen von der Bundesanstalt für Materialforschung und -prüfung (BAM)) verglichen, um nicht extrahierbare fluorierte Seitenkettenpolymere (SFPs) in funktionellen Textilien zu charakterisieren. Es konnte gezeigt

werden, dass mehrere Textilien hohe Konzentrationen an kurz- und langkettigen Perfluoralkyl-Seitenketten enthielten, die nicht extrahierbar waren und daher ohne vorherige chemische Umwandlung nicht direkt über Massenspektrometrie zugänglich sind.

Acknowledgements

First, I would like to thank Prof. Dr. Christian Zwiener for giving me the possibility to perform my research in his working group. I very much appreciate all the scientific knowledge that I could learn over the years in the group of Environmental Analytical Chemistry and especially all the helpful and extensive discussions about analytical chemistry and other topics. I really enjoyed the supervision that allowed me to be creative and provided me enough time to concentrate on novel ideas that could be worked out together by frequent feedback.

I further thank Prof. Dr. Peter Grathwohl and Prof. Dr. Torsten Schmidt for their role as the second supervisor and third examiner of my thesis.

Next, I thank Dr. Boris Bugsel who continuously supported me in every aspect of my work, in particular with his knowledge about analytical and instrumental aspects. Throughout the years I learned many important skills from our fruitful collaboration and there was not a single question that could not be asked and solved together. Every Spikeball session was a pleasure. I further want to thank Catharina Capitain for her excellent work in the frame of her Master's thesis that contributed to this dissertation. My special thanks go also to all group members of the Environmental Analytical Chemistry Group such as Stephanie Nowak, Melanie Schübler, and Miriam Haußecker for the pleasant working atmosphere, discussions, and all the help with issues in the lab.

I also acknowledge the Deutsche Bundesstiftung Umwelt (DBU) for the financial support from my PhD scholarship, my DBU supervisor Dr. Hedda Schlegel-Starmann, and all the interesting scholarship seminars that brought me in contact with other DBU scholars and provided lots of high-quality talks and discussions on environmental related topics besides my research.

I further thank all the collaborators who were part of this research.

I also would like to thank Cora Strobel for all lunches, walks, and tea or coffee breaks that were always a welcome timeout and offered useful new ideas to solve different tasks.

Moreover, I thank my girlfriend Madita Schulz for her constant help and support in every difficult situation. She supported me throughout my time at the University and all the fun times and living together were of great importance to always stay motivated.

Last but not least I deeply thank my parents who supported me throughout my academic career. Their constant help made my education at the University possible.

List of Publications

Publication 1:

Zweigle, J., Bugsel, B., & Zwiener, C. (2023). Efficient PFAS prioritization in non-target HRMS data: systematic evaluation of the novel MD/C-m/C approach. *Analytical and Bioanalytical Chemistry*, 415(10), 1791-1801.

Author contributions: JZ planned the study and conducted the data evaluation. BB and CZ were part of the interpretation of the data and of the MD/C-m/C approach. JZ wrote the first draft of the manuscript which was reviewed and edited by all authors.

Publication 2:

Zweigle, J., Bugsel, B., & Zwiener, C. (2022). FindPFAS: Non-Target Screening for PFAS — Comprehensive Data Mining for MS2 Fragment Mass Differences. *Analytical Chemistry*, 94(30), 10788-10796.

Author contributions: All authors planned the study, JZ conducted the experimental part, method development, and data evaluation. JZ and BB wrote the Python algorithm. JZ wrote the first draft of the manuscript and all authors provided critical reviewing and editing of the manuscript.

Publication 3:

Zweigle, J.* , Bugsel, B.* , Röhler, K., Haluska, A. A., & Zwiener, C. (2023). PFAS-Contaminated Soil Site in Germany: Nontarget Screening before and after Direct TOP Assay by Kendrick Mass Defect and FindPFAS. *Environmental Science & Technology*, 57(16), 6647-6655.

Author contributions: *JZ and BB contributed equally to this publication and share first authorship. Experimental work and data evaluation were performed by JZ and BB. Interpretation and final identification of PFAS was done by JZ, BB, and CZ. KR and AAH performed soil sampling, KR conducted the direct TOP assay. JZ and BB wrote the first draft of the manuscript and all authors reviewed the final version of the manuscript.

Publication 4:

Zweigle, J., Bugsel, B., Fabregat-Palau, J., & Zwiener, C. (2023). PFAScreen — An open-source tool for automated PFAS feature prioritization in non-target HRMS data. *Analytical and Bioanalytical Chemistry*.

Author contributions: JZ planned the study and had the main role in designing and writing the Python-based PFAScreen tool. BB was part of writing the Python codes. JF-P extracted the soils and reviewed the manuscript. All authors reviewed the manuscript.

Publication 5:

Bugsel, B.*, Zweigle, J.*, & Zwiener, C.* (2023). Nontarget Screening Strategies for PFAS Prioritization and Identification by High Resolution Mass Spectrometry: A Review. *Trends in Environmental Analytical Chemistry*.

Author contributions: *BB and JZ contributed equally to this publication and share first authorship. This review paper was planned and designed together; every author was responsible for writing selected paragraphs. All authors reviewed and edited the manuscript.

Publication 6:

Zweigle, J., Bugsel, B., Capitain, C., & Zwiener, C. (2022). PhotoTOP: PFAS Precursor Characterization by UV/TiO₂ Photocatalysis. *Environmental Science & Technology*, 56(22), 15728-15736.

Author contributions: JZ, BB, and CZ planned the study. JZ and CC conducted the experimental part. JZ performed the data evaluation. JZ, BB, and CZ were part of the interpretation of the data. JZ wrote the first draft of the manuscript. All authors reviewed the manuscript.

Publication 7:

Zweigle, J., Capitain, C., Simon, F., Roesch, P., Bugsel, B., & Zwiener, C. (2023). Non-extractable PFAS in functional textiles—characterization by complementary methods: oxidation, hydrolysis, and fluorine sum parameters. *Environmental Science: Processes & Impacts*, 25(8), 1298-1310.

Author contributions: JZ planned the study, supervised the experimental part, and wrote the first draft of the manuscript. CC conducted the oxidation and hydrolysis experiments and was part of writing the first draft. FS performed EOF measurements and reviewed the manuscript. PR performed TF measurements and reviewed the manuscript. BB reviewed the manuscript. CZ supervised the study and reviewed the manuscript.

Additional publications published during the research of this thesis that are not included:

- Zweigle, J., Bugsel, B., Schmitt, M., & Zwiener, C. (2021). Electrochemical Oxidation of 6: 2 Polyfluoroalkyl Phosphate Diester—Simulation of Transformation Pathways and Reaction Kinetics with Hydroxyl Radicals. *Environmental Science & Technology*, 55(16), 11070-11079.
- Bugsel, B., Schübler, M., Zweigle, J., Schmitt, M., & Zwiener, C. (2023). Photocatalytic transformation of fluorotelomer- and perfluorosulfonamide-based PFAS on mineral surfaces and soils in aqueous suspensions. *Science of The Total Environment*, 164907.

Oral and Poster presentations

- Bugsel, B., Zweigle, J., Schmitt, M., Zwiener, C.; 2021. Photo- und elektrochemischer Abbau von poly- und perfluorierten Alkylsubstanzen (PFAS) – LC-HRMS-Screening von Transformationsprodukten. Poster presentation at Wasser 2021 (online).
- Zweigle, J., Bugsel, B., Zwiener, C.; 2021. Non-target screening for PFAS – Searching for $\Delta(\text{CF}_2)_n$ mass differences in fragmentation spectra. Poster presentation at the International Conference on Non-Target-Screening (ICNTS) in Erding.
- Zweigle, J., Bugsel, B., Schmitt, M., Zwiener, C.; 2021. Electrochemical oxidation of 6:2 polyfluoroalkyl phosphate diester – simulation of transformation pathways and reaction kinetics with $\bullet\text{OH}$. Poster presentation at Langenauer Wasserforum (online).
- Zweigle, J., Bugsel, B., Zwiener, C.; 2021. Non-target screening for PFAS – Comprehensive data mining for MS^2 fragment mass distances. Poster presentation at the PFAS Σ -it at the Geo- and Environmental Center in Tübingen.
- Zweigle, J., Bugsel, B., Zwiener, C.; 2022. Non-target screening for PFAS – Searching for mass distances in data-dependent MS^2 spectra. Poster presentation at Wasser 2022 (online).
- Zweigle, J., Bugsel, B., Zwiener, C.; 2023. Neues zur PFAS-Kontamination eines bekannten Falls in NRW – Priorisierung relevanter Daten im Non-Target Screening durch Massendifferenzen. Oral presentation at Wasser 2023 in Augsburg.
- Zweigle, J., Bugsel, B., Zwiener, C.; 2023. Highly PFAS contaminated field site in Germany: Non-target screening via fragment mass differences and Kendrick mass defect analysis. Oral presentation at the International Conference on Chemistry and the Environment (ICCE) in Venice.
- Zweigle, J., Bugsel, B., Zwiener, C.; 2023. Highly PFAS-contaminated soil site in Germany: Non-target screening via fragment mass differences and Kendrick mass defect analysis. Oral presentation at FLUOROS 2023 in Idstein.
- Zweigle, J., Bugsel, B., Zwiener, C.; 2023. Non-target screening via fragment mass differences and Kendrick mass defect: Application to highly PFAS-contaminated soil in Germany. Oral presentation at the International Conference on Non-Target-Screening (ICNTS) in Erding.



1. Introduction

1.1. Per- and polyfluoroalkyl substances (PFAS)

Per- and polyfluoroalkyl substances (PFAS) are a large group of anthropogenic chemicals that are characterized by their carbon fluorine bonds (C-F) (Evich et al., 2022). To harmonize the PFAS terminology, several approaches were undergone. Originally, chemicals exhibiting at least one fully fluorinated carbon atom, a perfluoroalkyl ($C_nF_{2n+1}-$) or a perfluoroether chain were considered as PFAS (Buck et al., 2011). However, recently, every chemical containing a CF_2- or CF_3- group is considered a PFAS which increased the number of compounds being classified as PFAS drastically (Wang et al., 2021). The total number of existing PFAS is not known and varies depending on the underlying assumptions and databases (Schymanski et al., 2023). Several different PFAS lists emerged over time, while one of the most prominent ones is a list from the Organisation for Economic Co-operation and Development (OECD) that includes approximately 4700 PFAS (OECD, 2018). When considering large chemical online databases such as PubChem, according to the new PFAS definition, the total number increased to over 7 million chemicals (Schymanski et al., 2023). This number reduces to approximately 200,000 PFAS that have more than a CF_2 or CF_3 within their chemical formula. In the following, when talking about PFAS in this dissertation, it is referred to “classical” PFAS with perfluoroalkyl or perfluoroether chains. This usually means that their molecular structure is dominated by C and F rather than by hydrocarbon moieties (see Figure 1).

The C-F bond is one of the strongest bonds in organic chemistry which is why perfluorinated carbon chains are extremely stable against chemical transformation, biological degradation and heat (Buck et al., 2011; Kissa, 2001). This high stability combined with the unique chemical properties of PFAS is desired in numerous applications and industrial processes (Wang et al., 2017). Perfluoroalkyl chains are considered fluorophilic, which means that they do neither interact with polar, nor with non-polar solvents and can, therefore, repel water, oil, and stain. Due to these unique properties that distinguish PFAS from most other chemistries, they are used commercially since the 1950s (Lindstrom et al., 2011). Over the decades, PFAS were increasingly used in everyday products as well as in different industrial processes. Therefore, PFAS have become an integral part of many products or processes of the modern life. In total, today more than 200 use categories for 1400 individual PFAS could be determined which are not considered to be

exhaustive, also since much information regarding PFAS structures is insufficiently reported or falls under the trade secret (Glüge et al., 2020; Ng et al., 2021). Examples of prominent PFAS uses are as surfactants in the chemical synthesis (Kissa, 2001), coatings for textiles (Gremmel et al., 2016; Holmquist et al., 2016), food contact materials (Schwartz-Narbonne et al., 2023), personal-care products (Whitehead et al., 2021), paints (Cahuas et al., 2022; Jia et al., 2021), fire-fighting foams (aqueous film forming foams) (Barzen-Hanson et al., 2017), in electroplating (Joerss et al., 2020), pesticides (Nascimento et al., 2018), in electronic devices (Gaines, 2023), photography (Gaines, 2023), in medical devices (Glüge et al., 2020), as polymers (Lohmann et al., 2020), and many more.

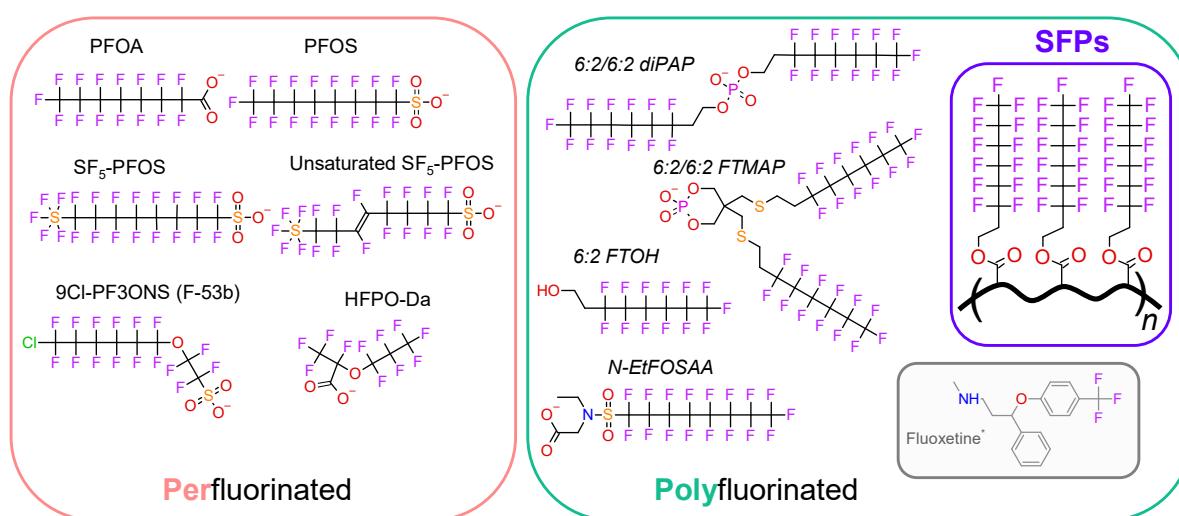


Figure 1: Example of chemical substances considered as PFAS according to the OECD definition. Compounds within the red box are perfluorinated while the green box includes polyfluorinated compounds. Side-chain fluorinated polymers (SFPs, blue box) fall within the class of polymers. Polyfluorinated compounds are also referred to as precursors. The pharmaceutical Fluoxetine (grey box) is also a PFAS per definition, however, such compounds are not addressed when talking about PFAS in this dissertation.

Within the PFAS classification, perfluorinated substances are distinguished from polyfluorinated substances. While a perfluorinated substance does not contain any C-H-bonds, a polyfluorinated substance is partially fluorinated and hence contains hydrocarbon moieties (Figure 1) (Buck et al., 2011). The class of PFAS consists of both monomers and polymers. The group of monomers is highly diverse and includes a very wide variety of different chemistries. PFAS polymers can be classified in fluoropolymers such as polytetrafluoroethylene (PTFE, also called Teflon), perfluoropolyethers and side-chain fluorinated polymers (SFPs). SFPs are copolymers consisting of a non-fluorinated hydrocarbon backbone with perfluoroalkyl side chains that provide unique properties (Washington et al., 2015).

The two main chemical syntheses for PFAS are electrochemical fluorination (ECF) and telomerization (Buck et al., 2011; Martin et al., 2004). The ECF process for instance starts with

a raw material [e.g., perfluorooctanesulfonyl fluoride (POSF)] and eventually results in a mixture of linear and branched perfluoroalkyl chains (e.g., 80%/20%) of a particular chain length. Historically, mainly C₆-, C₈-, and C₁₀-based ECF-based PFAS were produced. On the other hand, telomerization yields even numbered perfluoroalkyl chains with a C₂H₄-spacer followed by a functional group. Telomer-based PFAS have usually exclusively linear perfluoroalkyl chains (Johansson et al., 2018).

1.2. PFAS in the environment

The above discussed unique properties of PFAS that are beneficial in countless applications, are also the main drivers for the adverse effects of PFAS on both humans and the environment (Evich et al., 2022; Lindstrom et al., 2011). Due to the extreme stability of the perfluoroalkyl chain, many PFAS are very persistent in the environment and in biota (Cousins et al., 2020; Knepper & Lange, 2012). The most well-known PFAS are perfluorooctanoic acid (PFOA), a perfluorocarboxylic acid (PFCA), and perfluorooctanesulfonic acid (PFOS), a perfluorosulfonic acid (PFSA) that both belong to the group of perfluoroalkyl acids (PFAAs). PFOA and its homologues (C₄-C₁₄) were extensively used in the past for instance as surfactants for the synthesis of fluoropolymers which led to estimated global emissions of 2000 up to 20000 t into the environment from the 1950s till 2015 (Wang et al., 2014). For PFOS, global emission estimates of 450 - 2700 t in the period from 1970 – 2012 were made (Paul et al., 2009). It should be noted that these numbers are subject to high uncertainties. PFAS emissions into the environment originate from both point sources such as production facilities, wastewater treatment plants (WWTP) or airports (from fire-fighting training), as well as from diffuse sources such as leaching, or volatilization from products containing them (Guelfo et al., 2021). PFAS such as PFAAs are considered very persistent which is why they are also called “Forever Chemicals” (Brunn et al., 2023). Due to this extreme persistence combined with bioaccumulation potential and toxicity, for instance PFOA and PFOS are classified as “Persistent Organic Pollutants” that are regulated globally under the Stockholm Convention (Stockholm Convention, 2022; Wang et al., 2017). Since they are neither biotically nor abiotically degraded in the environment, PFAAs undergo Long-Range-Transport (LRT) into remote regions such as the arctic or Antarctica (Wang et al., 2015; Zhao et al., 2012). Furthermore, the bioaccumulation and biomagnification potential of several PFAS such as long-chain PFAAs (PFCAs > C₇, and PFSAs > C₆) result in strong enrichment in biota along the food web (Buck et al., 2011; De Silva et al., 2021; Huang et al., 2022). As a result of these chemical properties, PFAS were detected worldwide in all environmental

compartments and biota such as in the oceans (Sawidou et al., 2023), surface waters (Loos et al., 2009), groundwater (Schaefer et al., 2015), drinking water (Kaboré et al., 2018), soil (Bugsel & Zwiener, 2020), air (Kim et al., 2012; Yu et al., 2020), indoor air (Morales-McDevitt et al., 2021; Winkens et al., 2017), dust (Gustafsson et al., 2022; Wang et al., 2022), food (Yang et al., 2023), wildlife (Rupp et al., 2023; Sun et al., 2019), and in humans (Aro et al., 2022; D'Eon & Mabury, 2011; Yeung & Mabury, 2016).

Besides PFAAs, many polyfluorinated PFAS which are still in use can transform through several processes like e.g., microbial transformation or atmospheric radical chemistry into persistent transformation products (TPs) (Ahrens, 2011; Benskin et al., 2012; Eriksson et al., 2017; Schenker et al., 2008; Zhang et al., 2021). Therefore, they are also referred to as precursors. Often, these TPs are PFAAs, depending on the underlying chemistry as exemplified in Figure 2. Prominent examples of precursors are fluorotelomer alcohols (FTOHs), polyfluoroalkyl phosphate esters, many AFFF compounds and SFPs (Figure 2) (Ahrens & Bundschuh, 2014). Understanding the fate of precursors in the environment is highly important for an overall understanding of the behavior of the PFAS class (Macorps et al., 2023; Martin et al., 2019; McDonough et al., 2022).

To prevent further distribution of selected PFAS, several regulatory measures and voluntary phase-outs were undertaken in the past (Brennan et al., 2021). Recently, for instance stricter drinking water thresholds and a tolerable weekly intake for four PFAS of only 4.4 ng/kg/week from food of the European Food Safety Authority (EFSA) were established (DIRECTIVE (EU) 2020/2184, 2020; Schrenk et al., 2020). Resulting from the wide-spread detection of C₈-based PFAS such as PFOA and PFOS combined with restrictions, leading production companies have developed several replacement compounds [e.g., dodecafluoro-3H-4,8-dioxanonanoate (ADONA) and hexafluoropropylene oxide dimer acid (HFPO-Da)]. Furthermore, due to less bioaccumulation potential, a shift towards a production of shorter perfluoroalkyl chains (e.g., C₆ or C₄) occurred (Brendel et al., 2018). Unfortunately, most replacement compounds showed rather similar properties and most importantly were of equal persistence compared to restricted PFAS (Brendel et al., 2018; Li et al., 2020). As a result of their higher water solubility and lower sorption, shorter chain PFAS are also much more mobile within the water cycle, posing a high risk for ground- and drinking water resources (Li et al., 2020; Neuwald et al., 2022). In the year 2023, within the European Union, PFAS are planned to be restricted as a whole chemical class resulting from scientific concerns (ECHA, 2023). This intervention is unique because usually only one single chemical at a time is restricted. Such a comprehensive restriction would have a wide influence on the chemical industry, many products and companies which led to a strong media attention of

PFAS. However, it is a long-lasting process with several exceptions for instance for pharmaceuticals or pesticides that are considered PFAS according to the OECD definitions.

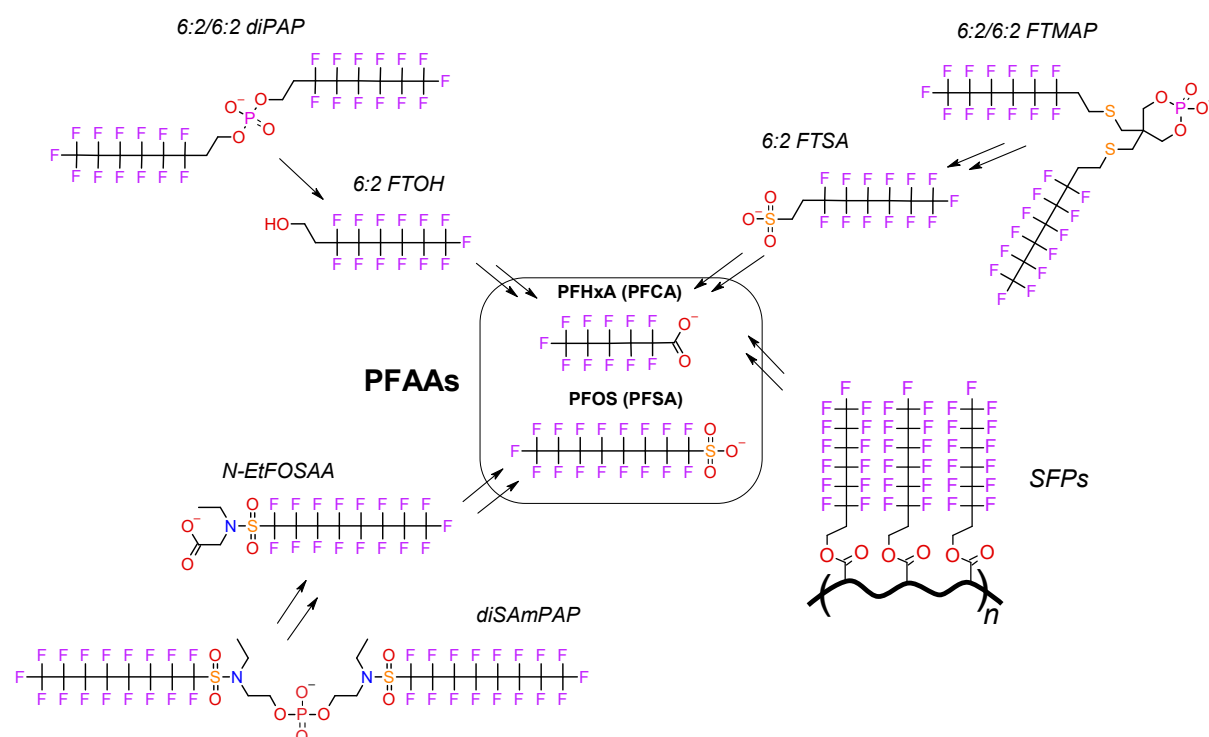


Figure 2: Schematic examples of known transformation reactions of precursors to PFAAs in the environment or biota. Transformation can include both abiotic (e.g., OH-radicals) and biotic (microbial transformation) reactions. Note that double arrows indicate multiple intermediates that are not shown here. Details on transformation reactions can be found in the following literature: (Benskin et al., 2012; D'Eon J & Mabury, 2011; D'Eon & Mabury, 2007; Liu & Mejia Avendano, 2013; Rhoads et al., 2008; Rosenmai et al., 2013)

1.3. Analytical chemistry of PFAS

The sheer number of PFAS that can potentially occur in samples of interest makes a comprehensive analytical detection very challenging (McDonough et al., 2019; Ruan & Jiang, 2017). Well-known PFAS such as the anionic PFAAs for which authentic reference standards are available are routinely analyzed by liquid chromatography coupled to mass spectrometry (LC-MS) (Dodds et al., 2021). This technique relies on the injection of a liquid sample which is usually water or a mixture of water with organic solvent. In case of complex matrices such as soils or consumer products, PFAS need to be extracted from the matrix before they can be measured with LC-MS. In the first step (LC), the dissolved (complex) mixture of organic molecules can be separated on a chromatographic column according to the interaction with its stationary phase (e.g., reversed phase, C_{18}). Subsequently, compounds eluting from the column are ionized by electrospray ionization (ESI) and after a separation by their mass to charge ratio (m/z) in the mass spectrometer (MS) they finally are detected by a detector (Gross, 2017). For quantification,

usually triple quadrupole (QqQ) mass spectrometry, also often referred to as tandem MS (MS/MS), is used which provides both very high sensitivity and selectivity (Harris, 2014). QqQ-MS provides unit mass resolution which means that integer masses are separable. This usually limits this approach to known compounds with reference standards for verification of retention time (RT) and typically two mass transitions (fragments).

Since the sheer number of PFAS makes a comprehensive use of authentic analytical reference standards practically impossible, high-resolution mass spectrometry (HRMS) provides several advantages and also allows identification of novel compounds (Jia et al., 2022). The most frequently used HRMS instruments are time-of-flight- (TOF) or Orbitrap systems (Hollender et al., 2017). If the resolution and mass accuracy is high enough, chemical formulas can be assigned to measured signals by using accurate masses and isotopic patterns (Hollender et al., 2023). When using HRMS detection, usually large amounts of data are acquired, aiming to detect as many molecules in a sample as possible. In a second step, computational techniques are used to detect so-called features (MS signals that are characterized by typical patterns of natural occurring isotopes and chromatographic peak shapes) in the MS-raw data followed by several steps from prioritization of potential features of interest, grouping, and eventually identification (if possible) (Hulleman et al., 2023; Renner & Reuschenbach, 2023). Note that in the literature features have different terminologies and are often also referred to as components. This approach is also called non-target screening (NTS) and is complementary to target screening (e.g., by LC-QqQ-MS) (Hollender et al., 2023). Depending on the polarity of the analyte, different separation and ionization techniques such as LC combined with ESI for polar analytes or gas-chromatography (GC) with atmospheric pressure chemical ionization (APCI) for more hydrophobic compounds might be required (Portoles et al., 2012). Depending on the research question, NTS can be a time-consuming process since usually some manual verification or interpretation of mass spectral data is required and cannot entirely be automated. It is further important to note that techniques based on chromatography and mass spectrometry are usually only suited to detect monomeric PFAS while characterization of polymeric PFAS need complementary analytical techniques (Henry et al., 2018).

Since during NTS approaches, a comprehensive identification of all PFAS in a sample is usually not possible except for special cases, additional analytical techniques have been developed in the past (see Figure 3 for a schematic overview of selected approaches). For example, the total oxidizable precursor (TOP) assay aims to convert unknown precursors within a sample extract to quantifiable PFCAs (Houtz & Sedlak, 2012). Water samples or sample extracts are oxidized by peroxodisulfate ($K_2S_2O_8$) at a pH value of 12 and a temperature of 85 °C which leads to

decomposition of $K_2S_2O_8$ into two sulfate radicals ($SO_4^{\bullet-}$). The sulfate radicals react with OH^- to form sulfate and hydroxyl radicals ($\bullet OH$) which are very strong and unselective oxidizing agents that react with the hydrocarbon moieties of the polyfluorinated precursors. Finally, the formed PFCAs can be quantified by LC-MS target analysis allowing an estimation of the total precursor content within a sample (Janda et al., 2019). When applying the TOP assay, valuable analytical information can be generated, however, the information on the exact structure of precursors is lost. There exist several modifications of the original TOP assay such as the direct TOP (dTOP) in which the sample is directly oxidized which therefore accounts also for non- or difficult to extract precursors in complex samples (Göckener et al., 2020).

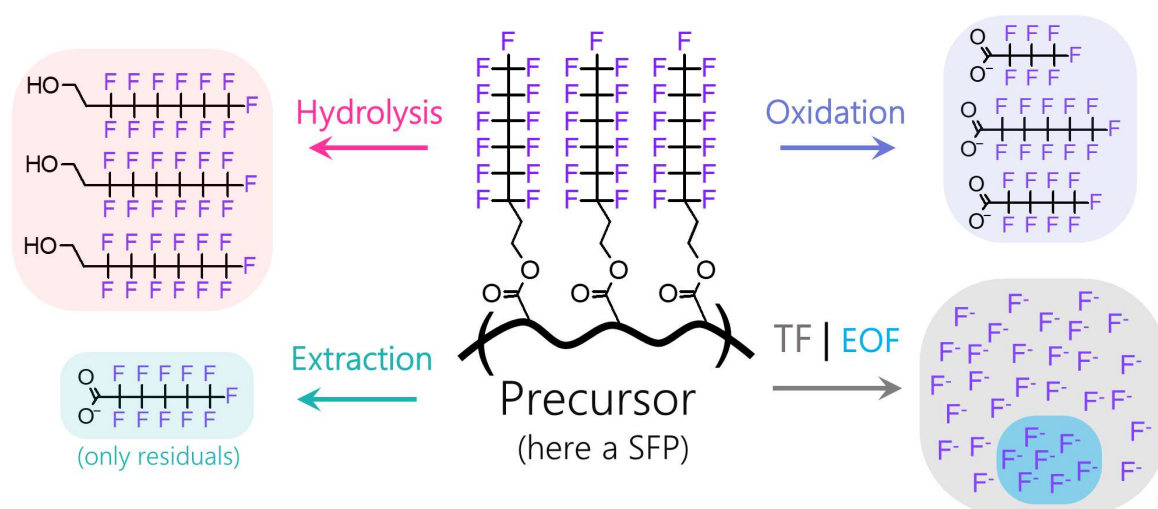


Figure 3: Schematic overview of methods to characterize precursors by oxidation [e.g., total oxidizable precursor (TOP) assay (here direct TOP assay)], hydrolysis [total hydrolysable precursors (THP)], fluorine sum parameters [extractable organic fluorine (EOF), and total fluorine (TF)] compared to conventional extraction. This is exemplified schematically with a side-chain fluorinated polymer (SFP) that might contain also other PFAS residuals that are not shown in the SFP structure in this scheme.

Besides the TOP assay, sum parameters such as the extractable organic fluorine (EOF) or the total fluorine (TF) were developed which open an even wider analytical window (McDonough et al., 2019; Miaz et al., 2020). For detection of the EOF, often combustion ion chromatography (CIC) is used. First, a sample extract is combusted assuring a quantitative conversion of PFAS into HF and CO_2 followed by detection of fluoride (F^-) via ion chromatography (Gehrenkemper et al., 2021). Recently, modifications were developed that use high resolution-continuum source-graphite furnace molecular absorption spectroscopy (HR-CS-GFMAS) which is faster and more sensitive (Simon et al., 2022). TF is able to capture all fluorine within a sample by combusting the whole sample followed by detection of F^- (Schultes et al., 2018). When comparing analytical information generated by such fluorine sum parameters with quantification of specific PFAS, mass balance approaches can be applied verify the comprehensiveness of the individual techniques to

capture PFAS in environmental, biological, or consumer product samples (Aro, Eriksson, Karrman, et al., 2021; Cioni et al., 2023; Jiao et al., 2023; Spaan et al., 2023).

Besides the herein discussed analytical tools, there exist more techniques that rely on spectroscopy such as for example ^{19}F nuclear magnetic resonance spectroscopy (NMR) (Gauthier & Mabury, 2023), particle-induced gamma ray emission (PIGE) (Ritter et al., 2017), or X-ray photoelectron spectroscopy (Tokranov et al., 2018) which are in particular valuable for PFAS analysis in products (Koch et al., 2020; Nordic Council of Ministers, 2022).

Albeit the rapid development and growing research on analytical techniques to tackle identification of unknown PFAS, countless studies report large fraction of unidentified organic fluorine, showing the high importance of innovative new approaches to be able to identify and eventually quantify potential hazardous PFAS in our surrounding environment (Aro, Eriksson, Kärrman, et al., 2021; Aro, Eriksson, Karrman, et al., 2021; Cioni et al., 2023; Simon et al., 2023; Yeung & Mabury, 2016). Robust analytical techniques are the absolute basis for subsequent toxicological risk assessment of chemicals and are especially necessary for establishing safety thresholds in drinking water, soil, food, and consumer products.

2. Aim of the thesis

Despite the rapid improvement of instrumental technology for the analytical detection of chemicals such as PFAS in the environment or consumer products, only small fractions of these chemicals are routinely detected since often target screening approaches are applied that only cover previously known substances. Therefore, a continuous development of novel NTS techniques to efficiently handle the complex data that is generated during HRMS measurements is of high importance for a significantly broader analytical window. In such NTS approaches most often the data evaluation is one major bottleneck for an efficient detection and identification of novel PFAS.

Therefore, the first goal of this thesis is the development, validation, and application of NTS-techniques to prioritize detected features in MS data by making use of the intrinsic properties of PFAS. Unlike common organic molecules, PFAS exhibit several unique chemical properties such as their typical mass defect (MD), the occurrence in homologues, common mass fragments and isotopic ratios that can be used to differentiate them from other organic compounds that are not dominated by fluorine. For such a prioritization both analytical information on the MS¹ and MS²-level will be used to increase the analytical confidence. To make the developed computational workflows accessible to a wider community, the focus was set on vendor-independency and open-source data evaluations. To show the applicability of the developed PFAS-prioritization techniques to highly complex samples, several contaminated soils from Germany with different origins of contamination (Brilon-Scharfenberg, Rastatt, and Mannheim) were investigated in detail. This also allows the deduction of useful mass spectrometric information from a much wider range of PFAS chemistries that can be transferred for the detection of other PFAS classes. To overcome limitations of single approaches the workflows should be combined together into a step-wise procedure to gain more information and increase efficiency during the identification.

The second goal is the investigation of PFAS classes that are not directly amenable to mass spectrometric detection at the first place which are much less studied than PFAS which can directly be detected. Since the fluorine mass balance can often not be closed by the identified PFAS even with NTS approaches (here often estimated by semi-quantification), the application of oxidative conversion to such unknown PFAA-precursors was further studied. Since those precursors often have strong sorption affinity to surfaces, high molecular weights or are even covalently bound to surfaces such as in the case of side-chain fluorinated polymers (SFPs), the application of the oxidative conversion techniques should be applicable directly to the samples themselves rather than to sample extracts. This guarantees that even non-extractable PFAS can be captured by the

subsequent analysis after conversion. The developed oxidation method was directly compared with several complementary methods such as the TOP assay, EOF, TF and others in a case study with SFP-coated textiles to show its applicability and performance.

3. Methods

3.1. Non-target screening (NTS)

In the following section, all steps used during the applied NTS workflows which include sample extraction, measurement, feature prioritization and eventually identification of PFAS are briefly described. The focus is set on the NTS data evaluation which was one central aspect of this dissertation. Details can be found in the respective publications in the appendix (A2-A4 and A6-A7).

3.1.1. PFAS extraction and HRMS measurements

The three matrices investigated during this work were soil, paper, and textile. Soil samples originated from agricultural fields around the region of Rastatt and Mannheim in south-western Germany where PFAS contaminated paper sludge was brought out in the past [see “Rastatt case” e.g., in Nürnberg et al. (2018) or Bugsel and Zwiener (2020)] and from one contaminated site near Brilon-Scharfenberg in North Rhine-Westphalia (NRW) (Röhler et al., 2021; Skutlarek et al., 2006) where contaminated waste materials were suspected as the cause of contamination. Paper samples originated from previous projects (Bugsel et al., 2022), while the textiles were ordered online in the year 2022. Samples intended for NTS were extracted with methanol (MeOH) for several hours with additional ultrasonication. MeOH was shown to be a suitable extraction solvent especially for anionic PFAS from different matrices (Ahmadireskety et al., 2021; Mertens et al., 2023). Selected samples were enriched by evaporation under N₂ followed by resuspension. For the HRMS measurements of sample extracts, no solid phase extraction (SPE) was performed since NTS aims to detect a wide spectrum of analytes of different physico-chemical properties. Due to their selectivity, SPE and other sample preparation steps can add a bias when used for enrichment or cleanup (Hollender et al., 2023; Simon et al., 2022). Sample extracts were measured by using an Agilent 1260 Infinity high-performance liquid chromatography (HPLC) system equipped with a C₁₈ reversed-phase column (Agilent Poroshell 120, 2.1 mm × 100 mm) with 2.7 μm particle size coupled to an Agilent 6550 quadrupole time-of flight (QTOF) mass spectrometer with a mass resolution of 20000 and a mass accuracy below 5 ppm via an ESI interface. The analytes were separated by gradient elution with eluent A [95/5 H₂O/MeOH with 2 mM ammonium acetate (NH₄Ac)] and eluent B (95/5 MeOH/H₂O + 2 mM NH₄Ac) and ionized

in separate measurements both in negative and positive ESI. Details on the respective methods can be found in the publications A2-A4 and A6-A7.

The acquisition range in the MS¹ was 100 – 1700 *m/z* while in MS² *m/z* 70 – 1700 were acquired to be able to detect diagnostic ions from typical functional groups of PFAS such as for example SO₃F⁻. Usually, an acquisition rate of 3 spectra per second was used which was adjusted for GC-APCI-QTOF measurements (10 spectra/s) due to much narrower peaks from GC separation. The QTOF-MS was operated in iterative data-dependent mode (DDA). In DDA, the instrument algorithm automatically sets the isolation window of the quadrupole to the unit mass (*m/z*) of a detected signal if an ion above a predefined threshold (e.g., 10⁴ counts) is detected and a defined number of MS² spectra for this precursor *m/z* is acquired. Note that precursor in this context refers to an intact ion that is fragmented subsequently (not a PFAS precursor). With this technique, abundant ions are automatically fragmented to gain structural information which is necessary for confirmation and identification of novel chemicals. To further increase the MS² coverage, the iterative mode was used where the sample is injected *n*-times and precursor masses for which MS² was acquired in previous runs are subsequently excluded (Koelmel et al., 2017). For the MS² fragmentation, either a set of fixed collision energies (CEs) (e.g., 20 and 40 eV) or a linear *m/z*-dependent CE was used so that heavier ions are subject to higher CEs [e.g., CE(*m/z*) = 4 $\frac{m/z}{100}$ + 15 eV]. Besides using HPLC for compound separation, selected samples with suspected volatile PFAS (e.g., FTOHs) were additionally measured by coupling an Agilent 7890B GC via an APCI interface with the QTOF-MS. A 30 m × 0.25 mm HP-5MS UI GC column with a 21 min temperature gradient was used for separation (for details see publication A6-A7).

3.1.2. NTS data evaluation

To make the developed workflows more accessible to the scientific community, most data evaluations were performed on open-source mass spectrometric raw data with the open-source language Python. Therefore, the Agilent data files (.d) were converted via the MSConvert tool from the ProteoWizard into open formats such as .ms2 and .mzML (Chambers et al., 2012; Deutsch, 2012; McDonald et al., 2004). To detect so-called features within the MS¹ raw data, either the MolecularFeatureExtraction algorithm from the Agilent MassHunter software (Version 10.0) or different algorithms from the OpenMS library (accessed via pyOpenMS) were used (Pfeuffer et al., 2017; Röst et al., 2014; Sturm et al., 2008). Due to the coupling of chromatography with mass spectrometry, features can be extracted from MS¹ spectra by their characteristic peak shape of consecutive *m/z* values of low variance combined with coeluting isotopic traces that result from the natural abundance of isotopes of common elements in organic molecules such as ¹³C, ³⁴S, ³⁷Cl

etc. Feature detection results in a list of signals characterized by m/z , retention time (RT) and intensity. Due to the high sensitivity of mass spectrometric detection, several filtering steps were applied to remove background signals (e.g., blank subtraction) followed by further prioritization steps to reduce the number of features. At this point, features are abstract data structures that bear valuable chemical information but are not yet identified.

3.1.3. Theoretical evaluation of the MD/C-m/C approach

Due to the intrinsic properties of PFAS, that are for instance a large fraction of hydrogen substituted by fluorine, features were prioritized by various approaches according to their likelihood of being a PFAS. From the accurate mass of all features, the chemical mass defect (MD) which is widely used in mass spectrometry and refers to the difference of the exact mass and the nominal mass was determined (Sleno, 2012). By definition, the MD of carbon is zero (because its mass is defined as 12.0000) while hydrogen exhibits a positive MD of +0.0078 and fluorine a slightly negative one (-0.0015). Since molecular formulas of PFAS are usually dominated by fluorine instead of hydrogen, the MD can be used to partially separate them from other common organic molecules (Liu et al., 2022). However, the MD alone has limitations due to overlapping with molecules that strongly exceed a MD of +0.5 resulting from a high H content or lower MDs from elements such as Cl or Br. Kaufmann et al. (2022) proposed a promising approach by normalizing the MD and the mass to the number of carbons (MD/C vs. m/C) for every feature. The carbon number (C) can be retrieved from the ratio of the intensity of the M+1 isotope (I_{M+1}) and the monoisotopic intensity divided by the natural abundance of ^{13}C ($\approx 1.11\%$) according to Equation 1:

$$C \approx I_{M+1}/I_M/0.011145 \quad (1)$$

By plotting MD/C vs. m/C , Kaufmann et al. were able to efficiently separate PFAAs from most of the endogenous matrix features from fish liver and muscle extracts which was the first prove of concept of this approach. Due to the fact that a PFAS' mass is dominated by fluorine rather than carbon, PFAAs have a much higher m/C (≈ 50) than fish matrix compounds.

To systematically evaluate the advantages and limitations of this approach for a PFAS prioritization in HRMS NTS data, a theoretical data evaluation based on a large number of compounds was performed. Therefore, approximately 490,000 chemical formulas from the PubChem database and from Koch et al. (2007) were downloaded, and separated into three groups which were PFAS, typical organic contaminants [from suspect lists of the CompTox Dashboard and the NORMAN network (Grulke et al., 2019; Mohammed Taha et al., 2022)], and

natural organic matter (NOM). From these datasets, it was calculated which PFAS can be separated from which type of organic compounds depending on their fluorine content, e.g., expressed as F/C ratio or mass percentage (%F) within a PFAS molecule. It was further evaluated whether molecular information such as the F/C ratio can be estimated based on the location of a feature within the MD/C-m/C plot.

3.1.4. Fragment mass differences

Due to the fact that PFAS usually have common molecular moieties such as perfluoroalkyl chains or perfluoroether chains, different diagnostic fragment masses can be used to detect MS² spectra that are potentially from a PFAS (Koelmel et al., 2020; Wang et al., 2018). To achieve this, exact masses of diagnostic fragments are matched with the accurate mass MS² data. Diagnostic fragments can be unspecific but are also often rather specific and might not be known for novel unknown PFAS. Fragments differences (often also referred to as neural losses) are commonly used for identification purposes in mass spectrometry and were also used for PFAS identification as they are suspected to have advantages over diagnostic fragments (Wang et al., 2020). To further investigate the comprehensive use of mass differences for a PFAS MS² spectra prioritization, measured LC-HRMS data from a PFAS standard mix (38 compounds from 10 classes), extracts of impregnated papers, and extracts of contaminated soils from the Rastatt case in south-western Germany [details on paper and soil samples in Bugsel et al. (2022)] and additional 20000 HR-MS² spectra from the online library database MassBank (Horai et al., 2010) were collected. To calculate all mass differences in every MS² spectrum comprehensively, mass difference matrices were calculated and used to identify the most frequent mass differences typical for PFAS. With the use of annotated MS² spectra from MassBank, the influence of parameters such as mass tolerance or intensity threshold on the false-positive identification rate was evaluated. The developed approach was used to identify PFAS within paper and soil samples and the identification performance was compared to previous approaches. To this end, a simple Python-based tool was developed which allows searching for PFAS typical fragment mass differences in vendor-independent MS² raw data (.ms2 files).

3.1.5. NTS application to contaminated soil from NRW

To prioritize and identify potential unknown PFAS in a composite sample from the contaminated site near Brilon-Scharfenberg, the developed fragment mass difference approach, combined with diagnostic fragments, suspect-screening, and Kendrick mass defect (KMD) analysis was used. KMD analysis, originally established by Kendrick (1963) for CH₂ repeating units, was used to

detect PFAS homologous series (HS) within the MS¹ data (e.g., CF₂-based). In case of CF₂, first, the Kendrick mass (KM) is calculated according to Equation 2:

$$\text{KM} = m/z_{\text{measured}} \cdot \frac{\text{CF}_{2\text{nominal}}}{\text{CF}_{2\text{exact}}} \quad (2)$$

Where m/z_{measured} refers to the accurate m/z of a feature, $\text{CF}_{2\text{nominal}}$ refers to the nominal mass of the CF₂ repeating unit (= 50) and $\text{CF}_{2\text{exact}}$ to the exact mass of CF₂ (= 49.9968). By subtracting the exact KM from the nominal KM, the KMD can be determined by Equation 3:

$$\text{KMD} = \text{KM}_{\text{exact}} - \text{KM}_{\text{nominal}} \quad (2)$$

The KMD for a particular HS of the form (CF₂)_n-R is then identical within the measurement error of the HRMS instrument since it is determined by the organic rest or functional group R. KMD analysis was performed via a Python script to detect potential PFAS within the feature lists. The workflow was applied to measurements of the soil extract (pre-TOP assay) and after oxidation with the direct TOP assay (post-TOP). The dTOP assay was performed based on Göckener et al. (2020). After feature prioritization, PFAS identifications were confirmed and verified by manual mass spectra interpretation. For details see publication A3.

3.1.6. Open-source PFAS NTS tool development

Several individual Python functions that were developed for different PFAS NTS purposes were eventually combined into an easy to use open-source NTS tool. With the use of the tkinter library, a basic graphical user interface (GUI) was developed which allows the end-user to utilize the tool without programming knowledge. Raw mass spectrometric data (.mzML) or custom feature lists (e.g., from vendor software) from a sample and a blank control can be read in by the tool and feature detection, MS² alignment and blank correction are performed. Functions to perform a PFAS feature prioritization include KMD analysis, MD filtering, MD/C-m/C filtering, and suspect-screening in the MS¹ data, and diagnostic fragment matching and fragment mass differences for MS². Additional Python functions were written that allow the user to visualize MS raw data such as building extracted ion chromatograms (EICs), visualized MS¹ and MS² spectra (MS² also with annotations), match theoretical with acquired isotope patterns and perform a basic EIC correlation to detect potential in-source fragments and adducts that are characterized by their strong coelution.

To demonstrate the functionality of the developed NTS tool, four soils from the region around Rastatt and Mannheim were extracted and measured by HPLC-QTOF and the raw data was used to perform an in-depth NTS to prioritize and identify novel PFAS.

3.1.7. PFAS NTS review

Within this dissertation, a critical review article dealing with promising techniques to identify PFAS with chromatographic techniques coupled to HRMS was written. A literature review was conducted that mainly included articles from the year 2018 onwards and the most promising and widely used approaches were compiled while advantages and limitations were discussed.

3.2. PFAS characterization via oxidation and hydrolysis

3.2.1. PhotoTOP development

Since a comprehensive identification of PFAA-precursors is often not possible and there are also polymeric PFAA-precursors such as side-chain fluorinated polymers (SFPs) that are neither extractable from a sample of interest nor ionizable and therefore not amenable to mass spectrometry, an oxidation technique based on photocatalysis was developed to convert precursors to their terminal end products. The method should be applicable to both sample extract but also directly to the sample itself and aims to quantitatively convert PFAA-precursors to PFCAs. In general, this method is similar to the TOP assay (Houtz & Sedlak, 2012), however, due to the catalytic nature of UV irradiation with suspended TiO_2 , the production of OH-radicals is not limited by the amount of reagent added, and the oxidation solution has no salt content at all. These differences should have several benefits for downstream analysis of the formed oxidation products. After developing a suitable setup, several oxidation experiments with standards of known PFAA-precursors such as diPAPs, FTSA, FTCA, PFOSA and N-EtFOSAA were performed in aqueous suspensions with anatase titanium dioxide (TiO_2) under UV irradiation in a UVA-CUBE 400 equipped with a 1200 W lamp. For oxidation, 20 mg of TiO_2 per 23 mL water was used and irradiated for 5 h. PFAA-precursors and PFCAs were quantified by using a 1290 Infinity II HPLC system coupled to a 6490 iFunnel QqQ MS (Agilent Technologies). All PFAS target analytes were quantified in the multiple reaction monitoring (MRM) mode by two mass transitions (except for perfluorobutanoic and perfluoropentanoic acid) with reference standards. After development and validation, the oxidation method was applied to extracts of PFAS impregnated papers, a PFAS polymer mixture and a textile that was suspected to contain SFPs. The method was named PhotoTOP.

3.2.2. SFP characterization in functional textiles

For a detailed investigation of potential SFPs that are not detectable directly by mass spectrometry, several water-repellent functional textiles (potentially coated with SFPs) were used

to compare several different methods to characterize potential PFAS. Contact angle measurements of both water and oil were used to prioritize the textiles since fluorinated durable water repellent (DWR) formulations are usually able to repel both phases (Schellenberger et al., 2018; Schellenberger, Hill, et al., 2019). The textiles were extracted, and the extracts were (1) screened for PFAAs and potential unknown PFAS by HPLC-QTOF-MS, (2) measured for EOF [in cooperation with the working group Inorganic Trace Analysis of the Federal Institute for Materials Research and Testing (BAM)]. The textiles were also (3) directly oxidized by the developed PhotoTOP, (4) oxidized by the TOP assay, (5) hydrolyzed by the total hydrolysable precursor (THP) assay (Nikiforov, 2021), and (6) finally also the total fluorine (TF) content was measured via CIC [from the working group Contaminant Transfer and Environmental Technologies of the Federal Institute for Materials Research and Testing (BAM)]. For the PhotoTOP, 20 mg of textile strips were oxidized for at least 5 h and PFCAs were quantified in the samples. For the direct TOP assay, a modified method from Liagkouridis et al. (2021) was applied. Briefly, 20 mg of textiles was mixed with 10 ng of isotopically labeled internal PFCAs standards, 0.48 g of potassium persulfate, 4.56 mmol of NaOH and 30 mL water. After thorough mixing, samples were placed in a water bath for 6 h at 85 °C. Afterwards, the pH value was adjusted with HCl, and samples were cleaned up via SPE. The THP assay was performed according to Nikiforov (2021) and the formed FTOHs < 10:2 were quantified and FTOHs \geq 10:2 were semi-quantified via GC-HRMS. More details and the methodologies of EOF and TF measurements can be found in publication A7.



4. Results and Discussion

The results focusing on development and application of NTS approaches for identification of PFAS by HRMS in environmental and product samples are individually discussed as separate subsections for each publication (4.1 – 4.5). The respective original publications are reprinted in the appendix (A1 – A5). Section 4.6 and 4.7 summarize the applied methods that focus on oxidative conversion of PFAA precursor in product samples such as papers and textiles (publications A6 and A7).

4.1. Theoretical evaluation of the MD/C-m/C approach

The novel MD/C-m/C approach first proposed by Kaufmann et al. (2022) was systematically evaluated with ~490,000 chemical formulas from online databases that were separated into PFAS, common organic contaminants and NOM substances. Using the carbon number C that can be retrieved from the intensity ratio of the M+1 isotope and the monoisotopic mass (M) in HRMS data, valuable information is used to separate potential PFAS from other substances by this approach. The high number of chemicals from online sources provides a robust data basis of potentially occurring chemicals in LC- or GC-HRMS data and was therefore used to evaluate advantages and limitations of the MD/C and m/C dimensions. A strong overlap of PFAS with low F-content with organic contaminants and NOM was observed, while with increasing F/C ratio or fluorine mass percentage (%F) a clear separation in the MD/C-m/C plot can be achieved (Figure 4). PFAS with at least a F/C ratio > 0.8, a H/F ratio < 0.8 or at least 55 mass% of fluorine were well separated from both other groups. This includes most “classical” PFAS as exemplified in Figure 4c, while compounds with very low F-content that have for instance only one CF₃-group, are not separable. It is important to note that these calculations should be considered a worst-case scenario since in usual HRMS measurements the number of non-PFAS features that competes with potential PFAS features is much lower than the number of chemical formulas used for this data evaluation. A major advantage of using both MD/C and m/C in NTS is the fact that the location of features is usually linked to a certain chemical composition and compounds with similar chemical formulas are often clustered together which might be useful for identification purposes. For instance, an increasing m/C is linked to the occurrence of heavy heteroatoms such as F, Cl, Br, I, O, P, S, or metals etc. and a decreasing MD/C indicates higher content of elements with negative MDs. Even homologous compounds that differ in their carbon chain length have similar locations due to the normalization to C. Especially, the m/C dimension is very powerful

since it can separate hydrocarbon features that are not separable from PFAS by their MD. Whenever a certain number of hydrogens in an organic molecule is reached, the MD strongly exceeds +0.5 (e.g., +0.9) and is therefore erroneously interpreted as a negative MD (-0.1) that is typical for PFAS. Such compounds however have a much lower m/C that PFAS (e.g., around m/C of 14 for a pure hydrocarbon and m/C = 50 for a perfluorinated compound) and can therefore be discarded.

With the basis of a subset of PFAS with a certain F-content (~55000 compounds), the MD/C-m/C domain was binned and the mean and standard deviation of certain fluorine measures such as the F/C ratio and %F in each bin were calculated. It was shown that the F/C can be predicted to estimate the number of fluorine atoms with a reasonable accuracy while the other F-measures did not sufficiently correlate with the location in the MD/C-m/C domain. Such an estimation could be used in the future to narrow down the atom number to be able to calculate chemical formulas with less false positives. Overall, the MD/C-m/C approach is highly promising to decrease the number of detected features during NTS to a manageable, much smaller number that drastically decreases false positives for downstream analysis such as suspect-screening, fragments mass difference, or diagnostic fragment matching. Since this approach only requires MS¹ data it is very easy to apply to every HRMS dataset.

Detailed information and methodology can be found in publication 1 in the Appendix (A1).

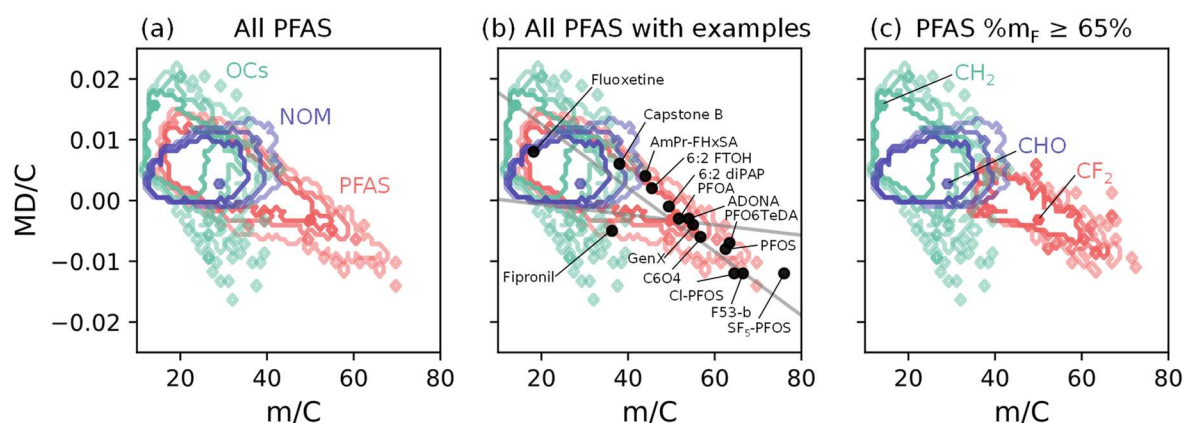


Figure 4: (a) Positions of organic contaminants (OCs, green) from the EPA DSSTox and NORMAN (182,503), NOM (blue) (124,782), and PFAS (red) (all: 209,760) in the MD/C-m/C plot. Note that the PFAS dataset is dominated by compounds with a single CF₃-group. The contour lines delimit the positions of 80% (center), 90% (middle), and 95% (external) of each group. (b) Positions of known PFAS in the MD/C-m/C plot. (c) In case of PFAS with more than 65% mass fluorine, an almost complete separation is possible from the other datasets. More details can be found in publication A1 in the appendix.

4.2. Fragment mass differences to prioritize MS² spectra

To evaluate the use of fragment mass differences, also often referred to as neutral losses, for a PFAS MS² spectra prioritization, HRMS spectra from 38 PFAS standards (10 compound classes), extracts from PFAS coated paper samples and contaminated soils (from the Rastatt region) as well as approximately 20,000 annotated spectra from MassBank were collected. The MassBank dataset included approximately 40 spectra of PFAS with perfluoroalkyl chains and 900 spectra of compounds with a CF₃-group. Within all spectra, mass differences were calculated comprehensively. Therefore, difference matrices were calculated that result in n^2 mass differences for n MS² peaks per spectrum. With this data, several mass differences such as $\Delta(\text{CF}_2)_n$, $\Delta(\text{HF})_n$, $\Delta\text{C}_n\text{H}_3\text{F}_{2n-3}$, $\Delta\text{C}_n\text{F}_{2n}\text{SO}_3$, ΔCF_3 , $\Delta\text{CF}_2\text{O}$, and modifications were identified as frequent occurring differences in many PFAS spectra. Depending on the mass difference, both generic and rather specific occurrences were observed. For instance, mass differences such as $\Delta(\text{HF})_n$, $\Delta\text{C}_n\text{H}_3\text{F}_{2n-3}$, were specific and formed during the fragmentation of telomer-based PFAS (general structure: $\text{R}-\text{C}_2\text{H}_4-(\text{CF}_2)_n-\text{F}$) while $\Delta(\text{CF}_2)_n$ was more often observed and is therefore suitable to prioritize spectra of a wide range of PFAS chemistries. Examples of spectra detectable by the identified mass differences are provided in Figure 5.

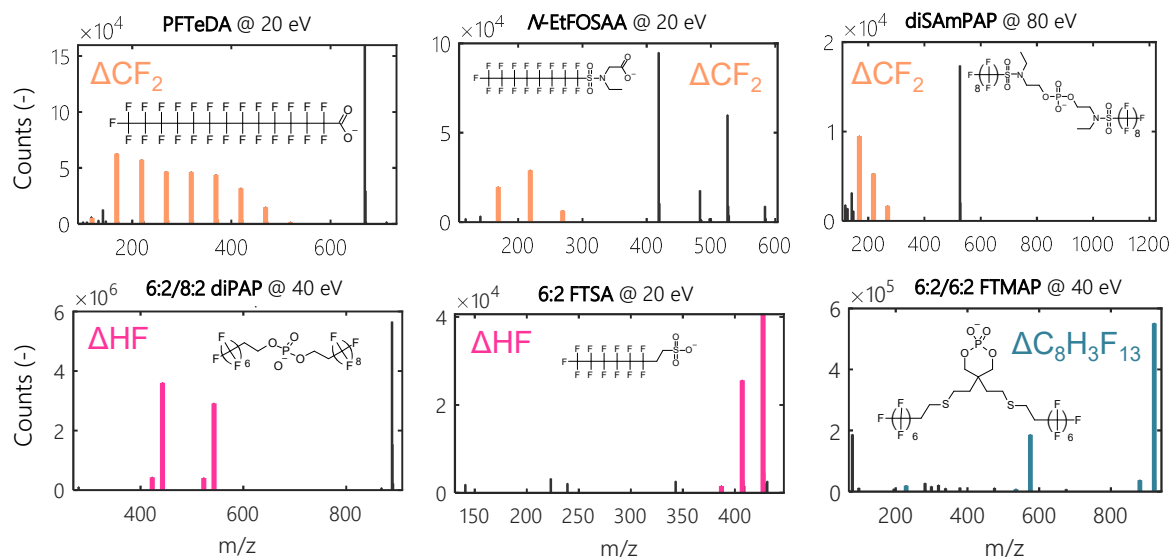


Figure 5: Example of fragment mass differences that can be used to prioritize PFAS MS² spectra. The top row shows ΔCF_2 for a PFCAs, N-EtFOSAA, and diSAmPAP, while on the bottom ΔHF , $\Delta\text{C}_n\text{H}_3\text{F}_{2n-3}$ is shown for telomer-based PFAS. Obviously, in all spectra abundant peaks are detectable by this small set of mass differences.

The use of fragment mass differences allowed to detect 94% of the PFAS in the standard mixture and using the MassBank spectra, a mass tolerance around ± 1 mDa and an intensity threshold of at least 3% were found to be suitable to keep false positive identifications low. However, those parameters should be adjusted dependent on the data quality and the instrument

used for data acquisition. The application of this approach to the pre-characterized paper and soil samples (by Bugsel et al. (2022)) led to the identification of several novel isomeric TPs of fluorotelomer mercapto alkyl phosphates (FTMAPs) in the paper sample (see an example in Figure 6). Those include several oxidation states of the thiol-groups from one up to three oxygen atoms. By looking retrospectively into older HRMS data from soils, those TPs could also be found in soils from the Mannheim region.

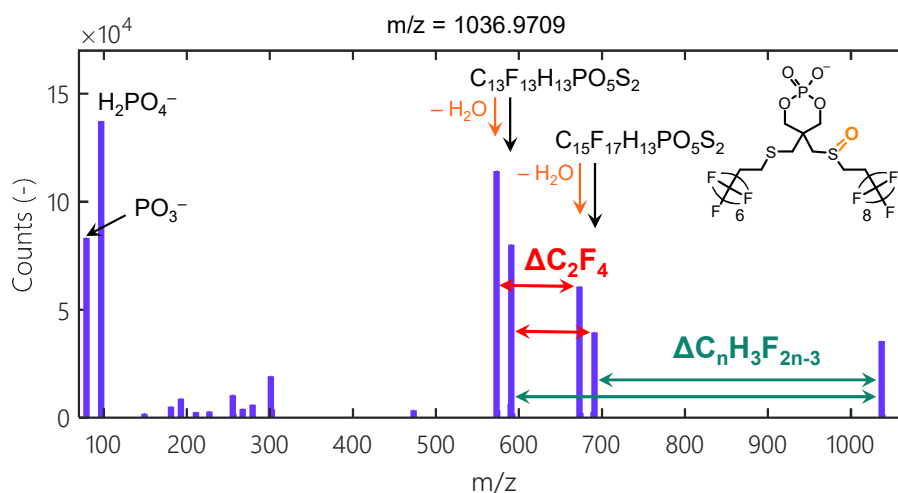


Figure 6: Example of the MS² spectrum of the newly identified FTMAP TPs FTMAP sulfoxide and the respective mass differences that led to its detection.

In summary, a major advantage of the fragment mass difference approach is the fact the fragments can be detected without knowing their mass. This is of particular importance, since a comprehensive use of diagnostic fragments is usually not possible and in case of TPs, adducts or in-source fragments the fragment masses change and might not appear on fragment mass lists anymore. Those unknown fragments are often still detectable via certain mass differences showing the potential for true NTS approaches. To this end, a Python tool named FindPFAS, was developed that allows to search in MS² raw data for fragment mass differences, independent on the used instrument. This allows a prioritization of potential PFAS fragmentation spectra.

Detailed information and methodology can be found in publication 2 in the Appendix (A2).

4.3. PFAS NTS in soil from NRW

For a characterization of a complex PFAS contamination, the mass difference approach combined with diagnostic fragments and KMD analysis was applied to a composite soil sample from a contaminated agricultural site near Brilon-Scharfenberg in NRW. In 2006, elevated concentrations of selected PFAAs were detected in the Möhnetalsperre, in the river Ruhr and some tributaries as well as in drinking water in this region. Skutlarek et al. (2006) were able to locate a 10 ha

agricultural field as a main source of this widespread contamination of PFAAs. Although there are other studies that investigated this soil, for instance regarding the long-term leaching of PFAS, no comprehensive NTS was performed there, and studies concentrated on known PFAS (LANUV, 2011; Röhler et al., 2021). The composite soil was therefore extracted (pre-TOP) and oxidized by the dTOP assay (post-TOP) and both samples were subjected to an in-depth NTS to identify potential unknown PFAS. After data evaluation and partially manual identification, the combined PFAS-specific NTS approaches led to the identification of more than 70 PFAS from 10 substance classes that were not known to occur in this soil before (see Figure 7). The identified PFAS also included entirely novel compounds that were to our best knowledge not reported in literature before (for one example see Figure 8). With a fraction of 40%, the SF₅-PFASs seem to be one of the main PFAS classes in the soil. Previously, they were usually detected in much lower concentrations compared to other PFAS in AFFF formulations or biosolids (Barzen-Hanson et al., 2017; Munoz et al., 2022).

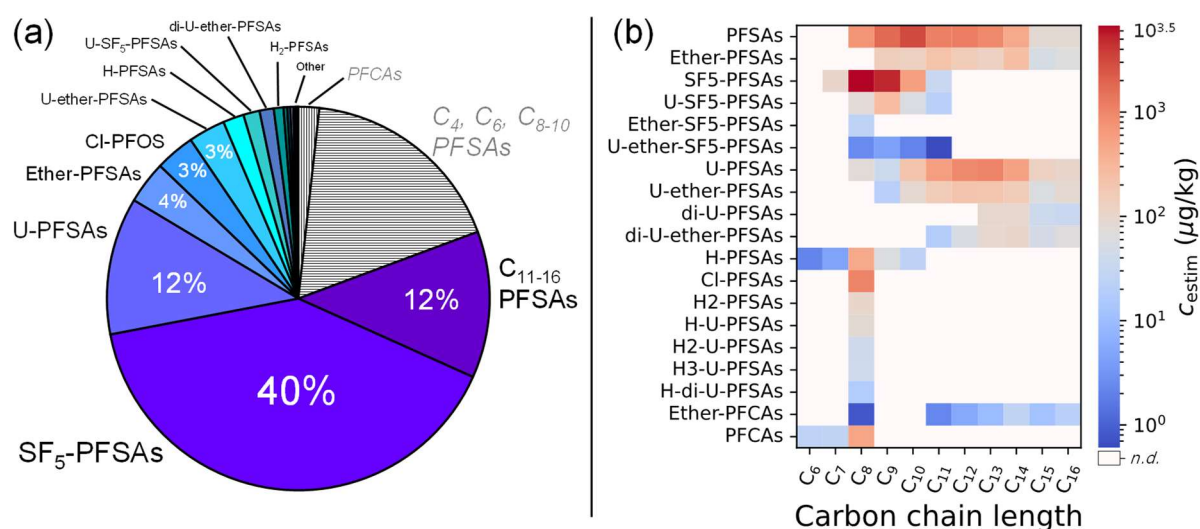


Figure 7: Overview of the identified PFAS in the Brilon-Scharfenberg soil, (a) Percentage of the semi- and quantified PFAS in the soil. The grey shaded area (~23%) highlights the previously known PFAS, while the blue color scales show the identified PFAS which also include generally novel PFAS. (b) Estimated concentration (C_{estim}) in $\mu\text{g}/\text{kg}$ soil of single PFAS subdivided into individual carbon chain lengths. Note that the identifications include complex isomeric mixtures. For details and abbreviations see publication A3.

Since almost all PFAS comprised sulfonic acid functional groups, they were semi-quantified by using PFSA reference standards. A total concentration of $> 30 \text{ mg}/\text{kg}$ was estimated which results in more than 2 t of PFAS on that field site when extrapolated from the composite sample to the whole area. A unique characteristic of the PFAS contamination in Brilon-Scharfenberg is the fact that it is dominated by perfluorinated PFAS. Approximately 97% of the identified PFAS were perfluorinated (no CH-bonds) and only ~3% had CH-bonds, i.e., they can act as precursors. This is a rather unique characteristic since many PFAS soil contaminations were typically described to

be dominated by precursors such AFFF-impacted sites or paper chemicals such as in the Rastatt case (Nickerson et al., 2020; Röhler, Susset, et al., 2023). By using the dTOP assay, 37% of the formed PFCAs could be explained by the semi-quantified precursors which is in a reasonable range. The discrepancy could be explained by either the presence of further precursors that were not captured by the NTS or by systematic errors from the semi-quantification or both. The identified perfluorinated PFAS were not transformed in the dTOP assay, however, it could be shown that due to the aqueous setup of the dTOP, long chain PFAS exhibit strong sorption and are therefore partially lost during the sample treatment. Furthermore, the NTS after the dTOP assay revealed C₆-C₁₀ perfluoroalkyl diacids with both a carboxylic and sulfonic acid group (PFCSA). Their estimated concentration after dTOP oxidation was ~41 ng/g which is only slightly less than the formed PFSAs (~64 ng/g) (Röhler, Haluska, et al., 2023), which demonstrates that besides PFAAs also other PFAS TPs can be relevant after TOP oxidation.

Overall, since most of the identified PFAS were perfluorinated and structurally rather similar to PFAAs (at respective chain lengths), it can be expected that they also distributed in the past and contaminated the ecosystem since the contamination was already discovered in 2006. This study shows the high importance of NTS approaches for a more comprehensive characterization of complex PFAS contaminations, since even the TOP assay combined with target analysis could only capture less than ~25% of this particular contamination pattern and lead to an analytical blind spot.

Detailed information and methodology can be found in publication 3 in the Appendix (A3).

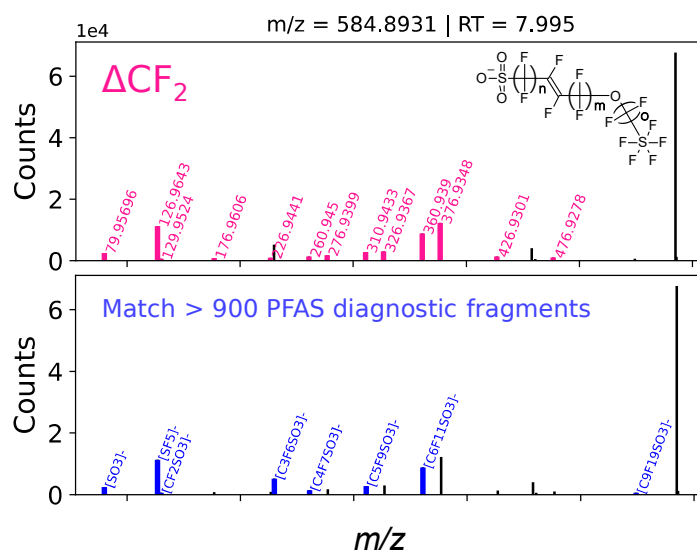


Figure 8: Example of the detection of fragments via the mass difference (ΔCF_2) (top) compared to matching the spectrum with over 900 PFAS-specific diagnostic fragments (bottom). The example shows the MS2 spectrum of an entirely novel PFAS, an unsaturated ether-SF₅-PFSA. Without the knowledge of specific fragment masses, still most fragments can be detected allowing a MS² prioritization.

4.4. Combination of workflows into a NTS tool

To combine several existing and developed PFAS-specific NTS approaches, a Python-based tool, PF Δ Screen, was developed. It is fully open-source and has a graphical user interface (GUI) to make its use as easy as possible. Its basic functionality allows the input of vendor-independent MS raw data (.mzML) from a sample and a blank file. In the first step, feature detection is performed by the FeatureFinderMetabo algorithm which is accessed via the pyOpenMS interface (Kenar et al., 2014; Röst et al., 2014). Originally designed for metabolomics datasets, it is very powerful for small molecules in general and also used for environmental NTS (Helmus et al., 2021). After feature detection, the MS² raw data is assigned to respective features by setting a certain *m/z* and RT tolerance and a subsequent blank correction can be performed that removes features from the sample of interest that also appear in the blank sample. As a result, a blank corrected feature list is generated that includes basic information such as *m/z*, RT, and intensity but also MS² spectra and isotope abundances that are needed to determine the carbon number which is a requirement for the MD/C-m/C approach. In the second step, a PFAS specific feature prioritization can be performed which includes the following techniques: (1) MD/C-m/C filtering, (2) MD filtering, (3) screening for homologous series by KMD analysis with predefined repeating units (e.g., CF₂), (4) searching for specific fragment mass differences (e.g., Δ CF₂), (5) matching of MS² spectra with PFAS-typical diagnostic fragments, and (6) perform a suspect-screening with a custom suspect list. Figure 9 provides an overview of the functionalities of the PF Δ Screen workflow.

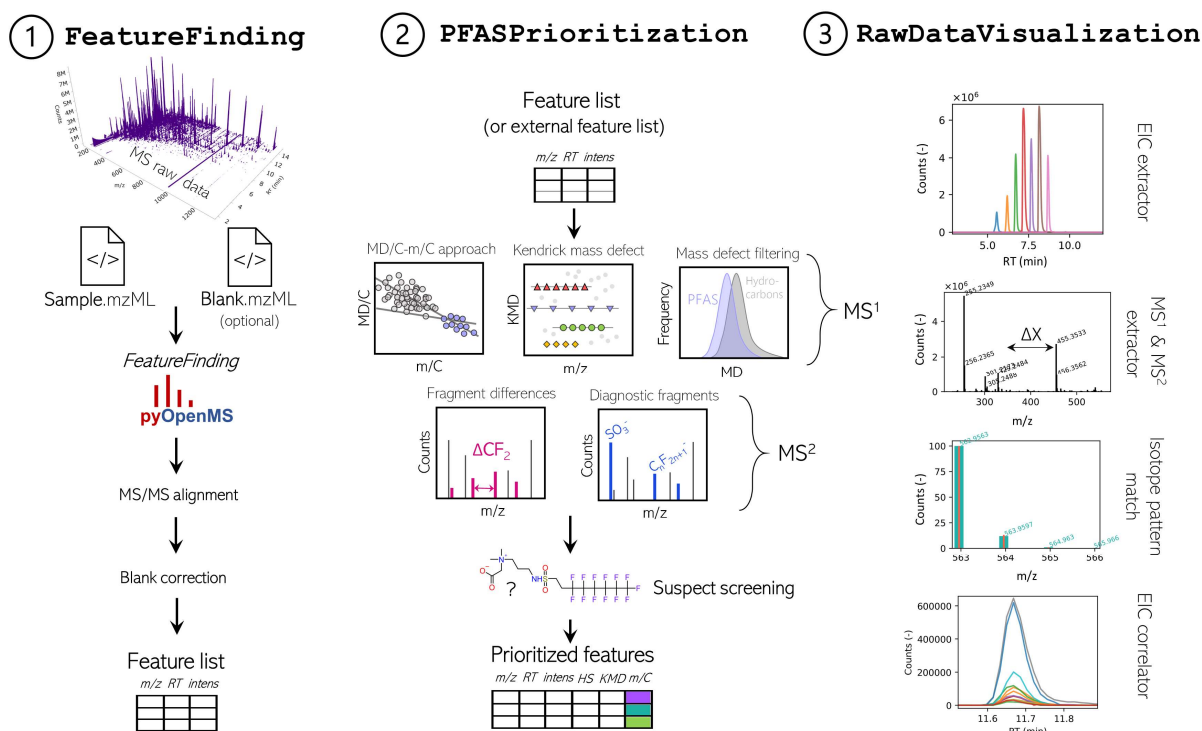


Figure 9: Schematic overview of the PFAScreen workflow in the structure of the GUI which includes feature detection, PFAS feature prioritization and a final raw data visualization that includes manual identification of adducts and in-source fragments via coelution correlation.

The result of the workflow is a table with prioritized and partially annotated features and several plots such as a KMD vs. m/z plot, the MD/C- m/C plot and MS² spectra. Since in NTS, a manual verification of features with a tentative hit (e.g., suspect hit) is crucial, the PFAScreen interface allows the user to visualize the MS raw data after running the workflow. This includes the generation of EIC, MS¹ and MS² spectra (with detected mass differences and diagnostic fragments) as well as matching of theoretical with measured isotope patterns (see also Figure 9). Furthermore, to manually cluster potential in-source fragments (e.g., neutral loss of HF) or adducts (e.g., $[M-H]^-$ and $[M+CH_3COO]^-$) together, it is possible to correlate the EIC of a particular feature of interest with all EICs of coeluting features and detect only highly correlating EICs since those potentially originate from the same compound (Guo et al., 2021; Kuhl et al., 2012).

To present the workflow, two soils from Rastatt (R1 & R2) and two soils from Mannheim (M1 & M2) were extracted and measured by HPLC-QTOF-MS and the MS raw data was processed with PFAScreen. By removing features with an m/C ratio < 30, which is unlikely low for highly fluorinated PFAS, 92% of the detected features could be removed which shows how powerful the m/C dimension is with respect to prioritization purposes in real MS data (see Figure 10).

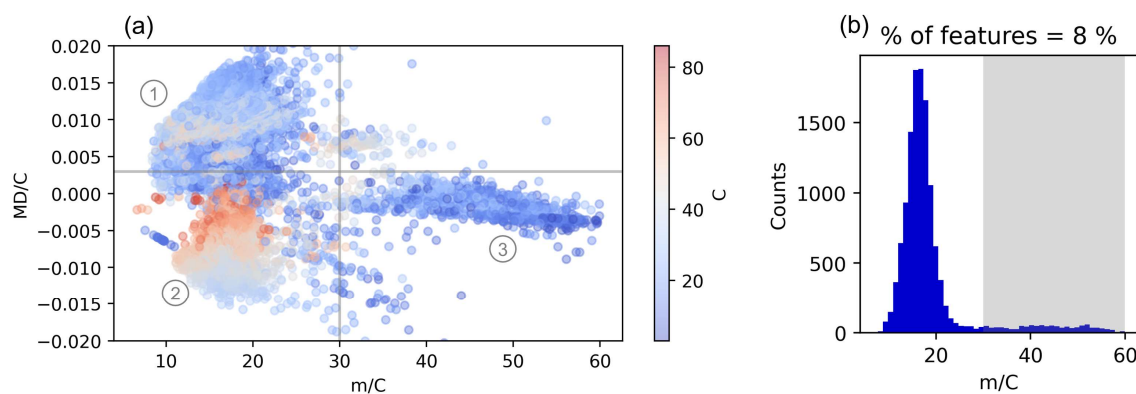


Figure 10: (a) MD/C-m/C plot of 12692 features detected in all four soils. The colorbar corresponds to the estimated carbon number. In the MD/C-m/C plot, potential PFAS (number 3) are clearly separated from hydrocarbons (number 1) and hydrocarbons with overlapping MD (number 2) (that exceed a MD of +0.5 Da due to high numbers of hydrogen atoms). They overlap in the MD/C dimension, however, by the more powerful m/C they can be easily separated. (b) Histogram of the feature numbers over the m/C dimension, which again highlights that most features in the soil extracts strongly differ from typical m/C ratios of PFAS.

As exemplified on soil M1, the application of CF_2 -based KMD analysis to the subset of features with $m/C > 30$ led to the detection of 26 homologous series and in the MS^2 data, 30 and 47 spectra exhibited PFAS-specific fragment mass differences and diagnostic fragments, respectively. It is important to note that further potential PFAS MS^2 spectra were detected in iterative measurements where other precursor masses were triggered. During suspect screening, 176 tentative hits by accurate mass were found in soil M1. Manual verification of the potential PFAS hits prioritized by PFAScreen resulted in the identification of more than 80 single PFAS with several isomers in the four soils (see Figure 11). Identified PFAS included classes such as PFCAs, PFSAs, fluorotelomer alkyl phosphate diesters (diPAPs), n:3 fluorotelomer carboxylic acids (FTCAs), fluorotelomer sulfonic acids (FTSAs), fluorotelomer mercapto alkyl phosphate esters (FTMAPs), and single PASF-based compounds such as perfluorooctane sulfonamide (PFOSA), N-ethylperfluoro-1-octanesulfonamidoacetic acid (N-EtFOSAA), and N-ethyl perfluorooctane sulfonamide ethanol-based phosphate diester (diSAM-PAP). Furthermore, several novel FTMAP related substances or TPs could be identified in the soils from Mannheim. The identification was possible with the correlation tool of PFAScreen since several adducts and in-source fragments (but no typical $[\text{M}-\text{H}]^-$ ions) were detected because the identified FTMAP related compounds were diols that are usually not ionizable in a deprotonated form. The FTMAP chemistries were only detected in the soils from Mannheim indicating a different source of contamination. In conclusion, the PFAScreen tool can be efficiently used to perform PFAS-prioritization and assistance during identification in HRMS raw data. The tool is available via GitHub and can be easily installed via batch files.

Detailed information and methodology can be found in publication 4 in the Appendix (A4).

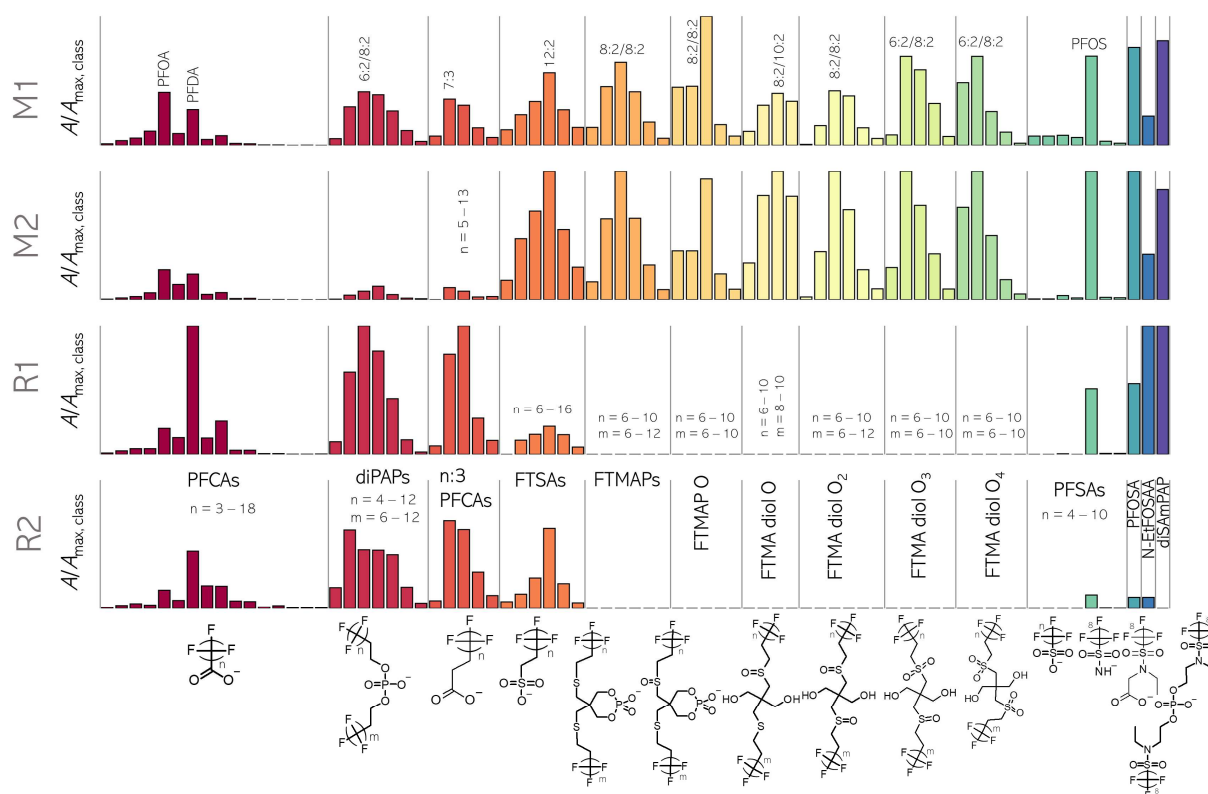


Figure 11: Overview of the identified PFAS classes in the four soils from Mannheim and Rastatt. The peak areas of each compound class were normalized to the highest peak area of the highest homologue in all four soils to allow a relative comparison.

4.5. PFAS HRMS review

During this dissertation, I was part of writing a critical review article discussing advantages and limitations of promising techniques for PFAS prioritization and identification by chromatographic techniques (LC and GC) coupled to HRMS. Resulting from the literature review, the most important methods relying on MS^1 data (full scan) were MD filtering, KMD analysis, the novel MD/C-m/C approach, chemical formula assignment with restricted elements towards detection of fluorinated compounds, and suspect screening (that also includes mass spectral library matching). In the MS^2 space, diagnostic fragments and mass differences or neutral losses are important techniques. Another promising approach is the so-called fragment ion flagging which uses either the elution profiles of PFAS specific in-source fragments or fragments during data-independent acquisition (DIA) to locate RT-ranges where potential PFAS elute. An overview is depicted in Figure 12. More recent instrumental advances that add another dimension to HRMS data such as ion mobility spectrometry (IMS) can further improve identification confidence and are able to separate for instance important and often ignored PFAS isomers.

Overall, more than 750 novel PFAS were identified in the environment in the last years highlighting the importance of NTS as a much wider analytical window compared to conventional target screening (Liu et al., 2019).

Detailed information and methodology can be found in publication 5 in the Appendix (A5).

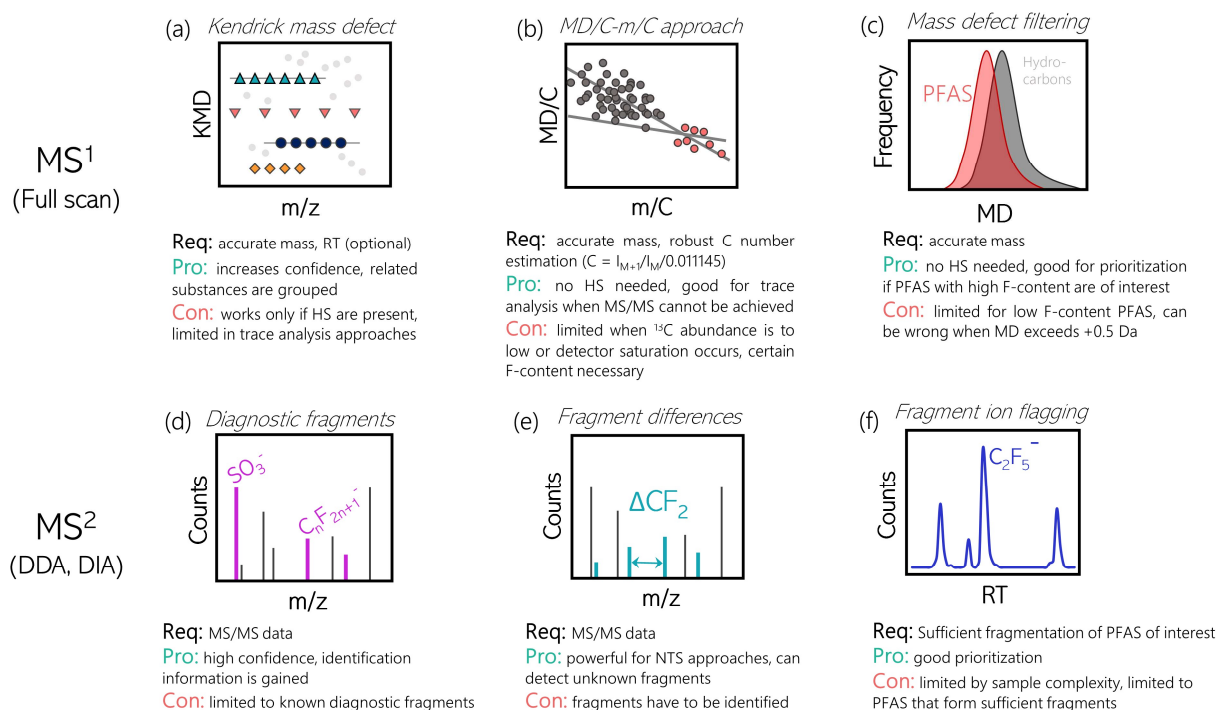


Figure 12: Overview of the most important prioritization and identification approaches used for PFAS NTS by chromatographic techniques coupled to HRMS. Abbreviations: KMD: Kendrick mass defect, HS: homologous series, RT: retention time, MD: mass defect, C: carbon atom, m: mass, Da: Dalton, DDA: data-dependent acquisition, DIA: data-independent acquisition.

4.6. Precursor oxidation via UV/TiO₂

As an alternative to the existing TOP assay which generates OH-radicals from thermal decomposition of peroxydisulfate at a high pH for oxidative conversion of PFAA-precursors, the “PhotoTOP” was developed which relies on photocatalytic generation of OH-radicals via UV/TiO₂. Estimating concentrations of precursors via oxidation is an important complementary approach to conventional extraction and mass spectrometric detection and can cover for instance also non-ionizable or non-extractable precursors. It was shown in spike experiments that a quantitative conversion with the PhotoTOP setup of known PFAA-precursors within less than 4 h of oxidation was possible resulting in a closed mass balance for diPAPs, FTCAs, FTSA, PFOSA, and N-EtFOSAA by transformation to PFCAs (Figure 13a). A major advantage of the PhotoTOP is the fact that the perfluoroalkyl chains are mostly conserved in the form of n-1. For example, the

oxidation of 8:2 FTSA (8 perfluorinated carbon atoms; $n = 8$) yielded mostly PFOA which means that one CF_2 -unit was oxidized as PFOA has 7 perfluorinated carbon atoms ($n = 7$) and a carboxylic acid group. Minor fractions of the yielded PFCAs exhibit the original perfluoroalkyl chain length (perfluorononanoic acid) or are shortened by more than one CF_2 -unit (Figure 13a). This allows to partially elucidate the chain length of precursors. Furthermore, due to the absence of any salts, the subsequent sample preparation steps are less time consuming compared to the TOP assay and allow direct injection with conventional ESI-MS without discriminating SPE. This can be beneficial especially for complex samples where no information on potential precursors, and therefore, on expected oxidation products is available. Another potential benefit of the PhotoTOP is the photocatalytic nature of the OH-radical production. While in the TOP assay only a defined amount of oxidizing agent is available which is consumed over time also by other compounds than PFAA-precursors in case of high dissolved organic carbon content, in the PhotoTOP, the oxidation time can be extended, and the OH-radical production continues. In theory this can be done until all precursors are quantitatively oxidized to PFAAs. However, this should be investigated in more detail in the future.

To present the conservation of the chain length distribution of precursors with more complex real samples, extracts of PFAS-coated papers where the precursors were known previously were oxidized and the formed PFAA chain lengths were correlated with the precursor chain lengths (Figure 13b). Direct oxidation of selected papers was also included.

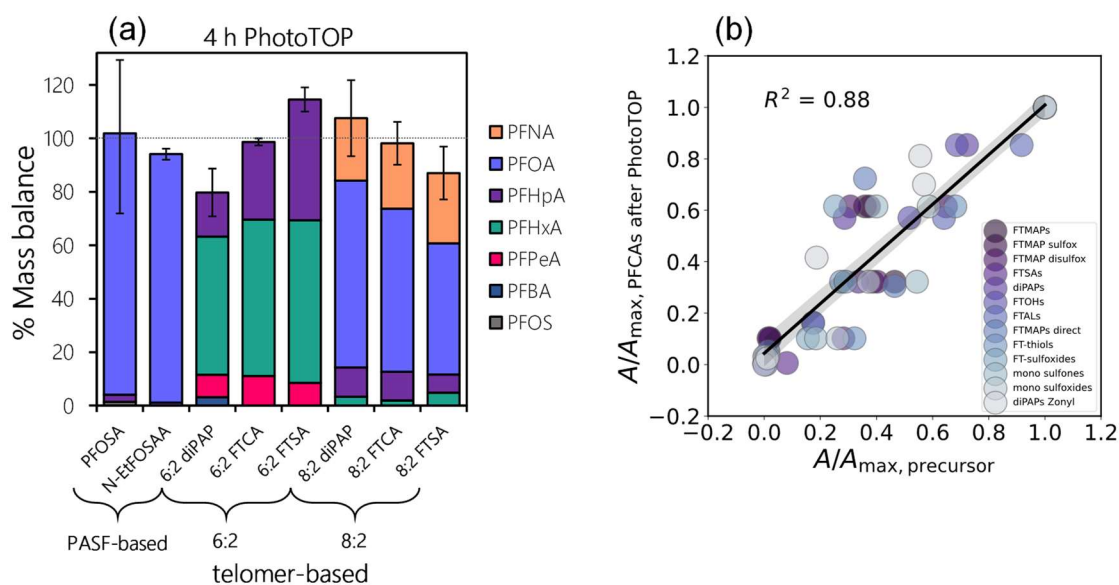


Figure 13: (a) Mass balance of the formed PFCAs from 8 known precursors after an application of the PhotoTOP oxidation for 4 hours. (b) Normalized peak areas of even-numbered PFCAs after PhotoTOP oxidation vs. normalized peak areas of different precursors from several paper extracts and direct paper oxidation. The correlation shows that the perfluoroalkyl chain lengths of precursors are conserved overall after oxidative conversion.

This shows that even in case of complex mixtures, relevant information on perfluoroalkyl chain lengths of unknown precursors is available. This is of particular relevance due to the restriction and bioaccumulation potential of longer chain PFAS. In the course of the NTS for the PFAA-precursors in the paper sample two novel classes of FTMAP TPs could be identified.

Finally, a commercial polymeric PFAS standard that was used as a water and grease repellent coating for different products and a textile sample that was suspected to be coated with SFPs were investigated with the PhotoTOP. When extracted with MeOH, no PFAS could be detected in the extracts. After direct oxidation, high concentrations of PFAAs formed which shows that also non-extractable and potentially non-ionizable precursors are amenable to the PhotoTOP. Such compounds are very important because they are often overlooked even by NTS approaches although they can be present in high concentrations in products and they were also shown to emit both volatile FTOHs (in indoor environment, e.g., from carpets) and PFAAs into the environment.

Detailed information and methodology can be found in publication 6 in the Appendix (A6).

4.7. Characterization of SFPs in textiles

To compare the performance of the developed PhotoTOP with complementary techniques for a characterization of SFPs in functional textiles, several samples that were suspected to contain fluorinated durable water repellent (DWR) coatings were ordered in 2022. SFPs are usually not amenable to mass spectrometry since the perfluoroalkyl side chains are covalently bound to the polymer backbone. Therefore, they are either non-extractable, or if partially extractable, molecular weights are too high for ESI. Examples for different textiles ordered were shower curtain, sunbed fabric, umbrella fabric, awning fabric, outdoor fabric, and Cordura. A subset of the textiles was prioritized by contact angle measurements with oil and water and several methods were applied. Extracts were screened for PFAAs and other common PFAS (before oxidation/hydrolysis), textiles were directly oxidized and hydrolyzed via PhotoTOP, dTOP, and THP, and additionally EOF and TF measurements were performed. It could be shown that both conventional extraction and detection of PFAAs as well as EOF were not able to comprehensively capture the organic fluorine present in the textiles. After oxidation or hydrolysis, the amount of organic fluorine (in the form of PFAAs or FTOHs) increased by a factor of 50 compared to the extractable PFAS, clearly indicating the presence of non-extractable SFPs. The chain length distribution of SFPs in the textiles could be described best by the THP assay since the original chain length is conserved when precursors are hydrolyzed. Also, the PhotoTOP resulted in much less chain shortening than the dTOP (Figure

14). It should be noted that the results also indicated that the THP assay is more selective due to hydrolysis compared to OH-radicals in case of dTOP and PhotoTOP.

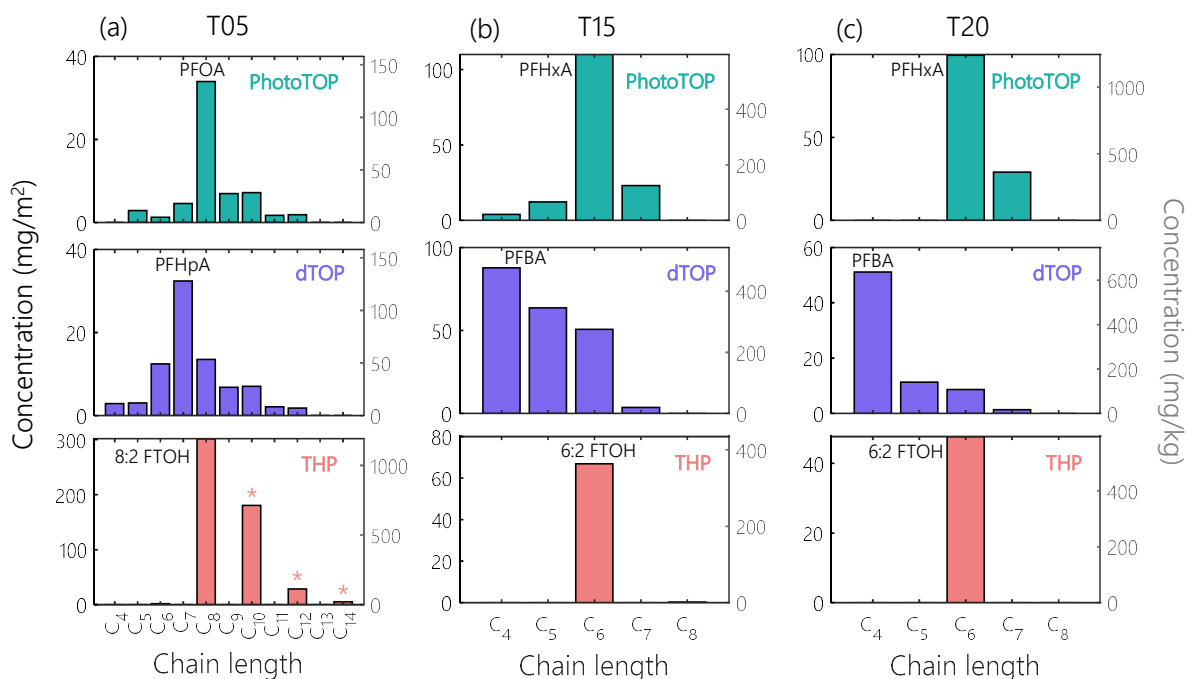


Figure 14: Comparison of concentrations of PFCAs and FTOHs formed from application of PhotoTOP (green), dTOP (blue), and THP (red) in the textiles T05, T15, and T20. Note that in the case of PFCAs, the total chain length (including carboxylic acid) is shown (e.g., PFOA = C8) while for FTOHs the perfluoroalkyl chain length was used (e.g., 8:2 FTOH = C8). The PhotoTOP was able to conserve the main perfluoroalkyl chain to $(n - 1)$ PFCAs. Asterisks highlight semi-quantified FTOHs.

A correlation between the formed PFCAs after PhotoTOP and dTOP and both EOF and TF measurements was observed (Figure 15). While the EOF was much lower, approximately 50% of the TF could be explained by fluorinated side chains generated by the oxidative methods. In previous studies, the explainable TF via PFCA formation from the dTOP was in the range of only 1% (Liagkouridis et al., 2021). Overall, the concentrations of SFPs in the textiles were in a comparable range compared to other studies. For oxidation/hydrolysis they range from <LOQ to over ~ 1000 mg F kg⁻¹ and for TF from <LOQ to > 2000 mg F kg⁻¹, while the EOF and target PFAS in extracts were detected at much lower concentrations (up to ~ 60 mg F kg⁻¹). The amount of fluorine in the investigated textiles was in the order of extraction \ll EOF \ll oxidation/hydrolysis $<$ TF. With over one mass percent of fluorine, the highest concentration of perfluoroalkyl side chains was detected in an outdoor fabric that was certified by the OekoTex Standard 100. Such certificates are usually based on extraction which further highlights the importance of methods such as PhotoTOP, dTOP or fluorine sum parameters. In conclusion, this study shows that even with restrictions, long-chain PFAA precursors such as SFPs are still used in high amounts in consumer products such as textiles today. Those SFPs were shown to emit both

PFAAs and FTOHs into the environment during their lifecycle and especially after their disposal for instance in waste incineration or landfills (Schellenberger, Jonsson, et al., 2019; Washington et al., 2015).

Detailed information and methodology can be found in publication 7 in the Appendix (A7).

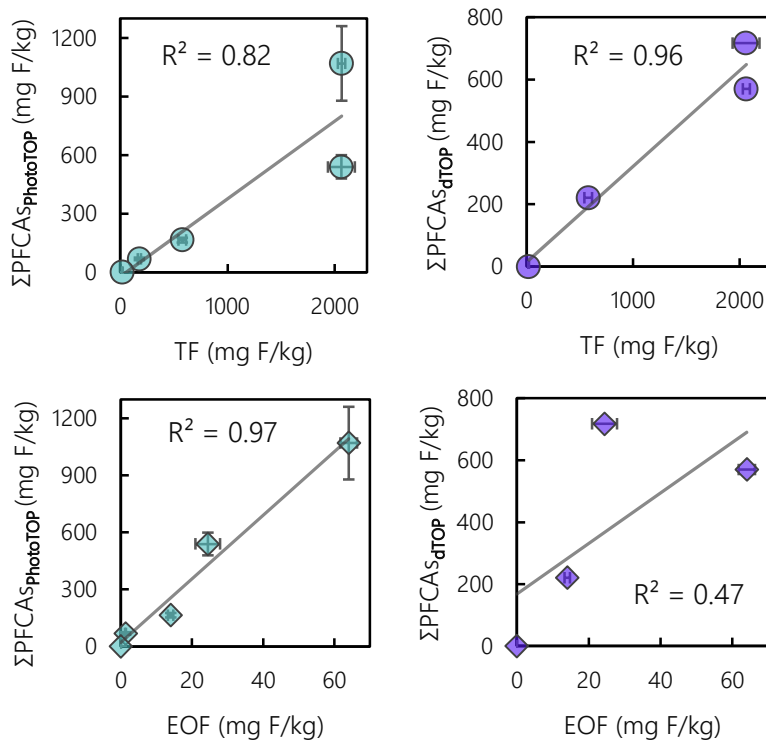


Figure 15: Correlation of fluorine in the sum of formed PFCAs after PhotoTOP and dTOP oxidation vs. fluorine from TF and EOF measurements. Compared with TF, an almost complete conversion (~50%) of SFPs to PFCAs was possible via oxidation when directly applied to the textiles. The measured EOF was much lower due insufficient extraction of SFPs, which is also reflected by low concentrations of PFCAs in oxidized textile extracts. Error bars from PhotoTOP measurements correspond to duplicate sampling (error calculated using Gaussian error propagation), while for EOF and TF they represent triplicate measurements.



5. Conclusions and outlook

In this dissertation both, NTS approaches for the identification of PFAS in complex samples were developed and applied as well as chemical conversion techniques (oxidation and hydrolysis) were used to unravel PFAS that are usually not amenable to mass spectrometry. During NTS, the MD/C-m/C approach that normalizes the mass defect (MD) and the measured mass to the carbon number C which can be estimated from the isotopic abundance of ^{13}C was evaluated and shown to be able to remove large fractions of background signals and signals that originate from non- or very low-fluorinated compounds. This resulted in an efficient data reduction in complex samples of the detected MS^1 signals allowing downstream approaches with considerably less false positive detections. To perform also MS^2 prioritization, fragment mass differences were combined with diagnostic fragments to detect spectra that originate from PFAS with a high probability. With the developed NTS approaches, an efficient prioritization of PFAS in complex HRMS datasets was possible and soil contaminations were characterized both from the Rastatt region and a contaminated site in Brilon-Scharfenberg. This resulted in identification of in total more than 100 single PFAS which also included several novel PFAS classes that were not reported before. In soil from Brilon-Scharfenberg, the NTS was combined with a semi-quantification approach which showed that more than $\sim 75\%$ of the PFAS were overlooked by previous target analyses. This could clearly demonstrate the importance of HRMS in combination with efficient data evaluation to characterize complex PFAS contaminations in more detail compared to target analysis which often missed significant fractions of PFAS in the past. Although accurate concentrations of identified analytes cannot be directly determined via NTS, it is a necessary and important first step because methods that rely on reference standards for each analyte are often unable to cover large fractions of the PFAS found in the environment.

Eventually, several NTS methods that were used and developed individually during this dissertation were combined into the step-wise data processing tool PFAScreen that is openly accessible and can easily be used by other analytical chemists for PFAS NTS. It works independently on the used mass spectrometric vendor with data dependent acquisition (DDA) MS raw data (LC- and GC with ESI or APCI) and allows both prioritization and tentative identification. Open-source software is an important part of the NTS community, makes the identification of organic contaminants in the environment and biological samples more reproducible and accelerates the discovery of new compounds.

Nevertheless, there are still limitations in NTS approaches that need to be addressed in the future. Although many PFAS could be identified, the identification of true unknowns is still very difficult and time consuming since it often has to be done manually. Manual identification and structure elucidation are very tedious and require expert knowledge on interpretation of mass spectra. Therefore, it is very important to report all identifications and annotated fragmentation spectra into publicly available databases such as PubChem. If chemical information on already known compounds is missing in chemical databases, their manual identification is rather time consuming while access to their structures allows faster identification via suspect screening.

Furthermore, for confident identification, MS² spectra are a prerequisite. The used DDA methods usually cover only a fraction of the detected ions and potential PFAS MS² spectra cannot be detected since they can be missing in the acquired datasets. This makes manual fragmentation experiments necessary. To overcome this incompleteness, data-independent acquisition (DIA) approaches could be used, which in principle, produce fragments of all ions. DIA datasets are more complex than DDA and the relation between precursor and fragmentation spectra is not given, however, more advanced data processing algorithms can be used in the future to potentially cover an even wider range of PFAS. Potentially, fragment mass differences can also be applied to DIA data to extract fragments of interest that are likely originating from fluorinated compounds.

Another important aspect of comprehensiveness in the mass spectrometric detection of PFAS is the usage of other chromatographic separations besides LC such as supercritical fluid chromatography (SFC) or GC that allow the coverage of analytes of very high polarity and high hydrophobicity, respectively. This should be considered in future studies, since analytes not detected by the used instrumental methods cannot be recognized and even the best algorithm or data processing approach will fail. Therefore, whenever extended chromatographic separation (or ion-mobility spectrometry) is available, it should be applied to increase the coverage of potential detectable analytes. There are of course also complementary techniques such as ¹⁹F-NMR that allow a different perspective on potential fluorinated compounds in samples of interest and increase the chemical information when combined with MS.

In the second part of this dissertation, several methods based on chemical conversion such as the developed PhotoTOP and the sum parameter TF were used to capture also PFAS that are not extractable and are therefore often not considered when only mass spectrometric detection is used. This further widens the analytical window to compounds that are not ionizable. The PhotoTOP assay generated relevant information such as chain-length distributions of precursors whose structure was unknown. Although a quantitative conversion was only possible in selected samples, the application of long enough oxidation times could cover more than 50% of the fluorine

in side-chain fluorinated polymers (SFPs) which was not possible in previous studies. Since the discrepancy between fluorine sum parameters and individual detected compounds is still significantly large in many environmental and consumer product samples, future work should be invested in optimization and standardization of those methods relying on chemical conversion towards fully quantitative information. Meanwhile, the structural information generated by chemical conversion is highly valuable and most other sum parameters lose this information. This knowledge can serve also as a prioritization for subsequent measurements with other techniques to obtain the identity of PFAS that form the detected oxidation or hydrolysis products. The ideal conversion should have rather mild conditions to retain as much structural information as possible but still be able to answer quantitative questions. In conclusion, it is always important to use a set of complementary tools to gain a deeper understanding of the chemistry of PFAS found in the environment and biota.

Robust analytical approaches are the basis for the identification of harmful chemicals around us and can provide the required information to act and stop emission and also production of toxic, mobile and persistent chemicals such as PFAS. A general principle is that reducing emissions at the source is always more efficient and cost-effective than removing widespread emissions from the environment. In fact, the latter is usually impossible within a reasonable framework of effort and cost. This is impressively illustrated by the large-scale contamination of the Rastatt and Brilon-Scharfenberg cases.



6. References

- Ahmadireskety, A., Da Silva, B. F., Townsend, T. G., Yost, R. A., Solo-Gabriele, H. M., & Bowden, J. A. (2021). Evaluation of extraction workflows for quantitative analysis of per- and polyfluoroalkyl substances: A case study using soil adjacent to a landfill. *Sci Total Environ*, *760*, 143944. <https://doi.org/10.1016/j.scitotenv.2020.143944>
- Ahrens, L. (2011). Polyfluoroalkyl compounds in the aquatic environment: a review of their occurrence and fate. *J Environ Monit*, *13*(1), 20-31. <https://doi.org/10.1039/c0em00373e>
- Ahrens, L., & Bundschuh, M. (2014). Fate and effects of poly- and perfluoroalkyl substances in the aquatic environment: a review. *Environ Toxicol Chem*, *33*(9), 1921-1929. <https://doi.org/10.1002/etc.2663>
- Aro, R., Eriksson, U., Kärrman, A., Chen, F., Wang, T., & Yeung, L. W. Y. (2021). Fluorine Mass Balance Analysis of Effluent and Sludge from Nordic Countries. *ACS ES&T Water*, *1*(9), 2087-2096. <https://doi.org/10.1021/acsestwater.1c00168>
- Aro, R., Eriksson, U., Kärrman, A., Jakobsson, K., & Yeung, L. W. Y. (2022). Extractable organofluorine analysis: A way to screen for elevated per- and polyfluoroalkyl substance contamination in humans? *Environ Int*, *159*, 107035. <https://doi.org/10.1016/j.envint.2021.107035>
- Aro, R., Eriksson, U., Kärrman, A., & Yeung, L. W. Y. (2021). Organofluorine Mass Balance Analysis of Whole Blood Samples in Relation to Gender and Age. *Environ Sci Technol*, *55*(19), 13142-13151. <https://doi.org/10.1021/acs.est.1c04031>
- Barzen-Hanson, K. A., Roberts, S. C., Choyke, S., Oetjen, K., McAlees, A., Riddell, N., McCrindle, R., Ferguson, P. L., Higgins, C. P., & Field, J. A. (2017). Discovery of 40 Classes of Per- and Polyfluoroalkyl Substances in Historical Aqueous Film-Forming Foams (AFFFs) and AFFF-Impacted Groundwater. *Environ Sci Technol*, *51*(4), 2047-2057. <https://doi.org/10.1021/acs.est.6b05843>
- Benskin, J. P., Ikonomidou, M. G., Gobas, F. A., Woudneh, M. B., & Cosgrove, J. R. (2012). Observation of a novel PFOS-precursor, the perfluorooctane sulfonamido ethanol-based phosphate (SAmPAP) diester, in marine sediments. *Environ Sci Technol*, *46*(12), 6505-6514. <https://doi.org/10.1021/es300823m>
- Brendel, S., Fetter, E., Staude, C., Vierke, L., & Biegel-Engler, A. (2018). Short-chain perfluoroalkyl acids: environmental concerns and a regulatory strategy under REACH. *Environ Sci Eur*, *30*(1), 9. <https://doi.org/10.1186/s12302-018-0134-4>
- Brennan, N. M., Evans, A. T., Fritz, M. K., Peak, S. A., & von Holst, H. E. (2021). Trends in the Regulation of Per- and Polyfluoroalkyl Substances (PFAS): A Scoping Review. *Int J Environ Res Public Health*, *18*(20). <https://doi.org/10.3390/ijerph182010900>
- Brunn, H., Arnold, G., Körner, W., Rippen, G., Steinhäuser, K. G., & Valentin, I. (2023). PFAS: forever chemicals—persistent, bioaccumulative and mobile. Reviewing the status and the need for their

-
- phase out and remediation of contaminated sites. *Environmental Sciences Europe*, 35(1). <https://doi.org/10.1186/s12302-023-00721-8>
- Buck, R. C., Franklin, J., Berger, U., Conder, J. M., Cousins, I. T., de Voogt, P., Jensen, A. A., Kannan, K., Mabury, S. A., & van Leeuwen, S. P. (2011). Perfluoroalkyl and polyfluoroalkyl substances in the environment: terminology, classification, and origins. *Integr Environ Assess Manag*, 7(4), 513-541. <https://doi.org/10.1002/ieam.258>
- Bugsel, B., Bauer, R., Herrmann, F., Maier, M. E., & Zwiener, C. (2022). LC-HRMS screening of per- and polyfluorinated alkyl substances (PFAS) in impregnated paper samples and contaminated soils. *Anal Bioanal Chem*, 414(3), 1217-1225. <https://doi.org/10.1007/s00216-021-03463-9>
- Bugsel, B., & Zwiener, C. (2020). LC-MS screening of poly- and perfluoroalkyl substances in contaminated soil by Kendrick mass analysis. *Anal Bioanal Chem*, 412(20), 4797-4805. <https://doi.org/10.1007/s00216-019-02358-0>
- Cahuas, L., Muensterman, D. J., Kim-Fu, M. L., Reardon, P. N., Titaley, I. A., & Field, J. A. (2022). Paints: A Source of Volatile PFAS in Air horizontal line Potential Implications for Inhalation Exposure. *Environ Sci Technol*, 56(23), 17070-17079. <https://doi.org/10.1021/acs.est.2c04864>
- Chambers, M. C., Maclean, B., Burke, R., Amodei, D., Ruderman, D. L., Neumann, S., Gatto, L., Fischer, B., Pratt, B., Egertson, J., Hoff, K., Kessner, D., Tasman, N., Shulman, N., Frewen, B., Baker, T. A., Brusniak, M. Y., Paulse, C., Creasy, D., Flashner, L., Kani, K., Moulding, C., Seymour, S. L., Nuwaysir, L. M., Lefebvre, B., Kuhlmann, F., Roark, J., Rainer, P., Detlev, S., Hemenway, T., Huhmer, A., Langridge, J., Connolly, B., Chadick, T., Holly, K., Eckels, J., Deutsch, E. W., Moritz, R. L., Katz, J. E., Agus, D. B., MacCoss, M., Tabb, D. L., & Mallick, P. (2012). A cross-platform toolkit for mass spectrometry and proteomics. *Nat Biotechnol*, 30(10), 918-920. <https://doi.org/10.1038/nbt.2377>
- Cioni, L., Plassmann, M., Benskin, J. P., Coelho, A., Nost, T. H., Rylander, C., Nikiforov, V., Sandanger, T. M., & Herzke, D. (2023). Fluorine Mass Balance, including Total Fluorine, Extractable Organic Fluorine, Oxidizable Precursors, and Target Per- and Polyfluoroalkyl Substances, in Pooled Human Serum from the Tromsø Population in 1986, 2007, and 2015. *Environ Sci Technol*, 57(40), 14849-14860. <https://doi.org/10.1021/acs.est.3c03655>
- Cousins, I. T., DeWitt, J. C., Glüge, J., Goldenman, G., Herzke, D., Lohmann, R., Ng, C. A., Scheringer, M., & Wang, Z. (2020). The high persistence of PFAS is sufficient for their management as a chemical class. *Environ Sci Process Impacts*, 22(12), 2307-2312. <https://doi.org/10.1039/d0em00355g>
- D'Eon J. C., & Mabury, S. A. (2011). Exploring indirect sources of human exposure to perfluoroalkyl carboxylates (PFCAs): evaluating uptake, elimination, and biotransformation of polyfluoroalkyl phosphate esters (PAPs) in the rat. *Environ Health Perspect*, 119(3), 344-350. <https://doi.org/10.1289/ehp.1002409>
- D'Eon, J. C., & Mabury, S. A. (2007). Production of perfluorinated carboxylic acids (PFCAs) from the biotransformation of polyfluoroalkyl phosphate surfactants (PAPS): exploring routes of human contamination. *Environ Sci Technol*, 41(13), 4799-4805. <https://doi.org/10.1021/es070126x>
- D'Eon, J. C., & Mabury, S. A. (2011). Is indirect exposure a significant contributor to the burden of perfluorinated acids observed in humans? *Environ Sci Technol*, 45(19), 7974-7984. <https://doi.org/10.1021/es200171y>

-
- De Silva, A. O., Armitage, J. M., Bruton, T. A., Dassuncao, C., Heiger-Bernays, W., Hu, X. C., Karrman, A., Kelly, B., Ng, C., Robuck, A., Sun, M., Webster, T. F., & Sunderland, E. M. (2021). PFAS Exposure Pathways for Humans and Wildlife: A Synthesis of Current Knowledge and Key Gaps in Understanding. *Environ Toxicol Chem*, *40*(3), 631-657. <https://doi.org/10.1002/etc.4935>
- Deutsch, E. W. (2012). File formats commonly used in mass spectrometry proteomics. *Mol Cell Proteomics*, *11*(12), 1612-1621. <https://doi.org/10.1074/mcp.R112.019695>
- DIRECTIVE (EU) 2020/2184. (2020). *DIRECTIVE (EU) 2020/2184 OF THE EUROPEAN PARLIAMENT AND OF THE COUNCIL* (Official Journal of the European Union, Issue. <https://eur-lex.europa.eu/legal-content/EN/TXT/PDF/?uri=CELEX:32020L2184>
- Dodds, J. N., Alexander, N. L. M., Kirkwood, K. I., Foster, M. R., Hopkins, Z. R., Knappe, D. R. U., & Baker, E. S. (2021). From Pesticides to Per- and Polyfluoroalkyl Substances: An Evaluation of Recent Targeted and Untargeted Mass Spectrometry Methods for Xenobiotics. *Anal Chem*, *93*(1), 641-656. <https://doi.org/10.1021/acs.analchem.0c04359>
- ECHA. (2023). *ECHA publishes PFAS restriction proposal*. Retrieved 21.09.2023 from <https://echa.europa.eu/de/-/echa-publishes-pfas-restriction-proposal>
- Eriksson, U., Haglund, P., & Karrman, A. (2017). Contribution of precursor compounds to the release of per- and polyfluoroalkyl substances (PFASs) from waste water treatment plants (WWTPs). *J Environ Sci*, *61*, 80-90. <https://doi.org/10.1016/j.jes.2017.05.004>
- Evich, M. G., Davis, M. J. B., McCord, J. P., Acrey, B., Awkerman, J. A., Knappe, D. R. U., Lindstrom, A. B., Speth, T. F., Tebes-Stevens, C., Strynar, M. J., Wang, Z., Weber, E. J., Henderson, W. M., & Washington, J. W. (2022). Per- and polyfluoroalkyl substances in the environment. *Science*, *375*(6580), eabg9065. <https://doi.org/10.1126/science.abg9065>
- Gaines, L. G. T. (2023). Historical and current usage of per- and polyfluoroalkyl substances (PFAS): A literature review. *Am J Ind Med*, *66*(5), 353-378. <https://doi.org/10.1002/ajim.23362>
- Gauthier, J. R., & Mabury, S. A. (2023). Identifying Unknown Fluorine-Containing Compounds in Environmental Samples Using (19)F NMR and Spectral Database Matching. *Environ Sci Technol*, *57*(23), 8760-8767. <https://doi.org/10.1021/acs.est.3c01220>
- Gehrenkemper, L., Simon, F., Roesch, P., Fischer, E., von der Au, M., Pfeifer, J., Cossmer, A., Wittwer, P., Vogel, C., Simon, F. G., & Meermann, B. (2021). Determination of organically bound fluorine sum parameters in river water samples-comparison of combustion ion chromatography (CIC) and high resolution-continuum source-graphite furnace molecular absorption spectrometry (HR-CS-GFMAS). *Anal Bioanal Chem*, *413*(1), 103-115. <https://doi.org/10.1007/s00216-020-03010-y>
- Glüge, J., Scheringer, M., Cousins, I. T., DeWitt, J. C., Goldenman, G., Herzke, D., Lohmann, R., Ng, C. A., Trier, X., & Wang, Z. (2020). An overview of the uses of per- and polyfluoroalkyl substances (PFAS). *Environ Sci Process Impacts*, *22*(12), 2345-2373. <https://doi.org/10.1039/d0em00291g>
- Göckener, B., Eichhorn, M., Lammer, R., Kotthoff, M., Kowalczyk, J., Numata, J., Schafft, H., Lahrssen-Wiederholt, M., & Bucking, M. (2020). Transfer of Per- and Polyfluoroalkyl Substances (PFAS) from Feed into the Eggs of Laying Hens. Part 1: Analytical Results Including a Modified Total

-
- Oxidizable Precursor Assay. *J Agric Food Chem*, 68(45), 12527-12538. <https://doi.org/10.1021/acs.jafc.0c04456>
- Gremmel, C., Fromel, T., & Knepper, T. P. (2016). Systematic determination of perfluoroalkyl and polyfluoroalkyl substances (PFASs) in outdoor jackets. *Chemosphere*, 160, 173-180. <https://doi.org/10.1016/j.chemosphere.2016.06.043>
- Gross, J. H. (2017). *Mass Spectrometry - A Textbook*. <https://doi.org/10.1007/978-3-319-54398-7>
- Grulke, C. M., Williams, A. J., Thillanadarajah, I., & Richard, A. M. (2019). EPA's DSSTox database: History of development of a curated chemistry resource supporting computational toxicology research. *Comput Toxicol*, 12. <https://doi.org/10.1016/j.comtox.2019.100096>
- Guelfo, J. L., Korzeniowski, S., Mills, M. A., Anderson, J., Anderson, R. H., Arblaster, J. A., Conder, J. M., Cousins, I. T., Dasu, K., Henry, B. J., Lee, L. S., Liu, J., McKenzie, E. R., & Willey, J. (2021). Environmental Sources, Chemistry, Fate, and Transport of Per- and Polyfluoroalkyl Substances: State of the Science, Key Knowledge Gaps, and Recommendations Presented at the August 2019 SETAC Focus Topic Meeting. *Environ Toxicol Chem*, 40(12), 3234-3260. <https://doi.org/10.1002/etc.5182>
- Guo, J., Shen, S., Xing, S., Yu, H., & Huan, T. (2021). ISFrag: De Novo Recognition of In-Source Fragments for Liquid Chromatography-Mass Spectrometry Data. *Anal Chem*, 93(29), 10243-10250. <https://doi.org/10.1021/acs.analchem.1c01644>
- Gustafsson, A., Bergman, A., & Weiss, J. M. (2022). Estimated daily intake of per- and polyfluoroalkyl substances related to different particle size fractions of house dust. *Chemosphere*, 303(Pt 2), 135061. <https://doi.org/10.1016/j.chemosphere.2022.135061>
- Harris, D. C. (2014). *Lehrbuch der Quantitativen Analyse*. Springer.
- Helmus, R., Ter Laak, T. L., van Wezel, A. P., de Voogt, P., & Schymanski, E. L. (2021). patRoom: open source software platform for environmental mass spectrometry based non-target screening. *J Cheminform*, 13(1), 1. <https://doi.org/10.1186/s13321-020-00477-w>
- Henry, B. J., Carlin, J. P., Hammerschmidt, J. A., Buck, R. C., Buxton, L. W., Fiedler, H., Seed, J., & Hernandez, O. (2018). A critical review of the application of polymer of low concern and regulatory criteria to fluoropolymers. *Integrated Environmental Assessment and Management*, 14(3), 316-334. <https://doi.org/10.1002/ieam.4035>
- Hollender, J., Schymanski, E. L., Ahrens, L., Alygizakis, N., Béen, F., Bijlsma, L., Brunner, A. M., Celma, A., Fildier, A., Fu, Q. G., Gago-Ferrero, P., Gil-Solsona, R., Haglund, P., Hansen, M., Kaserzon, S., Krueve, A., Lamoree, M., Margoum, C., Meijer, J., Merel, S., Rauert, C., Rostkowski, P., Samanipour, S., Schulze, B., Schulze, T., Singh, R. R., Slobodnik, J., Steininger-Mairinger, T., Thomaidis, N. S., Togola, A., Vorkamp, K., Vulliet, E., Zhu, L. Y., & Krauss, M. (2023). NORMAN guidance on suspect and non-target screening in environmental monitoring. *Environmental Sciences Europe*, 35(1). <https://doi.org/10.1186/s12302-023-00779-4>
- Hollender, J., Schymanski, E. L., Singer, H. P., & Ferguson, P. L. (2017). Nontarget Screening with High Resolution Mass Spectrometry in the Environment: Ready to Go? *Environ Sci Technol*, 51(20), 11505-11512. <https://doi.org/10.1021/acs.est.7b02184>

-
- Holmquist, H., Schellenberger, S., van der Veen, I., Peters, G. M., Leonards, P. E., & Cousins, I. T. (2016). Properties, performance and associated hazards of state-of-the-art durable water repellent (DWR) chemistry for textile finishing. *Environ Int*, *91*, 251-264. <https://doi.org/10.1016/j.envint.2016.02.035>
- Horai, H., Arita, M., Kanaya, S., Nihei, Y., Ikeda, T., Suwa, K., Ojima, Y., Tanaka, K., Tanaka, S., Aoshima, K., Oda, Y., Kakazu, Y., Kusano, M., Tohge, T., Matsuda, F., Sawada, Y., Hirai, M. Y., Nakanishi, H., Ikeda, K., Akimoto, N., Maoka, T., Takahashi, H., Ara, T., Sakurai, N., Suzuki, H., Shibata, D., Neumann, S., Iida, T., Tanaka, K., Funatsu, K., Matsuura, F., Soga, T., Taguchi, R., Saito, K., & Nishioka, T. (2010). MassBank: a public repository for sharing mass spectral data for life sciences. *J Mass Spectrom*, *45*(7), 703-714. <https://doi.org/10.1002/jms.1777>
- Houtz, E. F., & Sedlak, D. L. (2012). Oxidative conversion as a means of detecting precursors to perfluoroalkyl acids in urban runoff. *Environ Sci Technol*, *46*(17), 9342-9349. <https://doi.org/10.1021/es302274g>
- Huang, K., Li, Y., Bu, D., Fu, J., Wang, M., Zhou, W., Gu, L., Fu, Y., Cong, Z., Hu, B., Fu, J., Zhang, A., & Jiang, G. (2022). Trophic Magnification of Short-Chain Per- and Polyfluoroalkyl Substances in a Terrestrial Food Chain from the Tibetan Plateau. *Environmental Science & Technology Letters*, *9*(2), 147-152. <https://doi.org/10.1021/acs.estlett.1c01009>
- Hulleman, T., Turkina, V., O'Brien, J. W., Chojnacka, A., Thomas, K. V., & Samanipour, S. (2023). Critical Assessment of the Chemical Space Covered by LC-HRMS Non-Targeted Analysis. *Environ Sci Technol*, *57*(38), 14101-14112. <https://doi.org/10.1021/acs.est.3c03606>
- Janda, J., Nodler, K., Scheurer, M., Happel, O., Nurenberg, G., Zwiener, C., & Lange, F. T. (2019). Closing the gap - inclusion of ultrashort-chain perfluoroalkyl carboxylic acids in the total oxidizable precursor (TOP) assay protocol. *Environ Sci Process Impacts*, *21*(11), 1926-1935. <https://doi.org/10.1039/c9em00169g>
- Jia, S., Marques Dos Santos, M., Li, C., & Snyder, S. A. (2022). Recent advances in mass spectrometry analytical techniques for per- and polyfluoroalkyl substances (PFAS). *Anal Bioanal Chem*, *414*(9), 2795-2807. <https://doi.org/10.1007/s00216-022-03905-y>
- Jia, X., Guan, H., Guo, Z., Qian, C., Shi, Y., & Cai, Y. (2021). Occurrence of Legacy and Emerging Poly- and Perfluoroalkyl Substances in Fluorocarbon Paint and Their Implications for Emissions in China. *Environmental Science & Technology Letters*, *8*(11), 968-974. <https://doi.org/10.1021/acs.estlett.1c00709>
- Jiao, E., Larsson, P., Wang, Q., Zhu, Z., Yin, D., Karrman, A., van Hees, P., Karlsson, P., Qiu, Y., & Yeung, L. W. Y. (2023). Further Insight into Extractable (Organo)fluorine Mass Balance Analysis of Tap Water from Shanghai, China. *Environ Sci Technol*, *57*(38), 14330-14339. <https://doi.org/10.1021/acs.est.3c02718>
- Joerss, H., Schramm, T. R., Sun, L., Guo, C., Tang, J., & Ebinghaus, R. (2020). Per- and polyfluoroalkyl substances in Chinese and German river water - Point source- and country-specific fingerprints including unknown precursors. *Environ Pollut*, *267*, 115567. <https://doi.org/10.1016/j.envpol.2020.115567>
- Johansson, J. H., Shi, Y., Salter, M., & Cousins, I. T. (2018). Spatial variation in the atmospheric deposition of perfluoroalkyl acids: source elucidation through analysis of isomer patterns. *Environ Sci Process Impacts*, *20*(7), 997-1006. <https://doi.org/10.1039/c8em00102b>

-
- Kaboré, H. A., Vo Duy, S., Munoz, G., Méité, L., Desrosiers, M., Liu, J., Sory, T. K., & Sauvé, S. (2018). Worldwide drinking water occurrence and levels of newly-identified perfluoroalkyl and polyfluoroalkyl substances. *Sci Total Environ*, *616-617*, 1089-1100. <https://doi.org/10.1016/j.scitotenv.2017.10.210>
- Kaufmann, A., Butcher, P., Maden, K., Walker, S., & Widmer, M. (2022). Simplifying Nontargeted Analysis of PFAS in Complex Food Matrixes. *J AOAC Int*, *105*(5), 1280-1287. <https://doi.org/10.1093/jaoacint/qsac071>
- Kenar, E., Franken, H., Forcisi, S., Wormann, K., Haring, H. U., Lehmann, R., Schmitt-Kopplin, P., Zell, A., & Kohlbacher, O. (2014). Automated label-free quantification of metabolites from liquid chromatography-mass spectrometry data. *Mol Cell Proteomics*, *13*(1), 348-359. <https://doi.org/10.1074/mcp.M113.031278>
- Kendrick, E. (1963). A Mass Scale Based on CH₂ = 14.0000 for High Resolution Mass Spectrometry of Organic Compounds. *Analytical Chemistry*, *35*(13), 2146-2154. <https://doi.org/10.1021/ac60206a048>
- Kim, S.-K., Shoeib, M., Kim, K.-S., & Park, J.-E. (2012). Indoor and outdoor poly- and perfluoroalkyl substances (PFASs) in Korea determined by passive air sampler. *Environmental Pollution*, *162*, 144-150. <https://doi.org/10.1016/j.envpol.2011.10.037>
- Kissa, E. (2001). *Fluorinated surfactants and repellents* (Vol. 97). CRC Press.
- Knepper, T., & Lange, F. T. (2012). Polyfluorinated Chemicals and Transformation Products. *Springer*. <https://doi.org/10.1007/978-3-642-21872-9>
- Koch, A., Aro, R., Wang, T., & Yeung, L. W. Y. (2020). Towards a comprehensive analytical workflow for the chemical characterisation of organofluorine in consumer products and environmental samples. *Trac-Trends in Analytical Chemistry*, *123*, 115423. <https://doi.org/10.1016/j.trac.2019.02.024>
- Koch, B. P., Dittmar, T., Witt, M., & Kattner, G. (2007). Fundamentals of molecular formula assignment to ultrahigh resolution mass data of natural organic matter. *Anal Chem*, *79*(4), 1758-1763. <https://doi.org/10.1021/ac061949s>
- Koelmel, J. P., Kroeger, N. M., Gill, E. L., Ulmer, C. Z., Bowden, J. A., Patterson, R. E., Yost, R. A., & Garrett, T. J. (2017). Expanding Lipidome Coverage Using LC-MS/MS Data-Dependent Acquisition with Automated Exclusion List Generation. *J Am Soc Mass Spectrom*, *28*(5), 908-917. <https://doi.org/10.1007/s13361-017-1608-0>
- Koelmel, J. P., Paige, M. K., Aristizabal-Henao, J. J., Robey, N. M., Nason, S. L., Stelben, P. J., Li, Y., Kroeger, N. M., Napolitano, M. P., Savvides, T., Vasiliou, V., Rostkowski, P., Garrett, T. J., Lin, E., Deigl, C., Jobst, K., Townsend, T. G., Godri Pollitt, K. J., & Bowden, J. A. (2020). Toward Comprehensive Per- and Polyfluoroalkyl Substances Annotation Using FluoroMatch Software and Intelligent High-Resolution Tandem Mass Spectrometry Acquisition. *Analytical Chemistry*, *92*(16), 11186-11194. <https://doi.org/10.1021/acs.analchem.0c01591>
- Kuhl, C., Tautenhahn, R., Bottcher, C., Larson, T. R., & Neumann, S. (2012). CAMERA: an integrated strategy for compound spectra extraction and annotation of liquid chromatography/mass spectrometry data sets. *Anal Chem*, *84*(1), 283-289. <https://doi.org/10.1021/ac202450g>

-
- LANUV. (2011). LANUV Fachbericht - Verbreitung von PFT in der Umwelt. *LANUV*.
- Li, F., Duan, J., Tian, S. T., Ji, H. D., Zhu, Y. M., Wei, Z. S., & Zhao, D. Y. (2020). Short-chain per- and polyfluoroalkyl substances in aquatic systems: Occurrence, impacts and treatment. *Chemical Engineering Journal*, *380*, 122506. <https://doi.org/10.1016/j.cej.2019.122506>
- Liagkouridis, I., Awad, R., Schellenberger, S., Plassmann, M. M., Cousins, I. T., & Benskin, J. P. (2021). Combined Use of Total Fluorine and Oxidative Fingerprinting for Quantitative Determination of Side-Chain Fluorinated Polymers in Textiles. *Environmental Science & Technology Letters*, *9*(1), 30-36. <https://doi.org/10.1021/acs.estlett.1c00822>
- Lindstrom, A. B., Strynar, M. J., & Libelo, E. L. (2011). Polyfluorinated compounds: past, present, and future. *Environ Sci Technol*, *45*(19), 7954-7961. <https://doi.org/10.1021/es2011622>
- Liu, J., & Mejia Avendano, S. (2013). Microbial degradation of polyfluoroalkyl chemicals in the environment: a review. *Environ Int*, *61*, 98-114. <https://doi.org/10.1016/j.envint.2013.08.022>
- Liu, L., Lu, M., Cheng, X., Yu, G., & Huang, J. (2022). Suspect screening and nontargeted analysis of per- and polyfluoroalkyl substances in representative fluorocarbon surfactants, aqueous film-forming foams, and impacted water in China. *Environment International*, *167*. <https://doi.org/10.1016/j.envint.2022.107398>
- Liu, Y., D'Agostino, L. A., Qu, G., Jiang, G., & Martin, J. W. (2019). High-resolution mass spectrometry (HRMS) methods for nontarget discovery and characterization of poly- and per-fluoroalkyl substances (PFASs) in environmental and human samples. *TrAC Trends in Analytical Chemistry*, *121*. <https://doi.org/10.1016/j.trac.2019.02.021>
- Lohmann, R., Cousins, I. T., DeWitt, J. C., Glüge, J., Goldenman, G., Herzke, D., Lindstrom, A. B., Miller, M. F., Ng, C. A., Patton, S., Scheringer, M., Trier, X., & Wang, Z. (2020). Are Fluoropolymers Really of Low Concern for Human and Environmental Health and Separate from Other PFAS? *Environ Sci Technol*, *54*(20), 12820-12828. <https://doi.org/10.1021/acs.est.0c03244>
- Loos, R., Gawlik, B. M., Locoro, G., Rimaviciute, E., Contini, S., & Bidoglio, G. (2009). EU-wide survey of polar organic persistent pollutants in European river waters. *Environmental Pollution*, *157*(2), 561-568. <https://doi.org/10.1016/j.envpol.2008.09.020>
- Macorps, N., Labadie, P., Lestremau, F., Assoumani, A., & Budzinski, H. (2023). Per- and polyfluoroalkyl substances (PFAS) in surface sediments: Occurrence, patterns, spatial distribution and contribution of unattributed precursors in French aquatic environments. *Sci Total Environ*, *874*, 162493. <https://doi.org/10.1016/j.scitotenv.2023.162493>
- Martin, D., Munoz, G., Mejia-Avendano, S., Duy, S. V., Yao, Y., Volchek, K., Brown, C. E., Liu, J., & Sauve, S. (2019). Zwitterionic, cationic, and anionic perfluoroalkyl and polyfluoroalkyl substances integrated into total oxidizable precursor assay of contaminated groundwater. *Talanta*, *195*, 533-542. <https://doi.org/10.1016/j.talanta.2018.11.093>
- Martin, J. W., Kannan, K., Berger, U., de Voogt, P., Field, J., Franklin, J., Giesy, J. P., Harner, T., Muir, D. C., Scott, B., Kaiser, M., Jarnberg, U., Jones, K. C., Mabury, S. A., Schroeder, H., Simcik, M., Sottani, C., van Bavel, B., Karrman, A., Lindstrom, G., & van Leeuwen, S. (2004). Analytical challenges hamper perfluoroalkyl research. *Environ Sci Technol*, *38*(13), 248A-255A. <https://doi.org/10.1021/es0405528>

-
- McDonald, W. H., Tabb, D. L., Sadygov, R. G., MacCoss, M. J., Venable, J., Graumann, J., Johnson, J. R., Cociorva, D., & Yates, J. R., 3rd. (2004). MS1, MS2, and SQT-three unified, compact, and easily parsed file formats for the storage of shotgun proteomic spectra and identifications. *Rapid Commun Mass Spectrom*, *18*(18), 2162-2168. <https://doi.org/10.1002/rcm.1603>
- McDonough, C. A., Guelfo, J. L., & Higgins, C. P. (2019). Measuring total PFASs in water: The tradeoff between selectivity and inclusivity. *Current Opinion in Environmental Science & Health*, *7*, 13-18. <https://doi.org/https://doi.org/10.1016/j.coesh.2018.08.005>
- McDonough, C. A., Li, W., Bischel, H. N., De Silva, A. O., & DeWitt, J. C. (2022). Widening the Lens on PFASs: Direct Human Exposure to Perfluoroalkyl Acid Precursors (pre-PFAAs). *Environ Sci Technol*, *56*(10), 6004-6013. <https://doi.org/10.1021/acs.est.2c00254>
- Mertens, H., Noll, B., Schwerdtle, T., Abraham, K., & Monien, B. H. (2023). Less is more: a methodological assessment of extraction techniques for per- and polyfluoroalkyl substances (PFAS) analysis in mammalian tissues. *Anal Bioanal Chem*, *415*(24), 5925-5938. <https://doi.org/10.1007/s00216-023-04867-5>
- Miaz, L. T., Plassmann, M. M., Gyllenhammar, I., Bignert, A., Sandblom, O., Lignell, S., Glynn, A., & Benskin, J. P. (2020). Temporal trends of suspect- and target-per/polyfluoroalkyl substances (PFAS), extractable organic fluorine (EOF) and total fluorine (TF) in pooled serum from first-time mothers in Uppsala, Sweden, 1996-2017. *Environ Sci Process Impacts*, *22*(4), 1071-1083. <https://doi.org/10.1039/c9em00502a>
- Mohammed Taha, H., Aalizadeh, R., Alygizakis, N., Antignac, J. P., Arp, H. P. H., Bade, R., Baker, N., Belova, L., Bijlsma, L., Bolton, E. E., Brack, W., Celma, A., Chen, W. L., Cheng, T., Chirsir, P., Cirka, L., D'Agostino, L. A., Djoumbou Feunang, Y., Dulio, V., Fischer, S., Gago-Ferrero, P., Galani, A., Geueke, B., Glowacka, N., Glüge, J., Groh, K., Grosse, S., Haglund, P., Hakkinen, P. J., Hale, S. E., Hernandez, F., Janssen, E. M., Jonkers, T., Kiefer, K., Kirchner, M., Koschorreck, J., Krauss, M., Krier, J., Lamoree, M. H., Letzel, M., Letzel, T., Li, Q., Little, J., Liu, Y., Lunderberg, D. M., Martin, J. W., McEachran, A. D., McLean, J. A., Meier, C., Meijer, J., Menger, F., Merino, C., Muncke, J., Muschket, M., Neumann, M., Neveu, V., Ng, K., Oberacher, H., O'Brien, J., Oswald, P., Oswaldova, M., Picache, J. A., Postigo, C., Ramirez, N., Reemtsma, T., Renaud, J., Rostkowski, P., Rudel, H., Salek, R. M., Samanipour, S., Scheringer, M., Schliebner, I., Schulz, W., Schulze, T., Sengl, M., Shoemaker, B. A., Sims, K., Singer, H., Singh, R. R., Sumarah, M., Thiessen, P. A., Thomas, K. V., Torres, S., Trier, X., van Wezel, A. P., Vermeulen, R. C. H., Vlaanderen, J. J., von der Ohe, P. C., Wang, Z., Williams, A. J., Willighagen, E. L., Wishart, D. S., Zhang, J., Thomaidis, N. S., Hollender, J., Slobodnik, J., & Schymanski, E. L. (2022). The NORMAN Suspect List Exchange (NORMAN-SLE): facilitating European and worldwide collaboration on suspect screening in high resolution mass spectrometry. *Environ Sci Eur*, *34*(1), 104. <https://doi.org/10.1186/s12302-022-00680-6>
- Morales-McDevitt, M. E., Becanova, J., Blum, A., Bruton, T. A., Vojta, S., Woodward, M., & Lohmann, R. (2021). The Air that we Breathe: Neutral and volatile PFAS in Indoor Air. *Environ Sci Technol Lett*, *8*(10), 897-902. <https://doi.org/10.1021/acs.estlett.1c00481>
- Munoz, G., Michaud, A. M., Liu, M., Vo Duy, S., Montenach, D., Resseguier, C., Watteau, F., Sappin-Didier, V., Feder, F., Morvan, T., Houot, S., Desrosiers, M., Liu, J., & Sauve, S. (2022). Target and Nontarget Screening of PFAS in Biosolids, Composts, and Other Organic Waste Products for Land Application in France. *Environ Sci Technol*, *56*(10), 6056-6068. <https://doi.org/10.1021/acs.est.1c03697>

-
- Nascimento, R. A., Nunoo, D. B. O., Bizkarguenaga, E., Schultes, L., Zabaleta, I., Benskin, J. P., Spano, S., & Leonel, J. (2018). Sulfluramid use in Brazilian agriculture: A source of per- and polyfluoroalkyl substances (PFASs) to the environment. *Environ Pollut*, *242*(Pt B), 1436-1443. <https://doi.org/10.1016/j.envpol.2018.07.122>
- Neuwald, I. J., Hubner, D., Wiegand, H. L., Valkov, V., Borchers, U., Nodler, K., Scheurer, M., Hale, S. E., Arp, H. P. H., & Zahn, D. (2022). Ultra-Short-Chain PFASs in the Sources of German Drinking Water: Prevalent, Overlooked, Difficult to Remove, and Unregulated. *Environ Sci Technol*, *56*(10), 6380-6390. <https://doi.org/10.1021/acs.est.1c07949>
- Ng, C., Cousins, I. T., DeWitt, J. C., Gluge, J., Goldenman, G., Herzke, D., Lohmann, R., Miller, M., Patton, S., Scheringer, M., Trier, X., & Wang, Z. (2021). Addressing Urgent Questions for PFAS in the 21st Century. *Environ Sci Technol*, *55*(19), 12755-12765. <https://doi.org/10.1021/acs.est.1c03386>
- Nickerson, A., Maizel, A. C., Kulkarni, P. R., Adamson, D. T., Kornuc, J. J., & Higgins, C. P. (2020). Enhanced Extraction of AFFF-Associated PFASs from Source Zone Soils. *Environ Sci Technol*, *54*(8), 4952-4962. <https://doi.org/10.1021/acs.est.0c00792>
- Nikiforov, V. A. (2021). Hydrolysis of FTOH precursors, a simple method to account for some of the unknown PFAS. *Chemosphere*, *276*, 130044. <https://doi.org/10.1016/j.chemosphere.2021.130044>
- Nordic Council of Ministers. (2022). *Analytical Methods for PFAS in Products and the Environment* (Nordic Council of Ministers, Issue).
- Nürenberg, G., Nödler, K., T, L. F., Schäfer, C., Huber, K., & Scheurer, M. (2018). Nachweis von polyfluorierten Alkylphosphateestern (PAP) und Perfluoroktansulfonamidoethanol-basierten Phosphateestern (SAMPAP) in Böden. *Mitt Umweltchem Ökotox*.
- OECD. (2018). *Toward a new comprehensive global database of per- and polyfluoroalkyl substances (PFASs): Summary report on updating the OECD 2007 list of per- and polyfluoroalkyl substances (PFASs)* (OECD, Issue. <https://www.norman-network.com/sites/default/files/files/suspectListExchange/190618Update/ENV-JM-MONO%282018%297.pdf>
- Paul, A. G., Jones, K. C., & Sweetman, A. J. (2009). A first global production, emission, and environmental inventory for perfluorooctane sulfonate. *Environ Sci Technol*, *43*(2), 386-392. <https://doi.org/10.1021/es802216n>
- Pfeuffer, J., Sachsenberg, T., Alka, O., Walzer, M., Fillbrunn, A., Nilse, L., Schilling, O., Reinert, K., & Kohlbacher, O. (2017). OpenMS - A platform for reproducible analysis of mass spectrometry data. *J Biotechnol*, *261*, 142-148. <https://doi.org/10.1016/j.jbiotec.2017.05.016>
- Portoles, T., Mol, J. G., Sancho, J. V., & Hernandez, F. (2012). Advantages of atmospheric pressure chemical ionization in gas chromatography tandem mass spectrometry: pyrethroid insecticides as a case study. *Anal Chem*, *84*(22), 9802-9810. <https://doi.org/10.1021/ac301699c>
- Renner, G., & Reuschenbach, M. (2023). Critical review on data processing algorithms in non-target screening: challenges and opportunities to improve result comparability. *Anal Bioanal Chem*, *415*(18), 4111-4123. <https://doi.org/10.1007/s00216-023-04776-7>

-
- Rhoads, K. R., Janssen, E. M., Luthy, R. G., & Criddle, C. S. (2008). Aerobic biotransformation and fate of N-ethyl perfluorooctane sulfonamidoethanol (N-EtFOSE) in activated sludge. *Environ Sci Technol*, *42*(8), 2873-2878. <https://doi.org/10.1021/es702866c>
- Ritter, E. E., Dickinson, M. E., Harron, J. P., Lunderberg, D. M., DeYoung, P. A., Robel, A. E., Field, J. A., & Peaslee, G. F. (2017). PIGE as a screening tool for Per- and polyfluorinated substances in papers and textiles. *Nuclear Instruments and Methods in Physics Research Section B: Beam Interactions with Materials and Atoms*, *407*, 47-54. <https://doi.org/10.1016/j.nimb.2017.05.052>
- Röhler, K., Haluska, A. A., Abramov, S., Thompson, K., Straub, D., Kleindienst, S., Bugsel, B., Zweigle, J., Zwiener, C., & Grathwohl, P. (2023). PFAS contaminated soil site in Germany: Comparison of laboratory batch incubation and field derived release rates. *Unpublished manuscript (04/2023)*.
- Röhler, K., Haluska, A. A., Susset, B., Liu, B., & Grathwohl, P. (2021). Long-term behavior of PFAS in contaminated agricultural soils in Germany. *J Contam Hydrol*, *241*, 103812. <https://doi.org/10.1016/j.jconhyd.2021.103812>
- Röhler, K., Susset, B., & Grathwohl, P. (2023). Production of perfluoroalkyl acids (PFAAs) from precursors in contaminated agricultural soils: Batch and leaching experiments. *Sci Total Environ*, *902*, 166555. <https://doi.org/10.1016/j.scitotenv.2023.166555>
- Rosenmai, A. K., Nielsen, F. K., Pedersen, M., Hadrup, N., Trier, X., Christensen, J. H., & Vinggaard, A. M. (2013). Fluorochemicals used in food packaging inhibit male sex hormone synthesis. *Toxicol Appl Pharmacol*, *266*(1), 132-142. <https://doi.org/10.1016/j.taap.2012.10.022>
- Röst, H. L., Schmitt, U., Aebersold, R., & Malmstrom, L. (2014). pyOpenMS: a Python-based interface to the OpenMS mass-spectrometry algorithm library. *Proteomics*, *14*(1), 74-77. <https://doi.org/10.1002/pmic.201300246>
- Ruan, T., & Jiang, G. (2017). Analytical methodology for identification of novel per- and polyfluoroalkyl substances in the environment. *TrAC Trends in Analytical Chemistry*, *95*, 122-131. <https://doi.org/10.1016/j.trac.2017.07.024>
- Rupp, J., Guckert, M., Berger, U., Drost, W., Mader, A., Nodler, K., Nurenberg, G., Schulze, J., Sohlmann, R., & Reemtsma, T. (2023). Comprehensive target analysis and TOP assay of per- and polyfluoroalkyl substances (PFAS) in wild boar livers indicate contamination hot-spots in the environment. *Sci Total Environ*, *871*, 162028. <https://doi.org/10.1016/j.scitotenv.2023.162028>
- Sawidou, E. K., Sha, B., Salter, M. E., Cousins, I. T., & Johansson, J. H. (2023). Horizontal and Vertical Distribution of Perfluoroalkyl Acids (PFAAs) in the Water Column of the Atlantic Ocean. *Environ Sci Technol Lett*, *10*(5), 418-424. <https://doi.org/10.1021/acs.estlett.3c00119>
- Schaefer, C. E., Andaya, C., Urriaga, A., McKenzie, E. R., & Higgins, C. P. (2015). Electrochemical treatment of perfluorooctanoic acid (PFOA) and perfluorooctane sulfonic acid (PFOS) in groundwater impacted by aqueous film forming foams (AFFFs). *J Hazard Mater*, *295*, 170-175. <https://doi.org/10.1016/j.jhazmat.2015.04.024>
- Schellenberger, S., Gillgard, P., Stare, A., Hanning, A., Levenstam, O., Roos, S., & Cousins, I. T. (2018). Facing the rain after the phase out: Performance evaluation of alternative fluorinated and non-fluorinated durable water repellents for outdoor fabrics. *Chemosphere*, *193*, 675-684. <https://doi.org/10.1016/j.chemosphere.2017.11.027>

-
- Schellenberger, S., Hill, P. J., Levenstam, O., Gillgard, P., Cousins, I. T., Taylor, M., & Blackburn, R. S. (2019). Highly fluorinated chemicals in functional textiles can be replaced by re-evaluating liquid repellency and end-user requirements. *Journal of Cleaner Production*, *217*, 134-143. <https://doi.org/10.1016/j.jclepro.2019.01.160>
- Schellenberger, S., Jonsson, C., Mellin, P., Levenstam, O. A., Liagkouridis, I., Ribbenstedt, A., Hanning, A. C., Schultes, L., Plassmann, M. M., Persson, C., Cousins, I. T., & Benskin, J. P. (2019). Release of Side-Chain Fluorinated Polymer-Containing Microplastic Fibers from Functional Textiles During Washing and First Estimates of Perfluoroalkyl Acid Emissions. *Environ Sci Technol*, *53*(24), 14329-14338. <https://doi.org/10.1021/acs.est.9b04165>
- Schenker, U., Scheringer, M., MacLeod, M., Martin, J. W., Cousins, I. T., & Hungerbuhler, K. (2008). Contribution of volatile precursor substances to the flux of perfluorooctanoate to the Arctic. *Environ Sci Technol*, *42*(10), 3710-3716. <https://doi.org/10.1021/es703165m>
- Schrenk, D., Bignami, M., Bodin, L., Chipman, J. K., Del Mazo, J., Grasl-Kraupp, B., Hogstrand, C., Hoogenboom, L. R., Leblanc, J. C., Nebbia, C. S., Nielsen, E., Ntzani, E., Petersen, A., Sand, S., Vleminckx, C., Wallace, H., Barregard, L., Ceccatelli, S., Cravedi, J. P., Halldorsson, T. I., Haug, L. S., Johansson, N., Knutsen, H. K., Rose, M., Roudot, A. C., Van Loveren, H., Vollmer, G., Mackay, K., Riolo, F., & Schwerdtle, T. (2020). Risk to human health related to the presence of perfluoroalkyl substances in food. *EFSA J*, *18*(9), e06223. <https://doi.org/10.2903/j.efsa.2020.6223>
- Schultes, L., Vestergren, R., Volkova, K., Westberg, E., Jacobson, T., & Benskin, J. P. (2018). Per- and polyfluoroalkyl substances and fluorine mass balance in cosmetic products from the Swedish market: implications for environmental emissions and human exposure. *Environmental Science: Processes & Impacts*, *20*(12), 1680-1690. <https://doi.org/10.1039/c8em00368h>
- Schwartz-Narbonne, H., Xia, C., Shalin, A., Whitehead, H. D., Yang, D., Peaslee, G. F., Wang, Z., Wu, Y., Peng, H., Blum, A., Venier, M., & Diamond, M. L. (2023). Per- and Polyfluoroalkyl Substances in Canadian Fast Food Packaging. *Environ Sci Technol Lett*, *10*(4), 343-349. <https://doi.org/10.1021/acs.estlett.2c00926>
- Schymanski, E. L., Zhang, J., Thiessen, P. A., Chirsir, P., Kondic, T., & Bolton, E. E. (2023). Per- and Polyfluoroalkyl Substances (PFAS) in PubChem: 7 Million and Growing. *Environ Sci Technol*, *57*(44), 16918-16928. <https://doi.org/10.1021/acs.est.3c04855>
- Simon, F., Gehrenkemper, L., Au, M. V., Wittwer, P., Roesch, P., Pfeifer, J., Cossmer, A., & Meermann, B. (2022). A fast and simple PFAS extraction method utilizing HR-CS-GFMAS for soil samples. *Chemosphere*, 133922. <https://doi.org/10.1016/j.chemosphere.2022.133922>
- Simon, F., Gehrenkemper, L., Becher, S., Dierkes, G., Langhammer, N., Cossmer, A., von der Au, M., Gockener, B., Flidner, A., Rudel, H., Koschorreck, J., & Meermann, B. (2023). Quantification and characterization of PFASs in suspended particulate matter (SPM) of German rivers using EOF, dTOPA, (non-)target HRMS. *Sci Total Environ*, *885*, 163753. <https://doi.org/10.1016/j.scitotenv.2023.163753>
- Skutlarek, D., Exner, M., & Farber, H. (2006). Perfluorinated surfactants in surface and drinking waters. *Environ Sci Pollut Res Int*, *13*(5), 299-307. <https://doi.org/10.1065/espr2006.07.326>
- Sleno, L. (2012). The use of mass defect in modern mass spectrometry. *J Mass Spectrom*, *47*(2), 226-236. <https://doi.org/10.1002/jms.2953>

-
- Spaan, K. M., Seilitz, F., Plassmann, M. M., de Wit, C. A., & Benskin, J. P. (2023). Pharmaceuticals Account for a Significant Proportion of the Extractable Organic Fluorine in Municipal Wastewater Treatment Plant Sludge. *Environmental Science & Technology Letters*, *10*(4), 328-336. <https://doi.org/10.1021/acs.estlett.3c00108>
- Stockholm Convention. (2022). *The new POPs under the Stockholm Convention*. Retrieved 21.03.2023 from <http://www.pops.int/TheConvention/ThePOPs/TheNewPOPs/tabid/2511/Default.aspx>
- Sturm, M., Bertsch, A., Gropl, C., Hildebrandt, A., Hussong, R., Lange, E., Pfeifer, N., Schulz-Trieglaff, O., Zerck, A., Reinert, K., & Kohlbacher, O. (2008). OpenMS - an open-source software framework for mass spectrometry. *BMC Bioinformatics*, *9*, 163. <https://doi.org/10.1186/1471-2105-9-163>
- Sun, J., Bossi, R., Bustnes, J. O., Helander, B., Boertmann, D., Dietz, R., Herzke, D., Jaspers, V. L. B., Labansen, A. L., Lepoint, G., Schulz, R., Sonne, C., Thorup, K., Tøttrup, A. P., Zubrod, J. P., Eens, M., & Eulaers, I. (2019). White-Tailed Eagle (*Haliaeetus albicilla*) Body Feathers Document Spatiotemporal Trends of Perfluoroalkyl Substances in the Northern Environment. *Environ Sci Technol*, *53*(21), 12744-12753. <https://doi.org/10.1021/acs.est.9b03514>
- Tokranov, A. K., Nishizawa, N., Amadei, C. A., Zenobio, J. E., Pickard, H. M., Allen, J. G., Vecitis, C. D., & Sunderland, E. M. (2018). How Do We Measure Poly- and Perfluoroalkyl Substances (PFASs) at the Surface of Consumer Products? *Environmental Science & Technology Letters*, *6*(1), 38-43. <https://doi.org/10.1021/acs.estlett.8b00600>
- Wang, B., Yao, Y., Wang, Y., Chen, H., & Sun, H. (2022). Per- and Polyfluoroalkyl Substances in Outdoor and Indoor Dust from Mainland China: Contributions of Unknown Precursors and Implications for Human Exposure. *Environ Sci Technol*, *56*(10), 6036-6045. <https://doi.org/10.1021/acs.est.0c08242>
- Wang, X., Yu, N., Qian, Y., Shi, W., Zhang, X., Geng, J., Yu, H., & Wei, S. (2020). Non-target and suspect screening of per- and polyfluoroalkyl substances in Chinese municipal wastewater treatment plants. *Water Res*, *183*, 115989. <https://doi.org/10.1016/j.watres.2020.115989>
- Wang, Y., Yu, N., Zhu, X., Guo, H., Jiang, J., Wang, X., Shi, W., Wu, J., Yu, H., & Wei, S. (2018). Suspect and Nontarget Screening of Per- and Polyfluoroalkyl Substances in Wastewater from a Fluorochemical Manufacturing Park. *Environ Sci Technol*, *52*(19), 11007-11016. <https://doi.org/10.1021/acs.est.8b03030>
- Wang, Z., Buser, A. M., Cousins, I. T., Demattio, S., Drost, W., Johansson, O., Ohno, K., Patlewicz, G., Richard, A. M., Walker, G. W., White, G. S., & Leinala, E. (2021). A New OECD Definition for Per- and Polyfluoroalkyl Substances. *Environ Sci Technol*, *55*(23), 15575-15578. <https://doi.org/10.1021/acs.est.1c06896>
- Wang, Z., Cousins, I. T., Scheringer, M., Buck, R. C., & Hungerbuehler, K. (2014). Global emission inventories for C4-C14 perfluoroalkyl carboxylic acid (PFCA) homologues from 1951 to 2030, Part I: production and emissions from quantifiable sources. *Environ Int*, *70*, 62-75. <https://doi.org/10.1016/j.envint.2014.04.013>
- Wang, Z., Cousins, I. T., Scheringer, M., & Hungerbuehler, K. (2015). Hazard assessment of fluorinated alternatives to long-chain perfluoroalkyl acids (PFAAs) and their precursors: status quo, ongoing challenges and possible solutions. *Environ Int*, *75*, 172-179. <https://doi.org/10.1016/j.envint.2014.11.013>

-
- Wang, Z., DeWitt, J. C., Higgins, C. P., & Cousins, I. T. (2017). A Never-Ending Story of Per- and Polyfluoroalkyl Substances (PFASs)? *Environ Sci Technol*, *51*(5), 2508-2518. <https://doi.org/10.1021/acs.est.6b04806>
- Washington, J. W., Jenkins, T. M., Rankin, K., & Naile, J. E. (2015). Decades-scale degradation of commercial, side-chain, fluorotelomer-based polymers in soils and water. *Environ Sci Technol*, *49*(2), 915-923. <https://doi.org/10.1021/es504347u>
- Whitehead, H. D., Venier, M., Wu, Y., Eastman, E., Urbanik, S., Diamond, M. L., Shalin, A., Schwartz-Narbonne, H., Bruton, T. A., Blum, A., Wang, Z., Green, M., Tighe, M., Wilkinson, J. T., McGuinness, S., & Peaslee, G. F. (2021). Fluorinated Compounds in North American Cosmetics. *Environmental Science & Technology Letters*, *8*(7), 538-544. <https://doi.org/10.1021/acs.estlett.1c00240>
- Winkens, K., Koponen, J., Schuster, J., Shoeib, M., Vestergren, R., Berger, U., Karvonen, A. M., Pekkanen, J., Kiviranta, H., & Cousins, I. T. (2017). Perfluoroalkyl acids and their precursors in indoor air sampled in children's bedrooms. *Environmental Pollution*, *222*(Supplement C), 423-432. <https://doi.org/https://doi.org/10.1016/j.envpol.2016.12.010>
- Yang, Z., Shojaei, M., & Guelfo, J. L. (2023). Per- and polyfluoroalkyl substances (PFAS) in grocery store foods: method optimization, occurrence, and exposure assessment. *Environ Sci Process Impacts*. <https://doi.org/10.1039/d3em00268c>
- Yeung, L. W. Y., & Mabury, S. A. (2016). Are humans exposed to increasing amounts of unidentified organofluorine? *Environmental Chemistry*, *13*(1), 102-110. <https://doi.org/10.1071/en15041>
- Yu, N., Wen, H., Wang, X., Yamazaki, E., Taniyasu, S., Yamashita, N., Yu, H., & Wei, S. (2020). Nontarget Discovery of Per- and Polyfluoroalkyl Substances in Atmospheric Particulate Matter and Gaseous Phase Using Cryogenic Air Sampler. *Environ Sci Technol*, *54*(6), 3103-3113. <https://doi.org/10.1021/acs.est.9b05457>
- Zhang, W., Pang, S., Lin, Z., Mishra, S., Bhatt, P., & Chen, S. (2021). Biotransformation of perfluoroalkyl acid precursors from various environmental systems: advances and perspectives. *Environ Pollut*, *272*, 115908. <https://doi.org/10.1016/j.envpol.2020.115908>
- Zhao, Z., Xie, Z., Moller, A., Sturm, R., Tang, J., Zhang, G., & Ebinghaus, R. (2012). Distribution and long-range transport of polyfluoroalkyl substances in the Arctic, Atlantic Ocean and Antarctic coast. *Environ Pollut*, *170*, 71-77. <https://doi.org/10.1016/j.envpol.2012.06.004>

Appendix 1

Publication 1

Efficient PFAS prioritization in non-target HRMS data: systematic evaluation of the novel MD/C-m/C approach

Jonathan Zweigle,⁺ Boris Bugsel,⁺ Christian Zwiener⁺

⁺Environmental Analytical Chemistry, Department of Geosciences, University of Tübingen,
Schnarrenbergstraße 94-96, 72076 Tübingen, Germany

Published in: Analytical and Bioanalytical Chemistry 415(10), 1791-1801

DOI: 10.1007/s00216-023-04601

Reprinted from Analytical & Bioanalytical Chemistry: Zweigle, J., Bugsel, B., & Zwiener, C. (2023). Efficient PFAS prioritization in non-target HRMS data: systematic evaluation of the novel MD/C-m/C approach. Anal Bioanal Chem, 415(10), 1791-1801. <https://doi.org/10.1007/s00216-023-04601-1>



Efficient PFAS prioritization in non-target HRMS data: systematic evaluation of the novel MD/C-m/C approach

Jonathan Zweigle¹ · Boris Bugsel¹ · Christian Zwiener¹

Received: 16 December 2022 / Revised: 3 February 2023 / Accepted: 8 February 2023
© The Author(s) 2023

Abstract

Non-target screening (NTS) based on high-resolution mass spectrometry (HRMS) is necessary to comprehensively characterize per- and polyfluoroalkyl substances (PFAS) in environmental, biological, and technical samples due to the very limited availability of authentic PFAS reference standards. Since in trace analysis, MS/MS information is not always achievable and only selected PFAS are present in homologous series, further techniques to prioritize measured HRMS data (features) according to their likelihood of being PFAS are highly desired due to the importance of efficient data reduction during NTS. Kaufmann et al. (*J AOAC Int*, 2022) presented a very promising approach to separate selected PFAS from sample matrix features by plotting the mass defect (MD) normalized to the number of carbons (MD/C) vs. mass normalized to the number of C (m/C). We systematically evaluated the advantages and limitations of this approach by using ~490,000 chemical formulas of organic chemicals (~210,000 PFAS, ~160,000 organic contaminants, and 125,000 natural organic matter compounds) and calculating how efficiently, and especially which, PFAS can be prioritized. While PFAS with high fluorine content (approximately: F/C > 0.8, H/F < 0.8, mass percent of fluorine > 55%) can be separated well, partially fluorinated PFAS with a high hydrogen content are more difficult to prioritize, which we discuss for selected PFAS. In the MD/C-m/C approach, even compounds with highly positive MDs above 0.5 Da and hence incorrectly assigned to negative MDs can still be separated from true negative mass defect features by the normalized mass (m/C). Furthermore, based on the position in the MD/C-m/C plot, we propose the estimation of the fluorine fraction in molecules for selected PFAS classes. The promising MD/C-m/C approach can be widely used in PFAS research and routine analysis. The concept is also applicable to other compound classes like iodinated compounds.

Keywords PFAS · High-resolution mass spectrometry · Non-target-screening · Feature prioritization · Data reduction · Elemental composition

Abbreviations

F/C	Fluorine to carbon ratio (number)
H/C	Hydrogen to carbon ratio (number)
m/C	Mass to carbon value
MD/C	Mass defect to carbon value
NOM	Natural organic matter
OCs	Organic contaminants
PFAS	Per- and polyfluoroalkyl substances

%m _F	Mass percentage of fluorine in a chemical formula
%n _F	Molar percentage of fluorine in a chemical formula

Introduction

Per- and polyfluoroalkyl substances (PFAS) are an immense class of anthropogenic chemicals with useful properties for countless commercial applications [1, 2]. PFAS characterized by C_nF_{2n+1}- or C_nF_{2n+1}-O-C_mF_{2m}-units exhibit non-stick properties and extreme stability [3, 4]. This high persistence, of either PFAS themselves or their perfluorinated transformation products, led to a global distribution of perfluoroalkyl acids (PFAAs) [5, 6]. As a reason of this property, combined with their bioaccumulation potential and

✉ Christian Zwiener
christian.zwiener@uni-tuebingen.de

¹ Environmental Analytical Chemistry, Department of Geosciences, University of Tübingen, Schnarrenbergstraße 94-96, 72076 Tübingen, Germany

observed adverse health effects, much effort was put into regulations for selected long-chain PFAS (perfluoroalkyl carboxylic and sulfonic acids) [7]. However, the development of replacement compounds and the large market for PFAS continuously increases the number of individual fluorinated substances and their production volume [8]. Several studies showed considerable fractions of unidentified organic fluorine in numerous samples, including human serum, showing that much more unknown PFAS must be present in the environment [9–12].

Since the sheer number of PFAS makes a comprehensive use of authentic analytical reference standards practically impossible, non-target screening (NTS) approaches based on high-resolution mass spectrometry (HRMS) are a necessary tool for PFAS identification in all kinds of samples [13, 14].

In NTS, data reduction and prioritization of features is always a crucial step for an efficient workflow. The chemical mass defect (MD), which is typically slightly negative for PFAS with high fluorine content, can be used as a first prioritization approach [15, 16]. For PFAS that occur as homologous series in samples of interest, Kendrick mass defect (KMD) analysis is a powerful tool for data prioritization and compound identification [17, 18]. In case of relatively high PFAS concentrations compared to the sample matrix, approaches relying on MS² data using diagnostic fragments and/or fragment mass differences are efficient in detecting potential PFAS candidates and further identifying them [19, 20]. However, approaches that rely on MS² data for prioritization are often impractical in trace analysis, because achieving a broad MS/MS coverage can be very time consuming and exhaustive coverage is usually not possible due to detection limits and hence noisy mass spectra. Furthermore, unknown PFAS not occurring as homologues cannot be captured by KMD analysis and if present in trace concentrations further homologues might not be present in sufficient concentrations for the peak picking algorithm or lost during certain data reduction steps. Depending on the sample matrix, even the MD approach may fail for compounds with a high positive MD that exceeds +0.5 Da that can be erroneously interpreted as negative MD and therefore incorrectly assigned to PFAS (see Fig. S1). Data filtering with too strict MD ranges on the other hand may exclude true positives (mainly critical for PFAS with high H-content or other halogens).

In a recent publication, Kaufmann et al. (2022) presented a highly promising approach for an efficient prioritization of potential PFAS in complex matrices (fish extracts) [21]. Compounds with high fluorine content (composed mainly of C and F) have much lower carbon numbers compared to compounds dominated by C and H at a similar mass. The carbon number can be retrieved from HRMS data from the abundance of the ¹³C isotope [M + 1] according to the following equation: $C = I_{M+1}/I_M/0.011145$, where I_{M+1} and I_M correspond to the

intensities of the first isotopic and monoisotopic peak, respectively [21]. Therefore, a compound mass normalized to the number of C atoms (m/C) can be used as a separation criterion for potential PFAS features (for CF₂, m/C = 50) from matrix features (for CH₂, m/C = 14). A further criterion for PFAS selection is the MD normalized to the number of C atoms (MD/C), for which Kaufmann et al. (2022) observed a strong separation of PFAAs from fish matrix in NTS data due to the typically more negative MD/C of PFAS compared to other CHO compounds. The general concept of the MD/C-m/C plot is illustrated in Fig. 1. Compounds with an increased number of heavier elements compared to H are shifted to higher m/C values, while compounds with a higher number of elements with negative MD are shifted to a more negative MD/C. As an example, a PFAS for which the chemical formula approaches (CF₂)_n would plot at m/C ≈ 50 and MD/C ≈ -0.003 while a compound mainly composed of (CH₂O)_n would plot at m/C = 30 and MD/C = +0.0106, showing that such a separation generally works. Therefore, if we consider compounds which are mainly characterized by the transition from a saturated hydrocarbon (CH₂) to a perfluoroalkyl substance (CF₂) (CH_xF_{2-x}, x = 0, 1, 2) all plot along the following line:

$$\text{MD}/\text{C}_{\text{CH}_x\text{F}_{2-x}} \approx -5.24 \times 10^{-4} \cdot \text{m}/\text{C} + 0.023 \quad (1)$$

The same principle holds for compounds that are characterized by the transition between CF and CF₂:

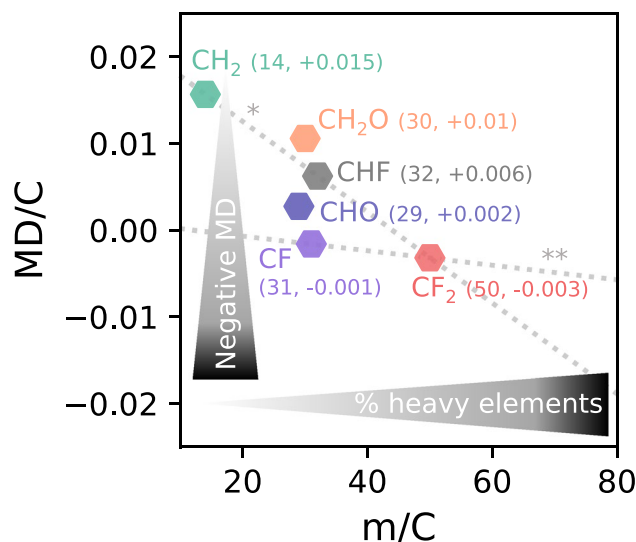


Fig. 1 Schematic explanation of the MD/C-m/C plot. Important positions of compounds composed on average of CH₂, CH₂O, CHO, CHF, CF, and CF₂ are shown. The general trend of increasing m/C with increasing percentage of heavy elements (e.g., halogens, O, N, P, S, and heavy metals) and the decreasing trend of MD/C with increasing numbers of elements that have a negative mass defect are highlighted. Furthermore, the CH_xF_{2-x}-line (*, with 0 ≤ x ≤ 2, see Eq. 1) and the CF_x-line (**, with 0 ≤ x ≤ 2, see Eq. 2) are given as orientations (see Fig. S2 for discrete points that fall on those lines)

$$\text{MD}/C_{\text{CF}_x} \approx -8.406 \times 10^{-5} \cdot m/C + 0.001 \quad (2)$$

with $0 \leq x \leq 2$. Both lines can be used as a very helpful orientation when using the MD/*m*/C plot for PFAS feature prioritization (discussed later, see also Fig. 1). One further important and useful intrinsic property of the MD/*m*/C plot is that structurally related compounds are clustered together.

To investigate the efficiency of the MD/*m*/C approach and its robustness to prioritize features as potential PFAS in GC or LC-HRMS data, we used chemical formulas of ~490,000 organic chemicals from online sources (PubChem (<https://pubchem.ncbi.nlm.nih.gov>) and Koch et al. 2007) [22, 23]. We systematically evaluated which chemical composition of PFAS classes (~210,000 compounds) can be separated from natural organic matter (NOM) compounds (~125,000) representing a typical matrix of environmental samples and from other organic contaminants (~160,000) and how explicitly that is possible. The degree of fluorination in a PFAS was expressed as F/C ratio (number of fluorine atoms divided by number of carbon atoms), H/F ratio (number of hydrogen atoms divided by number of fluorine atoms), mass percentage of fluorine (%*m*_F), and by the molar percentage of F atoms per molecule (%*n*_F) to determine the range of elemental compositions (chemical formulas) for a clear separation from matrix components. General advantages and limitations of the MD/*m*/C approach are discussed in detail. Furthermore, we discuss the possibility to estimate the degree of fluorination of a compound based on its position in the MD/*m*/C plot for a statistically relevant number of PFAS.

Methods

Data collection

To perform a data evaluation with a robust amount of organic chemicals, raw data was downloaded from the PubChem Classification Browser and from the Supporting Information of Koch et al. 2007 [22–24] and preprocessed in three individual datasets which are PFAS, organic compounds (OCs), and NOM compounds. From PubChem, the EPA DSSTox dataset (245,545 compounds) [25], the NORMAN Suspect List Exchange (113,737 compounds) [26] and from the “PFAS and Fluorinated Compounds in PubChem Tree” PFAS with parts larger than CF₂ or CF₃ that fall into the OECD definition (224,017 compounds) were downloaded as CSV and TXT files [27, 28]. The EPA DSSTox dataset includes any kind of toxic substances while the NORMAN database includes emerging environmental contaminants. To also include natural substances (NOM) which are typical

matrix compounds in LC–MS (and GC) measurements, chemical formulas of 124,782 NOM constituents derived from ESI FT-ICR-MS measurements of a Suwannee River Fulvic Acid Standard (SRFA II) were included [22].

Data cleanup

Data cleanup and calculations were performed with Python 3.9.13. Each CSV file was imported, and several cleanup steps and basic chemical calculations were performed which are presented in the following bullet points:

- Masses below 100 Da and above 2000 Da were removed to obtain a reasonable GC- and LC-MS mass range.
- All inorganic compounds were removed (mainly present in the EPA DSSTox dataset).
- All salts were removed via periods in their SMILES code.
- All organometallic compounds were removed since they usually play a minor role in typical environmental matrices and in addition most of them can rather easily be distinguished from other organic molecules by their unique isotopic pattern. Approximately 5% organometallic compounds were present in the three PubChem databases. Only compounds containing C, H, N, O, P, S, Si, F, Cl, Br, and I were kept for further calculations.
- The exact mass was calculated for each compound from its molecular formula. In case of charged compounds (e.g., quaternary ammonium compounds), charges were removed for the mass calculation.
- The number of C, F, and H atoms and the total number of atoms per compound were calculated.
- Both exact MD (theoretical; sum of MDs of all elements in the chemical formula) and the calculable MD (MD = accurate mass – integer mass) were determined.
- Finally, *m*/C and MD/C were calculated for all compounds. Additionally, the MD/C was calculated with the calculable MD.

In the following step, the EPA DSSTox and NORMAN database were combined and most overlapping compounds (the EPA DSSTox already contains part of NORMAN) were removed by keeping only unique SMILES and InChIKeys. Then all fluorine-containing compounds were removed. This final dataset contained 182,503 organic contaminants without fluorine which are denoted as OCs in the following. The NOM dataset was kept in its original form with 124,782 compounds containing C, H, O, N, S, and P.

For the PFAS dataset (210,091 PFAS), four parameters were calculated that describe the amount of fluorine in PFAS molecules in different ways: F/C ratio, H/F ratio, the mass percentage of fluorine (%*m*_F), and the fraction of fluorine atoms per molecule (%*n*_F).

Data evaluation

Separation of PFAS from OCs and NOM

To determine how well PFAS can be separated from compounds without fluorine (OCs and NOM) in the MD/C-m/C plot a MD/C vs. m/C domain from $-0.05 \leq \text{MD/C} \leq 0.025$ and $10 \leq \text{m/C} \leq 100$ and was chosen which included > 99.8% of all compounds of the three groups. Compounds that fall out of this domain were not included in the data evaluation (mainly compounds with less than two C atoms and heavy elements such as I or Cl and P).

To determine the position of each class in the MD/C-m/C domain, this was subdivided in a rectangular grid of 2D bins. A grid size of either 70×70 or 100×100 bins was chosen which corresponds to bin sizes of $0.0011 \text{ MD/C} \times 1.28 \text{ m/C}$ or $0.00075 \text{ MD/C} \times 0.9 \text{ m/C}$. For the binned data, a 2D histogram was calculated for all three compound groups. The resulting matrix with the number of compounds in each bin (counts) was normalized to the total number of compounds present to obtain the fraction of compounds relative to all compounds in each bin (the sum of the normalized matrix corresponds to 100%) (Fig. S3). To find the position of a certain percentage of compounds (e.g., 90%) around the region with highest density of compounds, the bins were summed up in decreasing order until the desired percentage criterion was reached (a schematic explanation of this procedure is depicted in Fig. S3). Now the matrix of PFAS can be compared to the matrix of the other compound classes (OCs or NOM) to find the overlapping region of both classes and determine the fraction of compounds that overlap for both classes (Fig. S4). Since OCs with high amounts of heavy elements (e.g., Br or I) always overlap with some PFAS, the calculations were performed for different percentages of each class. With this general procedure, the overlap was simulated for different fluorine content by varying the parameters F/C, H/F, %m_F, and %n_F and considering PFAS that fall into the criterion (e.g., PFAS with %m_F ≥ 50%).

Position of PFAS in the MD/C-m/C plot as a function of fluorine content

To determine the distribution of F/C, H/F, %m_F, and %n_F in the MD/C-m/C plot for PFAS, the mean and standard deviation of PFAS with %m_F > 50% in each bin of the 2D histogram were calculated (see Fig. S3b for a schematic explanation). The 2D matrices with the mean of F/C, H/F, %m_F, and %n_F in each bin were used to investigate how well single bins represent these parameters (F/C, H/C etc.) and therefore how well MD/C-m/C positions can be used to predict those (F/C, H/C etc.) for PFAS. Furthermore, the overall error distribution was determined from the

standard deviation matrices to conclude on the precision of such a prediction.

Results and discussion

Separation of PFAS from NOM and organic contaminants (OCs)

The position of organic compounds in the MD/C-m/C plot depends on their average mass per C atom and their average MD per C atom which are both strongly correlated with chemical composition. Molecules with multiple heavy elements (e.g., halogens, O, S, P, heavy metals) rather than H are shifted to the lower right corner (lower MD/C and higher m/C). This can be used to separate features that are highly fluorinated from other organic contaminants (OCs) and NOM (Fig. 2). The positions for 80%, 90%, and 95% of OCs (182,503 compounds from the EPA DSSTox and NORMAN database), typical NOM constituents (124,782), and PFAS (209,760 with more than one CF₂ or CF₃ group according to the OECD) were calculated and visualized in the MD/C-m/C plot. Their exact distribution in the MD/C-m/C domain is shown in 2D histograms (Fig. S5).

Overall, many partly fluorinated PFAS which are dominated by CH from the PubChem dataset overlap with both OCs and NOM while highly fluorinated PFAS are well separable if they are characterized by %m_F > ~ 65% or F/C ratios ≥ ~ 1.1 (Fig. 2). High fluorine content draws the compounds the lower right corner of the MD/C-m/C plot. In Fig. S6, another representation of the overlap is provided as additional information.

To put the overlap into a quantitative context, the separation of PFAS from both NOM and OCs was simulated individually by varying F/C, H/F, %m_F, and %n_F (Fig. 3). In general, NOM compounds show more overlap with PFAS in the critical lower MD/C and higher m/C range. From these calculations, approximate boundaries for an efficient PFAS separation can be estimated. In the case of NOM, 90% of the PFAS are separated from 90% of the NOM constituents (or in other words less than 10% of PFAS are in overlapping regions with NOM features), if the F/C ratio of PFAS is higher than ~ 1.03, or the H/F ratio smaller than ~ 0.59, or the %m_F higher than ~ 58% or the fraction of fluorine atoms in the chemical formula is at least ~ 36% (for details, see Fig. 3). For the OCs, the boundaries (90%/90%) are F/C ~ 0.65, H/F ~ 1.17, %m_F ~ 47%, or %n_F ~ 25%. Histograms for PFAS are given in Fig. 4, where non-separable PFAS that fall below the thresholds of F/C, %m_F, and %n_F or above H/F are covered by a grey area (90%/90% boundary). It is important to

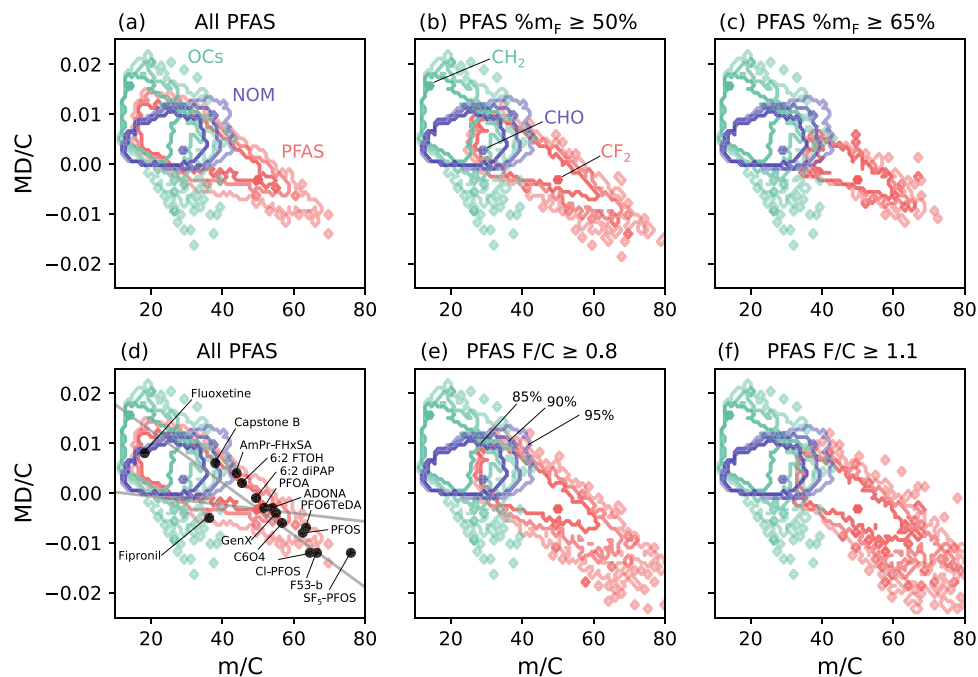


Fig. 2 Positions of organic contaminants (OCs, green) from the EPA DSSTox and NORMAN (182,503), NOM (blue) (124,782), and PFAS (red) (all: 209,760) with different amounts of fluorine (according to mass percent F (%m_F) (a–c) and F/C ratio (d–f)) in the MD/C-m/C plot. The contour lines delimit the positions of 80% (center), 90% (middle), and 95% (external) of each group. In case of PFAS with %m_F ≥ 65% or F/C ≥ 1.1, an almost complete separa-

tion is possible. Details on the known PFAS shown in subplot (d) are given in Table 1. The CH_xF_{2-x}-line (with 0 ≤ x ≤ 2) and the CF_x-line (with 0 ≤ x ≤ 2) are given as orientations (see also Fig. 1; for discrete data points of PFAS that fall on the CH_xF_{2-x}-line and CF_x-line, see Fig. S2). Figure S6 provides another representation of the overlap as further information

note that the determined boundaries should be considered as smooth transitions, as they are shown in Fig. 3 and the PFAS in the grey area are not necessarily “non-separable”.

In principle, these calculations reflect a worst-case scenario because in typical HRMS measurements, only a much smaller number of features is present (especially because a sufficient ¹³C isotope signal is required which further reduces the feature number) that directly compete with potential PFAS in the MD/C-m/C plot. However, the potential overlap in real-world measurements is always highly dependent on the sample matrix. In the case of fish extracts measured by Kaufmann et al. (2022), a complete separation of PFAS from co-extracted matrix from liver and muscle tissue was achieved. We further included four MD/C-m/C plots of PFAS in extracts of agricultural soils (raw data from Bugsel and Zwiener 2020 [17]) to demonstrate the applicability of the approach in the SI (details in Fig. S7).

In the case of the presence of compounds with low MD/C and high m/C (e.g., halogenated substances, organometallic compounds, and others), a distinct separation from PFAS might not always be possible. Nonetheless, such compounds can often be separated from PFAS by their distinct isotopic patterns (e.g., Cl, Br, many heavy metals). This is more

difficult for compounds with I or high percentages of O, P, or S. The MD/C-m/C plot is therefore also highly useful to find other compound classes such as iodinated substances, since they are located at even higher m/C and lower MD/C values than PFAS. The MD/C-m/C approach for PFAS feature prioritization has a further key advantage over the use of the MD alone. Compounds with a high positive MD above +0.5 Da (for the simplest case (CH₂)₃₂ = 448.5008 Da, becomes more important with increasing mass) may erroneously be interpreted as negative MD (rounding to the nearest integer) and hence incorrectly assigned to highly halogenated compounds like PFAS (see Fig. S1). In particular, this becomes more important for samples with high-molecular weight PFAS. In the MD/C-m/C plot, this unavoidable issue becomes much less of a problem because such features (high H content and MD > +0.5 Da) are still separated by the m/C dimension. For example, m/C of (CH₂)₃₂ = 14 compared to m/C of CHF (= 32) or CF₂ (= 50) (see Fig. S8).

To classify the positions of selected examples of known PFAS in the MD/C-m/C plot, they were included in Fig. 2d (abbreviations are given in the caption of Table 1). For high fluorine-containing PFAS, a separation is clearly possible with limitations in case of the telomer-based aqueous film-forming foam (AFFF) compound Capstone B and the

Table 1 m/C, MD/C, H/F, F/C, %m_F, and %n_F for well-known PFAS which are shown in Fig. 1. Abbreviations: SF₅-PFOS, pentafluoro-sulfanyl perfluorooctane sulfonic acid [29]; F53-b, 6:2 Cl-perfluoro ether sulfonic acid; PFO6TeDA, perfluoro- (3,5,7,9,11,13-hexaooxa-tetradecanoic) acid [30]; PFOS, perfluorooctane sulfonic acid; C6O4, perfluoro ([5-methoxy-1,3-dioxolan-4-yl]oxy) acetic acid; GenX or HFPO-DA, hexafluoropropylene oxide dimer acid; ADONA, dodecafluoro-3H-4,8-dioxananoate; PFOA, perfluorooctanoic acid;

Compound	Formula	m/C	MD/C	H/F	F/C	%m _F	%n _F	Predicted F/C
SF ₅ -PFOS	C ₈ F ₂₁ O ₃ S ₂	76.0	-0.012	0.05	2.63	66	60	-
F53-b	C ₈ HCIF ₁₆ O ₄ S	66.5	-0.012	0.06	2.00	57	52	2.0
Cl-PFOS	C ₈ HF ₁₆ ClO ₃ S	64.5	-0.012	0.06	2.00	59	53	-
PFO6TeDA	C ₇ HF ₁₃ O ₇	63.4	-0.007	0.08	1.86	56	46	2.2
PFOS	C ₈ HF ₁₇ O ₃ S	62.5	-0.008	0.06	2.13	65	57	2.2
C6O4	C ₆ HF ₉ O ₆	56.7	-0.006	0.11	1.50	50	41	1.9
GenX	C ₆ HF ₁₁ O ₃	55.0	-0.004	0.09	1.83	63	52	1.9
ADONA	C ₇ H ₂ F ₁₂ O ₄	54.0	-0.003	0.17	1.71	60	48	1.9
PFOA	C ₈ HF ₁₅ O ₂	51.7	-0.003	0.07	1.88	69	58	1.9
6:2 diPAP	C ₁₆ H ₉ F ₂₆ O ₄ P	49.4	-0.001	0.35	1.63	63	46	1.8
6:2 FTOH	C ₈ H ₅ F ₁₃ O	45.5	+0.002	0.38	1.63	68	48	1.5
AmPr-FHxSA	C ₁₁ H ₁₃ F ₁₃ N ₂ O ₂ S	44.0	+0.004	1.00	1.18	51	32	1.4
Capstone B	C ₁₅ H ₁₉ F ₁₃ N ₂ O ₄ S	38.0	+0.006	1.46	0.87	43	24	1.2
Fipronil	C ₁₂ H ₄ Cl ₂ F ₆ N ₄ OS	36.3	-0.005	0.67	0.50	26	20	-
Fluoxetine	C ₁₇ H ₁₈ F ₃ NO	18.2	+0.008	6.00	0.18	18	8	-

6:2 diPAP, 6:2 polyfluoroalkyl phosphate diester; 6:2 FTOH, 6:2 fluorotelomer alcohol; AmPr-FHxSA, N-dimethyl ammonio propyl perfluorohexane sulfonamide [31]; Capstone B (also 6:2 FTAB), 6:2 fluorotelomer sulfonamide alkylbetaine [32]. For the predicted F/C, the table provided as Electronic Supplementary Material was used. Compounds without prediction fell either in bins outside the used MD/C-m/C domain or were located in bins with less than 5 entries which were excluded in data analysis.

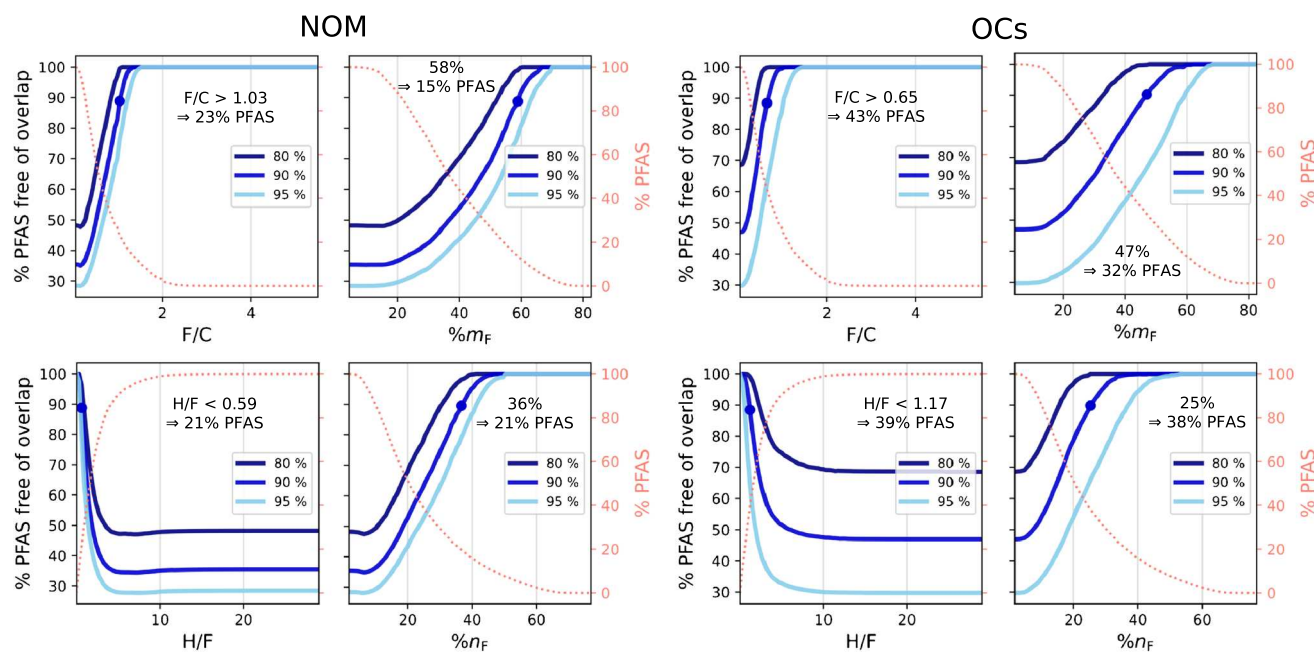
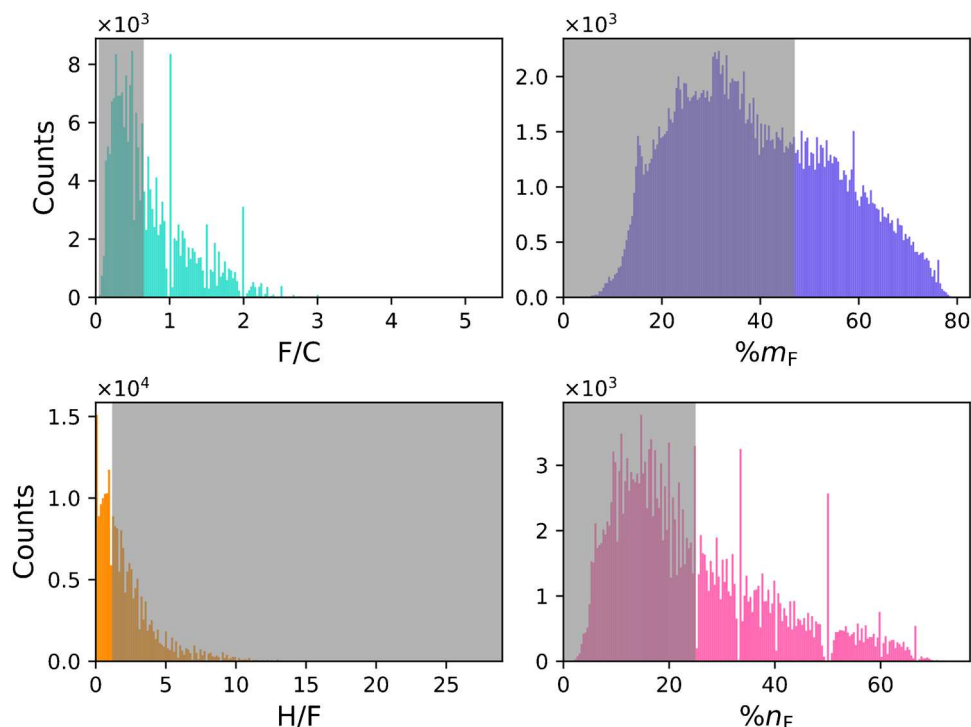


Fig. 3 Simulation of the separation of PFAS dependent on their fluorine content (>F/C, <H/F, >%m_F, and >%n_F) from NOM compounds and organic contaminants (OCs) in the MD/C-m/C plot for 80%, 90%, and 95% of both classes (NOM vs. PFAS and OCs vs. PFAS). Blue dots mark the position where 90% of PFAS overlap less than 10% with 90% of the other class. The secondary y-axis shows the PFAS

fraction that is above (F/C, %m_F, %n_F) or below (H/F) each fluorine quantity parameter. The text within each subplot gives the exact fluorine quantity and how much PFAS fall into that range (PFAS that have >F/C, %m_F, and %n_F for H/F PFAS that have <H/F for 90% of both classes). The underlying concept of the calculation of one data point is exemplified in Fig. S4

Fig. 4 Histograms of the distributions of PFAS with larger parts than CF_2 or CF_3 (210,091 compounds) from PubChem for F/C, H/F, $\%m_F$, and $\%n_F$. Grey areas indicate PFAS that cannot be easily separated by the MD/C-m/C approach based on the 90%/90% boundaries from Fig. 3 since they overlap with other compounds. The grey areas are given according to the calculations based on OCs. The data for each histogram was separated in 200 bins. Note which molecular compositions of PFAS are frequent. Note that the PFAS inside the grey area are not necessarily “non-separable PFAS”



pharmaceutical fluoxetine. The separation works also very well for ether-PFAS such as C6O4, ADONA, GenX, and PFO6TeDA due to an additional high O content. AmPr-FHxSA (electrochemically fluorinated AFFF), 6:2 FTOH, and fipronil are examples (low MD/C due to 2 Cl atoms and high m/C resulting from a high fraction of heteroatoms) that fall in regions closer to some OCs and NOM. Fluoxetine has only one CF_3 -group and is an example for a compound that cannot be prioritized due to the dominance of CH in the chemical formula. This is generally the case for all compounds with low CF compared to CH groups which are therefore shifted to the upper left part of the MD/C-m/C-plot and hence overlapping with NOM constituents (CHO) and many other organic chemicals. Information on the F/C, H/F, $\%m_F$, and $\%n_F$ of those PFAS examples are given in Table 1. In general, all examples with longer perfluoroalkyl (or perfluoroether) chains are in the vicinity of the $\text{CH}_x\text{F}_{2-x}$ -line as indicated in Fig. 2d (see also Fig. 1 and Eq. 1). This line can be used as a helpful tool to estimate the elemental composition of features that are located closely and helps as an orientation in the MD/C-m/C plot. Compounds with more H atoms are shifted upwards in MD/C (e.g., 6:2 FTOH, or the AFFF compounds) while the presence of 2 Cl atoms in fipronil results in a lower MD/C which shifts downwards (and a shift to the right at higher m/C).

Generally, the prioritization of features as potential PFAS in the MD/C-m/C plot should either be performed elliptically outwards from the CF_2 position ($\text{MD}/\text{C} \approx -0.003$ and $\text{m}/\text{C} \approx 50$) along the slope of the $\text{CH}_x\text{F}_{2-x}$ -line (see Eq. 1) or along the

$\text{CH}_x\text{F}_{2-x}$ -line from right to left (increasing MD/C and decreasing m/C). To facilitate the procedure, we propose to rotate the MD/C vs. m/C data by the angle of the $\text{CH}_x\text{F}_{2-x}$ -line and to shift the CF_2 position to the origin (0,0) (Eqs. 3 and 4):

$$\text{m}/\text{C}_m = (\text{m}/\text{C} - \text{m}/\text{C}_{\text{CF}_2}) \cos(m) - (\text{MD}/\text{C} - \text{MD}/\text{C}_{\text{CF}_2}) \sin(m) \quad (3)$$

$$\text{MD}/\text{C}_m = (\text{m}/\text{C} - \text{m}/\text{C}_{\text{CF}_2}) \sin(m) + (\text{MD}/\text{C} - \text{MD}/\text{C}_{\text{CF}_2}) \cos(m) \quad (4)$$

where m/C_m and MD/C_m are the new shifted and rotated locations, $\text{m}/\text{C}_{\text{CF}_2}$ and $\text{MD}/\text{C}_{\text{CF}_2}$ are the respective CF_2 positions (49.9968, -0.00319), and m is the positive slope of the $\text{CH}_x\text{F}_{2-x}$ -line ($+5.23 \times 10^{-4}$). For prioritization of subsets of the features, suitable ranges for MD/C_m and m/C_m can now be set more easily (e.g., ± 10 m/C and ± 0.001 MD/C) (see Fig. S9). Furthermore, if a continuous feature prioritization is desired (ranking), the elliptical radii of features from the shifted CF_2 position (0,0) can be calculated according to Eq. 5:

$$r_{\text{CF}_2} = \sqrt{\left(\frac{\text{m}/\text{C}_m}{\lambda}\right)^2 + \text{MD}/\text{C}_m^2} \quad (5)$$

where r_{CF_2} corresponds to the radial distance from the CF_2 position and λ is a factor that determines the aspect ratio of the ellipse. Since the m/C range of PFAS with high F content (e.g., $\%m_F > 60\%$) is approximately 3000 times the MD/C range (see Figs. S9 and S10), a reasonable λ would

be ~ 3000 ; however, this parameter should be adjusted. After calculating r_{CF_2} , features can be prioritized by sorting them by increasing r_{CF_2} . It should be noted that λ is an empirical parameter that should be interpreted as an approximate value.

Estimation of the degree of fluorination

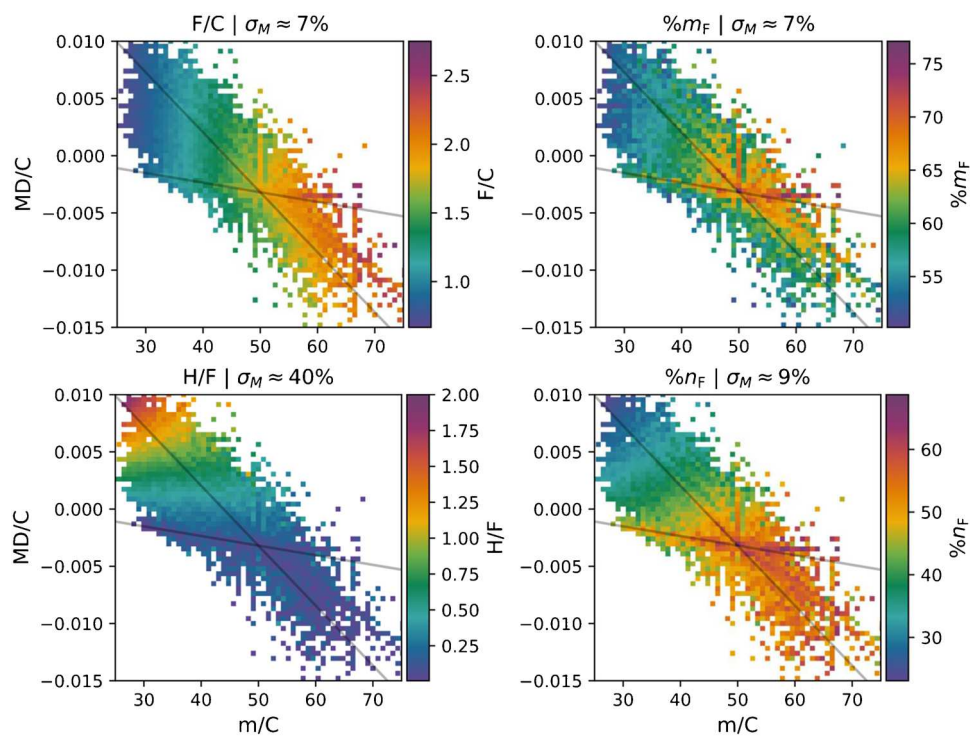
To determine whether the degree of fluorination can be estimated from the position of a PFAS feature in the MD/C-m/C plot, the mean and standard deviations of PFAS with $\%m_F > 50\%$ in each MD/C-m/C bin (70×70 grid) were calculated for F/C, H/F, $\%m_F$, and $\%n_F$ (Fig. 5). Only PFAS with more than 50% m_F were used in this data analysis because 50% m_F was approximately determined to be sufficient for a separation of PFAS from other compounds (see Fig. 3). Bins in which less than 5 PFAS are located were excluded from the analysis since 5 compounds have been considered as minimum for statistical calculations like mean and standard deviation. It is important to mention that the standard deviation in each bin is dependent on the grid size, since a very fine grid (only one compound per bin) would result in a variance of zero. We have chosen a grid size of 70×70 bins for this data evaluation (for the dependency of the standard error on grid size, see Fig. S11; further details on calculations in Fig. S3).

For F/C, H/F, $\%m_F$, and $\%n_F$, overall reproducible distributions in the MD/C-m/C plot were observed (Fig. 5). The F/C ratio increases with increasing m/C (from left to right). H/F shows a decreasing trend with decreasing MD/C with particularly small

values slightly above and below the CF_x -line. $\%m_F$ shows an elliptical decreasing trend (along the CH_xF_{2-x} -line and other specific positions) with increasing distance to the CF_2 -point and maxima along the specific lines (Fig. 5). A similar distribution was observed for $\%n_F$; however, in the region higher than $m/C = 50$, it still increases with increasing m/C. For all four fluorine parameters (F/C, H/F, etc.), there are exceptions which originate from the underlying dataset.

To estimate how well the four fluorine parameters can be estimated from a position in the MD/C-m/C plot, they were predicted based on the respective calculated 2D mean matrices. Those predicted values were then correlated with the true values (see Fig. 6 for F/C, and Fig. S12 for H/C, $\%m_F$, and $\%n_F$). Obviously, for F/C and H/F, the strongest correlation ($R^2 = 0.88$) was observed while for $\%n_F$ and $\%m_F$, it was lower (0.72 and 0.41, respectively). The distribution of the standard errors of the mean in all bins reveals that H/F has by far the largest standard error (see Fig. 7; the detailed standard deviations in each bin in Fig. S12). While the standard error distribution of all bins for F/C and $\%m_F$ was the lowest (around $\sim 7\% \pm$ approx. 7%), that for $\%n_F$ was medium (range of $\sim 25\%$), and that for H/F was very large (up to 300%). This results from the fact that for highly fluorinated compounds, H/F becomes very small and close to zero ($H = 1$ or even 0 if F is very high) and in case of the standard error, the standard deviation is divided by this very small value of H/F (see also H/F plot in Fig. S13 close to the origin). Therefore, a prediction of H/F is not possible with reasonable precision. However, the F/C ratio of a compound can be estimated depending on its position in the MD/C-m/C

Fig. 5 Average F/C, H/F, $\%m_F$, and $\%n_F$ for PFAS with $\%m_F > 50\%$ in the MD/C-m/C plot (70×70 bins). The F/C ratio can be roughly estimated from a feature position in the MD/C-m/C plot (for correlation, see Fig. 6). Plot titles (σ_M) provide the median overall standard error (for standard error distribution, see Fig. 7). Exact standard deviations in each bin are provided in Fig. S12. Due to the higher variability of H/F, $\%m_F$, and $\%n_F$ independent on the position in the MD/C-m/C plot, no accurate predictions can be performed (see Fig. S13 for correlation plots)



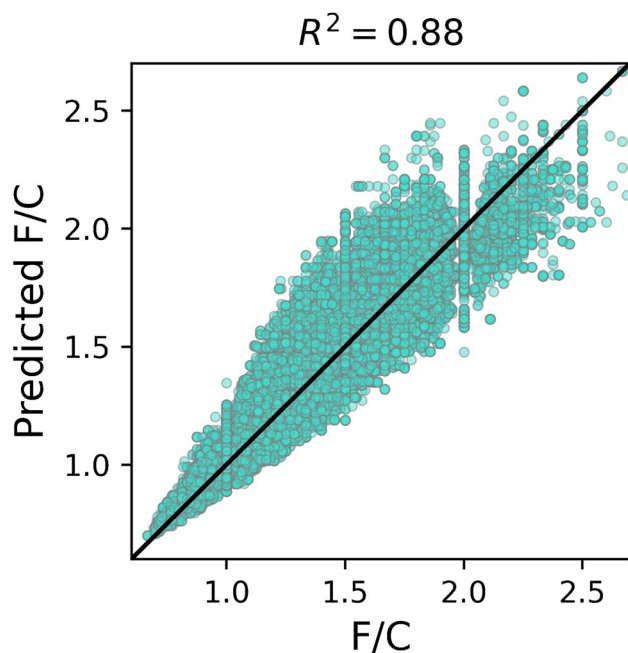


Fig. 6 Predicted F/C ratios based on the MD/C-m/C position in the mean matrix of F/C (F/C subplot in Fig. 5 and the Excel table of the ESI) vs. calculated real F/C ratios for chemical formulas of 52,769 PFAS with $\%m_F > 50\%$. Predictions for H/F, $\%m_F$, and $\%n_F$ are given in Fig. S13

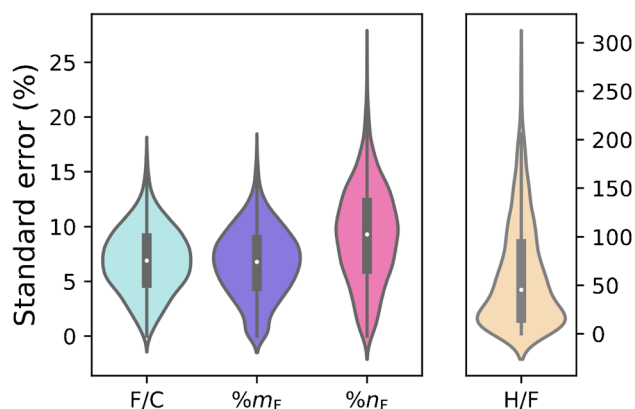


Fig. 7 Distribution of the standard error of F/C, $\%m_F$, $\%n_F$, and H/F in all bins from the MD/C-m/C plot for the calculations in Fig. 5 (for detailed standard deviations and calculations, see Figs. S3 and S12). While F/C, $\%m_F$, and $\%n_F$ have reproducible errors, as H/F approaches close to zero, the standard error becomes very high due to division by a very small mean H/F (see also Fig. S13). Therefore, a reasonable prediction of H/F cannot be achieved from a position in the MD/C-m/C plot

plot with meaningful accuracy (see Fig. 6). Examples for F/C predictions from the mean matrix for the above PFAS examples are given in Table 1. With the estimated F/C ratio, the number of F atoms can further be calculated, since the number of C atoms is known. Furthermore, with the mass and number of F atoms, even $\%m_F$ can be estimated. For that purpose, an Excel

sheet with the mean matrix (and standard deviation) of the F/C ratio and corresponding MD/C and m/C-bins is provided as Electronic Supplementary Material.

This general estimation approach, however, should be handled with care, because compounds in the MD/C-m/C plot can deviate from a CHF composition strongly making predictions more difficult. Also, measurement artifacts (e.g., errors in ^{13}C isotope intensity due to detector saturation) should be considered in this approach. Overall, however, such a prediction provides useful information and a rough estimate of fluorine content of a measured feature based only on accurate mass measurements.

Conclusions and implication for PFAS NTS

Overall, the MD/C-m/C approach is a highly promising tool for data reduction in NTS measurements and, therefore, to improve and accelerate non-targeted identification of highly fluorinated PFAS in highly complex samples. Since the prioritization does not require MS/MS data or several homologues, it is especially valuable in trace analysis approaches. It can efficiently be used to select potential PFAS candidates with high fluorine content for subsequent MS/MS experiments at a high probability. This increases the identification throughput since broad MS/MS coverage can be time consuming (multiple measurements per sample). Furthermore, during suspect screening approaches, the number of features can be substantially reduced to potential PFAS compounds so that the false positive rate (which is often very high, when using large PFAS lists) can be kept in a manageable extent. Special care should be taken when considering features at very high or low signal intensity, because of increased uncertainty of the determination of the ^{13}C isotope abundance (and therefore MD/C and m/C). In the case of signals at or near MS detector saturation (e.g., in highly contaminated samples), the number of C atoms will be likely overestimated, shifting a feature to a lower m/C (stronger overlap with CH compounds) and lower MD/C. Therefore, it must be noted that both values are always subject to a certain error (e.g., $\pm 10\%$). However, if the MD/C of a feature is close to -0.003 and m/C close to 50, there is a high probability that this indicates a highly fluorinated compound. Additionally, when the structure of a compound is known, the intrinsic property of the MD/C-m/C to cluster compounds of high elemental similarity can be used to get potential information on features that plot closely to known compounds.

In particular, we want to highlight the advantages of this approach over the use of MD only. Additionally, the MD/C-m/C position allows preliminary estimates on the elemental composition of a feature of interest.

We recommend an inside-out sequence of feature prioritization of HRMS data in an elliptical shape (starting from the CF_2 location) along the $\text{CH}_x\text{F}_{2-x}$ -line (see e.g., Eqs. 3–5, the PFAS region shown in Fig. 2c, or Figs. S9 and S10).

In addition, besides PFAS, the MD/C-m/C approach is highly promising for other compound classes like iodinated

compounds (e.g., iodine-containing disinfection byproducts which are highly toxic [33]) since they are even better separated from non-halogenated features in both dimensions due to their high m/C and low MD/C from to the contribution of I. Overall, we hope that this approach will be adapted by a wide range of PFAS researchers as well as analytical laboratories.

Supplementary Information The online version contains supplementary material available at <https://doi.org/10.1007/s00216-023-04601-1>.

Acknowledgements The authors acknowledge the scholarship of JZ by the Deutsche Bundesstiftung Umwelt.

Funding Open Access funding enabled and organized by Projekt DEAL. Deutsche Bundesstiftung Umwelt (DBU) funded the PhD scholarship of JZ.

Declarations

Conflict of interest The authors declare no competing interests.

Open Access This article is licensed under a Creative Commons Attribution 4.0 International License, which permits use, sharing, adaptation, distribution and reproduction in any medium or format, as long as you give appropriate credit to the original author(s) and the source, provide a link to the Creative Commons licence, and indicate if changes were made. The images or other third party material in this article are included in the article's Creative Commons licence, unless indicated otherwise in a credit line to the material. If material is not included in the article's Creative Commons licence and your intended use is not permitted by statutory regulation or exceeds the permitted use, you will need to obtain permission directly from the copyright holder. To view a copy of this licence, visit <http://creativecommons.org/licenses/by/4.0/>.

References

- Glüge J, Scheringer M, Cousins IT, DeWitt JC, Goldenman G, Herzke D, Lohmann R, Ng CA, Trier X, Wang Z. An overview of the uses of per- and polyfluoroalkyl substances (PFAS). *Environ Sci Process Impacts*. 2020;22(12):2345–73. <https://doi.org/10.1039/d0em00291g>.
- Evich MG, Davis MJB, McCord JP, Acrey B, Awkerman JA, Knappe DRU, Lindstrom AB, Speth TF, Tebes-Stevens C, Strynar MJ, Wang Z, Weber EJ, Henderson WM, Washington JW. Per- and polyfluoroalkyl substances in the environment. *Science*. 2022;375(6580):eabg9065. <https://doi.org/10.1126/science.abg9065>.
- Cousins IT, DeWitt JC, Glüge J, Goldenman G, Herzke D, Lohmann R, Ng CA, Scheringer M, Wang Z. The high persistence of PFAS is sufficient for their management as a chemical class. *Environ Sci Process Impacts*. 2020;22(12):2307–12. <https://doi.org/10.1039/d0em00355g>.
- Kissa E. Fluorinated surfactants and repellents, vol. 97. CRC Press; 2001.
- Cousins IT, Johansson JH, Salter ME, Sha B, Scheringer M. Outside the safe operating space of a new planetary boundary for per- and polyfluoroalkyl substances (PFAS). *Environ Sci Technol*. 2022;56(16):11172–9. <https://doi.org/10.1021/acs.est.2c02765>.
- Jian JM, Guo Y, Zeng L, Liang-Ying L, Lu X, Wang F, Zeng EY. Global distribution of perfluorochemicals (PFCs) in potential human exposure source—a review. *Environ Int*. 2017;108:51–62. <https://doi.org/10.1016/j.envint.2017.07.024>.
- Stockholm Convention. The new POPs under the Stockholm Convention. 2022. <http://www.pops.int/TheConvention/ThePOPs/TheNewPOPs/tabid/2511/Default.aspx>. Accessed 7 July 2022.
- Wang Z, DeWitt JC, Higgins CP, Cousins IT. A never-ending story of per- and polyfluoroalkyl substances (PFASs)? *Environ Sci Technol*. 2017;51(5):2508–18. <https://doi.org/10.1021/acs.est.6b04806>.
- Aro R, Carlsson P, Vogelsang C, Karrman A, Yeung LW. Fluorine mass balance analysis of selected environmental samples from Norway. *Chemosphere*. 2021;283:131200. <https://doi.org/10.1016/j.chemosphere.2021.131200>.
- Aro R, Eriksson U, Kärrman A, Chen F, Wang T, Yeung LWY. Fluorine mass balance analysis of effluent and sludge from Nordic countries. *ACS ES&T Water*. 2021;1(9):2087–96. <https://doi.org/10.1021/acsestwater.1c00168>.
- Kaiser AM, Forsthuber M, Aro R, Karrman A, Gundacker C, Zeisler H, Foessleitner P, Salzer H, Hartmann C, Uhl M, Yeung LWY. Extractable organofluorine analysis in pooled human serum and placental tissue samples from an Austrian subpopulation—a mass balance analysis approach. *Environ Sci Technol*. 2021;55(13):9033–42. <https://doi.org/10.1021/acs.est.1c00883>.
- Yeung LWY, Mabury SA. Are humans exposed to increasing amounts of unidentified organofluorine? *Environ Chem*. 2016;13(1):102–10. <https://doi.org/10.1071/en15041>.
- Ruan T, Jiang G. Analytical methodology for identification of novel per- and polyfluoroalkyl substances in the environment. *TrAC, Trends Anal Chem*. 2017;95:122–31. <https://doi.org/10.1016/j.trac.2017.07.024>.
- Jia S, Marques Dos Santos M, Li C, Snyder SA. Recent advances in mass spectrometry analytical techniques for per- and polyfluoroalkyl substances (PFAS). *Anal Bioanal Chem*. 2022;414:2795–807. <https://doi.org/10.1007/s00216-022-03905-y>.
- Gonzalez de Vega R, Cameron A, Clases D, Dodgen TM, Doble PA, Bishop DP. “Simultaneous targeted and non-targeted analysis of per- and polyfluoroalkyl substances in environmental samples by liquid chromatography-ion mobility-quadrupole time of flight-mass spectrometry and mass defect analysis.” *J Chromatogr A*. 2021;1653:462423. <https://doi.org/10.1016/j.chroma.2021.462423>.
- Liu Y, D’Agostino LA, Qu G, Jiang G, Martin JW. High-resolution mass spectrometry (HRMS) methods for nontarget discovery and characterization of poly- and per-fluoroalkyl substances (PFASs) in environmental and human samples. *TrAC Trends Anal Chem*. 2019;121:115420. <https://doi.org/10.1016/j.trac.2019.02.021>.
- Bugsel B, Zwiener C. LC-MS screening of poly- and perfluoroalkyl substances in contaminated soil by Kendrick mass analysis. *Anal Bioanal Chem*. 2020;412(20):4797–805. <https://doi.org/10.1007/s00216-019-02358-0>.
- Munoz G, Michaud AM, Liu M, Vo Duy S, Montenach D, Resseguier C, Watteau F, Sappin-Didier V, Feder F, Morvan T, Houot S, Desrosiers M, Liu J, Sauve S. Target and nontarget screening of PFAS in biosolids, composts, and other organic waste products for land application in France. *Environ Sci Technol*. 2022;56(10):6056–68. <https://doi.org/10.1021/acs.est.1c03697>.
- Koelmel JP, Stelben P, McDonough CA, Dukes DA, Aristizabal-Henao JJ, Nason SL, Li Y, Sternberg S, Lin E, Beckmann M, Williams AJ, Draper J, Finch JP, Munk JK, Deigl C, Rennie EE, Bowden JA, Godri Pollitt KJ. FluoroMatch 2.0-making automated and comprehensive non-targeted PFAS annotation a reality. *Anal Bioanal Chem*. 2022;414(3):1201–15. <https://doi.org/10.1007/s00216-021-03392-7>.
- Zweigle J, Bugsel B, Zwiener C. FindPFAS: non-target screening for PFAS - comprehensive data mining for MS2 fragment mass differences. *Anal Chem*. 2022;94(30):10788–96. <https://doi.org/10.1021/acs.analchem.2c01521>.
- Kaufmann A, Butcher P, Maden K, Walker S, Widmer M. Simplifying nontargeted analysis of PFAS in complex food matrices. *J*

- AOAC Int. 2022;105:1280–7. <https://doi.org/10.1093/jaoacint/qsac071>.
22. Koch BP, Dittmar T, Witt M, Kattner G. Fundamentals of molecular formula assignment to ultrahigh resolution mass data of natural organic matter. *Anal Chem.* 2007;79(4):1758–63. <https://doi.org/10.1021/ac061949s>.
 23. Kim S, Chen J, Cheng T, Gindulyte A, He J, He S, Li Q, Shoemaker BA, Thiessen PA, Yu B, Zaslavsky L, Zhang J, Bolton EE. PubChem in 2021: new data content and improved web interfaces. *Nucleic Acids Res.* 2021;49(D1):D1388–95. <https://doi.org/10.1093/nar/gkaa971>.
 24. PubChem. PFAS and fluorinated compounds in PubChem Tree. 2022. <https://pubchem.ncbi.nlm.nih.gov/classification/#hid=120>. Accessed 7 July 2022.
 25. Grulke CM, Williams AJ, Thillanadarajah I, Richard AM. EPA's DSS-Tox database: history of development of a curated chemistry resource supporting computational toxicology research. *Comput Toxicol.* 2019;12:100096. <https://doi.org/10.1016/j.comtox.2019.100096>.
 26. Mohammed Taha H, Aalizadeh R, Alygizakis N, Antignac JP, Arp HPH, Bade R, Baker N, Belova L, Bijlsma L, Bolton EE, Brack W, Celma A, Chen WL, Cheng T, Chirsir P, Cirka L, D'Agostino LA, Djoumbou Feunang Y, Dulio V, Fischer S, Gago-Ferrero P, Galani A, Geueke B, Glowacka N, Gluge J, Groh K, Grosse S, Haglund P, Hakkinen PJ, Hale SE, Hernandez F, Janssen EM, Jonkers T, Kiefer K, Kirchner M, Koschorreck J, Krauss M, Krier J, Lamoree MH, Letzel M, Letzel T, Li Q, Little J, Liu Y, Lunderberg DM, Martin JW, McEachran AD, McLean JA, Meier C, Meijer J, Menger F, Merino C, Muncke J, Muschket M, Neumann M, Neveu V, Ng K, Oberacher H, O'Brien J, Oswald P, Oswaldova M, Picache JA, Postigo C, Ramirez N, Reemtsma T, Renaud J, Rostkowski P, Rudel H, Salek RM, Samanipour S, Scheringer M, Schliebner I, Schulz W, Schulze T, Sengl M, Shoemaker BA, Sims K, Singer H, Singh RR, Sumarah M, Thiessen PA, Thomas KV, Torres S, Trier X, van Wezel AP, Vermeulen RCH, Vlaanderen JJ, von der Ohe PC, Wang Z, Williams AJ, Willighagen EL, Wishart DS, Zhang J, Thomaidis NS, Hollender J, Slobodnik J, Schymanski EL. The NORMAN Suspect List Exchange (NORMAN-SLE): facilitating European and worldwide collaboration on suspect screening in high resolution mass spectrometry. *Environ Sci Eur.* 2022;34(1):104. <https://doi.org/10.1186/s12302-022-00680-6>.
 27. Wang Z, Buser AM, Cousins IT, Demattio S, Drost W, Johansson O, Ohno K, Patlewicz G, Richard AM, Walker GW, White GS, Leinala E. A new OECD definition for per- and polyfluoroalkyl substances. *Environ Sci Technol.* 2021;55(23):15575–8. <https://doi.org/10.1021/acs.est.1c06896>.
 28. Barnabas SJ, Böhme T, Boyer SK, Irmer M, Ruttkies C, Wetherbee I, Kondić T, Schymanski EL, Weber L. Extraction of chemical structures from literature and patent documents using open access chemistry toolkits: a case study with PFAS. *Digital Discovery.* 2022;1:490–501. <https://doi.org/10.1039/d2dd00019a>.
 29. Barzen-Hanson KA, Roberts SC, Choyke S, Oetjen K, McAlees A, Riddell N, McCrindle R, Ferguson PL, Higgins CP, Field JA. Discovery of 40 classes of per- and polyfluoroalkyl substances in historical aqueous film-forming foams (AFFFs) and AFFF-impacted groundwater. *Environ Sci Technol.* 2017;51(4):2047–57. <https://doi.org/10.1021/acs.est.6b05843>.
 30. Xia X, Zheng Y, Tang X, Zhao N, Wang B, Lin H, Lin Y. Nontarget identification of novel per- and polyfluoroalkyl substances in cord blood samples. *Environ Sci Technol.* 2022;56:17061–9. <https://doi.org/10.1021/acs.est.2c04820>.
 31. Tenorio R, Maizel AC, Schaefer CE, Higgins CP, Strathmann TJ. Application of high-resolution mass spectrometry to evaluate UV-sulfite-induced transformations of per- and polyfluoroalkyl substances (PFASs) in aqueous film-forming foam (AFFF). *Environ Sci Technol.* 2022;56:14774–87. <https://doi.org/10.1021/acs.est.2c03228>.
 32. Shaw DMJ, Munoz G, Bottos EM, Duy SV, Sauve S, Liu J, Van Hamme JD. Degradation and defluorination of 6:2 fluorotelomer sulfonamidoalkyl betaine and 6:2 fluorotelomer sulfonate by *Gordonia* sp. strain NB4-1Y under sulfur-limiting conditions. *Sci Total Environ.* 2019;647:690–8. <https://doi.org/10.1016/j.scitotenv.2018.08.012>.
 33. Dong H, Qiang Z, Richardson SD. Formation of iodinated disinfection byproducts (I-DBPs) in drinking water: emerging concerns and current issues. *Acc Chem Res.* 2019;52(4):896–905. <https://doi.org/10.1021/acs.accounts.8b00641>.

Publisher's note Springer Nature remains neutral with regard to jurisdictional claims in published maps and institutional affiliations.



Jonathan Zweigle is a PhD candidate (German Federal Environmental Foundation scholar) in the lab of Christian Zwiener. His current research includes analysis of per- and polyfluoroalkyl substances (PFAS) and their transformation products by GC and LC-HRMS and PFAS precursor characterization by oxidative conversion. One focus is the development of data analysis approaches to enhance PFAS identification in HRMS data.



Boris Bugsel is a postdoctoral researcher in the lab of Christian Zwiener at the University of Tübingen. His research covers the analysis, occurrence, and environmental fate of per- and polyfluoroalkyl substances (PFAS) and their transformation products. His interests particularly lie in the development of novel screening techniques by liquid and gas chromatography coupled to high-resolution mass spectrometry and an enhanced understanding of the complex and wide-ranging impacts of PFAS on the environment.



Christian Zwiener is head of the group of Environmental Analytical Chemistry in the Department of Geosciences at the Eberhard Karls Universität Tübingen. His research focuses on the analysis, occurrence, and fate of organic micropollutants in the environment and in water treatment (e.g., disinfection byproducts, pharmaceuticals, personal care products, pesticides, poly- and perfluorinated compounds). This includes the development of analytical approaches for non-target and suspect screening by LC-high-resolution mass spectrometry, field investigations and lab scale experiments for photochemistry, biodegradation, and electrochemical oxidation to identify transformation products.

Supporting Information

Efficient PFAS Prioritization in Non-Target HRMS Data: Systematic Evaluation of the novel MD/C-m/C Approach

Jonathan Zweigle,⁺ Boris Bugsel,⁺ Christian Zwiener^{+,*}

⁺Environmental Analytical Chemistry, Department of Geosciences, University of Tübingen, Schnarrenbergstraße 94-96, 72076 Tübingen, Germany

*Corresponding author.

Contents

ABBREVIATIONS & VARIABLES	1
Supporting data.....	2
Fig. S 1: True mass defect (MD) vs calculable MD for PFAS, NOM [1], and organic contaminants (OCs).	2
Fig. S 2: Examples for PFAS with %m _F ≥ 60% that fall along the CH _x F _{2-x} and the CF _x -line.	2
Fig. S 3: Schematic explanation of matrix calculations.	3
Fig. S 4: Example for the calculation of the overlapping regions of PFAS with organic contaminants (OCs).....	3
Fig. S 5: 2D histograms of the positions of PFAS, organic contaminants (OCs), and NOM compounds in the MD/C-m/C plot.	4
Fig. S 6: Further representation of the overlap of PFAS with organic contaminants (OCs).	5
Fig. S 7: Examples of four experimental MD/C-m/C plots from extracts of PFAS contaminated agricultural soils measured by Bugsel and Zwiener 2020 [2].	5
Fig. S 8: Positions of 90% 95% and, 97% of the organic contaminants (OCs) with the true and the calculable MD (determined by rounding: MD = Exact mass – Integer mass).....	6
Fig. S 9: Shifting and rotating the MD/C-m/C data.	6
Fig. S 10: Contour lines (black) of Equation 5 with λ = 3000 for PFAS prioritization in the MD/C-m/C plot.....	6
Fig. S 11: Dependency of the mean of the standard error matrix and the standard deviation of the standard error matrix of F/C, H/F, %m _F , and %n _F on grid size.....	7
Fig. S 12: Standard deviation of F/C, H/F, %m _F , and %n _F (shown as color bars) for PFAS with %m _F > 50% in the MD/C-m/C plot	8
Fig. S 13: Predicted H/F, %m _F , and %n _F based on the MD/C-m/C position in the respective mean matrix vs. real values for 52769 PFAS with %m _F > 50%.	8
REFERENCES	8

Abbreviations & Variables

F/C	Fluorine to carbon ratio (number)
H/C	Hydrogen to carbon ratio (number)
m/C	Mass to carbon value
MD/C	Mass defect to carbon value
NOM	Natural organic matter
OCs	Organic contaminants
PFAS	Per- and polyfluoroalkyl substances
%m _F	Mass percentage of fluorine in a chemical formula
%n _F	Molar percentage of fluorine atoms in a chemical formula

Supporting data

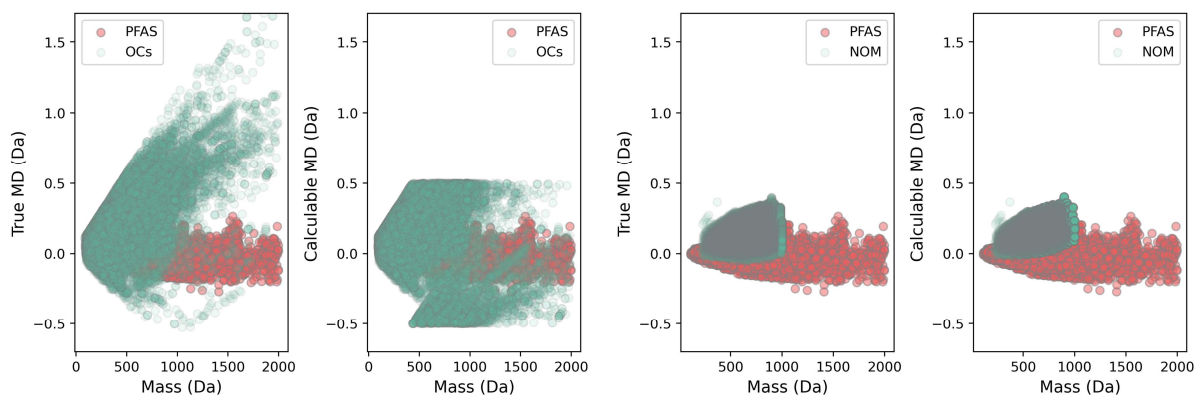


Fig. S 1: True mass defect (MD) vs calculable MD for PFAS, NOM [1], and organic contaminants (OCs). Obviously, numerous compounds exceed a mass defect of +0.5 Da, shifting them erroneously into the negative MD range which leads to overlapping with PFAS (left plot). This is not the case for NOM features.

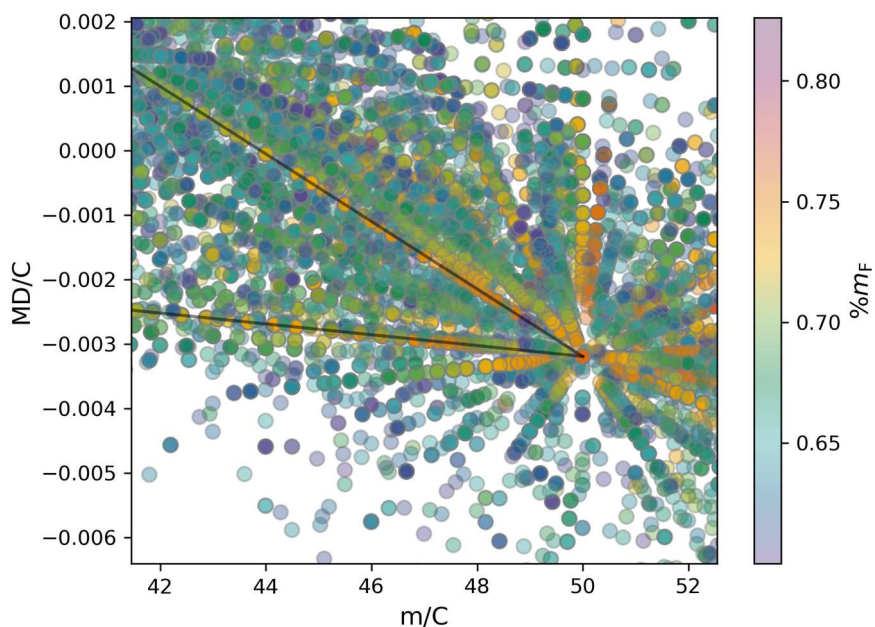


Fig. S 2: Examples for PFAS with $\%m_F \geq 60\%$ that fall along the $\text{CH}_x\text{F}_{2-x}$ and the CF_x -line. The color bar corresponds to the respective $\%m_F$. For details on the lines see Equation 1 and 2.

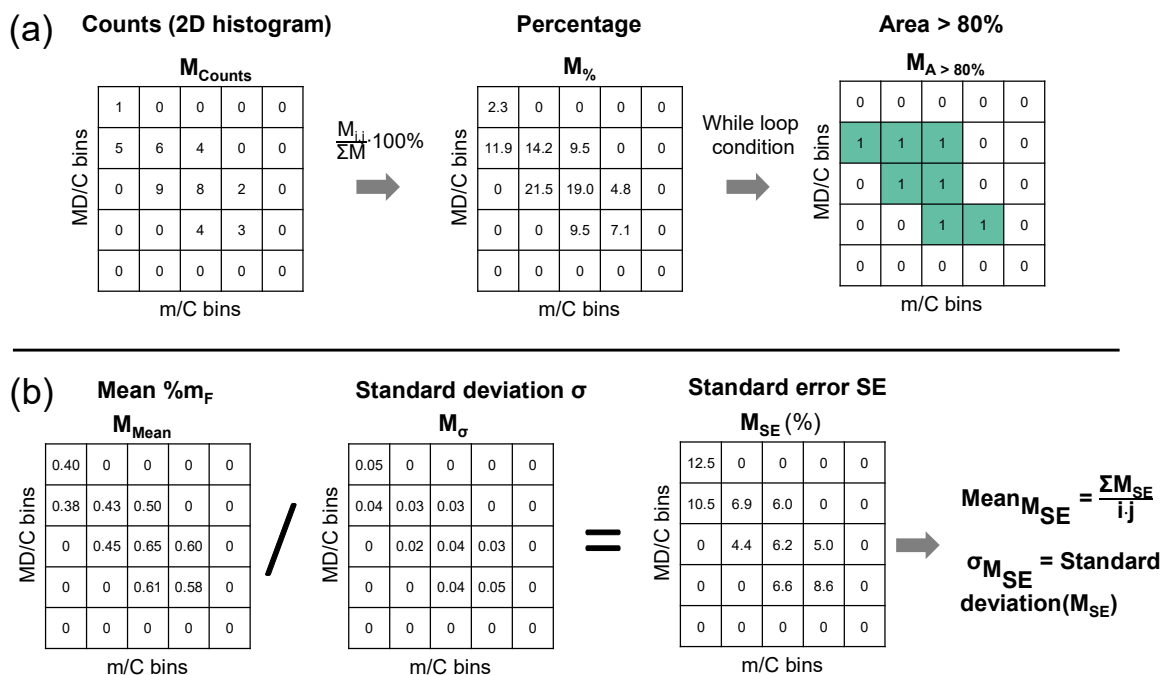


Fig. S 3: Schematic explanation of matrix calculations. (a) To find the area of a certain percentage of compounds in the MD/C–m/C plot the 2D histogram was normalized to its sum (percent compounds in each entry) and a while loop was used to find the area of x% in decreasing order (see also Fig. S4). (b) For F/C, H/F, %m_F, and %m_F the mean and standard deviation matrices (see Fig. 5 and Fig. S12, for standard error distribution see Fig. 6) of PFAS with %m_F > 50% that fall in each bin were calculated. The standard deviation matrix was divided by the mean matrix to obtain a matrix with the standard errors. For the grid size dependent standard error, the mean and standard deviation of the whole standard error matrix were plotted against grid size (Formulas for Mean_{M_{SE}} and $\sigma_{M_{SE}}$, see also Fig. S11).

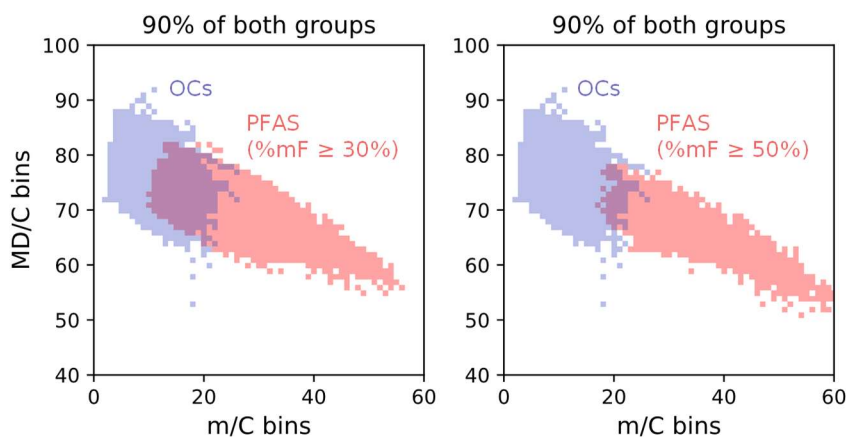


Fig. S 4: Example for the calculation of the overlapping regions of PFAS with organic contaminants (OCs). (Left) 90% of PFAS with %m_F > 30% vs. 90% of OCs and (right) PFAS with %m_F > 50% vs. 90% of OCs in a 100 × 100 binned grid. For continuous simulations see Fig. 5.

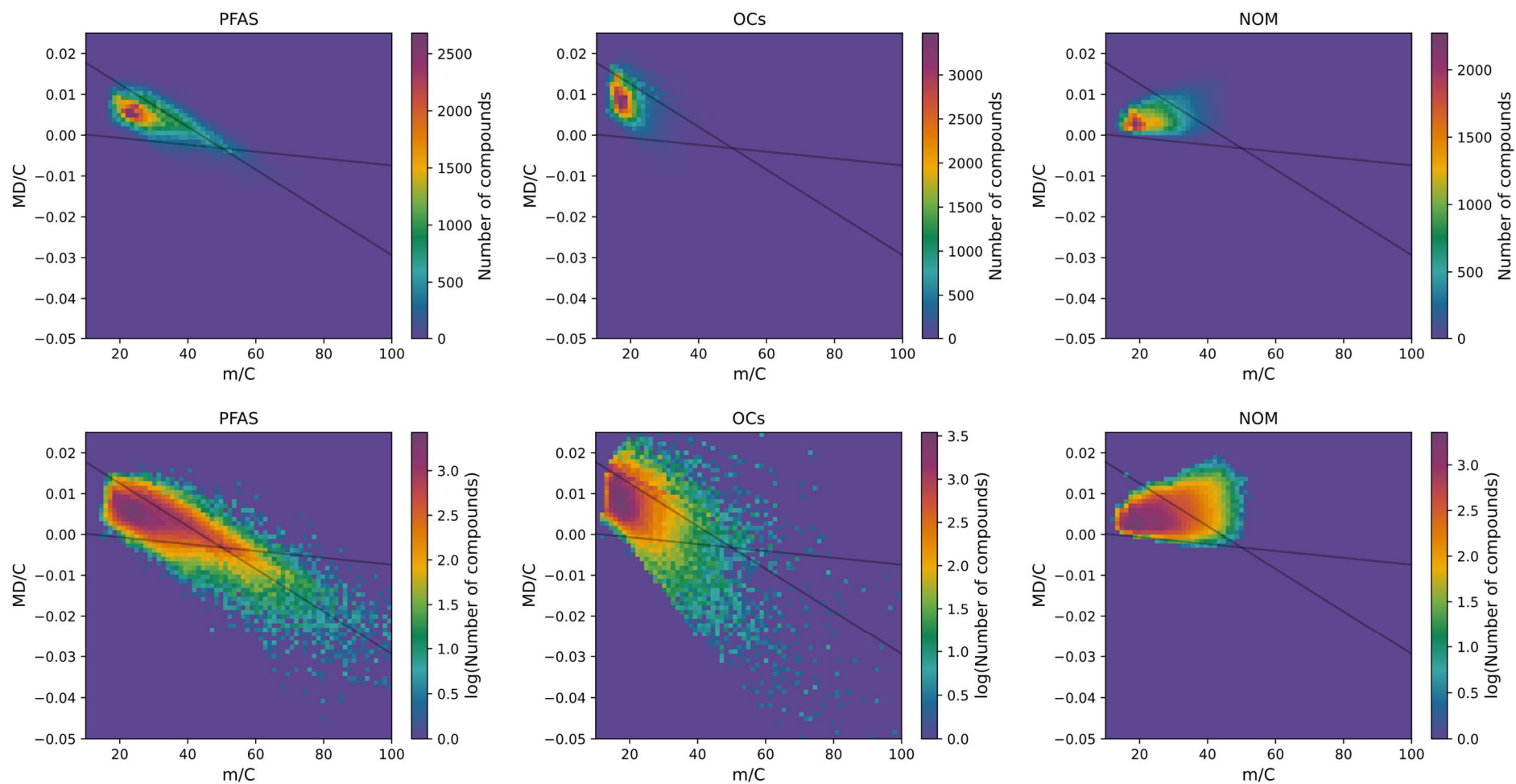


Fig. S 5: 2D histograms of the positions of PFAS, organic contaminants (OCs), and NOM compounds in the MD/C–m/C plot. Data is shown both in linear and log scale. In total, 210,091 PFAS, 159,236 OCs, and 124,782 NOM compounds are shown in a 70×70 bin grid.

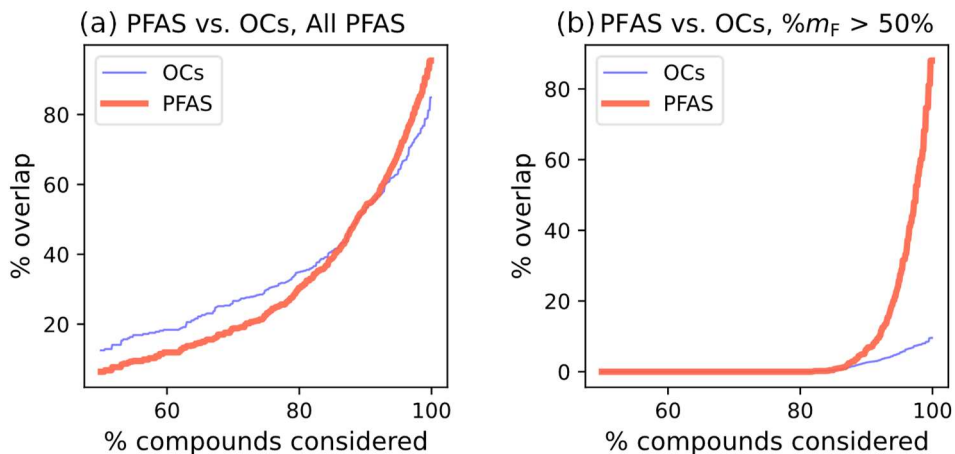


Fig. S 6: Further representation of the overlap of PFAS with organic contaminants (OCs). (a) % Overlap of PFAS and OCs vs. percent compounds considered for calculating this overlap. (b) Similar calculation but only PFAS with $\%m_F > 50\%$ were considered. The % compounds considered was calculated by summing up bins in decreasing order of compounds present.

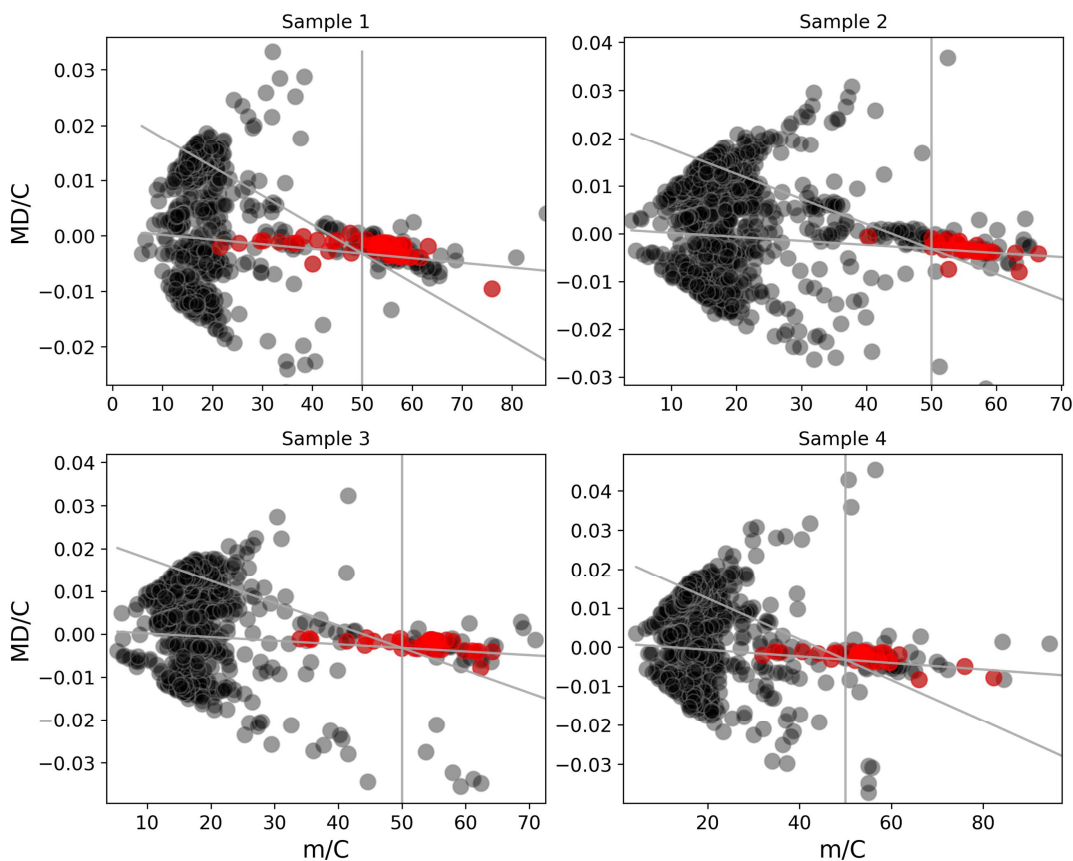


Fig. S 7: Examples of four experimental MD/C-m/C plots from extracts of PFAS contaminated agricultural soils measured by Bugsel and Zwiener 2020 [2]. Samples were measured by high-performance liquid chromatography quadrupole time-of-flight mass spectrometry and MS1 features above a certain intensity threshold are shown as black dots (details on the samples, sample preparation and identification can be found in [2]). Red dots are features that were identified as PFAS (e.g., perfluoroalkyl acids, polyfluoroalkyl phosphate esters, fluorotelomer carboxylic acids etc.). Overall an efficient separation from a significant fraction of matrix features can be observed which is generally concentrated along the proposed lines (see equation 1 and 2). The vertical line highlights m/C of 50 ($= CF_2$). Note: The sample numbers correspond to the sample numbers in [2].

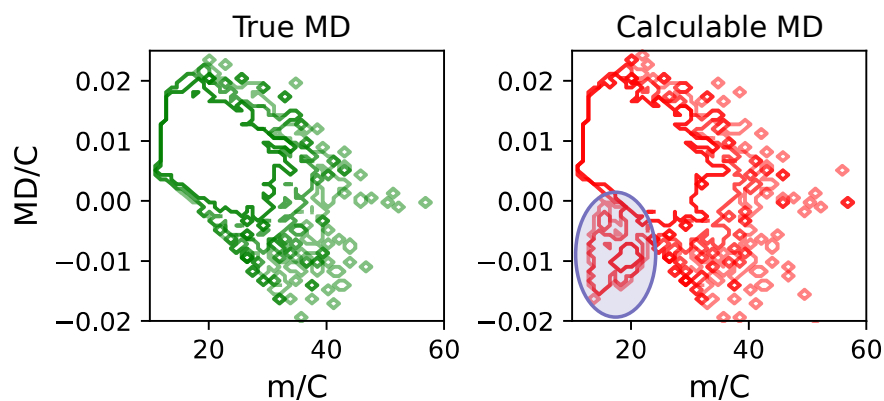


Fig. S 8: Positions of 90% 95% and, 97% of the organic contaminants (OCs) with the true and the calculable MD (determined by rounding: $MD = \text{Exact mass} - \text{Integer mass}$). It becomes obvious that the compounds with erroneously negative MD are unproblematic since they can be separated from PFAS in the m/C dimension. This is not the case when considering the MD alone (see Fig. S1).

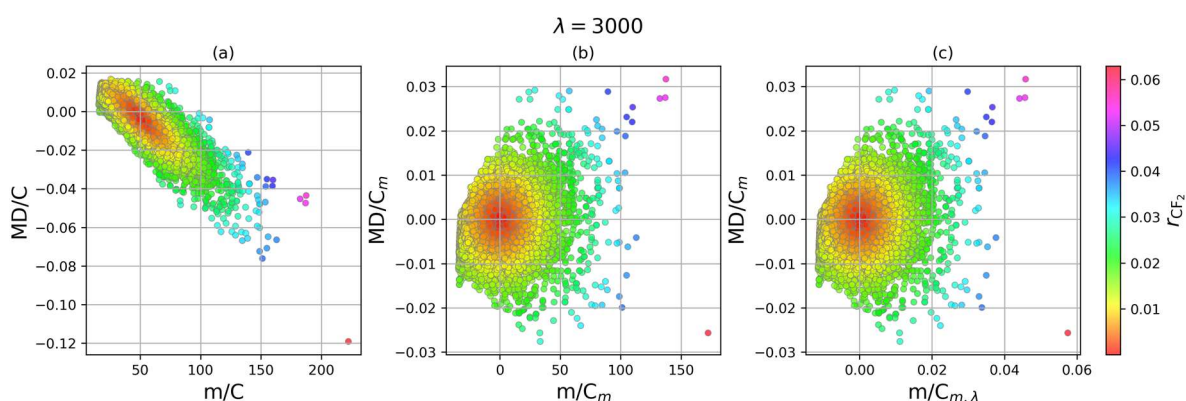


Fig. S 9: Shifting and rotating the $MD/C - m/C$ data. (a) $MD/C - m/C$ plot with calculated r_{CF_2} as color bar according to Equation 5 with $\lambda = 3000$ for PFAS with $\%m_F > 20\%$. (b) Data shifted to the origin and rotated by the slope of the CH_xF_{2-x} line according to Equation 3 and 4. (c) Compression of m/C dimension through the factor λ .

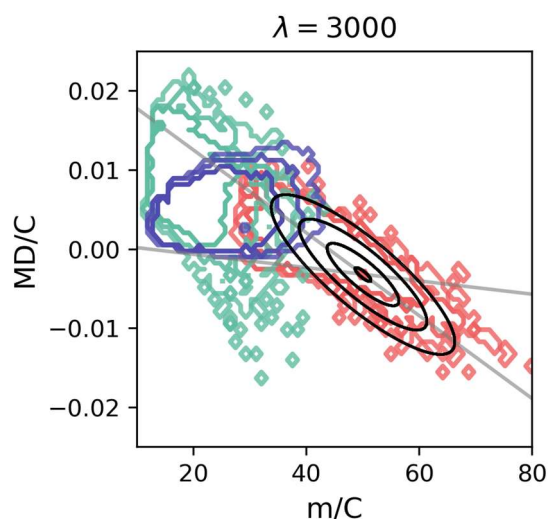


Fig. S 10: Contour lines (black) of Equation 5 with $\lambda = 3000$ for PFAS prioritization in the $MD/C - m/C$ plot. Positions of OCs (green), NOM (blue) and PFAS with $\%m_F > 55\%$ (red) are shown. The colored contour lines delimit the positions of 80% (center), 90% (middle), and 95% of each group (see also Fig. 2).

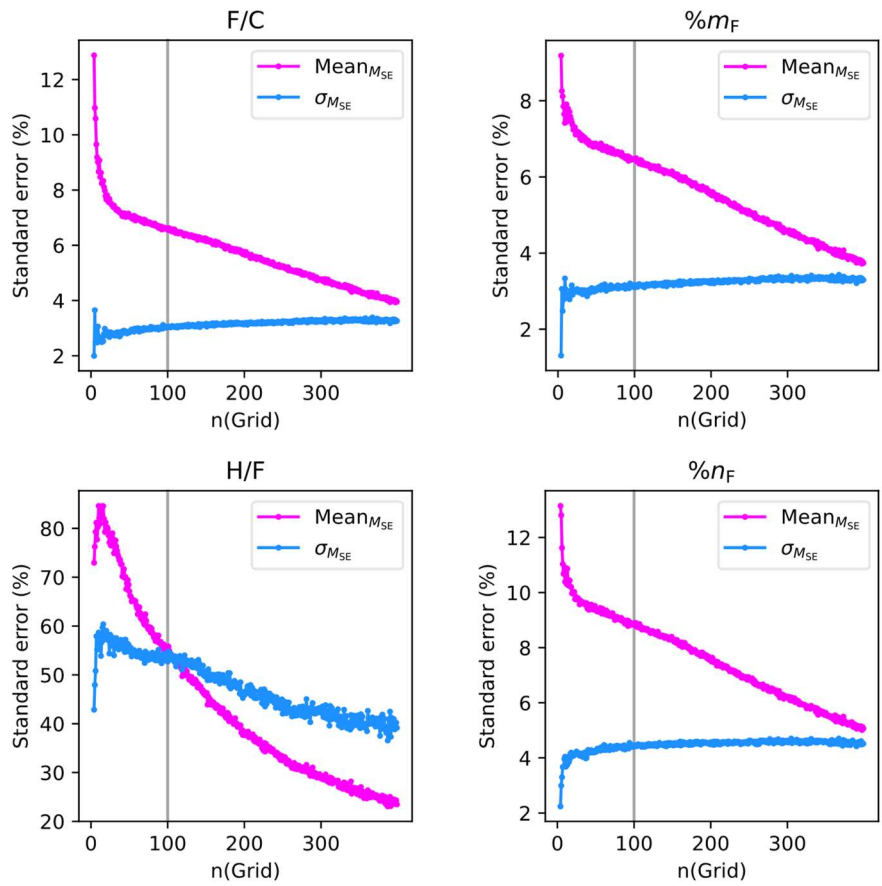


Fig. S 11: Dependency of the mean of the standard error matrix and the standard deviation of the standard error matrix of F/C, H/F, %m_F, and %n_F on grid size (for schematic explanations see also Fig. S3b).

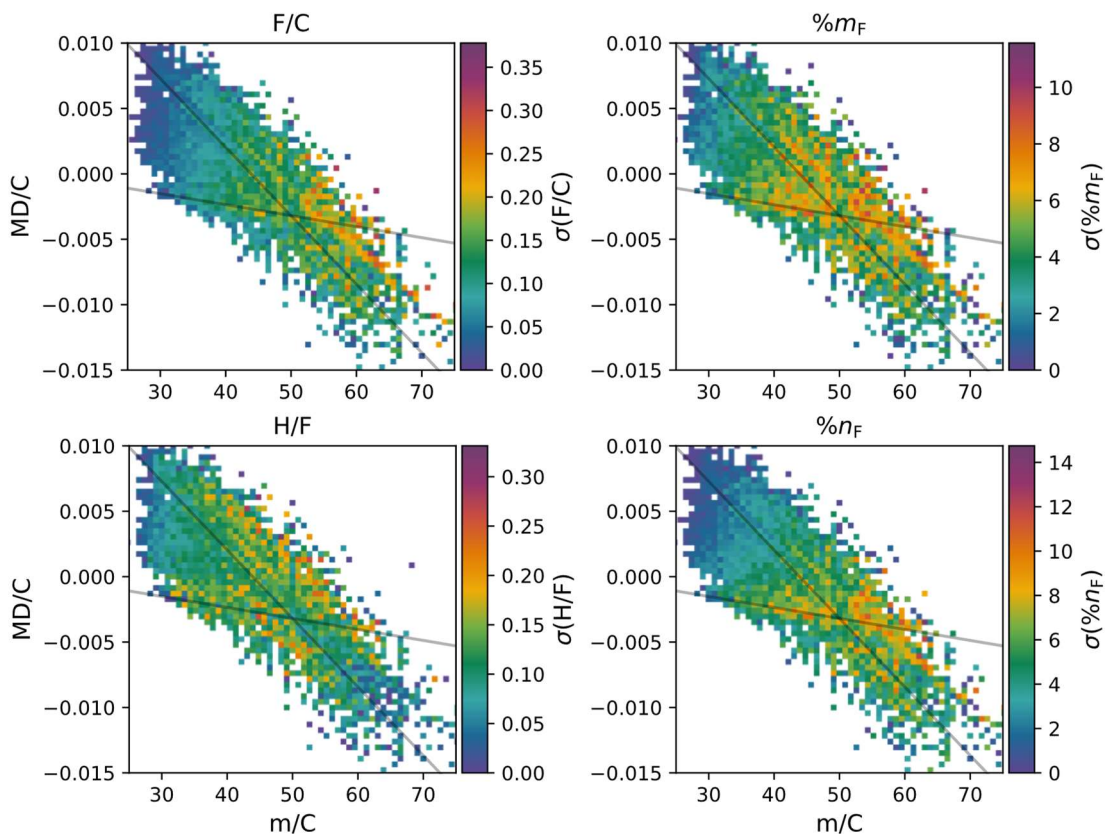


Fig. S 12: Standard deviation of F/C, H/F, $\%m_F$, and $\%n_F$ (shown as color bars) for PFAS with $\%m_F > 50\%$ in the MD/C–m/C plot (70×70 bins). For standard error distribution see Fig. 7. Note that the large standard error distribution of H/F result from the fact that in selected bins with highly fluorinated substances H/F approaches close to zero.

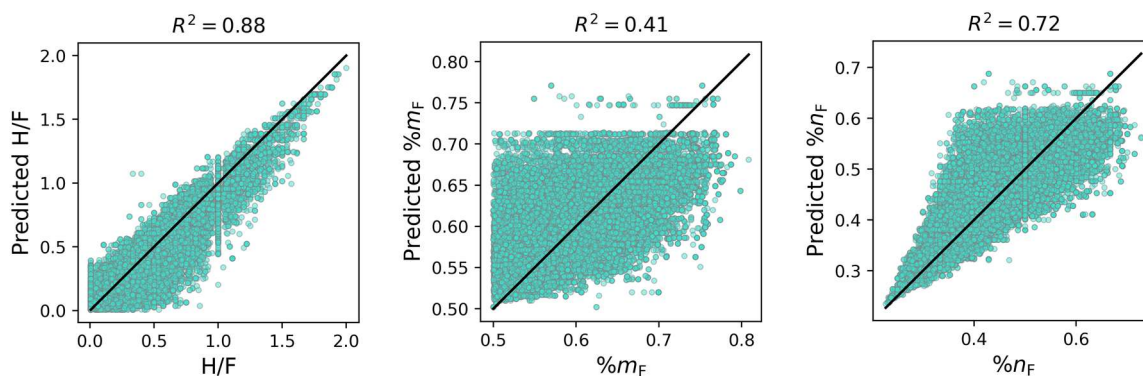


Fig. S 13: Predicted H/F, $\%m_F$, and $\%n_F$ based on the MD/C–m/C position in the respective mean matrix vs. real values for 52769 PFAS with $\%m_F > 50\%$. Note that the large standard error of H/F (see Fig. 7) results from the variability in the low H/F range (compounds with much higher number of F than H), where it gets closer to zero.

References

1. Koch, B.P., et al., *Fundamentals of molecular formula assignment to ultrahigh resolution mass data of natural organic matter*. *Anal Chem*, 2007. **79**(4): p. 1758-63.
2. Bugsel, B. and C. Zwiener, *LC-MS screening of poly- and perfluoroalkyl substances in contaminated soil by Kendrick mass analysis*. *Anal Bioanal Chem*, 2020. **412**(20): p. 4797-4805.

Appendix 2

Publication 2

FindPFAS: Non-Target Screening for PFAS - Comprehensive Data Mining for MS² Fragment Mass Differences

Jonathan Zweigle,⁺ Boris Bugsel,⁺ Christian Zwiener^{+,*}

⁺Environmental Analytical Chemistry, Center for Applied Geoscience, University of Tübingen,
Schnarrenbergstraße 94-96, 72076 Tübingen, Germany

Published in: Analytical Chemistry 94 (30):10788-10796.

DOI: 10.1021/acs.analchem.2c015

Reprinted from Analytical Chemistry: Zweigle, J., Bugsel, B., & Zwiener, C. (2022). FindPFAS: Non-Target Screening for PFAS - Comprehensive Data Mining for MS² Fragment Mass Differences. Anal Chem, 94(30), 10788-10796. <https://doi.org/10.1021/acs.analchem.2c01521>

which takes advantage of typical repeating units of PFAS homologues (e.g., CF_2).^{8,25–27} Furthermore, specific in-source fragments (in-source fragmentation flagging) such as C_2F_5^- were successfully used to identify PFAS in water.²⁸ Similar approaches were applied with data-independent acquisition using PFAS-specific fragments and neutral losses.^{29,30} Diagnostic fragments were also combined with in silico fragmentation prediction as automated PFAS NTS software on MS (KMD analysis) and MS^2 -level.³¹ Further methods focusing on computational approaches with in silico predicted fragments and PFAS TPs also exist.^{32,33} However, the above-mentioned methods also have drawbacks: Suspect-screening is often limited due to high false positive rates and high uncertainties if MS^2 information is missing. Diagnostic fragments are only described for a limited number of known PFAS classes and in silico models with rule-based or combinatorial fragmentation are not able to predict fragments formed by molecular rearrangements sufficiently.³⁴

Besides diagnostic PFAS fragments, the use of neutral losses strongly increased the information on PFAS identity in several studies.^{35–37} Here, mainly only mass differences of one fragment to the observed molecular ion were used (e.g., $[\text{M}-\text{H}-\text{HF}]^-$). Despite the large variety of chemical structures of PFAS, they include common substructures such as perfluoroalkyl chains ($\text{C}_n\text{F}_{2n+1}-\text{R}$), perfluoro-ether groups ($\text{C}_n\text{F}_{2n+1}-\text{O}-\text{C}_m\text{F}_{2m}-\text{R}$), or just a CF_3 -group in the case of compounds with low F-content such as, for example, pesticides and pharmaceuticals.³⁸ Hence, MS^2 -fragmentation patterns of PFAS typically contain several fragment specific mass differences associated with these common substructures. Therefore, we investigated in this work a comprehensive use of mass differences for PFAS identification in accurate mass MS^2 data. This general approach has several advantages: Mass differences are more generally applicable for truly non-targeted approaches because they occur between different, so far not pre-defined fragment ions, in contrast to diagnostic fragments which need to be known beforehand. Similar statements were hypothesized by Wang et al. 2020.³⁶ Additionally, diagnostic fragments of TPs may be shifted compared to the precursor compound by a certain mass, making detection via diagnostic fragments sometimes more difficult, while their mass differences often remain identical. An advantage of MS^2 fragment differences compared to KMD analysis is the identification of single compounds which do not occur in a homologous series. Because the advantages of mass differences were only partly used and discussed in past publications, the main goal of the present study was to investigate their occurrence and use for PFAS identification in more detail and provide an algorithm to extract and use relevant fragment differences from HR- MS^2 -data. Therefore, an in-house written algorithm (FindPFAS = FindPolyFluoroDeltas) based on Python 3.9.7 was developed, optimized, and validated with analytical PFAS standards (38 substances from 10 compound classes), 2 previously characterized PFAS-coated paper extracts, 2 soil extracts and finally with a larger extent of spectra retrieved from MassBank database.^{39,40} The focus here was on PFAS according to the OECD definition.³⁸ The impact of selected fragment differences, applied collision energies (CEs), and parameters such as mass tolerance and intensity thresholds on the rate of correct identifications versus false positive detections were investigated. FindPFAS is provided open source on GitHub (source code), as well as an executable windows application.

MATERIALS AND METHODS

FindPFAS Code. A fully automated Python (3.9.7) data processing workflow was developed to find PFAS in high-resolution MS/MS data. Raw data input is achieved by the MS^2 -format (.ms2), which is a simple and commonly used format to store and exchange vendor-independent MS^2 raw data.^{41,42} MS^2 files can easily be generated vendor-independently by using the open source MSConvert software from the ProteoWizard tools (centroid data, only one CE at a time recommended; for details see Figure S1).⁴³

In the first step, raw data (.ms2) (all precursor masses, their TIC intensity, RT and all MS^2 fragment peaks) are imported via Pyteomics, an open source Python MS package.⁴⁴ The subsequent steps of the algorithm are presented simplified (details in Supporting Information, Section S1):

- Data, background, and noise reduction (frequently occurring background masses, noise below a certain threshold in spectra).
- Calculate the differences between each peak in all MS^2 -spectra [n MS^2 peaks result in $n(n - 1)/2$ mass differences].
- Search differences for defined mass shifts (e.g., ΔCF_2 and $\Delta\text{C}_2\text{F}_4$) and save data.
- Rank data according to intensity or number of occurrences of selected mass shifts.
- Optional: search for diagnostic fragments and/or compare precursor masses to a suspect list.

A simplified scheme and explanations how to use the graphical user interface (GUI) and which output files are generated by FindPFAS are given in Figure S1.

Converted MS^2 -files (generated with MSConvert) from several vendor raw data files [Agilent (.d), Bruker (.baf), AB Sciex (.wiff), Shimadzu (.lcd), Thermo (.raw)] were tested for error-free data reading and evaluation with FindPFAS.

Note that this workflow was initially written in MATLAB R2021b (9.11.0.1809720) [reads in dd MS^2 XML-files (.CEF) resulting from the Agilent “FindByAutoMSMS” algorithm] for which reason some tasks for data evaluation were also performed in MATLAB.

Chemicals and Sample Preparation. The specifications and origins of chemicals are shown in the Supporting Information (Table S1). A PFAS standard mixture (20 $\mu\text{g}/\text{L}$) containing 38 different compounds from 10 compound classes [13 PFCAs, 8 PFSA, 4 FTCA, 3 PASF-based PFAS (diSAMPA, N-EtFOSAA, PFOSA), 2 FTUCAs, 2 diPAPs, 2 PFECAs [HFPO-DA (GenX), ADONA], 2 PFESAs (F-53B), 6:2 FTSA, and 6:6 PFPiA; acronyms in Table S1] was prepared in MeOH for optimization of the dd MS^2 -method and the validation of FindPFAS. Two raw paper samples (P1 and P2, provided by the Fraunhofer Institute, for details see⁴⁰) and two agricultural soil samples (S1 contaminated with PFAS, S2 without known contamination, but background input) were used to test and verify the performance of FindPFAS in real sample matrix (sample preparation details in Supporting Information, Section S2).

Non-Target Analysis and Data Acquisition. Measurements were performed using high-performance liquid chromatography-quadrupole time-of-flight mass spectrometry (HPLC-QTOF-MS). Compounds were separated using a 1260 Infinity HPLC system (Agilent Technologies, Waldbronn, Germany) equipped with a Poroshell 120 EC- C_{18} column (2.1 mm \times 100 mm) with a particle size of 2.7 μm at a flow rate of

0.3 mL/min (Oven temperature = 40 °C) coupled to a 6550 QTOF-mass spectrometer (Agilent Technologies, Santa Clara, USA). A 23 min gradient program (A: 95/5 H₂O/MeOH + 2 mM NH₄Ac; B: 95/5 MeOH/H₂O + 2 mM NH₄Ac) was applied and the ESI source was operated in the negative mode (Tables S2 and S3 for details).

Data were acquired in an iterative data-dependent MS/MS mode (ddMS² or AutoMSMS) with static and rolling exclusion lists (details in Supporting Information, Section S2 and Figure S2). Each measurement sequence included a solvent and an extraction blank and a quality control for every 20th sample (PFAS standard mixture). Data acquisition started at 1 min (prior waste line) with 3 scans/s in the MS (m/z 100–1700) and in the MS/MS range (m/z 70–1700). MS/MS was acquired from m/z 70 to include diagnostic fragments such as PO₃⁻, H₂PO₄⁻, and SO₃⁻. The threshold for precursor selection was set to 1000 counts with a narrow isolation width (≈ 1.3 m/z). Two different CEs (20 and 40 eV) and a linear, mass-dependent CE were used for MS/MS experiments [CE (m/z) = $4 \frac{m/z}{100} + 15$ eV, formula based on fragmentation experiments of known PFAS] for precursor m/z -dependent collision.

Retrospective Analysis. For selected PFAS MS² spectra, the number of all mass differences was calculated to find the most important differences for single substances, and substance classes by combining multiple spectra of each PFAS class. The number was calculated by counting the occurrences of all differences within a certain mass tolerance. Note that typically the isotope peaks also contribute to this number.

Furthermore, to also consider intensity, a number weighted by intensity (N_{iw}) was determined by assigning the lower intensity of two fragments x and y to their difference and summing up the intensities of all identical fragment differences (within a mass tolerance).

$$N_{iw,x,y} = \sum_{n=0}^{N_{x,y}} I_{x,y \min}(n) \quad (1)$$

The lower intensity was chosen because always the lower fragment peak determines whether a difference can be calculated or the peak disappears in noise which is essential for sensitivity. A large N_{iw} means that a difference is both frequent and has a high intensity.

Application of FindPFAS to MassBank. To determine ideal mass tolerance and intensity threshold and quantify their influence on identification- and false positive rate, FindPFAS was applied to the database MassBank.³⁹ Only HR-MS² spectra (QTOF- and FT-MS instruments) with ≥ 2 peaks (prerequisite for mass differences) were included resulting in 20,998 MS²-spectra from 1921 compounds (filtered by unique compound name). MassBank spectra were mainly searched for ΔCF_2 , ΔHF , and ΔCF_3 and compounds with chemical formulae ≥ 3 F atoms [942 spectra $F_{\geq 3}$ from 99 compounds $F_{\geq 3}$ (40 with perfluoroalkyl chain); searching via SMILES ["C(F)(F)F"] showed that >94% have a CF₃-group (including perfluoroalkyl chains)] were considered as hits (details in Supporting Information, Section S3).

RESULTS AND DISCUSSION

Retrospective Analysis with PFAS Standards and Paper Extracts. The retrospective analysis was performed with numerous PFAS spectra (standards and pre-characterized

paper extracts).⁴⁰ The most frequent and most intense fragment mass differences ($\Delta_{\text{fragments}}$) were calculated to identify the most important ones and further to deduce general rules of fragmentation. The intensity of $\Delta_{\text{fragments}}$ was calculated based on the lower intense fragment. The overall procedure is exemplified in Figure 1 for the MS/MS spectrum

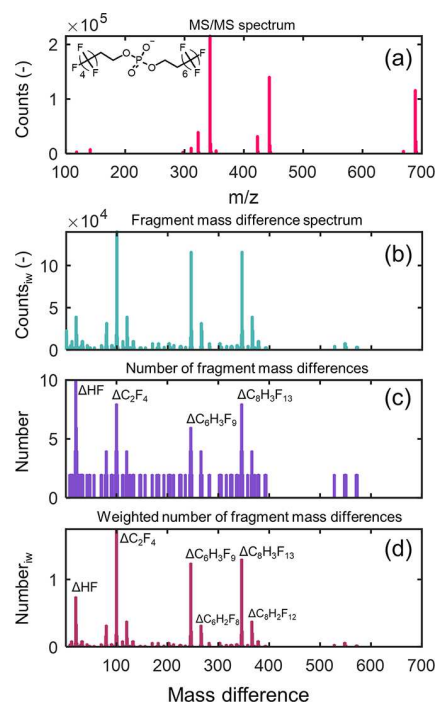


Figure 1. Example of the calculation of the number of mass differences in the spectrum of 4:2/6:2 diPAP ($m/z = 688.9825$) at 40 eV from paper extract P2. Note: MS/MS peaks below m/z 100 are not shown (H₂PO₄⁻ and PO₃⁻). (a) Spectrum of 4:2/6:2 diPAP (n peaks). (b) Calculated mass difference spectrum [$n(n-1)$ mass difference peaks]. Each mass difference gets the intensity value of the fragment with the lower intensity. (c) Number of each mass difference (tolerance ± 1 mDa). (d) Number of each mass difference weighted by the intensities (N_{iw}) of the respective fragments (see eq 1).

of 4:2/6:2 diPAP. The most important mass differences for 4:2/6:2 diPAP at 40 eV are ΔHF , ΔC_2F_4 , and larger differences with general formulae $\Delta C_nH_3F_{2n-3}$ and $\Delta C_nH_2F_{2n-4}$. While just by number, ΔHF is the most important difference, ΔC_2F_4 is both frequent and has a high relative intensity, as shown by the intensity weighted number (N_{iw} in Figure 1).

With this procedure, all 38 PFAS MS/MS spectra were investigated for their mass differences at different applied CEs. Furthermore, these calculations were also performed for substance classes such as PFCAs, PFSAs, diPAPs, fluorotelomer mercapto alkyl phosphates (FTMAPs), FTSA, and some important PFAS in-source fragments (all fragment mass difference plots for compound classes in Figure S4). The overall results are summarized in Table 1 and are discussed in the following.

ΔCF_2 . ΔCF_2 is the most general difference for PFAS because it occurs when the perfluoroalkyl chain is fragmented twice between two different CF₂ units (Table 1 row 1). Depending on the functional group, either the perfluoroalkyl chain itself (C_nF_{2n+1}) or the other rest R keeps the charge (examples in Table 1), meaning that besides typical $C_nF_{2n+1}^-$

Table 1. Summary of the Most Important Observed Fragment Mass Differences ($\Delta_{\text{fragments}}$), Their Proposed Underlying Fragmentation Reactions, Compound Classes They Occur in, and Examples of Compounds Where They Were Observed^a

Fragment difference	Exact mass	Fragmentation reactions	Compound classes	Compound examples
ΔCF_2 $\Delta(\text{CF}_2)_n$	49.99681		PFAS with perfluoroalkyl chains F-containing molecules	PFCAs (R = CO ₂), PFSAs (R = SO ₃), PASF-based [e.g. N-EtFOSAA (R = SO ₂ NC ₄ H ₉ O ₂)] diSAmPAP, FOSA], Capstone A & B, PFPiAs, PFECAs ^{21, 36}
$\Delta(\text{C}_2\text{F}_4)_n$ $\Delta(\text{C}_2\text{F}_4 - \text{H}_2\text{O})$ $\Delta(\text{C}_2\text{F}_4 + \text{H}_2\text{O})$	99.99361 81.98305 118.00418		n:2/(n+2):2 telomer-based PFAS	8:2/10:2 diPAP (R = PO ₄), 10:2/12:2 FTMAPs (R = C ₇ H ₁₂ S ₂ PO ₄), 10:2/12:2 FTMAP disulfoxide
ΔHF $\Delta(\text{H}_2\text{F}_2)$ $\Delta(\text{C}_2\text{F}_4 - \text{HF})$ $\Delta(\text{HF})_n(\text{CO}_2)_m$ ^{35, 36}	20.00623 40.01246 79.98738		telomer-based PFAS F-containing molecules H-substituted PFAS ³⁵⁻³⁷	diPAPs [R = PO ₄ C ₂ H ₄ (CF ₂) _n F], FTMAPs, FTMAP sulfoxides FTSs (R = SO ₃), FTCAs, FTUCAs H-PFCAs ³⁷
$\Delta\text{C}_n\text{H}_3\text{F}_{2n-3}$ $\Delta\text{C}_n\text{H}_2\text{F}_{2n-4}$ $\Delta\text{C}_n\text{HF}_{2n-5}$ $\Delta(\text{C}_n\text{H}_3\text{F}_{2n-3}\text{H}_2\text{O})$	for n = 8 346.00271 325.99648 305.99025 364.01327		telomer-based PFAS	diPAPs [R = PO ₄ C ₂ H ₄ (CF ₂) _n F], FTMAPs, FTMAP sulfoxides, FTSs (R = SO ₃).
$\Delta\text{C}_n\text{F}_{2n}\text{SO}_3$ $\Delta\text{C}_n\text{F}_2\text{SO}_3 + \text{HF}$ ³⁶ $\Delta\text{C}_n\text{F}_2\text{SO}_3 + \text{HF} + \text{CF}_2\text{O}$ ³⁶	for n = 3 229.94723		PFESAs, PFECAs, PFESAs H-substituted PFESAs ³⁶	PFOS [R = (CF ₂) _n F], 9Cl-PF3ONS (R = OC ₆ F ₁₂ Cl), 11Cl-PF3ONS
ΔCF_3	68.99521	different reactions	CF ₃ -containing molecules	e.g. pesticides, pharmaceuticals containing F ₂₃ , unsaturated ether PFAS ²⁷
$\Delta\text{CF}_2\text{O}$ ^{21, 35, 36}	65.99172		PFECAs, UPFAs, PFEAs Cl-substituted unsaturated alcohols ^{21, 35, 36}	4:4 PFESA ²¹ (R ₁ = C ₃ F ₇ , R ₂ = C ₄ F ₈ SO ₃)

^aR refers to any organic or inorganic rest and is exemplified for several compounds (see right column). Fragment mass differences highlighted in blue were not observed in this study but found in MS/MS spectra from literature. Note: besides the identified fragmentation reactions there might be more that generate these mass differences.

fragments, R-C_nF_{2n+1} fragments also occur. Furthermore, longer perfluoroalkyl chains also lead to multiples of ΔCF_2 [$\Delta(\text{CF}_2)_n$]. The occurrence of $\Delta(\text{CF}_2)_n$ can be used to get additional structural information regarding the chain length of the precursor. Because the extent of fragmentation strongly depends on CE for a given structure, functional group and molar mass, CEs of 20, 40 eV and higher according to a linear dependency on mass were used to achieve meaningful PFAS fragmentation (MS/MS spectra with ΔCF_2 in Figure S5). While for PFCAs and FTCAs, usually a CE of 20 eV was sufficient even for long-chain homologues (up to C₁₈), PFSAs, diSAmPAP, ADONA, and, for example, 6:6 PFPiA needed much higher CEs. The occurrence of ΔCF_2 in spectra of further compound classes such as pesticides or pharmaceuticals with only one CF₃-group will be discussed in the next section.

$\Delta\text{C}_2\text{F}_4$. $\Delta\text{C}_2\text{F}_4$ also appears in the context of the perfluoroalkyl chain cleavage [$\Delta(\text{CF}_2)_2$]; however, it can also occur from telomer-based PFAS such as diPAPs or FTMAPs which typically occur as mixtures of homologues with C₂F₄-repeating units (Table 1 row 2).⁴⁵ $\Delta\text{C}_2\text{F}_4$ is generated by fragmentation if one or the other telomer-chain breaks off, if they differ by C₂F₄ [formula: n:2/(n + 2):2 (e.g., 6:2/8:2 diPAP)] (Figure S6 for $\Delta\text{C}_2\text{F}_4$ examples). $\Delta\text{C}_2\text{F}_4$ was also often observed in combination with the loss or addition of H₂O [$\Delta(\text{C}_2\text{F}_4 \pm \text{H}_2\text{O})$]. To our best knowledge, the use of mass differences made up by a combination of two losses such as $\Delta(\text{C}_2\text{F}_4 - \text{H}_2\text{O})$ has not been reported in literature before. Generally, for diPAPs and FTMAPs, CEs of 20 and 40 eV were sufficient, while 60 eV led to decreased numbers of fragments (Figure S7). For these substance classes, a further fragmentation of the perfluoroalkyl chain was not observed

(independent of CE), meaning that n:2/n:2 diPAPs/FTMAPs neither form ΔCF_2 nor $\Delta\text{C}_2\text{F}_4$.

ΔHF . For telomer-based PFAS, ΔHF becomes the relevant difference (CH bound in vicinity to a CF₂-group), but also other PFAS (e.g., H-substituted PFCAs) typically have one or more neutral HF losses [$\Delta(\text{HF})_n$] during fragmentation when forming C=C and eventually C≡C bonds (Table 1 row 3).^{35-37,46} ΔHF was observed for FTSAs, FTCAs, FTUCAs, diPAPs, and FTMAPs and can also appear in combination with one or two CO₂ losses from carboxylic acids [$\Delta(\text{HF})_n(\text{CO}_2)_m$ with n, m = 1,2]³⁷ (examples in Figure S8).^{35-37,46} Furthermore, in combination with $\Delta\text{C}_2\text{F}_4$, the HF loss also combines to the difference $\Delta(\text{C}_2\text{F}_4 - \text{HF})$. ΔHF was also observed for more organofluorine compounds (next section).

$\Delta\text{C}_n\text{H}_3\text{F}_{2n-3}$. The R-CH₂-CH₂-C_{2n-2}F_{2n-3} moiety of telomer-based PFAS is a further unique structural feature that can be used for identification. When cleaved off in the collision cell while forming a C=C bond (Table 1, row 4), the differences $\Delta\text{C}_n\text{H}_3\text{F}_{2n-3}$ can form depending on the chain length (n = 6, 8, 10, etc.; note: perfluoroalkyl chain length = n-2). The fragment can even occur twice for PFAS with two telomer chains. These differences were further observed in combination with one or two HF losses or H₂O loss ($\Delta\text{C}_n\text{H}_2\text{F}_{2n-4}$; $\Delta\text{C}_n\text{HF}_{2n-5}$; $\Delta\text{C}_n\text{H}_3\text{F}_{2n-3}\text{H}_2\text{O}$). One major advantage of those differences is that they reveal the PFAS chain length (examples in Figure S9). To our best knowledge, the use of these mass differences was reported for the first time.

$\Delta\text{C}_n\text{F}_{2n}\text{SO}_3$. PFAS with sulfonate groups directly attached to a perfluoroalkyl chain generate the useful difference $\Delta\text{C}_n\text{F}_{2n}\text{SO}_3$. However, PFSAs, PFESAs, or Cl-PFESAs often barely form fragments and typically need higher CEs than other PFAS with similar masses³⁵ (Table 1 row 5, spectra in

Figure S10). $\Delta C_n F_{2n} SO_3$ was also observed elsewhere in combination with a HF loss and CF_2O for H-substituted Cl-PFESAs ($\Delta C_n F_{2n} SO_3 HF$ and $\Delta C_n F_{2n} SO_3 HF CF_2 O$).^{21,36}

ΔCF_3 . All compounds with at least one CF_3 -group are considered as PFAS. Mainly compounds with a CF_3 -group attached to an aromatic or heterocyclic ring and without any extended perfluoroalkyl chain form ΔCF_3 during fragmentation, especially observed for compounds with low F-content (next section).

ΔCF_2O . Not only for ether PFAS such as PFESAs, PFECAs, and perfluoroalkyl ether alcohols but also for unsaturated perfluoroalkyl alcohols (UPFAs) and Cl-substituted UPFAs, ΔCF_2O was observed in several MS/MS spectra by others, showing its importance for these substance classes.^{21,35,36} Besides ΔCF_2O , Wang et al. 2018 described further differences such as ΔOCF_2CO_2 , $\Delta C_2H_4F_2O_2$, $\Delta C_2H_4F_2O_3$, $\Delta HFCH_2CO_2$, and $\Delta HFOCH_2CO_2$ for several (unsaturated) polyfluorinated ether PFAS.³⁵

In general, the list of meaningful mass differences can be easily extended to detect further PFAS or other compounds (e.g., novel ether PFAS, aromatic PFAS, or chlorofluorocarbons, etc.) which have not yet been considered in our work.^{47,48}

Application to MassBank. To evaluate how mass tolerance and intensity threshold are affecting the identification efficiency and the rate of false positive detection, FindPFAS was applied to a subset of mass spectra in MassBank. It is important to note that MassBank comprises both PFAS with low F-content ($\approx 60\%$ with $F_{\leq 7}$) and PFAS with perfluoroalkyl chains ($\approx 40\%$; compound distribution in Figure S3). When using ΔCF_2 the number of detected compounds depended on the used mass tolerance and intensity threshold [see Figure 2; $F_{\geq 3}$ compounds detected in Table S4 (± 1 mDa and 1% base peak normalized intensity)]. It becomes obvious that by increasing the mass tolerance from ± 0.05 to ± 1 mDa, the identification rate increased on average between 20 and 25%,

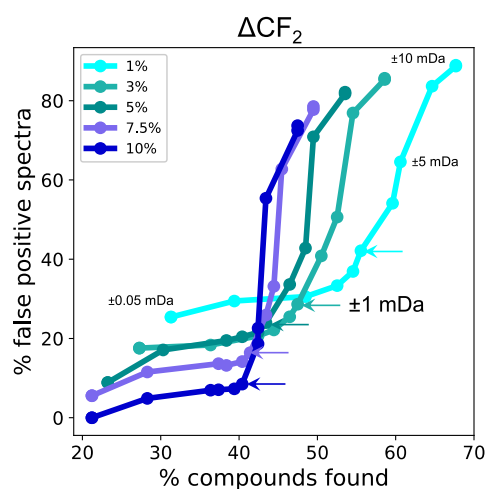


Figure 2. Percentage of false positive spectra findings vs correctly assigned unique compound spectra detected by FindPFAS in selected MassBank spectra for the difference ΔCF_2 (hit: compounds with at least three fluorine atoms). The mass tolerance was varied in the following order: $\pm(0.05, 0.075, 0.1, 0.25, 0.5, 0.75, 1, 2, 3, 5, 7.5, \text{ and } 10 \text{ mDa})$ for five intensity thresholds (1, 3, 5, 7.5, and 10%). Note: data points are partially labeled. For detailed calculations, see Supporting Information, Section S3.

while the fraction of false positives did not change much (lower end of S-shaped curve). Mass tolerances above ± 1 mDa, however, increased the false positives rapidly (examples in Table S5 and Figure S17), resulting in too many false positive assignments above ± 2 mDa (also dependent on intensity threshold). It is important to note that the applicable mass tolerance depends on the mass accuracy of the acquired data. It should therefore be adjusted for each instrument type and acquisition parameters (MassBank spectra are from different instruments and different vendors).

In contrast, the intensity threshold showed an opposite trend: the false positive rate increased if the relative intensity of fragments is decreased (the curve shifts upward). However, by also considering smaller peaks, more compounds are detected correctly by FindPFAS (curve shifts to the right). From 3 to 1%, there was a big difference, showing that false positives mainly arise from low intensity peaks, which is due to the strong increase of the number of peaks with the decrease in relative intensity (Figure S11). Observed trends for ΔCF_3 , ΔHF , and combination of all three differences are shown in Figures S12 and S13.

Nearly all PFAS with perfluoroalkyl chains (e.g., PFCAs, PFASs, N-Et- and N-MeFOSAA, FOSAA, and 6:2 FTUCA) present in MassBank were detected via FindPFAS (Table S4 and Figure S14). However, FindPFAS was also able to detect a much wider range of F-containing compounds such as pharmaceuticals and pesticides with CF_3 -groups (Table S4; note: in MassBank often several spectra with different CEs are available per compound). This shows the general broad application range of FindPFAS for non-target screening purposes. The detection of compounds is strongly dependent on the used differences: in case of ΔCF_2 , compounds from the whole F-containing range were detected (F_3 up to F_{27}) in MassBank (but nearly all high F-content compounds; Figure S14), while ΔCF_3 and ΔHF were much more selective for compounds of lower F-content (mainly $F_{\leq 6}$; Figure S15), which is very beneficial for preselection of specific compounds in HR-MS²-data.

MassBank fragment annotations of positively assigned fragments by FindPFAS were used to distinguish true from false positive differences and to identify the chemical formulae leading to false positive identifications. Also, compounds with only 3 F atoms showed ΔCF_2 , which was not further investigated in detail (spectra in Figure S16). False positive differences arose from combinations of fragments such as $(CH_4OS-N) = 49.9978 \text{ Da}$ mimicking $\Delta CF_2 (= 49.9968)$ or $(C_3-O) = 20.0051$ mimicking $\Delta HF (= 20.0062)$, all at a mass tolerance of 1 mDa (more false positive ΔCF_2 differences in Table S5 and Figure S17). It is important to note that besides the above discussed universal differences, other differences are much more selective. For instance, spectra of 8:2 monoPAP- and diPAP were easily detected in MassBank by FindPFAS when using $\Delta C_8H_3F_{13}$, which was highly selective resulting in not even one single false positive detection [2 out of 20,998 spectra detected, mass tolerance ± 1 mDa, intensity threshold = 3%]. For $\Delta C_{10}H_3F_{17}$ (10:2 monoPAP detected) and $\Delta C_2F_4SO_3$ [9Cl-PF3ONS (F-53B) detected], similar results were observed.

Finally, two general rules for the use of mass differences were deduced from the application to MassBank: (1) increasing mass differences can statistically be composed of more possible chemical formulae, but they are also exponentially less frequent (Figure S18). Furthermore,

precursor masses which are smaller than the mass difference do not give any false positives. (2) mass differences with negative mass defects lead to less false positives because their chemical formulae have higher specificities due to the involvement of elements with negative mass defects. For example, ΔHF led to much more false positives ($\text{MD} = +0.006$) than ΔCF_2 or ΔCF_3 ($\text{MD} = -0.003$ and -0.005), which is presumably due to the higher probability of the occurrence of the ($\text{C}_3\text{-O}$) difference in spectra of the huge number of CHO compounds (Figure S13).

Validation with PFAS Standards, Paper, and Soil Extracts. For systematic validation, FindPFAS was applied to the PFAS standard mix, two paper and two soil samples with known PFAS contamination at three CEs (20, 40 eV and a CE linearly dependent on mass; iterative ddMS², three injections per sample). All identified compounds in paper and soil samples discussed in this section have MS/MS information and one standard per homologous series and are therefore considered as level 2a for homologues and level 1 if a reference standard is available according to the identification levels by Schymanski et al. 2014 and to the new levels for PFAS.^{8,49,50}

PFAS Standards. When using ΔCF_2 , $\Delta\text{C}_2\text{F}_4$, ΔHF , and $\Delta\text{C}_2\text{F}_4\text{SO}_3$ together (tolerance ± 1 mDa, absolute intensity threshold = 1000 counts), 94% of all compounds were correctly assigned by FindPFAS. Only PFBA and PFPeA were not found due to missing fragment ions (for PFBA also at 5 and 10 eV no fragments were found except for the loss of CO_2). At 20 eV however, PFPeA was found resulting in 97% detection. Several PFCAs, FTCAs, and HFPO-DA (GenX) were identified as in-source fragments (e.g., $[\text{M}-\text{H}-\text{CO}_2]^-$, presumably due to fragmentation in ion- source and funnel). The results clearly show that the use of mass differences works efficiently for a variety of PFAS classes. $\Delta\text{CF}_2\text{O}$ was suspected for ether PFAS such as ADONA but was not observed in this work, however, in the literature (e.g., for 4:4 PFESA).²¹

Paper Extracts. Now we applied the algorithm to extracts of previously characterized paper samples⁴⁰ [differences: ΔCF_2 , $\Delta\text{C}_2\text{F}_4$, ΔHF , $\Delta\text{C}_n\text{H}_3\text{F}_{n-3}$ ($n = 8, 10, 12$), $\Delta\text{C}_n\text{F}_{2n}\text{SO}_3$ ($n = 2, 3$), $\Delta(\text{C}_2\text{F}_4-\text{H}_2\text{O})$, and $\Delta(\text{C}_2\text{F}_4-\text{HF})$; tolerance ± 1 mDa; absolute intensity threshold = 1000 counts]. In the paper extract P1 several homologues of FTSAAs (e.g., 6:2 up to 12:2), FTMAPs (e.g., 6:2/8:2 up to 8:2/12:2 and numerous isomers; Figure S6), and PFCAs were found by FindPFAS. P2 showed numerous diPAP homologues (4:2/6:2 up to 12:2/12:2 with several isomers) and PFCAs with similar chain lengths (C_7 to C_{13}). FTMAPs and diPAPs were assigned efficiently only at CE = 40 eV, while higher CEs led to insufficient fragments. The identification results in paper samples are similar as described by Bugsel et al. 2021.⁴⁰ In addition, further tentatively assigned PFAS have been detected with FindPFAS according to specific fragment differences (see the following section).

Soil Extracts. In the contaminated soil extract (identical search criteria as used for paper extracts) homologues of diPAPs, PFCAs, PFSAs, *N*-EtFOSAA, and diSAmPAP were found, while in the extract from the PFAS free soil sample only one precursor mass with three HF losses could be found but not further identified. The absence of mass difference matches in the non-contaminated soil sample clearly shows that almost no false positive detections were observed despite the complex composition of the soil matrix.

Generally, it is important to note that FindPFAS was always applied first to a MeOH blank injection. All precursor masses in the blank were manually discarded whenever they appeared

in a sample. Noisy spectra of bad quality were also manually excluded. Generally, the data reduction based on mass differences worked very efficiently for samples as shown in Figure 3 where the differences in all triggered MS/MS spectra

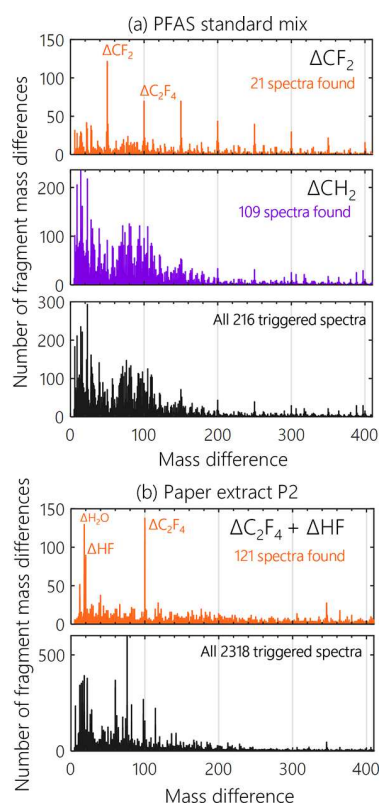


Figure 3. Efficient data reduction by selection of meaningful mass differences. (a) 216 triggered spectra in the PFAS standard (black) are reduced to 109 spectra by the more general mass difference ΔCH_2 for hydrocarbons (blue) and further to 21 spectra by the PFAS-specific mass difference ΔCF_2 (orange) (CE = 20 eV, mass tolerance = ± 2 mDa, second iterative injection). (b) 2318 triggered spectra in the paper extract P2 are reduced to 121 spectra considering the mass differences $\Delta\text{C}_2\text{F}_4$ and/or ΔHF (orange) typical for PFAS (CE = 40 eV, mass tolerance = ± 1 mDa). Note that in the paper extract P2, mainly telomer-based PFAS are present which do not generate ΔCF_2 because the perfluoroalkyl chain cannot be further fragmented; see the discussion of $\Delta\text{C}_2\text{F}_4$. These plots can further be used to get a first idea whether to expect PFAS in a sample.

are compared to the spectra selected by FindPFAS for ΔCH_2 (hydrocarbons) and ΔCF_2 (PFAS). These plots can also be used to get a first idea whether to expect PFAS in a sample.

Identification of Unknowns in Paper Extracts. Besides the discussed compounds, in both paper extracts, further compounds found by FindPFAS could be tentatively identified. For example, within the spectrum of m/z 1036.9709, the differences $\Delta\text{C}_2\text{F}_4$ and $\Delta\text{C}_n\text{H}_3\text{F}_{n-3}$ ($n = 8, 10$) were detected, indicating a telomer-based PFAS with both 6 and 8 perfluorinated carbon atoms (Figure 4). The mass spectrum shows a similar fragmentation pattern compared to 6:2/8:2 FTMAP (including H_2PO_4^- and PO_3^-) but two fragments and the molecular ion are shifted by 15.9931 Da which is reasonably oxygen (= 15.9949 Da). Further fragments of m/z 1036.9709 can be assigned to the loss of water (18.01 Da), leading to the assumption that one thioether group is oxidized to a sulfoxide (spectra and further information in

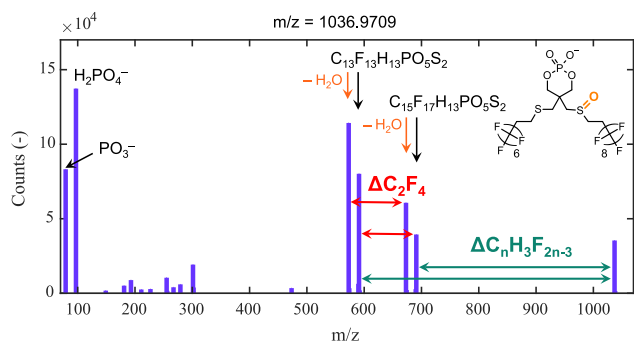


Figure 4. MS/MS spectrum of 6:2/8:2 FTMAP sulfoxide ($m/z = 1036.9709$) at a CE of 40 eV in the paper extract P1. Mass differences leading to its detection via FindPFAS are highlighted [further differences detected: for example, $\Delta(C_2F_4 \pm H_2O)$]. Note: the structure shown also includes two isomers depending on the position of the oxygen.

Figures S19–S21). A loss of OH was observed elsewhere for sulfoxides such as, for example, methiocarb sulfoxide supporting this observation. In total, 6 O homologues of FTMAP (C_2F_4 -repeating unit, with isomers evidenced by MS/MS) were detected via FindPFAS. The FTMAP sulfoxides are either oxidative TPs of FTMAP-treated papers or technical byproducts formed during FTMAP production.

FindPFAS found further 6 O_2 homologues of FTMAP (and isomers evidenced by MS/MS) with similar MS/MS patterns. Either both S atoms are oxidized (two sulfoxide groups) or one S is oxidized to a sulfone-group ($-SO_2-$). Partially resolved chromatographic double peaks support this observation (Figure S22). FTMAP sulfoxides with different chain lengths [for example $n:2/(n+2):2$] form isomers due to the position of O. Suspect screening for accurate masses of FTMAPs with three oxygen atoms also resulted in four peaks. Due to low abundances (Figure S22) only one MS/MS spectrum could be acquired, which is in good agreement with the other spectra (Figure S20). Further oxidation of the FTMAP sulfones consequently yields FTSA which were already described in literature and detected in the paper extract.^{40,51} Considering all pieces of information, the identification level is 2b.⁵⁰ Besides being present in the paper sample, some FTMAP sulfoxides/sulfones have been retrospectively found (by accurate mass, Figure S23) in a contaminated soil sample where FTMAPs and FTSA were previously identified,⁴⁰ indicating their presence also in environmental samples. Similar observations were made for diPAPs in paper extract P2. Here, in total five homologues of hydroxylated diPAPs were observed (based on ΔC_2F_4 and $\Delta C_nH_3F_{2n-3}$ from FindPFAS) which are likely TPs of diPAPs (details in Figures S24 and S25). Hydroxylation of the C_2H_4 -groups can also potentially occur for other telomer-based PFAS.

CONCLUSIONS

The overall results demonstrate well that specific fragment mass differences considerably improve the discovery and the classification of untargeted PFAS in HR-MS²-data. The algorithm FindPFAS also detects single PFAS which are not members of homologues series but requires MS²-data of sufficient quality. Therefore, MS²-spectra have to be inspected manually to reduce false positives. In general, we recommend a stepwise NTS workflow which starts with the use of suitable, single fragment differences at low mass tolerances and rather

high intensity thresholds. In the next steps, multiple differences with less strict parameters may be used to increase the number of detected PFAS but also the risk to detect false positives. We recommend using a linear mass-dependent CE if there is no information available on the structure of the PFAS of interest. The output of FindPFAS can be easily enhanced by further specific mass differences of PFAS which were not yet in focus. FindPFAS could be also applied to MS²-data from data-independent acquisition (e.g., all ion fragmentation, SWATH, etc.) which appears still to be challenging due to the high number of mass fragments and the superimposed spectra of coeluting compounds. The general approach of using mass differences can also be transferred to other compound classes which are characterized by specific mass fragmentation patterns.

ASSOCIATED CONTENT

Supporting Information

The Supporting Information is available free of charge at <https://pubs.acs.org/doi/10.1021/acs.analchem.2c01521>.

FindPFAS algorithm, graphical user interface, and output; chemicals, sample preparation, and data acquisition; MassBank calculations; fragment differences and MS² spectra; application of FindPFAS to MassBank; and identification of unknowns (PDF)

AUTHOR INFORMATION

Corresponding Author

Christian Zwiener – Environmental Analytical Chemistry, Center for Applied Geoscience, University of Tübingen, Tübingen 72076, Germany; orcid.org/0000-0002-6682-5828; Email: christian.zwiener@uni-tuebingen.de

Authors

Jonathan Zweigle – Environmental Analytical Chemistry, Center for Applied Geoscience, University of Tübingen, Tübingen 72076, Germany; orcid.org/0000-0002-7194-1567

Boris Bugsel – Environmental Analytical Chemistry, Center for Applied Geoscience, University of Tübingen, Tübingen 72076, Germany

Complete contact information is available at: <https://pubs.acs.org/doi/10.1021/acs.analchem.2c01521>

Notes

The authors declare no competing financial interest.

ACKNOWLEDGMENTS

The authors acknowledge the DBU (Deutsche Bundesstiftung Umwelt) for the scholarship of J.Z., funding of the project FluorTECH by the state of Baden-Württemberg (BWPFC19010), Katja Wack for support during sample extraction, and several members of the expert committee Non-target Screening (Water Chemical Society, GDCh) who provided MS²-files from different MS instruments for functionality testing.

REFERENCES

- (1) Kissa, E. *Fluorinated Surfactants and Repellents*; CRC Press, 2001; Vol. 97.

- (2) Buck, R. C.; Franklin, J.; Berger, U.; Conder, J. M.; Cousins, I. T.; de Voogt, P.; Jensen, A. A.; Kannan, K.; Mabury, S. A.; van Leeuwen, S. P. *Integr. Environ. Assess. Manage.* **2011**, *7*, 513–541.
- (3) Glüge, J.; Scheringer, M.; Cousins, I. T.; DeWitt, J. C.; Goldenman, G.; Herzke, D.; Lohmann, R.; Ng, C. A.; Trier, X.; Wang, Z. *Environ. Sci.: Processes Impacts* **2020**, *22*, 2345–2373.
- (4) Evich, M. G.; Davis, M. J. B.; McCord, J. P.; Acrey, B.; Awkerman, J. A.; Knappe, D. R. U.; Lindstrom, A. B.; Speth, T. F.; Tebes-Stevens, C.; Strynar, M. J.; Wang, Z.; Weber, E. J.; Henderson, W. M.; Washington, J. W. *Science* **2022**, *375*, No. eabg9065.
- (5) Morales-McDevitt, M. E.; Becanova, J.; Blum, A.; Bruton, T. A.; Vojta, S.; Woodward, M.; Lohmann, R. *Environ. Sci. Technol. Lett.* **2021**, *8*, 897–902.
- (6) D'Agostino, L. A.; Mabury, S. A. *Environ. Sci. Technol.* **2017**, *51*, 13603–13613.
- (7) Kaboré, H. A.; Vo Duy, S.; Munoz, G.; Méité, L.; Desrosiers, M.; Liu, J.; Sory, T. K.; Sauvé, S. *Sci. Total Environ.* **2018**, *616*–617, 1089–1100.
- (8) Bugsel, B.; Zwiener, C. *Anal. Bioanal. Chem.* **2020**, *412*, 4797–4805.
- (9) Sun, J.; Bossi, R.; Bustnes, J. O.; Helander, B.; Boertmann, D.; Dietz, R.; Herzke, D.; Jaspers, V. L. B.; Labansen, A. L.; Lepoint, G.; Schulz, R.; Sonne, C.; Thorup, K.; Tøttrup, A. P.; Zubrod, J. P.; Eens, M.; Eulaers, I. *Environ. Sci. Technol.* **2019**, *53*, 12744–12753.
- (10) Kaiser, A. M.; Forsthuber, M.; Aro, R.; Kärrman, A.; Gundacker, C.; Zeisler, H.; Foessler, P.; Salzer, H.; Hartmann, C.; Uhl, M.; Yeung, L. W. Y. *Environ. Sci. Technol.* **2021**, *55*, 9033–9042.
- (11) Stockholm Convention The new POPs under the Stockholm Convention. <http://www.pops.int/TheConvention/ThePOPs/TheNewPOPs/tabid/2511/Default.aspx> (accessed on 23 03, 2022).
- (12) US Environmental Protection Agency. *PFAS Strategic Roadmap: EPA's Commitments to Action 2021-2024*; US Environmental Protection Agency, 2021.
- (13) Barnabas, S. J.; Böhme, T.; Boyer, S. K.; Irmer, M.; Ruttkies, C.; Wetherbee, I.; Kondić, T.; Schymanski, E. L.; Weber, L. *Digit. Discov.* **2022**, DOI: 10.1039/d2dd00019a.
- (14) Chen, M.; Wang, Q.; Shan, G.; Zhu, L.; Yang, L.; Liu, M. *Sci. Total Environ.* **2018**, *634*, 251–259.
- (15) Cousins, I. T.; DeWitt, J. C.; Glüge, J.; Goldenman, G.; Herzke, D.; Lohmann, R.; Ng, C. A.; Scheringer, M.; Wang, Z. *Environ. Sci.: Processes Impacts* **2020**, *22*, 2307–2312.
- (16) Li, F.; Duan, J.; Tian, S. T.; Ji, H. D.; Zhu, Y. M.; Wei, Z. S.; Zhao, D. Y. *Chem. Eng. J.* **2020**, *380*, 122506.
- (17) Yeung, L. W. Y.; Mabury, S. A. *Environ. Chem.* **2016**, *13*, 102–110.
- (18) Aro, R.; Carlsson, P.; Vogelsang, C.; Kärrman, A.; Yeung, L. W. *Chemosphere* **2021**, *283*, 131200.
- (19) Aro, R.; Eriksson, U.; Kärrman, A.; Chen, F.; Wang, T.; Yeung, L. W. Y. *ACS ES&T Water* **2021**, *1*, 2087–2096.
- (20) McCord, J.; Strynar, M. J. *Environ. Sci. Technol.* **2019**, *53*, 4717–4727.
- (21) Kang, Q.; Gao, F.; Zhang, X.; Wang, L.; Liu, J.; Fu, M.; Zhang, S.; Wan, Y.; Shen, H.; Hu, J. *Environ. Int.* **2020**, *139*, 105686.
- (22) Ruan, T.; Jiang, G. *Trac. Trends Anal. Chem.* **2017**, *95*, 122–131.
- (23) Yukioka, S.; Tanaka, S.; Suzuki, Y.; Echigo, S.; Kärrman, A.; Fujii, S. *Water Res.* **2020**, *184*, 116207.
- (24) Wang, R.; Ching, C.; Dichtel, W. R.; Helbling, D. E. *Environ. Sci. Technol. Lett.* **2020**, *7*, 954–960.
- (25) Strynar, M. J.; Dagnino, S.; McMahan, R.; Liang, S.; Lindstrom, A. B.; Andersen, E.; McMillan, L.; Thurman, M.; Ferrer, I.; Ball, C. *Environ. Sci. Technol.* **2015**, *49*, 11622–11630.
- (26) Barzen-Hanson, K. A.; Roberts, S. C.; Choyke, S.; Oetjen, K.; McAlees, A.; Riddell, N.; McCrindle, R.; Ferguson, P. L.; Higgins, C. P.; Field, J. A. *Environ. Sci. Technol.* **2017**, *51*, 2047–2057.
- (27) Jacob, P.; Barzen-Hanson, K. A.; Helbling, D. E. *Environ. Sci. Technol.* **2021**, *55*, 2346–2356.
- (28) Liu, Y.; Pereira, S.; Martin, J. W. *Anal. Chem.* **2015**, *87*, 4260–4268.
- (29) Hensema, T. J.; Berendsen, B. J. A.; van Leeuwen, S. P. J. *Chemosphere* **2021**, *265*, 128599.
- (30) Gonzalez de Vega, R.; Cameron, A.; Clases, D.; Dodgen, T. M.; Doble, P. A.; Bishop, D. P. *J. Chromatogr., A* **2021**, *1653*, 462423.
- (31) Koelmel, J. P.; Stelben, P.; McDonough, C. A.; Dukes, D. A.; Aristizabal-Henao, J. J.; Nason, S. L.; Li, Y.; Sternberg, S.; Lin, E.; Beckmann, M.; Williams, A. J.; Draper, J.; Finch, J. P.; Munk, J. K.; Deigl, C.; Rennie, E. E.; Bowden, J. A.; Godri Pollitt, K. J. *Anal. Bioanal. Chem.* **2022**, *414*, 1201–1215.
- (32) Getzinger, G. J.; Higgins, C. P.; Ferguson, P. L. *Anal. Chem.* **2021**, *93*, 2820–2827.
- (33) Getzinger, G. J.; Ferguson, P. L. *ACS ES&T Water* **2021**, *1*, 1240–1251.
- (34) Chao, A.; Al-Ghoul, H.; McEachran, A. D.; Balabin, I.; Transue, T.; Cathey, T.; Grossman, J. N.; Singh, R. R.; Ulrich, E. M.; Williams, A. J.; Sobus, J. R. *Anal. Bioanal. Chem.* **2020**, *412*, 1303–1315.
- (35) Wang, Y.; Yu, N.; Zhu, X.; Guo, H.; Jiang, J.; Wang, X.; Shi, W.; Wu, J.; Yu, H.; Wei, S. *Environ. Sci. Technol.* **2018**, *52*, 11007–11016.
- (36) Wang, X.; Yu, N.; Qian, Y.; Shi, W.; Zhang, X.; Geng, J.; Yu, H.; Wei, S. *Water Res.* **2020**, *183*, 115989.
- (37) Li, Y.; Yu, N.; Du, L.; Shi, W.; Yu, H.; Song, M.; Wei, S. *Environ. Sci. Technol.* **2020**, *54*, 3407–3416.
- (38) Wang, Z.; Buser, A. M.; Cousins, I. T.; Demattio, S.; Drost, W.; Johansson, O.; Ohno, K.; Patlewicz, G.; Richard, A. M.; Walker, G. W.; White, G. S.; Leinala, E. *Environ. Sci. Technol.* **2021**, *55*, 15575–15578.
- (39) Horai, H.; Arita, M.; Kanaya, S.; Nihei, Y.; Ikeda, T.; Suwa, K.; Ojima, Y.; Tanaka, K.; Tanaka, S.; Aoshima, K.; Oda, Y.; Kakazu, Y.; Kusano, M.; Tohge, T.; Matsuda, F.; Sawada, Y.; Hirai, M. Y.; Nakanishi, H.; Ikeda, K.; Akimoto, N.; Maoka, T.; Takahashi, H.; Ara, T.; Sakurai, N.; Suzuki, H.; Shibata, D.; Neumann, S.; Iida, T.; Tanaka, K.; Funatsu, K.; Matsuura, F.; Soga, T.; Taguchi, R.; Saito, K.; Nishioka, T. *J. Mass Spectrom.* **2010**, *45*, 703–714.
- (40) Bugsel, B.; Bauer, R.; Herrmann, F.; Maier, M. E.; Zwiener, C. *Anal. Bioanal. Chem.* **2022**, *414*, 1217–1225.
- (41) McDonald, W. H.; Tabb, D. L.; Sadygov, R. G.; MacCoss, M. J.; Venable, J.; Graumann, J.; Johnson, J. R.; Cociorva, D.; Yates, J. R., 3rd *Rapid Commun. Mass Spectrom.* **2004**, *18*, 2162–2168.
- (42) Deutsch, E. W. *Mol. Cell. Proteomics* **2012**, *11*, 1612–1621.
- (43) Chambers, M. C.; Maclean, B.; Burke, R.; Amodei, D.; Ruderman, D. L.; Neumann, S.; Gatto, L.; Fischer, B.; Pratt, B.; Egertson, J.; Hoff, K.; Kessner, D.; Tasman, N.; Shulman, N.; Frewen, B.; Baker, T. A.; Brusniak, M. Y.; Paulse, C.; Creasy, D.; Flashner, L.; Kani, K.; Moulding, C.; Seymour, S. L.; Nuwaysir, L. M.; Lefebvre, B.; Kuhlmann, F.; Roark, J.; Rainer, P.; Detlev, S.; Hemenway, T.; Huhmer, A.; Langridge, J.; Connolly, B.; Chadick, T.; Holly, K.; Eckels, J.; Deutsch, E. W.; Moritz, R. L.; Katz, J. E.; Agus, D. B.; MacCoss, M.; Tabb, D. L.; Mallick, P. *Nat. Biotechnol.* **2012**, *30*, 918–920.
- (44) Levitsky, L. I.; Klein, J. A.; Ivanov, M. V.; Gorshkov, M. V. *J. Proteome Res.* **2019**, *18*, 709–714.
- (45) Gebbink, W. A.; Ullah, S.; Sandblom, O.; Berger, U. *Environ. Sci. Pollut. Res.* **2013**, *20*, 7949–7958.
- (46) Trier, X.; Granby, K.; Christensen, J. H. *Environ. Sci. Pollut. Res. Int.* **2011**, *18*, 1108–1120.
- (47) Myers, A. L.; Jobst, K. J.; Mabury, S. A.; Reiner, E. J. *J. Mass Spectrom.* **2014**, *49*, 291–296.
- (48) Li, X.; Chevez, T.; De Silva, A. O.; Muir, D. C. G.; Kleywegt, S.; Simpson, A.; Simpson, M. J.; Jobst, K. J. *Environ. Sci. Technol.* **2021**, *55*, 15912–15920.
- (49) Schymanski, E. L.; Jeon, J.; Gulde, R.; Fenner, K.; Ruff, M.; Singer, H. P.; Hollender, J. *Environ. Sci. Technol.* **2014**, *48*, 2097–2098.
- (50) Charbonnet, J. A.; McDonough, C. A.; Xiao, F.; Schwichtenberg, T.; Cao, D.; Kaserzon, S.; Thomas, K. V.; Dewapriya, P.; Place, B. J.; Schymanski, E. L.; Field, J. A.; Helbling, D. E.; Higgins, C. P. *Environ. Sci. Technol. Lett.* **2022**, *9*, 473–481.

(51) Lee, H.; Mabury, S. A. *Environ. Sci. Technol.* **2011**, *45*, 8067–8074.

Recommended by ACS

Optimization of Parameters for ROI Data Compression for Nontargeted Analyses Using LC–HRMS

Sonia Schöneich, Robert E. Synovec, *et al.*

DECEMBER 23, 2022

ANALYTICAL CHEMISTRY

READ 

MS2Tox Machine Learning Tool for Predicting the Ecotoxicity of Unidentified Chemicals in Water by Nontarget LC-HRMS

Pilleriin Peets, Anneli Kruve, *et al.*

OCTOBER 21, 2022

ENVIRONMENTAL SCIENCE & TECHNOLOGY

READ 

PICA: Pixel Intensity Correlation Analysis for Deconvolution and Metabolite Identification in Mass Spectrometry Imaging

Yonghui Dong, Asaph Aharoni, *et al.*

JANUARY 03, 2023

ANALYTICAL CHEMISTRY

READ 

AntDAS-DDA: A New Platform for Data-Dependent Acquisition Mode-Based Untargeted Metabolomic Profiling Analysis with Advantage of Recognizing Insource Fragme...

Xing-Cai Wang, Yuanbin She, *et al.*

JANUARY 04, 2023

ANALYTICAL CHEMISTRY

READ 

[Get More Suggestions >](#)

Supporting Information

FindPFAS: Non-target screening for PFAS – Comprehensive data mining for MS² fragment mass differences

Jonathan Zweigle,⁺ Boris Bugsel,⁺ Christian Zwiener^{+,*}

⁺Environmental Analytical Chemistry, Center for Applied Geoscience, University of Tübingen,
Schnarrenbergstraße 94-96, 72076 Tübingen, Germany

^{*}Corresponding author

Contents

S1 FINDPFAS ALGORITHM, GRAPHICAL USER INTERFACE AND OUTPUT	2
FindPFAS algorithm	2
Figure S 1: Graphical user interface of FindPFAS	3
S2 CHEMICALS, SAMPLE PREPARATION AND DATA ACQUISITION	4
Chemicals	4
Table S 1: Summary of the 38 PFAS	4
Sample preparation	4
Table S 2: Summary of instrument and ESI source parameters	5
Table S 3: Gradient program	5
Data acquisition	5
Figure S 2: Iterative ddMS ²	6
S3 MASSBANK CALCULATIONS	6
Figure S 3: Distribution of F-containing compounds in MassBank	7
S4 FRAGMENT DIFFERENCES AND MS ² SPECTRA	8
Figure S 4: Mass	8
Figure S 5: ΔCF ₂ spectra	9
Figure S 6: ΔC ₂ F ₄ spectra	10
Figure S 7: diPAP fragments dependent on applied CE	10
Figure S 8: ΔHF spectra	11
Figure S 9: ΔC _n H ₃ F _{2n-3} and ΔC _n H ₂ F _{2n-4} spectra	11
Figure S 10: ΔC _n F _{2n} SO ₃ spectra	12
S5 APPLICATION OF FINDPFAS TO MASSBANK	12
Figure S 11: Histogram of the number of intensities within the MassBank dataset	12
Table S 4: Examples of unique correctly detected compounds by FindPFAS in MassBank	12
Figure S 12: False positive vs. correct detections for ΔCF ₃ and ΔHF	13
Figure S 13: False positive vs. correct detection for combinations of mass	13
Figure S 14: Distribution of found compounds with ΔCF ₂	14
Figure S 15: Distribution of found compounds with ΔCF ₃ and ΔHF	14
Figure S 16: Arbitrary examples of correctly detected spectra by FindPFAS within the MassBank	15
Figure S 17: Arbitrary examples of false positive detected spectra by FindPFAS within the MassBank	16
Table S 5: False positive	17
Figure S 18: Exponential decrease of the frequency of integer mass	17
S6 IDENTIFICATION OF UNKNOWNNS	18
Figure S 19: MS/MS spectra of FTMAP, FTMAP sulfoxide and FTMAP disulfoxide/sulfone	18
Figure S 20: MS/MS spectrum of 6:2/8:2 FTMAP sulfoxide-sulfone	19
Figure S 21: Proposed fragmentation reactions	19
Figure S 22: EICs (scan) of 6 homologous of FTMAP sulfoxides and FTMAP disulfoxides/FTMAP sulfones	20
Figure S 23: EICs of FTMAPs, FTMAP sulfoxide and one FTMAP disulfoxide/sulfone in the soil extract	20
Figure S 24: MS/MS spectra of the tentatively identified Hydroxy-diPAPs	21
Figure S 25: EICs (scan) of 5 Hydroxy-diPAP homologous	21
REFERENCES	22

S1 FindPFAS algorithm, graphical user interface and output

FindPFAS algorithm: Explanation of each step performed by the FindPFAS algorithm is given in the following:

- All identical precursor masses (m/z) that appear n -times with MS^2 -spectra can be removed (user specific input, e.g. 20 times), because these are typically persistent background signals originating from the analytical system with no peak shape.
- Cleanup of each MS^2 -spectrum with a certain intensity threshold (e.g. 1000 counts or 5%) to remove noise and background peaks.
- Find all associated MS^2 -spectra (identical precursor m/z but more than one MS^2 -spectrum over the chromatographic peak) and store only the spectrum with the highest TIC precursor intensity (peak maximum or highest TIC selected for MS/MS).
- Calculate the differences between each peak in all MS^2 -spectra [n MS^2 peaks result in $n(n-1)/2$ mass differences].
- Search within fragment mass differences for defined mass differences ($\Delta_{\text{Fragments}}$) of interest at a defined mass tolerance in mDa. (user input, e.g. 1 mDa and $\Delta_{\text{Fragments}}$ e.g. ΔCF_2 and ΔC_2F_4).
- Save data of all precursor masses with n positively matched $\Delta_{\text{Fragments}}$ (user specific input, e.g. $n = 3$ means that at least 3 differences are required for a positive match) in their MS^2 spectra.
- Rank the positively assigned spectra according to their precursor TIC intensity or their number of detected mass differences $\Delta_{\text{Fragments}}$ (n).
- *Optional:* Compare positively assigned precursor masses with a suspect list at a defined mass tolerance (user specific input, e.g. 1 mDa).
- *Optional:* Search for diagnostic fragments within MS^2 -spectra of positively assigned masses. (e.g. $C_3F_7^-$, $C_4F_9^-$, SO_3F^- etc.).
- *Optional:* Screen both precursor- and fragment masses for abundant mass differences. The repeated occurrence of identical mass differences indicates abundant repeating units.
- Generate KMD plots for precursor masses.

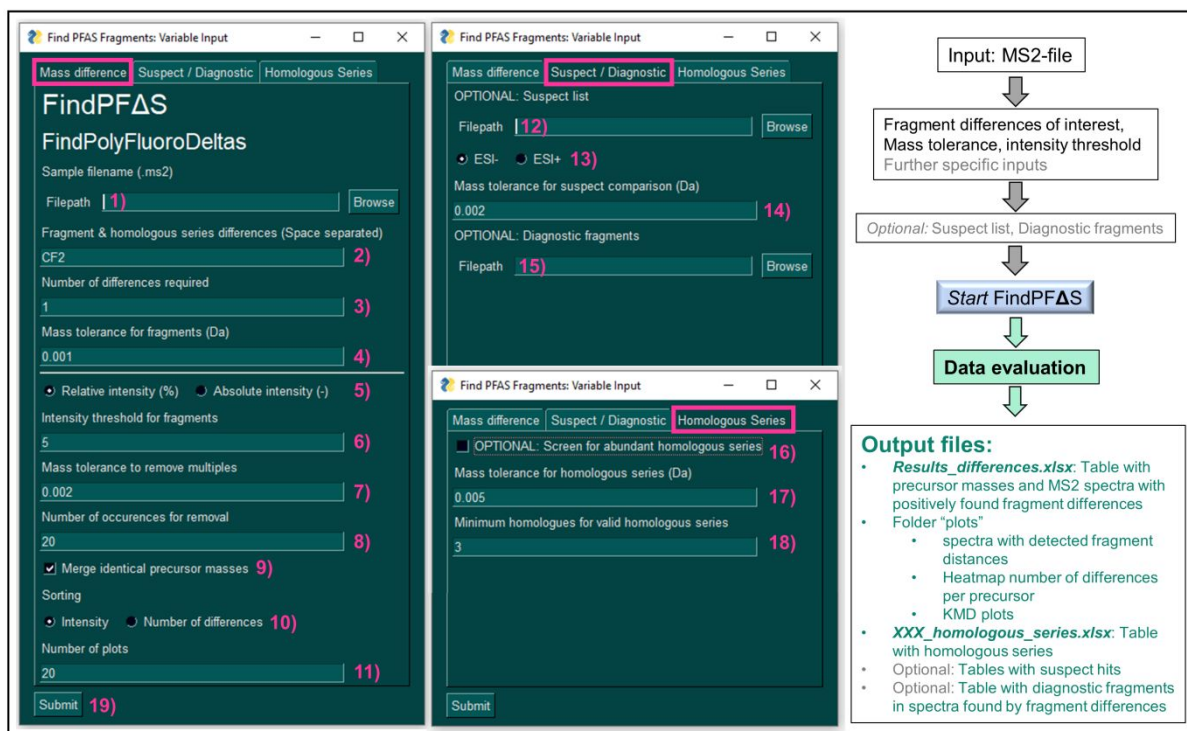


Figure S 1: Graphical user interface of FindPFAS (programmed with PySimpleGUI), a schematic workflow, and the generated output files. (1) Specification of file path to the .ms2-file (MS² files can be generated vendor independently from raw data by using the MSConvert software from the ProteoWizard tools; prerequisite on raw data: FindPFAS only works for centroid data. If data was acquired in the profile mode, centroid data can be generated with the “peak picking” function of MSConvert when converting raw data to MS²-files. It is further recommended to use FindPFAS with only one collision energy at a time (or e.g. one linear formula). If multiple collision energies were acquired, each collision energy can be separately converted to one MS²-file by using the “subset” function of MSConvert). (2) Input of desired fragment mass differences (separated by space) either as chemical formula or exact mass. It is recommended to start by using only one difference per run to keep the results simple in the beginning and to later use multiple differences. (3) Number of differences desired for positive assignment: e.g. a difference has to be present at least 3 times per spectra (1 by default). (4) Absolute mass tolerance (Da). It is recommended to start with a small tolerance (≤ 0.001 Da, depending on mass accuracy of the instrument) to keep the high false positive rates low in the beginning. (5) Radio button to specify whether relative of absolute intensities should be used. (6) Absolute or relative intensity threshold for fragments that should be considered. (7) Mass tolerance (Da) to remove persistent background precursor masses that are triggered n-times for MS². (8) Number n above which precursor masses should be excluded from data evaluation (e.g. if a compound is triggered 20 times for MS² it is likely a background signal without a peak shape. Important note: If the instrument algorithm stays on one precursor to collect several spectra, this number has to be chosen larger, otherwise FindPFAS will potentially exclude compounds of interest). (9) Checkbox to decide whether multiple spectra from identical precursors should be merged together (e.g. if a chromatographic peak has 5 MS² scans only the spectrum with the highest precursor intensity will be considered for data evaluation). Note: If unchecked, the data evaluation will take much more time because every single MS²-spectrum in the dataset will be searched for fragment differences. (10) Radio button to decide how the data should be sorted. (11) Specifies how many spectra of positive precursors should be plotted. (12) Optional file path for a suspect list to compare hits found by FindPFAS. (13) Radio button to specify whether the data was acquired in positive or negative ionization, which is necessary to specify for suspect screening. Note that either only [M-H]⁻ or [M+H]⁺ adducts can be considered for suspect comparison. (14) Desired mass tolerance (Da) for suspect comparison. (15) Optional input for a list with diagnostic fragment. All spectra detected by FindPFAS will additionally be searched for the given diagnostic fragments. (16) Checkbox whether the MS¹ masses should be screened for abundant repeating units (unchecked by default; Note: If checked, the runtime can increase drastically). (17) Mass tolerance to screen for homologous series within the MS¹ masses. (18) Minimum number of homologues to be assigned as a series. (19) Button to run FindPFAS.

S2 Chemicals, sample preparation and data acquisition

Chemicals. Water, methanol (MeOH) and ammonium acetate (NH₄Ac) for analysis and extraction were LC-MS grade and purchased from Fisher scientific. PFAS standards (with acronyms) are given in Table S1.

Table S 1: Summary of the 38 PFAS used in the standard mixture and their origin. [PFCAs = Perfluoroalkyl carboxylic acids, PFSAs = Perfluoroalkyl sulfonic acids, PASF = Perfluoroalkane sulfonyl fluoride (PFOSA = Perfluorooctanesulfonamide, *N*-EtFOSAA = *N*-Ethylperfluoro-1-octanesulfonamidoacetic acid, diSAmPAP = *N*-Ethyl perfluorooctane sulfonamide ethanol-based phosphate diester acid), FTCAs = Fluorotelomer carboxylic acids, FTUCAs = Fluorotelomer unsaturated carboxylic acids, diPAPs = Polyfluorinated dialkylated phosphate esters, PFECAs = Perfluoroalkyl ether carboxylic acids (HFPO-DA = Hexafluoropropylene oxide-dimer acid, ADONA = Dodecafluoro-3H-4,8-dioxanonoate), PFESAs = Perfluoroalkyl ether sulfonic acids (9Cl-PF3ONS = 9-Chlorohexadecafluoro-3-Oxanone-1-Sulfonic Acid, 9Cl-PF3OUdS = 11-Chloroeicosafluoro-3-oxaundecane-1-sulfonic acid), 6:2 FTSA = 6:2 Fluorotelomer sulfonic acid, 6:6 PFPiA = 6:6 Perfluoroalkyl phosphinic acid]

Substance	Origin	Substance	Origin
PFCAs		PASF-based PFAS	
PFBA	Wellington Laboratories	PFOSA	Wellington Laboratories
PFPeA	Wellington Laboratories	<i>N</i> -EtFOSAA	Wellington Laboratories
PFHxA	Wellington Laboratories	diSAmPAP	Wellington Laboratories
PFHpA	Wellington Laboratories	FTCAs	
PFOA	Wellington Laboratories	6:2 FTCA	Wellington Laboratories
PFNA	Wellington Laboratories	8:2 FTCA	Wellington Laboratories
PFDA	Wellington Laboratories	5:3 FTCA	Wellington Laboratories
PFUdA	Wellington Laboratories	7:3 FTCA	Wellington Laboratories
PFDoA	Wellington Laboratories	FTUCAs	
PFTTrDA	Wellington Laboratories	6:2 FTUCA	Wellington Laboratories
PFTeDA	Wellington Laboratories	8:2 FTUCA	Wellington Laboratories
PFHxDA	Wellington Laboratories	diPAPs	
PFODA	Wellington Laboratories	6:2 diPAP	Toronto Research Chemicals
PFSAs		8:2 diPAP	Wellington Laboratories
PFBS	Wellington Laboratories	PFECAs	
PFPeS	Wellington Laboratories	HFPO-DA (GenX)	Wellington Laboratories
PFHxS	Wellington Laboratories	ADONA	Wellington Laboratories
PFHpS	Wellington Laboratories	PFESAs	
PFOS	Wellington Laboratories	9Cl-PF3ONS (F-53B)	Wellington Laboratories
PFNS	Wellington Laboratories	11Cl-PF3OUdS (F-53B)	Wellington Laboratories
PFDS	Wellington Laboratories	Others	
PFDoS	Wellington Laboratories	6:2 FTSA	Wellington Laboratories
		6:6 PFPiA	Toronto Research Chemicals

Sample preparation. The two paper samples were cut into squares (10 × 10 cm, ≈ 0.4 g) with MeOH rinsed scissors and 5 g portions of soil were weighted in PP tubes and samples were covered with 20 mL MeOH. The tubes were placed in the overhead-shaker overnight and eventually sonicated for 1 h. 7 mL of supernatant was removed (soil samples were centrifuged beforehand, 15 min @ 4000 rcf) and split in two 3.5 mL fractions which were evaporated until

dryness under a gentle N₂-stream (40 °C) and redissolved in 0.35 mL MeOH leading to a 10-fold enrichment. Afterwards, all extracts were centrifuged for 10 min @ 8900 rcf and the supernatant was taken for analysis. Additionally, always extraction blanks were prepared for consideration of background contamination.

Table S 2: Summary of instrument and ESI source parameters of the 6550 QTOF-MS.

Instrument Parameters	
Gas Temp (°C)	150
Gas Flow (L/min)	16
Nebulizer pressure (psig)	35
Sheath gas temperature (°C)	380
Sheath gas flow (L/min)	12
Fragmentor voltage (V)	360
Scan Source Parameter	
Capillary voltage (V)	3000
Nozzle voltage (V)	300

Table S 3: Gradient program used for HPLC separation. A = 95/5 H₂O/MeOH + 2 mM NH₄Ac and B = 95/5 MeOH/H₂O + 2 mM NH₄Ac. Flow = 0.3 mL/min.

Time (min)	A (%)	B (%)
0	85	15
2.0	30	70
5.0	10	90
10.0	0	100
15.0	0	100
15.1	85	15
22.0	85	15

Data acquisition. During iterative ddMS² a rolling exclusion list was automatically generated during multiple sample injections to subsequently exclude peaks at a certain RT window which were already selected for MS/MS experiments in prior injections. This greatly enhances the MS/MS coverage (see Figure S2).¹ An additional static exclusion list (generated from MeOH blank injections) was used to exclude persistent background signals originating from the analytical system over the complete RT-range. During selected injections active exclusion was enabled allowing the QTOF to exclude each triggered m/z for a certain RT after acquiring a certain number of MS/MS scans, which further increased the number of precursors selected

for MS/MS. For each measurement 2 to 5 μL of sample was injected followed by a threefold needle wash with isopropanol.

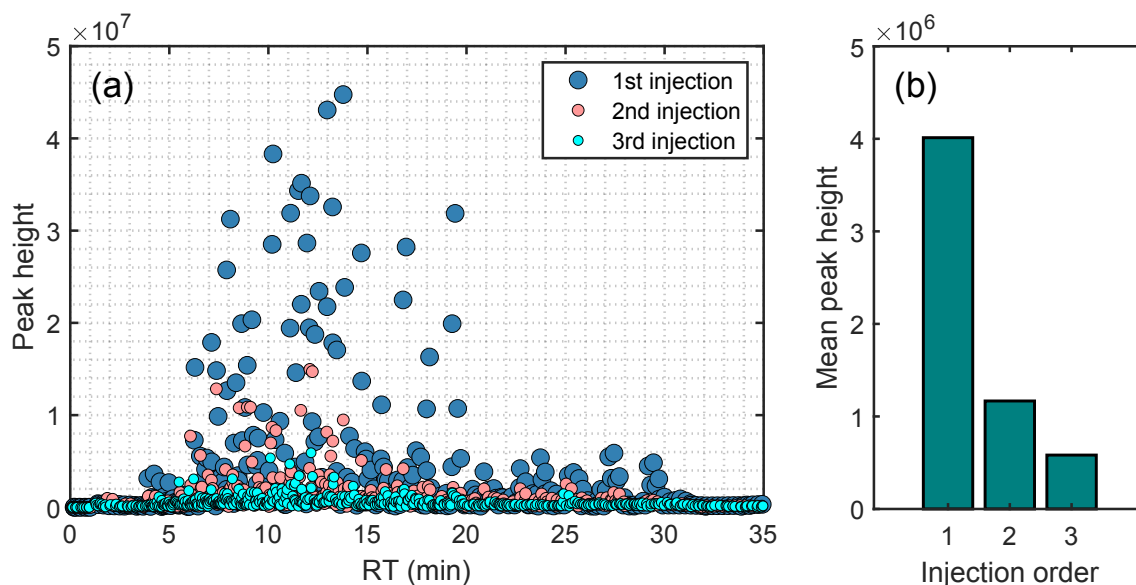


Figure S 2: Iterative ddMS². (a) Peak height of precursors triggered for MS/MS during iterative ddMS², showing the strongly enhanced coverage of small peaks with multiple injections. (b) Average peak height of all triggered peaks of each injection.

S3 MassBank calculations

MassBank was downloaded from the MoNA website (MassBank of North America, <https://mona.fiehnlab.ucdavis.edu/downloads>) as a JSON-file and was preprocessed with Python. 20998 single HR-MS²-spectra (with at least 2 peaks) were searched for ΔCF_2 , $\Delta\text{C}_2\text{F}_4$ and ΔCF_3 (and selected others) since the PFAS present in MassBank are mainly compounds with one CF_3 -group and some perfluorinated compounds while only very few telomer-based PFAS (often with insufficient fragments) are present (see Figure S3). Mass tolerance and intensity threshold were subsequently changed [mass tolerance: $\pm(0.05, 0.075, 0.1, 0.25, 0.5, 0.75, 1, 2, 3, 5, 7.5, 10 \text{ mDa})$, relative intensity threshold: 10, 7.5, 5, 3, 1%] and the percentage of identification and false positive rates were calculated. All compounds having a sum formulae with ≥ 3 fluorine atoms [in MassBank: 942 single spectra $\text{F}_{\geq 3}$ from 99 unique compounds $\text{F}_{\geq 3}$; it was also searched via SMILES ('C(F)(F)F') showing that more than 94% of the 942 spectra are from compounds with a CF_3 -group (including PFAS with perfluoroalkyl

chains since they also have one CF₃-group)] were considered as hits. 40 of the 99 compounds are PFAS with perfluoroalkyl chains (more than 7 fluorine atoms) (161 of 942 spectra). On the one hand, these results are considered as best-case scenario, since multiple spectra at different CEs per compound were present (see Equation S1-2). On the other hand, the number of spectra against which FindPFAS was tested is much larger than the number of spectra acquired in a typical ddMS²-run. Positive and false positive assigned spectra were manually inspected for correctness.

The percent of identification was calculated by dividing the number of unique hits with at least 3 fluorine atoms by the number of all unique compounds in MassBank with at least 3 fluorine atoms:

$$\% \text{ compounds found} = \frac{\text{Unique hits } F_{\geq 3}}{\text{All unique compounds in MassBank } F_{\geq 3}} \cdot 100 \% \quad (\text{S1})$$

The rate of false positive spectra was calculated by dividing all spectra of compounds with at least 3 fluorine atoms by the total number of spectra found by FindPFAS:

$$\% \text{ false positive spectra} = \left(1 - \frac{\text{All hits } F_{\geq 3}}{\text{All hits}} \right) \cdot 100 \% \quad (\text{S2})$$

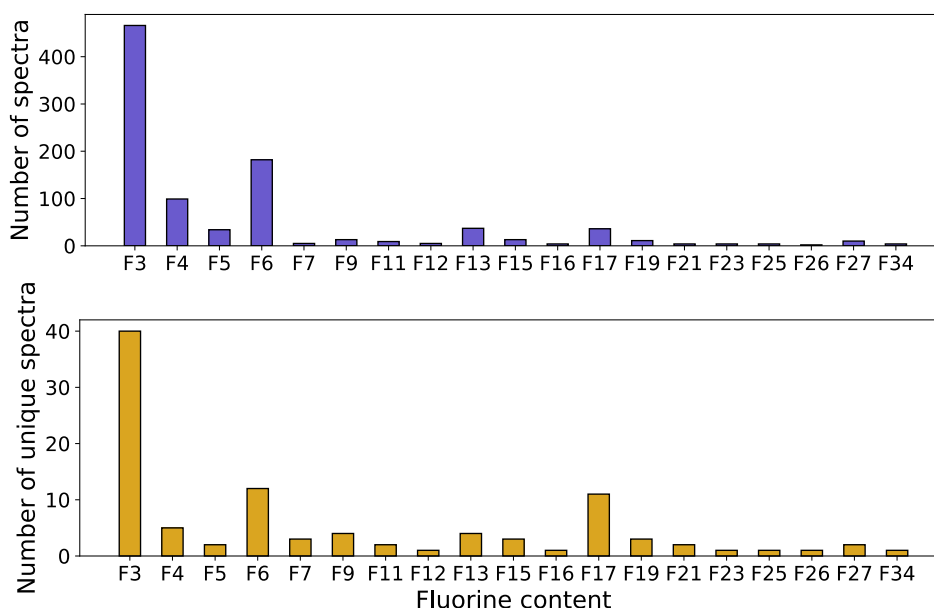


Figure S 3: Distribution of F-containing compounds in MassBank. Total number of spectra (942 spectra) containing at least 3 fluorine atoms (filtered by chemical formula) and unique compound spectra (filtered by name) containing at least 3 F (99 compounds).

S4 Fragment differences and MS² spectra

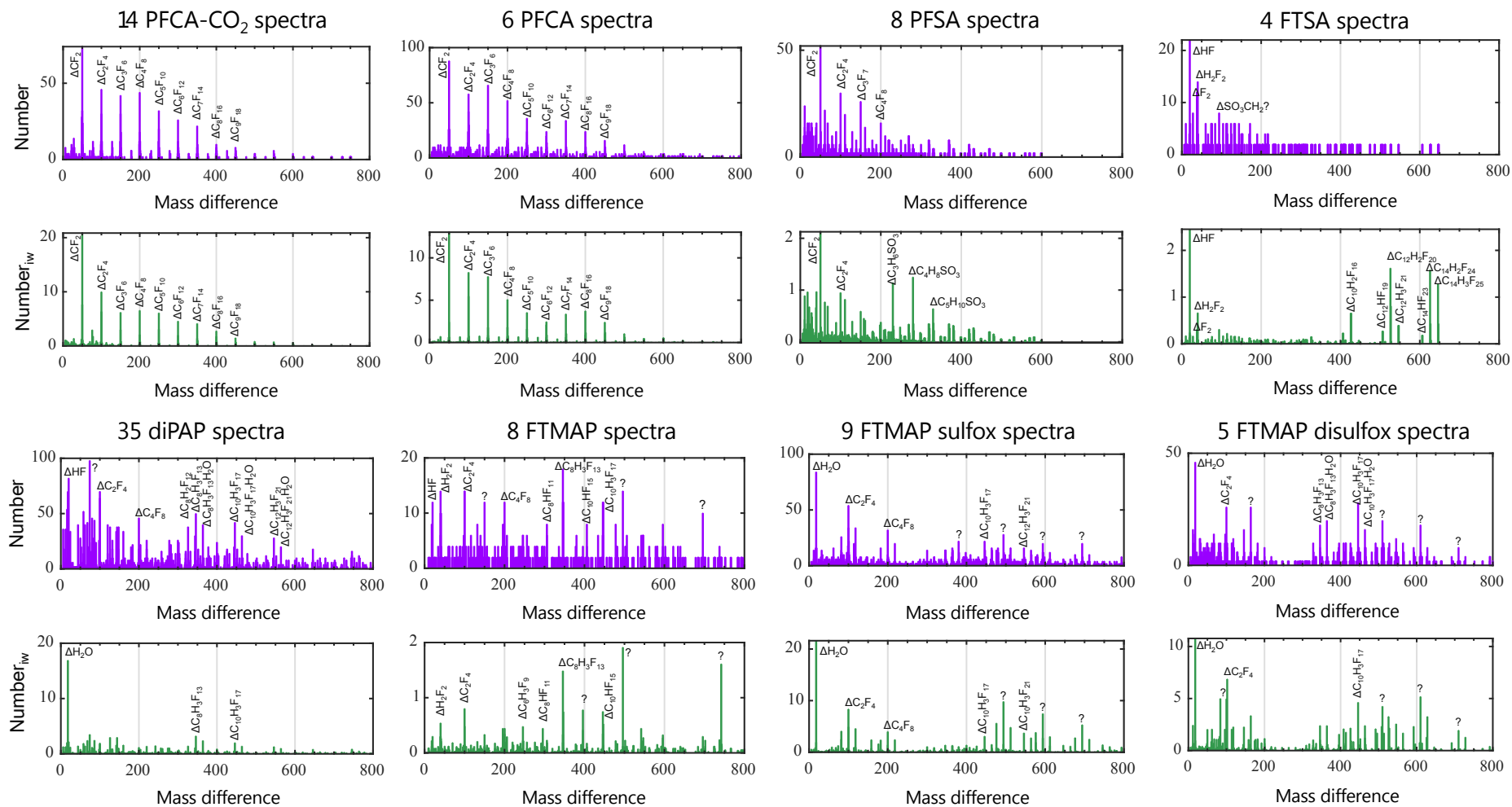


Figure S 4: Mass difference plots. Number of observed mass differences and intensity weighted number for all measured compound classes. Note: e.g. the diPAP spectra include multiples of isomeric peaks, meaning that the same precursor can be present more than once.

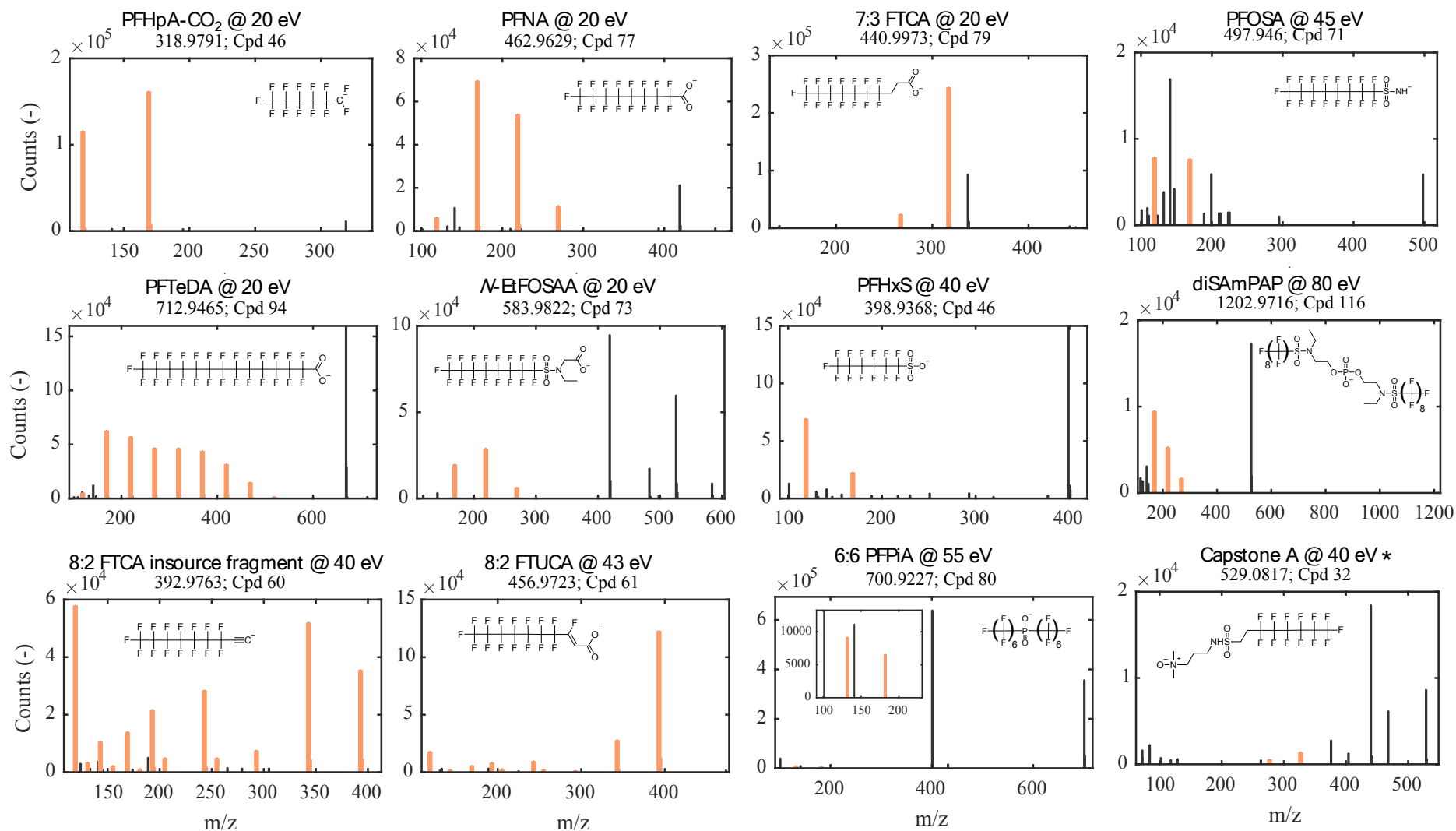


Figure S 5: ΔCF_2 spectra. Examples of spectra with the occurrence of ΔCF_2 differences (highlighted in yellow) from the standard mix at different CEs. Mass tolerance ± 1 mDa, intensity threshold 1000 counts. *Note: In case of Capstone A the ionization mode was positive, the intensity threshold was 500 counts, and the standard had a concentration of 100 $\mu\text{g/L}$.

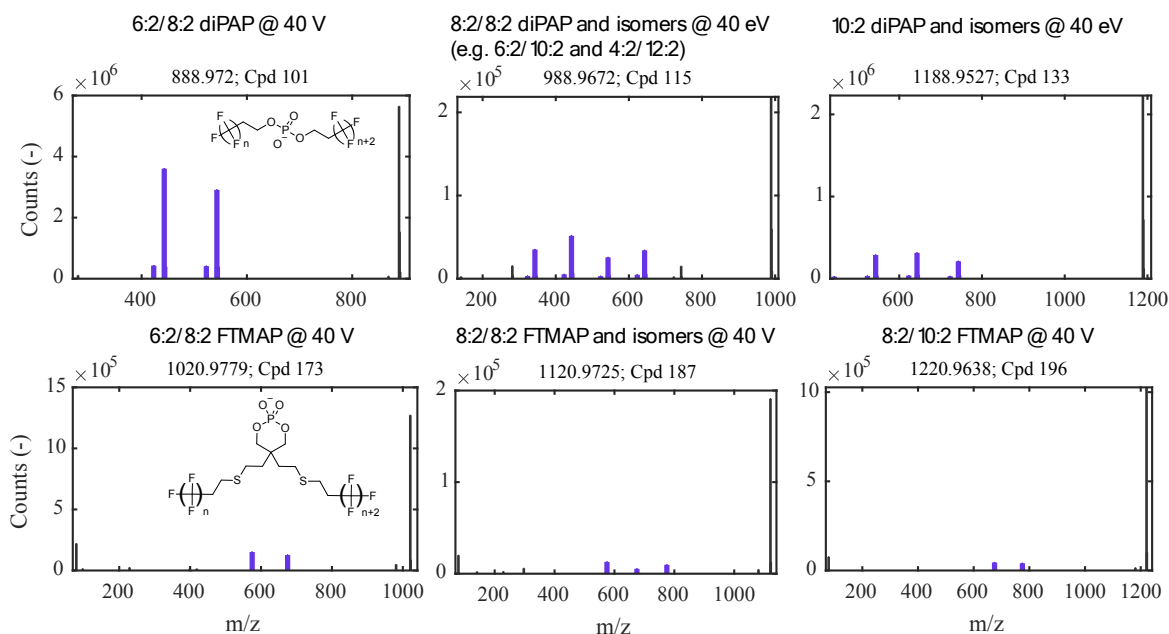


Figure S 6: ΔC_2F_4 spectra. Examples of spectra with ΔC_2F_4 (highlighted in blue) arising from the two fluorinated telomer-based $n:2/(n+2):2$ arms in the paper extracts of paper P1 and P2 at 40 eV. Mass tolerance ± 1 mDa, intensity threshold 1000 counts. Note that e.g. in case of 8:2/8:2 diPAP there are isomers presents in the form $n:2/n:2$, $n:2/(n+2):2$ and $n:2/(n+4):2$. This spectrum results from coeluting isomers and represents a mixture. Peaks below m/z 100 are not shown (e.g. H_2PO_4 and PO_3).

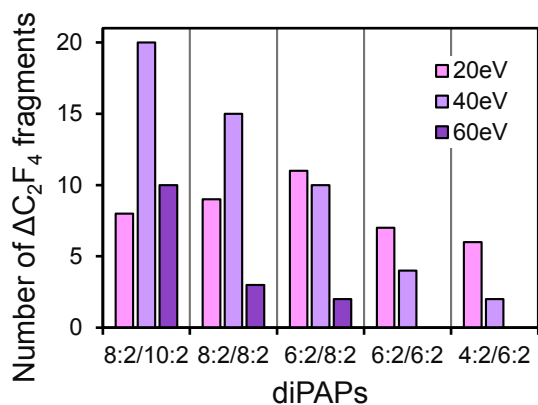


Figure S 7: diPAP fragments dependent on applied CE. Number of ΔC_2F_4 fragment differences observed in the paper sample extract P2 depending on the applied CE. Note that the number of ΔC_2F_4 also results from isomers (e.g. 6:2/12:2 in case of 8:2/10:2 diPAP).

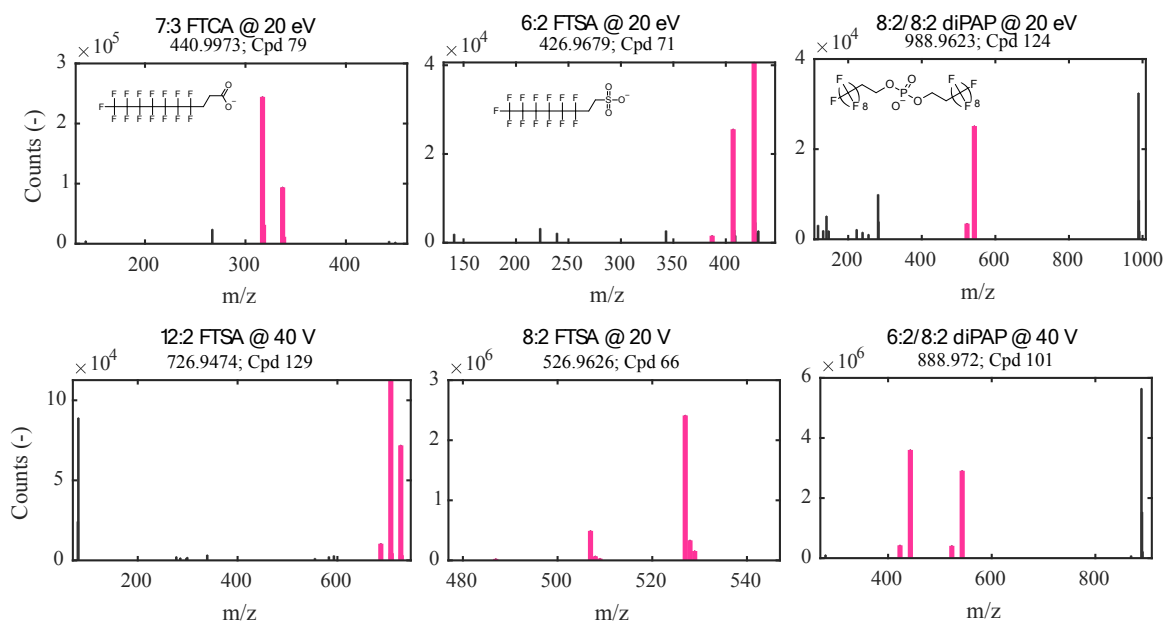


Figure S 8: Δ HF spectra. Examples of spectra with Δ HF (highlighted in red) arising from one or more neutral losses of HF in the PFAS standard and paper extract P2. Mass tolerance ± 1 mDa, intensity threshold 1000 counts. Those differences typically occur when at least one H is bound to a C neighboring a CF_2 -group.

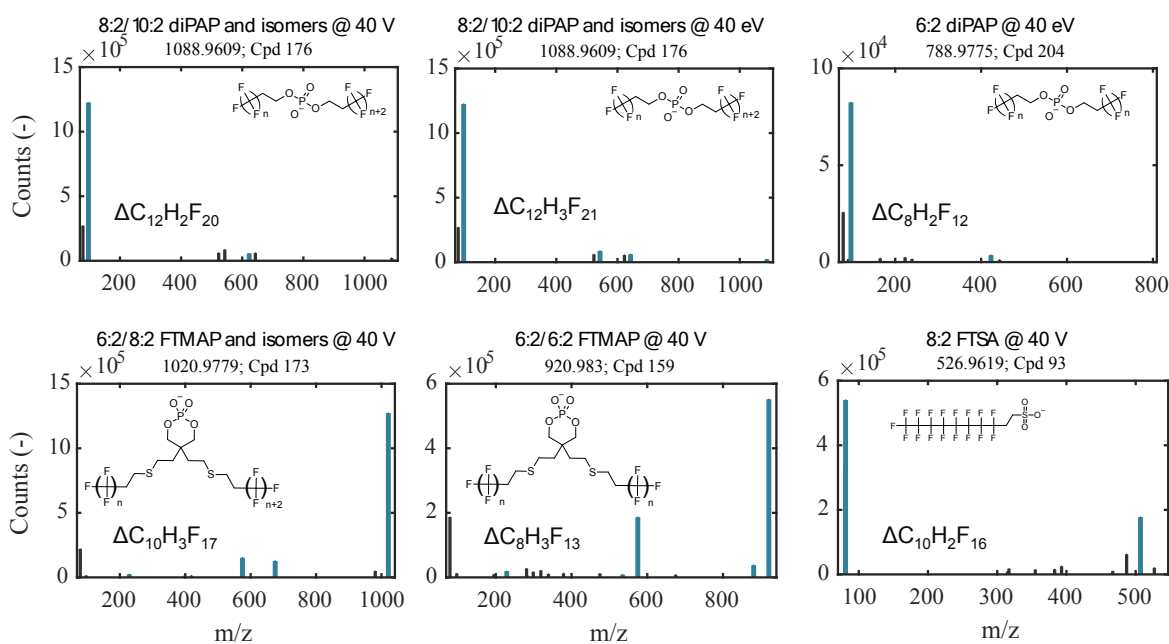


Figure S 9: $\Delta\text{C}_n\text{H}_3\text{F}_{2n-3}$ and $\Delta\text{C}_n\text{H}_2\text{F}_{2n-4}$ spectra. Examples of spectra found with $\Delta\text{C}_n\text{H}_3\text{F}_{2n-3}$ and $\Delta\text{C}_n\text{H}_2\text{F}_{2n-4}$ (highlighted in green) from the paper sample extracts. Mass tolerance ± 1 mDa, intensity threshold 1000 counts. Note the perfluoroalkyl chain length equals $n-2$.

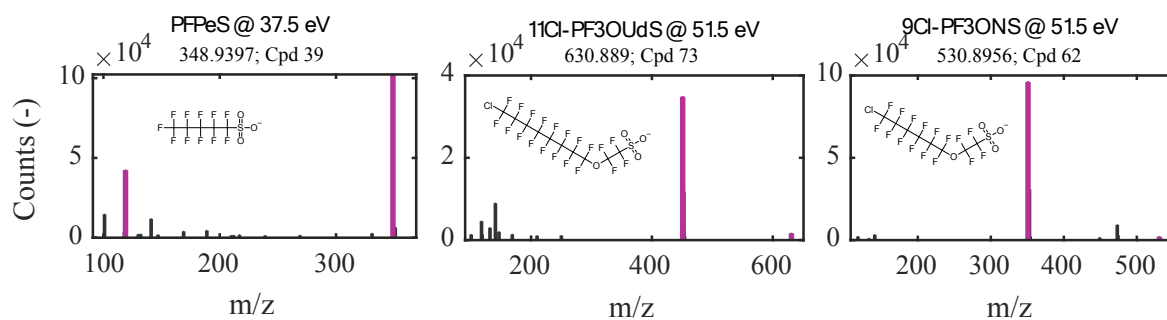


Figure S 10: $\Delta C_n F_{2n} SO_3$ spectra. Examples of spectra containing $\Delta C_n F_{2n} SO_3$ (highlighted in purple) from the PFAS standard mixture. Mass tolerance ± 1 mDa, intensity threshold 1000 counts.

S5 Application of FindPFAS to MassBank

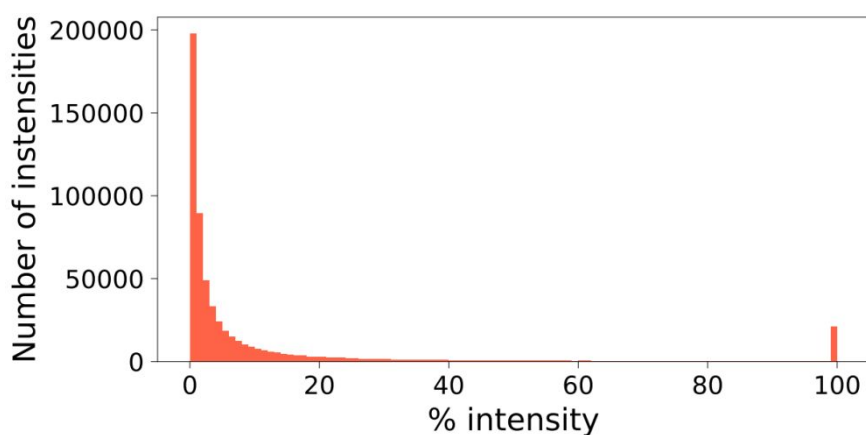


Figure S 11: Histogram of the number of intensities within the MassBank dataset, showing the high frequency of peaks $\leq 3\%$ relative intensity.

Table S 4: Examples of unique correctly detected compounds by FindPFAS in MassBank with the difference ΔCF_2 , a mass tolerance of ± 1 mDa and relative intensity threshold of 1%. Note: very few compounds appear twice due to the filtering by unique compound name.

Compound name	Chemical formula	Compound name	Chemical formula
Mabuterol	C13H18ClF3N2O	Nilotinib	C28H22F3N7O
Flunixin	C14H11F3N2O2	Flurtamone	C18H14F3NO2
Niflumic acid	C13H9F3N2O2	Picolinafen	C19H12F4N2O2
Norfenfluramine	C10H12F3N	Perfluorobutane sulfonic acid (PFBuS)	C4HF9O3S
N-Nitrosufenfluramine	C12H15F3N2O	Flunitrazepam	C16H12FN3O3
Diflufenican	C19H11F5N2O2	Flunixin	C14H11F3N2O2
Fluazifop	C15H12F3NO4	Fluometuron	C10H11F3N2O
Fipronil	C12H4Cl2F6N4OS	6:2 fluorotelomer unsaturated carboxylic acid	C8H2F12O2
Fipronil-sulfone	C12H4Cl2F6N4O2S	Celecoxib	C17H14F3N3O2S
Fipronil-sulfide	C12H4Cl2F6N4S	Perfluorooctanesulfonic acid	C8HF17O3S
Perfluoroheptanoic acid	C7HF13O2	Perfluorotetradecanoic acid	C14HF27O2
Perfluorooctanoic acid	C8HF15O2	Fipronil desulfinyl	C12H4Cl2F6N4
Perfluorononanoic acid	C9HF17O2	Fluvoxamine	C15H21F3N2O2
Perfluorodecanoic acid	C10HF19O2	Fluticasone propionate	C25H31F3O5S
N-Ethylperfluorooctansulfonamid	C10H6F17NO2S	N-Ethylperfluorooctane sulfonamidoacetic acid	C12H8F17NO4S
Tritosulfuron	C13H9F6N5O4S	Flonicamid	C9H6F3N3O

1-(3-(Trifluoromethyl)phenyl)piperazine	C11H13F3N2	Flecainide	C17H20F6N2O3
Sitagliptin	C16H15F6N5O	Fluazifop-butyl	C19H20F3NO4
Perfluorooctane sulfonamidoacetic acid	C10H4F17NO4S	Lansoprazole	C16H14F3N3O2S
N-methylperfluorooctane sulfonamidoacetic acid	C11H6F17NO4S	N-MeFOSAA	C11H6F17NO4S
Oxyfluorfen	C15H11ClF3NO4	Perfluorooctanoic acid (PFOA)	C8HF15O2
Trifloxystrobin	C20H19F3N2O4	Perfluorononanoic acid (PFNA)	C9HF17O2
Triflusulfuron-methyl	C17H19F3N6O6S	Perfluorodecanoic acid (PFDA)	C10HF19O2
Efavirenz	C14H9ClF3NO2	Perfluoroundecanoic acid (PFUnDA)	C11HF21O2
Isoxaflutole	C15H12F3NO4S	Perfluorododecanoic acid (PFDoDA)	C12HF23O2
Haloxypop	C15H11ClF3NO4	Perfluorotridecanoic acid (PFTTrDA)	C13HF25O2
Flufenamic acid	C14H10F3NO2	Perfluorotetradecanoic acid (PFTeDA)	C14HF27O2
Acifluorfen	C14H7ClF3NO5	Thiazopyr	C16H17F5N2O2S

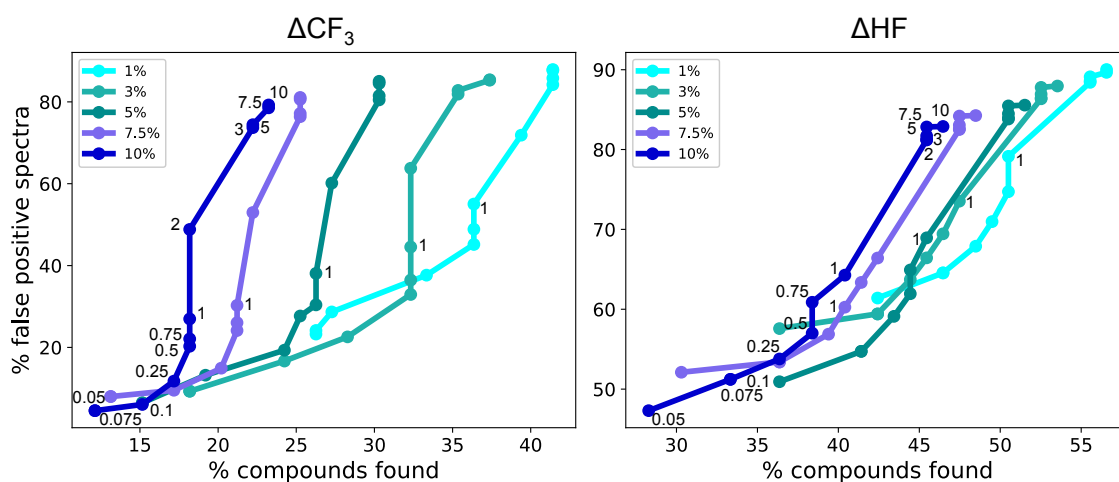


Figure S 12: False positive vs. correct detections for ΔCF_3 and ΔHF . Percentage of correctly assigned unique compound spectra with ΔCF_3 and ΔHF (hit: compounds with at least 3 fluorine atoms) detected by FindPFAS in the MassBank plotted against the rate of false positive detected total spectra. Numbers correspond to the mass tolerance in mDa (only one curve fully labeled, 1 mDa marked for all), colors to intensity thresholds.

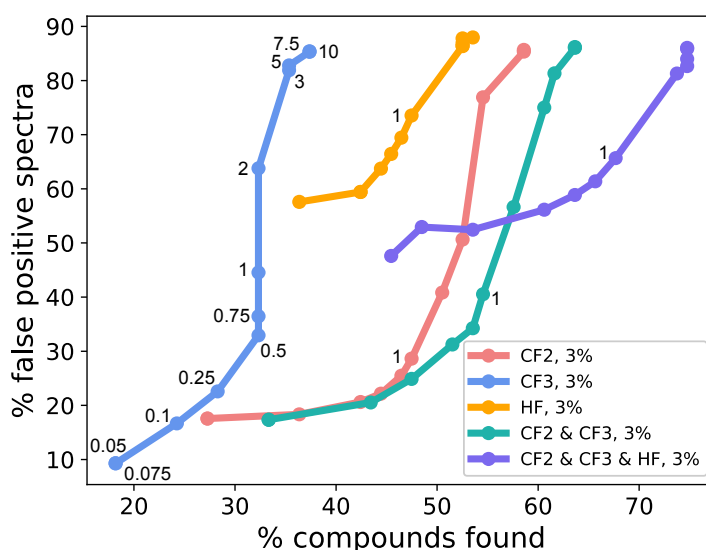


Figure S 13: False positive vs. correct detection for combinations of mass differences. Percentage of correctly assigned unique compound spectra (hit: compounds with at least 3 fluorine atoms) detected by FindPFAS in the MassBank plotted against the rate of false positive detected total spectra. Comparison of different mass differences and combinations with an intensity threshold of 3%. Note that by using ΔHF the number of false positives strongly increased. Numbers correspond to the mass tolerance in mDa (only one curve fully labeled, 1 mDa marked for all).

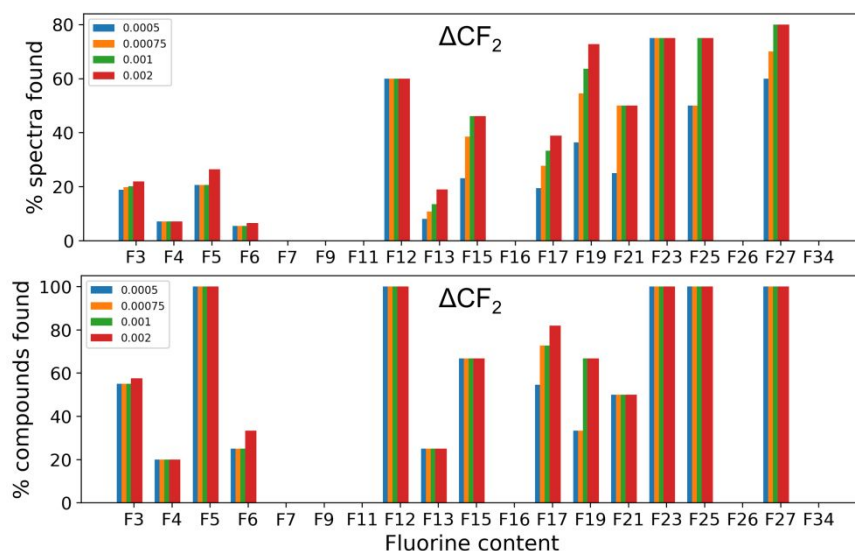


Figure S 14: Distribution of found compounds with ΔCF_2 . % spectra found and % compounds found when using ΔCF_2 with FindPFAS in MassBank for different F-containing compounds depending on mass difference [legend = $\pm(0.5, 0.75, 1$ and 2 mDa)] with a fixed intensity threshold of 3%. Note: F₂₆ and F₃₄ are diPAP spectra, F₁₆ is 9Cl-PF3ONS with 3 peaks which were found when using other mass differences. F₇ is PFBA (only 2 peaks), F₉ and F₁₁ are PFBA and PFH_xA which were not detected due to insufficient fragments. Missing F amounts means that no such compounds were present in MassBank.

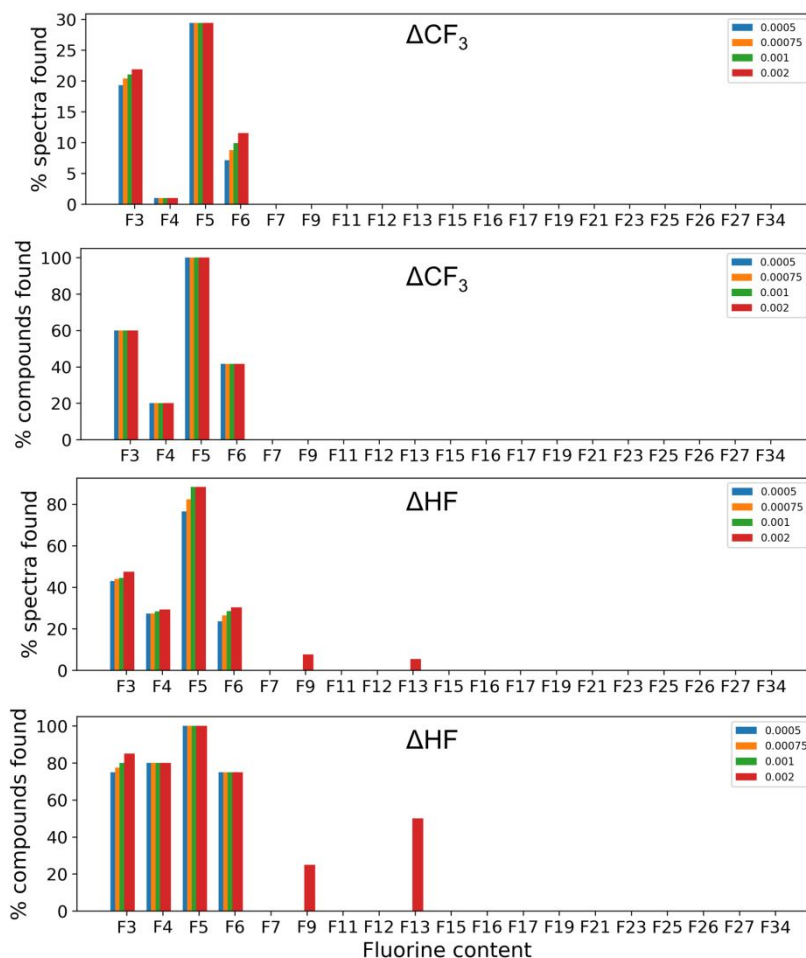


Figure S 15: Distribution of found compounds with ΔCF_3 and ΔHF . % spectra found and % compounds found with ΔCF_3 and ΔHF in MassBank for different F-containing compounds depending on mass difference with a fixed intensity threshold of 3%. Compare to Figure S14.

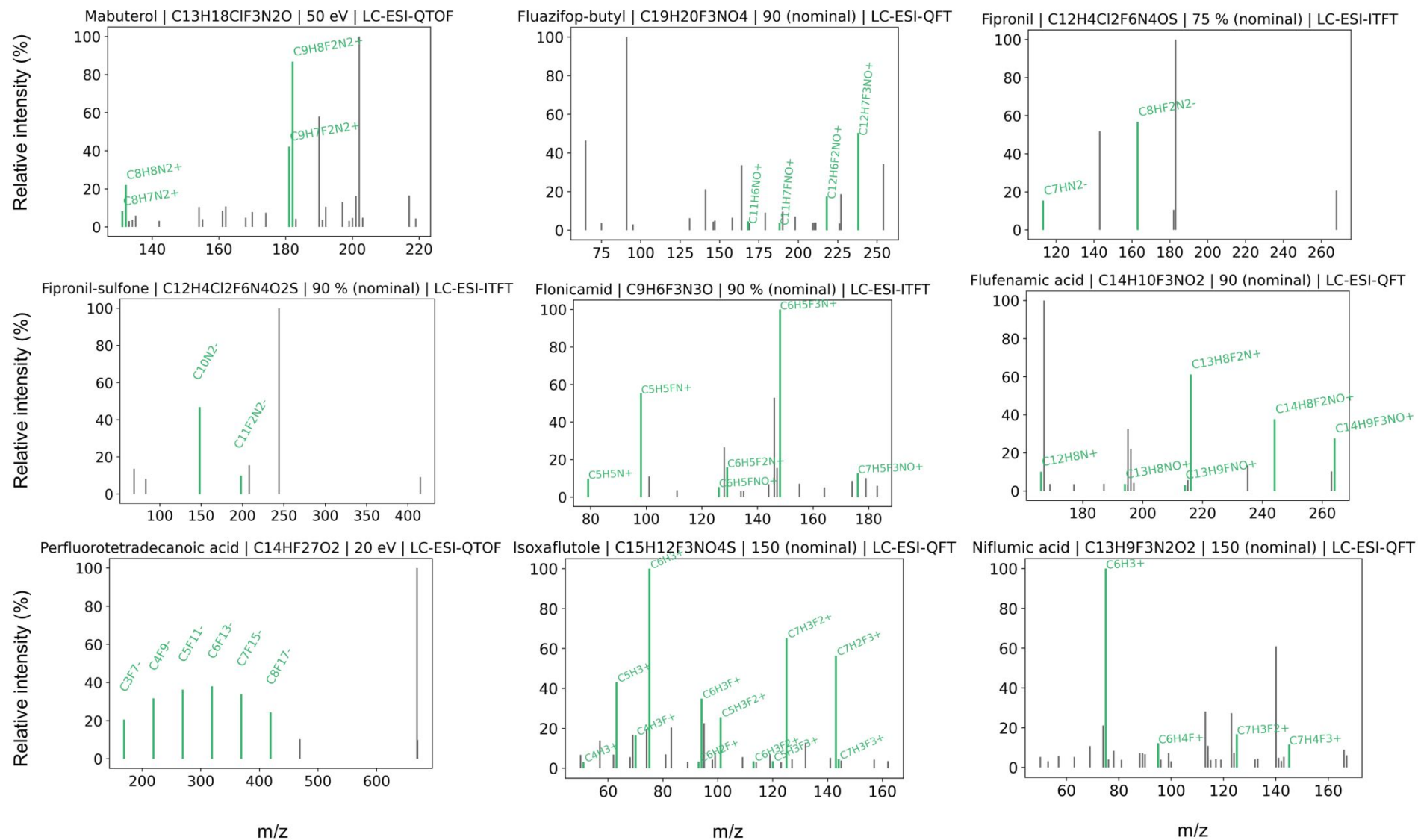


Figure S 16: Arbitrary examples of correctly detected spectra by FindPFAS within the MassBank dataset (mass difference ΔCF_2 , mass tolerance ± 1 mDa, intensity threshold 3%). Note that there can still be false positives within correct detected spectra.

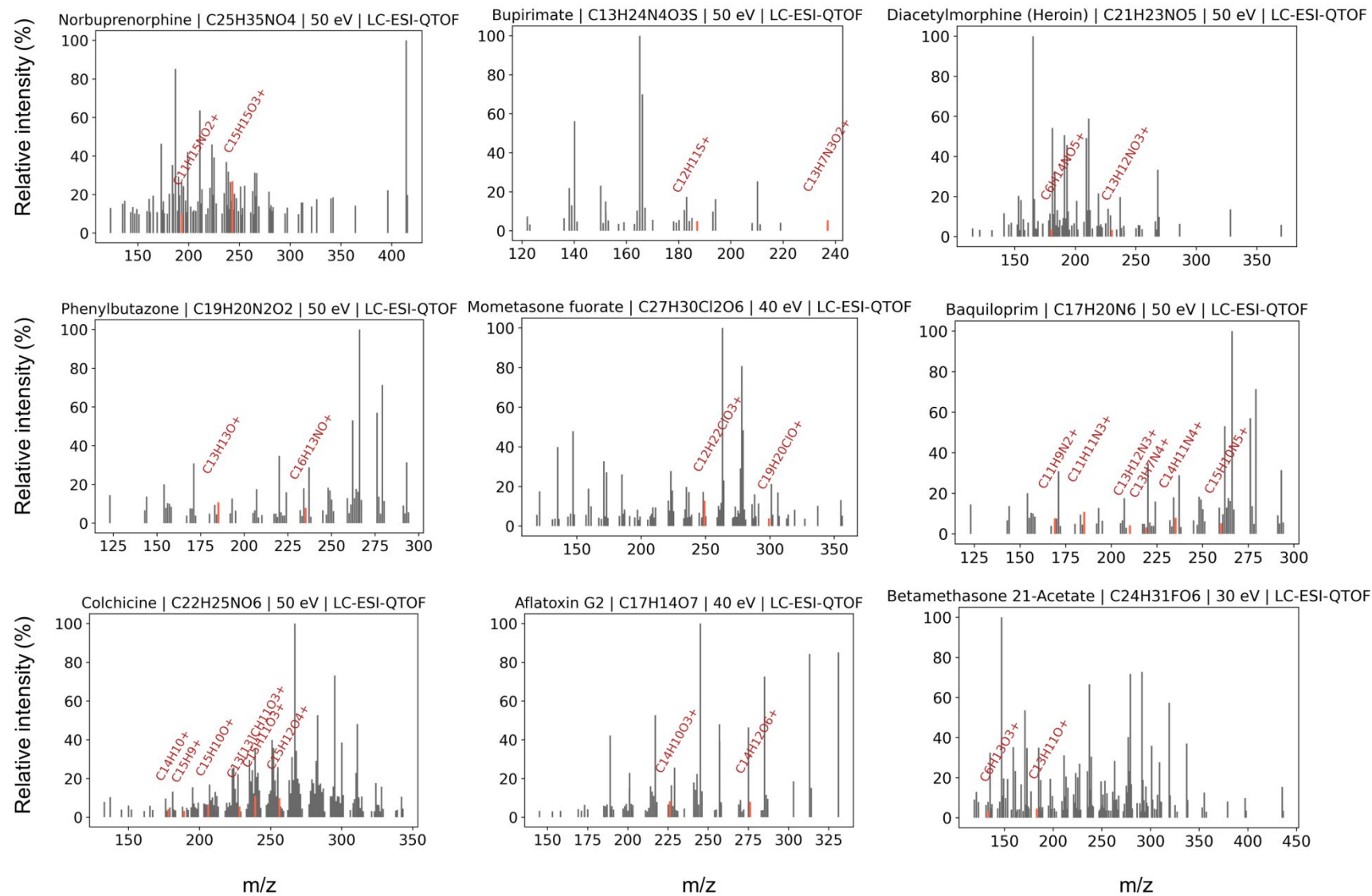


Figure S 17: Arbitrary examples of false positive detected spectra by FindPFAS within the MassBank dataset (mass difference ΔCF_2 , mass tolerance ± 1 mDa, relative intensity threshold 3%).

Table S 5: False positive differences for ΔCF_2 . Examples of fragments from MS/MS spectra in MassBank which led to false positive hits for the mass difference ΔCF_2 (= 49.9968 Da). Highlighted in blue are sometimes observed false positives which actually arose from compounds containing one F.

Fragment 1	Fragment 2	Difference contributing atoms	Exact Mass (Da)	Deviation from ΔCF_2 (mDa)
C ₈ H ₉ OS	C ₇ H ₅ N	CH ₄ OS – N	49.9978	0.99
C ₁₅ H ₁₃ NO ₄	C ₈ H ₁₅ NO ₆	C ₇ – H ₂ O ₂	49.9945	2.3
C ₁₇ H ₁₃ N ₂	C ₁₃ H ₁₃ NO	C ₄ O – N	49.9918	4.9
C ₁₃ H ₇ N ₄	C ₁₁ H ₉ N ₂	C ₂ N ₂ – H ₂	49.9904	6.4
C ₃₃ H ₃₈ O ₄	C ₃₃ H ₃₆ O	H ₂ O ₃	50.0004	3.6
C ₁₄ H ₈ N ₄	C ₁₀ H ₉ O	C ₄ F – OH	49.9956	1.2
C ₁₅ H ₈ ClFN	C ₁₂ H ₄ N ₃ O	C ₃ H ₄ ClF	49.9975	0.7
C ₁₁ H ₁₃ O ₃	C ₈ H ₁₂ OF	C ₃ HO ₂ – F	49.9992	2.5

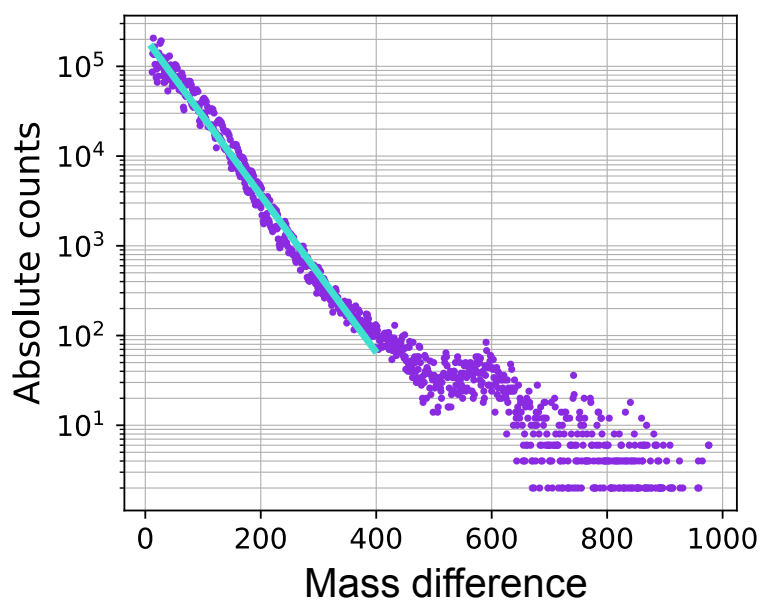


Figure S 18: Exponential decrease of the frequency of integer mass differences with increasing mass difference within 20998 HR-MS/MS spectra in MassBank. Note: y-axis is in log-scale. R^2 for the fit until mass difference 400 Da equals 0.992.

S6 Identification of unknowns

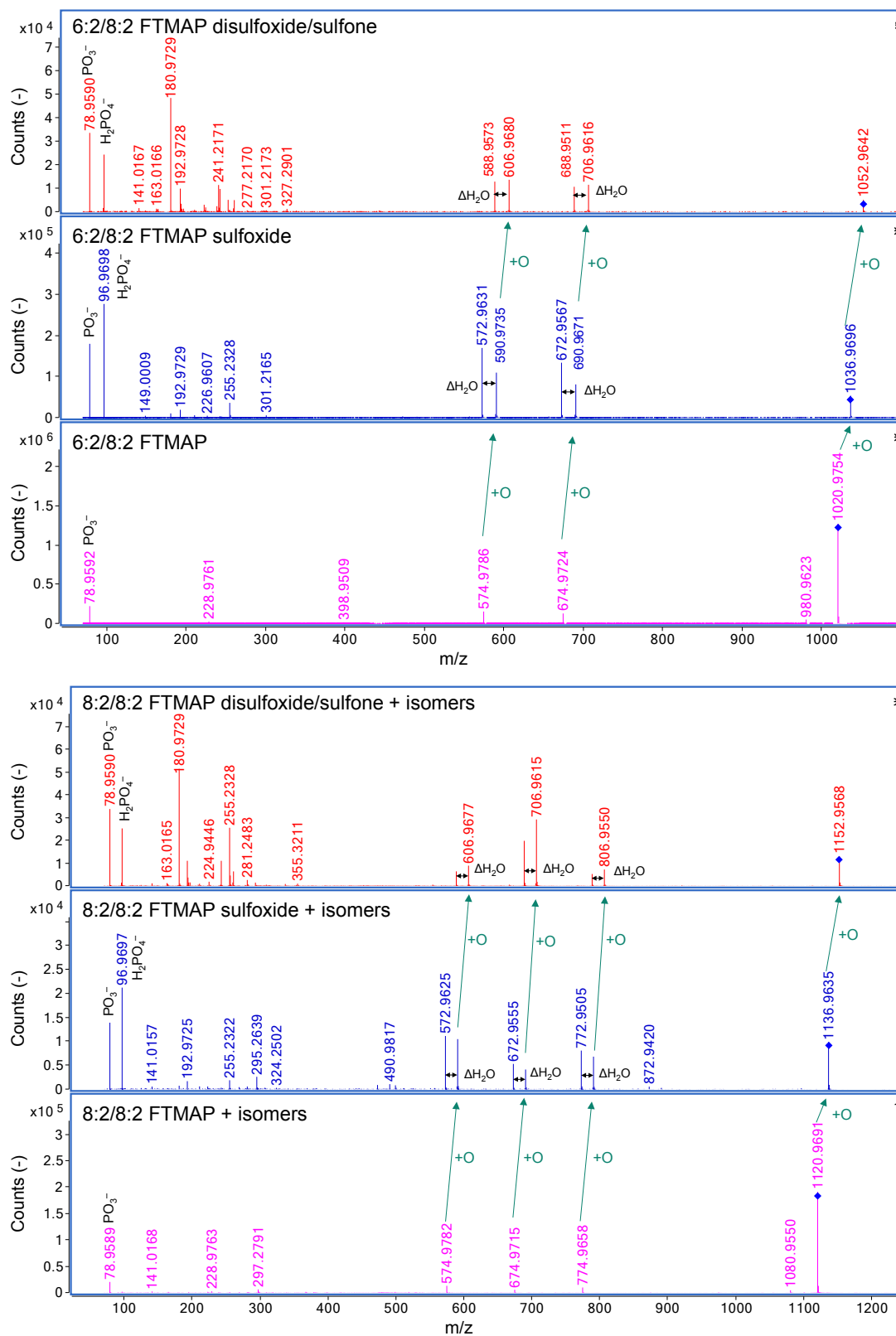


Figure S 19: MS/MS spectra of FTMAP, FTMAP sulfoxide and FTMAP disulfoxide/sulfone [6:2/8:2 and 8:2/8:2 with additional isomers (telomer chain length and position of oxygen)] at 40 eV in paper extract P1. Highlighted are the oxygen shifts of the fragments from the different oxidation states.

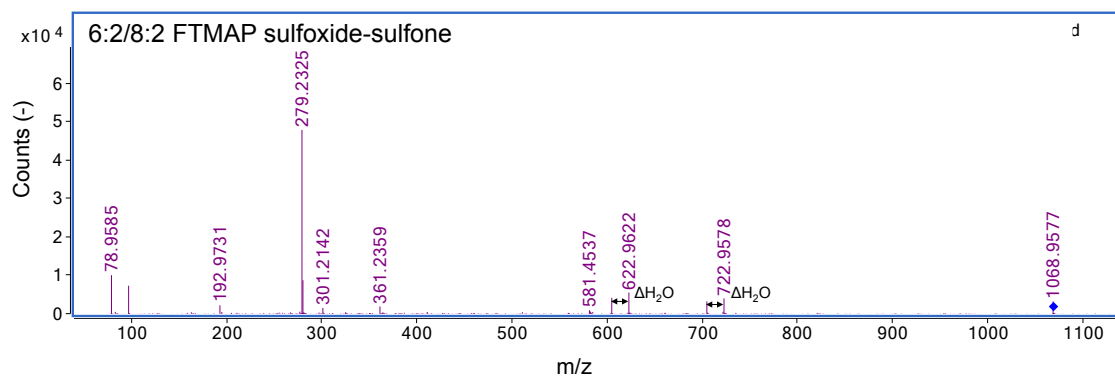


Figure S 20: MS/MS spectrum of 6:2/8:2 FTMAP sulfoxide-sulfone at 40 eV in paper extract P1.

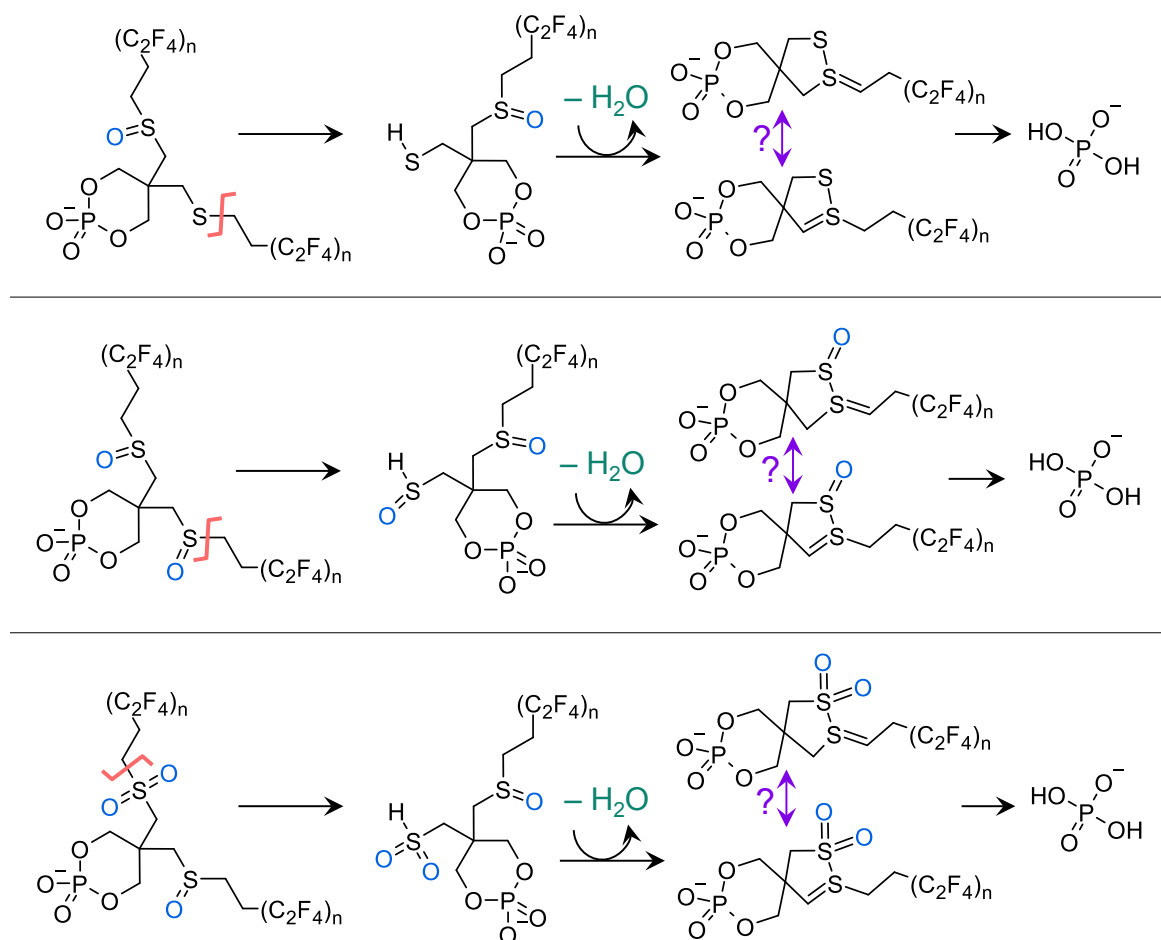


Figure S 21: Proposed fragmentation reactions for FTMAP sulfoxide, FTMAP disulfoxide/sulfone and FTMAP disulfoxide-sulfone homologues. Note that the position of the S=C double bond was not determined.

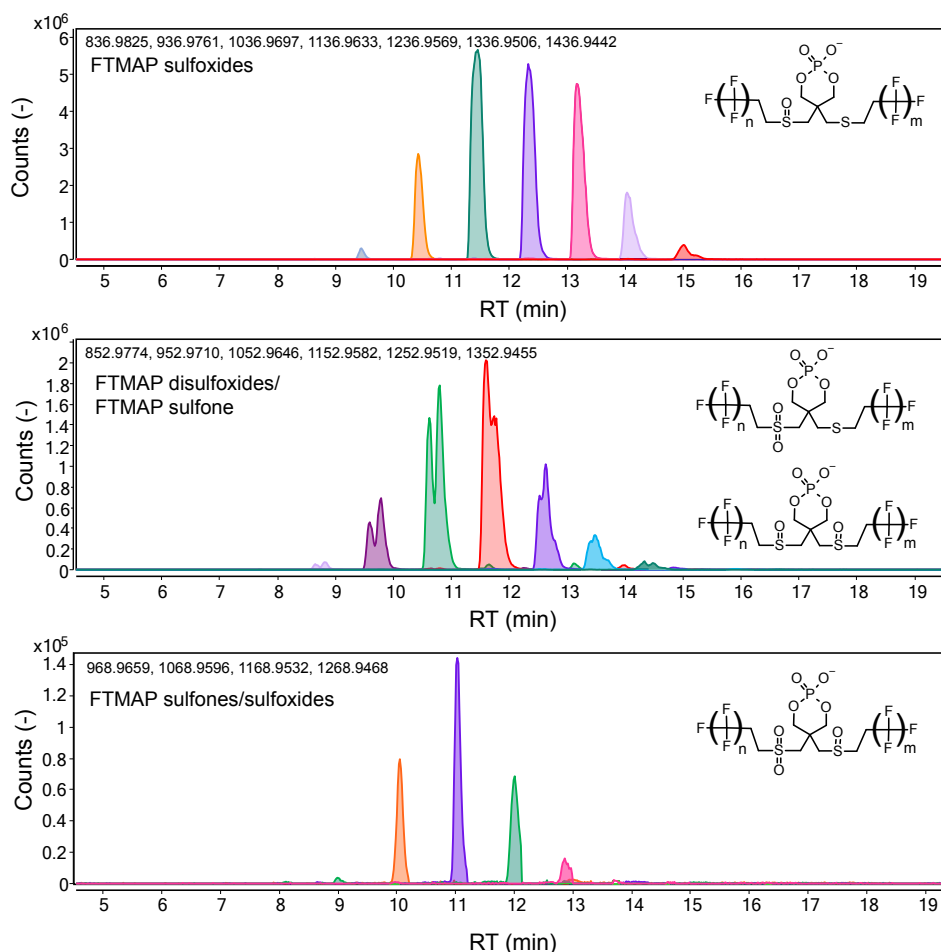


Figure S 22: EICs (scan) of 6 homologous of FTMAP sulfoxides and FTMAP disulfoxides/FTMAP sulfones in paper extract P1. Note that the peak shape is indicative of isomers of disulfoxides/sulfones and additionally $n:2/(n+2):2$ compounds can have further isomers depending on the positions of oxygen.

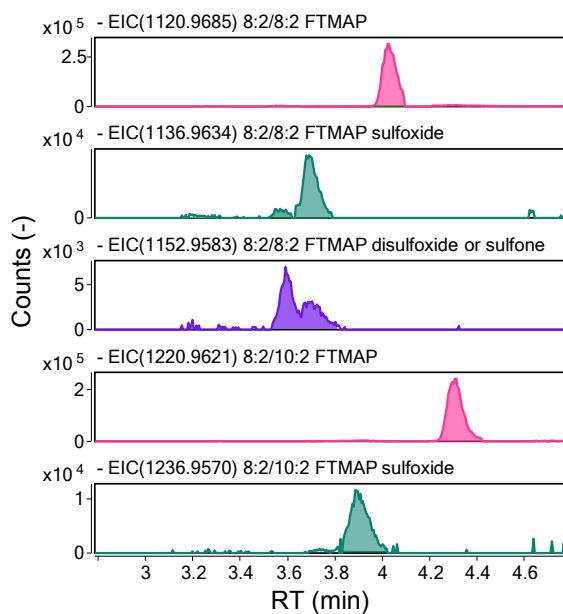


Figure S 23: EICs of FTMAPs, FTMAP sulfoxide and one FTMAP disulfoxide/sulfone in the soil extract from Mannheim.² Note: the strong RT-differences in comparison to Figure S22 arise from the fact that here a UHPLC system was used for chromatographic separation.

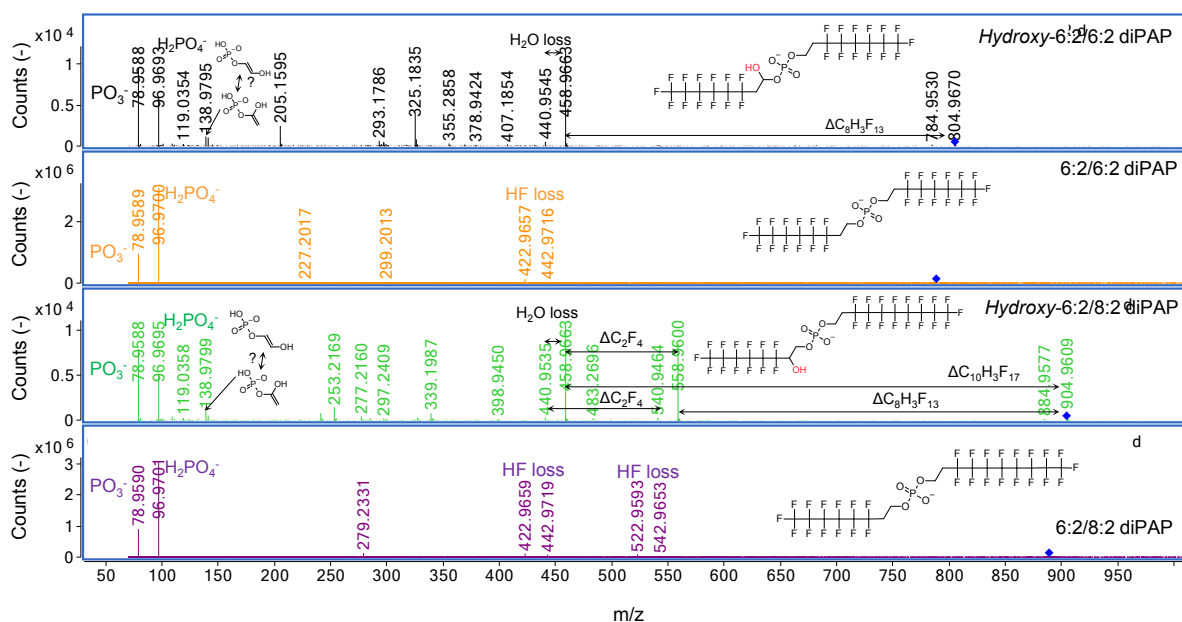


Figure S 24: MS/MS spectra of the tentatively identified Hydroxy-diPAPs and comparison to 6:2/6:2 diPAP, 6:2/8:2 diPAP at 40 eV in paper extract P2 (with additional isomers depending on the position of the hydroxy group). Note that the exact position of the OH-group was not determined (it can be bound to the C-atom next to the perfluoroalkyl chain or to the C-atom next to the oxygen of the phosphate group; both positions are shown on one structure respectively). Highlighted are the fragment mass differences which led to detection with FindPFAS. Hydroxy-diPAPs were also retrospectively found based on their accurate mass (and RT shift with respect to diPAPs) in a soil from the region around Rastatt (Hügelsheim).

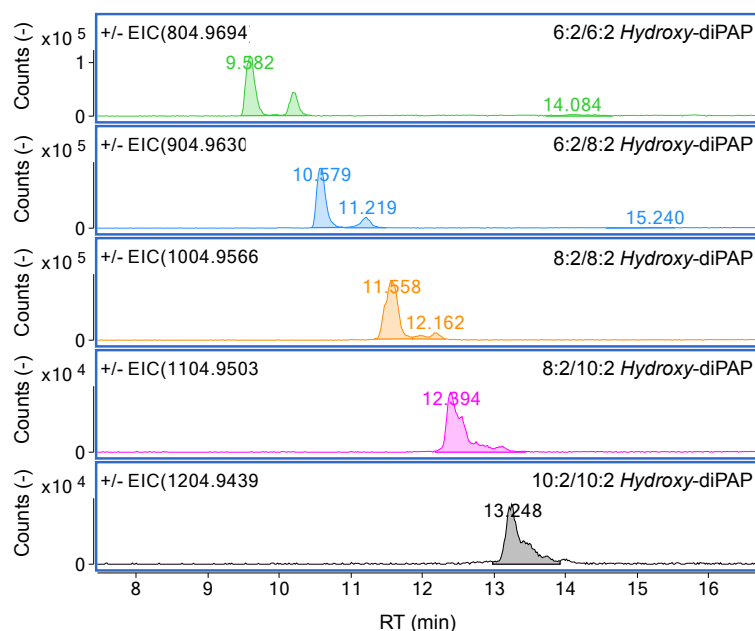


Figure S 25: EICs (scan) of 5 Hydroxy-diPAP homologous in the paper extract P2. The two peaks presumably arise from different positions of the OH-group. All Hydroxy-diPAPs have a slightly shorter RT compared to diPAPs as expected for hydroxylated compounds. Hydroxy-diPAPs were also retrospectively found based on their accurate mass (and RT shift with respect to diPAPs) in a soil from the region around Rastatt (Hügelsheim).

References

1. Koelmel, J. P.; Kroeger, N. M.; Gill, E. L.; Ulmer, C. Z.; Bowden, J. A.; Patterson, R. E.; Yost, R. A.; Garrett, T. J., Expanding Lipidome Coverage Using LC-MS/MS Data-Dependent Acquisition with Automated Exclusion List Generation. *J Am Soc Mass Spectrom* **2017**, *28*, (5), 908-917.
2. Bugsel, B.; Bauer, R.; Herrmann, F.; Maier, M. E.; Zwiener, C., LC-HRMS screening of per- and polyfluorinated alkyl substances (PFAS) in impregnated paper samples and contaminated soils. *Anal Bioanal Chem* **2021**.

Appendix 3

Publication 3

PFAS-Contaminated Soil Site in Germany: Nontarget Screening before and after Direct TOP Assay by Kendrick Mass Defect and FindPFAS

Jonathan Zweigle,^{+||} Boris Bugsel,^{+||} Klaus Röhler,[‡] Alexander Haluska,[‡] Christian Zwiener^{+,*}

⁺Environmental Analytical Chemistry, Department of Geosciences, University of Tübingen, Schnarrenbergstraße 94-96, 72076 Tübingen, Germany

[‡]Hydrogeochemistry, Department of Geosciences, University of Tübingen, Schnarrenbergstraße 94-96, 72076 Tübingen, Germany

^{||}The authors contributed equally to this work and share first authorship.

Published in: *Environmental Science and Technology* 57(16), 6647-6655.

DOI: 10.1021/acs.est.2c07969

Reprinted with permission from *Environmental Science & Technology*: Zweigle, J., Bugsel, B., Röhler, K., Haluska, A. A., & Zwiener, C. (2023). PFAS-Contaminated Soil Site in Germany: Nontarget Screening before and after Direct TOP Assay by Kendrick Mass Defect and FindPFAS. *Environ Sci Technol*, 57(16), 6647-6655. <https://doi.org/10.1021/acs.est.2c07969>

PFAS-Contaminated Soil Site in Germany: Nontarget Screening before and after Direct TOP Assay by Kendrick Mass Defect and FindPFAS

Jonathan Zweigle,^{||} Boris Bugsel,^{||} Klaus Röhler, Alexander Arthur Haluska, and Christian Zwiener^{*}



Cite This: *Environ. Sci. Technol.* 2023, 57, 6647–6655



Read Online

ACCESS |



Metrics & More



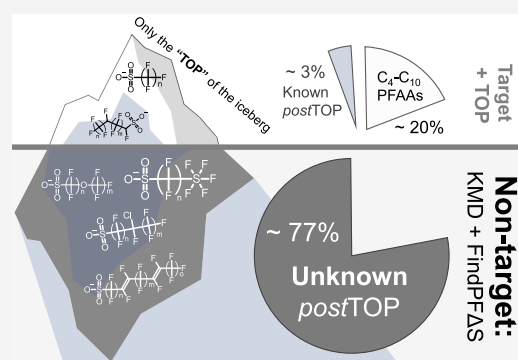
Article Recommendations



Supporting Information

ABSTRACT: Soil contaminations with per- and polyfluoroalkyl substances (PFAS) are of great concern due to their persistence, leading to continuous, long-term groundwater contamination. A composite sample from contaminated agricultural soil from northwestern Germany (Brilon-Scharfenberg, North Rhine-Westphalia) was investigated in depth with nontarget screening (NTS) (Kendrick mass defect and MS² fragment mass differences with FindPFAS). Several years ago, selected PFCAs and PFSAs were identified on this site by detection in nearby surface and drinking water. We identified 10 further PFAS classes and 7 C₈-based PFAS (73 single PFAS) previously unknown in this soil including some novel PFAS. All PFAS classes except for one class comprised sulfonic acid groups and were semi-quantified with PFSA standards from which ~97% were perfluorinated and are not expected to be degradable. New identifications made up >75% of the prior known PFAS concentration, which was estimated to >30 μg/g. Pentafluorosulfanyl (–SF₅) PFASs are the dominant class (~40%). Finally, the soil was oxidized with the direct TOP (dTOP) assay, revealing PFAA precursors that were covered to a large extent by identified H-containing PFAS and additional TPs (perfluoroalkyl diacids) were detected after dTOP. In this soil, however, dTOP + target analysis covers <23% of the occurring PFAS, highlighting the importance of NTS to characterize PFAS contaminations more comprehensively.

KEYWORDS: PFAS, high-resolution mass spectrometry, nontarget screening, TOP assay, TOP direct, fragment mass differences, FindPFAS, Kendrick mass defect



INTRODUCTION

Per- and polyfluoroalkyl substances (PFAS) form an exclusively man-made group of substances.¹ According to the OECD definition, all substances with a perfluorinated methyl group (–CF₃) or a perfluorinated methylene group (–CF₂–) are considered PFAS.² The online database PubChem contains more than 6 million individual compounds that meet this definition.³ This considerable number of substances results from the unique properties that PFAS offer and their wide range of applications: for example, they are used as repelling agents in textiles and food contact materials and as surfactants in aqueous film-forming foams (AFFFs) and in the electronics and semiconductor industry.^{4–7} While the stability of PFAS is advantageous for industry, this property has disadvantages for their environmental behavior. Due to their wide range of applications and persistence, PFAS have become a major environmental concern as more and more PFAS-contaminated sites are discovered.^{8–10} For many of the PFAS-contaminated sites, it is vastly problematic that the individual PFAS are only partially known. Compared to the 6 million PFAS in the PubChem database, only a few PFAS are usually detected and quantified by target analysis.¹¹

To address this problem, the total oxidizable precursor (TOP) assay and modifications (conversion via UV/TiO₂), as well as hydrolysis-based reactions, are applied to estimate the amount of PFAA precursors (i.e., compounds that can be oxidatively converted to PFAAs or hydrolyzed to, e.g., fluorotelomer alcohols), which are not captured by conventional target analysis.^{12–15} In brief, the TOP assay oxidizes PFAS precursors to PFAAs by hydroxyl radicals. An increase in PFAA concentrations after the TOP assay can therefore be attributed to unknown precursors and therefore is a means to estimate the amount of precursors. Although the TOP assay is a valuable tool that only requires a triple-quadrupole (QqQ) instrument for the estimation of the PFAS pollution at contaminated sites, only those precursors that form PFCAs

Received: November 16, 2022

Revised: April 3, 2023

Accepted: April 3, 2023

Published: April 14, 2023



and PFASs as oxidation or hydrolysis products can be detected.¹⁶ For example, many of the novel replacement compounds such as GenX, ADONA, or C6O4 belong to the group of perfluorinated ether carboxylic acids (PFECAs), which cannot be converted to PFCAs in the TOP assay.¹⁷

In 2006, a small-scale PFAS-contaminated site in Germany (Brilon-Scharfenberg, North Rhine-Westphalia) was discovered.¹⁸ Presumably, the application of inorganic and organic waste materials on agricultural areas led to PFAS-contaminated soils and receiving rivers. Target analytes included PFCAs and PFASs, with the highest measured concentration of 33,900 ng/L perfluorooctanoic acid (PFOA) in the Steinbecke River. Recently, Röhler et al. (2022) applied the direct TOP (dTOP) assay to one of the contaminated agricultural soils (BS-NRW) and found a high production of PFAAs, which indicates the presence of so-far undetected precursors.¹⁹ However, a full characterization of the contaminated site is crucial to estimate further environmental impacts since a contamination with precursors can act as a long-term source by a continuous transformation to PFAAs, which can leach to receiving rivers and groundwater bodies.

The objective of this study was to apply (i) nontarget screening (NTS) approaches based on Kendrick mass defect analysis and fragment mass differences (FindPFAS)²⁰ to characterize the contamination of the BS-NRW site and (ii) NTS after the dTOP assay to screen for possible oxidation products that are not measured by conventional target analysis.

MATERIALS AND METHODS

Chemicals and Reagents. Origin and specifications of used chemicals are given in the SI (Section S1).

Field Site. The soil sample was collected in October 2021 from a 10 ha PFAS-contaminated agriculture site in Brilon-Scharfenberg, North Rhine-Westphalia (BS-NRW), Germany. The site is suspected to have periodically received a PFAS-containing compost between 2004 and 2006. However, the origin of the PFAS is not known. More details about the field site can be found in previous publications.^{18,21}

Sample Preparation and dTOP Assay. The composite sample (1 g) was weighed in a 50 mL Falcon tube, covered with 10 mL of MeOH, and put to an overhead shaker overnight. After sonication for 1 h, the mixture was centrifuged (at 4000 rcf for 10 min) and 1 mL of aliquots from the supernatant were taken for subsequent analysis with high-resolution mass spectrometry (HRMS). An extraction blank without adding soil to the centrifuge tube was also prepared and measured. For the dTOP assay, briefly, 100 mg of the soil sample was weighed in 100 mL glass bottles and 10 ng of internal standards was spiked (C₄–C₁₂ PFCAs, C₄, C₆, and C₈ PFASs). A volume of 100 mL of a 200 mM potassium persulfate and 500 mM sodium hydroxide solution was then added. The bottles were then put in an oven at 85 °C for 7 h and shaken periodically. After adjustment to pH 7 and solid-phase extraction (Chromabond HR-XAW, Macherey-Nagel), the SPE eluates were dried and reconstituted with 50/50 MeOH/H₂O (v/v) and analyzed by LC-HRMS. Details on solid-phase extraction are given in the SI (Section S1).

NTS Data Acquisition. Soil extracts and SPE eluates from dTOP were analyzed with HPLC-QTOF-MS. Compound separation was achieved with an Agilent 1260 Infinity HPLC system (Poroshell 120 EC-C₁₈ column; 2.1 mm × 100 mm; 2.7 μm particle size; 40 °C) at a flow rate of 0.3 mL/min, which was coupled to an Agilent 6550 QTOF-mass spectrometer. A

23 min gradient program was used ((A) 95/5 H₂O/MeOH + 2 mM NH₄Ac and (B) 5/95 H₂O/MeOH + 2 mM NH₄Ac) and the ionization source was operated separately in positive and negative modes (details in Tables S1 and S2).

The QTOF was operated in the iterative data-dependent MS² (ddMS²) mode [3 scans/s in MS (*m/z* 100–1700) and MS/MS range (*m/z* 70–1700)] with both static exclusion (generated from blank injections) and a rolling exclusion list, which subsequently excluded already triggered masses from previous injections to maximize MS² coverage. Precursors above 1000 counts were selected (narrow isolation width ≈ 1.3 *m/z*) and actively excluded for 0.5 min after acquiring three spectra. All experiments were performed with a linear *m/z*-dependent collision energy (CE(*m/z*) = 3^{*m/z*}/100 + 15 eV). The injection volume was 5 μL and samples were measured at least in 3 iterations but up to 6. A three-fold needle wash in three separate vials with isopropanol was applied between each injection. Each measurement series included two blanks and a PFAA standard solution to monitor instrument drift.

Semi-Quantification via PFASs. All identified PFAS that comprised sulfonic acid headgroups (–SO₃[–]) were semi-quantified based on calibration curves of C₄–C₁₀ and C₁₂ PFASs (0.1, 1, 5, 10, and 20 μg/L) with the respective carbon chain length. Therefore, all slopes were extrapolated up to C₁₆ and used to estimate concentrations (*c*_{estim}) for identified PFAS in soil (Figure S1). One PFAS class with a carboxylic headgroup (perfluorinated ether carboxylic acids) was similarly semi-quantified with PFCAs ([M – H][–] and [M – H – CO₂][–] ions). Soil extracts were measured in dilutions of 1:10 to decrease matrix effects for semi-quantification. Matrix effects in this 1:10 diluted soil extract were quantified for C₅–C₁₂, C₁₄ PFCAs and C₄, C₆, and C₈ PFASs with the use of isotopically labeled internal standards (see Table S3). All matrix effects were in the range between 93 and 112%. Due to the strong structural similarity of most identified PFAS to PFASs in combination with the observed general weak dependency of PFSA chain length on the ESI efficiency, we expect the semi-quantification to be comparatively accurate. This is further supported by the similar polarity shown by the RT vs chain length correlation (see the next section and Figure 3).

NTS Workflow and Data Mining. In the first step, MS¹-peak-finding was performed with the FindByMolecularFeature (MFE) algorithm (Agilent MassHunter Qualitative Software; peak height ≥ 600 counts; [M – H][–], [M + Cl][–], [M + HCOO][–], and [M + CH₃COO][–] adducts), resulting in 5294 features in the ESI[–] mode (soil extract). CSV files with *m/z*, RT, and peak area were extracted and analyzed for (CF₂)_{*n*}-based Kendrick mass defect with a Python script (at least 5 homologues, 5 mDa absolute mass tolerance). This resulted in 43 homologous series (HS, 526 features, including multiples resulting from isomeric chromatographic peaks), which were manually inspected, compared to extraction and solvent blanks, and inspected for their characteristic RT shift with increasing *m/z*. Twenty-five HS (206 features) were manually discarded due to detection in blanks, very low intensities, bad peak shape, or no systematic RT shift.

In the following step, FindPFAS²⁰ was used to extract potential PFAS masses by the occurrence of characteristic fragment mass differences [Δ(CF₂)_{*n*}, *n* = 1–3; ΔCF₃(CF₂)_{*n*}, *n* = 0–2; ΔCF(CF₂)_{*n*}, *n* = 0–3; ΔF; ΔSF₃; ΔCF₂O; and ΔHF; absolute mass tolerance 2 mDa, minimum MS² intensity 3000 counts; further details in the SI (Section S2 and Figure S2)] in

Table 1. Summary of All Identified PFAS in the Soil Sample and Their Behavior during the dTOP Assay^a

Name	General structure	n, m, o, p	$\sum C_{estim}$ ($\mu\text{g/g soil}$)	dTOP assay
SF ₅ -PFASs		n = 7 to 10	12.5	stable
PFASs ^a		n = 4 to 18	9.3	Target analysis
Unsaturated PFASs		n + m = 6 to 14	3.5	stable
Ether-PFASs		n + m = 9 to 16	1.1	stable
Cl-PFOS		n + m = 7	1.0	stable
Unsaturated-ether-PFASs		n + m + o = 7 to 14	1.0	stable
PFCAs ^a		n = 6 to 8	0.5	Target analysis
H-PFASs		n + m = 5 to 9	0.5	TOP oxidizable
Unsaturated-SF ₅ -PFCAs		n + m = 6 to 9	0.4	stable
di-unsaturated-ether-PFASs		n + m + o + p = 7 to 12	0.4	stable
di-unsaturated PFASs		n + m + o = 9 to 12	0.3	stable
H ₂ -PFASs		n = 7	0.1	TOP oxidizable
H-unsaturated-PFASs		n + m = 5	0.08	TOP oxidizable
Ether-PFCAs		n + m = 7, 10 to 15	0.08	unclear
H ₃ -unsaturated-PFASs		n + m + o = 5	0.04	TOP oxidizable
H ₂ -unsaturated-PFASs		n + m = 4	0.04	TOP oxidizable
Ether-SF ₅ -PFASs ^N		n = 8	0.02	stable
H-di-unsaturated-PFASs		n + m + o = 4	0.02	TOP oxidizable
Unsaturated-ether-SF ₅ -PFASs ^N		n + m + o = 6 to 9	9.3×10^{-3}	stable
Generated during dTOP				
PFCAs		n = 5 to 9	0.3	TOP products

^aCompounds are sorted according to their decreasing estimated concentration in soil. Observed carbon chain lengths are given as the sum of n + m + o + p. Since all compounds were observed as complex isomeric mixtures (evidenced by chromatography and MS/MS), the positions of, for example, double bonds, ether bonds, or further branched isomers could not be determined and are therefore given as variables. Note that the variables can also be 0 and in special cases their positions are exchangeable. More details are provided in Figure 1. Compound classes marked with ^a were previously identified in this soil,^{18,21} classes without mark were previously unknown in the BS-NRW soil, and classes marked with ^N were to our best knowledge not reported in the literature before.

their MS² spectra (6 iterations with the total 4268 unique MS² spectra; persistent background masses removed by FindPFAS), which resulted in 208 potential hits (including

multiples resulting from variance in mass accuracy). This m/z list was compared to the m/z list from KMD analysis to remove overlapping masses and was further reduced by

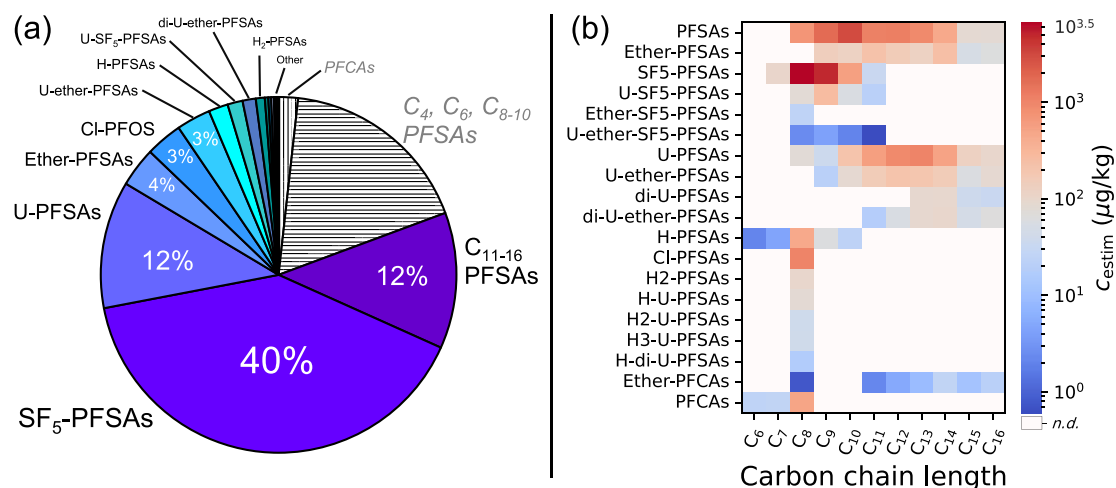


Figure 1. (a) Percentage of identified PFAS classes based on the estimated concentrations of all identified PFAS. Previously identified PFAS in the BS-NRW soil are shown as gray-shaded areas with italic gray labels.^{18,21} New identifications make up more than 77% of the total found PFAS based on c_{estim} . (b) Heatmap of the estimated concentrations (c_{estim} , log scale) for each homologue of the respective compound class. For more details on PFAS structures, see Table 1.

removing $[M + 1]$, $[M + 2]$ (from both ^{34}S and two ^{13}C atoms) isotopes (which are often selected for MS/MS in later iterations if they have very high intensities) as well as dimers and further adducts (adducts and dimers were exported from CEF files (XML) from the MFE) to 40 masses, which were then manually investigated. Finally, the resulting total mass list was used for manual identification. Mass spectrometry fragmentation theory, typical PFAS properties (e.g., negative mass defect, decreasing mass defect with increasing chain length, etc.), and an RT vs total chain length correlation were used to increase confidence (Figure 3). To improve identification performance, an additional Python script was used to automatically annotate MS^2 peaks in the MS^2 spectra of interest with 934 diagnostic fragments for PFAS (collected from Koelmel et al. 2022²²) and assign fragment mass differences of interest, which greatly enhanced the efficiency during manual visual MS^2 spectra inspection. Peaks identified as PFAS were manually checked for being in-source fragments. Due to complex isomeric mixtures (multiple peak maxima), both RTs (see Table S4) and especially peak shapes were compared to exclude potential in-source fragmentation (examples in Figure S3) since for selected overlapping peaks, checking the RT alone is not sufficient. This workflow was similarly applied to the SPE eluate after dTOP oxidation in both negative and positive ionization modes.

RESULTS AND DISCUSSION

Identified PFAS and PFAS Classes. With the application of KMD analysis (MS^1) and FindPFAS (MS^2 fragment mass difference approach), besides previously detected PFAAs, 10 PFAS substance classes with multiple homologues and 7 C_8 -based PFAS could be identified in the BS-NRW soil extract, all of which exclusively comprised sulfonic acids (one exception). This allowed a semi-quantification (c_{estim}) based on PFSA and PFCA calibration standards. In the following, structurally related compounds will be discussed together in decreasing order of their estimated concentration in the soil (for more details, see Table 1 and Figure 1). Further detailed information to support all PFAS identifications (chromatograms and annotated MS/MS spectra) is provided in the SI.

Pentafluorosulfanyl Perfluoroalkyl Sulfonic Acids (SF_5 -PFASs). C_7 – C_{11} SF_5 -PFASs were identified with the highest estimated concentration of $\sum c_{\text{estim}} \sim 12.5 \mu\text{g/g}$ soil with the highest concentrations of the C_8 and C_9 homologues. The sum concentration of SF_5 -PFASs made up more than $\sim 40\%$ of all identified PFAS in the BS-NRW sample. Mixtures of different linear and branched isomers (evidenced by partially separated peaks and MS/MS) were detected, which indicate an electrochemical fluorination-based origin. SF_5 -PFASs showed characteristic CF_2 mass shifts ($= 49.9968 \text{ Da}$) and SF_5^- fragments (EICs and MS/MS details in Figures S4 and S9).

Unsaturated SF_5 -PFASs (U-SF_5 -PFASs) were identified at much lower concentrations ($\sum c_{\text{estim}} \sim 0.4 \mu\text{g/g}$; Figures S5 and S10). Furthermore, a C_8 ether- SF_5 -PFAS was detected with FindPFAS ($c_{\text{estim}} \sim 0.02 \mu\text{g/g}$; Figures S8 and S11) in even lower concentrations and four U-ether- SF_5 -PFAS homologues ($\sum c_{\text{estim}} \sim 9.4 \text{ ng/g}$; Figures S6 and S12) were identified. Figure 2 exemplifies how powerful fragment mass differences are based on a U-ether- SF_5 -PFOS MS/MS spectrum. ΔCF_2 already detects most of the fragments, while matches with 932 PFAS diagnostic fragments miss several peaks because the fragments are not present in the list. U- SF_5 -PFASs were previously identified in an AFFF formulation;²² however, to the best of our knowledge, the occurrence of ether- SF_5 -PFASs and U-ether- SF_5 -PFASs are reported for the first time in the environment, and no entry in PubChem was found. The relative chain length distribution of SF_5 -PFASs was similar to U- SF_5 -PFASs, while the distribution of U- SF_5 -PFASs and U-ether- SF_5 -PFASs was almost identical, which indicates that they are related side products. Since SF_5 -PFASs are perfluorinated and were not transformed in the dTOP assay (see the following section), the unsaturated SF_5 -PFASs are expected to be side products rather than transformation products. In general, PFAS with SF_5 groups were detected in AFFFs and commercial products,^{7,22,23} in biosolids and organic waste,²⁴ as well as in landfill leachates,²⁵ and waste water related to electronics fabrication,²⁶ however, to our knowledge never as the primary PFAS contamination. Barzen-Hanson et al. (2017)⁷ found SF_5 -PFASs in 3M patents from 1992²⁷ and detected them in technical products but not in groundwater. The patent states that their hydrophobic and oleophobic

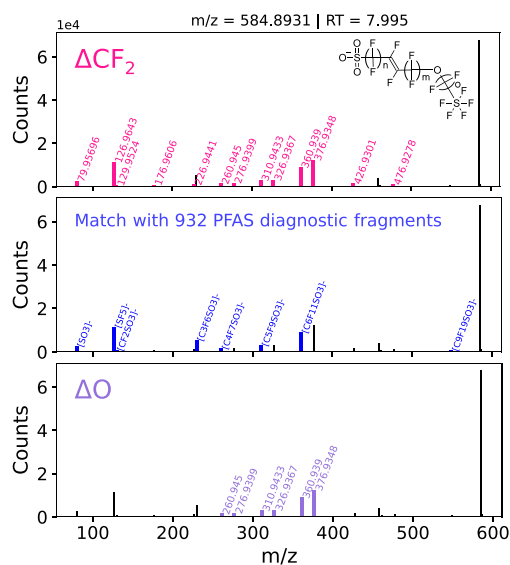


Figure 2. Example of an MS/MS spectrum of an unsaturated-ether-SF₅-perfluorooctanesulfonic acid. Fragments were detected via fragment differences (CF₂, red; O, purple) and matches with a list of diagnostic fragments (blue). It clearly shows how powerful fragment mass differences such as ΔCF₂ are, which can detect almost all fragments.

performance can be even superior to the CF₃ group, making them ideal for repellent coatings for textiles and papers. We found another patent from 1994 by the same authors for the electrochemical production of pentafluorosulfanyl fluorides.²⁸ Due to the fact that SF₅-PFASs seem to be the major PFAS contaminants in the BS-NRW soil, it is reasonable to assume that the contamination of the BS-NRW soil goes back to specific sources and unknown products. Previously reported SF₅-PFAS in environmental samples were minor contaminants compared to other detected PFAS.^{7,25}

Perfluoroalkyl Sulfonic Acids (PFASs). C₄, C₆, and C₈ PFASs were already detected in 2006 in the BS-NRW soil (later also C_{9–10}),^{18,21} in the adjacent creek Steinebecke, in following downstream rivers such as the Möhne River, and in drinking water.¹⁸ With a total concentration of 5.4 μg/g, C₄, C₆, and C₈ PFASs contributed 18% of the identified PFAS, with PFDS being present at the highest concentrations (PFASs were confirmed by authentic reference standards; Figures S4 and S13). Further C_{11–16} PFASs were detected by NTS with a total concentration of 3.8 μg/g (composing 13% of all identifications). Partially co-eluting peaks in the chromatograms hint to linear and branched isomers of all PFASs. We further identified unsaturated PFASs (U-PFASs), which exhibited a dominance of C₈–C₁₆ chain lengths with a total estimated concentration of $\sum c_{\text{estim}} \sim 3.6 \mu\text{g/g}$, which demonstrates their high importance. Their fragmentation patterns confirmed their linear or branched structure but excluded cyclic structures such as perfluoroethylcyclohexane sulfonate or related homologues (commonly known as PFECHS) due to the systematic observation of (CF₂)_nSO₃[−] and F(CF₂)_nC₂F₂[−] fragments with several CF₂ units. U-PFASs were identified as several positional isomers since they likely occurred as mixtures where the double bond position cannot be easily located (EICs and MS/MS in Figures S4 and S14). Furthermore, twice unsaturated PFASs (di-U-PFASs) were detected at $\sum c_{\text{estim}} \sim 0.3 \mu\text{g/g}$ (C₁₃–C₁₆; Figures S6 and S15).

Ether-Perfluoroalkyl Sulfonic Acids (Ether-PFASs). Ether-PFASs were found with $\sum c_{\text{estim}} \sim 1.1 \mu\text{g/g}$ with a similar carbon chain length distribution as U-PFASs (discussed later), while C₁₄-ether-PFSA showed the highest concentrations (EICs and MS/MS in Figures S5 and S16). Ether-PFASs were also identified in their unsaturated form (U-ether-PFASs) at lower concentrations at about 0.9 μg/g (Figures S5 and S17).

Chlorinated Perfluorooctanesulfonic Acid (Cl-PFOS). Cl-PFOS was found with FindPFAS based on MS² fragment mass differences. Only a C₈ homologue with different positional and/or branched isomers was observed ($c_{\text{estim}} \sim 1.0 \mu\text{g/g}$) (EIC and MS/MS in Figures S8 and S18). This indicates that this compound was likely used exclusively as a C₈-based homologue. The position of the Cl was not explicitly determined; however, the fragmentation pattern indicated its position between the third and the fifth C (from the functional group, see Figure S19). However, MS/MS was not acquired over the whole chromatographic peak, allowing more potential Cl-positions. Furthermore, Cl₂-PFOS was detected at approximately two orders of magnitude lower intensity, indicating it to be a potential impurity from synthesis.

Perfluorocarboxylic Acids (PFCAs). C₆–C₈ PFCAs were previously identified in BS-NRW and detected at a concentration of 0.55 μg/g.¹⁸ PFOA (C₈) was the dominating homologue (90% of the concentration), and longer-chained homologues had very low intensities and were therefore excluded in the semi-quantitative estimation (Figures S6 and S20). PFCAs comprised branched isomers observed by several partially co-eluting peaks, suggesting that they may be transformation products of branched precursors. The dominance of PFOA is in good agreement with the potentially degradable polyfluorinated (H-containing) precursors and the results from dTOP oxidation (see the following and next section).

Ether-Perfluorocarboxylic Acids (Ether-PFCAs). C₈ and C₁₁–C₁₆ ether-PFCAs were detected ($\sum c_{\text{estim}} \sim 0.08 \mu\text{g/g}$), with C₁₄ being the main homologue (Figures S7 and S21). Besides PFCAs, ether-PFCAs were the only compound class with a carboxylic acid functional group. They were, therefore, semi-quantified based on PFCAs. Chromatographic separation again indicated branched isomers, which were not investigated in more detail. Due to limited information from the MS/MS spectra, the position of the ether bond could not be determined.

Hydrogen-Substituted PFASs (Potential PFAS Precursors). Several H-substituted PFASs were identified in the BS-NRW soil. H-PFASs (C₆–C₁₀) were the polyfluorinated PFAS detected in the highest estimated concentrations of $\sum c_{\text{estim}}$ of $\sim 0.55 \mu\text{g/g}$ soil with C₈ making up >80% (Figures S7 and S22). Based on MS/MS data only, the position of the hydrogen could not be determined. H₂-PFOS (or *n*:1 PFOS, $c_{\text{estim}} \sim 0.1 \mu\text{g/g}$) and H-U-PFOS ($c_{\text{estim}} \sim 0.08 \mu\text{g/g}$) were detected via FindPFAS because no further homologues were observed (Figures S8, S23, and S24). Furthermore, U-H₃-PFOS U-H₂-PFOS and H-di-U-PFOS were identified in estimated concentrations of ~ 0.04 , ~ 0.04 , and $\sim 0.02 \mu\text{g/g}$, respectively (Figures S8 and S25–S27). In each case, the position of the H atoms could not be readily determined due to complex isomeric mixtures.

All above-discussed PFAS are classified as identification level 2b according to Charbonnet et al. (2022).²⁹ We are aware that our identifications are limited by the exact positions of double

bonds and/or hydrogen or chlorine atoms. But we still assigned identification level 2b because from an environmental point of view, each isomer has to be added to the contamination. Further evidence is provided by numerous matching fragment mass differences (FindPFD Δ S) and a strong match of the RT with the RT model (Figure 3). ESI measurements in the positive mode did not lead to any meaningful identification.

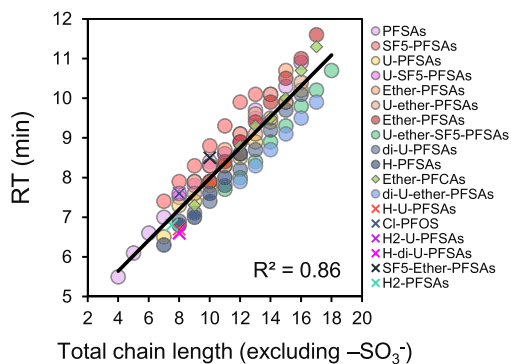


Figure 3. Correlation of total chain length (including ether bonds and SF₅ groups, excluding the charge-carrying polar sulfonic acid group and the carboxylic acid group in the case of ether-PFCAs) and chromatographic retention time (RT). Single substances are marked as crosses, and the only class with a carboxylic acid group is marked as diamonds. Besides accurate mass, MS/MS evidence from fragment mass differences and diagnostic fragments, and characteristic CF₂ mass shifts, the strong correlation for all identified compounds ($R^2 = 0.86$) provides further confidence in the form of a simple RT vs chain length model. Note that small peaks of further homologues were partially included in the correlation, while they were excluded from semi-quantification.

Interestingly, the dominant semi-quantified part of the identified PFAS (>97%) was perfluorinated and is, therefore, not expected to degrade in a short time frame on the contaminated soil in BS-NRW. This is of particular importance because the fraction of previously unknown PFAS on this site corresponds to over ~75% of all reported PFAS. Only six classes that make up approximately 3% of all semi-quantified PFAS in the sample are polyfluorinated and may potentially act as precursors on this field site (Table 1). Therefore, an estimated 3% of the overall contamination seems to continuously produce PFCAs over time. Due to slow biotransformation, this PFCA supply was also suspected to be the cause of long-term tailings in column tests observed by Röhler et al. (2021).²¹ The fact that most of the H-containing PFAS are C₈-based is in good agreement with the observed PFCA formation during the dTOP assay oxidation. Further details on degradability and persistence are discussed in the following TOP assay section.

dTOP Assay NTS and PFAS Stability. We performed NTS of soil samples after dTOP (postTOP) and in comparison to the non-oxidized extract (preTOP). Therefore, we examined the stability of all identified PFAS during dTOP by comparing their peak intensities in the original soil extract to those after dTOP. An NTS workflow was used to find potential unknown PFAS oxidation products, which may be present in addition to the well-investigated PFCAs and PFSAs.

Due to the general aqueous experimental setup of the dTOP assay, we observed a high chain length discrimination for all

identified perfluorinated PFAS (Figure 4), which expressed itself in a decreasing $A_{\text{postTOP}}/A_{\text{preTOP}}$ ratio with increasing

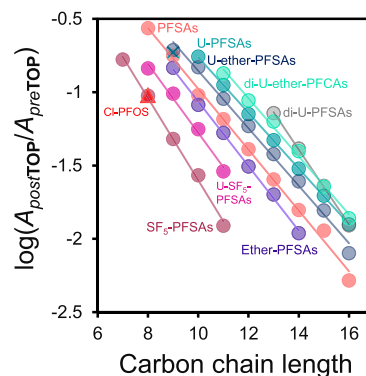


Figure 4. Correlation of the logarithmic ratio of peak areas of identified PFAS after dTOP oxidation (SPE eluate) and before dTOP (soil extract) with carbon chain length ($R^2 > 0.98$). The decreasing trend of $\log(A_{\text{postTOP}}/A_{\text{preTOP}})$ with increasing chain length represents the increasing loss of PFAS due to sorption to soil particles. Similar sorption relationships (linear relationship of $\log K_d$ vs carbon chain length) were often observed for PFAAs, supporting the idea of sorption rather than transformation.^{31,32} Note: Teal X indicates an outlier of the di-U-ether-PFCAs, which likely resulted from rather small chromatographic peaks.

chain length. This observation was not unexpected, which is why PFAAs are typically corrected by internal standards in order to correct this loss during the TOP assay.^{13,30} However, since reference standards are not available for most of our identified PFAS, such a correction was not possible. Due to the strong correlation of $\log(A_{\text{postTOP}}/A_{\text{preTOP}})$ with the PFAS carbon chain lengths, we conclude that sorption was the reason for decreasing intensities postTOP with increasing chain length rather than oxidation. Similar relationships were typically observed for PFAAs in sorption experiments ($\log K_d$ vs chain length).^{31,32} We also see a clear trend for the sorption behavior for different PFSAs, which may be useful for further investigations. At a given carbon chain length, a decreasing sorption can be observed in the order from SF₅-PFSAs, U-SF₅-PFSAs, ether-PFSAs, PFSAs, U-ether-PFSAs, U-PFSAs to di-U-ether-PFCAs, resulting in more than an order of magnitude difference of the $A_{\text{postTOP}}/A_{\text{preTOP}}$ ratio between SF₅-PFSAs and di-U-ether-PFCAs for this specific soil sample. Since most perfluorinated PFAS are typically not transformed by OH-radical-initiated reactions, sorptive losses to soil during the dTOP assay are reasonable and further confirm the hypotheses.

Furthermore, polyfluorinated PFAS (e.g., H-PFSAs, H₂-PFSAs, H₃-PFSAs, etc.) have not been found after dTOP oxidation, which reveals their potential for complete oxidation. Furthermore, this corroborates correct compound assignments since all proposed structures offer favorable attack sites for OH radicals (e.g., H atoms). From an analytical point of view, it is very important that polyfluorinated compounds made up only ~3% of all identified PFAS in the soil. As such, this reveals that >77% (based on our identifications) of the contamination was hidden prior to our NTS approach. Neither target analysis nor TOP assay or a combination of both would unravel the identity or quantity of those PFAS, highlighting the high importance of applying NTS approaches. To counteract the highlighted flaws of the TOP assay, we emphasize the

importance of internal standard correction and suggest an additional extraction step of the remaining soil particles after the dTOP assay with an appropriate organic solvent in the original vessel. It must be noted that even a correction with internal standards cannot account for possible differences that occur between spiking PFAAs directly to the dTOP assay solution and “aged” PFAAs, which were sorbed to the soil already for many years.

Besides PFAA formation, NTS after dTOP oxidation revealed C_6 – C_{10} perfluoroalkyl diacids with a carboxylic and a sulfonic acid group (PFCSA), which were found by KMD analysis. In MS/MS, they showed both a neutral loss of CO_2 and an abundant SO_3^- fragment as expected from the two functional groups. The RTs of these PFCASAs were much shorter than for both PFCAs and PFSAs, which likely results from two charges due to proton dissociation in solution. We estimated their concentration (based on $[M - H]^-$ and $[M - H - CO_2HF]^-$ ions) after dTOP to ~ 41 ng/g, which is slightly less than the formation of PFSAs (≈ 64 ng/g).¹⁹ This demonstrates that besides PFCAs and PFSAs, other TPs can become important in the TOP assay. Röhler et al. (2022) estimated 2.2 mg/kg precursors in the soil of BS-NRW based on PFAA formation after dTOP.¹⁹ In total, our semi-quantitative approach estimated oxidizable, polyfluorinated precursors at 0.82 mg/kg, which is at a rather similar level (about 37% of 2.2 mg/kg). Two possible reasons could cause the discrepancy between both approaches: (i) the occurrence of further precursors not captured by our NTS approach or (ii) systematic errors in the semi-quantitative approach, which commonly lead to differences in the estimated concentrations in the range of a factor of two.

Fragment Mass Differences vs Diagnostic Fragments vs Homologous Series. In this work, we combined established PFAS-screening methods, such as homologous series detection and diagnostic fragment screening, with our novel approach of mass difference screening (FindPFAS).²⁰ To illustrate the possibilities and limitations between the usage of a diagnostic fragment database (here mainly the list from Koelmel et al. (2022)²² with 872 F-containing fragments) and fragment mass differences (14 mass differences), we performed a simple comparison by using an HRMS/MS datafile from the PFAS-contaminated soil extract. In the first iterative measurement of the soil extract, 65 precursor masses were found by both approaches plus 17 only by fragment mass differences and plus 5 only by diagnostic fragments. Within the MS/MS fragmentation patterns in all detected precursor masses, 148 fragments were found by both approaches; in addition, 203 fragments were only found by the 14 mass differences and 73 fragments were only found by diagnostic fragments (Figure 5). These numbers illustrate that a combination of both approaches is most efficient and can explain more fragments than each single approach on its own. Furthermore, screening for mass differences with FindPFAS found the same compound classes that were also detected as homologous series; however, it further detected single substances. This underlines the effectiveness of the mass difference approach and opens new possibilities in the identification of PFAS that do not occur as homologous series.

Environmental Implications. Previous studies included target analysis coupled with the TOP assay to estimate the overall pollution of contaminated sites. Skutlarek et al. (2006) found that PFOA was the major contaminant among the investigated PFAAs in surface waters downstream of the BS-

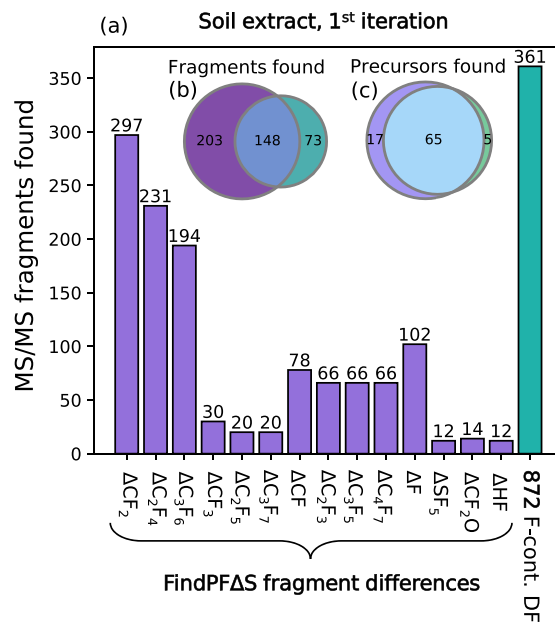


Figure 5. Exemplary comparison of two approaches to detect PFAS fragments in ddMS² data of the BS-NRW soil extract: based on fragment mass differences or on a list of diagnostic fragments (DFs). (a) Number of detected fragments based on 14 characteristic mass differences (violet) or on 872 fluorine-containing DFs (teal). (b) Comparison of unique detected fragments by both approaches: 203 unique fragments were only detected via mass differences, 148 were found by both approaches, and 73 only by the list of DFs. (c) Number of precursor masses of the MS/MS spectra that were either found exclusively by mass differences, DFs, or by both approaches. Since a fragment mass difference is always made up of two fragments, the criteria for positive assignment of precursor MS/MS spectra via diagnostic fragments were also set to two fragments. To keep false-positive fragments or mass differences as small as possible, the mass tolerance was 1 mDa and the intensity threshold of the fragments was at a minimum of 3000 counts.

NRW site.¹⁸ Sixteen years later, we discovered that PFCAs had much lower soil concentrations than many other PFAS. In our study, we showed that NTS revealed major, previously unknown contaminants that supposedly contaminated the whole ecosystem and potentially also found their way into nearby drinking water, showing that TOP and target analysis are insufficient to characterize the PFAS burden in this type of contamination.

Advanced analytical screening techniques are essential to identify and characterize contaminated field sites to further estimate the overall pollution. However, this does not address the root of the problem: the disposal of contaminated waste on agricultural soils like the herein-discussed BS-NRW site or other PFAS-impacted sites (e.g., the Rastatt case in SW Germany). These examples reveal the problematic nature of material recycling promoted by circular economy. During the recycling of material streams, unintended recycling of persistent contaminants has to be excluded. But this is rather challenging due to analytical limitations in detecting and identifying all trace organic compounds. The application of the precautionary principle may even prevent material recycling on agricultural soils like this is already largely practiced for sewage sludge (e.g., in Baden-Württemberg and other countries). To protect soil, groundwater, and drinking water, the discharge of

PFAS into the environment has to be considered as an issue of highest priority and must be discontinued.³³

■ ASSOCIATED CONTENT

SI Supporting Information

The Supporting Information is available free of charge at <https://pubs.acs.org/doi/10.1021/acs.est.2c07969>.

S1: Chemicals, reagents, and sample preparation. S2: Nontarget screening. Tables S1 and S2: Instrument parameters. Table S3: Matrix effects. Figure S1: Calibration curve extrapolation. Figure S2: Fragment mass differences. Figure S3: Peak shape comparison. Table S4: Retention times. Figures S4–S8: Extracted ion chromatograms. Figures S9–S27: Mass spectra (PDF)

■ AUTHOR INFORMATION

Corresponding Author

Christian Zwiener – Environmental Analytical Chemistry, Department of Geosciences, University of Tübingen, 72076 Tübingen, Germany; orcid.org/0000-0002-6682-5828; Email: christian.zwiener@uni-tuebingen.de

Authors

Jonathan Zweigle – Environmental Analytical Chemistry, Department of Geosciences, University of Tübingen, 72076 Tübingen, Germany; orcid.org/0000-0002-7194-1567

Boris Bugsel – Environmental Analytical Chemistry, Department of Geosciences, University of Tübingen, 72076 Tübingen, Germany; orcid.org/0000-0001-9752-9741

Klaus Röhler – Hydrogeochemistry, Department of Geosciences, University of Tübingen, 72076 Tübingen, Germany; orcid.org/0000-0002-7657-9579

Alexander Arthur Haluska – Hydrogeochemistry, Department of Geosciences, University of Tübingen, 72076 Tübingen, Germany

Complete contact information is available at: <https://pubs.acs.org/10.1021/acs.est.2c07969>

Author Contributions

J.Z. and B.B. contributed equally to this work and share first authorship.

Notes

The authors declare no competing financial interest.

■ ACKNOWLEDGMENTS

The authors acknowledge the DBU (Deutsche Bundesstiftung Umwelt) for the scholarship of J.Z. and funding of the project FluorTECH by the state of Baden-Württemberg (BWPF 19010).

■ REFERENCES

- (1) Kissa, E., *Fluorinated surfactants and repellents*, 2nd ed.; Marcel Dekker: New York, NY, 2001.
- (2) Wang, Z.; Buser, A. M.; Cousins, I. T.; Demattio, S.; Drost, W.; Johansson, O.; Ohno, K.; Patlewicz, G.; Richard, A. M.; Walker, G. W.; White, G. S.; Leinala, E. A new OECD definition for per- and polyfluoroalkyl substances. *Environ. Sci. Technol.* **2021**, *55*, 15575–15578.
- (3) PubChem PubChem: PFAS and Fluorinated Compounds in PubChem. <https://pubchem.ncbi.nlm.nih.gov/classification/#hid=120> (accessed Oct 24, 2022).
- (4) Glüge, J.; Scheringer, M.; Cousins, I.; DeWitt, J. C.; Goldenman, G.; Herzke, D.; Lohmann, R.; Ng, C.; Trier, X.; Wang, Z. An overview

of the uses of per- and polyfluoroalkyl substances (PFAS). *Environ. Sci.: Processes Impacts* **2020**, *22*, 2345–2373.

(5) Schellenberger, S.; Liagkouridis, I.; Awad, R.; Khan, S.; Plassmann, M.; Peters, G.; Benskin, J. P.; Cousins, I. T. An Outdoor Aging Study to Investigate the Release of Per- and Polyfluoroalkyl Substances (PFAS) from Functional Textiles. *Environ. Sci. Technol.* **2022**, *56*, 3471–3479.

(6) Trier, X.; Taxvig, C.; Rosenmai, A. K.; Pedersen, G. A. *PFAS in paper and board for food contact: Options for risk management of poly- and perfluorinated substances*. Nordic Council of Ministers, 2018.

(7) Barzen-Hanson, K. A.; Roberts, S. C.; Choyke, S.; Oetjen, K.; McAlees, A.; Riddell, N.; McCrindle, R.; Ferguson, P. L.; Higgins, C. P.; Field, J. A. Discovery of 40 Classes of Per- and Polyfluoroalkyl Substances in Historical Aqueous Film-Forming Foams (AFFFs) and AFFF-Impacted Groundwater. *Environ. Sci. Technol.* **2017**, *51*, 2047–2057.

(8) Bugsel, B.; Zwiener, C. LC-MS screening of poly- and perfluoroalkyl substances in contaminated soil by Kendrick mass analysis. *Anal. Bioanal. Chem.* **2020**, *412*, 4797–4805.

(9) McCord, J.; Strynar, M. Identification of Per- and Polyfluoroalkyl Substances in the Cape Fear River by High Resolution Mass Spectrometry and Nontargeted Screening. *Environ. Sci. Technol.* **2019**, *53*, 4717–4727.

(10) Washington, J. W.; Rosal, C. G.; McCord, J. P.; Strynar, M. J.; Lindstrom, A. B.; Bergman, E. L.; Goodrow, S. M.; Tadesse, H. K.; Pilant, A. N.; Washington, B. J.; Davis, M. J.; Stuart, B. G.; Jenkins, T. M. Nontargeted mass-spectral detection of chloroperfluoropolyether carboxylates in New Jersey soils. *Science* **2020**, *368*, 1103–1107.

(11) Shoemaker, J.; Tettenhorst, D., *Method 537.1: Determination of Selected Per- and Polyfluorinated Alkyl Substances in Drinking Water by Solid Phase Extraction and Liquid Chromatography/Tandem Mass Spectrometry (LC/MS/MS)*; US Environmental Protection Agency, Office of Research and Development, National Center for Environmental Assessment: Washington, DC, 2018.

(12) Houtz, E. F.; Sedlak, D. L. Oxidative conversion as a means of detecting precursors to perfluoroalkyl acids in urban runoff. *Environ. Sci. Technol.* **2012**, *46*, 9342–9349.

(13) Janda, J.; Nödler, K.; Brauch, H.-J.; Zwiener, C.; Lange, F. T. Robust trace analysis of polar (C 2-C 8) perfluorinated carboxylic acids by liquid chromatography-tandem mass spectrometry: method development and application to surface water, groundwater and drinking water. *Environ. Sci. Pollut. Res.* **2019**, *26*, 7326–7336.

(14) Nikiforov, V. A. Hydrolysis of FTOH precursors, a simple method to account for some of the unknown PFAS. *Chemosphere* **2021**, *276*, No. 130044.

(15) Zweigle, J.; Bugsel, B.; Capitain, C.; Zwiener, C. PhotoTOP: PFAS Precursor Characterization by UV/TiO₂ Photocatalysis. *Environ. Sci. Technol.* **2022**, *56*, 15728–15736.

(16) Göckener, B.; Lange, F. T.; Lesmeister, L.; Gökçe, E.; Dahme, H. U.; Bandow, N.; Biegel-Engler, A. Digging deep—implementation, standardisation and interpretation of a total oxidisable precursor (TOP) assay within the regulatory context of per- and polyfluoroalkyl substances (PFASs) in soil. *Environmental Sciences. Europe* **2022**, *34*, 52.

(17) Zhang, C.; Hopkins, Z. R.; McCord, J.; Strynar, M. J.; Knappe, D. R. U. Fate of Per- and Polyfluoroalkyl Ether Acids in the Total Oxidizable Precursor Assay and Implications for the Analysis of Impacted Water. *Environ. Sci. Technol. Lett.* **2019**, *6*, 662–668.

(18) Skutlarek, D.; Exner, M.; Farber, H. Perfluorinated surfactants in surface and drinking waters. *Environ. Sci. Pollut. Res. Int.* **2006**, *13*, 299–307.

(19) Röhler, K.; Haluska, A. A.; Abramov, S.; Thompson, K.; Straub, D.; Kleindienst, S.; Bugsel, B.; Zweigle, J.; Zwiener, C.; Grathwohl, P. PFAS on a contaminated soil site in Germany: Comparison of laboratory batch incubation- and field-derived release rates. (unpublished manuscript 04/2023)

(20) Zweigle, J.; Bugsel, B.; Zwiener, C. FindPFAS: Non-Target Screening for PFAS - Comprehensive Data Mining for MS2 Fragment Mass Differences. *Anal. Chem.* **2022**, *94*, 10788–10796.

(21) Röhler, K.; Haluska, A. A.; Susset, B.; Liu, B.; Grathwohl, P. Long-term behavior of PFAS in contaminated agricultural soils in Germany. *J. Contam. Hydrol.* **2021**, *241*, No. 103812.

(22) Koelmel, J. P.; Stelben, P.; McDonough, C. A.; Dukes, D. A.; Aristizabal-Henao, J. J.; Nason, S. L.; Li, Y.; Sternberg, S.; Lin, E.; Beckmann, M.; Williams, A. J.; Draper, J.; Finch, J. P.; Munk, J. K.; Deigl, C.; Rennie, E. E.; Bowden, J. A.; Godri Pollitt, K. J. FluoroMatch 2.0-making automated and comprehensive non-targeted PFAS annotation a reality. *Anal. Bioanal. Chem.* **2022**, *414*, 1201–1215.

(23) Young, R. B.; Pica, N. E.; Sharifan, H.; Chen, H.; Roth, H. K.; Blakney, G. T.; Borch, T.; Higgins, C. P.; Kornuc, J. J.; McKenna, A. M.; Blotevogel, J. PFAS Analysis with Ultrahigh Resolution 21T FT-ICR MS: Suspect and Nontargeted Screening with Unrivaled Mass Resolving Power and Accuracy. *Environ. Sci. Technol.* **2022**, *56*, 2455–2465.

(24) Munoz, G.; Michaud, A. M.; Liu, M.; Vo Duy, S.; Montenach, D.; Resseguier, C.; Watteau, F.; Sappin-Didier, V.; Feder, F.; Morvan, T.; Houot, S.; Desrosiers, M.; Liu, J.; Sauve, S. Target and Nontarget Screening of PFAS in Biosolids, Composts, and Other Organic Waste Products for Land Application in France. *Environ. Sci. Technol.* **2021**, *56*, 6056–6068.

(25) Maldonado, V. Y.; Schwichtenberg, T.; Schmokel, C.; Witt, S. E.; Field, J. A. Electrochemical Transformations of Perfluoroalkyl Acid (PFAA) Precursors and PFAAs in Landfill Leachates. *ACS ES&T Water* **2022**, *2*, 624–634.

(26) Jacob, P.; Barzen-Hanson, K. A.; Helbling, D. E. Target and nontarget analysis of per- and polyfluoroalkyl substances in wastewater from electronics fabrication facilities. *Environ. Sci. Technol.* **2021**, *55*, 2346–2356.

(27) Hansen, J. C.; Savu, P. M. Higher pentafluorosulfanyl-fluoroaliphatic carbonyl and sulfonyl fluorides, and derivatives. *U.S. Patent* 1992, *5*, 159,105.

(28) Hansen, J. C.; Savu, P. M. Electrochemical production of higher pentafluorosulfanyl acid fluorides. *U.S. Patent* 1994, *5*, 286,352.

(29) Charbonnet, J. A.; McDonough, C. A.; Xiao, F.; Schwichtenberg, T.; Cao, D.; Kaserzon, S.; Thomas, K. V.; Dewapriya, P.; Place, B. J.; Schymanski, E. L.; Field, J. A.; Helbling, D. E.; Higgins, C. P. Communicating Confidence of Per- and Polyfluoroalkyl Substance Identification via High-Resolution Mass Spectrometry. *Environ. Sci. Technol. Lett.* **2022**, *9*, 473–481.

(30) Göckener, B.; Fliedner, A.; Rüdell, H.; Fettig, I.; Koschorreck, J. Exploring unknown per- and polyfluoroalkyl substances in the German environment—The total oxidizable precursor assay as helpful tool in research and regulation. *Sci. Total Environ.* **2021**, *782*, No. 146825.

(31) Higgins, C. P.; Luthy, R. G. Sorption of perfluorinated surfactants on sediments. *Environ. Sci. Technol.* **2006**, *40*, 7251–7256.

(32) Guelfo, J. L.; Higgins, C. P. Subsurface transport potential of perfluoroalkyl acids at aqueous film-forming foam (AFFF)-impacted sites. *Environ. Sci. Technol.* **2013**, *47*, 4164–4171.

(33) Cousins, I. T.; Johansson, J. H.; Salter, M. E.; Sha, B.; Scheringer, M. Outside the Safe Operating Space of a New Planetary Boundary for Per- and Polyfluoroalkyl Substances (PFAS). *Environ. Sci. Technol.* **2022**, *56*, 11172–11179.

Recommended by ACS

Centurial Persistence of Forever Chemicals at Military Fire Training Sites

Bridger J. Ruyle, Elsie M. Sunderland, *et al.*

MAY 15, 2023

ENVIRONMENTAL SCIENCE & TECHNOLOGY

READ 

The Total Oxidizable Precursor (TOP) Assay as a Forensic Tool for Per- and Polyfluoroalkyl Substances (PFAS) Source Apportionment

Edmund H. Antell, David L. Sedlak, *et al.*

JULY 05, 2023

ACS ES&T WATER

READ 

Per- and Polyfluoroalkyl Substances (PFAS) in the Fountain Creek Watershed, Colorado Springs, CO, USA: A Yearlong Investigation of PFAS Levels in Water, Soils, and Sediments

Jose Caleb Quezada Davalos, Janel E. Owens, *et al.*

DECEMBER 07, 2022

ACS ES&T WATER

READ 

Software Comparison for Nontargeted Analysis of PFAS in AFFF-Contaminated Soil

Sara L. Nason, Krystal J. Godri Pollitt, *et al.*

NOVEMBER 23, 2020

JOURNAL OF THE AMERICAN SOCIETY FOR MASS SPECTROMETRY

READ 

Get More Suggestions >

Supporting Information

PFAS-Contaminated Soil Site in Germany: Nontarget Screening before and after Direct TOP Assay by Kendrick Mass Defect and FindPFAS

Jonathan Zweigle,^{+||} Boris Bugsel,^{+||} Klaus Röhler,[‡] Alexander Arthur Haluska,[‡]
Christian Zwiener^{+,*}

⁺Environmental Analytical Chemistry, Department of Geosciences, University of Tübingen,
Schnarrenbergstraße 94-96, 72076 Tübingen, Germany

[‡]Hydrogeochemistry, Department of Geosciences, University of Tübingen, Schnarrenbergstraße 94-
96, 72076 Tübingen, Germany

^{||}The authors contributed equally to this work and share first authorship.

*Corresponding author.

Contents

S1 CHEMICALS, REAGENTS, AND SAMPLE PREPARATION.....	2
Solid phase extraction.....	2
S2 NON-TARGET SCREENING.....	2
Table S 1: Gradient elution of the HPLC-QTOF method.....	2
Table S 2: Summary of instrument and scan source parameters.....	3
Table S 3: Quantification of matrix effects for selected PFCAs and PFASs in the 1:10 diluted soil extract.....	3
Figure S 1: Regression of the slopes of calibration curves.....	3
FindPFAS:.....	4
Figure S 2: Frequent fragment mass differences.....	4
Figure S 3: Comparison of selected peak shapes to distinguish individual compounds from in-source fragmentation.....	4
Table S 4: Retention times (RTs) of all identified PFAS.....	5
Figure S 4: Extracted ion chromatograms (EICs).....	6
Figure S 5: Extracted ion chromatograms (EICs).....	7
Figure S 6: Extracted ion chromatograms (EICs).....	8
Figure S 7: Extracted ion chromatograms (EICs).....	9
Figure S 8: Extracted ion chromatograms (EICs).....	10
Figure S 9: Fragmentation spectrum of m/z 606.8967.....	10
Figure S 10: Fragmentation spectrum of m/z 618.8970.....	11
Figure S 11: Fragmentation spectrum of m/z 622.8920.....	11
Figure S 12: Fragmentation spectrum of m/z 634.8953.....	12
Figure S 13: Fragmentation spectrum of m/z 498.9298.....	12
Figure S 14: Fragmentation spectrum of m/z 460.9334.....	13
Figure S 15: Fragmentation spectrum of m/z 722.9180.....	13
Figure S 16: Fragmentation spectrum of m/z 564.9218.....	14
Figure S 17: Fragmentation spectrum of m/z 526.9251.....	14
Figure S 18: Fragmentation spectrum of m/z 514.9010.....	15
Figure S 19: Fragmentation spectrum of Cl-PFOS.....	15
Figure S 20: Fragmentation spectrum of m/z 412.9664.....	16
Figure S 21: Fragmentation spectrum of m/z 828.9354.....	16
Figure S 22: Fragmentation spectrum of m/z 480.9396.....	17
Figure S 23: Fragmentation spectrum of m/z 462.9490.....	17

46	Figure S 24: Fragmentation spectrum of m/z 442.9427	18
47	Figure S 25: Fragmentation spectrum of m/z 406.9620	18
48	Figure S 26: Fragmentation spectrum of m/z 424.9520	19
49	Figure S 27: Fragmentation spectrum of m/z 404.9460	19
50	NOTES	20
51	REFERENCES	20
52		

S1 Chemicals, reagents, and sample preparation

Water, methanol (MeOH), ammonium acetate (NH₄Ac) were LC-MS grade and purchased from Fisher scientific. The origin of perfluoroalkyl sulfonic acids (PFSAs; C₄ – C₁₀ and C₁₂) and perfluoroalkyl carboxylic acids (PFCAs; C₄ – C₁₄ and C₁₆) for semi-quantification of identified PFAS was Wellington laboratories.

Solid phase extraction

The cartridges (Chromabond HR-XAW, 3mL, 200 mg, Macherey-Nagel) were conditioned with 6 mL of 0.1 % NH₄OH in MeOH with 3 mL of MeOH and 6 mL H₂O. The samples were passed through the cartridge using a vacuum at approximately one drop per second. Afterward, the cartridges were washed with 6 mL H₂O and sucked dry under vacuum until visually no liquid was left. Elution was achieved with 3 mL MeOH and 6 mL of MeOH with 0.1 % NH₄.

S2 Non-target screening

Table S 1: Gradient elution of the HPLC-QTOF method. A = 95/5 H₂O/MeOH + 2 mM NH₄Ac and B = 95/5 MeOH/H₂O + 2 mM NH₄Ac.

Time (min)	A (%)	B (%)
0	85	15
2.0	30	70
5.0	10	90
10.0	0	100
15.0	0	100
15.1	85	15
22.0	85	15

68 **Table S 2:** Summary of instrument and scan source parameters used for HPLC-QTOF measurements.

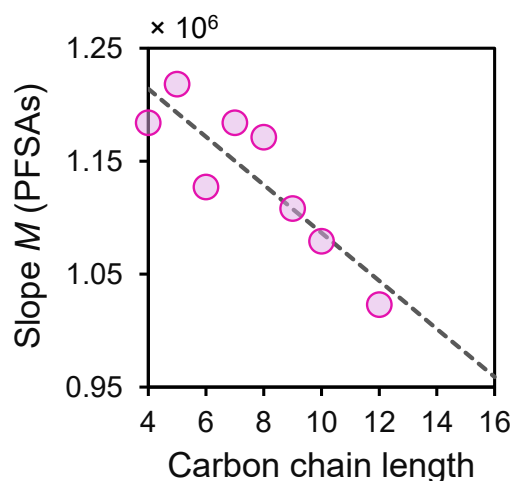
Instrument Parameters	
Gas Temp (°C)	150
Gas Flow (L/min)	16
Nebulizer pressure (psig)	35
Sheath gas temperature (°C)	380
Sheath gas flow (L/min)	12
Fragmentor voltage (V)	380
Scan Source Parameter	
Capillary voltage (V)	3000
Nozzle voltage (V)	300

69

70 **Table S 3:** Quantification of matrix effects for selected PFCAs and PFSA in the 1:10 diluted soil extract. A
 71 blank sample and the soil extract were spike with the internal standards (Origin: Wellington laboratories) and
 72 measured in duplicates to calculate the matrix effect.

Compound	Internal standard	Matrix effect
PFPeA	M5PFPeA	108 ± 7%
PFHxA	M5PFHxA	108 ± 6%
PFHpA	M4PFHpA	107 ± 5%
PFOA	M8PFOA	105 ± 9%
PFNA	M9PFNA	101 ± 3%
PFDA	M6PFDA	107 ± 1%
PFUdA	M7PFUdA	93 ± 1%
PFDoA	MPFDoA	96 ± 2%
PFTeDA	M2PFTeDA	98 ± 2%
PFBS	M3PFBS	112 ± 9%
PFHxS	M3PFHxS	110 ± 6%
PFOS	M8PFOS	104 ± 4%

73



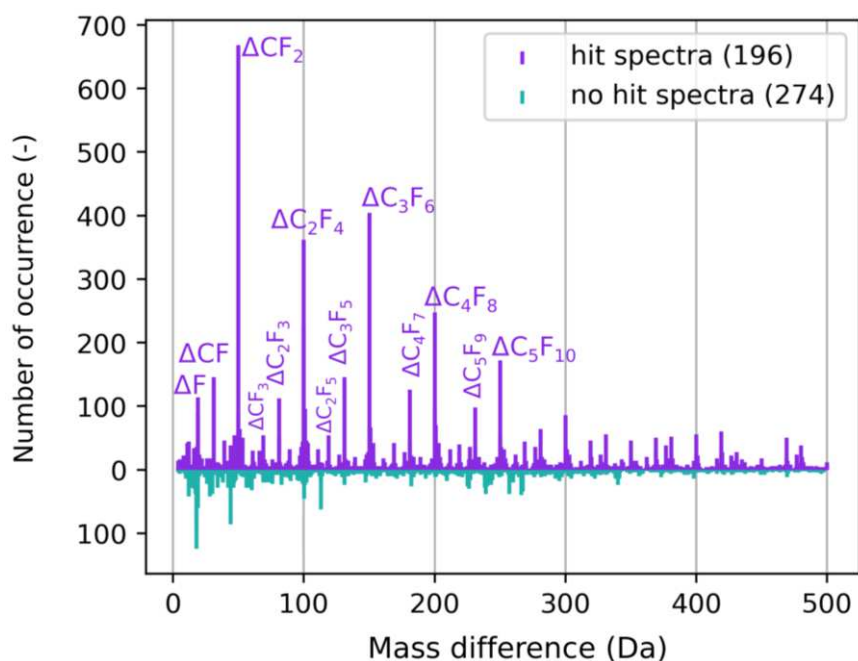
74

75 **Figure S 1:** Regression of the slopes of calibration curves (0.1, 1, 5, 10 and 20 µg/L) of C₄–C₁₀ and C₁₂ PFASs
 76 from a PFAA reference standard mixture. Note that the responses of PFASs were not strongly chain length
 77 dependent. PFAS with a sulfonic acid group and chain lengths from C₄ to C₁₆ were semi-quantified with intra-
 78 and extrapolated slopes.

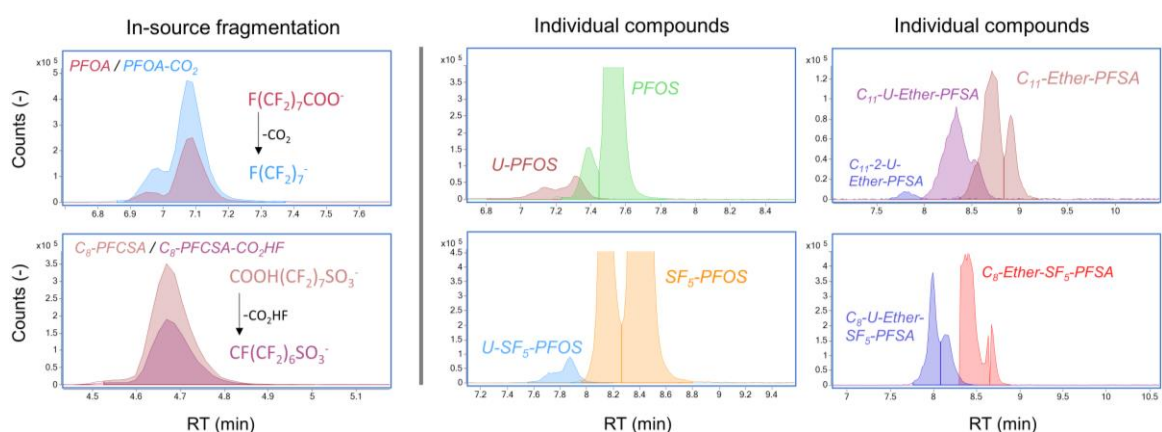
79

80 **FindPFAS:**

81 To find the most relevant fragment mass differences in the BS-NRW soil extract the most
 82 frequent mass differences in spectra that have e.g. several $\Delta(\text{CF}_2)_n$ were plotted (Figure S2).
 83 The resulting differences and selected others (ΔSF_5 , $\Delta\text{CF}_2\text{O}$, and ΔHF) were then used for
 84 NTS. For further details on FindPFAS see Zweigle et al. 2022.³



85 **Figure S 2:** Frequent fragment mass differences in 196 MS/MS spectra in the first iteration of the soil extract
 86 potentially identified as PFAS with FindPFAS vs. not as hits classified spectra (274). The most frequent mass
 87 differences were $\Delta(\text{CF}_2)_n$, $\Delta\text{CF}(\text{CF}_2)_n$, $\Delta\text{CF}_3(\text{CF}_2)_n$, and ΔF . Besides those fragments which are powerful to
 88 generally find compounds that are likely PFAS, there are more specific differences such as ΔSF_5 which further
 89 help in structure elucidation.
 90

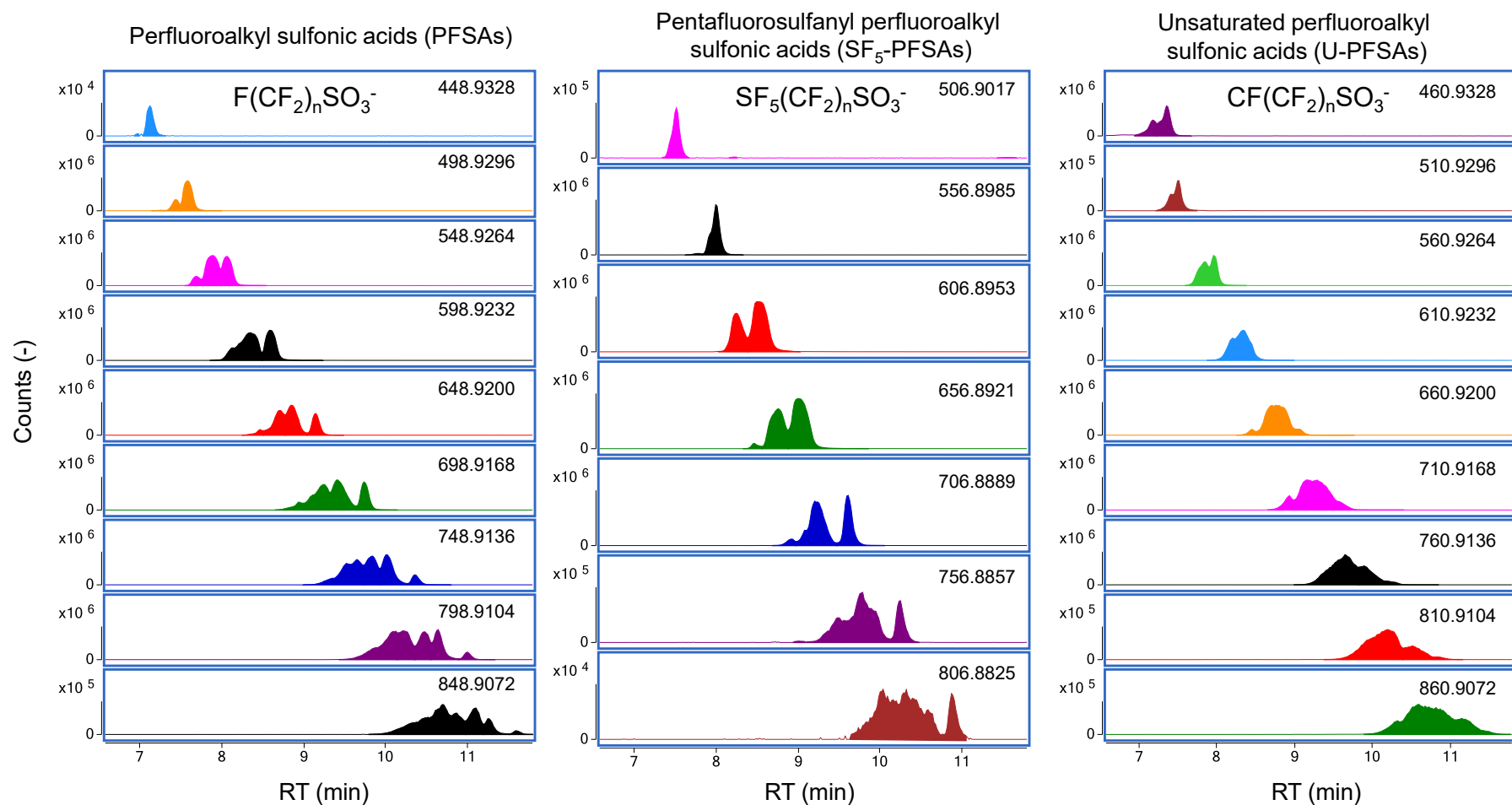


91 **Figure S 3:** Comparison of selected peak shapes to distinguish individual compounds from in-source
 92 fragmentation. The left two subplots are examples of the co-elution of typical in-source fragments of PFCAs and
 93 PFCSAs, while the right four show distinct differences of peak shapes and RT for unsaturated PFAS compared
 94 to potential saturated PFAS precursors, which clearly disprove the unsaturated PFAS as in-source fragments of
 95 the saturated PFAS. Note that from peaks with multiple maxima from complex isomeric mixtures RT alone is
 96 often an insufficient criterion.
 97

99 **Table S 4:** Retention times (RTs) (min) of all identified PFAS. It is important to note that due to complex isomeric mixtures for selected compounds (see e.g., longer chain PFCAs
 100 in Figure S4) no unique RT can be determined (here we chose the peak center) since those isomeric mixture can result in multiple peak maxima. Therefore, peak shapes together
 101 with RT should always be checked carefully to clearly distinguish in-source fragmentation from coelution of individual compounds (for examples see Figure S3).

Carbon chain length	PFSAs	SF ₅ -PFSAs	U-PFSAs	U-SF ₅ -PFSAs	Ether-PFSAs	U-ether-PFSAs	di-U-PFSAs	H ₂ -PFSAs	H-U-PFSAs	Cl-PFOS	H-PFSAs
C ₆		7.7									5.9
C ₇	7.1	8.0	7.2	7.6							6.4
C ₈	7.6	8.4	7.5	7.9			7.0	6.9	6.8	7.6	6.9
C ₉	8.0	8.9	7.9	8.4	8.0	7.7					7.2
C ₁₀	8.3	9.2	8.2	8.8	8.4	8.0	7.5				7.7
C ₁₁	8.9	9.7	8.8	9.2	8.9	8.4	7.8				8.1
C ₁₂	9.4	10.2	9.2	9.7	9.4	9.0	8.4				8.6
C ₁₃	9.9		9.8		9.9	9.4	8.7				
C ₁₄	10.4		10.2		10.5	9.9	9.2				
C ₁₅	10.9		10.7		11.0	10.2	9.7				
C ₁₆					11.6	10.8	10.2				

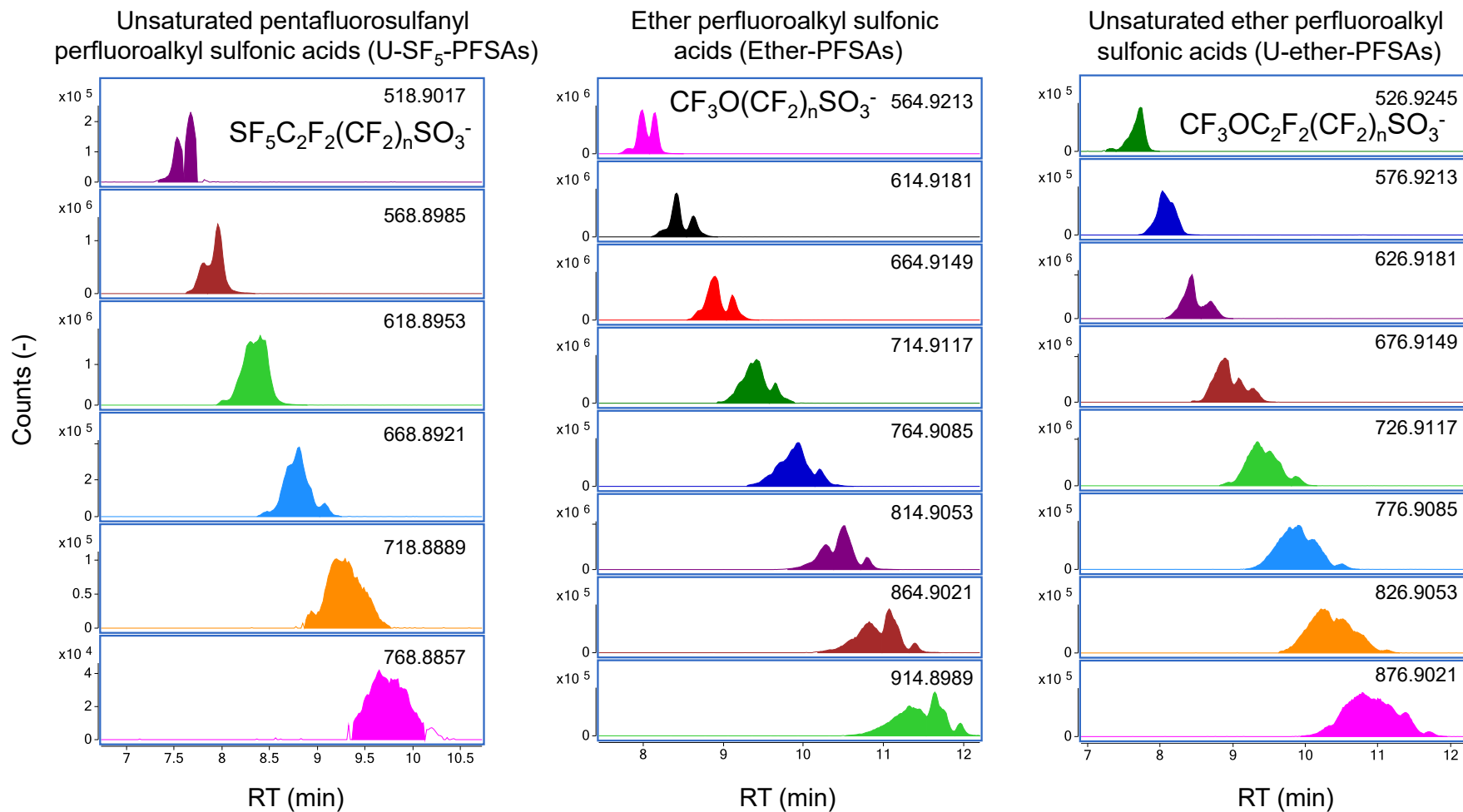
Carbon chain length	H ₃ -U-PFSAs	U-ether-SF ₅ -PFSAs	H ₂ -U-PFSAs	H-di-U-PFSAs	Ether-SF ₅ -PFSAs	di-U-ether-PFSAs	Ether-PFCAs	PFCAs	PFCAs-CO ₂	PFCAs
C ₆								6.1	6.1	1.4
C ₇								6.6	6.6	3.4
C ₈	6.3	8.0	6.7	6.7	8.4			7.1	7.1	4.7
C ₉		8.5						7.6		5.0
C ₁₀		8.9				7.7	9.2	8.2		5.3
C ₁₁		9.5				8.0	9.6	8.6		
C ₁₂						8.4	10.2	9.0		
C ₁₃						8.9	10.7	9.6		
C ₁₄						9.3	11.1	10.1		
C ₁₅						9.8				
C ₁₆						10.2				



104

105 **Figure S 4:** Extracted ion chromatograms (EICs) of perfluoroalkyl sulfonic acids (PFSA, n = 7–15), pentafluorosulfanyl perfluoroalkyl sulfonic acids (SF₅-PFSA, n = 6–12)
 106 and unsaturated PFSA (U-PFSA, n = 6–14). Note that due to simultaneously occurring isomers (e.g. branched isomers or positional isomers) chromatographic peaks are only
 107 partially resolved.

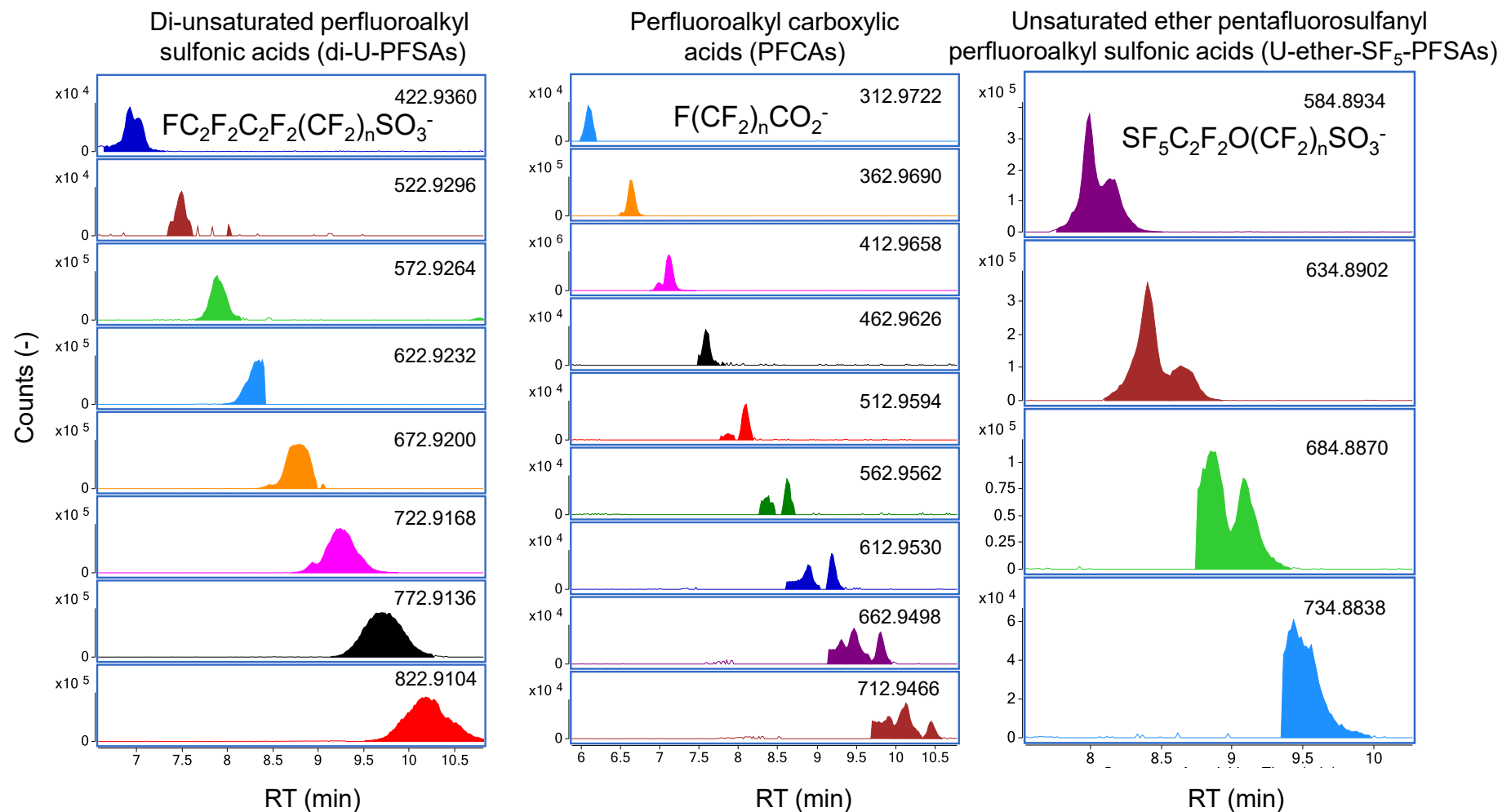
108



109

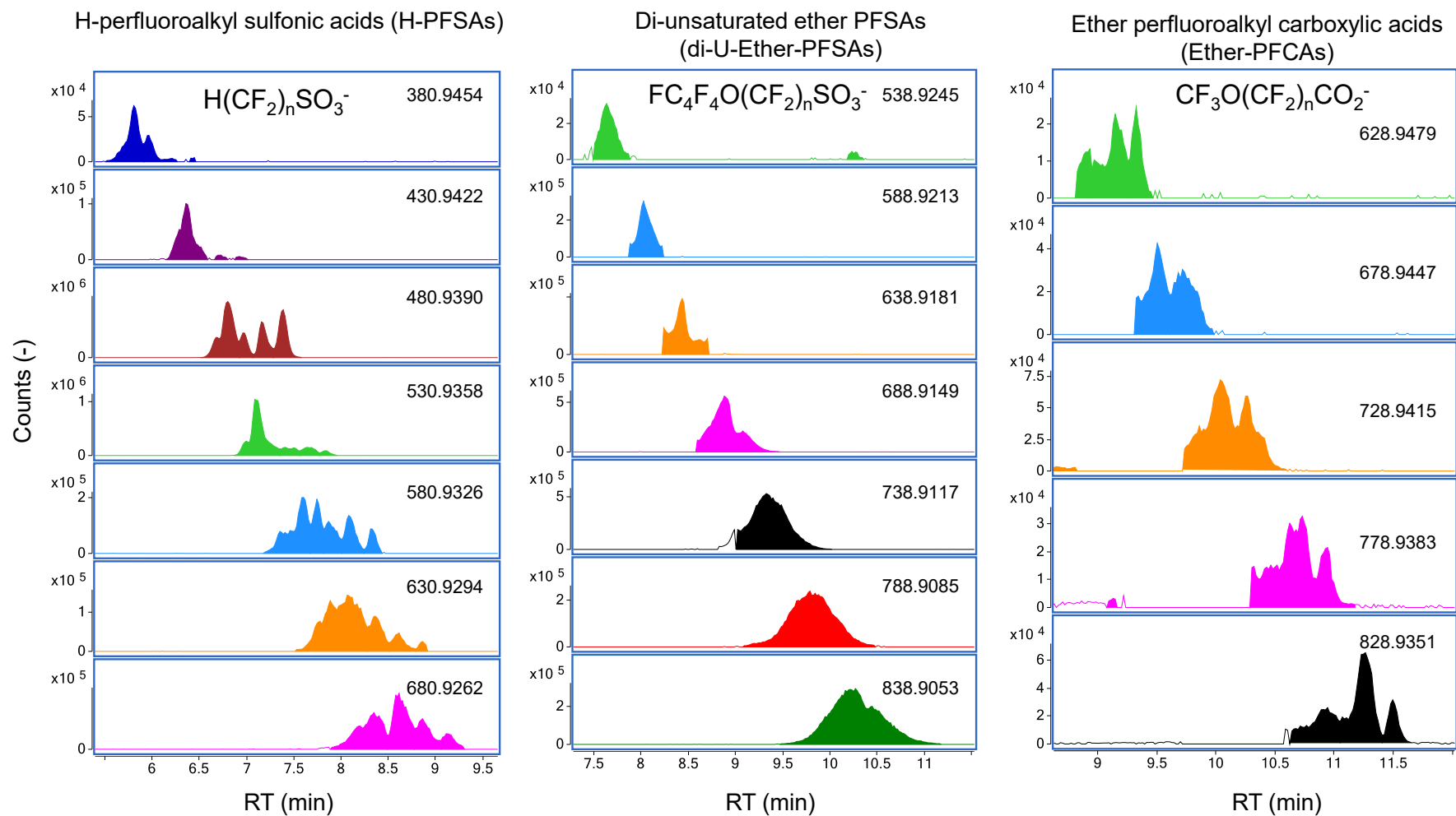
110 **Figure S 5:** Extracted ion chromatograms (EICs) of unsaturated pentafluorosulfanyl perfluoroalkyl sulfonic acids (U-SF₅-PFSAs, n = 5–10), ether perfluoroalkyl sulfonic acids
 111 (Ether-PFSAs, n = 8–15) and unsaturated ether PFSAs (U-ether-PFSAs, n = 6–13). Note that due to many simultaneously occurring isomers (e.g. branched isomers or positional
 112 isomers) chromatographic peaks are only partially resolved.

113



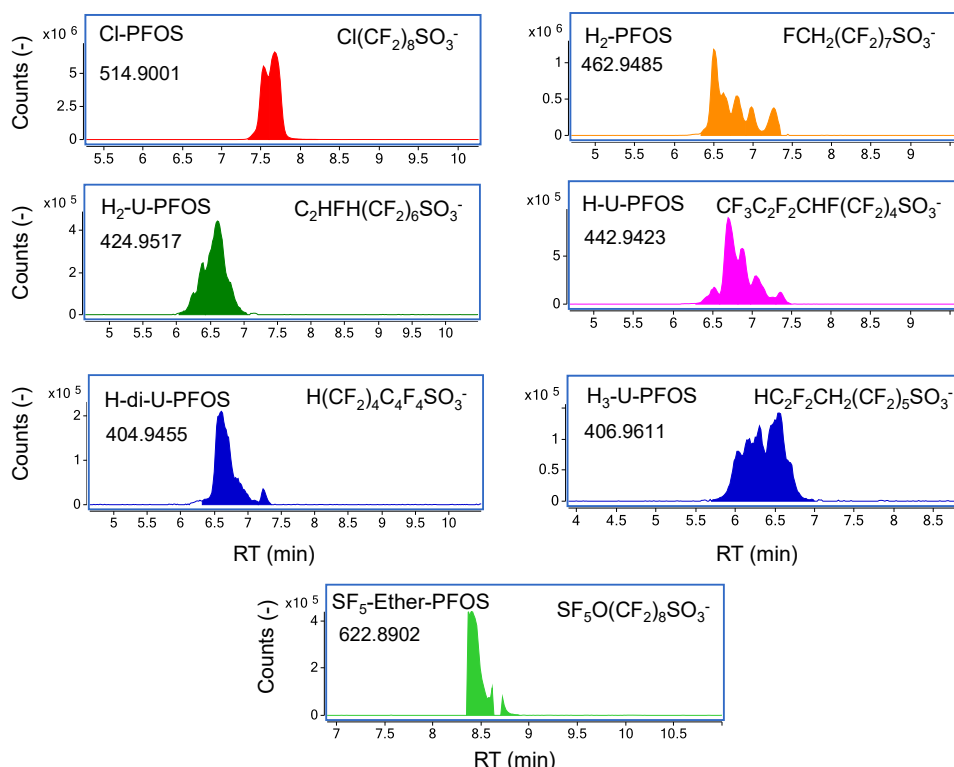
115

116 **Figure S 6:** Extracted ion chromatograms (EICs) of twice unsaturated perfluoroalkyl sulfonic acids (2-U-PFSAs, $n = 4-12$, $n \neq 5$), perfluoroalkyl carboxylic acids (PFCAs, $n =$
 117 $5-13$, note that several intensities were very low) and unsaturated ether pentafluorosulfanyl PFSAs (U-ether-SF₅-PFCAs, $n = 6-9$). Note that due to many simultaneously
 118 occurring isomers (e.g. branched isomers or positional isomers) chromatographic peaks are only partially resolved.



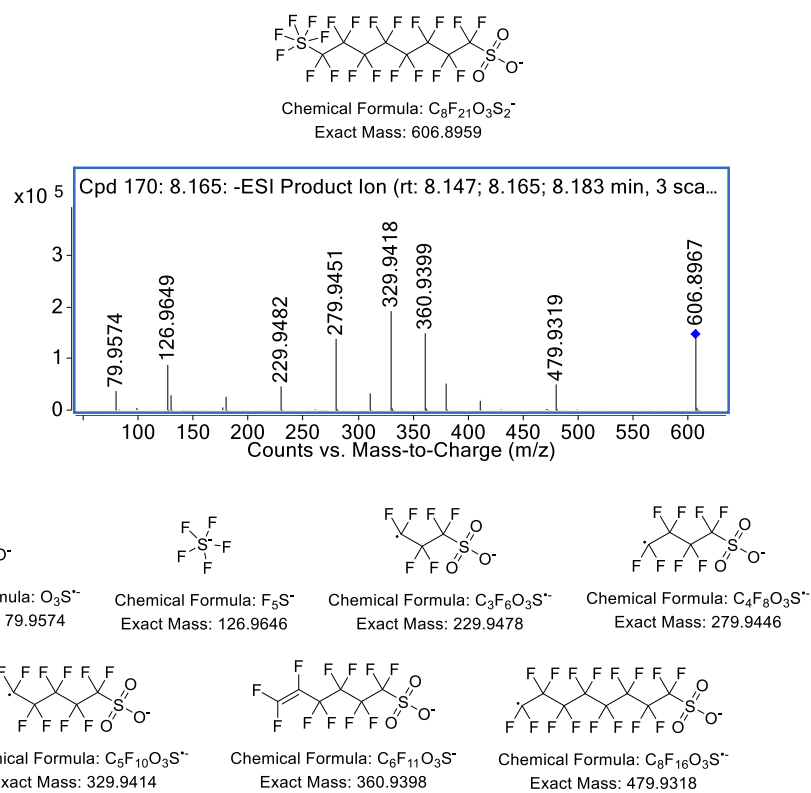
120

121 **Figure S 7:** Extracted ion chromatograms (EICs) of H-PFSAs (n = 6–12), twice unsaturated ether PFSA (2-U-ether-PFSAs, n = 6–12), and ether-PFCAs (n = 10–14). Note that
 122 due to many simultaneously occurring isomers (e.g. branched isomers or positional isomers) chromatographic peaks are only partially resolved.



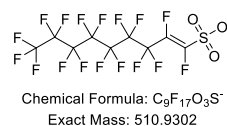
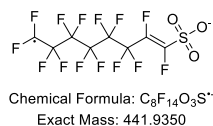
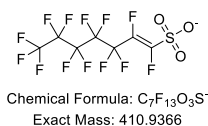
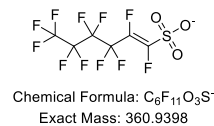
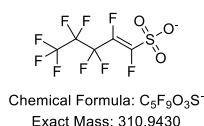
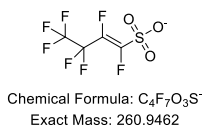
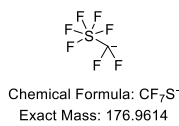
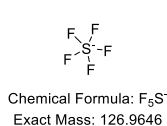
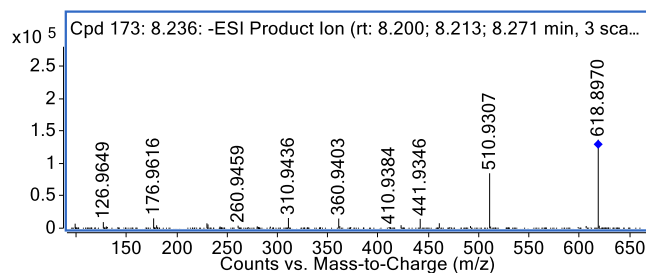
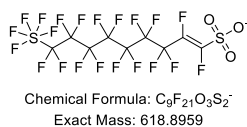
123
124
125
126
127

Figure S 8: Extracted ion chromatograms (EICs) of Cl-PFOS, H₂-PFOS, H₂-U-PFOS, H-U-PFOS, H-di-U-PFOS, H₃-U-PFOS, and SF₅-ether-PFOS. Note that due to many simultaneously occurring isomers (e.g. branched isomers or positional isomers) chromatographic peaks are only partially resolved. Note that those compounds were exclusively detected by FindPFAS via fragment mass differences because they did not occur as homologues.



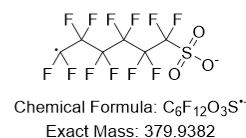
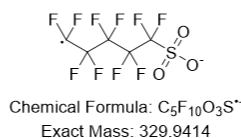
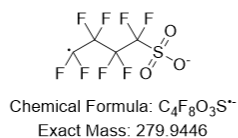
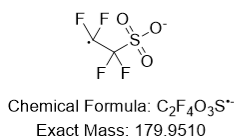
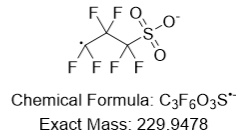
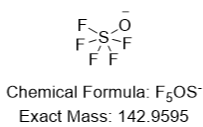
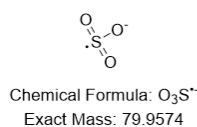
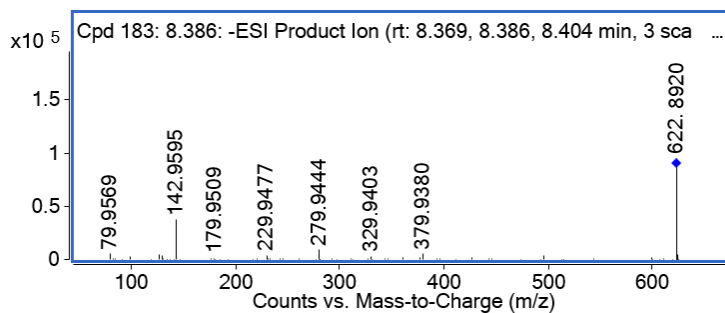
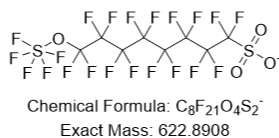
128
129
130
131

Figure S 9: Fragmentation spectrum of m/z 606.8967 @ 33.2 eV and a narrow isolation window (± 0.7 Da), identified as a SF₅-PFSA. The exact position of the SF₅-group remains undetermined, partially resolved peaks indicate further, branched isomers.



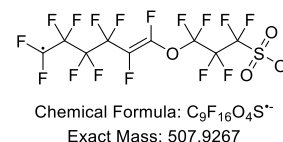
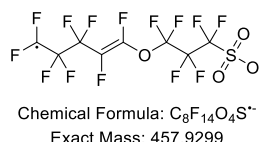
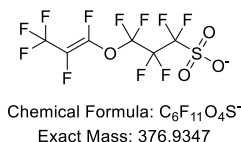
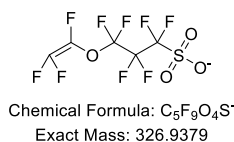
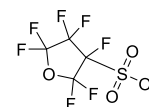
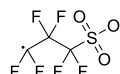
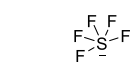
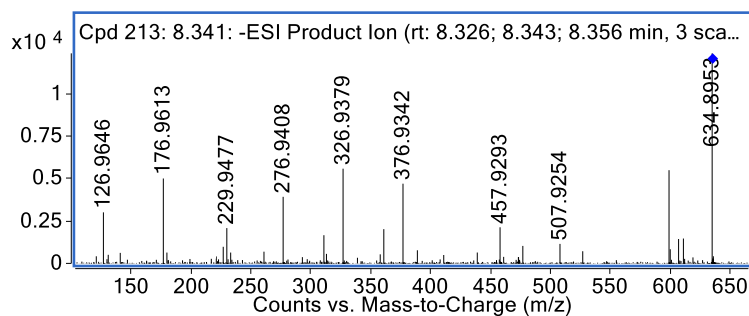
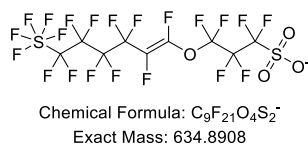
132
133
134
135

Figure S 10: Fragmentation spectrum of m/z 618.8970 @ 33.6 eV and a narrow isolation window (± 0.7 Da), identified as an unsaturated SF_5 -PFSA. The exact position of both the SF_5 -group and the double bond remain undetermined, chromatographic split peaks indicate further, branched isomers.



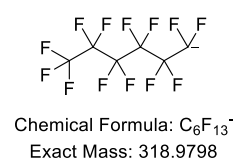
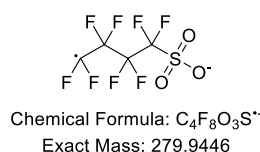
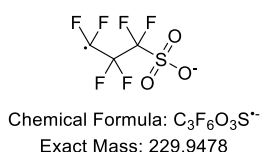
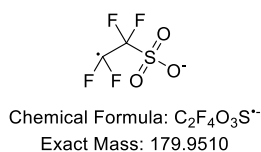
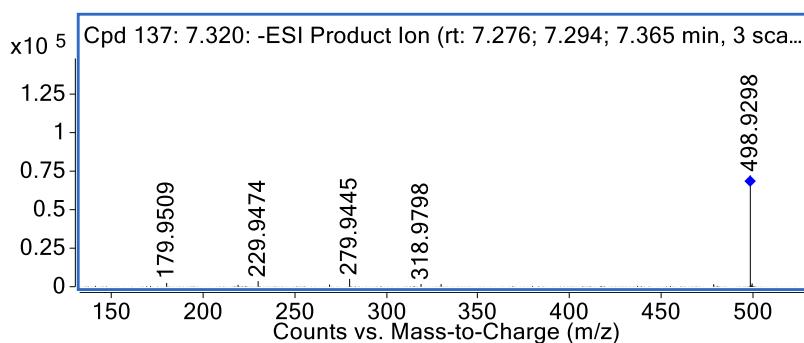
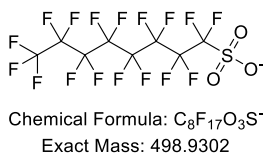
136
137
138
139

Figure S 11: Fragmentation spectrum of m/z 622.8920 @ 33.7 eV and a narrow isolation window (± 0.7 Da), identified as unsaturated SF_5 -ether-PFSA. The exact position of both the SF_5 -group and the ether linkage remain undetermined, chromatographic split peaks indicate further, branched isomers.



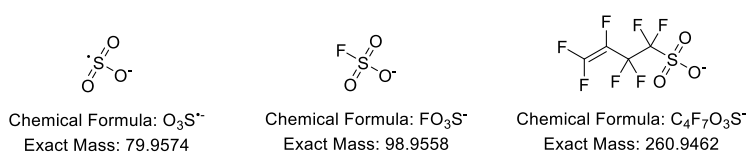
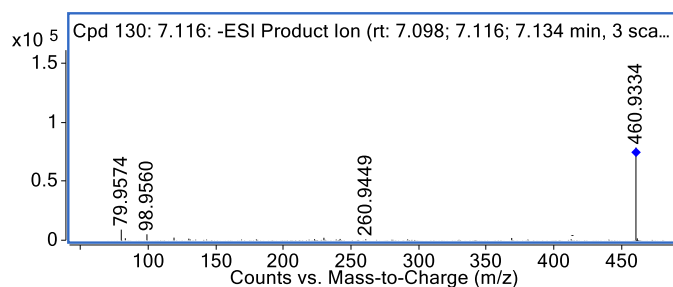
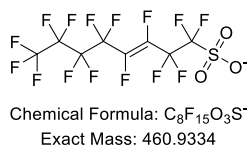
140
141
142
143

Figure S 12: Fragmentation spectrum of m/z 634.8953 @ 34.1 eV and a narrow isolation window (± 0.7 Da), identified as an unsaturated ether SF_5 -PFSA. The exact positions of the SF_5 -group, the double bond and the ether group remain undetermined, chromatographic split peaks indicate further, branched isomers.



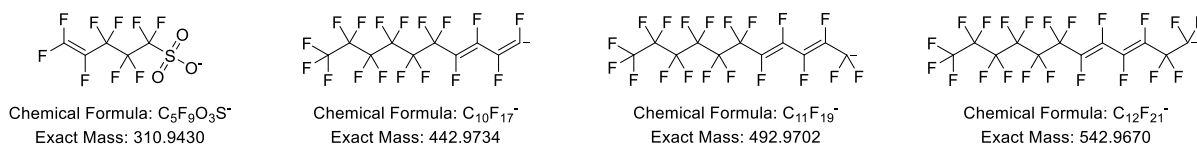
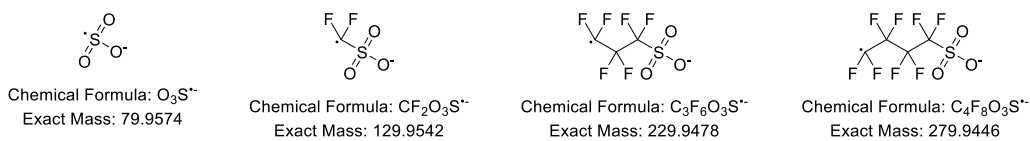
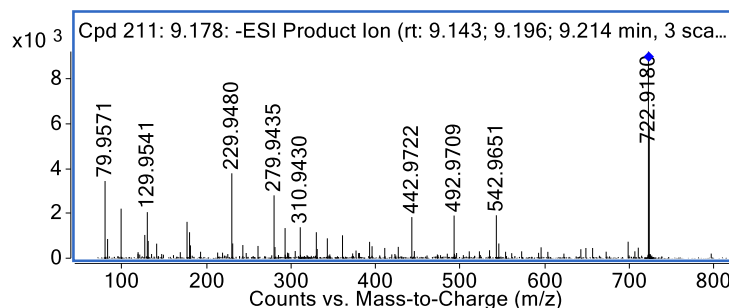
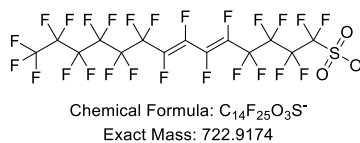
144
145
146

Figure S 13: Fragmentation spectrum of m/z 498.9298 @ 30.0 eV and a narrow isolation window (± 0.7 Da), identified as a PFSA. Split chromatographic peaks indicate further branched isomers.



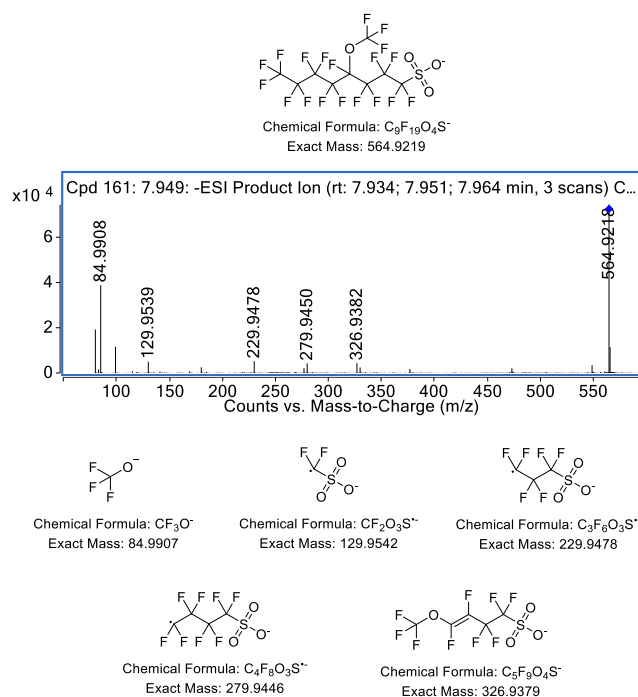
147
148
149
150

Figure S 14: Fragmentation spectrum of m/z 460.9334 @ 28.8 eV and a narrow isolation window (± 0.7 Da), identified as U-PFSA. The exact position of the double bond remains undetermined, chromatographic split peaks indicate further, branched isomers.



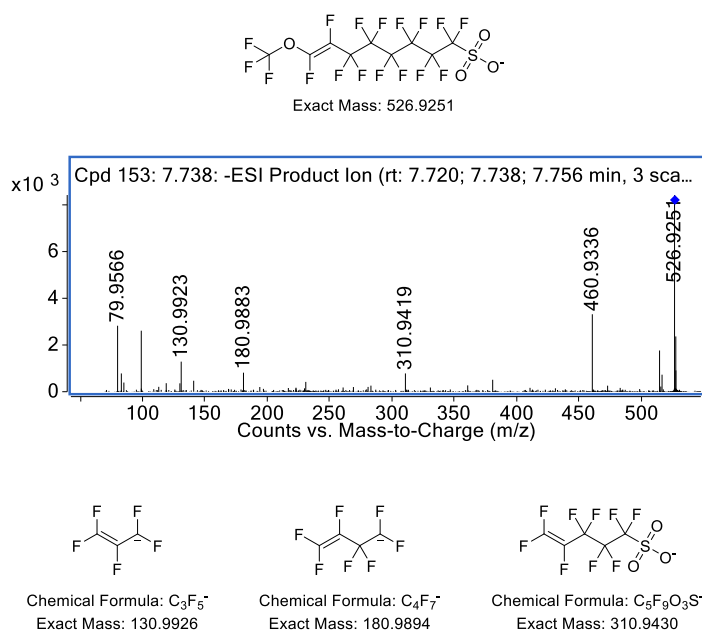
151
152
153
154
155

Figure S 15: Fragmentation spectrum of m/z 722.9180 @ 36.7 eV and a narrow isolation window (± 0.7 Da), identified as a di-unsaturated PFSA. The exact positions of the double bonds remain undetermined, chromatographic split peaks indicate further, branched isomers.



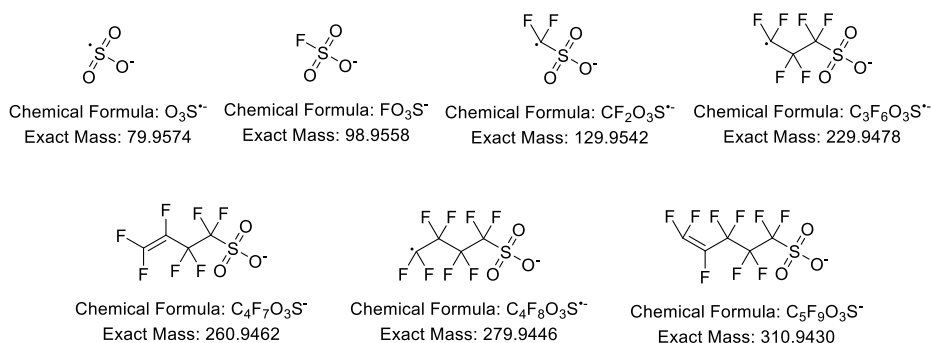
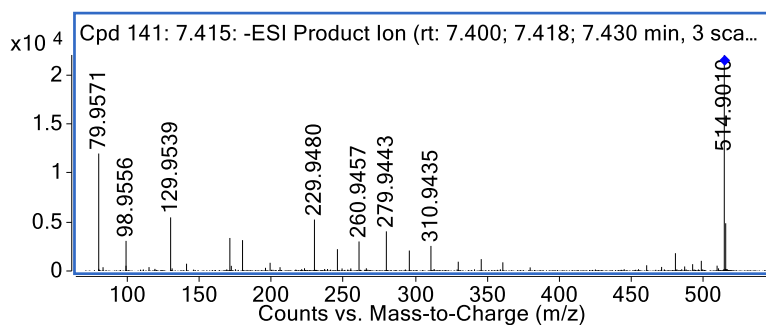
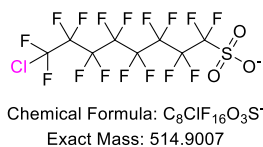
156
157
158
159

Figure S 16: Fragmentation spectrum of m/z 564.9218 @ 32.0 eV and a narrow isolation window (± 0.7 Da), identified as an ether-PFSA. The exact position of the ether group remains undetermined, chromatographic split peaks indicate further, branched isomers.



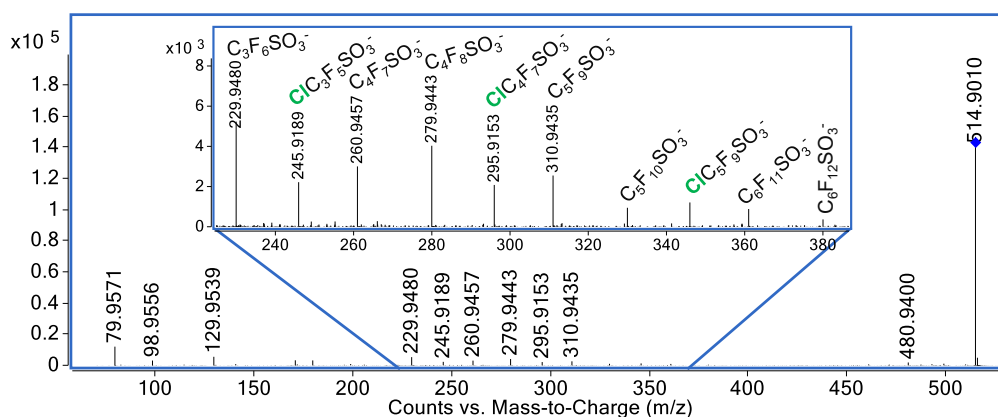
160
161
162
163

Figure S 17: Fragmentation spectrum of m/z 526.9251 @ 32.0 eV and a narrow isolation window (± 0.7 Da), identified as an unsaturated-ether-PFSA. The exact position of the ether linkage and the double bond remain undetermined, chromatographic split peaks indicate further, branched isomers.



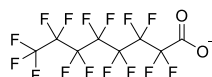
164
165
166
167
168

Figure S 18: Fragmentation spectrum of m/z 514.9010 @ 30.5 eV and a narrow isolation window (± 0.7 Da), identified as Cl-PFOS. The exact position of the chlorine atom remains undetermined, chromatographic split peaks indicate further, branched isomers. The relative abundance of the M+2 isotope (36.9 % measured vs. 37.5 % theoretical) further confirms a chlorinated compound.

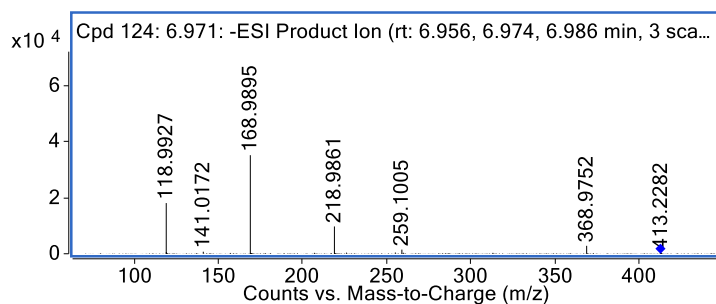


169
170
171
172

Figure S 19: Fragmentation spectrum of Cl-PFOS (m/z 514.9010 @ 30.5 eV) indicating the position of the Cl-atom to be at the third up to the fifth C-atom (from the functional group). It is important to note, however, that MS/MS was not acquired over the whole peak making more positions possible.



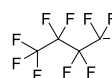
Chemical Formula: $C_8F_{15}O_2^-$
Exact Mass: 412.9664



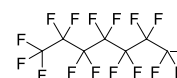
Chemical Formula: $C_2F_5^-$
Exact Mass: 118.9926



Chemical Formula: $C_3F_7^-$
Exact Mass: 168.9894



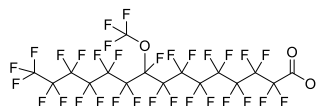
Chemical Formula: $C_4F_9^-$
Exact Mass: 218.9862



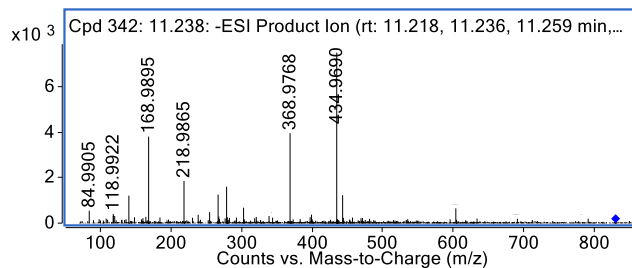
Chemical Formula: $C_7F_{15}^-$
Exact Mass: 368.9766

173
174
175

Figure S 20: Fragmentation spectrum of m/z 412.9664 @ 27.4 eV and a narrow isolation window (± 0.7 Da), identified as a PFCA.



Chemical Formula: $C_{16}F_{31}O_3^-$
Exact Mass: 828.9358



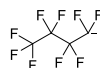
Chemical Formula: CF_3O^-
Exact Mass: 84.9907



Chemical Formula: $C_2F_5^-$
Exact Mass: 118.9926



Chemical Formula: $C_3F_7^-$
Exact Mass: 168.9894



Chemical Formula: $C_4F_9^-$
Exact Mass: 218.9862



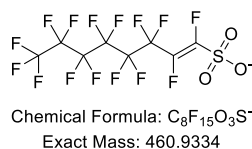
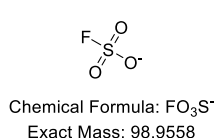
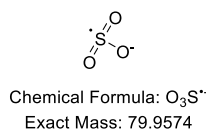
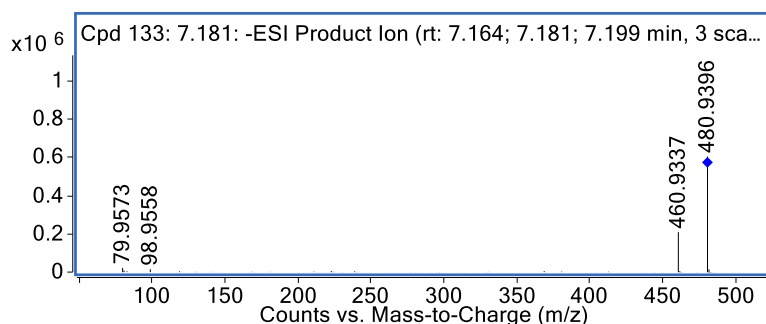
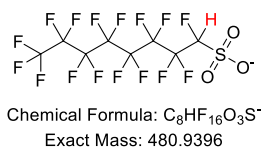
Chemical Formula: $C_7F_{15}^-$
Exact Mass: 368.9766



Chemical Formula: $C_8F_{17}O^-$
Exact Mass: 434.9683

176
177
178

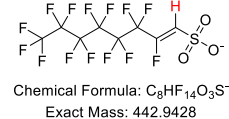
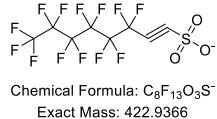
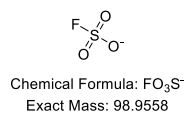
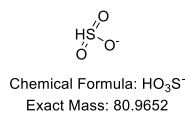
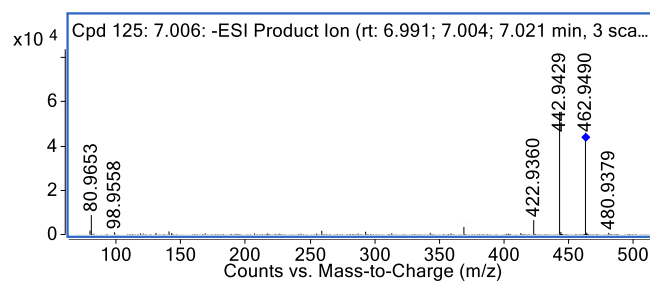
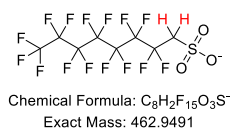
Figure S 21: Fragmentation spectrum of m/z 828.9354 @ 39.9 eV and a narrow isolation window (± 0.7 Da), identified as an ether-PFCA. The exact location of the ether linkage remains undetermined.



179

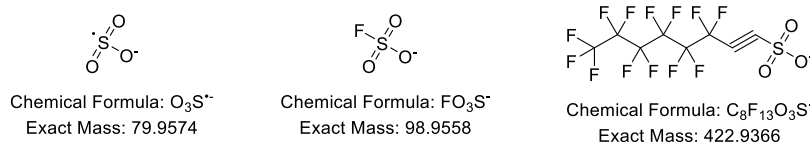
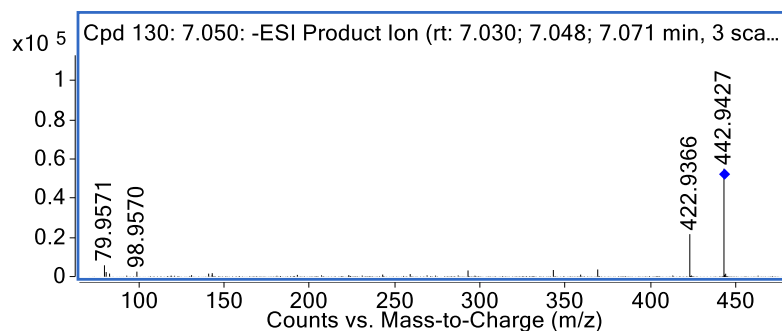
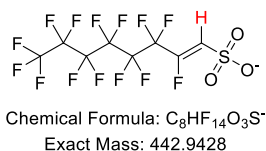
180 **Figure S 22:** Fragmentation spectrum of m/z 480.9396 @ 29.4 eV and a narrow isolation window (± 0.7 Da),
181 identified as H-PFOS. The exact position of the hydrogen atoms remains undetermined, chromatographic split
182 peaks indicate further, branched isomers.

183



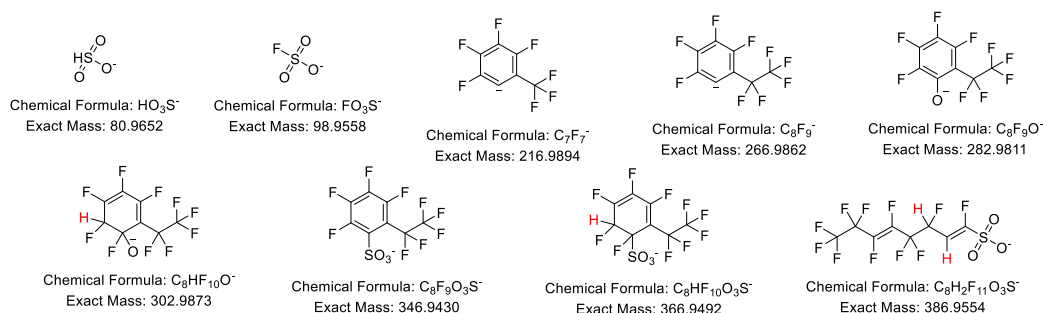
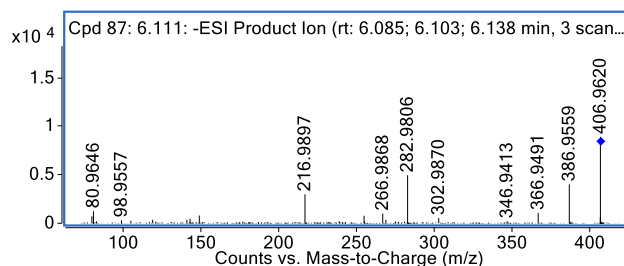
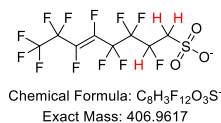
184

185 **Figure S 23:** Fragmentation spectrum of m/z 462.9490 @ 28.9 eV and a narrow isolation window (± 0.7 Da),
186 identified as H_2 -PFOS. The exact position of the hydrogens remain undetermined, chromatographic split
187 peaks indicate further, branched isomers.



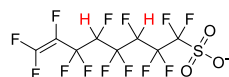
188
189
190
191

Figure S 24: Fragmentation spectrum of m/z 442.9427 @ 28.3 eV and a narrow isolation window (± 0.7 Da), identified as unsaturated H-PFOS. The exact position of the hydrogen remains undetermined, chromatographic split peaks indicate further, branched isomers.

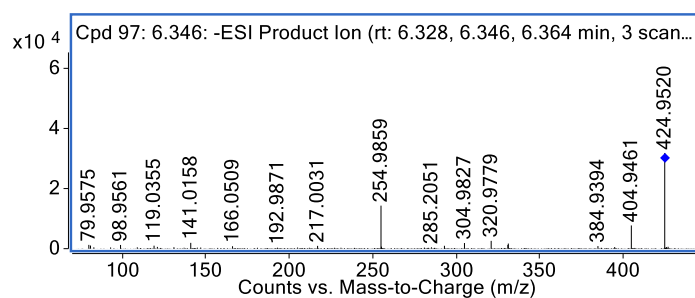


192
193
194
195

Figure S 25: Fragmentation spectrum of m/z 406.9620 @ 27.2 eV and a narrow isolation window (± 0.7 Da), identified as unsaturated H₃-PFOS. The exact positions of the double bonds and the hydrogen atoms remain undetermined, chromatographic split peaks indicate further, branched isomers.



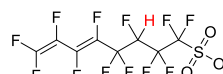
Chemical Formula: C₈H₂F₁₃O₃S⁻
Exact Mass: 424.9523



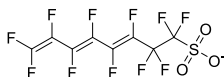
Chemical Formula: O₃S⁻
Exact Mass: 79.9574



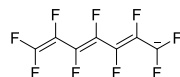
Chemical Formula: FO₃S⁻
Exact Mass: 98.9558



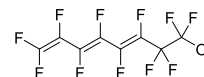
Chemical Formula: C₈HF₁₂O₃S⁻
Exact Mass: 404.9460



Chemical Formula: C₈F₁₁O₃S⁻
Exact Mass: 384.9398



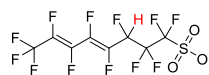
Chemical Formula: C₇F₉⁻
Exact Mass: 254.9862



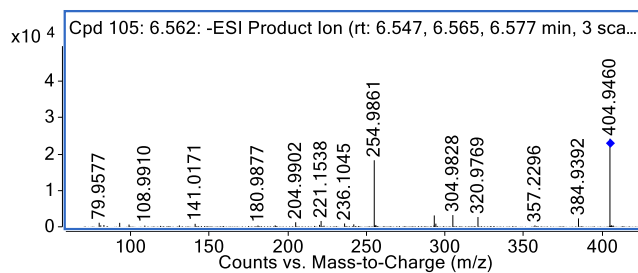
Chemical Formula: C₈F₁₀O⁻
Exact Mass: 320.9779

196
197
198
199

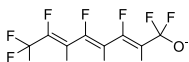
Figure S 26: Fragmentation spectrum of m/z 424.9520 @ 27.8 eV and a narrow isolation window (± 0.7 Da), identified as unsaturated H₂-PFOS. The exact positions of the double bond and the hydrogen atoms remain undetermined, chromatographic split peaks indicate further, branched isomers.



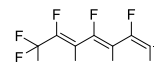
Chemical Formula: C₈HF₁₂O₃S⁻
Exact Mass: 404.9460



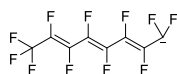
Chemical Formula: O₃S⁻
Exact Mass: 79.9574



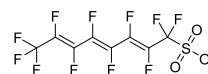
Chemical Formula: C₈F₁₁O⁻
Exact Mass: 320.9779



Chemical Formula: C₇F₉⁻
Exact Mass: 254.9862



Chemical Formula: C₈F₁₁⁻
Exact Mass: 304.9830



Chemical Formula: C₈F₁₁O₃S⁻
Exact Mass: 384.9398

200
201
202
203

Figure S 27: Fragmentation spectrum of m/z 404.9460 @ 27.2 eV and a narrow isolation window (± 0.7 Da), identified as unsaturated H-di-unsaturated PFOS. The exact positions of the double bonds and the hydrogen atom remain undetermined, chromatographic split peaks indicate further, branched isomers.

204 **Notes**

205 ‖The authors contributed equally to this work and share first authorship.

206 **References**

- 207 1. Portoles, T.; Mol, J. G.; Sancho, J. V.; Hernandez, F., Advantages of atmospheric pressure
208 chemical ionization in gas chromatography tandem mass spectrometry: pyrethroid insecticides as a
209 case study. *Anal Chem* **2012**, *84*, (22), 9802-9810.
- 210 2. Rosch, A.; Beck, B.; Hollender, J.; Singer, H., Picogram per liter quantification of pyrethroid
211 and organophosphate insecticides in surface waters: a result of large enrichment with liquid-liquid
212 extraction and gas chromatography coupled to mass spectrometry using atmospheric pressure chemical
213 ionization. *Anal Bioanal Chem* **2019**, *411*, (14), 3151-3164.
- 214 3. Zweigle, J.; Bugsel, B.; Zwiener, C., FindPFAS: Non-Target Screening for PFAS horizontal
215 line Comprehensive Data Mining for MS2 Fragment Mass Differences. *Anal Chem* **2022**, *94*, (30),
216 10788-10796.

217

Appendix 4

Publication 4

PF Δ Screen – An open-source tool for automated PFAS feature prioritization in non-target HRMS data

Jonathan Zweigle,⁺ Boris Bugsel,⁺ Joel Fabregat-Palau,[‡] Christian Zwiener^{+,*}

⁺Environmental Analytical Chemistry, Center for Applied Geoscience, University of Tübingen,
Schnarrenbergstraße 94-96, 72076 Tübingen, Germany

[‡]Hydrogeochemistry, Department of Geosciences, University of Tübingen, Schnarrenbergstraße 94-96,
72076 Tübingen, Germany

Published in: Analytical and Bioanalytical Chemistry

DOI: 10.1007/s00216-023-05070-2

Reprinted from Analytical & Bioanalytical Chemistry: Zweigle, J., Bugsel, B., Fabregat-Palau, J., & Zwiener, C. (2023). PF Δ Screen - an open-source tool for automated PFAS feature prioritization in non-target HRMS data. Anal Bioanal Chem. <https://doi.org/10.1007/s00216-023-05070-2>



PFAScreen — an open-source tool for automated PFAS feature prioritization in non-target HRMS data

Jonathan Zweigle¹ · Boris Bugsel¹ · Joel Fabregat-Palau² · Christian Zwiener¹

Received: 26 September 2023 / Revised: 17 November 2023 / Accepted: 21 November 2023
© The Author(s) 2023

Abstract

Per- and polyfluoroalkyl substances (PFAS) are a huge group of anthropogenic chemicals with unique properties that are used in countless products and applications. Due to the high stability of their C-F bonds, PFAS or their transformation products (TPs) are persistent in the environment, leading to ubiquitous detection in various samples worldwide. Since PFAS are industrial chemicals, the availability of authentic PFAS reference standards is limited, making non-target screening (NTS) approaches based on high-resolution mass spectrometry (HRMS) necessary for a more comprehensive characterization. NTS usually is a time-consuming process, since only a small fraction of the detected chemicals can be identified. Therefore, efficient prioritization of relevant HRMS signals is one of the most crucial steps. We developed PFAScreen, a Python-based open-source tool with a simple graphical user interface (GUI) to perform efficient feature prioritization using several PFAS-specific techniques such as the highly promising MD/C-m/C approach, Kendrick mass defect analysis, diagnostic fragments (MS^2), fragment mass differences (MS^2), and suspect screening. Feature detection from vendor-independent MS raw data (mzML, data-dependent acquisition) is performed via pyOpenMS (or custom feature lists) with subsequent calculations for prioritization and identification of PFAS in both HPLC- and GC-HRMS data. The PFAScreen workflow is presented on four PFAS-contaminated agricultural soil samples from south-western Germany. Over 15 classes of PFAS (more than 80 single compounds with several isomers) could be identified, including four novel classes, potentially TPs of the precursors fluorotelomer mercapto alkyl phosphates (FTMAPs). PFAScreen can be used within the Python environment and is easily automatically installable and executable on Windows. Its source code is freely available on GitHub (<https://github.com/JonZwe/PFAScreen>).

Keywords PFAS · Non-target screening · Feature prioritization · HRMS · Open-source software · Mass defect · MD/C-m/C · KMD

Introduction

Per- and polyfluoroalkyl substances (PFAS) are a large group of anthropogenic chemicals characterized by containing multiple C-F bonds [1, 2]. Due to their unique properties,

they are used in a wide array of daily products and different industrial applications [3]. Their high chemical resistance and water and oil repellency lead to the production of PFAS with a variety of different chemistries [4]. Due to the high stability of C-F bonds, the perfluoroalkyl chains of PFAS exhibit an intrinsic persistence that leads to a worldwide distribution of PFAS and their terminal transformation products (TPs) such as perfluoroalkyl acids (PFAAs) which were extensively produced and used in the past [5–8]. Nowadays, the number of known PFAS ranges from thousands to millions, depending on the definition and source of information. According to the updated OECD definition, all chemicals containing a CF_3 or isolated CF_2 group are considered PFAS, which has increased the number of PFAS considerably [9, 10]. Global regulatory efforts restricted the production of selected longer-chain PFAAs such as perfluorooctanoic

✉ Jonathan Zweigle
jonathan.zweigle@uni-tuebingen.de

✉ Christian Zwiener
christian.zwiener@uni-tuebingen.de

¹ Environmental Analytical Chemistry, Department of Geosciences, University of Tübingen, Schnarrenbergstraße 94-96, 72076 Tübingen, Germany

² Hydrogeochemistry, Department of Geosciences, University of Tübingen, Schnarrenbergstraße 94-96, 72076 Tübingen, Germany

acid (PFOA) and perfluorooctanesulfonic acid (PFOS) due to their persistence, bioaccumulation potential, and adverse effects on humans and the environment [11]. This resulted in the production of replacement compounds of rather similar persistence, increasing the number of different PFAS on the global market that are also eventually emitted into the environment [12]. Therefore, PFAS are considered to be regulated as a chemical class in the European Union in the future [13].

Several studies have shown that considerable fractions of organically bound fluorine (e.g., extractable organic fluorine) in environmental and human samples cannot be explained sufficiently by routinely analyzed PFAS (target screening), which usually include less than 50 analytes [14–17]. Since almost no fluorinated organic compounds occur naturally, unknown fractions of organically bound fluorine are clear indications of anthropogenic chemicals [18].

Due to the sheer number of different PFAS that transform into an even larger number of unknown TPs, a comprehensive use of authentic reference standards is usually not possible and most likely will not be soon [19, 20]. The fact that PFAS are industrial chemicals that often underlie the trade secrets even complicates the availability of standards. Therefore, non-target screening (NTS) based on high-resolution mass spectrometry (HRMS) is necessary for a more comprehensive characterization of PFAS [21, 22]. Several studies have shown that target analysis is insufficient to capture PFAS present in complex samples, which can easily result in the overlooking of important compounds even when present in high concentrations [23]. NTS approaches led to the identification of more than 750 novel PFAS in various samples in the past worldwide, showing their high relevance in analytical approaches [22, 24]. Since NTS is typically a time-consuming and often partially manual process, efficient prioritization techniques are needed to separate detected matrix components from the analytes of interest (often a data reduction from ~5000 detected compounds to 10–100 identified analytes or even less) [25].

The intrinsic properties of PFAS (with a certain fluorine percentage) allow the use of several techniques for their prioritization [21, 26]: The chemical mass defect (MD) of PFAS is typically lower ($MD_F = -0.0016$ Da) than the one of hydrocarbons ($MD_H = +0.0078$ Da) and has been used to remove detected features outside a predefined MD range (e.g., -0.25 to $+0.1$ Da) [27–29]. However, this range is not fixed, and depending on the structure, it is important to know that hydrocarbons of higher mass that exceed a MD of $+0.75$ Da can also fall into the same range. Similarly, polyfluorinated PFAS with a high H content may bear a positive MD exceeding $+0.1$ Da. Recently, a promising approach based on the MD normalized to the carbon number (MD/C) vs. the mass normalized to the carbon number (m/C) was proposed to separate PFAS much more efficiently from other

hydrocarbon features in HRMS data which was further systematically evaluated for ~200,000 PFAS from chemical databases [26, 30]. The carbon number can be easily estimated for all HRMS features by using the relative abundance of the M+1 isotope (^{13}C). PFAS have a much higher m/C when their mass is dominated by fluorine (e.g., $m/C \sim 50$), while hydrocarbons of similar mass are dominated by carbon ($m/C \sim 14$), allowing a convenient separation. Details on the MD/C-m/C approach are summarized in Zweigle et al. [26]. Especially, the m/C dimension can be used to remove large fractions of non-PFAS features when applied appropriately. This is illustrated in Fig. 1 with a 2D histogram of the MD/C-m/C locations of over 50,000 features from previous HRMS measurements of PFAS-contaminated soils and grease-repelling papers, where a clear separation of potentially highly fluorinated compounds is observed (region around $m/C \approx 40$, $MD/C = -0.002$). It is important to note, however, that the MD/C-m/C separation works better the higher the percentage of fluorine in a molecule is, with an accordingly higher F/C and a lower H/F ratio [26]. Like the MD, the MD/C-m/C approach cannot separate, for instance, hydrocarbons with one or two CF_3 groups from other hydrocarbons.

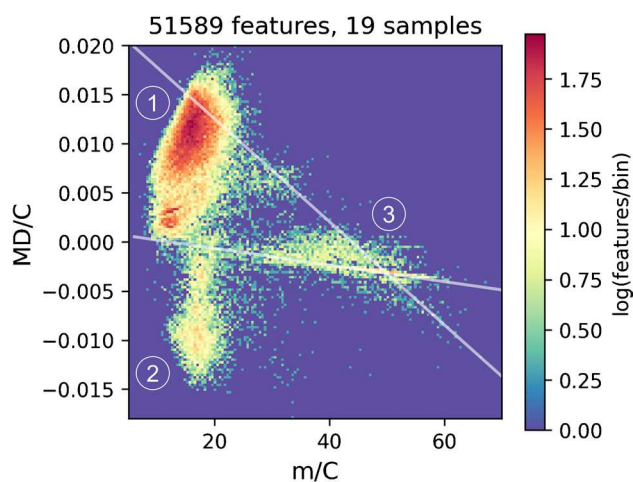


Fig. 1 2D histogram of the number of compounds (log scale) (compound density) in the MD/C-m/C plot of 19 measured samples used from several paper and soil extracts, standards, and blanks (19 samples with 51,589 features from [23, 31, 32]). Hydrocarbon features are located usually below m/C of 25 with a clearly positive MD/C (position 1), while at a certain C number the MD exceeds $+0.5$ Da yielding a position of a mathematical negative MD/C (position 2). Highly fluorinated compounds or compounds with other heavy heteroatoms are strongly shifted to higher m/C values (position 3). It becomes obvious that even with these high numbers of features in several samples from several different matrices, potential PFAS features with a certain fraction of fluorine within the molecule are efficiently separated from most matrix components. The gray lines mark the $CH_x F_{2-x}$ -line ($0 \leq x \leq 2$) and the CF_x -line ($0 \leq x \leq 2$) (for details on the MD/C-m/C plot, see Zweigle et al. [26])

Besides the MD and MD/C-m/C approach, the Kendrick mass defect (KMD) analysis to detect homologous series of PFAS (e.g., with CF₂ or CF₂O as repeating units) is of great relevance since it allows the grouping of structurally related PFAS, simplifying their identification [27, 33]. In the MS² data, lists of PFAS-specific diagnostic fragments (DFs) as well as fragment mass differences and neutral losses can be used to prioritize fragmentation spectra [28, 31, 34]. These techniques are often combined with suspect screening by matching accurate mass (or further evidence) with PFAS lists [22, 35].

KMD, DFs, fragment mass differences, and especially suspect screening with large lists (e.g., PFASMASTER, gathering over 12,000 compounds [36]) in combination with complex samples (thousands of features) are prone to a high number of false-positive detections (depending on mass tolerance) that often need to be excluded manually, which is a time-consuming process. Even with extremely high mass resolution, naturally occurring compounds can still mimic certain PFAS-specific repeating units such as CF₂, complicating KMD analysis and making retention time shifts a necessary criterion [37]. Therefore, if the number of features can be preliminarily reduced by the MD/C-m/C approach before applying those techniques, a faster and more accurate NTS workflow can be performed, decreasing both computational and manual effort regarding the further inspection of the features. Although many of the above discussed PFAS-specific techniques for prioritization and identification are applied, they are often not performed in a systematic way using open-source software [38]. Therefore, it is important to combine the data processing in a more systematic step-wise procedure.

To facilitate the non-targeted screening of PFAS in complex samples, we developed PFAScreen, an open-source Python-based software tool with a simple graphical user interface (GUI) that combines the discussed techniques to efficiently prioritize PFAS in LC- or GC-HRMS data acquired with electrospray (ESI) or atmospheric pressure chemical ionization (APCI). PFAScreen can be applied vendor-independently either on mass spectrometric raw data (mzML, automated feature finding via pyOpenMS) or on custom feature lists (external feature finding by other software tools). The PFAScreen workflow presented here is then applied to four PFAS-contaminated agricultural soil extracts from south-western Germany (Rastatt case [27, 39]), where several PFAS classes, including novel PFAS, were identified. The advantages of the combined workflow are discussed in detail. The source code is available via GitHub and can be easily automatically installed and executed via batch files on Windows within the Python environment. The Python source code can also be executed on other operating systems within the Python environment (without automatic installation).

Materials and methods

PFAScreen workflow

PFAScreen is a fully automated tool for detection and prioritization of potential PFAS features (LC- or GC-HRMS with ESI or APCI source) in raw mass spectrometric data written in Python (3.9.13) (Fig. 2). PFAScreen is structured in several individual Python functions that are executed from one main file that allows data and parameter input via a simple GUI programmed with the tkinter library (Fig. S1). It can easily be automatically installed and executed on Windows using batch files. Detailed instructions on installation and functionality are provided in the SI. Input MS raw data can be converted vendor-independently from data-dependent acquisition (ddMS²) files into the mzML data format (.mzML) by using the MSConvert software from ProteoWizard [40, 41]. Only mzML files with centroided spectra and one collision energy (CE) should be used. If profile data was acquired and MS² spectra from several different CEs per precursor m/z are present, the peak picking (for centroiding) and subset functions (to keep only one desired CE) from MSConvert can be used to generate the correct mzML input files.

In the following, the three main functionalities of PFAScreen are explained in the same order as they can be executed in the GUI (Fig. 2 and Fig. S1).

FeatureFinding

The first step usually performed in NTS is detection of features in the MS raw data characterized by chromatographic peak shapes of coeluting isotopes, resulting in a list of m/z, retention time (RT), and peak area. This task is performed with pyOpenMS, a Python interface to the C++ OpenMS library [42–46]. For feature detection, the FeatureFinderMetabo algorithm is used, which is designed for metabolites and small molecules [47–49]. Three parameters (mass error (ppm), intensity threshold, and an isotope model for more accurate detection of coeluting isotopologues) can be specified. The most important parameter is the intensity threshold, which is highly dependent on the instrument used, sample, and the underlying NTS question. After feature finding in the MS¹ data, MS² spectra can be aligned to their respective precursors by specifying an m/z and RT tolerance. Only one unique MS² spectrum with the highest precursor intensity is assigned to the respective MS¹ precursor.

With PFAScreen, a single sample with a corresponding (optional) blank can be processed at a time. Blank

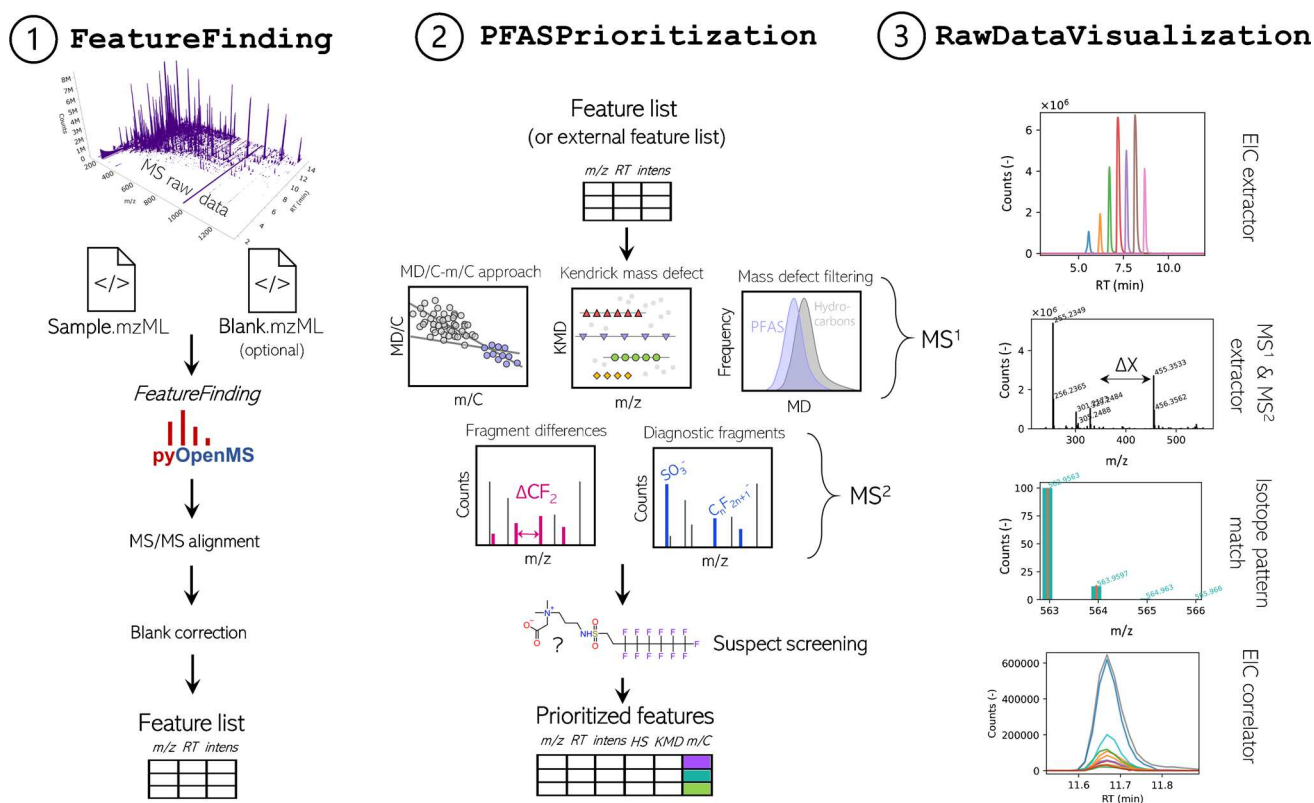


Fig. 2 Schematic overview of the PFAScreen workflow in the structure of the GUI (Fig. S1). The FeatureFinding tab (1) allows detection of feature via pyOpenMS in MS raw data followed by MS² alignment and blank correction resulting in a feature list for a sample of interest. PFAS feature prioritization (2) includes techniques such as the MD/C-m/C approach, KMD analysis, fragment matching, and frag-

ment mass differences which generates a strongly reduced feature list of potential PFAS. The data from this list can be visualized and verified by the RawDataVisualization tool (3) together with other output files such as interactive HTML plots which allow efficient NTS (Fig. S3–S5)

correction is performed by setting an m/z and RT tolerance as well as a fold change with the desired increase of abundance in the sample compared to the blank. Features appearing in both sample and blank within the specified criteria are removed from the dataset. After preprocessing, the raw data is ready for specific PFAS prioritization. If feature finding by an external software is desired (e.g., vendor software), the following steps can also be performed by loading a feature table (.csv, that requires m/z, RT, and intensities of the [M] and [M+1] isotopes) into PFAScreen without feature detection via OpenMS. However, the raw mzML files are still needed to assign MS² data to the features in the feature table (see SI). Besides pyOpenMS, the mass spectrometric Python library Pyteomics is used for selected calculations [50, 51].

PFASPrioritization

The PFAS prioritization workflow is intended in an iterative manner: after feature detection, the MD/C-m/C plot should firstly be manually inspected to determine

reasonable boundaries to remove most of the detected features (e.g., ~90%) that cannot be PFAS due to their MD/C-m/C locations (depending on the underlying question). After determination of these cutoffs, the PFAS feature prioritization can be executed again focused on a subset of features, which will strongly decrease false positives in KMD analysis, fragment matching, and suspect screening where the respective parameters can be adjusted accordingly without a strong increase of wrong assignments. Since the execution time of PFAScreen is usually below 1 min (e.g., for ~4000 spectra per sample), input parameters can easily be varied to test their influence on the outcome. After execution, a folder is generated named after the sample file where important results are saved, including a summary in an Excel sheet which is formatted as a table that can be easily inspected, sorted, and subset for a faster overview of the results as well as an additional CSV file that includes the same data (Fig. S2). Important plots are saved in the interactive HTML format which can easily be opened in any browser, allowing zooming and data inspection with interactive tooltips (Fig. S3).

In the workflow to prioritize features according to their likelihood of being PFAS, several pieces of evidence are calculated individually for all detected features in the first place. For all MS¹ features, the number of carbon atoms, MD, and both MD/C and m/C dimensions are determined. To detect homologues series (HS), the KMD (with a pre-defined repeating unit required; e.g., CF₂) is calculated and corresponding features belonging to a certain HS are aligned by providing a unique HS number (parameters: mass tolerance, minimum number of homologues).

For all MS² spectra, fragment mass differences are calculated comprehensively. Therefore, all fragment differences within each MS² spectrum are calculated and matched against a predefined list of PFAS typical mass differences (e.g., ΔCF₂, ΔC₂F₄, ΔHF, ΔC₁₀H₃F₁₇, more details can be found in [31]). This allows an efficient detection of fragments indicative for PFAS without prior knowledge on their actual mass [23, 31]. Furthermore, a list of typical PFAS diagnostic fragments (DFs, approximately 900 fragments) from literature are automatically matched with all fragmentation spectra (which is easily extendable) [52, 53]. Both negative and positive fragments are considered depending on the measurement polarity which can be specified in the GUI. The most important parameter is the MS² noise threshold, used to specify the lowest MS² intensity to be considered for DF, and mass difference matching. It is important to select a suitable instrument-specific threshold as a too low input value may result in a high number of false-positive annotations. Besides a mass tolerance for fragment matching, a minimal number of positive DFs or mass differences can be specified to flag a MS² spectrum as potential hit.

To enhance annotation in the MS², fragments that have a defined mass difference to another already annotated fragment (accurate mass match and therefore also a chemical formula) are also annotated by subtraction or addition of the respective mass difference (e.g., ΔC₂F₄) to an annotated chemical formula (e.g., C₁₂H₅F₁₂O₄S + ΔC₂F₄). This allows the calculation of unknown chemical formulas for fragment masses that are not present in the list of DFs (see Fig. S6).

In the third step, suspect screening by accurate mass match (with mass tolerance) can be performed. We used a custom PFAS suspect list format (.csv) which currently includes PFAS from the NIST suspect list [54]. This list which includes compound name, SMILES, chemical formula, and exact mass can easily be modified or extended with data from other suspect lists (e.g., from NORMAN or the CompTox Dashboard). For suspect screening, three adducts can be chosen which are [M–H][–] for negative polarity, and both [M+H]⁺ and [M]⁺ for positive polarity (compounds such as betaines present in various AFFF formulations are often detected as M⁺ ions) [55].

RawDataVisualization

After feature finding or the complete workflow, the MS raw data can be directly visualized via the PFAScreen GUI (Fig. 2 and S4).

EIC extractor Extracted ion chromatograms (EICs) can be generated by accurate m/z (e.g., from the Excel or CSV results file) and inspected in an external window. Several masses can be extracted together (comma separated) to investigate coelution or RT shifts. To verify the systematic RT shifts of detected HS, a repeating unit can be specified (e.g., CF₂) and *n* EICs are extracted at once (Fig. 2 and S4), allowing fast checking for reasonable peak shapes and elution order of suspected masses.

MS¹ extractor To visualize single MS¹ spectra, a certain RT of interest can be specified. Theoretical isotope patterns of chemical formulas from suspect hits can then be plotted on top of the experimental MS¹ isotope pattern (Fig. 2 and S4).

MS² extractor MS² spectra can also be directly accessed via the GUI by inputting the accurate m/z value. If DFs and fragment mass differences were detected, they are displayed within the respective MS² spectrum (Fig. S4).

EIC correlator To detect potential in-source fragments (e.g., [M–HF][–]) or adducts (e.g., [M+Br][–] or [M+Acetate][–]) by coelution correlation, an m/z of interest can be specified and all detected features within a certain RT range are correlated (EICs) and only highly correlating ions can be visualized (e.g., correlation of $R^2 > 0.95$). This can greatly enhance understanding of ionization processes and helps to find related ions that were not grouped during feature detection (more detailed explanation in the “Results and discussion” section, Fig. 6 and S9).

Soil collection and extraction

To present the feature prioritization procedure via PFAScreen, four different PFAS-contaminated composite agricultural topsoil samples from Rastatt (R1 and R2) and Mannheim (M1, M2) regions (Germany) were extracted and measured by HPLC-QTOF-MS (see sampling details and soil physicochemical properties in the SI (S3)). The R1, R2, S1, and S2 soil names correspond to soils B, A, D, and H from Röhler et al. [56], respectively. Agricultural fields in these regions were subjected to contaminated paper sludge in the past and found to be highly contaminated with several PFAS classes [27, 32, 56]. Information on all chemicals used can be found in SI (S4). Soil extraction was adapted from existing procedures [27]. Briefly, 5 g of dried soil (40 °C) was weighed in 50-mL polypropylene (PP) tubes and

combined with 10 mL of methanol (MeOH). The suspension was sonicated for 1 h and overhead shaken for 16 h. After centrifugation (10 min @ 4000 rcf), the supernatant was transferred into a 20-mL glass vessel, and extraction was repeated. The combined extracts (20 mL) were evaporated under a gentle stream of N₂ until dryness at 40 °C and reconstituted in 1 mL of MeOH, sonicated for 10 min, and thoroughly vortexed for 1 min. In the last step, the enriched extract was filtered through a 0.2- μ m regenerated cellulose syringe filter, transferred into PP HPLC vials, and stored in the fridge (4°C) until analysis. As quality control, an extraction blank following the identical extraction procedure but without adding any soil was prepared to account for background contamination.

LC-HRMS measurements and data acquisition

Soil extracts were analyzed with an Agilent 1260 Infinity HPLC system (Poroshell 120 EC-C₁₈ column; 2.1 mm \times 100 mm; 2.7 μ m particles at 40 °C) at a flow rate of 0.3 mL/min coupled to an Agilent 6550 QTOF-mass spectrometer. For compound separation, a 23-min gradient program was used (A: 95/5 H₂O/MeOH + 2 mM NH₄Ac; B: 5/95 H₂O/MeOH + 2 mM NH₄Ac) and both negative and positive measurements were performed (details in Table S1–S2). Data acquisition was performed in the data-dependent mode (ddMS²) using 3 scans/s (MS¹ range: m/z 100–1700 and MS² range m/z 70–1700) with a static exclusion list (resulting from prior MeOH blank injections) to avoid fragmentation of background signals. Furthermore, a rolling exclusion list was used to iteratively exclude previously triggered precursor masses from previous measurements (three injections) of the same sample to maximize the MS² coverage. The threshold for precursor selection was set to 1000 counts, and each precursor was excluded for 0.5 min after collection of three MS² spectra. For collision-induced dissociation, a linear m/z-dependent collision energy (CE) according to the following equation was used: $CE(m/z) = 3 \frac{m/z}{100} + 15$ eV. To prevent sample cross contamination, a threefold needle wash in MeOH was performed in-between each injection. Each measurement sequence included several blanks and quality controls (PFAS reference standard mixture) to monitor instrument drift.

Results and discussion

PFAS prioritization and identification with PF Δ Screen are aimed to be performed in an iterative process. This means that the program is executed multiple times allowing parameter adjustment to generate reasonable results. PF Δ Screen runtimes are usually below 1 min (e.g., for ~4000 spectra per sample) for the whole workflow. When changing specific

input parameters (e.g., tolerances, thresholds, mass differences), their effect on the output can directly be observed. In this way, input parameters can be conveniently adjusted depending on end-user needs and sample types. After feature detection, blank correction, and a short inspection of the results, the data can be reduced by the MD/C-m/C approach by setting an appropriate m/C cutoff value. Subsequent KMD analysis, fragment mass differences, DF matching, and suspect screening then result in a detailed table of a manageable size.

To demonstrate the PF Δ Screen workflow, it was applied here to four contaminated agricultural topsoils. The iterative identification process started with the soil extract of M1. After data preprocessing and application of prioritization techniques, the identified PFAS (including adducts and in-source fragments) were manually added to the suspect list, and the same workflow was applied to the next soil sample. In the following, the whole workflow starting from data reduction to final identification is discussed in detail.

Data preprocessing

After data-dependent acquisition (DDA), the raw MS data (.d files, Agilent) were converted into mzML with MSConvert [40]. For each soil, PF Δ Screen was executed individually together with the extraction blank to remove background signals originating from both the extraction procedure and the HPLC system. The mass error for feature detection was set to 10 ppm, the MS¹ intensity threshold was set to 2000 counts and the metabolites (5% RMS) isotope model from OpenMS was used to exclude features with unusual peak shapes of isotopic traces. Peaks reported after feature detection have to have a full width at half maximum (FWHM) above 1 s and below 1 min, and at least two isotopic traces. MS² spectra were aligned with a mass tolerance of 5 mDa and an RT tolerance of 0.2 min (these tolerances can be verified by an interactive m/z vs. RT plot (Fig S3a)). Features detected in both sample and extraction blank that deviated by <2 mDa at a RT difference of <0.1 min and were not at least fivefold more abundant in the sample were removed. Exemplified on soil M1, 4209 features were detected, which were reduced to 3750 features after blank correction in the ESI⁻ mode. A total of 1026 out of 2450 acquired MS² spectra corresponded to detected features, from which 417 unique spectra remained (~11% MS² coverage in first iteration).

Data reduction by m/C and MD/C

After these feature preprocessing steps, the m/C and MD/C dimensions were used for data reduction. When looking at the MD/C-m/C plot of all soils together (containing more than 12,000 features), a clear separation of three groups of

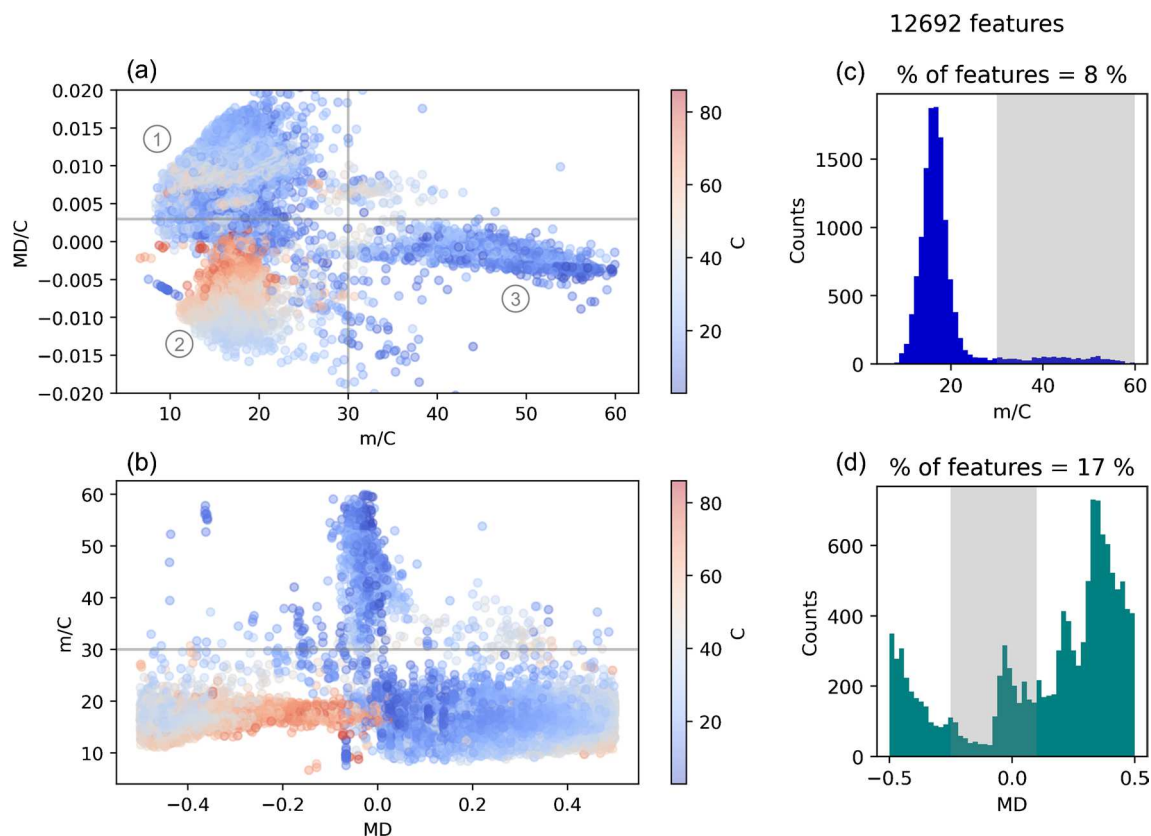


Fig. 3 Data reduction by the MD/C-m/C approach compared to the MD. **a** MD/C-m/C plot for all detected features (12,692) in the four soil extracts and **b** m/C vs. MD. The colorbars correspond to the calculated carbon number. In the MD/C-m/C plot, potential PFAS (3) are clearly separated from hydrocarbons (1) and hydrocarbons with many carbon atoms that exceed a MD of +0.5 and are therefore flipped to a similar MD region as the PFAS but are easily separated by m/C. The number of features is reduced to 8% by the m/C

dimension when cutting at $m/C > 30$ and to 7.4% when including a threshold of $MD/C < 0.003$ (gray lines in subplot a). **c** Histogram of m/C and of the MD (**d**), showing that the m/C works more efficiently than the MD (**d**), showing that the m/C remains when cutting at $-0.25 < MD < 0.1$ which includes 92% of the PFASOECDNA list [27]). Many features strongly exceeding a MD of +0.5 would be wrongly prioritized. Note how the m/C dimension allows a much clearer cutoff from hydrocarbon-based features compared to the MD

compounds can be observed (Fig. 3a). Most features were located below $m/C < 30$, which are a wide variety of different hydrocarbon molecules. A theoretical molecule exclusively consisting of $(CH_2)_n$ groups would be located at $m/C = 14$, while for the four soil extracts a clear peak distribution ranging from $m/C \approx 10$ –25 and reaching a maximum around $m/C \approx 16$ was observed (Fig. 3c). The determination of the carbon number strongly depends on the peak picking algorithm, since it is based on robustly integrated EICs from the monoisotopic mass and its corresponding $M+1$ isotope ($C \approx I_{M+1}/I_M/0.011145$). Therefore, a certain uncertainty should always be expected, which increases with decreasing ion abundance. Nonetheless, $\sim 92\%$ of all detected features are clearly located below $m/C = 30$ (e.g., humic substances) (Fig. 3c). Therefore, here a cutoff at $m/C = 30$ was chosen since PFAS that are dominated by fluorine usually have a higher m/C (e.g., $m/C_{6:2 \text{ diPAP}} \approx 49$; $m/C_{\text{PFOA}} \approx 51$; $m/C_{6:2 \text{ FTAB}} \approx 38$). 6:2 FTAB is an AFFF constituent which already has a considerable fraction of hydrogen ($C_{15}H_{19}F_{13}N_2O_4S$) compared

to other PFAS, while other organic compounds containing less fluorine (compared to hydrogen, high H/F ratio) such as the pharmaceutical fluoxetine with only three fluorine atoms ($C_{17}H_{18}F_3NO$, $m/C \approx 18$) fall below the applied cutoff. Depending on the underlying NTS question, this cutoff can be adjusted accordingly. Attempting to remove further features, an MD/C cutoff of $< +0.003$ was set, although as seen in Fig. 3a the m/C dimension was much more effective for data reduction. The MD/C-m/C approach was more efficient to reduce features compared to the MD, as shown in Fig. 3b and d. When applying a MD range from -0.25 to $+0.1$ Da, which would include 92% of the PFAS in the PFASOECDNA list (CompTox Dashboard [36, 57]), 17% of the features remained, while the combined m/C and MD/C cutoffs led to only 7.4% of remaining features. It is very important to note here that the number of features that strongly exceed a MD of +0.5 is not negligible, since a conventional calculation of the MD would result in a negative MD (e.g., -0.2 Da for a saturated hydrocarbon with

60 carbon atoms ($\text{H}(\text{CH}_2)_{60}\text{H}$), whereas the true MD would be +0.8 Da). As can be seen from the carbon number, a considerable number of features has more than 60 carbon atoms (up to 80 carbons) which are in a PFAS typical MD range (Fig. 3b). Therefore, setting an appropriate m/C cutoff is highly recommended, since these features are easily removed by this additional criterion. Eventually, when combining both m/C and MD/C cutoffs, only 949 features (7.4%) remain in all four soils together. This is an appropriate number of features for further PFAS-specific calculations such as KMD analysis, DFs, fragment mass differences, and suspect screening. It should be noted in particular that due to the removal of ~90% of the initial features, the false-positive rate decreases drastically (especially with large lists) and allows adjustment of selected tolerances with smaller effect on false positives.

KMD analysis, fragment differences, DFs, and suspect screening

For further prioritization and tentative identification, repeating units representative for PFAS such as $(\text{CF}_2)_n$ and CF_2O were applied to detect HS (mass tolerance was set at ± 2 mDa, with at least 3 homologues). Without any m/C cutoff, in soil M1, 74 $(\text{CF}_2)_n$ -based HS were detected, likely including numerous false positives (Fig. 4a) evidenced by a random RT pattern (no RT shift in linked KMD m/z vs. RT plot). The KMD analysis in *PFAScreen* is performed without checking the systematic RT shift, but the interactive KMD plot (HTML) allows a fast verification of RT shifts. Each HS can be highlighted individually by clicking on it, and the respective m/z vs. RT correlation is visualized (Fig. S5). Obviously, many hydrocarbon features were detected in the soil extract that are mimicking CF_2 -repeating units, which is a common issue of complex matrices [31, 37]. These compounds have a higher CF_2 -based KMD (e.g., 0.2 to 0.5, or lower if their MD strongly exceeds +0.5 Da) compared to that of PFAS (Fig. 4a). If the combined MD/C-m/C cutoff is applied, the number of detected HS in soil M1 is reduced to 26 (~65% data reduction, see Fig. 4b) which confirms the utility of this approach.

For detection of fragment mass differences and DFs in the MS^2 data, preliminary ΔCF_2 , $\Delta\text{C}_2\text{F}_4$, ΔHF , and the list of DFs were used (later specific mass differences were searched). This resulted in the detection of 30 MS^2 spectra that contained the specified mass differences, and 47 spectra with DF hits out of a total number of 373 unique MS^2 spectra at a mass tolerance set to ± 2 mDa and an MS^2 intensity threshold of 2000 counts in the M1 soil extract (first iteration).

In the suspect screening process, the hits by accurate mass (tolerance of 4 mDa) were reduced from 217 to 176 by the MD/C-m/C cutoff in soil M1.

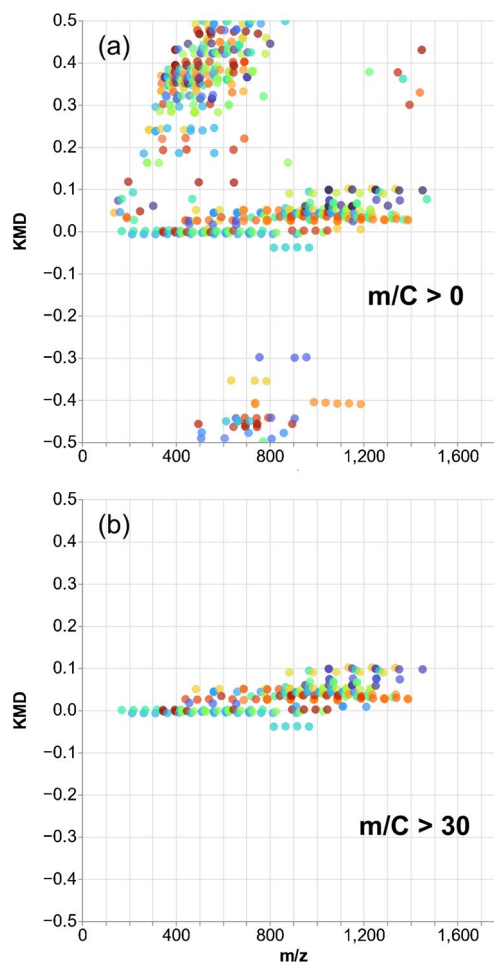


Fig. 4 True- and false-positive CF_2 -based HS in soil M1 **a** without ($m/C > 0$) and **b** with m/C cutoff ($m/C > 30$). An MS^1 noise threshold of 1000 counts was used for feature detection, and the KMD mass tolerance was set to ± 1 mDa with a minimum of three homologues. Even with the low mass tolerance of ± 1 mDa, many hydrocarbon matrix components are mimicking the CF_2 -repeating unit (see also Fig S5). Note: Multiple $(\text{CF}_2)_n$ differences within the KMD tolerance are also assigned to the respective HS; therefore, each datapoint has at least two HS partners

Manual identification process with the *PFAScreen* results table

The verification and (partially manual) identification process of prioritized features from the *PFAScreen* results table (Excel or CSV) was performed by sorting the table according to decreasing intensity, after removing features based on defined MD/C-m/C cutoffs. For soil M1, this resulted in a feature list with 305 potential compounds. Note that some features appear multiple times in the list due to structural isomerism, resulting in multiple features at multiple distinct RTs depending on the degree of separation and the peak finding algorithm. Each feature was verified manually for occurrence in the extraction blank and reasonable peak

shape (until <1% of the most abundant feature). Although a blank correction was performed, typical contaminations from the LC system with long tailing peaks can be integrated multiple times at different RTs. Therefore, they are not always correctly removed depending on the specified parameters. By using the RawDataVisualization tool of PFAScreen, EICs of every m/z belonging to one HS (using the integrated HS extrapolator) can be verified for RT shift and peak shape, eventually resulting in identification of homologues with very low abundances that were missed in the feature finding process due to the MS^1 intensity threshold. The chemical formulas from suspect hits were used to check for reasonable isotope patterns with the RawDataVisualization of PFAScreen. SMILES codes were used to verify at least one candidate per HS by an MS^2 spectrum.

In total, nine PFAS classes could be identified via PFAScreen in the four soils that exhibited at least one suspect hit per HS or compound (Fig. 5). Perfluoroalkyl carboxylic acids (PFCAs, C_4 – C_{20}), fluorotelomer alkyl phosphate diesters (diPAPs, 4:2/6:2–12:2/12:2), $n:3$ fluorotelomer

carboxylic acids (FTCAs, 5:3–13:3), fluorotelomer sulfonic acids (FTSAs, 6:2–16:2), perfluorosulfonic acids (PFSAs, C_4 – C_{10}), perfluorooctane sulfonamide (PFOSA), N-ethylperfluoro-1-octanesulfonamidoacetic acid (N-EtFOSAA), and N-ethyl perfluorooctane sulfonamide ethanol-based phosphate diester (diSAmPAP) were identified in all four soils. Different chain length distributions and abundances were observed (Fig. 5). diPAPs were detected as complex mixtures of several structural isomers depending on their chain length (e.g., 6:2/10:2 and 8:2/8:2, shown by MS/MS). Additionally, their EICs showed peaks at much later RTs corresponding to in-source fragments of triPAPs (Fig. S7). While all telomer-based PFAS were detected as linear chains, the PASF-based PFAS (PFSAs, N-EtFOSAA, PFOSA, and diSAmPAP) showed typical chromatographic peak shapes of mixtures of branched and linear isomers [58]. In these cases, the dominance of a C_8 -based chemistry can be observed (see PFSAs in Fig. 5).

All four soils had a similar contamination pattern. However, for soils M1 and M2 (Mannheim region), another very

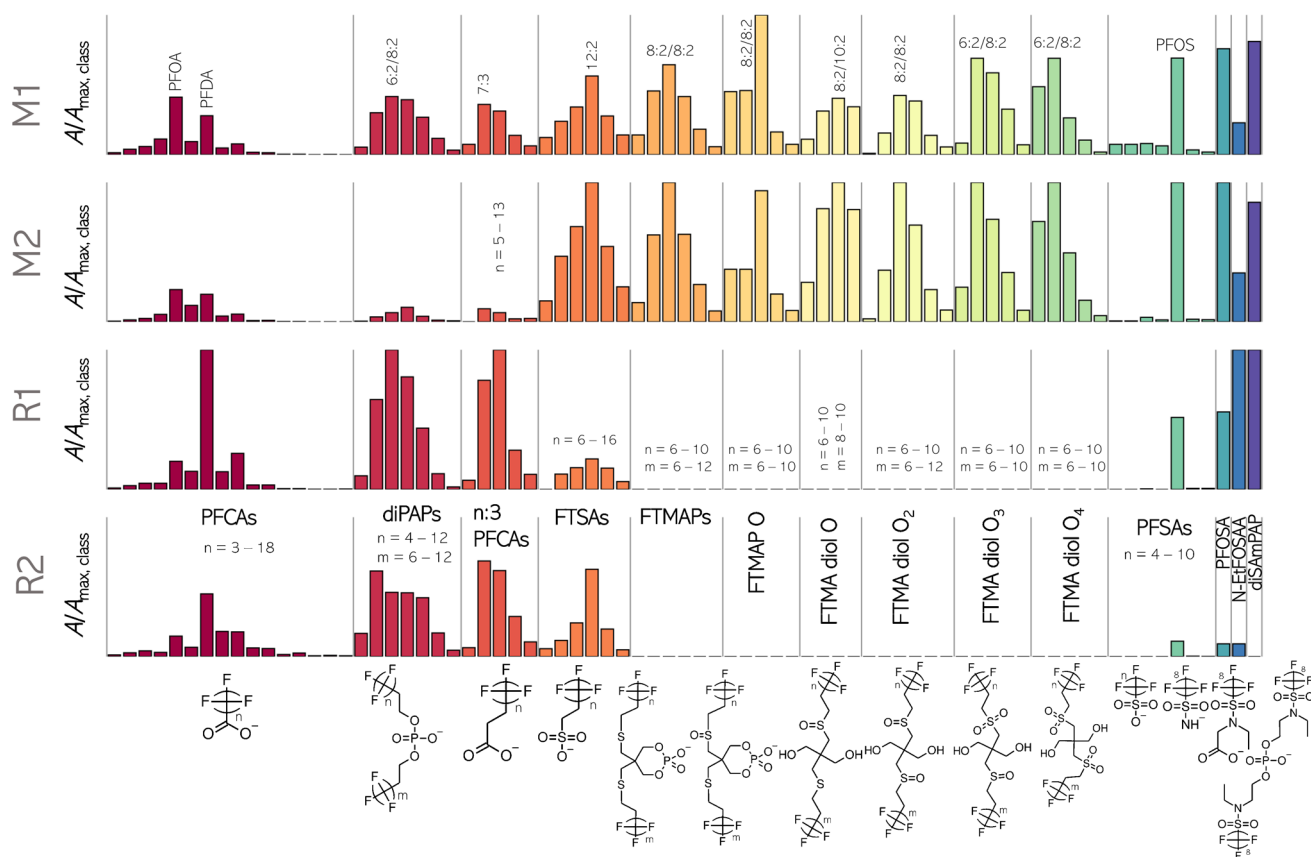


Fig. 5 Qualitative summary of identified PFAS in the four soils (M1, M2, R1, and R2). Each class (e.g., PFCAs, diPAPs) is normalized to the peak area of the most abundant homologue within all four samples. Further abbreviations: FTMAP O, FTMAP-sulfoxide; FTMA diol O, FTMA-diol-sulfoxide; FTMA diol O₂, FTMA-diol-disulfoxide or -sulfone; FTMA diol O₃, FTMA-diol-sulfoxide-sulfone; FTMA

diol O₄, FTMA-diol-disulfone. Note that depending on chain length and sulfur oxidation degree, diPAPs, FTMAPs, and FTMA-diols were detected as complex mixture of structural and positional isomers (e.g., 6:2/10:2 \neq 8:2/8:2, or disulfoxide \neq sulfone). Very small abundant identifications and triPAPs are not shown in the figure

abundant precursor class, namely FTMAPs, was detected (including isomeric profiles ranging 6:2/6:2 to 10:2/12:2), as well the previously identified TPs FTMAP-sulfoxides [31].

The 6:2 fluorotelomer mercapto alkyl phosphate esters (6:2/6:2 FTMAP) could be confirmed with an in-house synthesized reference standard, leading to identification levels of 1 for 6:2 FTMAP and 2a for the further homologues due to clear MS/MS evidence [59]. In general, all identified PFAS are in good agreement with previous studies including biotransformation that characterized other soil samples from both Rastatt and Mannheim [27, 31, 32, 39, 56].

The PF Δ Screen results table also revealed several unknown HS that were detected but did not have an accurate mass match with the suspect list. Their identification with the help of the EIC correlator of PF Δ Screen is discussed in the following.

EIC correlator: coelution correlation analysis for identification of unknowns

After identification of the PFAScreen results, there were several C₂F₄-based HS left without any hit in the suspect list. When looking at several MS¹ spectra of different homologues, many coeluting ions were observed, often characterized by HF losses and other mass differences (Fig. S8). This is an indication of in-source fragmentation of these classes [60, 61]. To be able to efficiently group corresponding in-source fragments and potential adduct ions together, the EIC correlator from the raw data visualization tools of PF Δ Screen was used to correlate the EICs of suspected features (from a given HS) with the EICs of

all detected features that coelute within a given RT range of ± 25 s. Strong correlation of EICs can be used to detect related ions and allows their isolation from other ions in consecutive MS¹ spectra without knowing their mass differences [62–65]. This is exemplified on the unknown *m/z* 966.9944 which is a member of a suspected HS. When correlating the EIC of *m/z* = 966.9944 with the EICs of all coeluting features within a RT range of 50 s, 12 out of 368 EICs correlated with an *R*² > 0.96 at an extraction width of 5 mDa (see Fig S9 for more details). The result is an MS¹ spectrum that only contains coeluting ions (correlation spectrum) of several in-source fragments and adducts (Fig. 6). Since well-known mass differences such as Δ C₂F₄ and Δ HF were found in this MS¹ spectrum, a telomer-based PFAS with potentially two telomer chains (e.g., 6:2/8:2) was suspected [31]. When looking at the mass differences of detected coeluting ions, [M+Cl]⁻, [M+Br]⁻, and [M+Ac]⁻ adducts and several other in-source fragments could be observed. The detection of [M+Cl]⁻ and [M+Br]⁻ ions was of great importance since they allowed the determination of [M] rather easily which then also allowed the identification of other adducts and the molecular formula. The *m/z* = 966.9944 (in-source fragment) corresponds to a FTMAP-related substance, which was tagged FTMA-diol-sulfone-sulfoxide or FTMA-diol-O₃ (see Figs. 5 and 6). With this correlation technique, several tens of unknown HS could be grouped into four novel FTMAP-related compound classes (Fig. 6). They were identified with one oxygen (sulfoxide) and up to 4 oxygens (disulfone) and to the best of our knowledge not reported in literature before. They could be microbial or

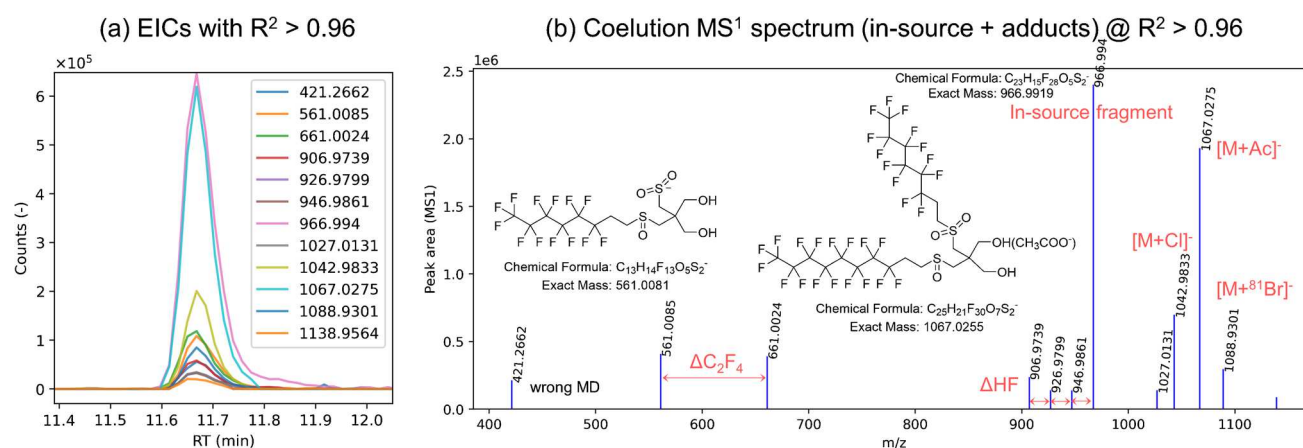


Fig. 6 Detection of coeluting in-source fragments and adducts via the EIC correlator of PF Δ Screen for the identification of 6:2/8:2 FTMA diol sulfoxide sulfone. The EIC of the unknown in-source fragment *m/z* = 966.9944 (which was detected as one member of a HS via KMD) was correlated with all EICs eluting at its RT ± 25 s resulting in non-targeted detection of related ions. In total, 4 HS corresponding to 21 novel FTMAP TPs were identified via the use of this tool

(see Fig. 5). A RT shift with increasing oxidation degree (1 O up to 4 O) was observed due to increasing polarity. Note that the EICs of [M+³⁷Cl] and [M+⁷⁹Cl] are also in the raw MS¹ spectra; however, they were combined into one feature by feature finding algorithm of pyOpenMS (in case of Br, a wrong isotope grouping occurred) and therefore not detectable by the correlation analysis

photochemical FTMAP TPs and close the unknown gap in a previous FTMAP-related transformation study [66], or they could be used intentionally or as side-products in PFAS-coated papers that contaminate these soils. These kinds of correlation spectra made identification possible since the MS² spectra of the adducts ([M-H]⁻ ions of the FTMA-diols were not detected at all which makes sense with ESI) barely formed useful fragments except for Br⁻ which made them hard to interpret. The use of in-source fragments for identification has the advantage that isotope patterns are available for all ions (features), which is often not the case in MS² spectra depending on the isolation width of the precursor ion. All these FTMAP-related substances form multiple in-source fragments (and adducts), all could be confirmed with rather high confidence (identification level of 2b). They all could be grouped by C₂F₄- and O-based KMD (for O-KMD, see Fig. S10) with systematic RTshifts, besides eluting at higher RT than FTMAPs due to their lower polarity attributed to the loss of the phosphoric acid group.

Conclusions

PFAScreen can be used efficiently for prioritizing features in both LC- and GC-HRMS (ESI and APCI) raw data in all kinds of samples independent of the vendor of the mass spectrometer used. Especially, the MD/C-m/C approach is a powerful tool to drastically decrease the number of features and thus reduce false-positive assignments, overcoming a common issue during NTS. Due to the short computational time of PFAScreen (less than 1 min for 4000 spectra), input parameters can be conveniently adjusted depending on the tested sample, instrument used, and end-user needs. Since the number of unknown PFAS in complex environmental and technical samples is still unknown, NTS approaches that combine several data reduction techniques for an efficient workflow are of importance to comprehensively elucidate the identity occurrence and fate of organic pollutants such as PFAS.

Supplementary Information The online version contains supplementary material available at <https://doi.org/10.1007/s00216-023-05070-2>.

Acknowledgements The authors would like to thank Axel Walter for his GitHub repository *ion-chromatogram-extractor* which inspired some functions related to building EICs in PFAScreen, Klaus Röhler for sampling the composite soil samples, and the DBU (Deutsche Bundesstiftung Umwelt) for the scholarship of JZ.

Author contribution JZ conceptualized the structure of PFAScreen, wrote most of the Python source code, and wrote the first draft of the manuscript. BB was part of writing and designing PFAScreen processes and reviewed the manuscript. JFP performed the soil extractions

and reviewed the manuscript. CZ supervised the study and reviewed the manuscript.

Funding Open Access funding enabled and organized by Projekt DEAL. Open Access funding enabled and organized by Projekt DEAL. Deutsche Bundesstiftung Umwelt (DBU) funded the PhD scholarship of JZ.

Code availability and license The Python source code of PFAScreen is available on GitHub (<https://github.com/JonZwe/PFAScreen>) together with example files. It is published under the LGPL-2.1 license.

Declarations

Conflict of interest The authors declare no competing interests.

Open Access This article is licensed under a Creative Commons Attribution 4.0 International License, which permits use, sharing, adaptation, distribution and reproduction in any medium or format, as long as you give appropriate credit to the original author(s) and the source, provide a link to the Creative Commons licence, and indicate if changes were made. The images or other third party material in this article are included in the article's Creative Commons licence, unless indicated otherwise in a credit line to the material. If material is not included in the article's Creative Commons licence and your intended use is not permitted by statutory regulation or exceeds the permitted use, you will need to obtain permission directly from the copyright holder. To view a copy of this licence, visit <http://creativecommons.org/licenses/by/4.0/>.

References

1. Evich MG, Davis MJB, McCord JP, Acrey B, Awkerman JA, Knappe DRU, Lindstrom AB, Speth TF, Tebes-Stevens C, Strynar MJ, Wang Z, Weber EJ, Henderson WM, Washington JW. Per- and polyfluoroalkyl substances in the environment. *Science* 2022;375(6580):eabg9065. <https://doi.org/10.1126/science.abg9065>.
2. Lindstrom AB, Strynar MJ, Libelo EL. Polyfluorinated compounds: past, present, and future. *Environ Sci Technol*. 2011;45(19):7954–61. <https://doi.org/10.1021/es2011622>.
3. Ng C, Cousins IT, DeWitt JC, Glüge J, Goldenman G, Herzke D, Lohmann R, Miller M, Patton S, Scheringer M, Trier X, Wang Z. Addressing urgent questions for PFAS in the 21st century. *Environ Sci Technol*. 2021. <https://doi.org/10.1021/acs.est.1c03386>.
4. Glüge J, Scheringer M, Cousins IT, DeWitt JC, Goldenman G, Herzke D, Lohmann R, Ng CA, Trier X, Wang Z. An overview of the uses of per- and polyfluoroalkyl substances (PFAS). *Environ Sci Process Impacts*. 2020;22(12):2345–73. <https://doi.org/10.1039/d0em00291g>.
5. Cousins IT, DeWitt JC, Glüge J, Goldenman G, Herzke D, Lohmann R, Ng CA, Scheringer M, Wang Z. The high persistence of PFAS is sufficient for their management as a chemical class. *Environ Sci Process Impacts*. 2020;22(12):2307–12. <https://doi.org/10.1039/d0em00355g>.
6. Wang Z, Cousins IT, Scheringer M, Buck RC, Hungerbühler K. Global emission inventories for C₄–C₁₄ perfluoroalkyl carboxylic acid (PFCA) homologues from 1951 to 2030, Part I: production and emissions from quantifiable sources. *Environ Int*. 2014;70:62–75. <https://doi.org/10.1016/j.envint.2014.04.013>.
7. Wang Z, Cousins IT, Scheringer M, Buck RC, Hungerbühler K. Global emission inventories for C₄–C₁₄ perfluoroalkyl carboxylic acid (PFCA) homologues from 1951 to 2030, part II: the

- remaining pieces of the puzzle. *Environ Int.* 2014;69:166–76. <https://doi.org/10.1016/j.envint.2014.04.006>.
8. Cousins IT, Johansson JH, Salter ME, Sha B, Scheringer M. Outside the safe operating space of a new planetary boundary for per- and polyfluoroalkyl substances (PFAS). *Environ Sci Technol.* 2022;56(16):11172–9. <https://doi.org/10.1021/acs.est.2c02765>.
 9. Wang Z, Buser AM, Cousins IT, Demattio S, Drost W, Johansson O, Ohno K, Patlewicz G, Richard AM, Walker GW, White GS, Leinala E. A new OECD definition for per- and polyfluoroalkyl substances. *Environ Sci Technol.* 2021;55(23):15575–8. <https://doi.org/10.1021/acs.est.1c06896>.
 10. Schymanski EL, Zhang J, Thiessen PA, Chirsir P, Kondic T, Bolton EE. Per- and polyfluoroalkyl substances (PFAS) in PubChem: 7 million and growing. *Environ Sci Technol.* 2023;57(44):16918–28. <https://doi.org/10.1021/acs.est.3c04855>.
 11. Stockholm Convention. The new POPs under the Stockholm Convention. 2022. <http://www.pops.int/TheConvention/ThePOPs/TheNewPOPs/tabid/2511/Default.aspx>. Accessed 21.03.2023
 12. Kwiatkowski CF, Andrews DQ, Birnbaum LS, Bruton TA, DeWitt JC, Knappe DRU, Maffini MV, Miller MF, Pelch KE, Reade A, Soehl A, Trier X, Venier M, Wagner CC, Wang Z, Blum A. Scientific basis for managing PFAS as a chemical class. *Environ Sci Technol Lett.* 2020;7(8):532–43. <https://doi.org/10.1021/acs.estlett.0c00255>.
 13. ECHA. ECHA publishes PFAS restriction proposal. 2023. <https://echa.europa.eu/de/-/echa-publishes-pfas-restriction-proposal>. Accessed 21.09.2023
 14. Aro R, Carlsson P, Vogelsang C, Karrman A, Yeung LW. Fluorine mass balance analysis of selected environmental samples from Norway. *Chemosphere.* 2021;283: 131200. <https://doi.org/10.1016/j.chemosphere.2021.131200>.
 15. Aro R, Eriksson U, Kärrman A, Chen F, Wang T, Yeung LWY. Fluorine mass balance analysis of effluent and sludge from Nordic countries. *ACS ES&T Water.* 2021;1(9):2087–96. <https://doi.org/10.1021/acsestwater.1c00168>.
 16. Simon F, Gehrenkemper L, Becher S, Dierkes G, Langhammer N, Cossmer A, von der Au M, Gockener B, Flidner A, Rudel H, Koschorreck J, Meermann B. Quantification and characterization of PFASs in suspended particulate matter (SPM) of German rivers using EOF, dTOPA, (non-)target HRMS. *Sci Total Environ.* 2023;885: 163753. <https://doi.org/10.1016/j.scitotenv.2023.163753>.
 17. Koch A, Aro R, Wang T, Yeung LWY. Towards a comprehensive analytical workflow for the chemical characterisation of organofluorine in consumer products and environmental samples. *TrAC Trend Anal Chem.* 2020;123: 115423. <https://doi.org/10.1016/j.trac.2019.02.024>.
 18. Aro R, Eriksson U, Karrman A, Yeung LWY. Organofluorine mass balance analysis of whole blood samples in relation to gender and age. *Environ Sci Technol.* 2021;55(19):13142–51. <https://doi.org/10.1021/acs.est.1c04031>.
 19. Ruan T, Jiang G. Analytical methodology for identification of novel per- and polyfluoroalkyl substances in the environment. *TrAC Trends Anal Chem.* 2017;95:122–31. <https://doi.org/10.1016/j.trac.2017.07.024>.
 20. Jia S, Marques Dos Santos M, Li C, Snyder SA. Recent advances in mass spectrometry analytical techniques for per- and polyfluoroalkyl substances (PFAS). *Anal Bioanal Chem.* 2022;414(9):2795–807. <https://doi.org/10.1007/s00216-022-03905-y>.
 21. Strynar M, McCord J, Newton S, Washington J, Barzen-Hanson K, Trier X, Liu Y, Dimzon IK, Bugsel B, Zwiener C, Munoz G. Practical application guide for the discovery of novel PFAS in environmental samples using high resolution mass spectrometry. *J Expo Sci Environ Epidemiol.* 2023. <https://doi.org/10.1038/s41370-023-00578-2>.
 22. Joerss H, Menger F. The complex ‘PFAS world’ - how recent discoveries and novel screening tools reinforce existing concerns. *Curr Opin Green Sustain Chem.* 2023. <https://doi.org/10.1016/j.cogsc.2023.100775>.
 23. Zweigle J, Bugsel B, Röhler K, Haluska AA, Zwiener C. PFAS-contaminated soil site in Germany: nontarget screening before and after direct TOP assay by Kendrick mass defect and FindPFAS. *Environ Sci Technol.* 2023;57(16):6647–55. <https://doi.org/10.1021/acs.est.2c07969>.
 24. Liu Y, D'Agostino LA, Qu G, Jiang G, Martin JW. High-resolution mass spectrometry (HRMS) methods for nontarget discovery and characterization of poly- and per-fluoroalkyl substances (PFASs) in environmental and human samples. *TrAC Trends Anal Chem.* 2019;121. <https://doi.org/10.1016/j.trac.2019.02.021>.
 25. Hulleman T, Turkina V, O'Brien JW, Chojnacka A, Thomas KV, Samanipour S. Critical assessment of the chemical space covered by LC-HRMS non-targeted analysis. *Environ Sci Technol.* 2023. <https://doi.org/10.1021/acs.est.3c03606>.
 26. Zweigle J, Bugsel B, Zwiener C. Efficient PFAS prioritization in non-target HRMS data: systematic evaluation of the novel MD/C-m/C approach. *Anal Bioanal Chem.* 2023. <https://doi.org/10.1007/s00216-023-04601-1>.
 27. Bugsel B, Zwiener C. LC-MS screening of poly- and perfluoroalkyl substances in contaminated soil by Kendrick mass analysis. *Anal Bioanal Chem.* 2020;412(20):4797–805. <https://doi.org/10.1007/s00216-019-02358-0>.
 28. Koelmel JP, Paige MK, Aristizabal-Henao JJ, Robey NM, Nason SL, Stelben PJ, Li Y, Kroeger NM, Napolitano MP, Savvaides T, Vasiliou V, Rostkowski P, Garrett TJ, Lin E, Deigl C, Jobst K, Townsend TG, Godri Pollitt KJ, Bowden JA. Toward comprehensive per- and polyfluoroalkyl substances annotation using FluoroMatch software and intelligent high-resolution tandem mass spectrometry acquisition. *Anal Chem.* 2020;92(16):11186–94. <https://doi.org/10.1021/acs.analchem.0c01591>.
 29. Dickman RA, Aga DS. Efficient workflow for suspect screening analysis to characterize novel and legacy per- and polyfluoroalkyl substances (PFAS) in biosolids. *Anal Bioanal Chem.* 2022. <https://doi.org/10.1007/s00216-022-04088-2>.
 30. Kaufmann A, Butcher P, Maden K, Walker S, Widmer M. Simplifying nontargeted analysis of PFAS in complex food matrices. *J AOAC Int.* 2022. <https://doi.org/10.1093/jaoacint/qsac071>.
 31. Zweigle J, Bugsel B, Zwiener C. FindPFAS: non-target screening for PFAS - comprehensive data mining for MS2 fragment mass differences. *Anal Chem.* 2022;94(30):10788–96. <https://doi.org/10.1021/acs.analchem.2c01521>.
 32. Bugsel B, Bauer R, Herrmann F, Maier ME, Zwiener C. LC-HRMS screening of per- and polyfluorinated alkyl substances (PFAS) in impregnated paper samples and contaminated soils. *Anal Bioanal Chem.* 2022;414(3):1217–25. <https://doi.org/10.1007/s00216-021-03463-9>.
 33. Munoz G, Michaud AM, Liu M, Vo Duy S, Montenach D, Resseguier C, Watteau F, Sappin-Didier V, Feder F, Morvan T, Houot S, Desrosiers M, Liu J, Sauve S. Target and nontarget screening of PFAS in biosolids, composts, and other organic waste products for land application in France. *Environ Sci Technol.* 2022;56(10):6056–68. <https://doi.org/10.1021/acs.est.1c03697>.
 34. Liu L, Lu M, Cheng X, Yu G, Huang J. Suspect screening and nontargeted analysis of per- and polyfluoroalkyl substances in representative fluorocarbon surfactants, aqueous film-forming foams, and impacted water in China. *Environ Int.* 2022;167. <https://doi.org/10.1016/j.envint.2022.107398>.
 35. Ng K, Alygizakis N, Androulakakis A, Galani A, Aalizadeh R, Thomaidis NS, Slobodnik J. Target and suspect screening of 4777 per- and polyfluoroalkyl substances (PFAS) in river water, wastewater, groundwater and biota samples in the Danube River Basin.

- J Hazard Mater. 2022;436: 129276. <https://doi.org/10.1016/j.jhazmat.2022.129276>.
36. Grulke CM, Williams AJ, Thillanadarajah I, Richard AM. EPA's DSSTox database: history of development of a curated chemistry resource supporting computational toxicology research. *Comput Toxicol.* 2019;12. <https://doi.org/10.1016/j.comtox.2019.100096>.
 37. Young RB, Pica NE, Sharifan H, Chen H, Roth HK, Blakney GT, Borch T, Higgins CP, Kornuc JJ, McKenna AM, Blotvogel J. PFAS analysis with ultrahigh resolution 21T FT-ICR MS: suspect and nontargeted screening with unrivaled mass resolving power and accuracy. *Environ Sci Technol.* 2022;56(4):2455–65. <https://doi.org/10.1021/acs.est.1c08143>.
 38. Bugsel B, Zweigle J, Zwiener C. Nontarget screening strategies for PFAS prioritization and identification by high resolution mass spectrometry: a review. *Trends Environ Anal Chem.* 2023;40. <https://doi.org/10.1016/j.teac.2023.e00216>.
 39. Nürenberg G, Nödler K, T LF, Schäfer C, Huber K, Scheurer M. Nachweis von polyfluorierten Alkylphosphatestern (PAP) und Perfluoroktansulfonamidoethanol-basierten Phosphatestern (SAM-PAP) in Böden. *Mitt Umweltchem Ökotox*; 2018.
 40. Chambers MC, Maclean B, Burke R, Amodei D, Ruderman DL, Neumann S, Gatto L, Fischer B, Pratt B, Egertson J, Hoff K, Kessner D, Tasman N, Shulman N, Frewen B, Baker TA, Brusniak MY, Paulse C, Creasy D, Flashner L, Kani K, Moulding C, Seymour SL, Nuwaysir LM, Lefebvre B, Kuhlmann F, Roark J, Rainer P, Detlev S, Hemenway T, Huhner A, Langridge J, Connolly B, Chadick T, Holly K, Eckels J, Deutsch EW, Moritz RL, Katz JE, Agus DB, MacCoss M, Tabb DL, Mallick P. A cross-platform toolkit for mass spectrometry and proteomics. *Nat Biotechnol.* 2012;30(10):918–20. <https://doi.org/10.1038/nbt.2377>.
 41. Martens L, Chambers M, Sturm M, Kessner D, Levander F, Shofstahl J, Tang WH, Rompp A, Neumann S, Pizarro AD, Montecchi-Palazzi L, Tasman N, Coleman M, Reisinger F, Souda P, Hermjakob H, Binz PA, Deutsch EW (2011) mzML—a community standard for mass spectrometry data. *Mol Cell Proteomics.* 2011;10(1):R110 000133. <https://doi.org/10.1074/mcp.R110.000133>.
 42. Röst HL, Schmitt U, Aebersold R, Malmstrom L. pyOpenMS: a Python-based interface to the OpenMS mass-spectrometry algorithm library. *Proteomics.* 2014;14(1):74–7. <https://doi.org/10.1002/pmic.201300246>.
 43. Röst HL, Sachsenberg T, Aiche S, Bielow C, Weisser H, Aicheler F, Andreotti S, Ehrlich HC, Gutenbrunner P, Kenar E, Liang X, Nahnsen S, Nilse L, Pfeuffer J, Rosenberger G, Rurik M, Schmitt U, Veit J, Walzer M, Wojnar D, Wolski WE, Schilling O, Choudhary JS, Malmstrom L, Aebersold R, Reinert K, Kohlbacher O. OpenMS: a flexible open-source software platform for mass spectrometry data analysis. *Nat Methods.* 2016;13(9):741–8. <https://doi.org/10.1038/nmeth.3959>.
 44. Sturm M, Bertsch A, Gropf C, Hildebrandt A, Hussong R, Lange E, Pfeifer N, Schulz-Trieglaff O, Zerck A, Reinert K, Kohlbacher O. OpenMS - an open-source software framework for mass spectrometry. *BMC Bioinformatics.* 2008;9:163. <https://doi.org/10.1186/1471-2105-9-163>.
 45. Sachsenberg T, Pfeuffer J, Bielow C, Wein S, Jeong K, Netz E, Walter A, Alka O, Nilse L, Colaiani P, McCloskey D, Kim J, Rosenberger G, Bichmann L, Walzer M, Veit J, Boudaud B, Bernt M, Patikas N, Pilz M, Startek MP, Kutuzova S, Heumos L, Charkow J, Sing J, Feroz A, Siraj A, Weisser H, Dijkstra T, Perez-Riverol Y, Röst H, Kohlbacher O. OpenMS 3 expands the frontiers of open-source computational mass spectrometry. Preprint. 2023. <https://doi.org/10.21203/rs.3.rs-3286368/v1>.
 46. Pfeuffer J, Sachsenberg T, Alka O, Walzer M, Fillbrunn A, Nilse L, Schilling O, Reinert K, Kohlbacher O. OpenMS - a platform for reproducible analysis of mass spectrometry data. *J Biotechnol.* 2017;261:142–8. <https://doi.org/10.1016/j.jbiotec.2017.05.016>.
 47. Kenar E, Franken H, Forcisi S, Wormann K, Haring HU, Lehmann R, Schmitt-Kopplin P, Zell A, Kohlbacher O. Automated label-free quantification of metabolites from liquid chromatography-mass spectrometry data. *Mol Cell Proteomics.* 2014;13(1):348–59. <https://doi.org/10.1074/mcp.M113.031278>.
 48. Helmus R, Ter Laak TL, van Wezel AP, de Voogt P, Schymanski EL. patRoom: open source software platform for environmental mass spectrometry based non-target screening. *J Cheminform.* 2021;13(1):1. <https://doi.org/10.1186/s13321-020-00477-w>.
 49. Kontou EE, Walter A, Alka O, Pfeuffer J, Sachsenberg T, Mohite OS, Nuhamunada M, Kohlbacher O, Weber T. UmetaFlow: an untargeted metabolomics workflow for high-throughput data processing and analysis. *J Cheminform.* 2023;15(1):52. <https://doi.org/10.1186/s13321-023-00724-w>.
 50. Goloborodko AA, Levitsky LI, Ivanov MV, Gorshkov MV. Pyteomics—a Python framework for exploratory data analysis and rapid software prototyping in proteomics. *J Am Soc Mass Spectrom.* 2013;24(2):301–4. <https://doi.org/10.1007/s13361-012-0516-6>.
 51. Levitsky LI, Klein JA, Ivanov MV, Gorshkov MV. Pyteomics 4.0: five years of development of a Python proteomics framework. *J Proteome Res.* 2019;18(2):709–714. <https://doi.org/10.1021/acs.jproteome.8b00717>.
 52. Koelmel JP, Stelben P, McDonough CA, Dukes DA, Aristizabal-Henao JJ, Nason SL, Li Y, Sternberg S, Lin E, Beckmann M, Williams AJ, Draper J, Finch JP, Munk JK, Deigl C, Rennie EE, Bowden JA, Godri Pollitt KJ. FluoroMatch 2.0-making automated and comprehensive non-targeted PFAS annotation a reality. *Anal Bioanal Chem.* 2022;414(3):1201–1215. <https://doi.org/10.1007/s00216-021-03392-7>.
 53. Barzen-Hanson KA, Roberts SC, Choyke S, Oetjen K, McAlees A, Riddell N, McCrindle R, Ferguson PL, Higgins CP, Field JA. Discovery of 40 classes of per- and polyfluoroalkyl substances in historical aqueous film-forming foams (AFFFs) and AFFF-impacted groundwater. *Environ Sci Technol.* 2017;51(4):2047–57. <https://doi.org/10.1021/acs.est.6b05843>.
 54. Place B. Suspect list of possible per- and polyfluoroalkyl substances (PFAS). National Institute of Standards and Technology; 2021. <https://data.nist.gov/od/id/mds2-2387>. Accessed 14 Nov 2023.
 55. Xiao F, Golovko SA, Golovko MY. Identification of novel non-ionic, cationic, zwitterionic, and anionic polyfluoroalkyl substances using UPLC-TOF-MS(E) high-resolution parent ion search. *Anal Chim Acta.* 2017;988:41–9. <https://doi.org/10.1016/j.aca.2017.08.016>.
 56. Röhler K, Susset B, Grathwohl P. Production of perfluoroalkyl acids (PFAAs) from precursors in contaminated agricultural soils: batch and leaching experiments. *Sci Total Environ.* 2023;902: 166555. <https://doi.org/10.1016/j.scitotenv.2023.166555>.
 57. OECD. Toward a new comprehensive global database of per- and polyfluoroalkyl substances (PFASs): summary report on updating the OECD 2007 list of per- and polyfluoroalkyl substances (PFASs). OECD; 2018.
 58. Londhe K, Lee C-S, McDonough CA, Venkatesan AK. The need for testing isomer profiles of perfluoroalkyl substances to evaluate treatment processes. *Environ Sci Technol.* 2022. <https://doi.org/10.1021/acs.est.2c05518>.
 59. Charbonnet JA, McDonough CA, Xiao F, Schwichtenberg T, Cao D, Kaserzon S, Thomas KV, Dewapriya P, Place BJ, Schymanski EL, Field JA, Helbling DE, Higgins CP. Communicating confidence of per- and polyfluoroalkyl substance identification via high-resolution mass spectrometry. *Environ Sci Technol Lett.* 2022;9(6):473–81. <https://doi.org/10.1021/acs.estlett.2c00206>.
 60. Berger U, Langlois I, Oehme M, Kallenborn R. Comparison of three types of mass spectrometers for HPLC/MS analysis of

- perfluoroalkylated substances and fluorotelomer alcohols. *Eur J Mass Spectrom* (Chichester). 2004;10(5):579–88. <https://doi.org/10.1255/ejms.679>.
61. Trier X, Granby K, Christensen JH. Tools to discover anionic and nonionic polyfluorinated alkyl surfactants by liquid chromatography electrospray ionisation mass spectrometry. *J Chromatogr A*. 2011;1218(40):7094–104. <https://doi.org/10.1016/j.chroma.2011.07.057>.
 62. Kuhl C, Tautenhahn R, Bottcher C, Larson TR, Neumann S. CAMERA: an integrated strategy for compound spectra extraction and annotation of liquid chromatography/mass spectrometry data sets. *Anal Chem*. 2012;84(1):283–9. <https://doi.org/10.1021/ac202450g>.
 63. Godzien J, Armitage EG, Angulo S, Martinez-Alcazar MP, Alonso-Herranz V, Otero A, Lopez-Gonzalez A, Barbas C. In-source fragmentation and correlation analysis as tools for metabolite identification exemplified with CE-TOF untargeted metabolomics. *Electrophoresis*. 2015;36(18):2188–95. <https://doi.org/10.1002/elps.201500016>.
 64. Seitzer PM, Searle BC. Incorporating in-source fragment information improves metabolite identification accuracy in untargeted LC-MS data sets. *J Proteome Res*. 2019;18(2):791–6. <https://doi.org/10.1021/acs.jproteome.8b00601>.
 65. Tada I, Chaleckis R, Tsugawa H, Meister I, Zhang P, Lazarinis N, Dahlen B, Wheelock CE, Arita M. Correlation-based deconvolution (CorrDec) to generate high-quality MS2 spectra from data-independent acquisition in multisample studies. *Anal Chem*. 2020;92(16):11310–7. <https://doi.org/10.1021/acs.analchem.0c01980>.
 66. Bugsel B, Schussler M, Zweigle J, Schmitt M, Zwiener C. Photocatalytic transformation of fluorotelomer- and perfluorosulfonamide-based PFAS on mineral surfaces and soils in aqueous suspensions. *Sci Total Environ*. 2023;894: 164907. <https://doi.org/10.1016/j.scitotenv.2023.164907>.

Publisher's Note Springer Nature remains neutral with regard to jurisdictional claims in published maps and institutional affiliations.



Jonathan Zweigle is a PhD candidate (German Federal Environmental Foundation scholar) in the lab of Christian Zwiener. His current research includes analysis of per- and polyfluoroalkyl substances (PFAS) and their transformation products by GC- and LC-HRMS and PFAS precursor characterization by oxidative conversion. His main focus is on the development of non-target screening data analysis approaches for PFAS identification in HRMS data.



Boris Bugsel is a postdoctoral researcher in the lab of Christian Zwiener at the University of Tübingen. His research covers the analysis, occurrence, and environmental fate of per- and polyfluoroalkyl substances (PFAS) and their transformation products. His interests particularly lie in the development of novel screening techniques by liquid and gas chromatography coupled to high-resolution mass spectrometry and an enhanced understanding of the complex and wide-ranging impacts of PFAS on the environment.



Joel Fabregat-Palau holds a PhD in analytical chemistry and the environment, and is currently a postdoctoral researcher in the lab of Prof. Peter Grathwohl at the University of Tübingen. His research covers the environmental fate of organic pollutants in the soil environment. In particular, his main interests are the analysis, sorption, and biodegradation processes of per- and polyfluoroalkyl substances, as well as the application of remediation strategies to contaminated sites.



Christian Zwiener is Head of the Environmental Analytical Chemistry Group in the Department of Geosciences at the Eberhard Karls Universität Tübingen. His research focuses on the analysis, occurrence, and fate of organic micropollutants in the environment and in water treatment (e.g., disinfection byproducts, pharmaceuticals, personal care products, pesticides, poly- and perfluorinated compounds). This includes the development of analytical approaches for non-target and suspect screening by LC-

high-resolution mass spectrometry, field investigations and lab-scale experiments for photochemistry, biodegradation, and electrochemical oxidation to identify transformation products.

Supporting Information

PF Δ Screen – An open-source tool for automated PFAS feature prioritization in non-target HRMS data

Jonathan Zweigle,^{+,*} Boris Bugsel,⁺ Joel Fabregat-Palau,^{||} Christian Zwiener^{+,*}

⁺Environmental Analytical Chemistry, Department of Geosciences, University of Tübingen, Schnarrenbergstraße 94-96, 72076 Tübingen, Germany

^{||}Hydrogeochemistry, Department of Geosciences, University of Tübingen, Schnarrenbergstraße 94-96, 72076 Tübingen, Germany

^{*}Corresponding authors

Contents

S1 INSTALLATION OF PF Δ SCREEN	2
S2 PF Δ SCREEN FUNCTIONALITY AND OUTPUT	3
Fig. S 1: Current graphical user interface (GUI) of PF Δ Screen which is separated into three main functionalities.	3
Fig. S 2: PF Δ Screen results table (here as formatted Excel table, a CSV file is also provided).	5
Fig. S 3: PF Δ Screen interactive HTML plots.	5
Fig. S 4: PF Δ Screen interactive figure from the RawDataVisualization tool.	6
Fig. S 5: Interactive KMD tooltips to visualize RT-shifts with increasing m/z for each detected HS. (a) Systematic (fits to PFCAs) and (b) non-systematic RT-shift (potential false-positive unknown group of compounds).	7
Fig. S 6: Example of an MS ² spectrum where unknown chemical formulas (here only C ₈ F ₁₇) of fragments are calculated by propagation of chemical formulas from diagnostic fragments via fragment mass differences.	7
Figure S 7: EIC of 6:2/6:2 diPAP (RT = 9.6) with in-source fragments that correspond to isomeric triPAPs (e.g., 6:2/6:2/6:2 triPAP).	8
Fig. S 8: HF mass differences from in-source fragmentation of FTMAP-related compounds (e.g., m/z = 1251.0202 which is an [M+Acetate] ⁻ ion of FTMAP diol disulfoxide/sulfone, C ₂₇ H ₁₈ F ₃₈ O ₄ S ₂ (CH ₃ COO) ⁻ = 1251.0172).	8
Fig. S 9: Results from the EIC correlator from the RawDataVisualization tools of PF Δ Screen for the in-source fragment m/z = 966.9944.	8
Fig. S 10: Cutout from an O- and CF ₂ -based KMD vs. m/z plot from the soil extract of M1 showing the different sulfur oxidation states from one to four oxygen atoms.	9
S3 SOIL SAMPLING	9
S4 CHEMICALS	9
S5 INSTRUMENTAL PARAMETERS	10
Table S1: Gradient elution of the HPLC-QTOF method.	10
Table S2: Summary of instrument and scan source parameters used for HPLC-QTOF measurements.	10
REFERENCES	10

S1 Installation of PF Δ Screen

PF Δ Screen can be installed and executed within the standard Python environment or by using the Anaconda distribution. To make installation and use as easy as possible, PF Δ Screen can be automatically installed with the `Installation.bat` file and executed with the `Run_PFAScreen.bat` file. Of course, people familiar with Python can execute the source code with their own custom environment and editor. In the following, the two steps needed for a simple installation are explained.

- 1) **Download PF Δ Screen:** Download the PF Δ Screen source code from <https://github.com/JonZwe/PFAScreen> by clicking on the green “Code” button and click “Download ZIP”. When downloaded, unzip the folder and move it to a local folder on your computer.
- 2) **Automatic installation of Python and the required packages with Installation.bat:** Navigate into the folder where PF Δ Screen was copied (PFAScreen-main). Double click the `Installation.bat` file. Note that depending on your Windows safety settings a warning notification might open that needs to be accepted. The Windows command line interface will open, and the Microsoft Store opens automatically if you do not have Python installed on your computer. Click on “Install” and wait until the installation of Python is finished and close the Microsoft Store. Back to the Windows command line press any button to automatically install pip (Package Manager for Python) and in the following all required Python packages. Finally, when the message “Installation successfully finished” pops up, press any button and the installation is completed.

Note that the Python source code (without the automatic installation via batch files) can also be executed on other operating systems within the Python environment. Here, the respective packages need to be installed manually.

S2 PF Δ Screen functionality and output

To start PF Δ Screen, double click the Run_PFAScreen.bat file. Note that depending on your Windows safety settings a warning notification might open that needs to be accepted. Both the GUI and a Python console window will open (Fig. S1). To load a MS raw datafile, click the “Browse Sample.mzML” button (see Nr. 1 in Fig S1) and choose the mzML file of a sample and an optional mzML file of a blank control (Browse Blank.mzML).

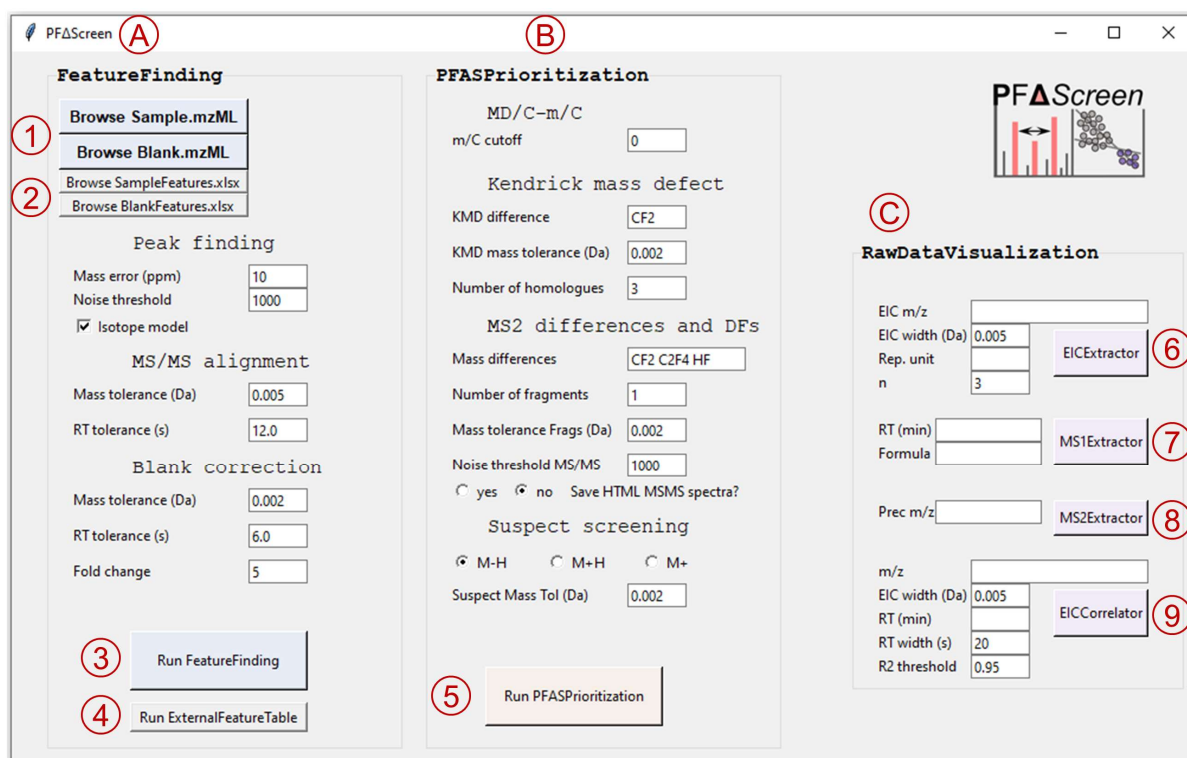


Fig. S 1: Current graphical user interface (GUI) of PF Δ Screen which is separated into three main functionalities. (A) FeatureFinding to detect features in MS raw data, align MS² spectra to detected features and perform a basic blank correction (optional: reading a custom feature list (.csv) from feature finding by another software); (B) PFASPrioritization to prioritize the features according to several techniques such as the MD/C-m/C approach, KMD analysis, fragment mass differences, diagnostic fragments and suspect screening resulting in output of several plots and a summary table (Excel and CSV); (C) RawDataVisualization to visualize MS raw data (EICs, MS¹ and MS² spectra) and correlate related ions to detect in-source fragments and adducts.

The samples should have been measured under data-dependent acquisition (ddMS²) with centroided spectra, ideally with one collision energy per precursor. Now, the parameters for peak finding, MS² alignment and blank correction can be specified and executed by pressing the “Run FeatureFinding” button (Nr. 3 in Fig S1). Since OpenMS and our MS² alignment and blank correction code are rather fast this task usually takes less than one minute (e.g., for

4000 spectra per sample), and runtime is mainly dependent on the selected MS¹ noise threshold. In case another feature finding procedure (e.g., from vendor software) is desired, custom feature lists (see `external_feature_list.xlsx` on GitHub) together with the respective mzML files can instead be included in *PFAScreen* (without peak finding by OpenMS). This is done by the “Browse SampleFeatures.xlsx” and “Browse BlankFeatures.xlsx” buttons, which are preprocessed by the “Run ExternalFeatureTable” button (Nr. 2 and 4 in Fig S1). Note that data evaluation only works when the corresponding mzML files are also given; otherwise MS² data would be missing. Whenever the **FeatureFinding** tab is completed, the **RawDataVisualization** (C in Fig S1) can be used even without PFAS-specific data. To perform the **PFASPrioritization** (B in Fig S1), appropriate input parameters can be set, and then PFAS-specific data evaluation is performed by clicking the “Run PFASPrioritization” button (Nr. 5 in Fig S1). This task is usually computed in less than one minute, allowing a convenient adjustment of input. Afterwards, MS² spectra displayed by the **RawDataVisualization** tool (MS² extractor), have highlighted fragment mass differences and diagnostic fragments, if some were detected. After executing the **PFASPrioritization** tab, the *PFAScreen* results table (Excel format and additional CSV file, Fig. S2) and several interactive HTML plots (Fig. S3) are saved in a folder named after the sample that can be easily inspected, including a MD/C-m/C plot, a m/z vs. RT plot (with and without MS² raw data), a KMD with linked m/z vs. RT plot (to verify systematic RT-shifts), and a m/C histogram. Data from the results table can be used to visualize EICs (and extrapolate HS with common repeating units such as CF₂), MS¹ and MS² spectra. Additionally, a coelution correlation can be performed with the **RawDataVisualization** tool. Also, the theoretical isotope patterns of suspect hits can be displayed over the experimental isotope patterns (MS¹) (see Fig. S4).

Index	m/z	m/z+1	m/z intens	RT (m)	RT	n diffs	n dias	C	MD	MD/C	m/C	KMD	HS Number	Unique Hom	hit in list	FORMULA	SMILES
2734	498.93062	499.933368	2273744.487	7.29678	437.807	0	0	7.112	-0.069	-0.00976	70.149	-0.03752	5528	2	Heptadecalf	[C8HF17O3S]	[C]C(C)C
4909	900.9085	901.912121	112198.5211	7.65217	459.13			13.53	-0.091	-0.00676	66.569	-0.03395	51	2	Bis[heptade	[C16HF34O2P]	[C]C(C)C
4030	669.96207	670.96497	1260132.474	9.81982	589.189	0	1	10.55	-0.038	-0.0036	63.529	0.004859	2180	1	N-methylpe	[C13H6F21NO]	[CN]C(C)=
4294	714.95517	715.958482	2146242.525	9.81982	589.189	10	4	11.3	-0.045	-0.00397	63.276	0.000834	1584	1			
89	168.98971	169.993094	3074503.186	4.00965	240.579	0	0	2.732	-0.01	-0.00377	61.853	0.000505	2012	5	PFBA-CO2H	[nan]	[nan]
3793	636.64176	637.644494	374695.8686	11.6856	701.134			10.35	-0.358	-0.0346	61.487	-0.31757	4084	1			
2405	466.97464	467.978318	341997.3838	6.977	418.62			7.595	-0.025	-0.00334	61.482	0.004469	1792	2			
2735	498.93101	499.934109	6416312.064	7.43892	446.335	10	8	8.121	-0.069	-0.0085	61.436	-0.03712	5528	2	Heptadecalf	[C8HF17O3S]	[C]C(C)C
4073	676.61431	677.617707	129699.9687	11.6856	701.134			11.03	-0.386	-0.03495	61.318	-0.34247	2952	1			
5	110.9759	111.978379	1708890.157	12.0765	724.587			1.822	-0.024	-0.01323	60.916	-0.01701	1152	1			
4703	816.90908	817.913829	89497.34175	7.36783	442.07			13.48	-0.091	-0.00674	60.587	-0.03874	1786	4			
2851	510.96415	511.967239	324169.5619	6.977	418.62			8.629	-0.036	-0.00415	59.218	-0.00321	1153	4	Hydrogen-su	[C10H2F18O3]	[C]C(C)C
4813	866.90665	867.910247	370298.3747	7.59885	455.931			14.67	-0.093	-0.00636	59.101	-0.03798	1786	4			
4893	894.94479	895.948189	719920.3489	15.7741	946.446			15.38	-0.055	-0.00359	58.175	0.001951	5016	14			
3817	640.63765	641.640766	93397.00261	11.4546	687.275			11.12	-0.362	-0.03257	57.591	-0.32143	4536	1			
4957	916.90365	917.906737	311725.1191	7.7943	467.658			15.97	-0.096	-0.00603	57.426	-0.03778	1786	4			
2726	497.94682	498.948762	342366.7266	8.29177	497.506			8.686	-0.053	-0.00612	57.327	-0.02137	5482	2	Perfluoroc	[C8H2F17NO2]	[C]C(C)C

Fig. S 2: PFAScreen results table (here as formatted Excel table, a CSV file is also provided). This table summarizes most calculations performed in the PFAS feature prioritization steps and is directly formatted as a table to conveniently sort and slice data. m/z and RT values can easily be copied and for instance EICs or MS spectra (and coelution correlation) can be visualized in the RawDataVisualization tool of PFAScreen.

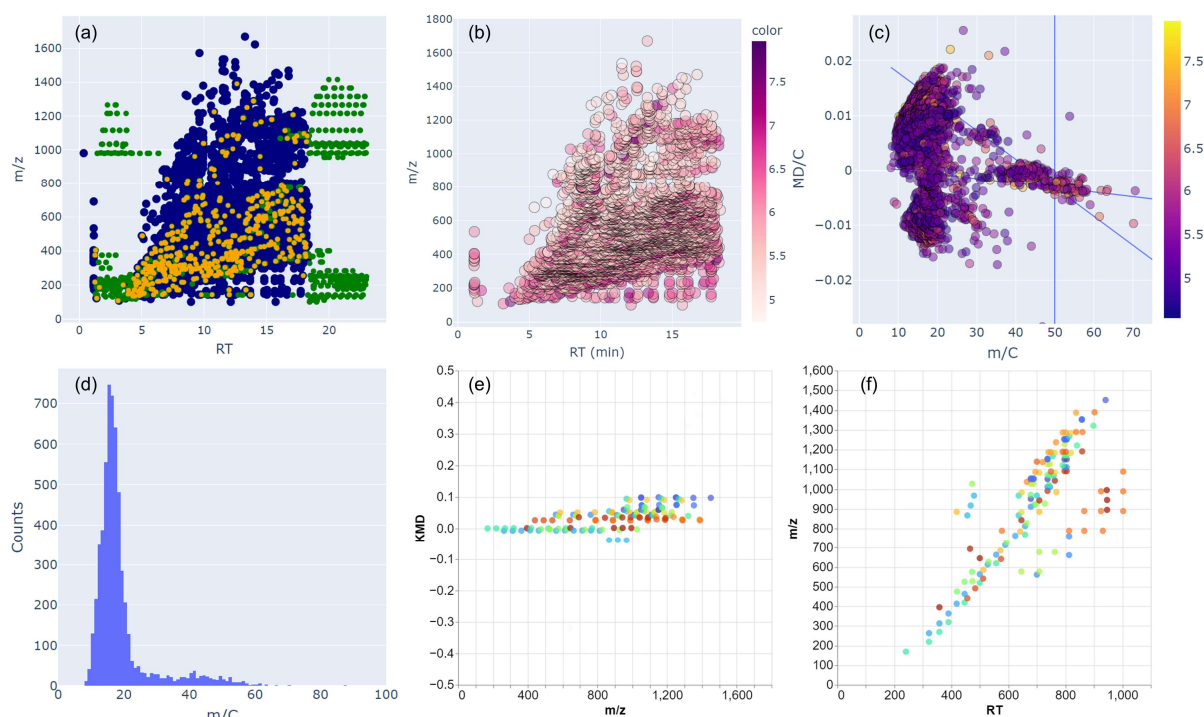


Fig. S 3: PFAScreen interactive HTML plots. (a) m/z vs. RT of all features and the precursors with MS² raw spectra. Blue color corresponds to a detected feature, yellow if an MS² spectrum was assigned and green displays all MS² spectra. This plot can be used to find suitable m/z and RT tolerances for MS² alignment depending on the chromatography (e.g., peak width) and the MS² scan rate. (b) m/z vs. RT overview with m/C as colormap. (c) MD/C-m/C plot to deduce reasonable cutoffs for data reduction depending on the sample matrix. (d) m/C histogram to visualize the m/C distribution of the measured sample. (e) KMD plot coupled to (f) m/z vs. RT to easily verify the systematic RT-shift of each detected homologous series (see Fig. S5).

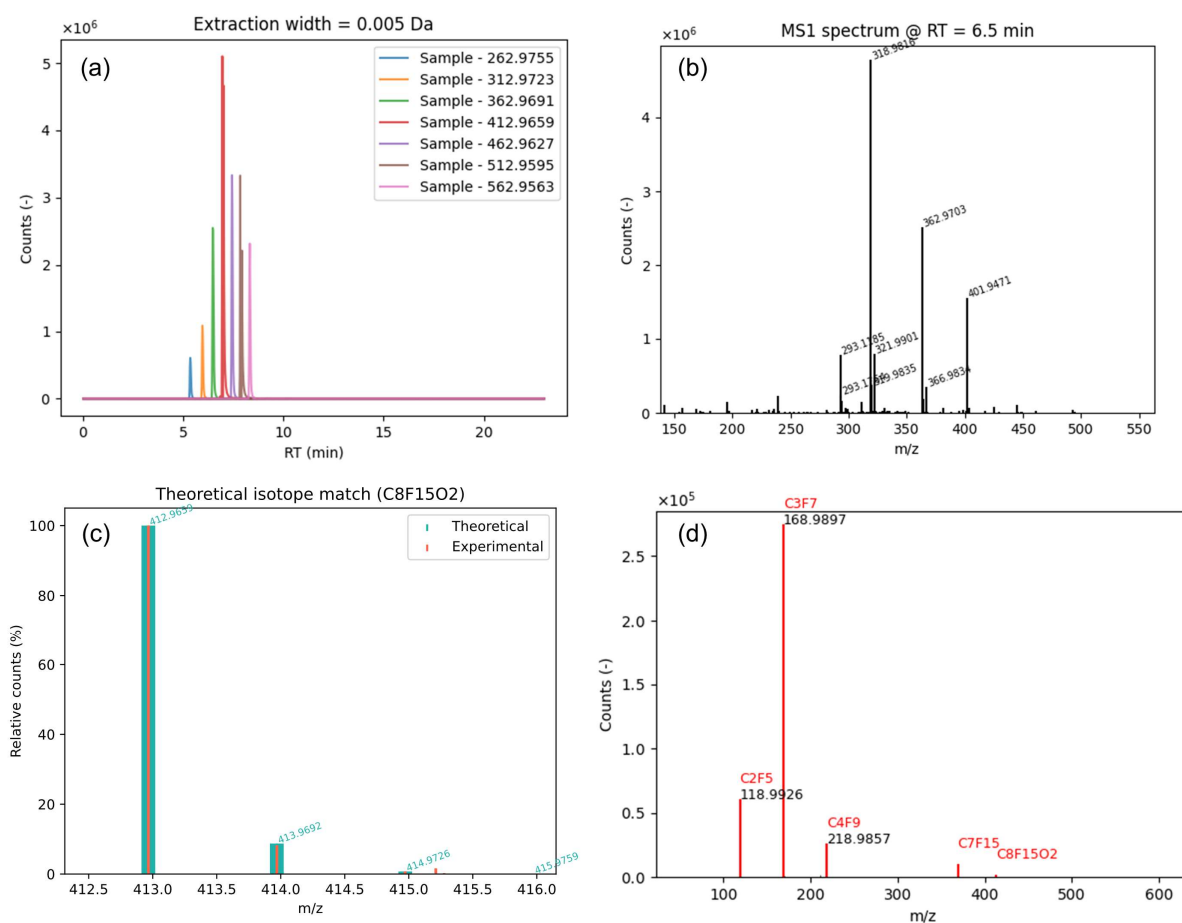


Fig. S 4: PFAScreen interactive figure from the RawDataVisualization tool. (a) EICs can be generated with comma separated lists of m/z values of for one m/z value n homologue of a common repeating unit (e.g., CF₂) are automatically generated. (b) Extracted MS¹ spectrum at a particular RT of interest. (c) When a chemical formula of a suspected compound (e.g., a suspect hit for PFOA, C₈F₁₅O₂ for [M-H]⁻) is given, the theoretical isotope pattern is overlaid with the normalized cutout at this specific m/z. (d) MS² spectra of an m/z of interest can also be visualized with annotations and fragment mass differences.

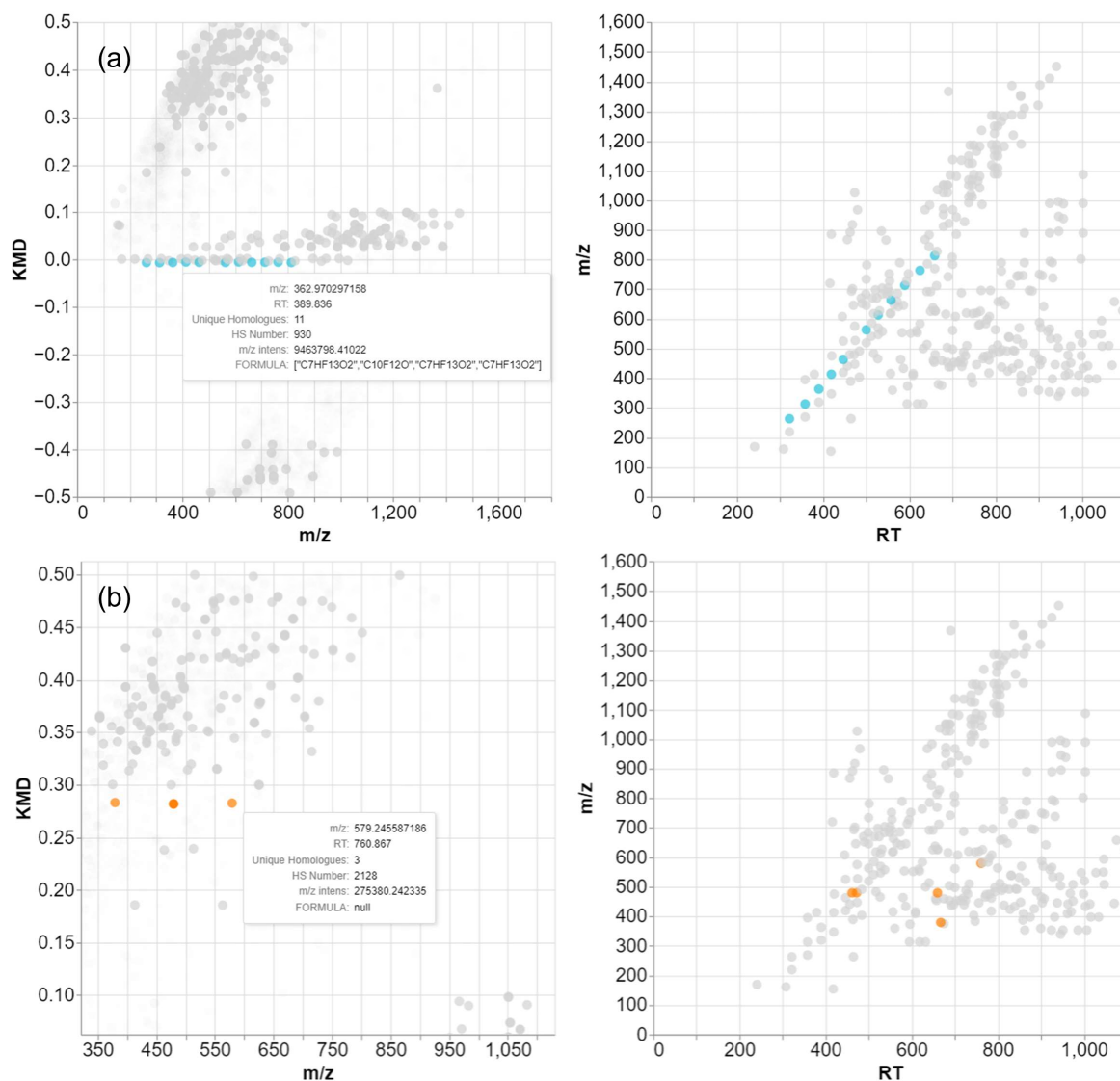


Fig. S 5: Interactive KMD tooltips to visualize RT-shifts with increasing m/z for each detected HS. (a) Systematic (fits to PFCAs) and (b) non-systematic RT-shift (potential false-positive unknown group of compounds).

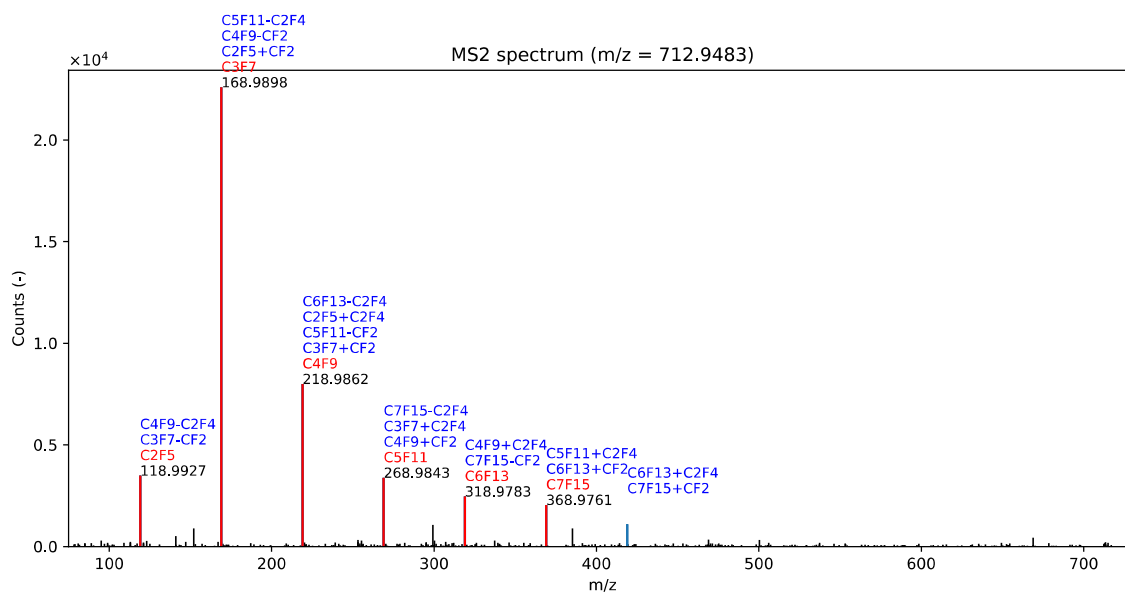


Fig. S 6: Example of an MS² spectrum where unknown chemical formulas (here only C₈F₁₇) of fragments are calculated by propagation of chemical formulas from diagnostic fragments via fragment mass differences.

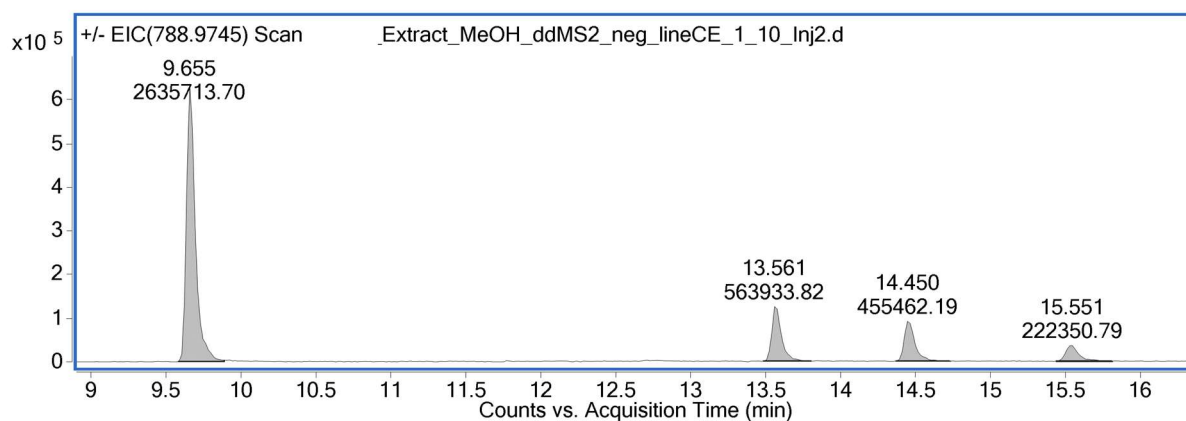


Figure S 7: EIC of 6:2/6:2 diPAP (RT = 9.6) with in-source fragments that correspond to isomeric triPAPs (e.g., 6:2/6:2/6:2 triPAP).

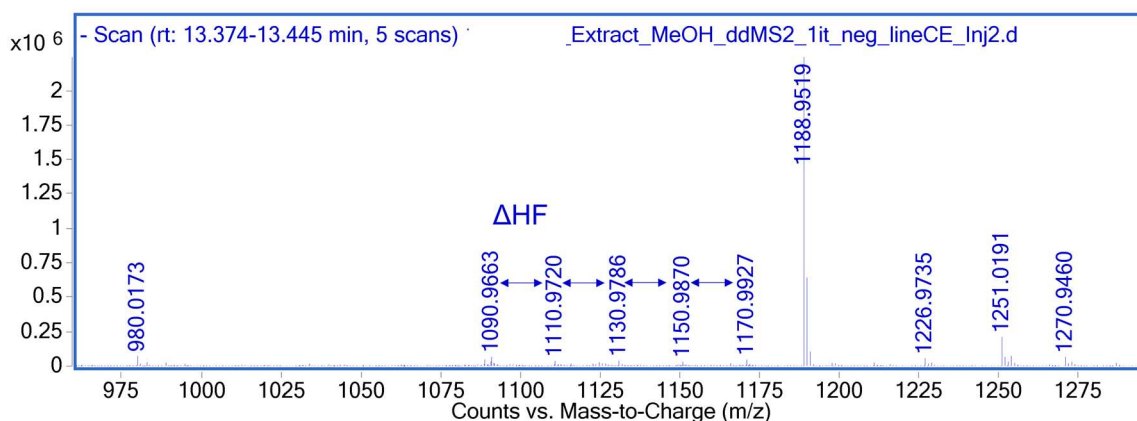


Fig. S 8: HF mass differences from in-source fragmentation of FTMAP-related compounds (e.g., $m/z = 1251.0202$ which is an $[M+Acetate]^-$ ion of FTMAP diol disulfoxide/sulfone, $C_{27}H_{18}F_{38}O_4S_2(CH_3COO)^- = 1251.0172$).

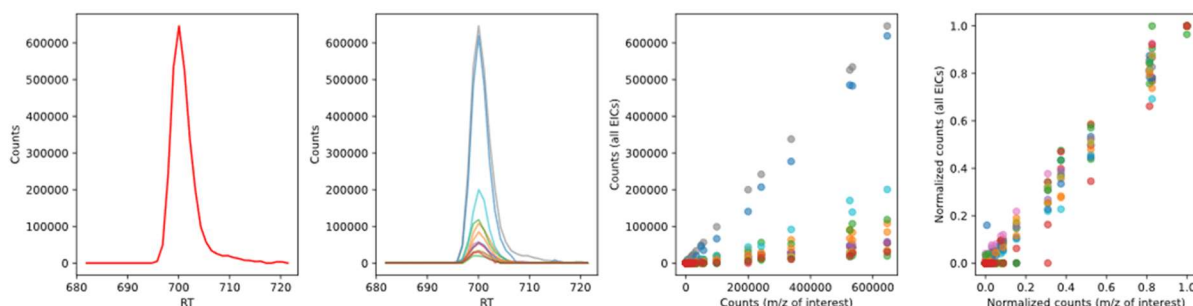


Fig. S 9: Results from the EIC correlator from the RawDataVisualization tools of PF Δ Screen for the in-source fragment $m/z = 966.9944$ (that corresponds to 6:2/8:2 FTMA diol sulfoxide sulfone) at a RT-width of 20 s and a R2 correlation threshold of > 0.95 .

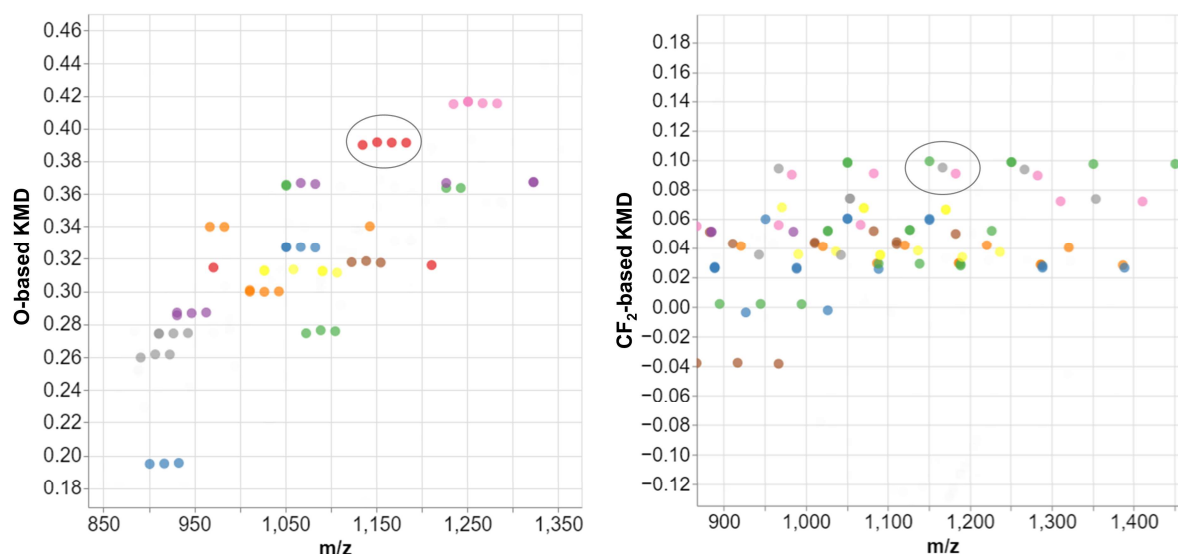


Fig. S 10: Cutout from an O- and CF₂-based KMD vs. m/z plot from the soil extract of M1 showing the different sulfur oxidation states from one to four oxygen atoms.

S3 Soil sampling

Soils were sampled on four agricultural fields in one diagonal over the respective area. Soils R1 and R2 were sampled near Rastatt, both within the 0 – 30 cm horizon. Soil R2 was a sandy loam soil, with pH 5.5 and organic content of 0.8%. Soil R1 was a loamy sand soil, with pH 6.9 and organic content of 2.3%. Soils M1 and M2 were sampled near Mannheim within the 0-30 and 0-50 cm horizon, respectively. Soil M1 was a loam soil, with pH 7.1 and organic content of 6.6%. Soil M2 was a clay loam soil, with pH 7.0 and organic content of 3.9%. All samples were homogenized and mixed thoroughly [1].

S4 Chemicals

Water and methanol (MeOH) were both LC-MS grade (Fisher Chemical). Ammonium acetate (NH₄Ac, ≥99%) was purchased from Fisherbrand. Reference standards of PFCAs, PFSA, 5:3 FTCA, 6:2 and 8:2 FTSA, and 6:2 and 8:2 diPAP, PFOSA, N-EtFOSAA, and diSAmPAP were purchased from Wellington laboratories. 6:2 FTMAP was previously synthesized (details in [2]).

S5 Instrumental parameters

Table S1: Gradient elution of the HPLC-QTOF method. A = 95/5 H₂O/MeOH + 2 mM NH₄Ac and B = 95/5 MeOH/H₂O + 2 mM NH₄Ac.

Time (min)	A (%)	B (%)
0	85	15
2.0	30	70
5.0	10	90
10.0	0	100
15.0	0	100
15.1	85	15
22.0	85	15

Table S2: Summary of instrument and scan source parameters used for HPLC-QTOF measurements.

Instrument Parameters	
Gas Temp (°C)	150
Gas Flow (L/min)	16
Nebulizer pressure (psig)	35
Sheath gas temperature (°C)	380
Sheath gas flow (L/min)	12
Fragmentor voltage (V)	380
Scan Source Parameter	
Capillary voltage (V)	3000
Nozzle voltage (V)	300

References

1. Röhler K, Susset B, Grathwohl P (2023) Production of perfluoroalkyl acids (PFAAs) from precursors in contaminated agricultural soils: Batch and leaching experiments. *Sci Total Environ* 902:166555. doi:10.1016/j.scitotenv.2023.166555
2. Bugsel B, Bauer R, Herrmann F, Maier ME, Zwiener C (2022) LC-HRMS screening of per- and polyfluorinated alkyl substances (PFAS) in impregnated paper samples and contaminated soils. *Anal Bioanal Chem* 414 (3):1217-1225. doi:10.1007/s00216-021-03463-9

Appendix 5

Publication 5

Nontarget Screening Strategies for PFAS Prioritization and Identification by High Resolution Mass Spectrometry: A Review

Boris Bugsel,^{+||} Jonathan Zweigle,^{+||} Christian Zwiener⁺

⁺Environmental Analytical Chemistry, Center for Applied Geoscience, University of Tübingen,
Schnarrenbergstraße 94-96, 72076 Tübingen, Germany

^{||}The authors contributed equally to this work and share first authorship.

Published in: Trends in Environmental Analytical Chemistry, 40.

DOI: 10.1016/j.teac.2023.e00216

Reprinted with permission from Trends in Environmental Analytical Chemistry: Bugsel, B., Zweigle, J., & Zwiener, C. (2023). Nontarget screening strategies for PFAS prioritization and identification by high resolution mass spectrometry: A review. Trends in Environmental Analytical Chemistry, 40. <https://doi.org/10.1016/j.teac.2023.e00216>



Nontarget screening strategies for PFAS prioritization and identification by high resolution mass spectrometry: A review

Boris Bugsel¹, Jonathan Zweigle¹, Christian Zwiener^{*}

Environmental Analytical Chemistry, Department of Geosciences, University of Tübingen, Schnarrenbergstraße 94–96, 72076 Tübingen, Germany

ARTICLE INFO

Keywords:

PFAS
Nontarget screening
High-resolution mass spectrometry
Kendrick mass
Mass defect
Diagnostic fragment
Fragment mass difference
Identification

ABSTRACT

Per- and polyfluoroalkyl substances (PFAS) are a large group of more than 4700 individual compounds which are applied in a wide range of applications in industrial processes and consumer products due to their water and oil repellency and surfactant properties. Concerns on PFAS arise from the very high stability, bioaccumulation potential and toxicity and the ubiquitous occurrence in humans, animals, soils, sediments, surface, ground and drinking waters. Advanced analytical methods are needed to investigate the input and fate of PFAS and potential transformation products in the environment and the exposure pathways for humans and wildlife. Therefore, nontarget screening (NTS) methods by high-resolution mass spectrometry (HRMS) coupled to chromatography are often applied to meet the analytical challenges arising from the high number and chemical diversity of individual compounds, the lack of authentic standards and information on identity and application areas. In this critical review we discuss the recent advances of NTS workflows applied to detect and identify PFAS based on the intrinsic information contained in data from chromatography and HRMS data on the MS¹ and MS² level. This includes retention time and peak shape characteristics, data on accurate mass and isotopologues, and high-resolution mass fragments. Successful approaches for prioritization and identification of PFAS are mostly based on mass defect filtering, Kendrick mass defect analysis, mass matches with suspect lists, assignment of chemical formulas, mass fragmentation patterns, diagnostic fragments and fragment mass differences. So far NTS approaches for PFAS were able to identify more than 750 compounds. However, still limited applicability of chromatography and ionization methods and limited mass resolving power and accuracy largely restrict a complete identification of a high number of unknown PFAS in complex samples from environmental compartments and biota.

1. Introduction

Per- and polyfluoroalkyl substances (PFAS) are a large chemical class with more than 4700 individual compounds with a wide variety of chemical compositions, molecular weights (e.g., 164 Da for perfluoropropionic acid and more than 2000 Da for phosphazenes which are used as reference compounds during mass spectral analysis), functional groups (e.g., carboxylic, sulfonic or phosphoric acids, betaines and phosphate esters) and fluorine percentages [1–3]. The database PubChem even shows more than 220,000 entries for compounds that contain more than one fully fluorinated methyl or methylene group (CF₂ or CF₃) and are therefore considered PFAS according to the Organisation for Economic Co-operation and Development (OECD) [1]. This also includes pharmaceuticals and pesticides [4].

PFAS exhibit unique properties due to the high thermal and chemical stability and the hydrophobic and concurrent lipophobic nature. Therefore, PFAS are used in a wide range of applications in industrial processes, consumer and household products, e.g., in metal plating, firefighting foams, electronics, photolithography, hydraulic fluids, textiles, paper, leather, cosmetics and cleaning products [5]. As a consequence, PFAS are discharged to the environment during production, use, disposal or recycling and can accumulate in environmental compartments and biota due to their extreme persistence under environmental conditions, which is why they are also called forever chemicals [6–8]. Therefore, PFAS are ubiquitously detected in humans and animals, soil, sediments, surface, ground and drinking waters [9–12]. Cousins et al. (2022) even suggested to define a separate planetary boundary for PFAS which is already exceeded based on the occurrence of four

* Corresponding author.

E-mail address: christian.zwiener@uni-tuebingen.de (C. Zwiener).

¹ The authors contributed equally to this work and share first authorship.

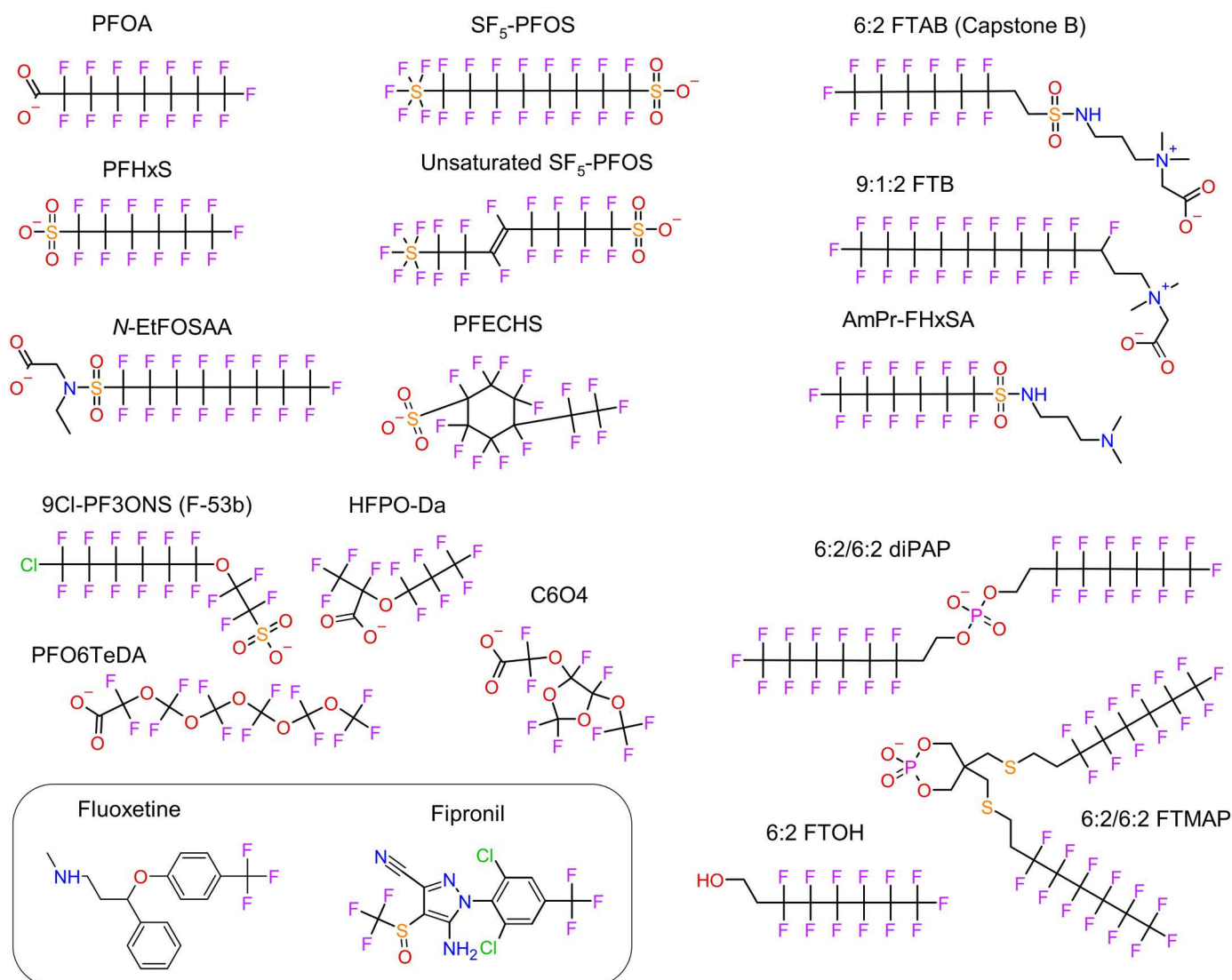


Fig. 1. General examples of different PFAS structures amenable to LC- or GC-HRMS measurements. The compounds inside the box are PFAS according to the OECD definition [1], however they are not in the scope of the techniques discussed in this review (except for diagnostic fragments or mass differences). There are examples of perfluorinated carboxylic and sulfonic acids (e.g., PFOA, PFHxS), telomer-based PFAS (e.g., diPAP, FTOH etc.), aqueous film-forming foam (AFFF) PFAS (e.g., FTAB, FTB), ether PFAS (e.g., HFPO-DA, C6O4) and sulfonamide-based PFAS (e.g., N-Et-FOSAA). Note that dependent on chemical synthesis the shown PFAS structures are also partially observed as branched isomers (e.g., typical for electrochemical fluorination).

perfluoroalkyl acids (PFOA, PFNA, PFOS, PFHxS) in rainwater, soils and surface waters and the poor reversibility of environmental exposure to PFAS [13]. PFAS are also affecting human and animal health including effects on the immune and hormone system, the lipid metabolism, liver and kidney [14–16].

To minimize emissions of PFAS and uptake by humans, animals and plants and to understand their input and fate in the environment and in industrial and treatment processes, there is an increasing need for analytical screening approaches which open the analytical window to detect a much larger fraction of PFAS and their transformation products (TPs) than routine measurements typically cover. The focus of standardized methods for PFAS quantification is on perfluoroalkyl carboxylic acids (PFCAs) and perfluoroalkyl sulfonic acids (PFSA), typically with much less than 50 analytes [17,18]. Recent reviews on target analysis and suspect screening considered the complete analytical process from sampling and sample preparation to analysis methods for air, water, solids and biota [11,19–22], others focused on PFOA and PFOS replacement chemicals like hexafluoropropylene oxide-dimer (HFPO-DA), 6:2 chlorinated polyfluoroalkyl ether sulfonate (F-53B), and also other ether PFAS [12,23].

The challenges of PFAS determination methods are based on the large number of single substances with quite different compound properties and the even larger number of transformation products (TPs), the lack of information on PFAS identity and application areas, and the scarcity of authentic standards. Therefore, nontarget screening (NTS) methods by high-resolution mass spectrometry (HRMS) coupled to chromatography and ion mobility are attractive approaches to meet these challenges. Since NTS workflows often result in tentative identifications which cannot always be confirmed by reference standards due to their unavailability, the confidence of the identification clearly needs to be communicated. For this purpose, a confidence scheme which was originally presented by Schymanski et al. [24] was adapted specifically for PFAS by Charbonnet et al. (2022), ranging from level 1a (confirmed by reference standard) to level 5a/5b (exact mass match) [25]. The more evidence there is available (e.g., a compound appears in a homologous series or MS² data further corroborate the structure of a PFAS), the higher the confidence level.

Various applications of NTS workflows including data evaluation detected more than 750 PFAS from 130 chemical classes in environmental samples, biofluids, and commercial products [26] and

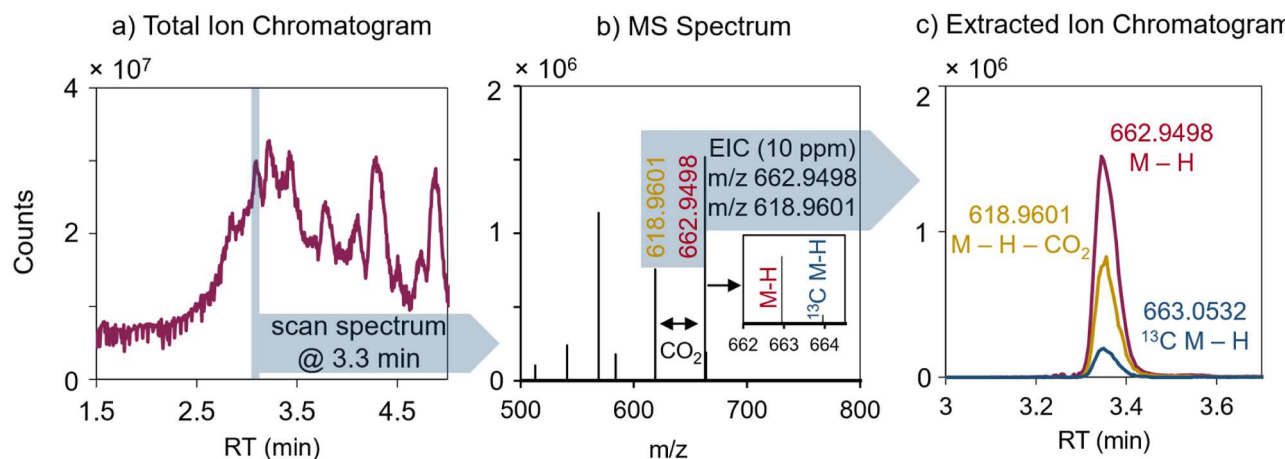


Fig. 2. Available information from fullscan measurements. a) Total ion chromatogram; b) MS spectrum of peak at 3.3 min with accurate mass, mass defect and the isotope ratio of the $M+1$ isotope (14.3% abundance; insert plot) of PFTTrDA (m/z 662.9498) and a potential fragment (m/z 618.9601) due to the neutral loss of CO_2 (43.9898 Da); c) The extracted ion chromatograms show a perfect co-elution of both ions (extracted with a 20 ppm window) and reveal m/z 618.9601 as in-source fragment of PFTTrDA.

demonstrated the high complexity of the worldwide PFAS contamination [27]. A further recent review discussed practical aspects and challenges of HRMS applications for the discovery of novel PFAS in environmental samples and demonstrated that various techniques have been developed and optimized for the analysis of PFAS in the recent years, however, the access to instruments and techniques which are required for a sophisticated NTS remain limited [28].

The objective of this critical review is therefore to compile and discuss the most promising tools and approaches used for NTS measurements and identification workflows for PFAS and their TPs in different sample matrices (air, water, soil, sediment, biota, industrial and consumer products). We will discuss the use of the intrinsic properties of LC- and GC-HRMS data on the MS^1 and the MS^2 level and their use for data prioritization and identification of PFAS and TPs. This includes information retrieval obtained from accurate mass, isotope patterns and retention times as well as mass fragmentation and its use in NTS workflows, libraries and computer-based algorithms. Typically, most approaches cover PFAS with a higher fluorine content (> 55% mass) or with at least three perfluorinated carbon atoms (CF_2 , CF_3). Therefore, for example pesticides, pharmaceuticals or PFAS with only one or two isolated CF_3 groups are not included.

2. MS^1 methods (fullscan)

HRMS data are typically acquired in a suitable mass range (typically between m/z 50–100 and 1300) which includes 98.3% of all PFAS in the curated OECD PFAS list in which compound mixtures and salts are removed, available as S25 in the NORMAN suspect list exchange [29] at a mass resolving power higher than 20,000 (at m/z 500) and a mass accuracy in the range between 1 and 10 ppm. Intrinsic information of HRMS data on the MS^1 level include the accurate mass of the molecular ion and its isotopologues and their intensities. Ultrahigh-resolution MS data at mass resolving power above 250,000 allows the identification of isotope fine structures of specific elements.

Further information on retention time and peak shapes (width, asymmetry) are obtained from chromatography (mostly LC or GC) coupled to HRMS. From high-resolution MS^1 data, advanced conclusions can be drawn on chemical formulas (elemental composition), compound characteristics and possible relationships between single analytes based on common repeating units of homologues (e.g. CF_2 or CF_2O units of PFAS). Furthermore, criteria to prioritize potential PFAS from a large list of nontarget features can be defined based on mass, mass defect or homologues. Data reduction, typically from several thousands of features to a few dozens of potential PFAS, is a crucial step in the NTS workflow

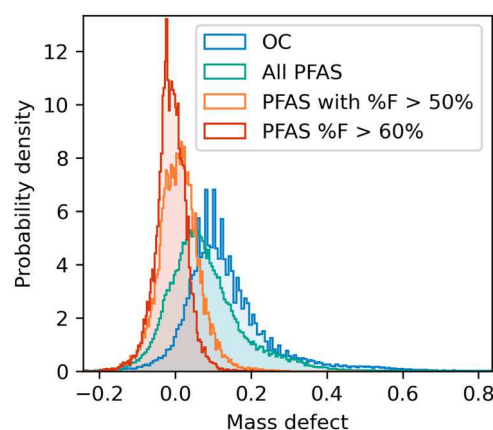


Fig. 3. Histogram of mass defects for different compound classes: hydrocarbons (blue, $n = 182\,503$), PFAS with parts larger than CF_2/CF_3 (teal, $n = 210\,091$), PFAS with $\%F > 50\%$ (orange, $n = 56\,239$) and PFAS with $\%F > 60\%$ (red, $n = 25\,590$). Formulas of PFAS were obtained from the “PFAS and Fluorinated Compounds in PubChem Tree”, of hydrocarbons from the EPA DSSTox dataset in PubChem [4,39] and the NORMAN Suspect List Exchange. The data was preprocessed according to Zweigle et al. (2023) [40].

since peak picking algorithms performed by instrument or open-source software (e.g., MZmine [30] or OpenMS [31]) provide long lists of features from sample and background constituents.

Furthermore, MS^1 information from “true” compounds which are present in the original sample have to be distinguished from possible in-source fragments. For example, negative ESI of PFCAs typically produces $[\text{M}-\text{H}]^-$ and $[\text{M}-\text{H}-\text{CO}_2]^-$ ions due to the neutral loss of CO_2 (Fig. 2) or telomer-based PFAS with adjacent CH and CF groups often produce $[\text{M}-\text{H}-\text{HF}]^-$ ions which erroneously can be interpreted as an unsaturated PFAS. This is where further information on retention time and peak shapes (width, asymmetry) obtained from chromatography (mostly LC or GC) coupled to HRMS can be beneficial. In-source fragments can be detected by chromatographic separation based on identical RT and peak shapes than their precursor compounds and thereby also be distinguished from real transformation products which would occur at different RT. However, it has to be noted that depending on the chromatographic separation, the difference in the retention time might only be small if the molecular structures are similar and cannot always be clearly distinguished. Also branched vs. linear isomers of PFAS display identical mass but are often partially separated by chromatography.

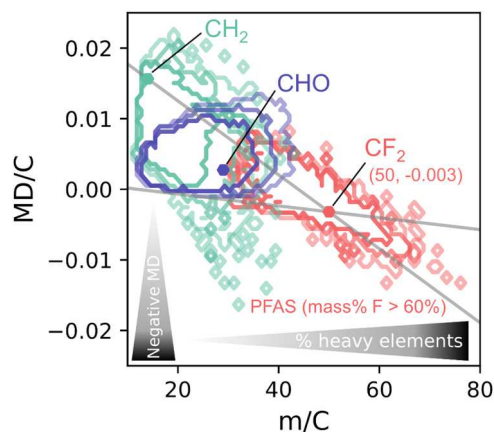


Fig. 4. Positions of different chemical classes in the MD/C-m/C plot. Typical organic contaminants (green, ~180,000 compounds), NOM (blue, ~125,000) and PFAS with a fluorine mass percentage higher than 60% (~25,000). Circles delineate the zones for 85%, 90% and 95% of each compound class (from the inside to the outside).

Modified from Zweigle et al. [40].

2.1. Mass defect

The mass defect (MD) is often used for data reduction in NTS workflows to prioritize potential PFAS in complex samples. The MD of a molecule most commonly is defined by the difference between its exact mass and nominal mass [32,33]. The chemical formula of PFAS is often dominated by carbon (12.0000 Da) and fluorine (18.9984 Da) and to a lesser extent by hydrogen (1.0078 Da). Whereas carbon per definition does not alter the overall MD of a molecule, every fluorine accounts for a slightly negative and every hydrogen for a slightly positive MD. In sum, this typically leads to overall MDs of PFAS in the range between -0.25 Da and $+0.1$ Da (Fig. 3). This MD range also covers 92.8% of all PFAS of the curated OECD PFAS list (S25 in the NORMAN suspect list exchange) [29]. For example Bugsel and Zwiener [34], Koelmel et al. [35] and Dickman and Aga [36] filtered their datasets in that MD range, Liu et al. [37] between -0.15 Da and 0.15 Da. Koelmel et al. [38] flagged features between MD -0.11 Da and 0.12 Da as potential PFAS in the FluoroMatch 2.0 software, and Charbonnet et al. [25] used this MD range to assign features to a confidence level 5b of the updated PFAS confidence scheme.

The advantage of the application of the MD for PFAS prioritization in NTS workflows is the simple procedure and a rather complete prioritization of PFAS with high F-content above 60% mass. The limits are the incomplete separation of PFAS from other hydrocarbon compounds since other elements like bromine, chlorine, iodine, oxygen, phosphorus, and sulfur contribute to a negative mass defect. Also, PFAS with positive mass defects like most AFFF compounds are overlapping with many fluorine-free hydrocarbons. Furthermore, compounds with high positive mass defects like $C_{40}H_{80}$ with mass 560.6260 Da may be erroneously assigned to negative mass defect of -0.374 Da (Fig. 3).

- **Requirement:** Accurate mass
- **Pros:** Easy to apply, good prioritization for PFAS with high F-content, does not require the occurrence of PFAS homologues
- **Cons:** Mass defect range overlaps with hydrocarbons, limited usability for PFAS with low F-content, wrong calculation for largely positive MD exceeding $+0.5$ Da, other halogens (e.g., Cl and Br) can also lead to negative MDs

2.2. MD/C-m/C

A considerable improvement of the MD approach to separate PFAS from the sample matrix features is the novel approach proposed by

Kaufmann et al. [41] which plots the mass defect (MD) normalized to the number of carbon atoms (MD/C) vs. the mass normalized to the number of carbon atoms (m/C) (Fig. 4). The basic idea behind the use of MD per carbon and mass per carbon is a more complete separation by two individual dimensions that separate PFAS and other compounds with relatively high numbers of heteroatoms with negative mass defects (e.g. F, Cl, Br, P from hydrocarbons). For example, if compounds mainly characterized by CH_2 (hydrocarbons and natural organic matter) are compared to those dominated by CHF and CF_2 groups (PFAS), the MD/C dimension makes use of the negative mass defect of fluorine, shifting compounds with fluorine substitutions to more negative MD/C values. The concept behind the particularly powerful m/C dimension is that PFAS tend to be heavier molecules compared to their hydrocarbon counterpart with the same number of carbon atoms. Since the number of carbon atoms can be estimated relatively easily by the abundance of the M+1 isotope (1.1145% ^{13}C) in HRMS scan data, this information allows a highly efficient prioritization of features when screening for PFAS. Kaufmann et al. were able to efficiently separate PFAS from features originating from the extraction of complex fish muscle and liver matrix [41].

Zweigle et al. [40] systematically evaluated the efficiency of the MD/C-m/C approach by using chemical formulas of ~ 210,000 PFAS, ~ 180,000 organic contaminants and ~ 125,000 natural organic matter compounds. While PFAS with little fluorine substitutions expectedly were shown to be more difficult to prioritize, PFAS with high fluorine content ($F/C > 0.8$, $H/F < 0.8$, mass percent of fluorine $> 55\%$) can be effectively separated from other organic contaminants and natural organic matter (NOM) (Fig. 4). An additional advantageous intrinsic property of the MD/C-m/C plot is its ability to group structurally related compounds (e.g., homologous PFAS) together [40]. The recently developed open-source software PFAScreen combines multiple approaches in PFAS NTS and also includes an automated generation of the MD/C – m/C plot and data filtering from vendor-independent raw data (mzML) [42].

Even though the MD/C – m/C plot is not a part of the confidence scheme by Charbonnet et al. [25], the m/C dimension (e.g., $m/C > 30$) in particular is very useful to corroborate the likelihood that the regarded compound is a PFAS and should be included in further confidence schemes.

- **Requirements:** Accurate mass, robust determination of the number of carbons for each feature ($C = I_{M+1}/I_M/0.011145$).
- **Pros:** Very efficient prioritization of PFAS with high F-content, F-content can be roughly estimated, useful also in trace analytical approaches.
- **Cons:** Problematic in case of signals with very low or very high intensities because the M+1 abundance and therefore the C number becomes uncertain (interference of noise at very low intensity or erroneous M abundance due to detector saturation). Similar to the MD, the approach is limited to PFAS with high fluorine content.

2.2.1. Kendrick mass defect & homologous series

The Kendrick mass defect (KMD) analysis is one of the most powerful approaches used for PFAS analysis since many PFAS in products and environmental samples are derived from technical mixtures which are characterized by a number of homologues with a range of repeating units (e.g., CF_2 , C_2F_4 , CF_2O). In a recent review, 14 out of 17 publications used homologous patterns and CF_2 -mass defects for nontarget PFAS discovery [26]. Edward Kendrick [43] first proposed this approach for CH_2 homologues. To calculate the Kendrick mass (KM), the mass defect of the repeating unit is defined as zero (e.g. for CH_2 by multiplying the IUPAC mass with $14.0000/14.0157$). The Kendrick mass defect (KMD = integer mass - KM) for all members of a specific CH_2 homologous series is then identical, since it is dominated by the remaining part of the molecule and differs only in the number of CH_2

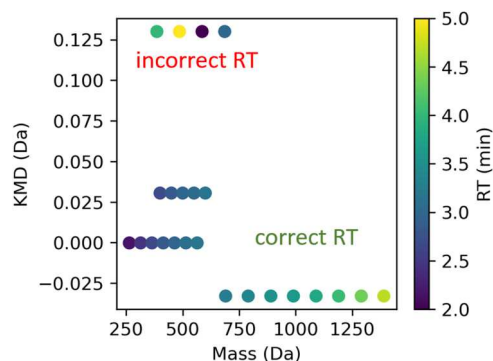


Fig. 5. Schematic demonstration of a KMD vs. mass plot. Even though four homologous series are detected, only three of them show a systematic retention time shift. The top row with four different features shows inconsistent ΔRT shifts, revealing this is a false-positive homologous series.

units. The KMD analysis was originally used to identify homologues of common compound classes in crude oil but can be used for polymers and homologues with any repeating units like PFAS (e.g. for CF_2 a factor of 50.0000/49.9968 is used). In KMD plots (KMD vs. mass), horizontal alignment of homologues from the same compound class occurs.

For example, in biosolids, composts and other organic waste products a KMD plot showed homologues with 2 (N-ethyl perfluoroalkane sulfonamide acetic acid, EtFASAA) to 15 (PFCA) members from 18 compound classes including PFASs and their hydrated derivatives (H-PFASs), fluorotelomer sulfonates (n:2 FTSAs) and their hydroxy derivatives (OH-n:2 FTSA), or bisfluoroalkyl phosphinic acids (n:m PhiA) [44]. In wastewater from electronics fabrication industries structures could be proposed for 15 homologous series out of 41 based on the repeating units CF_2 , CF_2O , C_2F_4 , and C_2F_4O . This revealed various fluorotelomer carboxylic acids and polyfluoroether carboxylic acids [45]. The KMD approach has been used successfully by many other researchers for the detection and identification of PFAS in various samples and matrices [45–50]. However, the limits of the KMD approach are seen in the often very small differences of KMDs between PFAS and matrix compounds with similar chemical formulas and in the finite mass accuracy. Therefore, typically a mass tolerance of 2 mDa must be considered to bin KMDs into one homologous series and the requirement of 3 or more homologues should reduce the number of false-positives. Young et al. [51] analyzed AFFF products and natural organic matter (NOM) samples by ultrahigh resolution FT-ICR MS at sub-ppm mass accuracy. Also, in the NOM sample they discovered in the HRMS spectra 3555 times the mass difference of CF_2 , although NOM should be PFAS-free. This example clearly demonstrates the probability of false-positives and therefore the limits of the KMD approach. A systematic retention time shift in chromatographic separation can be used as further criterium to validate members of a homologous series, since for every repeating unit which is added to a PFAS homologue, the retention time is typically shifted to longer times as shown by Bugsel and Zwiener [34] and used in the R package called “nontarget” which can be used to screen for homologous series [52] (Fig. 5). If no clear retention time trend for the homologues is observed, a false assignment of the homologous series can be assumed.

Instead of examining pre-defined repeating units like 49.9968 Da (CF_2) or 65.9917 Da (CF_2O), tools such as the R package nontarget (which also verifies systematic RT shifts) [52] also allow an automated search for abundant repeating units of homologous series in a sample. This approach also facilitates the detection of homologous series with so-far unknown repeating units which would otherwise be completely missed, although it must be noted that this approach also reveals many repeating units not related to PFAS.

The approach of mass defect filtering which was described in the previous section can also be used to filter for the KMD instead of the MD,

as described by Munoz et al. [44] who filtered potential PFAS for KMDs between -0.15 Da and 0.15 Da. The advantage of this approach is that variations in the number of repeating units do not alter the KMD in contrast to the MD. For example, the MDs of $(CF_2)_3$ and $(CF_2)_{10}$ are -0.010 Da and -0.032 Da, respectively, whereas the KMD in both cases is constant. The regular MD of compounds therefore tends to shift downwards with increasing chain length, whereas the KMD is stable. Both MD and KMD approaches have been increasingly used in recent years [54].

Aside from the benefits that homologous series detection offers, it is important to mention that the presence of few homologues can also increase the likelihood of false-positive homologous series, especially if the retention time criterion cannot be applied. Furthermore, compounds which do not occur as homologous series cannot be detected with this approach. This is true for PFAS that are only produced with a defined chain length (e.g., 8 fluorinated carbon atoms for N-ethyl perfluorooctane sulfonamido ethanol diester [diSAM-PAP] and N-ethyl perfluorooctane sulfonamidoacetic acid [EtFOSAA] [55]) or for which further homologues are of low abundance and therefore easily missed by the peak picking algorithm. Homologous series increase the confidence level and help during compound identification.

- **Requirements:** Accurate mass, RT (optional)
- **Pros:** Increase of confidence of the identification that can be based on only one or two members of a homologous series, compounds from the same class are grouped together
- **Cons:** Occurrence of several members of a homologous series is needed (does not reveal single compounds), limited in trace analysis approaches, few homologues increase the likelihood of false positives

2.3. Chemical formula assignment

In general, chemical formulas can be assigned to accurate mass measurements of sufficient accuracy since each element and its stoichiometry contributes to a specific mass defect [56]. In practice, limited resolving power and mass accuracy increase the number of possible chemical formulas with increasing mass exponentially (e.g., for a mass 500 Da, at 5 ppm mass accuracy the number of potential molecular formulas including the elements C, H, N, S, O and P is 115, and at 1 ppm only 21) [57]. Therefore, the number of elements and their stoichiometry must be restricted reasonably and the consideration of isotopologues can considerably improve the selection of the most probable chemical formulas (e.g., for a mass 500 Da at 5 ppm the number of potential molecular formulas is lowered to 33 if isotopes are considered at an abundance accuracy of 5%) [57].

The approach of direct chemical formula assignment was applied in numerous studies for PFAS screening, often in combination with KMD analysis or further filtering tools. Strynar et al. [58] used vendor software tools (Agilent MassHunter) to automatically generate formulas for a subset of negative MD features and discarded assignments below a certain formula scoring threshold. Similar workflows were applied by Newton et al. [59] and McCord and Strynar [60] leading to several new PFAS identifications in impacted surface waters.

A further approach, called isotope profile matching, was used by Baygi et al. [61] who first generated chemical formulas of potential PFAS with the general form $C_cO_oF_fCl_cH_hS_s$ on a theoretical basis. The stoichiometry was restricted for carbon ($c = 4 \dots 10$) and for oxygen ($o = 2 \dots 3$). Fluorine, chlorine and hydrogen were added so that all carbon atoms were fully saturated. The authors investigated Great Lakes fish extracts and applied a search algorithm to match accurate masses and their isotopes with the chemical formulas. From the identified tentative formula, a theoretical isotopic distribution was then calculated. In the case of multiple m/z matches at different RTs, an objective function was used to determine the compound with the best fitting isotope pattern. This approach allowed the authors to identify 30 PFAS which were not

previously reported in the literature. Among the identified compounds were novel polyfluoroalkyl sulfonates and ether carboxylic acids which are fluorinated to a lesser extent compared to conventional PFCAs and PFASs. The workflow established by Baygi et al. [61] was also successfully used by Ren et al. [62] to identify PFAS in Lake Ontario food web and by Singh et al. [63] to determine PFAS breakdown products in a plasma-based water treatment process.

It should be noted that formula generation alone is most often an insufficient technique due to the high number of formula assignments with increasing mass at a limited mass resolving power and accuracy. Therefore, it should be used in combination with other approaches such as KMD analysis or matches with high-resolution MS fragments to increase the confidence of identification. If this approach is used just by itself, the assignment of an unequivocal molecular formula allows a confidence level of 4 [25].

- **Requirements:** Accurate mass, robust determination of isotope abundance, useful restriction of chemical composition
- **Pros:** No homologous series needed, assignment of specific chemical formula possible
- **Cons:** Rather strict criteria in the chemical formula assignment, likelihood of missing compounds which do not match the restricted range of chemical formulas

2.4. Database / suspect screening

Accurate mass matches with exact masses in databases can be used to tentatively identify compounds by so-called suspect screening [64]. Typical suspect lists or databases used in the literature include publicly available lists such as the OECD PFAS list (available as No. S25 in the NORMAN suspect list exchange, used by Yukioka et al. [65], suspect lists compiled by researchers which include previously discovered PFAS by non-target HRMS (available as No. S46 in the NORMAN suspect list exchange, used by Yukioka et al. [65], Liu et al. [37]) or various in-house optimized lists [66–68]. Suspect screening approaches were also combined with retention time prediction to increase confidence and decrease the critical false positive rate [69].

Joerss and Menger [27] have compared three large PFAS libraries [NISTPFAS (n = 4948), PRIORISKPFAS (n = 4240), PFASMASTER (n = 8498)] and demonstrated that all three lists contain lots of PFAS which are unique, indicating the complexity of PFAS and also the risks to miss PFAS when relying on individual databases.

A match of a feature with a compound in a PFAS-database should always be verified (or falsified) with its isotopic pattern. From the chemical formula, the theoretical isotopic distribution can be calculated and compared to the acquired spectrum. The measured spectrum should agree with the theoretical spectrum in the range of an acceptable tolerance (e.g. 2%; M+1 isotope abundance from the number of carbon atoms or M+2 abundance if further halogens or sulfur are present).

While the size of the databases for suspect screening is not limited and larger databases cover a broader range of potential PFAS, the probability of false positive assignments increases in the same manner. For example, PubChem currently contains more than 6 million compounds with one fully fluorinated CF₂ or CF₃ group based on the OECD PFAS definition [70]. However, to minimize the number of false positive assignments, the content and extent of the suspect list (database) should be tailored to fit the analytical problem to be addressed (background information on environmental compartments, contamination sources, products used etc.) and the kind and type of analytes amenable to the analytical methods (e.g. compound classes and functional groups amenable to ESI).

Suspect screening can be ideally used in combination with other prioritization approaches like the KMD analysis to detect homologous series. A preselection of most probable PFAS by Kendrick mass defects of the repeating unit CF₂ considerably reduced the list of nontarget features and hence increased the number of true mass matches in a preceding

suspect screening approach to identify 61 PFAS from 12 compound classes [34]. Furthermore, using a subset of features from PFAS-likely MD/C-m/C regions (e.g., m/C > 30 and MD/C < 0.01) might be very promising to decrease the number of features for suspect screening.

While this section solely covers database screening on the MS¹ level, it has to be mentioned that this technique can also be applied on the MS² level by comparing fragment information with databases with accurate mass fragmentation information. However, the availability of such spectra is often limited (e.g., MassBank only contained MS² spectra of 40 unique PFAS that have a perfluoroalkyl chain in 2022 [53]). If more MS² spectra become available over time, this can be a further promising approach.

- **Requirements:** Accurate mass, database
- **Pros:** Powerful in combination with other prioritization techniques, assignment of specific compounds possible
- **Cons:** Rather high likelihood of false positive assignments if used alone

3. Methods based on fragmentation (MS²)

MS² fragmentation is commonly used to obtain structural information and confidence on the identity of analytes of interest [25]. Generally, the most common techniques for MS/MS generation are targeted MS/MS, data-dependent- (DDA) and data-independent acquisition (DIA). While in targeted MS/MS a list of analytes (m/z and RT) is used for precursor selection, during DDA, abundant ions are automatically triggered for fragmentation by the instrument software. Both approaches generate MS² spectra of single precursor ions. However, both approaches have the disadvantage of missing a large part of ions of interest. To efficiently enhance MS² coverage in DDA, iterative exclusion during multiple sample injections is very useful to subsequently exclude already selected signals [71]. On the other hand, DIA generates spectra of multiple precursor ions with restricted or without any precursor selection which can be more comprehensive since it is not dependent on precursor abundance. Especially in highly complex samples with a high likelihood of multiple coeluting compounds, MS² spectra after DIA cannot always be used to interpret mass spectral fragmentation since the fragments cannot always be easily assigned to their precursors but MS² spectra can still be checked for the occurrence of diagnostic fragments. If available, techniques such as SWATH or SONAR, specific variants of DIA available for SCIEX and WATERS instruments, respectively, can help to decrease the number of precursors per MS² spectrum by dividing the isolation to narrow time-scheduled m/z windows [72]. Furthermore, efficient deconvolution techniques help to cleanup DIA MS² spectra for easier interpretation. Overall, MS² coverage is one of the crucial parameters for successful NTS workflows for PFAS identification and the basis to accomplish high confidence. Therefore, besides the use of characteristic PFAS fragmentation which will be discussed in the following, optimizing the MS² acquisition is a very important precondition.

3.1. Diagnostic Fragments

Since PFAS with higher fluorine content are most often characterized by common repeating units such as perfluoroalkyl (C_nF_{2n+1}-R) or perfluoroether chains (C_nF_{2n+1}-O-C_mF_{2m}-R) and characteristic functional groups (e.g., SO₃, CO₂, PO₃, betaines, etc.), rather concise lists of diagnostic fragments and their exact masses can be used to match with accurate mass fragments. This way, mass spectra of potential PFAS can be prioritized and tentatively identified [35,73,74]. The PFAS NTS software FluoroMatch 2.0 performs various steps in data analysis such as feature detection (MZmine) and blank filtering and also screens for 777 pre-defined diagnostic fragments in MS² data [38]. Since FluoroMatch 2.0 runs fully automated, it facilitates the analysis for researchers significantly.

Table 1
Examples of typical PFAS diagnostic fragments (negative ESI) and fragment mass differences used during NTS approaches.

Diagnostic fragments	Explanation and occurrence
$C_nF_{2n+1}^-$	Negative perfluoroalkyl chains (e.g., PFCAs, sulfonamide-based AFFFs), less useful for PFAS with charge carrying functional groups (e.g. SO_3^-) or telomer-based PFAS
$C_nF_{2n}SO_3^-$, $C_nF_{2n+1}SO_3^-$, $C_nF_{2n-1}SO_3^-$	PFAS with a sulfonic acid group attached to a perfluoroalkyl chain (many different PFASs: unsaturated PFASs, SF_5 -PFASs etc.)
$C_nF_{2n+1}O^-$, $C_nF_{2n-1}O^-$, $C_nF_{2n-1}O_2^-$	Ether PFAS
$C_nHF_{2n-1}SO_3^-$, $C_nHF_{2n}SO_3^-$, SO_3F^- , SO_2F^- , PO_2F^- , SF_5^-	H-containing PFAS with sulfonic acid group Applicable for different functional groups, provides evidence for fluorine
$H_2PO_4^-$, PO_3^- , PO_2^- , SO_3^-	Functional groups; without fluorine nonspecific to PFAS
Mass differences & neutral losses	
$\Delta(CF_2)_n$, $\Delta(C_2F_4)_n$	Widely applicable
$\Delta(HF)_n$	Neutral loss, fluorotelomer-based or H-containing PFAS (CH in vicinity to CF)
$\Delta C_nH_3F_{2n-3}$	Neutral loss, fluorotelomer-based PFAS, provides chain length (e.g., diPAPs, FTSA, telomer-based AFFFs)
$\Delta C_nF_{2n}SO_3$	Mass difference, sulfonic acid directly attached to a perfluoroalkyl chain which breaks at different positions
ΔCF_2O	Mass difference, typical for ether PFAS
ΔF	Mass difference, e.g., from SO_3^- and SO_3F^- or unsaturation during fragmentation ($C_nF_{2n-1}SO_3^-$ and $C_nF_{2n}SO_3^-$)
$\Delta CF(CF_2)_n$, $\Delta CF_3(CF_2)_n$	Mass differences, e.g., from $C_nF_{2n}SO_3^-$ and $C_{n+1}F_{2n+1}SO_3^-$

Diagnostic Fragments were used in numerous studies while most studies concentrated on negative ESI but for identification of AFFF PFAS (often zwitterions, e.g., quaternary ammonium cations) positive ESI was used [35,37,38,47,58,73–79]. Also, for GC-HRMS applications (both electron ionization (EI) and chemical ionization (CI)) PFAS diagnostic fragments were collected experimentally [80] by rule-based predictions (e.g. from SMILES), or in-silico fragmentation modeling [35,75,81]. Some in-silico predictions led to new fragments for PFAS subclasses that could be manually verified [66]. Combinations of experimental and in-silico fragmentation were applied for instance by Shojaei et al. (2022) who were able to identify 8 novel PFAS in an AFFF mixture [79].

Due to the highly diverse PFAS chemistries, there are no entirely generic diagnostic fragments that work for all PFAS. However, there are both rather nonspecific diagnostic fragments that can be used in NTS approaches where no prior knowledge on PFAS structures is available and diagnostic fragments which are rather specific for single PFAS classes (see Table 1). Nonspecific fragments are for example $C_nF_{2n+1}^-$ which originate from a cleavage of the perfluoroalkyl chain (ESI). However, PFAS fragmentation is very much dependent on compound characteristics such as the type of functional group and degree and configuration of fluorination as well as instrumental operating parameters like the ionization polarity and the technique and energy of collision-induced dissociation (the application of collision energies based on the mass of unknowns can be helpful to obtain meaningful mass spectra [53]). For instance, fluorotelomer-based PFAS or PFAS with sulfonic acid group directly attached to the perfluoroalkyl chain barely form $C_nF_{2n+1}^-$ fragments while PFAS with carboxylic acid or sulfonamide groups do. One reason is that SO_3^- retains the negative charge which is well delocalized across the SO_3^- ion. In Table 1 we provide an overview of common diagnostic fragments with high F-content that were observed for numerous PFAS classes and are comparatively selective due to their negative mass defect.

Besides fluorinated diagnostic fragments, for PFAS with extended hydrocarbon moieties such as AFFF compounds also diagnostic fragments of the non-fluorinated moieties can be used to indicate PFAS, for example $C_4H_{10}O_2N^+$ for betaines or $C_3H_6O_3S^-$ for propyl sulfonate moieties (more positive ESI fragments can be found in Barzen-Hanson

et al. [75]). Specific diagnostic fragments can be selectively used if specific PFAS classes are of interest.

For PFAS spectra prioritization a list that covers meaningful diagnostic fragments of multiple classes and parts of PFAS molecules should be used to minimize false-negatives and therefore the chance to miss PFAS potentially occurring in samples. If at least 3 diagnostic MS^2 -fragments can be found, a confidence level of 2b is reached [25].

- **Requirements:** Good quality MS/MS data is a prerequisite for both identification and confirmation with the use of diagnostic fragments.
- **Pros:** Very useful for both spectra prioritization and compound identification. Matching with diagnostic fragments already advances the identification process by structural information.
- **Cons:** It is difficult to develop exhaustive lists of PFAS diagnostic fragments which should always be considered. MS/MS data is not always readily available for low abundance ions.

3.2. Fragment differences and neutral losses

Besides the use of diagnostic fragments, typical neutral losses (e.g., ΔHF , ΔCO_2) and fragment mass differences (e.g., ΔCF_2) or combinations with diagnostic fragments were used in various studies for PFAS identification or prioritization [37,73,74,77,82,83]. It is important to distinguish neutral losses from fragment mass differences. A typical neutral loss relates two fragments by a distinct neutral chemical formula such as HF that typically occurs when a carbon atom bearing a hydrogen atom is adjacent to a carbon atom bearing a fluorine atom (e.g., in telomer-based or H-containing PFAS). Fragment mass differences on the other hand may occur also between non-related fragments that differ by a certain formula but originate from different fragmentation pathways. The difference of ΔCF_2 for example between a $C_2F_6SO_3^-$ and a $C_3F_8SO_3^-$ ion would be an example for a fragment mass difference.

For the open-source tool FindPFAS, Zweigle et al. [53] used fragment mass differences in data-dependent fragmentation in a comprehensive manner by calculating the differences between all fragments in each MS/MS spectrum (difference matrix) which showed that many different unknown PFAS fragments are detectable by single mass differences (e.g., ΔC_2F_4 , $\Delta C_nH_3F_{2n-3}$) without any further knowledge on their chemical formula (see Fig. 7). Fragment mass differences can be ideally combined with diagnostic fragments since they can strongly enhance the detection of non-targeted fragments of PFAS [49]. A potential advantage of mass differences compared to diagnostic fragments is the fact that they may still occur unchanged in mass spectra of PFAS transformation products like those from oxidation processes (e.g., +O, $-H_2$), ester or ether hydrolysis. However, this is not mandatory as diagnostic fragments and mass differences from molecular moieties subjected to change are also shifted in the mass spectrum [53]. When matching diagnostic fragments or fragment mass differences with MS/MS spectra it is very important to consider the instrument mass accuracy to minimize false-positive detection. Fragment differences are not considered in confidence schemes so far. However, we propose to use them in the future.

The mass difference approach might also be promising when used with data-independent fragmentation data to cover a broader range of fragments which may not have been produced in data-dependent fragmentation. We therefore also encourage other researchers to try and experiment with this approach.

- **Requirements:** Good quality high-resolution MS/MS data is a prerequisite for the use of fragment mass differences and neutral losses.
- **Pros:** Powerful for NTS approaches since also unknown PFAS fragments are detectable. A rather small number of differences can already capture numerous fragments. PFAS transformation products can often still be detected because mass differences corresponding with unchanged molecular moieties are conserved in transformed compounds

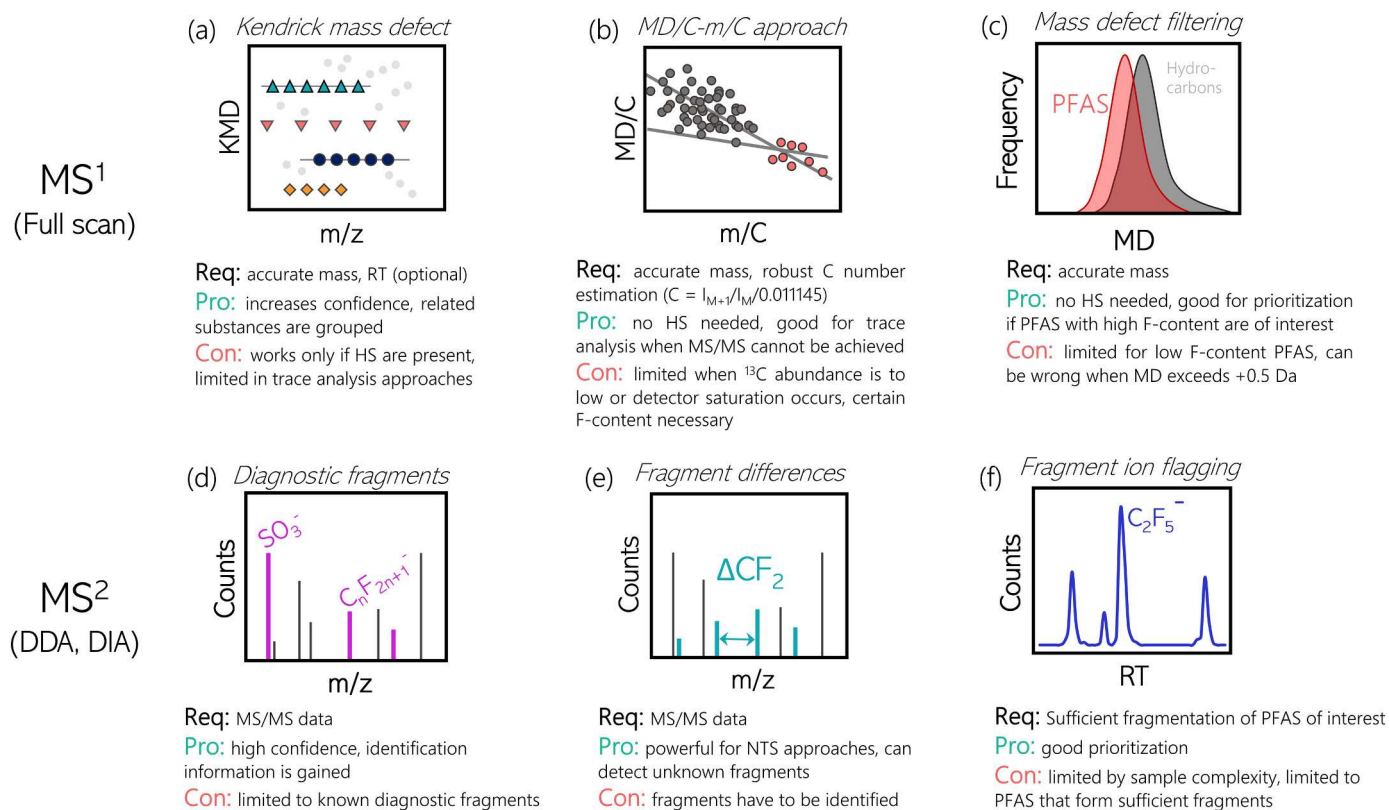


Fig. 6. Summary of six promising approaches for PFAS non-targeted screening with their respective requirements, advantages, and disadvantages. Abbreviations: KMD: Kendrick mass defect, HS: homologous series, RT: retention time, MD: mass defect, C: carbon atom, m: mass, Da: Dalton, DDA: data-dependent acquisition, DIA: data-independent acquisition.

- **Cons:** Fragment chemical composition is not directly known. MS/MS data is not always readily available for low abundance ions.

3.3. Fragment ion flagging

The approach of fragment ion flagging was first proposed by Liu et al. [84]. The workflow includes two injections. In the first injection, fragments of the analytes are produced in the ion source (in-source fragmentation) and the resulting chromatograms are screened for diagnostic PFAS fragments (e.g., C_nF_{2n+1} , C_nF_{2n-1} , SO_3F or Cl for chlorinated PFAS alternatives). The occurrence of the selected fragment ions was then used to find the potential corresponding PFAS which produced the fragment at the given RT. Candidates were then selected and subjected to a manual homologous series analysis. A second injection was then used to gather MS/MS information and confirm the proposed molecular formula for at least one candidate for every homologous series. Similar approaches were also successfully adapted by other researchers [82, 85–88]. Fragment ion flagging was also successfully applied for identification of PFAS from ionic liquids in surface waters in combination with MS³ fragmentation experiments for structure elucidation [89]. Different modifications were applied such as time-scheduled MS and in-source fragmentation experiments and a technique using DIA [90].

- **Requirements:** Accurate mass, knowledge about suitable source parameters if in-source fragmentation is desired, not necessary when DIA is used.
- **Pros:** Good prioritization, high likelihood of detecting PFAS that form the selected fragment ions. Selective for compounds with specific fragments.
- **Cons:** In case of in-source fragmentation, this approach is limited to PFAS which easily form in-source fragments, to preselected fragment ions; the high sample complexity exacerbates the assignment of PFAS

to the corresponding fragment ions, potentially dependent on type and geometry of the used ion-source. For DIA, high sample complexity might limit this approach to abundant ions.

3.4. Ion-mobility mass spectrometry

Mass spectrometers equipped with ion mobility spectrometers (IMS) can be used to add a further dimension to separate and characterize the analytes based on their size and shape. A big benefit of using IMS is that the separation occurs in the gas phase and is therefore fast and can be used without additional analysis time [91]. Dodds et al. [91] have characterized collision cross section (CCS) values for various PFAS classes and homologues and found linear PFAS mass / CCS trendlines within the same compound class. Foster et al. [92] and Kirkwood et al. [93] observed a good separation between biomolecules and halogenated xenobiotics, including PFAS, by the collision cross section determined in IMS-MS measurements. At similar mass (m/z), PFAS were shown to have a lower collision cross section (CCS) than hydrocarbons. This observation was attributed to the fact that halogens such as F increase the mass of a molecule, but the molecular size does not increase in the same manner. CCS data do not influence the confidence level, however, if the instruments and data are available, they can further help in the prioritization and identification of PFAS.

- **Requirements:** IMS-MS instrument, CCS data
- **Pros:** Adds one further dimension on compound characterization, is fast and helpful in the separation of isomers
- **Cons:** High requirements for instrumentation and software

4. Conclusions

The diverse, widespread use of PFAS, the longevity of the substances,

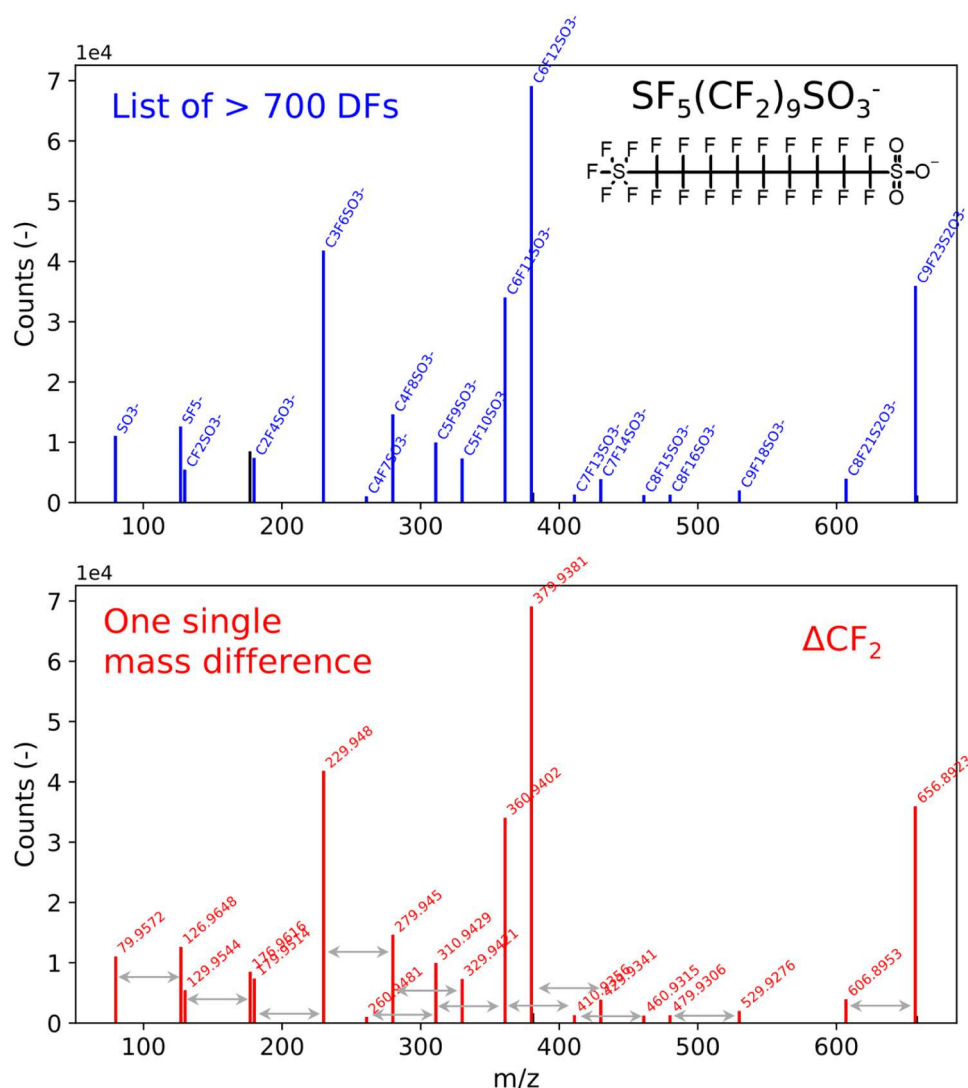


Fig. 7. Example of matching of a large list of diagnostic fragments (> 700) in comparison to the use of one single fragment mass difference (ΔCF_2) with an MS/MS spectrum of SF₅-perfluoronanesulfonic acid. While the chemical formula is not known, in this particular example ΔCF_2 detects most of the fluorine containing fragments showing that fragment mass differences can be very powerful for non-targeted approaches, especially when combined with diagnostic fragments. Note that potential branched or positional isomers of SF₅-perfluoronanesulfonic acid can be present (see also Zweigle et al. (2023) [49]).

and the continuing development of new PFAS cause an increasing complexity and challenge for monitoring PFAS in products and the environment. Since target analysis only tackles a very limited number of environmentally relevant PFAS, NTS approaches and their continuous further development are crucial which make use of PFAS-specific properties.

The intrinsic properties of PFAS include a relevant fraction of hydrogen atoms substituted by fluorine, common functional groups and molecular moieties such as perfluoroalkyl or perfluoroether chains, as well as the frequent occurrence of homologues. These characteristics constitute a useful basis to separate many PFAS from matrix features by the discussed techniques. Recently developed tools such as FluoroMatch and PFAScreen aim to combine several of the herein discussed techniques for efficient PFAS NTS. While in the absence of specific knowledge on PFAS of interest, the difficulty of prioritization increases with decreasing fluorine content for techniques such as the mass defect (MD) or the MD normalized to the number of carbon atoms (MD/C-m/C). While all approaches discussed in this review are valuable on their own, they become much more powerful when combined and applied in a suitable order so that the confidence of true positive findings increases significantly compared to the use of just a single approach.

CRediT authorship contribution statement

Boris Bugsel: conceptualization, writing of original draft (focus on Section 2., 2.1–2.5, 3.3, 3.4 and 4.), preparation of Figs. 2 and 5. **Jonathan Zweigle:** conceptualization, writing of original draft (focus on Sections 2.2, 3., 3.1, 3.2 and 4.), preparation of Figs. 1, 3, 4, 6 and 7. **Christian Zwiener:** conceptualization, supervision, writing of original draft (focus on abstract and Section 1.), review & editing.

Declaration of Competing Interest

The authors declare the following financial interests/personal relationships which may be considered as potential competing interests: Christian Zwiener reports financial support was provided by Federal Ministry of Education and Research Bonn Office. Jonathan Zweigle reports financial support was provided by German Federal Environmental Foundation.

Data availability

Data will be made available on request.

Acknowledgements

The authors acknowledge the DBU (Deutsche Bundesstiftung Umwelt) for the scholarship of JZ and the Federal Ministry of Education and Research (BMBF) for funding the project PFClean (O2WGW1665C).

References

- Z. Wang, A.M. Buser, I.T. Cousins, S. Demattio, W. Drost, O. Johansson, K. Ohno, G. Patlewicz, A.M. Richard, G.W. Walker, G.S. White, E. Leinala, *Environ. Sci. Technol.* 55 (2021) 15575–15578, <https://doi.org/10.1021/acs.est.1c06896>.
- Organisation for Economic Co-operation and Development (OECD), *Reconciling Terminology of the Universe of Per- and Polyfluoroalkyl Substances: Recommendations and Practical Guidance*. 2021.
- K.L. Olson, K.L. Rinehart Jr., J.C. Cook Jr., *Biomed. Mass Spectrom.* 4 (1977) 284–290, <https://doi.org/10.1002/bms.1200040503>.
- PubChem, PFAS and Fluorinated Compounds in PubChem. 2023.
- J. Glüge, M. Scheringer, I. Cousins, J.C. DeWitt, G. Goldenman, D. Herzke, R. Lohmann, C. Ng, X. Trier, Z. Wang, *Environ. Sci. Proc. Imp.* 22.12 (2020) 2345–2373, <https://doi.org/10.31224/osf.io/2eqac>.
- M.G. Evich, M.J.B. Davis, J.P. McCord, B. Acrey, J.A. Awkerman, D.R.U. Knappe, A.B. Lindstrom, T.F. Speth, C. Tebes-Stevens, M.J. Strynar, Z. Wang, E.J. Weber, W. M. Henderson, J.W. Washington, *eabg9065*, *Science* 375 (2022), <https://doi.org/10.1126/science.abg9065>.
- C. Sonne, M.S. Bank, B.M. Jenssen, T.M. Ciesielski, J. Rinklebe, S.S. Lam, M. Hansen, R. Bossi, K. Gustavson, R. Dietz, *Science* 379 (2023) 887–888, <https://doi.org/10.1126/science.adh0934>.
- H. Brunn, G. Arnold, W. Körner, G. Rippen, K.G. Steinhäuser, I. Valentin, *Environ. Sci. Eur.* 35 (2023), <https://doi.org/10.1186/s12302-023-00721-8>.
- G. Pitter, F. Da Re, C. Canova, G. Barbieri, M. Zare Jeddi, F. Dapra, F. Manea, R. Zolin, A.M. Bettega, G. Stopazzolo, S. Vittorini, L. Zambelli, M. Martuzzi, D. Mantoan, F. Russo, *Environ. Health Perspect.* 128 (2020) 27007, <https://doi.org/10.1289/EHP5337>.
- C.A. McDonough, W. Li, H.N. Bischel, A.O. De Silva, J.C. DeWitt, *Environ. Sci. Technol.* 56 (2022) 6004–6013, <https://doi.org/10.1021/acs.est.2c00254>.
- T. Teymoorian, G. Munoz, S.V. Duy, J.X. Liu, S. Sauve, *ACS Est. Water* (2023) 246–261, <https://doi.org/10.1021/acsestwater.2c00387>.
- G. Munoz, J. Liu, S. Vo Duy, S. Sauvé, *Trends Environ. Anal. Chem.* 23 (2019), e00066, <https://doi.org/10.1016/j.teac.2019.e00066>.
- I.T. Cousins, J.H. Johansson, M.E. Salter, B. Sha, M. Scheringer, *Environ. Sci. Technol.* 56 (2022) 11172–11179, <https://doi.org/10.1021/acs.est.2c02765>.
- E.M. Sunderland, X.C. Hu, C. Dassuncao, A.K. Tokranov, C.C. Wagner, J.G. Allen, *J. Expo. Sci. Environ. Epidemiol.* 29 (2019) 131–147, <https://doi.org/10.1038/s41370-018-0094-1>.
- E.C. Panel, Risk to human health related to the presence of perfluoroalkyl substances in food. EFSA J 18 e06223, <https://doi.org/10.2903/j.efsa.2020.6223>.
- S. Garg, P. Kumar, V. Mishra, R. Guijt, P. Singh, L.F. Dumée, R.S. Sharma, *J. Water Process Eng.* 38 (2020), 101683, <https://doi.org/10.1016/j.jwpe.2020.101683>.
- ISO 21275:2019. Water quality — Determination of perfluoroalkyl and polyfluoroalkyl substances (PFAS) in water — Method using solid phase extraction and liquid chromatography-tandem mass spectrometry (LC-MS/MS), 2019.
- United States Environmental Protection Agency, Draft Method 1633. Analysis of Per- and Polyfluoroalkyl Substances (PFAS) in Aqueous, Solid, Biosolids, and Tissue Samples by LC-MS/MS., 2021.
- S. Jia, M. Marques Dos Santos, C. Li, S.A. Snyder, *Anal. Bioanal. Chem.* 414 (2022) 2795–2807, <https://doi.org/10.1007/s00216-022-03905-y>.
- K.E. Pelch, T. McKnight, A. Reade, *Sci. Total Environ.* 876 (2023), 162978, <https://doi.org/10.1016/j.scitotenv.2023.162978>.
- L.A. Koroniaiou, C. Nannou, N. Xanthopoulou, G. Seretoudi, D. Bikiaris, D.A. Lambropoulou, *Microchem. J.* 179 (2022) 107457, <https://doi.org/10.1016/j.microc.2022.107457>.
- A.U. Rehman, M. Crimi, S. Andreescu, *Trends Environ. Anal. Chem.* (2023), e00198, <https://doi.org/10.1016/j.teac.2023.e00198>.
- L. Mullin, D. Katz, N. Riddell, R. Plumb, J.A. Burgess, L.W.Y. Yeung, I.E. Jogsten, *Trends Anal. Chem.* 118 (2019) 828–839, <https://doi.org/10.1016/j.trac.2019.05.015>.
- E.L. Schymanski, J. Jeon, R. Gulde, K. Fenner, M. Ruff, H.P. Singer, J. Hollender, *Environ. Sci. Technol.* 48 (2014) 2097–2098, <https://doi.org/10.1021/es5002105>.
- J.A. Charbonnet, C.A. McDonough, F. Xiao, T. Schwichtenberg, D. Cao, S. Kaserzon, K.V. Thomas, P. Dewapriya, B.J. Place, E.L. Schymanski, J.A. Field, D. E. Helbling, C.P. Higgins, *Environ. Sci. Technol. Lett.* 9 (2022) 473–481, <https://doi.org/10.1021/acs.estlett.2c00206>.
- Y. Liu, L.A. D'Agostino, G. Qu, G. Jiang, J.W. Martin, *TrAC Trends Anal. Chem.* 121 (2019), 115420, <https://doi.org/10.1016/j.trac.2019.02.021>.
- H. Joerss, F. Menger, *Curr. Opin. Green. Sustain. Chem.* 40 (2023), 100775, <https://doi.org/10.1016/j.cogsc.2023.100775>.
- M. Strynar, J. McCord, S. Newton, J. Washington, K. Barzen-Hanson, X. Trier, Y. Liu, B. Bugsel, I.K. Dimzon, C. Zwiener, G. Munoz, *J. Expo. Sci. Environ. Epidemiol.* (2023).
- H. Mohammed Taha, R. Aalizadeh, N. Alygizakis, J.P. Antignac, H.P.H. Arp, R. Bade, N. Baker, L. Belova, L. Bijlsma, E.E. Bolton, W. Brack, A. Celma, W. L. Chen, T. Cheng, P. Chirsir, L. Cirka, L.A. D'Agostino, Y. Djoumbou Feunang, V. Dulio, S. Fischer, P. Gago-Ferrero, A. Galani, B. Geueke, N. Glowacka, J. Gluge, K. Groh, S. Grosse, P. Haglund, P.J. Hakkinen, S.E. Hale, F. Hernandez, E. M. Janssen, T. Jonkers, K. Kiefer, M. Kirchner, J. Koschorreck, M. Krauss, J. Krier, M.H. Lamoree, M. Letzel, T. Letzel, Q. Li, J. Little, Y. Liu, D.M. Lunderberg, J. W. Martin, A.D. McEachran, J.A. McLean, C. Meier, J. Meijer, F. Menger, C. Merino, J. Muncke, M. Muschket, M. Neumann, V. Neveu, K. Ng, H. Oberacher, J. O'Brien, P. Oswald, M. Oswaldova, J.A. Picache, C. Postigo, N. Ramirez, T. Reemtsma, J. Renaud, P. Rostkowski, H. Rudel, R.M. Salek, S. Samanipour, M. Scheringer, I. Schliebner, W. Schulz, T. Schulz, M. Sengl, B.A. Shoemaker, K. Sims, H. Singer, R.R. Singh, M. Sumarah, P.A. Thiessen, K.V. Thomas, S. Torres, X. Trier, A.P. van Wezel, R.C.H. Vermeulen, J.J. Vlaanderen, P.C. von der Ohe, Z. Wang, A.J. Williams, E.L. Willighagen, D.S. Wishart, J. Zhang, N.S. Thomaidis, J. Hollender, J. Slobodnik, E.L. Schymanski, *Environ. Sci. Eur.* 34 (2022) 104, <https://doi.org/10.1186/s12302-022-00680-6>.
- R. Schmid, S. Heuckeroth, A. Korf, A. Smirnov, O. Myers, T.S. Dyrland, R. Bushuiev, K.J. Murray, N. Hoffmann, M. Lu, A. Sarvepalli, Z. Zhang, M. Fleischauer, K. Duhrkop, M. Wesner, S.J. Hoogstra, E. Rudt, O. Mokshyna, C. Brungs, K. Ponomarov, L. Mutabdzija, T. Damiani, C.J. Pudney, M. Earll, P. O. Helmer, T.R. Fallon, T. Schulze, A. Rivas-Ubach, A. Bilbao, H. Richter, L. F. Nothias, M. Wang, M. Oresic, J.K. Weng, S. Bocker, A. Jeibmann, H. Hayden, U. Karst, P.C. Dorrestein, D. Petras, X. Du, T. Pluskal, *Nat. Biotechnol.* 41 (2023) 447–449, <https://doi.org/10.1038/s41587-023-01690-2>.
- H.L. Rost, T. Sachsenberg, S. Aiche, C. Bielow, H. Weisser, F. Aicheler, S. Andreotti, H.C. Ehrlich, P. Gutenbrunner, E. Kenar, X. Liang, S. Nahnsen, L. Nilse, J. Pfeuffer, G. Rosenberger, M. Rurik, U. Schmitt, J. Veit, M. Walzer, D. Wojnar, W.E. Wolski, O. Schilling, J.S. Choudhary, L. Malmstrom, R. Aebersold, K. Reinert, O. Kohlbacher, *Nat. Methods* 13 (2016) 741–748, <https://doi.org/10.1038/nmeth.3959>.
- L. Sleno, *J. Mass Spectrom.* 47 (2012) 226–236, <https://doi.org/10.1002/jms.2953>.
- A.L. Myers, K.J. Jobst, S.A. Mabury, E.J. Reiner, *J. Mass Spectrom.* 49 (2014) 291–296, <https://doi.org/10.1002/jms.3340>.
- B. Bugsel, C. Zwiener, *Anal. Bioanal. Chem.* 412 (2020) 4797–4805, <https://doi.org/10.1007/s00216-019-02358-0>.
- J.P. Koelmel, M.K. Paige, J.J. Aristizabal-Henao, N.M. Robey, S.L. Nason, P. J. Stelben, Y. Li, N.M. Kroeger, M.P. Napolitano, T. Savvaides, V. Vasilou, P. Rostkowski, T.J. Garrett, E. Lin, C. Deigl, K. Jobst, T.G. Townsend, K.J. Godri Pollitt, J.A. Bowden, *Anal. Chem.* 92 (2020) 11186–11194, <https://doi.org/10.1021/acs.analchem.0c01591>.
- R.A. Dickman, D.S. Aga, *Anal. Bioanal. Chem.* 414 (2022) 4497–4507, <https://doi.org/10.1007/s00216-022-04088-2>.
- L. Liu, M. Lu, X. Cheng, G. Yu, J. Huang, *Environ. Int.* 167 (2022), 107398, <https://doi.org/10.1016/j.envint.2022.107398>.
- J.P. Koelmel, P. Stelben, C.A. McDonough, D.A. Dukes, J.J. Aristizabal-Henao, S. L. Nason, Y. Li, S. Sternberg, E. Lin, M. Beckmann, A.J. Williams, J. Draper, J. P. Finch, J.K. Munk, C. Deigl, E.E. Rennie, J.A. Bowden, K.J. Godri Pollitt, *Anal. Bioanal. Chem.* 414 (2022) 1201–1215, <https://doi.org/10.1007/s00216-021-03392-7>.
- C.M. Grulke, A.J. Williams, I. Thillanadarajah, A.M. Richard, *Comput. Toxicol.* 12 (2019), 100096, <https://doi.org/10.1016/j.comtox.2019.100096>.
- J. Zweigle, B. Bugsel, C. Zwiener, *Anal. Bioanal. Chem.* 415 (2023) 1791–1801, <https://doi.org/10.1007/s00216-023-04601-1>.
- A. Kaufmann, P. Butcher, K. Maden, S. Walker, M. Widmer, *J. AOAC Int* 105 (2022) 1280–1287, <https://doi.org/10.1093/jaoacint/qsac071>.
- J. Zweigle, B. Bugsel, J. Fabregat-Palau, C. Zwiener, *ChemRxiv*. Cambridge: Cambridge Open Engage; 2023; This content is a preprint and has not been peer-reviewed. (2023) <https://doi.org/10.26434/chemrxiv-2023-r843x>.
- E. Kendrick, *Anal. Chem.* 35 (1963) 2146–2154.
- G. Munoz, A.M. Michaud, M. Liu, S. Vo Duy, D. Montenach, C. Resseguier, F. Watteau, V. Sappin-Didier, F. Feder, T. Morvan, S. Houot, M. Desrosiers, J. Liu, S. Sauve, *Environ. Sci. Technol.* 56 (2022) 6056–6068, <https://doi.org/10.1021/acs.est.1c03697>.
- P. Jacob, K.A. Barzen-Hanson, D.E. Helbling, *Environ. Sci. Technol.* 55 (2021) 2346–2356, <https://doi.org/10.1021/acs.est.0c06690>.
- W. Li, H.N. Bischel, *Sci. Total Environ.* 837 (2022), 155850, <https://doi.org/10.1016/j.scitotenv.2022.155850>.
- Y.Q. Wang, L.X. Hu, T. Liu, J.H. Zhao, Y.Y. Yang, Y.S. Liu, G.G. Ying, *Environ. Int.* 163 (2022), 107219, <https://doi.org/10.1016/j.envint.2022.107219>.
- B. Bugsel, R. Bauer, F. Herrmann, M.E. Maier, C. Zwiener, *Anal. Bioanal. Chem.* 414 (2022) 1217–1225, <https://doi.org/10.1007/s00216-021-03463-9>.
- J. Zweigle, B. Bugsel, K. Rohler, A.A. Haluska, C. Zwiener, *Environ. Sci. Technol.* 57 (2023) 6647–6655, <https://doi.org/10.1021/acs.est.2c07969>.
- C.E. Schaefer, J.L. Hooper, L.E. Strom, I. Abusallout, E.R.V. Dickenson, K. A. Thompson, G.R. Mohan, D. Drennan, K. Wu, J.L. Guelfo, *Water Res* 233 (2023), 119724, <https://doi.org/10.1016/j.watres.2023.119724>.
- R.B. Young, N.E. Pica, H. Sharifan, H. Chen, H.K. Roth, G.T. Blakney, T. Borch, C. P. Higgins, J.J. Kornuc, A.M. McKenna, J. Blotvogel, *Environ. Sci. Technol.* 56 (2022) 2455–2465, <https://doi.org/10.1021/acs.est.1c08143>.
- M. Loos, H. Singer, *J. Chemin.-.* 9 (2017) 12, <https://doi.org/10.1186/s13321-017-0197-z>.
- J. Zweigle, B. Bugsel, C. Zwiener, *Anal. Chem.* 94 (2022) 10788–10796, <https://doi.org/10.1021/acs.analchem.2c01521>.
- S. Merel, *Chemosphere* 313 (2023), 137443, <https://doi.org/10.1016/j.chemosphere.2022.137443>.
- X. Trier, K. Granby, J.H. Christensen, *Environ. Sci. Pollut. R.* 18 (2011) 1108–1120, <https://doi.org/10.1007/s11356-010-0439-3>.
- A.G. Marshall, R.P. Rodgers, *Proc. Natl. Acad. Sci. USA* 105 (2008) 18090–18095, <https://doi.org/10.1073/pnas.0805069105>.

- [57] T. Kind, O. Fiehn, *BMC Bioinforma.* 7 (2006) 234, <https://doi.org/10.1186/1471-2105-7-234>.
- [58] M. Strynar, S. Dagnino, R. McMahan, S. Liang, A. Lindstrom, E. Andersen, L. McMillan, M. Thurman, I. Ferrer, C. Ball, *Environ. Sci. Technol.* 49 (2015) 11622–11630, <https://doi.org/10.1021/acs.est.5b01215>.
- [59] S. Newton, R. McMahan, J.A. Stoeckel, M. Chislock, A. Lindstrom, M. Strynar, *Environ. Sci. Technol.* 51 (2019) 1544–1552, <https://doi.org/10.1021/acs.est.6b05330>.
- [60] J. McCord, M. Strynar, *Environ. Sci. Technol.* 53 (2019) 4717–4727, <https://doi.org/10.1021/acs.est.8b06017>.
- [61] S. Fakouri Baygi, B.S. Crimmins, P.K. Hopke, T.M. Holsen, *Environ. Sci. Technol.* 50 (2016) 9460–9468, <https://doi.org/10.1021/acs.est.6b01349>.
- [62] J. Ren, S. Fernando, P.K. Hopke, T.M. Holsen, B.S. Crimmins, *Environ. Sci. Technol.* 56 (2022) 17626–17634, <https://doi.org/10.1021/acs.est.2c04321>.
- [63] R.K. Singh, S. Fernando, S.F. Baygi, N. Multari, S.M. Thagard, T.M. Holsen, *Environ. Sci. Technol.* 53 (2019) 2731–2738, <https://doi.org/10.1021/acs.est.8b07031>.
- [64] M. Paszkiewicz, K. Godlewska, H. Lis, M. Caban, A. Bia, P. Stepnowski, *Trends Anal. Chem.* 154 (2022), 116671, <https://doi.org/10.1016/j.trac.2022.116671>.
- [65] S. Yukioka, S. Tanaka, Y. Suzuki, S. Echigo, A. Karrman, S. Fujii, *Water Res* 184 (2020), 116207, <https://doi.org/10.1016/j.watres.2020.116207>.
- [66] G.J. Getzinger, C.P. Higgins, P.L. Ferguson, *Anal. Chem.* 93 (2021) 2820–2827, <https://doi.org/10.1021/acs.analchem.0c04109>.
- [67] R. Wang, C. Ching, W.R. Dichtel, D.E. Helbling, *Environ. Sci. Technol. Lett.* 7 (2020) 954–960, <https://doi.org/10.1021/acs.estlett.0c00736>.
- [68] X. Jia, H.Y. Guan, Z.B. Guo, C.J. Qian, Y.L. Shi, Y.Q. Cai, *Environ. Sci. Technol. Lett.* 8 (2021) 968–974, <https://doi.org/10.1021/acs.estlett.1c00709>.
- [69] K. Ng, N. Alygizakis, A. Androulakakis, A. Galani, R. Aalizadeh, N.S. Thomaidis, J. Slobodnik, *J. Hazard Mater.* 436 (2022), 129276, <https://doi.org/10.1016/j.jhazmat.2022.129276>.
- [70] E.L. Schymanski, E. Bolton, *Zenodo* (2023), <https://doi.org/10.5281/zenodo.7756622>.
- [71] J.P. Koelmel, N.M. Kroeger, E.L. Gill, C.Z. Ulmer, J.A. Bowden, R.E. Patterson, R. A. Yost, T.J. Garrett, *J. Am. Soc. Mass Spectrom.* 28 (2017) 908–917, <https://doi.org/10.1007/s13361-017-1608-0>.
- [72] C. Ludwig, L. Gillet, G. Rosenberger, S. Amon, B.C. Collins, R. Aebbersold, *Mol. Syst. Biol.* 14 (2018), e8126, <https://doi.org/10.15252/msb.20178126>.
- [73] Y. Wang, N. Yu, X. Zhu, H. Guo, J. Jiang, X. Wang, W. Shi, J. Wu, H. Yu, S. Wei, *Environ. Sci. Technol.* 52 (2018) 11007–11016, <https://doi.org/10.1021/acs.est.8b03030>.
- [74] X. Wang, N. Yu, Y. Qian, W. Shi, X. Zhang, J. Geng, H. Yu, S. Wei, *Water Res* 183 (2020), 115989, <https://doi.org/10.1016/j.watres.2020.115989>.
- [75] K.A. Barzen-Hanson, S.C. Roberts, S. Choyke, K. Oetjen, A. McAlees, N. Riddell, R. McCrindle, P.L. Ferguson, C.P. Higgins, J.A. Field, *Environ. Sci. Technol.* 51 (2017) 2047–2057, <https://doi.org/10.1021/acs.est.6b05843>.
- [76] Q. Kang, F. Gao, X. Zhang, L. Wang, J. Liu, M. Fu, S. Zhang, Y. Wan, H. Shen, J. Hu, *Environ. Int* 139 (2020), 105686, <https://doi.org/10.1016/j.envint.2020.105686>.
- [77] Y. Li, N. Yu, L. Du, W. Shi, H. Yu, M. Song, S. Wei, *Environ. Sci. Technol.* 54 (2020) 3407–3416, <https://doi.org/10.1021/acs.est.9b06505>.
- [78] T. Liu, L.X. Hu, Y. Han, L.L. Dong, Y.Q. Wang, J.H. Zhao, Y.S. Liu, J.L. Zhao, G. G. Ying, *Sci. Total Environ.* 844 (2022), 157021, <https://doi.org/10.1016/j.scitotenv.2022.157021>.
- [79] M. Shojaei, A.S. Joyce, P.L. Ferguson, J.L. Guelfo, *J. Hazard. Mater. Lett.* 3 (2022), <https://doi.org/10.1016/j.hazl.2022.100061>.
- [80] J.S. Casey, S.R. Jackson, J. Ryan, S.R. Newton, *J. Chromatogr. A* 1693 (2023), 463884, <https://doi.org/10.1016/j.chroma.2023.463884>.
- [81] N. Yu, H. Guo, J. Yang, L. Jin, X. Wang, W. Shi, X. Zhang, H. Yu, S. Wei, *Environ. Sci. Technol.* 52 (2018) 8205–8214, <https://doi.org/10.1021/acs.est.8b02492>.
- [82] R.G. de Vega, A. Cameron, D. Clases, T.M. Dodgen, P.A. Doble, D.P. Bishop, *J. Chromatogr. A* 1653 (2021), 462423, <https://doi.org/10.1016/j.chroma.2021.462423>.
- [83] N. Yu, H. Wen, X. Wang, E. Yamazaki, S. Taniyasu, N. Yamashita, H. Yu, S. Wei, *Environ. Sci. Technol.* 54 (2020) 3103–3113, <https://doi.org/10.1021/acs.est.9b05457>.
- [84] Y. Liu, S. Pereira Ados, J.W. Martin, *Anal. Chem.* 87 (2015) 4260–4268, <https://doi.org/10.1021/acs.analchem.5b00039>.
- [85] S. Yukioka, S. Tanaka, Y. Suzuki, S. Fujii, S. Echigo, *Chemosphere* 239 (2020), 124644, <https://doi.org/10.1016/j.chemosphere.2019.124644>.
- [86] T.J. Hensema, B.J.A. Berendsen, S.P.J. van Leeuwen, *Chemosphere* 265 (2021), 128599, <https://doi.org/10.1016/j.chemosphere.2020.128599>.
- [87] Y. Jeong, K.M. Da Silva, E. Iturraspe, Y. Fujii, T. Boogaerts, A.L.N. van Nuijs, J. Koelmel, A. Covaci, *J. Hazard Mater.* 437 (2022), 129378, <https://doi.org/10.1016/j.jhazmat.2022.129378>.
- [88] S. Yi, N. Morson, E.A. Edwards, D. Yang, R. Liu, L. Zhu, S.A. Mabury, *Environ. Sci. Technol.* 56 (2022) 907–916, <https://doi.org/10.1021/acs.est.1c05475>.
- [89] I.J. Neuwald, D. Zahn, T.P. Knepper, *Anal. Bioanal. Chem.* 412 (2020) 4881–4892, <https://doi.org/10.1007/s00216-020-02606-8>.
- [90] F. Xiao, S.A. Golovko, M.Y. Golovko, *Anal. Chim. Acta* 988 (2017) 41–49, <https://doi.org/10.1016/j.aca.2017.08.016>.
- [91] J.N. Dodds, Z.R. Hopkins, D.R.U. Knappe, E.S. Baker, *Anal. Chem.* 92 (2020) 4427–4435, <https://doi.org/10.1021/acs.analchem.9b05364>.
- [92] M. Foster, M. Rainey, C. Watson, J.N. Dodds, K.I. Kirkwood, F.M. Fernandez, E. S. Baker, *Environ. Sci. Technol.* 56 (2022) 9133–9143, <https://doi.org/10.1021/acs.est.2c00201>.
- [93] K.I. Kirkwood, J. Fleming, H. Nguyen, D.M. Reif, E.S. Baker, S.M. Belcher, *Environ. Sci. Technol.* 56 (2022) 3441–3451, <https://doi.org/10.1021/acs.est.1c06483>.

Appendix 6

Publication 6

PhotoTOP: PFAS Precursor Characterization by UV/TiO₂ Photocatalysis

Jonathan Zweigle,⁺ Boris Bugsel,⁺ Catharina Capitain,⁺ Christian Zwiener⁺

⁺Environmental Analytical Chemistry, Center for Applied Geoscience, University of Tübingen,
Schnarrenbergstraße 94-96, 72076 Tübingen, Germany

Published in: Environmental Science and Technology 56 (22):15728-15736

DOI: 10.1021/acs.est.2c05652

Reprinted with permission from Environmental Science & Technology: Zweigle, J., Bugsel, B., Capitain, C., & Zwiener, C. (2022). PhotoTOP: PFAS Precursor Characterization by UV/TiO₂ Photocatalysis. Environ Sci Technol, 56(22), 15728-15736. <https://doi.org/10.1021/acs.est.2c05652>

PhotoTOP: PFAS Precursor Characterization by UV/TiO₂ Photocatalysis

Jonathan Zweigle, Boris Bugsel, Catharina Capitain, and Christian Zwiener*



Cite This: *Environ. Sci. Technol.* 2022, 56, 15728–15736



Read Online

ACCESS |



Metrics & More

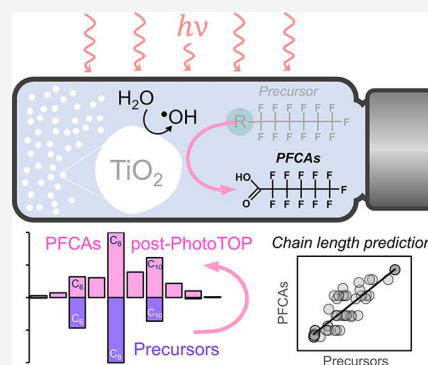


Article Recommendations



Supporting Information

ABSTRACT: To unravel the complexity of per- and polyfluoroalkyl substances (PFAS) in products and environmental samples, sum parameters that provide relevant information on chemical characteristics are necessary since not all PFAS can be captured by target analysis in case of missing reference standards or if they are not extractable or amenable to the analytical method. Therefore, we evaluated photocatalysis (UV/TiO₂) as a further total oxidizable precursor approach (PhotoTOP) to characterize perfluoroalkyl acid precursors via their conversion to perfluoroalkyl carboxylic acids (PFCAs). Photocatalysis has the advantage that no salts are needed, allowing direct injection with liquid chromatography-mass spectrometry without time-consuming and potentially discriminating sample cleanup. OH radicals were monitored with OH probes to determine the reactivity. For eight different precursors (diPAPs, FTSA, FTCAs, N-EtFOSAA, PFOSA), mass balance was achieved within 4 h of oxidation, and also, in the presence of matrix, complete conversion was possible. The PhotoTOP was able to predict the precursor chain length of known and here newly identified precursors qualitatively when applied to two PFAS-coated paper samples and technical PFAS mixtures. The length of the perfluorinated carbon chain (*n*) was mostly conserved in the form of PFCAs (*n*-1) with only minor fractions of shorter-chain PFCAs. Finally, an unknown fabric sample and a polymer mixture (no PFAS detectable in extracts) were oxidized, and the generated PFCAs indicated the occurrence of side-chain fluorinated polymers.



KEYWORDS: PFAS, PFAA precursors, precursors, PFCAs, TOP assay, photocatalysis, UV/TiO₂, transformation products, mass spectrometry

INTRODUCTION

Per- and polyfluoroalkyl substances (PFAS) form a huge group of diverse anthropogenic chemicals.¹ Recently, estimates categorized more than 6 million chemical structures of PFAS in PubChem based on the Organisation for Economic Co-operation and Development (OECD) definition (at least one isolated -CF₂- or -CF₃ group).² The unique properties of PFAS, for instance, water-, stain-, and oil repellency and their high chemical stability, led to widespread use with countless applications, which cannot be exhaustively characterized.³

The chemical nature of PFAS, particularly the extreme stability of the perfluoroalkyl chain (C_nF_{2n+1}-), arising from the strong C-F bond, in combination with their extensive use resulted in a worldwide distribution of PFAS and their transformation products (TPs).^{4,5} Especially perfluoroalkyl acids (PFAAs) were detected throughout the water cycle,^{6–8} in biota including humans,^{9,10} air, indoor environments,^{11,12} and in soils.¹³ Today, selected PFAAs fall under global regulations to restrict their use due to high persistence, bioaccumulation potential, and adverse health effects.¹⁴

However, regulatory actions combined with the demand for alternatives also lead to the use and production of many yet unknown PFAS. Although some PFAS might be degradable in

the environment their TPs are often dead-end products such as PFAAs. For example, over 85% of the 4730 OECD PFAS (PFAS containing a perfluoroalkyl moiety) are expected to potentially be PFAA precursors.¹⁵ For most PFAS this information is unknown. Since many studies showed high fractions of unknown organic fluorine in both environmental and product samples, it is important to further improve and develop methods to understand the origin of PFAAs from currently used PFAS.^{16–18}

Besides high-resolution mass spectrometry (HRMS), which considerably helped to increase knowledge about distinct identities of numerous new PFAS,^{19–22} there are also sum-parameter approaches that are necessary due to the fact that many PFAS are not readily ionizable or extractable from their matrix.²³ While parameters such as total fluorine (TF)²⁴ and absorbable and extractable organic fluorine (AOF, EOF)^{25,26}

Received: August 5, 2022

Revised: October 8, 2022

Accepted: October 19, 2022

Published: October 28, 2022



have their individual advantages they also go along with the loss of information on identity of individual PFAS, their properties, fate, and toxicity (e.g., chain length, bioaccumulation).²⁷

Therefore, further, partly more selective, techniques were developed to gain relevant information about the chemical structure of PFAA precursors in various matrices due to their complexity.^{28,29} The most prominent technique is the total oxidizable precursor (TOP) assay,³⁰ which uses peroxodisulfate to chemically convert precursors to PFAAs. Moreover, additional attempts were made with O₃ as oxidant in the TOP assay,³¹ a modified version that targets hydrolyzable precursors (THP)³² and electrochemistry to study the transformation of precursors.³³

While the TOP assay is conveniently applicable in most laboratories due to the low requirements on equipment and chemicals it also has drawbacks.^{34,35} During TOP there is a limited amount of oxidant in form of persulfate and hence OH radicals ($\cdot\text{OH}$) available. In the case of high matrix-to-PFAS ratios, persulfate may be consumed by matrix instead of the target PFAS precursors.³⁶ Furthermore, samples after TOP contain high salt concentrations, which is not amenable to electrospray ionization. Therefore, solid phase extraction (SPE) is needed, making it difficult to consider a wide range of formed TPs due to variable recoveries. SPE also affects the visualization of the time course of the reaction by sampling at different reaction times.

In this paper we evaluated the photocatalytic degradation by UV/TiO₂ (PhotoTOP) as a further method to characterize PFAA-precursors. The focus was set to PFAS in papers, textile, and technical mixtures. The photocatalyst TiO₂ can generate considerable concentrations of $\cdot\text{OH}$ and other reactive oxygen species under UV light while it is not consumed itself over time.^{37,38} The use of $\cdot\text{OH}$ -sensitive molecules such as terephthalic acid (and others) is a well-established technique to monitor the reactivity in a UV/TiO₂ system, which was used to improve understanding of the applied oxidation conditions.^{39,40} In addition, a UV/TiO₂ system does not require addition of any salts, having the main advantage that, in principle, no sample cleanup is required, which avoids the potentially unknown selectivity of SPE and allows direct injection with conventional liquid chromatography-mass spectrometry (LC-MS). Moreover, this can be of further benefit when screening with HRMS for unknown TPs from oxidation.

First, we optimized and characterized our UV/TiO₂ setup with the $\cdot\text{OH}$ probe terephthalic acid followed by verification of the stability of PFAAs under the applied conditions. In total we oxidized eight known PFAA precursors with the developed setup and discuss their degradation kinetics, TPs, and mass balances. To evaluate the effect of matrix (dissolved organic carbon; DOC) on the PhotoTOP oxidation we oxidized 8:2 fluorotelomer sulfonic acid (FTSA) with four different matrix dilutions. To this end, we applied the UV/TiO₂ oxidation to two precharacterized (regarding the occurrence of precursors)^{22,41} PFAS-coated paper samples and a technical grease-repellent PFAS standard as well as an acrylic PFAS copolymer and an unknown water-repellent fabric sample. We discuss the ability of the PhotoTOP to unravel the chain-length distribution of precursors in oxidized samples (already known precursors and in this study via non-target screening newly identified precursors) by the generated perfluoroalkyl carboxylic acids (PFCAs). Finally, we consider advantages and

disadvantages of our method for PFAS precursor characterization.

MATERIALS AND METHODS

Chemicals and Reagents. Origin and specifications of used chemicals are given in the [Supporting Information \(Section S1\)](#).

TiO₂ Characterization. The point of zero charge (PZC), the mean particle size, and the particle size distribution were determined to characterize the anatase TiO₂ used for oxidizing PFAA precursors ([Figures S1 & S2](#)).

UV/TiO₂ Oxidation Setup. Experiments were performed within a UVA-CUBE 400 (Hönle UV Technology) equipped with a 1200 W lamp (SOL 1200 RF2, solar simulator lamp). Within the UV chamber three battery-powered magnetic stirrers were placed on a turntable standing on a laboratory scissor jack below the lamp to guarantee uniform and reproducible irradiation of multiple samples ([Figures S3 & S4](#)). Samples were irradiated horizontally in conventional 20 mL Environmental Protection Agency (EPA) screw-cap vials (Pyrex borosilicate glass), which were filled with 23 mL of LC-MS grade water to keep the headspace as small as possible.

Sample Preparation. 10 or 20 mg of TiO₂ was weighed in an EPA vial (~430 or 860 mg/L), and 200 μL of MeOH together with the respective PFAS standard (100 $\mu\text{g}/\text{L}$) was spiked onto the particles. After mixing, the vial was sonicated for 1 min to break apart clumped particles and left open overnight to let the solvent evaporate. The next day 23 mL of water and a magnetic stir bar were added, and the mixture was sonicated for 5 min and thoroughly mixed. In selected experiments, $\cdot\text{OH}$ probes were spiked to a final concentration of 10 μM . In case of PFAS oxidation experiments terephthalic acid (TPA) was used as the $\cdot\text{OH}$ probe, while for mechanistic experiments also coumarin (COU) and coumarin-3-carboxylic acid (CCA) were used. For PFAS sampling 100 μL of the suspension was mixed with 900 μL of MeOH, vortexed, and centrifuged at 20 817 relative centrifugal forces (rcf), and 600 μL of supernatant was transferred in polypropylene (PP) high-performance liquid chromatography (HPLC) vials. The addition of organic solvent to the sample was performed to extract PFAS from the TiO₂ particles, which were sampled as suspension. Before placing the vial in the UV chamber the t_0 sample was taken. Samples were taken in duplicates. To determine the initial concentration of the PFAA precursor an identical dilution (100 $\mu\text{g}/\text{L}$) of the standard (identical standard for spiking the particles) was prepared because sampling of the suspension could not accurately determine the initial concentration of the more hydrophobic precursors (e.g., 8:2 polyfluorinated dialkylated phosphate ester (diPAP)) due to sorption. After finishing irradiation (4 or 5 h), the remaining suspension was placed in an oven overnight at 70 °C to evaporate the water. Then 23 mL of MeOH was added, mixed, and sonicated for 1 h to extract all remaining PFAS from the particles. This extraction control was performed to validate whether sampling over time was representative, which was the case for all PFCAs (very hydrophobic precursors need stronger extraction conditions; however, in the spike experiments they were already degraded after 4 h).

One experiment without irradiation (dark control) was performed ([Figure S9](#)).

For direct oxidation, paper and fabric samples were cut into about 1 mm stripes and mixed with the TiO₂ particles (details in [S1](#)). The technical standards (Zonyl RP, Cartafluor CFI)

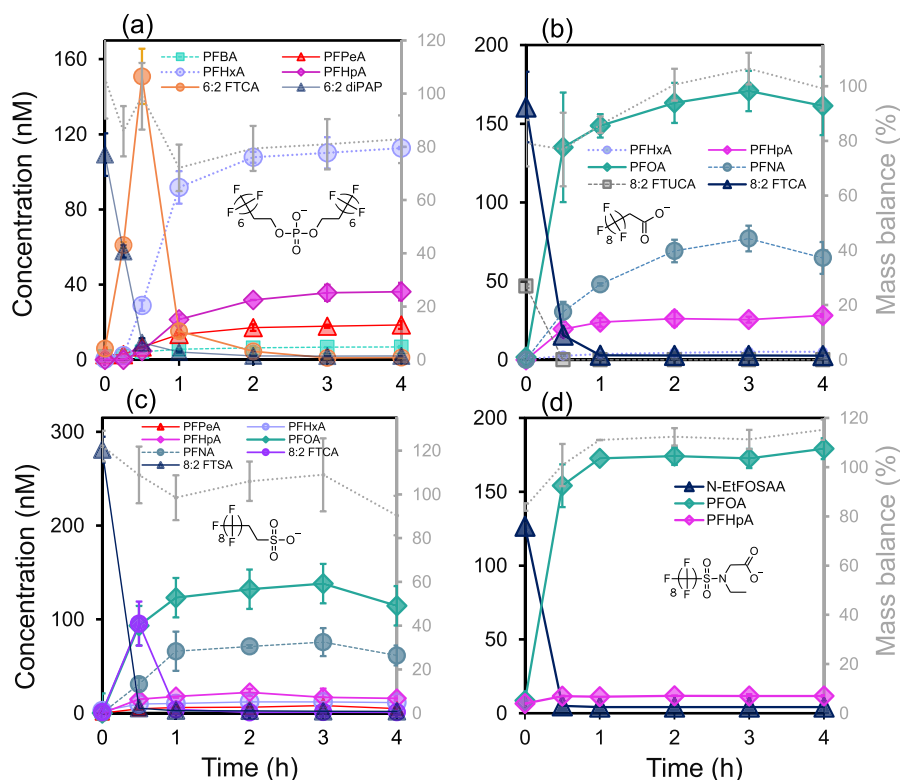


Figure 1. Examples of degradation curves of four PFAA precursors over 4 h of UV/TiO₂ oxidation ($c_0 = 100 \mu\text{g/L}$). (a) 6:2/6:2 diPAP, (b) 8:2 FTCA, (c) 8:2 FTSA, and (d) N-EtFOSAA. Mass balances were calculated on a molar basis. Note that, in case of 6:2/6:2 diPAP, two moles of PFCAs can be formed from one mole of diPAP. Error bars correspond to two standard deviations of duplicate samples. Error bars of the mass balance were calculated according to the Gaussian error propagation. Note: In case of the 8:2 FTCA its standard contained also 8:2 FTUCA probably arising from degradation over time due to its instability.⁴⁷

were directly added to the TiO₂ similar as PFAS standards. Zonyl RP is a polyfluorinated phosphate ester (PAP)-based grease-resistant coating, while Cartafleur CFI is an acrylic fluoro-copolymer mixture.^{42,43} To compare the postoxidation PFCA distribution with precursors prior to oxidation, selected samples were extracted and measured with HPLC-HRMS. Briefly, 10 cm² of sample was covered with 20 mL of MeOH and placed in the overhead shaker overnight followed by ultrasonication for 1 h. After centrifugation, the supernatant was concentrated under a gentle stream of N₂ (40 °C) by a factor of 10.

To determine the rate constants of the ·OH probes in selected experiments, 200 μL of the TiO₂ suspension was sampled at certain time points and centrifuged (8324 rcf), and 150 μL of supernatant was spiked with 4.5 μL of 1:10 diluted formic acid (FA) to guarantee protonation of the ·OH probes for HPLC-UV analysis.

Compound Analysis. Target analytes (C₄–C₁₀ PFCAs, C₄–C₈ perfluoroalkyl sulfonic acids (PFSAs), 6:2 and 8:2 fluorotelomer carboxylic acid (FTCA), 6:2 and 8:2 fluorotelomer unsaturated carboxylic acid (FTUCA), 6:2 and 8:2 diPAP, 6:2 and 8:2 FTSA, N-ethyl perfluorooctane sulfonamide ethanol-based phosphate diester acid (diSAmPAP), perfluorooctanesulfonamide (PFOSA), and N-ethylperfluorooctane sulfonamidoacetic acid (N-EtFOSAA); details in Table S1) were quantified with a 1290 Infinity II HPLC (Agilent Technologies) coupled to a 6490 iFunnel Triple Quadrupole MS (Agilent Technologies). Detailed information regarding chromatographic and instrument parameters is shown in section S2, Tables S2–S4). Quantification was

based on calibration standards (seven different concentrations), and calibration curves were measured before and after each sample set; quality controls were included approximately every 15th sample, and every sample batch contained two blanks.

Precursors without an available reference standard were detected with high-resolution mass spectrometry [1260 Infinity HPLC (Agilent Technologies) coupled to an Agilent 6550 quadrupole time-of-flight mass spectrometer (QTOF-MS)] based on their accurate mass (details in S2; Tables S2 and S4). Furthermore, selected volatile precursors (e.g., fluorotelomer alcohols (FTOHs) and FT-thiols) were detected by coupling an Agilent 7890B gas-chromatograph (GC) via an APCI interface with the QTOF-MS (method details in section S2; Table S5). For each homologous series one reference standard was used for validation, except for fluorotelomer mercapto alkyl phosphate (FTMAP) sulfoxide/sulfone homologues, which were previously identified,²² and newly tentatively identified PFAS (four further FTMAP-related compounds and fluorotelomer aldehydes (FTALs); for details on identification see section S4 and Figures S17–S21) in the paper extracts (for several precursors no reference standard was available). Each measurement sequence included a solvent and extraction blank (for sample extracts) and quality controls to monitor instrument performance similar as described above for target analysis. Qualitative chain-length distributions were determined by molar mass-based signal intensities (chromatographic peak area *A*). For this, *A* of the molecular ion [M-H][−] was multiplied with the molar mass of the respective compound. In case of PFCAs, the molar mass-based peak

areas of the predominant insource fragment ions $[M-CO_2]^-$ were also added. Furthermore, a more in-depth non-target screening (NTS) via FindPFAS and Kendrick mass defect analysis (MS¹, peak picking with the Agilent FindByMolecularFeature algorithm) was performed to search for unknown PFAS precursors in selected sample extracts (more details on identification level⁴⁴ and identity in section S4, further details on NTS described elsewhere).^{22,41} For raw data evaluation, the Agilent Mass Hunter Qualitative Analysis 10.0 and Quantitative Analysis 10.1 were used.

A 1260 Infinity HPLC (Agilent Technologies) equipped with a diode array detector (DAD) was used to separate and detect the $\cdot OH$ probes (details in section S2; Table S6). $\cdot OH$ probes were verified for correct retention time (RT) with reference standards.

$\cdot OH$ Concentration Estimation. To monitor the UV/TiO₂ reactivity, several experiments with $\cdot OH$ -sensitive molecules were conducted [terephthalic acid (TPA), coumarin (COU), and coumarin carboxylic acid (CCA)], and the steady-state $\cdot OH$ concentration ($[\cdot OH]_{ss}$) was determined (details in section S2, Table S6, and Figure S5).

RESULTS AND DISCUSSION

UV/TiO₂ Characterization and Method Development.

Due to the high reactivity, all experiments were performed with anatase TiO₂.⁴⁰ The PZC of washed TiO₂ was pH 3.6, and the mean particle size was 390 nm (Figures S1 & S2). Due to cheaper price and good availability and since $[\cdot OH]_{ss}$ (determined from $k_{obs,TPA}$) was only around a factor of 2 smaller in Pyrex glass vials compared to quartz glass, Pyrex was chosen. Pretests with TPA showed high reproducibility of the developed setup when comparing multiple samples (Figure S4). Since a pH change of the suspension (pH 3–10, Figure S6) only changed $[\cdot OH]_{ss}$ by a factor of 2, neutral pH without any addition of salts was considered ideal, because it allows direct injection with LC-MS without prior sample cleanup making it much faster and avoiding discrimination of unknown TPs during, for example, SPE. In the final setup $[\cdot OH]_{ss}$ was $(1.1-1.5) \times 10^{-12}$ M (TPA and COU) and an order of magnitude higher by CCA (1.1×10^{-11} M). CCA was described to be able to detect $\cdot OH$ near the TiO₂ surface (adsorbed $\cdot OH$) leading to the hypothesis of higher $[\cdot OH]_{ss}$ at the TiO₂ surface compared to the bulk solution (Figure S5).³⁹ The steady-state temperature in suspension was approximately 60 °C (Figure S7).

PhotoTOP with Known PFAA-Precursors. To evaluate the stability of PFAAs as oxidation end products, PFBA, PFHxA, PFOA, PFBA, PFHxS, and PFOS were irradiated for 4 h (430 mg/L TiO₂). None of them degraded under the applied conditions showing that neither the generated radicals nor direct hole reactions on the excited TiO₂ could oxidize them, being consistent with previous observations (Figure S8).^{45,46}

To investigate the suitability and performance of UV/TiO₂ to characterize PFAA-precursors, at first, the transformation of eight known precursors with available reference standards was investigated. Therefore, six telomer-based precursors (6:2/6:2 diPAP, 8:2/8:2 diPAP, 6:2 and 8:2 FTSA, and 6:2 and 8:2 FTCA) and two PASF-based-precursors (PFOSA and N-EtFOSAA) were oxidized, and samples were taken at 0, 0.5, 1, 2, 3, and 4 h and analyzed for targeted PFAS with HPLC-MS/MS (Figure 1a–d for selected degradation curves, mass balances after 4 h in Figure 2). Telomer-based precursors comprising a $F(CF_2)_n-C_2H_4-R$ group formed n:2 FTCAs as

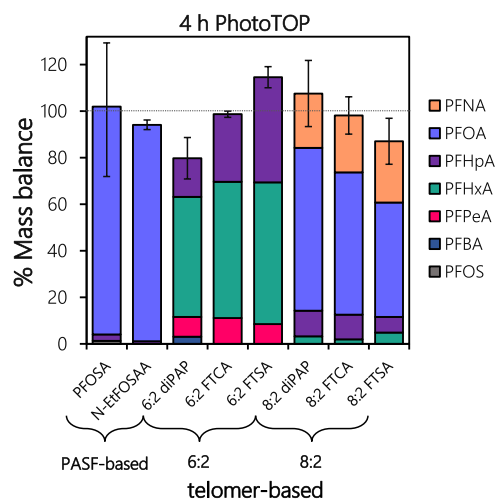


Figure 2. Mass balances for the eight PFAA-precursors after 4 h of photocatalytic oxidation by UV/TiO₂ ($c_0 = 100 \mu\text{g/L}$). Note how different precursors with identical chain length (e.g., 8:2 FTCA, and 8:2 FTSA) led to similar PFCA distributions. Mass balances were calculated on a molar basis. Error bars correspond to two standard deviations of duplicate samples calculated for the mass balance with the Gaussian error propagation.

intermediates (approximately 0.5 h) and further degraded to a mixture of PFCAs with the reaction being completed after around 2 h (Figures 1a–c and 2). 8:2 FTCA directly degraded to a PFCA mixture without intermediates. The main end product of 6:2 precursors was PFHxA (51–60%) followed by PFHpA (17–45%) and smaller amounts of PFPeA and in case of 6:2/6:2 diPAP also 3% PFBA. 8:2 precursors formed PFOA as the major end product (49–70%) followed by PFNA (23–26%), PFHpA (7–11%), and PFHxA below 5%. The total mass balance of all precursors ranged from 82% to 115% showing that a quantitative conversion from precursor to PFCAs is possible via UV/TiO₂ oxidation (Figure 2). From the mass balances it can be concluded that no significant concentrations of ultrashort-chain PFCAs were generated.

In general, the qualitative PFCA distribution after complete conversion of telomer-based precursors was very similar for the three different 6:2 and 8:2 precursors, respectively. In principle, this allows some prediction of the precursor perfluoroalkyl chain length. Since the main oxidation product was always shortened by one CF₂ unit (e.g., PFOA from an 8:2 precursor) and the relative distribution of PFCAs was very similar, the precursor chain length can be predicted for simple cases where only one precursor is present. However, it is important to note that the PFCA chain length distribution was temperature-dependent (tested for 6:2/6:2 diPAP, Figure S10). While a higher temperature led to higher fractions of perfluoroalkyl chain shortening, presumably due to a preferential HF loss (e.g., PFHxA from 6:2 precursor), at lower temperature PFHpA became the major end product and PFHxA a side product. The original TOP assay typically produces PFCAs with a broader distribution of perfluoroalkyl chain lengths. We hypothesize that the 85 °C of the TOP assay could be one result for the formation of ultrashort-chain PFCAs like trifluoroacetic acid (TFA).⁴⁸ Therefore, it is very important to keep the temperature constant when comparing

different samples. In case of the PASF-based precursors the perfluorooctanesulfonamide unit was completely transformed to PFOA in which the information on the identity of a sulfonamide group is lost after oxidation.

To examine the effect of the matrix on the oxidation of PFAA precursors in the UV/TiO₂ system, 50 g of standard soil (LUF A SP2.4, ~1.8% organic carbon) was extracted in 1 L of deionized water. The suspension was placed on an overhead shaker for 6 h and sonicated for 1 h. After centrifugation the extract was used in three dilutions (undiluted, 1:10, and 1:100) for oxidation of 8:2 FTSA ($c_0 = 100 \mu\text{g/L}$). The DOC concentration in the filtered extract was 15 mg/L (details in the Supporting Information Section S2), which corresponded to a matrix equivalent of 100. The initial PFCA formation was suppressed in the undiluted extract, while it was much less affected in the dilutions compared to the control in LC-MS-grade water (Figure S11). This suppression was also verified by $k_{\text{obs,TPA}}$ (first 15 min), which was proportionally suppressed to the initial PFCA formation (initial rate). Although this suppression was observed, after 4 h, 8:2 FTSA was completely transformed to PFCAs, and their distribution was identical within the previously observed variability. Mass balance was achieved independently of the matrix in all four experiments (90–109%) as shown in Figure 3. The discussed experiments

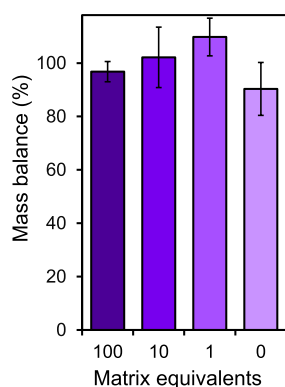


Figure 3. Mass balance of all PFCAs from the precursor 8:2 FTSA after 4 h of oxidation with four different matrix concentration equivalents (MEs). An ME value of 100 corresponded to 15 mg/L DOC. 50 g/L of soil was extracted (overhead shaker for 6 and 1 h of ultrasound in water), and oxidation was performed in the undiluted extract (100 MEs), in dilutions of 1:10 (10 MEs) and 1:100 (1 ME) as well as in matrix free water (0). Error bars correspond to the standard deviation of duplicate samples calculated for the mass balance with the Gaussian error propagation. Complete degradation curves over time are shown in Figure S11.

clearly show that the matrix has an influence on the degradation of PFAA precursors in the UV/TiO₂ system. However, when ensuring long enough oxidation, which was fulfilled by 4 h, matrix-independent oxidation can be achieved. Here, we hypothesize that the amount of TiO₂ does not need to be adapted to different kinds and amounts of matrix due to the steady oxidant supply during photocatalysis. Based on the time course of the PFCA formation the completeness of precursor oxidation can be proven, and oxidation time can be adapted to other matrices if necessary.

Qualitative Precursor Chain Length Prediction Via PhotoTOP for Paper, Fabric Samples, and Technical PFAS Mixtures. To evaluate the suitability of the PhotoTOP with real samples, it was applied to two previously

characterized PFAS-coated papers (P1 & P2),^{22,41} two technical PFAS mixtures [Zonyl RP (monomeric) and Cartafluor CFI (polymeric)], and one unknown water-repellent fabric (canvas).

First, papers P1 & P2 and Zonyl RP are discussed, because numerous PFAA precursors were already detected allowing a good comparison to PFCAs generated by PhotoTOP. In the case of paper P1 the amount of extract used in the PhotoTOP corresponded to about 10 mg paper/mL TiO₂ suspension, whereas for P2 the extract corresponded to only about 0.1 mg of paper/mL, which is a difference of 2 orders of magnitude (quantities of extracts are here expressed as mass of paper per milliliter of TiO₂ suspension). Both extracts were oxidized under identical conditions.

P1 is a paper coated with FTMAP homologous (6:2/6:2 to 10:2/10:2), and it contains further previously identified FTMAP (di)sulfoxide/sulfone homologues and FTSAs.²² In addition, four further homologous compound classes were tentatively identified here (details in section S4), which are presumably byproducts from production or TPs of FTMAPs due to their related chemical structure (Figure S17). Paper P2 is coated with diPAP homologues (4:2/6:2 to 12:2/12:2), and further FTOHs were detected. It is important to note that diPAPs, FTMAPs, and other two-armed precursors occurred in several structural isomers [e.g., $n:2/n:2$ & $(n-2):2/(n+2):2$ & $(n-4):2/(n+4):2$]. The following results are based on simple molar mass-based peak areas (A) that are typically acquired with HRMS.

Oxidation of the paper extracts by PhotoTOP generated several PFCAs with chain lengths of C₄ up to C₁₈ (PFBA to PFOA) over time. A snapshot of the relative signal intensities of the generated PFCAs (A/A_{max}) after 4 h of PhotoTOP reveals that their chain length distribution reflects well the initial chain length distribution of the precursors (e.g., FTMAPs, diPAPs, etc.) in both papers (Figure 4). The main products were even-numbered PFCAs, while odd numbers were less represented, which is due to the even-numbered telomer-based precursors. PFCAs > C₁₂ were only observed in P2, although no diPAPs with such chain lengths were detected in the extract. This could presumably be a result of decreasing recoveries of precursors (diPAPs) with increasing chain length due to decreasing ionization efficiency and solubility in MeOH.⁴⁹ However, FTOHs are further precursors detected in the extract of paper P2 by GC-QTOF-MS at chain lengths up to C₁₈, which must be considered as additional precursors of PFCAs (Figure S13).

After 4 h of oxidation, the rate of PFCA formation was still increasing in P1 (incomplete oxidation), while in P2 the formation levels off already (Figure S12a,b), which presumably results from the 100-fold lower amount of extract used for P2. Nevertheless, due to the parallel formation rate changes, the snapshot of PFCAs can predict the precursor chain length distribution independently of the completeness of oxidation and, therefore, on the amount of extract oxidized. Furthermore, although the signal intensities of the precursors (Figure 4, Figure S13, and Section S4) were different, all present precursor classes could similarly be represented by produced PFCAs. However, due to unavailable reference standards it cannot be verified which precursor class contributed to the PFCA formation in which extent in both samples.

Precursor chain length prediction was also possible for the paper coating formulation Zonyl RP directly (Figure S14a). Due to the fact that here the PFCA formation stopped after 4 h

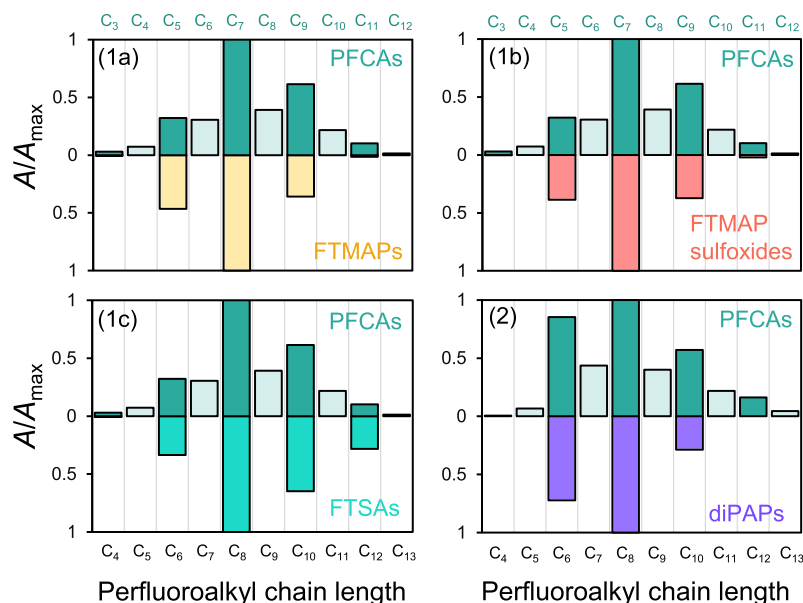


Figure 4. Relative signal intensities of precursors in two different PFAS-coated paper sample extracts before oxidation (negative y-axis) and relative signal intensities of PFCAs after 4 h of PhotoTOP oxidation (positive y-axis). Peak areas of asymmetrically substituted precursors (e.g., 6:2/8:2 diPAP) were divided among the PFCAs with corresponding chain lengths (e.g., PFHxA, PFOA). Odd-numbered PFCAs are shown in light green. Note that, e.g., a perfluoroalkyl chain length of C₇ corresponds to PFOA. (1a–c) Paper extract P1 coated with FTMAP homologues and related compounds. In 1b,c the precursors FTMAP sulfoxides and FTSAs are also shown. Note that the PFCA distribution data (positive y-axis) is identical. (2) Paper extract P2 from the paper sample coated with different diPAP homologues. Formation of PFCAs over time are shown in Figure S12a,b for both samples and further detected precursors in Figure S13 and section S4. Note that the amount of extract used for oxidation of P1 and P2 was different by 2 orders of magnitude.

we assume an almost complete conversion of perfluoroalkyl chains of the precursors to PFCAs.

To further verify whether the precursor chain length distribution can be estimated from the generated PFCAs also via direct oxidation of PFAS products, paper stripes from paper P1 (2 mg paper/mL TiO₂ suspension) were directly oxidized by PhotoTOP. Direct oxidation has the major advantage of being able to capture nonextractable precursors (e.g., too strong interactions with the matrix or covalently bound perfluoroalkyl chains on a polymer backbone). A third case could be an extractable but nonionizable precursor. The results showed that the PhotoTOP was also applicable by direct oxidation and generated PFCAs representative for the precursor chain length distribution (Figure S15). It is important to mention that the oxidation was approximately 10 times slower in comparison to extract oxidation.

To get a statistically meaningful estimate of the possibility to predict precursor chain lengths via PhotoTOP, relative signal intensities of 11 different precursor classes (for details on identification levels⁴⁴ and newly identified precursors see section S4) were correlated with the formation of even-numbered PFCAs from direct and extract oxidation experiments (Figure 5). Generally, a clear positive correlation was observed ($R^2 = 0.88$) demonstrating the potential of the PhotoTOP approach. We suggest excluding odd-numbered PFCAs since they were only of minor importance due to the dominance of the observed $n-1$ chain length (e.g., PFOA from 8:2 diPAP). In comparison to the original TOP assay (directly compared to results obtained by Houtz and Sedlak 2014³⁰ and Janda et al. 2019⁴⁸ in Figure S16) the UV/TiO₂ oxidation resulted in less chain shortening and, hence, could better conserve the original precursor chain length.

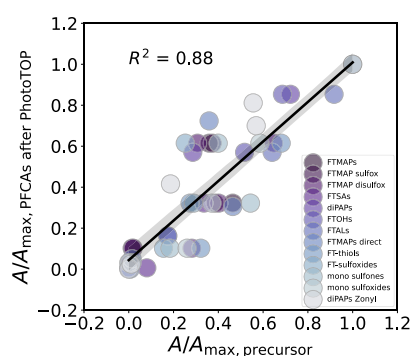


Figure 5. Correlation of relative signal intensities (peak area A/A_{\max}) of even-numbered PFCAs after 4 h of PhotoTOP oxidation with relative signal intensities of 11 different precursor classes in P1, P2, and Zonyl RP prior to oxidation (sample extracts) for different chain lengths. Data from direct oxidation of P1 are also included. Only even-numbered carbon chains were used since telomer-based precursors typically exclusively contain even perfluoroalkyl chains. Due to rather selective chain-shortening reactions in PhotoTOP, even-numbered PFCAs predicted the overall precursor chain lengths best when odd numbers were excluded (see Figures 4 and S13). Peak areas of asymmetrically substituted precursors ($n:m:2$, e.g., 6:2/8:2 diPAP) were divided among the PFCAs with corresponding chain lengths (e.g., PFHxA, PFOA). Further, more extreme asymmetric congeners ($n-m \geq 4$) have not been considered. $R^2 = 0.88$ shows a clear correlation; the 99% confidence interval of the regression is represented as a gray shaded area. We propose this as a verification that precursor chain lengths can be qualitatively predicted by the PhotoTOP. For information on identity and identification levels of precursors see section S4 and Figures S17–S21.

Finally, the PhotoTOP was applied to samples where the initial precursors could not be determined: the water-repellent

fabric (extract oxidation and direct oxidation) and the technical mixture Cartafluor CFI (direct). An in-depth non-target screening, including suspect screening with a list of well-known PFAS, Kendrick mass defect analysis of MS¹ peaks, and a MS/MS fragment mass difference search with FindPFAS, could not reveal any meaningful identification in the fabric extract and dilutions of Cartafluor CFI. This is also true for the oxidized extract of the fabric leading to the assumption that probably here no extractable PFAS were present. However, direct oxidation of the fabric itself generated plenty of PFCAs over time (a snapshot after 5 h is shown in Figure 6; PFCAs over time are shown in Figure S12c).

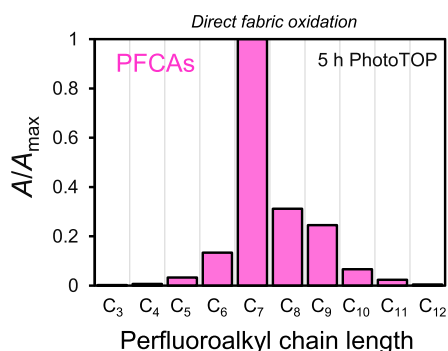


Figure 6. Normalized PFCAs signal intensity distribution after 5 h of direct UV/TiO₂ oxidation of the fabric sample (Note that, e.g., a perfluoroalkyl chain length of C₇ corresponds to PFOA). Neither in the fabric extract nor in the oxidized fabric extract PFAS were found (NTS with HRMS). This led to the assumption that the fabric either contained side-chain fluorinated polymers (SFPs) or precursors that were not extractable/ionizable or were overseen during NTS analyses. Due to the strong similarity to Cartafluor CFI (Figure S14b) we hypothesize the fabric to be coated with acrylate-based SFPs. Formation of PFCAs over time are shown in Figure S12c.

From this PFCAs distribution we assume the fabric to be coated with side-chain fluorinated polymers (SFPs), which cannot be extracted, but the perfluoroalkyl chains can be cleaved off during oxidation. The observed distribution indicates telomer-based SFPs similar to the fingerprints found by Liagkouridis et al. 2022 with TOP,²³ because we assume that sulfonamide-based SFPs would generate one distinct chain length as observed for PASF-based precursors. Cartafluor CFI showed a highly similar chain-length distribution further indicating that the PFCAs in the fabric originate from an acrylate-based SFP (Figure S14b). Note that sampling over time during oxidation of Cartafluor CFI indicated complete conversion of PFCAs meaning the distribution likely reflects most of the perfluoroalkyl chains present. The overall results show that the PhotoTOP was also applicable to real samples and generated relevant information on the identity and chemical characteristics of precursors. This is, in particular, the chain-length distribution of PFAA precursors in paper and fabric samples as well as in technical PFAS mixtures with relatively little laboratory effort. We believe that this can easily be expanded to further environmental matrices such as, for example, wastewater; however, this was outside the scope of this study.

In comparison to the original TOP assay, we assume a more constant ·OH radical generation over time due to the photocatalytic nature of the UV/TiO₂ system, which has advantages in the presence of quenching matrix compared to

peroxodisulfate. The absence of strong chain-shortening potentially results from milder conditions and the absence of sulfate radicals, which can mineralize PFCAs at high concentrations (they potentially play a minor role in the TOP due to high pH).⁴⁸ However, the effect of temperature on chain shortening should be investigated in more detail for both approaches. Another important advantage of the PhotoTOP is the absence of high salt concentrations that keep laboratory and sample cleanup efforts low and minimize matrix interferences.

A clear disadvantage of the PhotoTOP is the more complex setup that requires a UV chamber that is difficult to standardize and compare (e.g., uniform irradiation, distance to the UV source). However, ·OH probes can be used to monitor the reactivity and make results comparable. Furthermore, in the case of complex matrices, sampling over time can help to identify whether oxidation was complete. In general, the PhotoTOP is not intended as an alternative to the original TOP assay but can be considered a complementary method to better understand complex PFAS contaminations. Future work should investigate whether complete quantitative oxidation can also be accomplished when applied directly to product or environmental samples.

■ ASSOCIATED CONTENT

Supporting Information

The Supporting Information is available free of charge at <https://pubs.acs.org/doi/10.1021/acs.est.2c05652>.

Chemicals, reagents, and samples; Compound analysis; Supporting experiments; Precursor identification in paper extracts (PDF)

■ AUTHOR INFORMATION

Corresponding Author

Christian Zwiener – Environmental Analytical Chemistry, Center for Applied Geoscience, University of Tübingen, 72076 Tübingen, Germany; orcid.org/0000-0002-6682-5828; Email: christian.zwiener@uni-tuebingen.de

Authors

Jonathan Zweigle – Environmental Analytical Chemistry, Center for Applied Geoscience, University of Tübingen, 72076 Tübingen, Germany; orcid.org/0000-0002-7194-1567

Boris Bugsel – Environmental Analytical Chemistry, Center for Applied Geoscience, University of Tübingen, 72076 Tübingen, Germany; orcid.org/0000-0001-9752-9741

Catharina Capitain – Environmental Analytical Chemistry, Center for Applied Geoscience, University of Tübingen, 72076 Tübingen, Germany

Complete contact information is available at: <https://pubs.acs.org/doi/10.1021/acs.est.2c05652>

Notes

The authors declare no competing financial interest.

■ ACKNOWLEDGMENTS

The authors acknowledge the Deutsche Bundesstiftung Umwelt for the scholarship of J.Z., funding of the project FluorTECH by the state of Baden-Württemberg (BWPFC 19010), and M. Haußecker, M. Schüßler, and K. Wack for support during selected oxidation experiments.

REFERENCES

- (1) Buck, R. C.; Franklin, J.; Berger, U.; Conder, J. M.; Cousins, I. T.; de Voogt, P.; Jensen, A. A.; Kannan, K.; Mabury, S. A.; van Leeuwen, S. P. Perfluoroalkyl and polyfluoroalkyl substances in the environment: terminology, classification, and origins. *Integr Environ. Assess Manag* **2011**, *7* (4), 513–41.
- (2) PubChem PFAS and Fluorinated Compounds in PubChem Tree. Online at <https://pubchem.ncbi.nlm.nih.gov/classification/#hid=120>; accessed 2022-07-07.
- (3) Gluge, J.; Scheringer, M.; Cousins, I. T.; DeWitt, J. C.; Goldenman, G.; Herzke, D.; Lohmann, R.; Ng, C. A.; Trier, X.; Wang, Z. An overview of the uses of per- and polyfluoroalkyl substances (PFAS). *Environ. Sci. Process Impacts* **2020**, *22* (12), 2345–2373.
- (4) Evich, M. G.; Davis, M. J. B.; McCord, J. P.; Acrey, B.; Awkerman, J. A.; Knappe, D. R. U.; Lindstrom, A. B.; Speth, T. F.; Tebes-Stevens, C.; Strynar, M. J.; Wang, Z.; Weber, E. J.; Henderson, W. M.; Washington, J. W. Per- and polyfluoroalkyl substances in the environment. *Science* **2022**, *375* (6580), eabg9065.
- (5) Wang, Z.; DeWitt, J. C.; Higgins, C. P.; Cousins, I. T. A Never-Ending Story of Per- and Polyfluoroalkyl Substances (PFASs)? *Environ. Sci. Technol.* **2017**, *51* (5), 2508–2518.
- (6) Kaboré, H. A.; Vo Duy, S.; Munoz, G.; Méité, L.; Desrosiers, M.; Liu, J.; Sory, T. K.; Sauvé, S. Worldwide drinking water occurrence and levels of newly-identified perfluoroalkyl and polyfluoroalkyl substances. *Sci. Total Environ.* **2018**, *616–617*, 1089–1100.
- (7) Loos, R.; Gawlik, B. M.; Locoro, G.; Rimaviciute, E.; Contini, S.; Bidoglio, G. EU-wide survey of polar organic persistent pollutants in European river waters. *Environ. Pollut.* **2009**, *157* (2), 561–568.
- (8) Xiao, F. Emerging poly- and perfluoroalkyl substances in the aquatic environment: A review of current literature. *Water Res.* **2017**, *124*, 482–495.
- (9) Yeung, L. W. Y.; Mabury, S. A. Are humans exposed to increasing amounts of unidentified organofluorine? *Environmental Chemistry* **2016**, *13* (1), 102–110.
- (10) De Silva, A. O.; Armitage, J. M.; Bruton, T. A.; Dassuncao, C.; Heiger-Bernays, W.; Hu, X. C.; Karrman, A.; Kelly, B.; Ng, C.; Robuck, A.; Sun, M.; Webster, T. F.; Sunderland, E. M. PFAS Exposure Pathways for Humans and Wildlife: A Synthesis of Current Knowledge and Key Gaps in Understanding. *Environ. Toxicol. Chem.* **2021**, *40* (3), 631–657.
- (11) Kim, S.-K.; Shoeib, M.; Kim, K.-S.; Park, J.-E. Indoor and outdoor poly- and perfluoroalkyl substances (PFASs) in Korea determined by passive air sampler. *Environ. Pollut.* **2012**, *162*, 144–150.
- (12) Fraser, A. J.; Webster, T. F.; Watkins, D. J.; Nelson, J. W.; Stapleton, H. M.; Calafat, A. M.; Kato, K.; Shoeib, M.; Vieira, V. M.; McClean, M. D. Polyfluorinated compounds in serum linked to indoor air in office environments. *Environ. Sci. Technol.* **2012**, *46* (2), 1209–15.
- (13) Bugsel, B.; Zwiener, C. LC-MS screening of poly- and perfluoroalkyl substances in contaminated soil by Kendrick mass analysis. *Anal Bioanal Chem.* **2020**, *412* (20), 4797–4805.
- (14) Convention, S. The new POPs under the Stockholm Convention. Online at <http://www.pops.int/TheConvention/ThePOPs/TheNewPOPs/tabid/2511/Default.aspx>; accessed 2022-07-07.
- (15) OECD *Toward a new comprehensive global database of per- and polyfluoroalkyl substances (PFASs): Summary report on updating the OECD 2007 list of per- and polyfluoroalkyl substances (PFASs)*; 2018.
- (16) Aro, R.; Eriksson, U.; Kärrman, A.; Chen, F.; Wang, T.; Yeung, L. W. Y. Fluorine Mass Balance Analysis of Effluent and Sludge from Nordic Countries. *ACS ES&T Water* **2021**, *1* (9), 2087–2096.
- (17) Aro, R.; Carlsson, P.; Vogelsang, C.; Karrman, A.; Yeung, L. W. Fluorine mass balance analysis of selected environmental samples from Norway. *Chemosphere* **2021**, *283*, 131200.
- (18) Kaiser, A. M.; Aro, R.; Karrman, A.; Weiss, S.; Hartmann, C.; Uhl, M.; Forsthuber, M.; Gundacker, C.; Yeung, L. W. Y. Comparison of extraction methods for per- and polyfluoroalkyl substances (PFAS) in human serum and placenta samples—insights into extractable organic fluorine (EOF). *Anal Bioanal Chem.* **2021**, *413* (3), 865–876.
- (19) Barzen-Hanson, K. A.; Roberts, S. C.; Choyke, S.; Oetjen, K.; McAlees, A.; Riddell, N.; McCrindle, R.; Ferguson, P. L.; Higgins, C. P.; Field, J. A. Discovery of 40 Classes of Per- and Polyfluoroalkyl Substances in Historical Aqueous Film-Forming Foams (AFFFs) and AFFF-Impacted Groundwater. *Environ. Sci. Technol.* **2017**, *51* (4), 2047–2057.
- (20) Neuwald, I. J.; Hubner, D.; Wiegand, H. L.; Valkov, V.; Borchers, U.; Nodler, K.; Scheurer, M.; Hale, S. E.; Arp, H. P. H.; Zahn, D. Ultra-Short-Chain PFASs in the Sources of German Drinking Water: Prevalent, Overlooked, Difficult to Remove, and Unregulated. *Environ. Sci. Technol.* **2022**, *56* (10), 6380–6390.
- (21) Young, R. B.; Pica, N. E.; Sharifan, H.; Chen, H.; Roth, H. K.; Blakney, G. T.; Borch, T.; Higgins, C. P.; Kornuc, J. J.; McKenna, A. M.; Blotvogel, J. PFAS Analysis with Ultrahigh Resolution 21T FT-ICR MS: Suspect and Nontargeted Screening with Unrivaled Mass Resolving Power and Accuracy. *Environ. Sci. Technol.* **2022**, *56* (4), 2455–2465.
- (22) Zweigle, J.; Bugsel, B.; Zwiener, C. FindPFAS: Non-Target Screening for PFAS horizontal line Comprehensive Data Mining for MS2 Fragment Mass Differences. *Anal. Chem.* **2022**, *94*, 10788.
- (23) Liagkouridis, I.; Awad, R.; Schellenberger, S.; Plassmann, M. M.; Cousins, I. T.; Benskin, J. P. Combined Use of Total Fluorine and Oxidative Fingerprinting for Quantitative Determination of Side-Chain Fluorinated Polymers in Textiles. *Environmental Science & Technology Letters* **2022**, *9* (1), 30–36.
- (24) Ritter, E. E.; Dickinson, M. E.; Harron, J. P.; Lunderberg, D. M.; DeYoung, P. A.; Robel, A. E.; Field, J. A.; Peaslee, G. F. PIGE as a screening tool for Per- and polyfluorinated substances in papers and textiles. *Nuclear Instruments and Methods in Physics Research Section B: Beam Interactions with Materials and Atoms* **2017**, *407*, 47–54.
- (25) Miaz, L. T.; Plassmann, M. M.; Gyllenhammar, I.; Bignert, A.; Sandblom, O.; Lignell, S.; Glynn, A.; Benskin, J. P. Temporal trends of suspect- and target-per/polyfluoroalkyl substances (PFAS), extractable organic fluorine (EOF) and total fluorine (TF) in pooled serum from first-time mothers in Uppsala, Sweden, 1996–2017. *Environ. Sci. Process Impacts* **2020**, *22* (4), 1071–1083.
- (26) von Abercron, E.; Falk, S.; Stahl, T.; Georgii, S.; Hamscher, G.; Brunn, H.; Schmitz, F. Determination of adsorbable organically bound fluorine (AOF) and adsorbable organically bound halogens as sum parameters in aqueous environmental samples using combustion ion chromatography (CIC). *Sci. Total Environ.* **2019**, *673*, 384–391.
- (27) McDonough, C. A.; Guelfo, J. L.; Higgins, C. P. Measuring total PFASs in water: The tradeoff between selectivity and inclusivity. *Current Opinion in Environmental Science & Health* **2019**, *7*, 13–18.
- (28) Koch, A.; Aro, R.; Wang, T.; Yeung, L. W. Y. Towards a comprehensive analytical workflow for the chemical characterisation of organofluorine in consumer products and environmental samples. *Trac-Trend Anal Chem.* **2020**, *123*, 115423.
- (29) McDonough, C. A.; Li, W.; Bichel, H. N.; De Silva, A. O.; DeWitt, J. C. Widening the Lens on PFASs: Direct Human Exposure to Perfluoroalkyl Acid Precursors (pre-PFAAs). *Environ. Sci. Technol.* **2022**, *56* (10), 6004–6013.
- (30) Houtz, E. F.; Sedlak, D. L. Oxidative conversion as a means of detecting precursors to perfluoroalkyl acids in urban runoff. *Environ. Sci. Technol.* **2012**, *46* (17), 9342–9.
- (31) Kaiser, A. M.; Saracevic, E.; Schaar, H. P.; Weiss, S.; Hornek-Gausterer, R. Ozone as oxidizing agent for the total oxidizable precursor (TOP) assay and as a preceding step for activated carbon treatments concerning per- and polyfluoroalkyl substance removal. *J. Environ. Manage* **2021**, *300*, 113692.
- (32) Nikiforov, V. A. Hydrolysis of FTOH precursors, a simple method to account for some of the unknown PFAS. *Chemosphere* **2021**, *276*, 130044.
- (33) Zweigle, J.; Bugsel, B.; Schmitt, M.; Zwiener, C. Electrochemical Oxidation of 6:2 Polyfluoroalkyl Phosphate Diester-Simulation of Transformation Pathways and Reaction Kinetics with

Hydroxyl Radicals. *Environ. Sci. Technol.* **2021**, *55* (16), 11070–11079.

(34) Larsson, P. Total oxidizable precursor assay: Applications and limitations. A study on the occurrence of perfluoroalkyl and polyfluoroalkyl substances (PFASs) in Chinese Wastewater Treatment Plants. *MSc Thesis*, Örebro University, 2020.

(35) Göckener, B.; Lange, F. T.; Lesmeister, L.; Gökçe, E.; Dahme, H. U.; Bandow, N.; Biegel-Engler, A., Digging deep—implementation, standardisation and interpretation of a total oxidisable precursor (TOP) assay within the regulatory context of per- and polyfluoroalkyl substances (PFASs) in soil. *Environmental Sciences Europe* **2022**, *34*, (1). DOI: 10.1186/s12302-022-00631-1.

(36) Al Amin, M.; Luo, Y.; Shi, F.; Yu, L.; Liu, Y.; Nolan, A.; Mallavarapu, M.; Naidu, R.; Fang, C. Optimising TOP assay to detect PFAS in AFFFs and soil. *SSRN Preprints* **2022**. DOI: 10.2139/ssrn.4150349

(37) Pelizzetti, E.; Pramauro, E.; Minero, C.; Serpone, N. Sunlight photocatalytic degradation of organic pollutants in aquatic systems. *Waste Management* **1990**, *10* (1), 65–71.

(38) Pelizzetti, E.; Minero, C. Mechanism of the photo-oxidative degradation of organic pollutants over TiO₂ particles. *Electrochim. Acta* **1993**, *38* (1), 47–55.

(39) Zhang, J.; Nosaka, Y. Mechanism of the OH Radical Generation in Photocatalysis with TiO₂ of Different Crystalline Types. *J. Phys. Chem. C* **2014**, *118* (20), 10824–10832.

(40) Hirakawa, T.; Yawata, K.; Nosaka, Y. Photocatalytic reactivity for O₂^{•-} and OH radical formation in anatase and rutile TiO₂ suspension as the effect of H₂O₂ addition. *Applied Catalysis A: General* **2007**, *325* (1), 105–111.

(41) Bugsel, B.; Bauer, R.; Herrmann, F.; Maier, M. E.; Zwiener, C. LC-HRMS screening of per- and polyfluorinated alkyl substances (PFAS) in impregnated paper samples and contaminated soils. *Anal Bioanal Chem.* **2022**, *414* (3), 1217–1225.

(42) Gebbink, W. A.; Ullah, S.; Sandblom, O.; Berger, U. Polyfluoroalkyl phosphate esters and perfluoroalkyl carboxylic acids in target food samples and packaging—method development and screening. *Environmental Science and Pollution Research* **2013**, *20* (11), 7949–7958.

(43) Rosenmai, A. K.; Taxvig, C.; Svingen, T.; Trier, X.; van Vugt-Lussenburg, B. M.; Pedersen, M.; Lesne, L.; Jegou, B.; Vinggaard, A. M. Fluorinated alkyl substances and technical mixtures used in food paper-packaging exhibit endocrine-related activity in vitro. *Andrology* **2016**, *4* (4), 662–72.

(44) Charbonnet, J. A.; McDonough, C. A.; Xiao, F.; Schwichtenberg, T.; Cao, D.; Kaserzon, S.; Thomas, K. V.; Dewapriya, P.; Place, B. J.; Schymanski, E. L.; Field, J. A.; Helbling, D. E.; Higgins, C. P. Communicating Confidence of Per- and Polyfluoroalkyl Substance Identification via High-Resolution Mass Spectrometry. *Environ. Sci. Technol. Lett.* **2022**, *9* (6), 473–481.

(45) Javed, H.; Lyu, C.; Sun, R.; Zhang, D.; Alvarez, P. J. J. Discerning the inefficacy of hydroxyl radicals during perfluorooctanoic acid degradation. *Chemosphere* **2020**, *247*, 125883.

(46) Yao, Y.; Meng, Y.; Sun, H. Heterogeneous photooxidation of 6:2 polyfluoroalkyl phosphoric acid diester on dust mineral components under simulated sunlight and the influence of relative humidity and oxygen. *Chemosphere* **2021**, *281*, 130713.

(47) Loewen, M.; Halldorson, T.; Wang, F.; Tomy, G. Fluorotelomer carboxylic acids and PFOS in rainwater from an urban center in Canada. *Environ. Sci. Technol.* **2005**, *39* (9), 2944–51.

(48) Janda, J.; Nodler, K.; Scheurer, M.; Happel, O.; Nurenberg, G.; Zwiener, C.; Lange, F. T. Closing the gap - inclusion of ultrashort-chain perfluoroalkyl carboxylic acids in the total oxidizable precursor (TOP) assay protocol. *Environ. Sci. Process Impacts* **2019**, *21* (11), 1926–1935.

(49) Wang, Z. Y.; MacLeod, M.; Cousins, I. T.; Scheringer, M.; Hungerbühler, K. Using COSMOtherm to predict physicochemical properties of poly- and perfluorinated alkyl substances (PFASs). *Environmental Chemistry* **2011**, *8* (4), 389–398.

Recommended by ACS

Hydroxyl Radical Transformations of Perfluoroalkyl Acid (PFAA) Precursors in Aqueous Film Forming Foams (AFFFs)

Nicholas Gonda, Bettina Voelker, *et al.*

MAY 18, 2023

ENVIRONMENTAL SCIENCE & TECHNOLOGY

READ 

Degradation and Defluorination of Per- and Polyfluoroalkyl Substances by Direct Photolysis at 222 nm

Xiaoyue Xin, Ching-Hua Huang, *et al.*

JULY 06, 2023

ACS ES&T WATER

READ 

Oxidation of Per- and Polyfluoroalkyl Ether Acids and Other Per- and Polyfluoroalkyl Substances by Sulfate and Hydroxyl Radicals: Kinetic Insights from Experiments a...

Chuhui Zhang, Detlef R.U. Knappe, *et al.*

MAY 24, 2023

ENVIRONMENTAL SCIENCE & TECHNOLOGY

READ 

Generation Mechanism of Perfluorohexanesulfonic Acid from Polyfluoroalkyl Sulfonamide Derivatives During Chloramination in Drinking Water

Zhigang Li, Guibin Jiang, *et al.*

JANUARY 12, 2023

ENVIRONMENTAL SCIENCE & TECHNOLOGY

READ 

Get More Suggestions >

Supporting Information

PhotoTOP: PFAS precursor characterization via UV/TiO₂ photocatalysis

Jonathan Zweigle,⁺ Boris Bugsel,⁺ Catharina Capitain,⁺ Christian Zwiener^{+,*}

⁺Environmental Analytical Chemistry, Center for Applied Geoscience, University of Tübingen, Schnarrenbergstraße 94-96, 72076 Tübingen, Germany

*Corresponding author

Contents

S1 CHEMICALS, REAGENTS, AND SAMPLES.....	2
Table S 1: Origin of the PFAS target analytes.....	2
S2 COMPOUND ANALYSIS.....	3
HPLC-QqQ-MS.....	3
HPLC-QTOF-MS.....	3
GC-QTOF-MS.....	4
Table S 2: Gradient elution of the HPLC-QTOF and the HPLC-QqQ method.....	4
Table S 3: MRM parameters for the target compounds used with the Agilent 6490 QqQ.....	5
Table S 4: Summary of instrument and scan source parameters.....	6
Table S 5: Summary APCI and QTOF parameters.....	6
HPLC-UV.....	6
Table S 6: •OH-probes used to estimate [\bullet OH] _{ss}	7
Dissolved organic carbon (DOC):.....	7
S3 SUPPORTING EXPERIMENTS.....	8
Figure S 1: Point of zero charge (PZC).....	8
Figure S 2: Particle size distribution and mean particle size.....	8
Figure S 3: UV/TiO ₂ oxidation setup.....	8
Figure S 4: TPA degradation dependent on the amount of TiO ₂	9
Figure S 5: Pseudo first-order degradation of the •OH-probes and direct vs. indirect photolysis.....	9
Figure S 6: Dependency of $k_{\text{obs,TPA}}$ on pH and TiO ₂ concentration.....	9
Figure S 7: Temperature and pH change over time in the UV-chamber.....	10
Figure S 8: Two control experiments of different PFAAs.....	10
Figure S 9: Dark control without irradiation.....	10
Figure S 10: Changes of degradation kinetics with changing temperature during UV/TiO ₂ oxidation.....	11
Figure S 11: Influence of matrix on the oxidation of 8:2 FTSA in the UV/TiO ₂ system.....	11
Figure S 12: Formation of PFCAs from oxidation of paper extract P1 and P2 (a & b), and direct oxidation of fabric stripes (c).....	11
Figure S 13: Volatile and newly identified precursor chain-length distribution vs. PFCA-distribution after PhotoTOP.....	12
Figure S 14: PhotoTOP with technical PFAS mixtures.....	13
Figure S 15: Direct oxidation of paper P1.....	13
Figure S 16: Comparison of the reaction yields from several precursors between PhotoTOP and the original TOP assay.....	13
S4 PRECURSOR IDENTIFICATION IN PAPER EXTRACTS.....	14
Figure S 17: Summary of identified PFAA-precursors in paper P1 and P2.....	14
Table S 7: Summary of identifications in paper extract P1 and P2.....	15
Figure S 18: Newly tentatively identified compounds in P1 (mono sulfone FTMAPs).....	16
Figure S 19: EICs of the newly identified compounds in P1 (mono sulfoxide/sulfone FTMAPs).....	16
Figure S 20: EICs of FTOHs and FTALs measured by GC-APCI-QTOF in paper extract P2.....	17
Figure S 21: EICs of FT-thiols and FT-sulfoxides measured by GC-APCI-QTOF in paper extract P1.....	18
REFERENCES.....	19

S1 Chemicals, reagents, and samples

Water, methanol (MeOH), ammonium acetate (NH₄Ac) and formic acid (FA) were LC-MS grade and purchased from Fisher scientific. Sodium terephthalate (TPA) was purchased from Tokyo Chemical Industry (TCI). Coumarin (COU), Coumarin-3-carboxylic acid (CCA), and Titanium(IV)oxide (TiO₂ anatase, powder, 99.8% trace metal basis) was purchased from Sigma-Aldrich. Sodium chloride (NaCl) and MES (PUFFERAN®) buffer came from Carl Roth. Origins of PFAS standards are given in Table S1.

Table S 1: Origin of the PFAS target analytes. [PFCAs = Perfluoroalkyl carboxylic acids, PFSAs = Perfluoroalkyl sulfonic acids, PASF = Perfluoroalkane sulfonyl fluoride (PFOSA = Perfluorooctanesulfonamide, *N*-EtFOSAA = *N*-Ethylperfluoro-1-octanesulfonamidoacetic acid, diSAmPAP = *N*-Ethyl perfluorooctane sulfonamide ethanol-based phosphate diester acid), FTCAs = Fluorotelomer carboxylic acids, FTUCAs = Fluorotelomer unsaturated carboxylic acids, diPAPs = Polyfluorinated dialkylated phosphate esters. FTSA = Fluorotelomer sulfonic acids].

Substance	Origin	Substance	Origin
PFCAs		PASF-based PFAS	
PFBA	Wellington Laboratories	PFOSA	Wellington Laboratories
PFPeA	Wellington Laboratories	<i>N</i> -EtFOSAA	Wellington Laboratories
PFHxA	Wellington Laboratories	diSAmPAP	Wellington Laboratories
PFHpA	Wellington Laboratories	FTCAs	
PFOA	Wellington Laboratories	6:2 FTCA	Wellington Laboratories
PFNA	Wellington Laboratories	8:2 FTCA	Wellington Laboratories
PFDA	Wellington Laboratories	5:3 FTCA	Wellington Laboratories
PFSAs		7:3 FTCA	Wellington Laboratories
PFBS	Wellington Laboratories	FTUCAs	
PFPeS	Wellington Laboratories	6:2 FTUCA	Wellington Laboratories
PFHxS	Wellington Laboratories	8:2 FTUCA	Wellington Laboratories
PFHpS	Wellington Laboratories	diPAPs	
PFOS	Wellington Laboratories	6:2 diPAP	Toronto Research Chemicals
FTSAs		8:2 diPAP	Wellington Laboratories
6:2 FTSA	Wellington Laboratories		
8:2 FTSA	Wellington Laboratories		

The paper samples P1 and P2 were provided by the Fraunhofer Institute as described elsewhere.¹ An in-depth characterization of PFAA-precursors in these samples was performed previously.^{1,2} The fabric sample was ordered from online from a textile shop and was chosen due to its description to be water-repellent. The standard soil SP2.4 was purchased from LUFA Speyer. Zonyl RP paper fluoridizer (DuPont), and Cartafluor CFI (Clariant) were provided by the Technologiezentrum Wasser (TZW, Karlsruhe).

S2 Compound analysis

HPLC-QqQ-MS:

For target analyte separation a Waters Acquity BEH C₁₈ column (2.1 mm × 100 mm, particle size 1.7 μm) with a flow rate of 0.4 mL/min (T = 60 °C) was used with solvent A: 95/5 H₂O/MeOH + 2 mM NH₄Ac and solvent B: 95/5 MeOH/H₂O + 2 mM NH₄Ac. A gradient elution program was used (for details see Table S2). Electrospray ionization was operated in negative mode and every analyte was measured with two mass transitions [except for perfluorobutanoic acid (PFBA), perfluorooctane sulfonamide (PFOSA)] for which only one product ion was used (for details see Table S3; instrument parameter in Table S4). The injection volume was 5 μL for all samples.

HPLC-QTOF-MS:

For NTS, compounds were separated with a Poroshell 120 EC-C₁₈ column (2.1 mm × 100 mm, particle size 2.7 μm) at a flow rate of 0.3 mL/min (Oven temperature = 40 °C). A 23 min gradient program (identical solvents as for target analysis) was applied and the ESI source was operated in the negative mode and selected samples were also measured with ESI⁺ (Table S2 and S4 for details). Data acquisition started at 1 min with a prior waste line [3 scans/s in the MS (m/z 100 – 1700) and MS/MS range (m/z 70 – 1700)]. The threshold for precursor selection was set to 1000 counts with narrow isolation width (≈ 1.3 m/z) and a mass dependent CE was used for MS/MS experiments ($CE(m/z) = 4 \frac{m/z}{100} + 15$ eV). In case of iterative ddMS² a rolling exclusion list was automatically generated during two sample injections to exclude masses at a certain RT window which were already selected for MS/MS experiments during the first injection. Furthermore, a static exclusion list (generated from MeOH blank injections) was used to exclude persistent background signals originating from the analytical system over the complete RT-range. The injection volume was 2 to 5 μL with a prior needle wash in isopropanol.

GC-QTOF-MS:

Non-target screening for volatile PFAS was performed with an Agilent 7890B GC equipped with an Agilent HP-5MS UI column (30 m × 0.25 mm, 0.25 μm film) coupled to the 6550 QTOF via an atmospheric pressure chemical ionization (APCI) interface. The GC temperature program started at 50 °C for 1 min followed by an increase to 250 °C at a rate of 40 °C/min. The final temperature was kept constant till minute 21. The APCI source parameters can be found in Table S5. With the help of our HPLC system a constant flow of 0.1 mL/min of water (column oven at 75 °C) into the APCI source was achieved to keep the humidity high, which increases the ionization efficiency.^{3, 4} The corona current was turned on after 2.5 min to prevent the solvent peak entering the QTOF. Due to the sharp nature of GC peaks 10 spectra/s were acquired to guarantee enough data point over a chromatographic peak. m/z-Ranges were similar as during HPLC-QTOF analysis. The background mass 257.2475 was used as a reference mass in the QTOF. The injection volume (MeOH extracts) was 1 μL with pulsed splitless injection.

Table S 2: Gradient elution of the HPLC-QTOF and the HPLC-QqQ method. A = 95/5 H₂O/MeOH + 2 mM NH₄Ac and B = 95/5 MeOH/H₂O + 2 mM NH₄Ac.

6550 QTOF			6490 QqQ		
Time (min)	A (%)	B (%)	Time (min)	A (%)	B (%)
0	85	15	0	60	40
2.0	30	70	1.0	40	60
5.0	10	90	3.5	0	100
10.0	0	100	6.0	0	100
15.0	0	100	6.1	60	40
15.1	85	15	8.0	60	40
22.0	85	15			

Table S 3: MRM parameters for the target compounds used with the Agilent 6490 QqQ: precursor and corresponding product ion with the respective collision energy (CE setpoint in eV) and fragmentor voltage (FV). The dwell time used during MRM was 15 ms.

Compound name	Precursor ion	Product ion	FV (V)	CE (eV)
6:2 diPAP	789	443	380	30
6:2 diPAP	789	97	380	30
8:2 diPAP	989	543	380	40
8:2 diPAP	989	97	380	30
6:2 FTCA	377	292.7	380	20
6:2 FTCA	377	63	380	5
8:2 FTCA	477	392.9	380	15
8:2 FTCA	477	63.2	380	5
5:3 FTCA	341	236.9	380	10
5:3 FTCA	341	216.8	380	25
6:2 FTUCA	357	293	380	10
6:2 FTUCA	357	243	380	40
8:2 FTUCA	457	393	380	10
8:2 FTUCA	457	343	380	50
6:2 FTSA	427	406.7	380	20
6:2 FTSA	427	81.2	380	55
8:2 FTSA	527	506.7	380	20
8:2 FTSA	527	81.2	380	55
<i>N</i> -EtFOSAA	584	526	380	25
<i>N</i> -EtFOSAA	584	418.7	380	25
PFOSA	497.9	77.9	380	40
PFDA	512.9	468.8	380	10
PFDA	512.9	268.9	380	15
PFNA	462.9	418.8	380	5
PFNA	462.9	218.8	380	15
PFOA	412.9	368.7	380	5
PFOA	412.9	168.7	380	20
PFHpA	362.8	318.8	380	5
PFHpA	362.8	168.7	380	15
PFHxA	312.9	268.9	380	5
PFHxA	312.9	119	380	25
PFPeA	262.9	219	380	5
PFPeA	262.9	68.8	380	45
PFBA	212.9	168.8	380	5
PFOS	499	99	380	50
PFOS	499	79.7	380	55
PFHpS	449	98.9	380	44
PFHpS	449	79.7	380	52
PFHxS	398.8	98.9	380	45
PFHxS	398.8	79.9	380	45
PFPeS	349	98.9	380	40
PFPeS	349	79.7	380	40
PFBS	298.9	98.9	380	30
PFBS	298.9	79.8	380	40

Table S 4: Summary of instrument and scan source parameters used for HPLC-QTOF- and HPLC-QqQ-MS measurements.

	6490 QqQ	6550 QTOF
Instrument Parameters		
Gas Temp (°C)	150	150
Gas Flow (L/min)	16	16
Nebulizer pressure (psig)	45	35
Sheath gas temperature (°C)	380	380
Sheath gas flow (L/min)	12	12
Fragmentor voltage (V)	380	380
Scan Source Parameter		
Capillary voltage (V)	3000	3000
Nozzle voltage (V)	0	300

Table S 5: Summary APCI and QTOF parameters used for GC-QTOF measurements.

APCI/QTOF Parameter	Value
Gas Temp (°C)	270
Drying gas (L/min)	11
Fragmentor voltage (V)	150
Capillary voltage (V)	1000
Corona current (μA)	1

HPLC-UV:

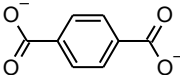
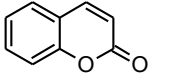
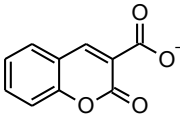
Separation of the $\cdot\text{OH}$ -probes was achieved which a Phenomenex column (150 mm \times 3 mm, particle size 4 μm , Synergi 4n polar RP 80 Å, T = 40 °C) with a flow rate of 0.5 mL/min. A 20 min isocratic method with eluent A (90/10 H₂O/MeOH + FA, pH 3) and B (MeOH) (80/20) was used. If only TPA was used the method run time was reduced to 8 min.

Three different $\cdot\text{OH}$ -probes were used to estimate the steady-state $\cdot\text{OH}$ concentration ($[\cdot\text{OH}]_{\text{ss}}$) and monitor effects of different parameters (e.g. pH, matrix concentration) on the oxidation conditions [terephthalic acid (TPA), coumarin (COU), and coumarin carboxylic acid (CCA)]. All $\cdot\text{OH}$ -probes were shown to react selectively with $\cdot\text{OH}$ during photocatalysis.^{5, 6} $[\cdot\text{OH}]_{\text{ss}}$ (mol/L) was calculated according to equation 1:

$$[\cdot\text{OH}]_{\text{ss}} = \frac{k_{\text{obs, probe}}}{k_{\cdot\text{OH, probe}}} \quad (1)$$

in which $k_{\text{obs,probe}}$ is the pseudo-first order rate constant (s^{-1}) and $k_{\text{OH,probe}}^{\bullet}$ is the bimolecular reaction constant ($\text{M}^{-1}\text{s}^{-1}$) of the respective probe with $\bullet\text{OH}$. $k_{\text{obs,probe}}$ was determined by fitting the normalized logarithmic UV-response over time (Figure S5).

Table S 6: $\bullet\text{OH}$ -probes used to estimate $[\bullet\text{OH}]_{\text{ss}}$ and their respective wavelengths used in HPLC-UV detection.

$\bullet\text{OH}$ -probe	Structure	Wavelength λ (nm)
Terephthalic acid (TPA)		245
Coumarin (COU)		277
Coumarin-3-carboxylic acid (CCA)		296

Dissolved organic carbon (DOC):

The centrifuged soil extract (LUFA SP2.4, 50 g/L) was filtered through a 0.45 μm mixed cellulose ester filter and analyzed with a TOC analyzer (Elementar HighTOC). Organic carbon is combusted to CO_2 which is detected by an infrared detector.

S3 Supporting experiments

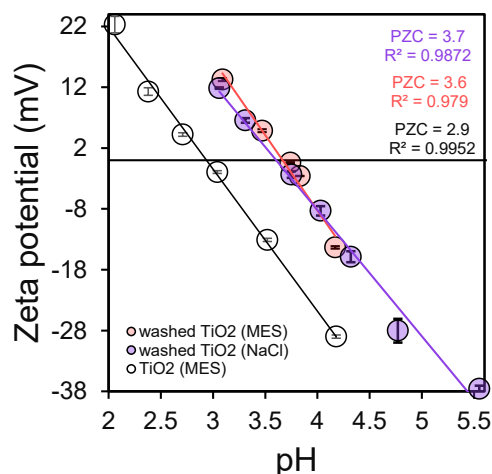


Figure S 1: Point of zero charge (PZC) of the original anatase TiO₂ and washed anatase TiO₂. The PZC was determined with a Zetasizer Nano ZSP (Malvern Pananalytical, Malvern, United Kingdom) with a folded capillary zeta cell (25 °C). Suspensions of 100 mg/L TiO₂ anatase were measured in 7 mM MES buffer and 10 mM NaCl solutions (triplicates) and the pH was adjusted with 0.1–1 M HCl and NaOH. A refractive index of 2.5 for TiO₂ anatase was used.

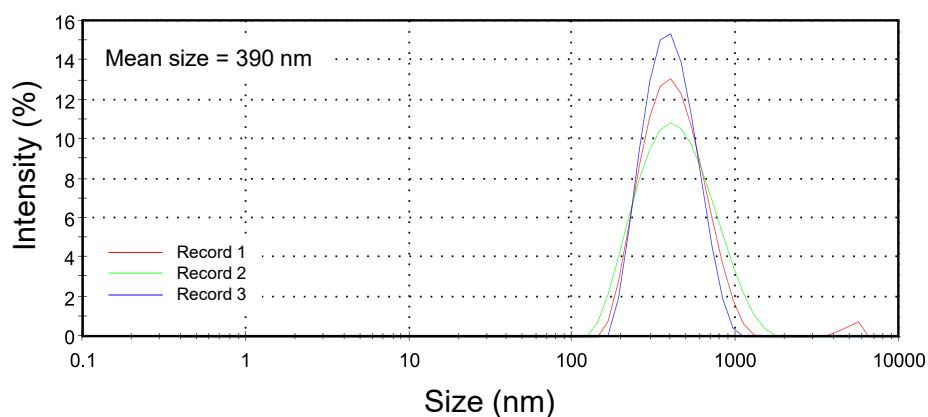


Figure S 2: Particle size distribution and mean particle size of the used anatase TiO₂. Measurements were performed on the Zetasizer Nano ZSP (see also Figure S1).

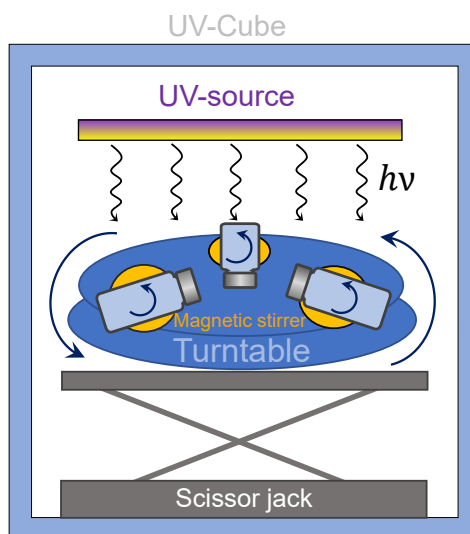


Figure S 3: UV/TiO₂ oxidation setup inside the UVA-CUBE to guarantee uniform and reproducible irradiation of multiple samples. Distance to the lamp was approximately 15 cm.

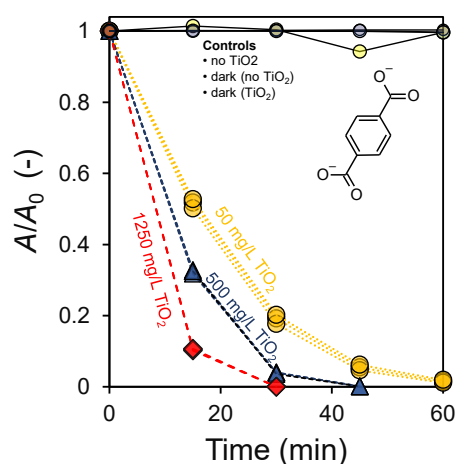


Figure S 4: TPA degradation dependent on the amount of TiO_2 . Note how reproducible triplicate experiments are due to rotating vials which are stirred at the same time. For this pre-experiment a 500 W lamp was used.

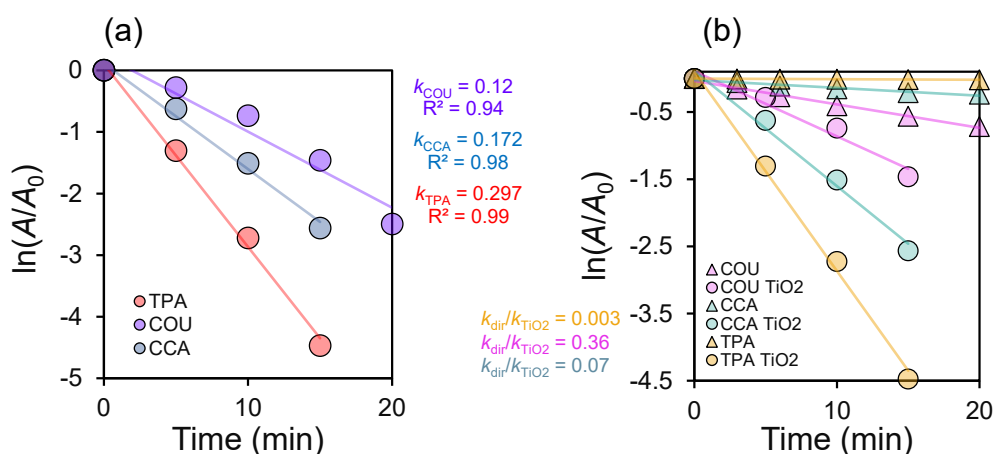


Figure S 5: Pseudo first-order degradation of the $\cdot\text{OH}$ -probes and direct vs. indirect photolysis. (a) Pseudo first-order degradation of terephthalic acid (TPA), coumarin (COU), and coumarin-3-carboxylic acid in the typical UV- TiO_2 setup. Steady state $\cdot\text{OH}$ -radical concentrations ($[\cdot\text{OH}]_{\text{ss}}$) were calculated based on the bimolecular reaction rate constants of each $\cdot\text{OH}$ -probe.^{5,7} TPA: $[\cdot\text{OH}]_{\text{ss}} = 1.1 \times 10^{-12}$ M, COU: $[\cdot\text{OH}]_{\text{ss}} = 1.5 \times 10^{-12}$ M, CCA: $[\cdot\text{OH}]_{\text{ss}} = 1.1 \times 10^{-11}$ M. (b) Direct vs. indirect rate constants for all three $\cdot\text{OH}$ -probes, showing that in case of COU a fraction of $> 30\%$ was degraded via direct irradiation. Note that in the TiO_2 -suspension the turbidity is high leading to a probably much smaller fraction of direct photolysis.

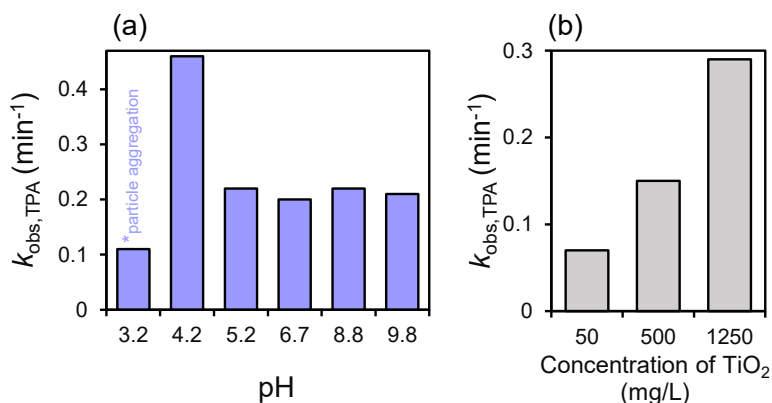


Figure S 6: Dependency of $k_{\text{obs,TPA}}$ on pH and TiO_2 concentration. (a) pH dependency of $k_{\text{obs,TPA}}$ with 500 mg/L TiO_2 . The pH was adjusted with H_3PO_4 and NaOH to keep quenching or further radical processes as small as possible. Overall $[\cdot\text{OH}]_{\text{ss}}$ was not strongly dependent on pH, while the maximum was at pH 4.2. However, this was likely due to the fact that at this pH a higher fraction of TPA is uncharged which decreases its water solubility while increasing sorption to TiO_2 . At pH 3.2 the TiO_2 particles aggregated and formed an unstable suspension. (b) Dependency $k_{\text{obs,TPA}}$ on TiO_2 concentration. For these pre-experiments a 500 W lamp was used.

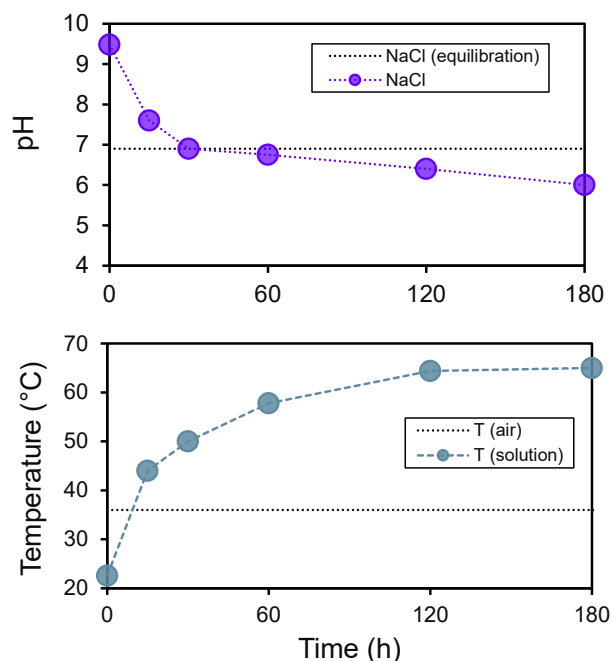


Figure S 7: Temperature and pH change over time in the UV-chamber measured in NaCl solutions of LC-MS grade water. NaCl equilibrium refers to a reference solution of LC-MS grade water which was measured with an equilibration time of 1 h of the pH electrode. Note that for all experiment only pure LC-MS grade without any other ingredient was used (pH between 6 and 8) and the high initial pH likely arose from measurement errors of the pH electrode.

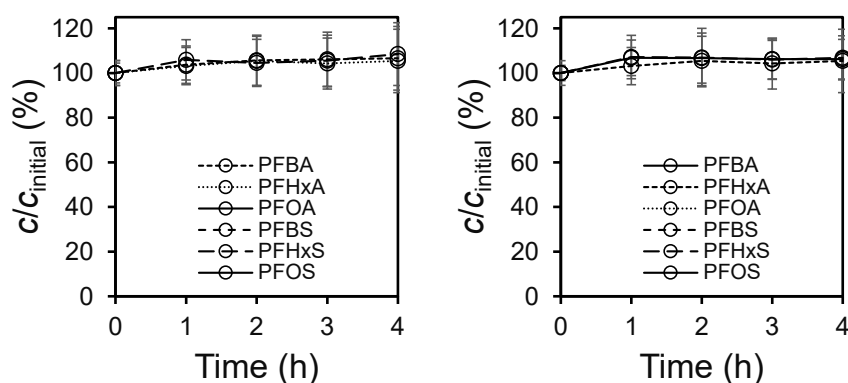


Figure S 8: Two control experiments of different PFAAs (PFBA, PFHxA, PFOA, PFBS, PFHxS, and PFOS) in the typical UV/TiO₂ oxidation setup (10 mg TiO₂, $c_0 = 100 \mu\text{g/L}$). Error bars correspond to two standard deviations of duplicate samples.

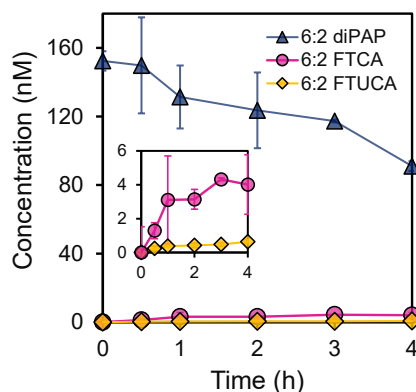


Figure S 9: Dark control without irradiation. Experiment with the precursor 6:2 diPAP + TiO₂ without irradiation. Approximately 40% of the initial 6:2 diPAP amount disappeared (also in the extract), however, no PFCA formation was observed only very low concentrations of 6:2 FTCA and 6:2 FTUCA. Presumably dark reactions or hydrolysis at this temperature led to e.g. 6:2 FTOH and 6:2 monoPAP or other products.

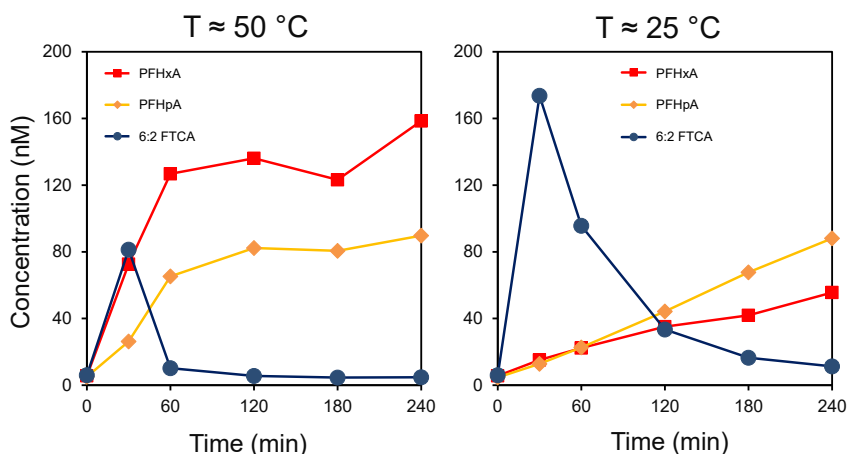


Figure S 10: Changes of degradation kinetics with changing temperature during UV/TiO₂ oxidation (precursor 6:2 diPAP). Note how the fraction of PFCA end products changed: Higher temperature led to a higher fraction of chain shortening leading to PFHxA as main end product at 50 °C vs. PFHpA at 25 °C.

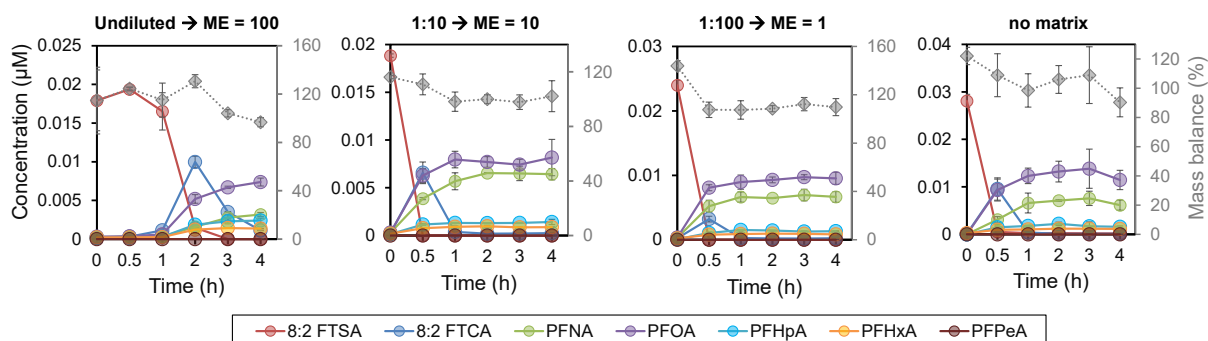


Figure S 11: Influence of matrix on the oxidation of 8:2 FTSA in the UV/TiO₂ system. 50 g/L of soil was extracted (overhead shaker for 6 h and 1 h ultrasound in water) and the oxidation was performed in the undiluted extract (100), twice diluted 1:10 and in matrix free water (0). Error bars correspond to two standard deviations of duplicate samples.

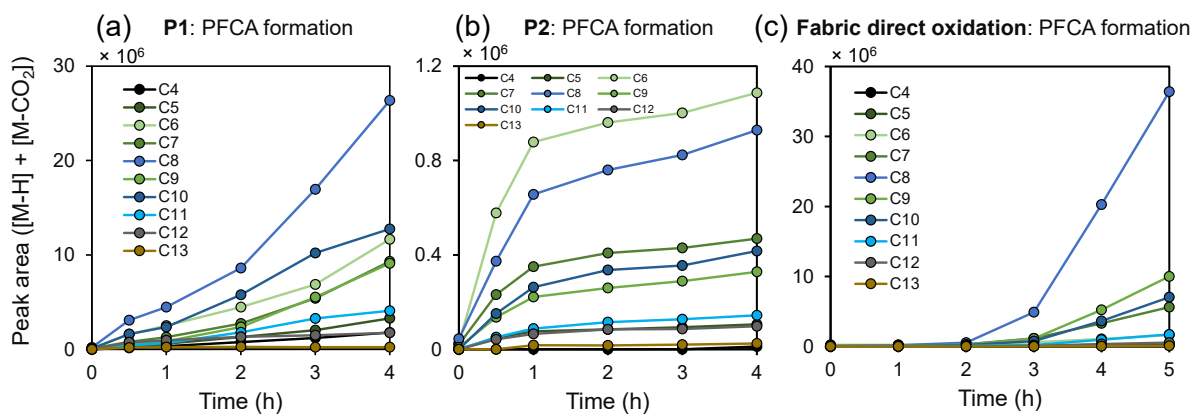


Figure S 12: Formation of PFCAs from oxidation of paper extract P1 and P2 (a & b), and direct oxidation of fabric stripes (c). Note that the amount of extract used for oxidation of P1 and P2 was different by two orders of magnitude.

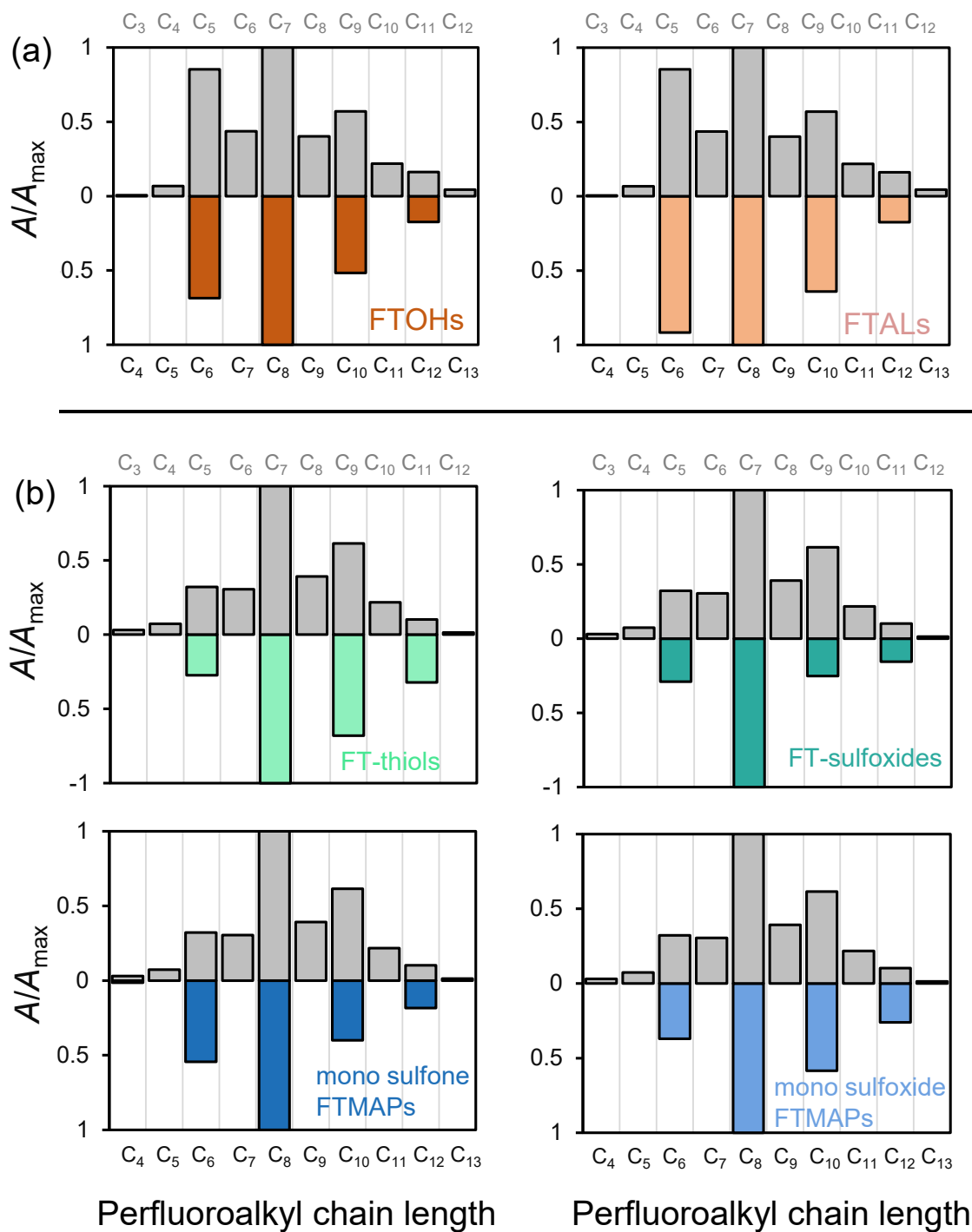


Figure S 13: Volatile and newly identified precursor chain-length distribution vs. PFCAs-distribution after PhotoTOP. Relative signal intensities normalized to the maximum peak area of precursors in (a) paper P2 and (b) paper P1 before oxidation (negative y-axis) vs. relative signal intensities of PFCAs after 4 h of UV/TiO₂ oxidation (positive y-axis). Note that e.g. a perfluoroalkyl chain length of C_7 corresponds to PFOA. For more information on newly identified compounds (GC and LC) see section S4 and Figure S17-21. Note that for some precursors even longer chains than C_{12} were detected in low abundances (e.g. up to C_{18} FTOH).

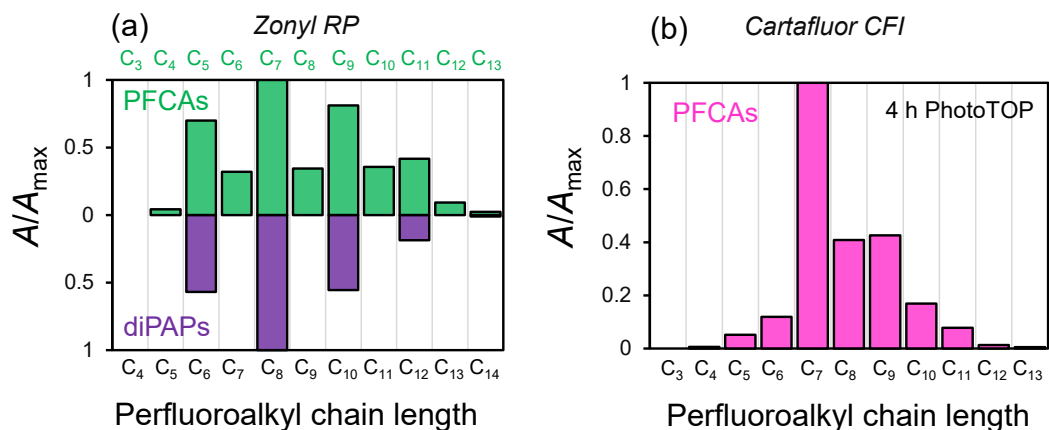


Figure S 14: PhotoTOP with technical PFAS mixtures. (a) PhotoTOP with Zonyl RP (1 μ L spiked) and (b) with Cartafluor CFI (1 μ L spiked). Note that the samples were diluted 1:10 due to high concentrations of PFCAs. In case of Cartafluor CFI the initial precursor cannot be determined. Note the similarity of the chain length distribution of PFCAs after PhotoTOP with the fabric sample (Figure 6).

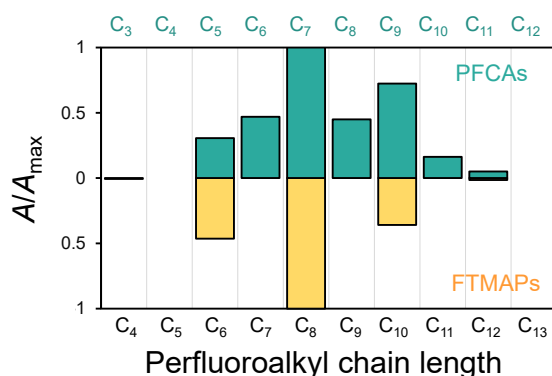


Figure S 15: Direct oxidation of paper P1. Relative signal intensities normalized to the maximum peak area of the precursors FTMAPs in paper extract P1 before oxidation (negative y-axis) vs. normalized signal intensities of PFCAs after 4 h of direct oxidation of paper stripes (positive y-axis). Note that e.g. a perfluoroalkyl chain length of C₇ corresponds to PFOA.

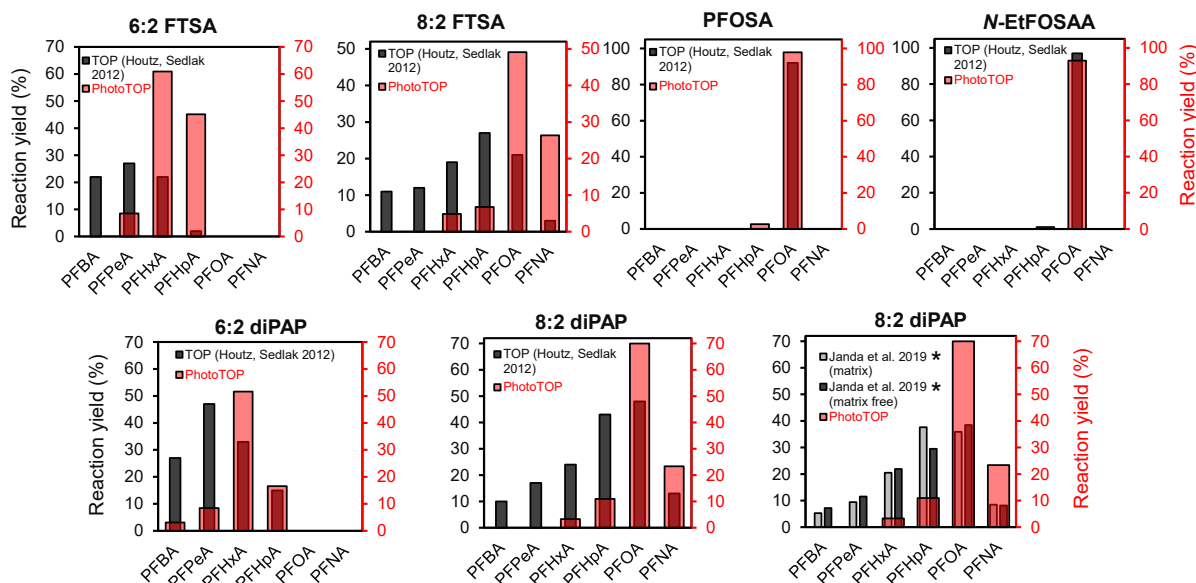


Figure S 16: Comparison of the reaction yields from several precursors between PhotoTOP and the original TOP assay. Data originates from Houtz and Sedlak 2012 and Janda et al. 2019.^{8,9} In case of Janda et al. (marked by asterisk) the data points were collected with the MATLAB grabit tool (grabit.m, freely available online) from the respective Figure in the publication. Note how the PhotoTOP can maintain the precursor chain length (n-1) as the main oxidation product.

Table S 7: Summary of identifications in paper extract P1 and P2. Note that the confidence levels also consider experimental evidence. For chemical structures see Figure S17.

Sample	LC/GC	Compound name	Exact mass (Da)	Deviation (ppm)	RT (min)	Confidence level
P1						
	LC					
		4:2/6:2 FTMAP	820.9881	-0.34	11.1	2b
		6:2/6:2 FTMAP	920.9817	-0.86	12.1	1
		6:2/8:2 FTMAP	1020.9754	1.16	12.9	2b
		8:2/8:2 FTMAP	1120.9690	0.60	13.8	2b
		8:2/10:2 FTMAP	1220.9626	1.04	14.6	2b
		10:2/10:2 FTMAP	1320.9562	0.34	15.6	2b
		6:2 FTSA	426.9679	-0.24	7.1	1
		8:2 FTSA	526.9615	0.72	8.0	1
		10:2 FTSA	626.9551	-0.04	9.1	2b
		12:2 FTSA	726.9487	-0.05	10.3	2b
		14:2 FTSA	826.9423	0.78	11.6	2b
		4:2/6:2 FTMAP sulfoxide	836.9830	0.60	9.6	2b
		6:2/6:2 FTMAP sulfoxide	936.9767	0.84	10.6	2b
		6:2/8:2 FTMAP sulfoxide	1036.9703	0.84	11.6	2b
		8:2/8:2 FTMAP sulfoxide	1136.9639	1.20	12.5	2b
		8:2/10:2 FTMAP sulfoxide	1236.9575	0.61	13.3	2b
		10:2/10:2 FTMAP sulfoxide	1336.9511	0.71	14.2	2b
		10:2/12:2 FTMAP sulfoxide	1436.9447	-0.03	15.2	2b
		6:2/6:2 FTMAP disulfoxide/sulfone	952.9716	0.60	9.8	2b
		6:2/8:2 FTMAP disulfoxide/sulfone	1052.9652	0.25	10.9	2b
		8:2/8:2 FTMAP disulfoxide/sulfone	1152.9588	0.13	11.8	2b
		8:2/10:2 FTMAP disulfoxide/sulfone	1252.9524	0.19	12.8	2b
		10:2/10:2 FTMAP disulfoxide/sulfone	1352.9460	0.46	13.6	2b
		10:2/12:2 FTMAP disulfoxide/sulfone	1452.9396	-0.81	14.6	2b
		6:2 monoFTMAP sulfoxide	559.0019	0.31	7.6	2b
		8:2 monoFTMAP sulfoxide	658.9955	-0.96	8.6	2b
		10:2 monoFTMAP sulfoxide	758.9891	0.46	9.8	2b
		12:2 monoFTMAP sulfoxide	858.9827	-0.06	11.1	2b
		6:2 monoFTMAP sulfone	574.9968	0.10	6.9	3d
		8:2 monoFTMAP sulfone	674.9904	-0.22	7.8	3d
		10:2 monoFTMAP sulfone	774.9840	0.05	9.0	3d
		12:2 monoFTMAP sulfone	874.9776	0.20	10.2	3d
	GC					
		6:2 FT-thiol	380.9977	-4.23	3.1	2b
		8:2 FT-thiol	480.9913	-5.66	3.6	2b
		10:2 FT-thiol	580.9849	-4.36	4.1	2b
		12:2 FT-thiol	680.9785	-0.07	4.5	2b
		6:2 FT-sulfoxide	396.9926	0.43	4.2	2b
		8:2 FT-sulfoxide	496.9862	-2.09	4.6	2b
		10:2 FT-sulfoxide	596.9798	-0.75	5.0	2b
		12:2 FT-sulfoxide	696.9734	-0.80	5.3	2b
P2						
	LC					
		4:2/6:2 diPAP	688.9814	-0.34	9.1	2b
		6:2/6:2 diPAP	788.9750	0.06	10.1	1
		6:2/8:2 diPAP	888.9686	0.38	11.2	2b
		8:2/8:2 diPAP	988.9622	1.34	12.0	1
		8:2/10:2 diPAP	1088.9558	1.11	13.0	2b
		10:2/10:2 diPAP	1188.9494	0.67	13.8	2b
		10:2/12:2 diPAP	1288.9431	0.38	14.6	2b
		12:2/12:2 diPAP	1388.9367	0.05	15.8	2b
	GC					
		6:2 FTOH	365.0205	1.76	3.0	1
		8:2 FTOH	465.0141	4.80	3.5	2b
		10:2 FTOH	565.0077	3.93	3.9	2b
		12:2 FTOH	665.0013	-3.59	4.3	2b
		6:2 FTAL	363.0049	2.18	3.0	2b
		8:2 FTAL	462.9985	3.85	3.5	2b
		10:2 FTAL	562.9921	2.78	3.9	2b
		12:2 FTAL	662.9857	-5.49	4.3	2b

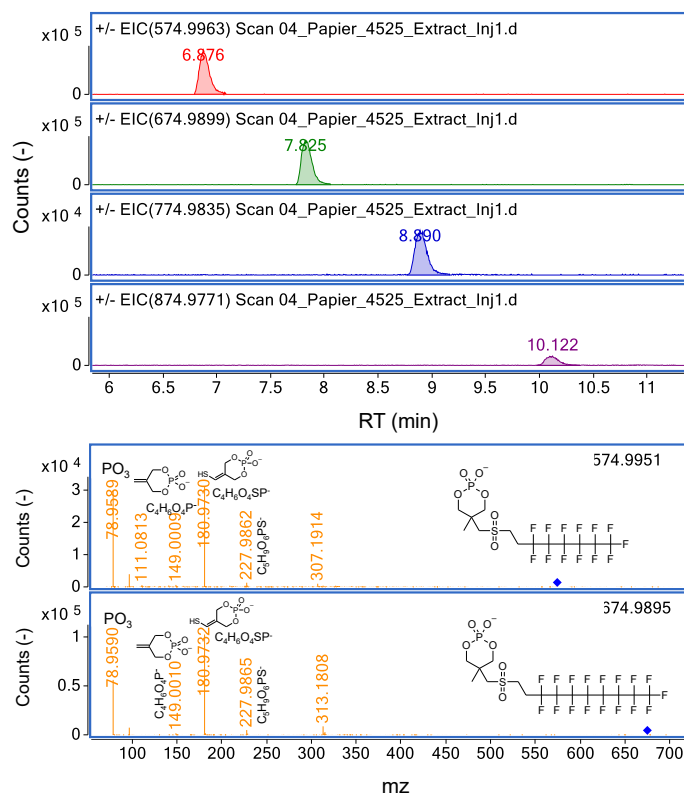


Figure S 18: Newly tentatively identified compounds in P1 (mono sulfone FTMAPs). Extracted ion chromatograms (EICs) of four tentatively identified FTMAP-related compounds in paper P1 and two respective MS/MS spectra acquired at a collision energy of 40 eV.

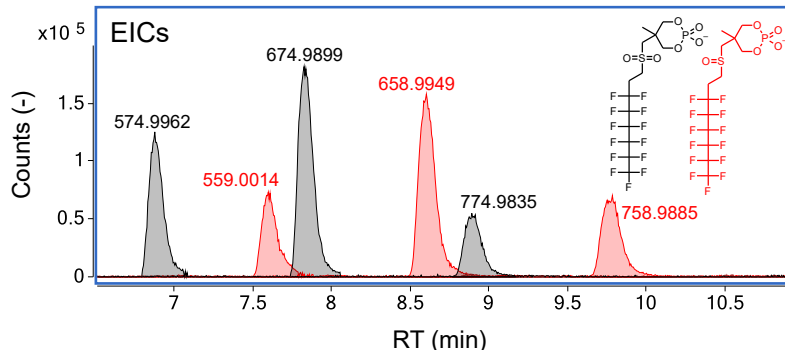


Figure S 19: EICs of the newly identified compounds in P1 (mono sulfoxide/sulfone FTMAPs). Compounds with a sulfone group were identified based on MS/MS (Note: the only 6:2 structures are shown). The related sulfoxide has no MS/MS evidence, however a characteristic RT shift from an expected lower polarity was observed and its homologous series distribution fits to the related compounds (e.g. FTMAPs etc.; see Figure 4 and S13).

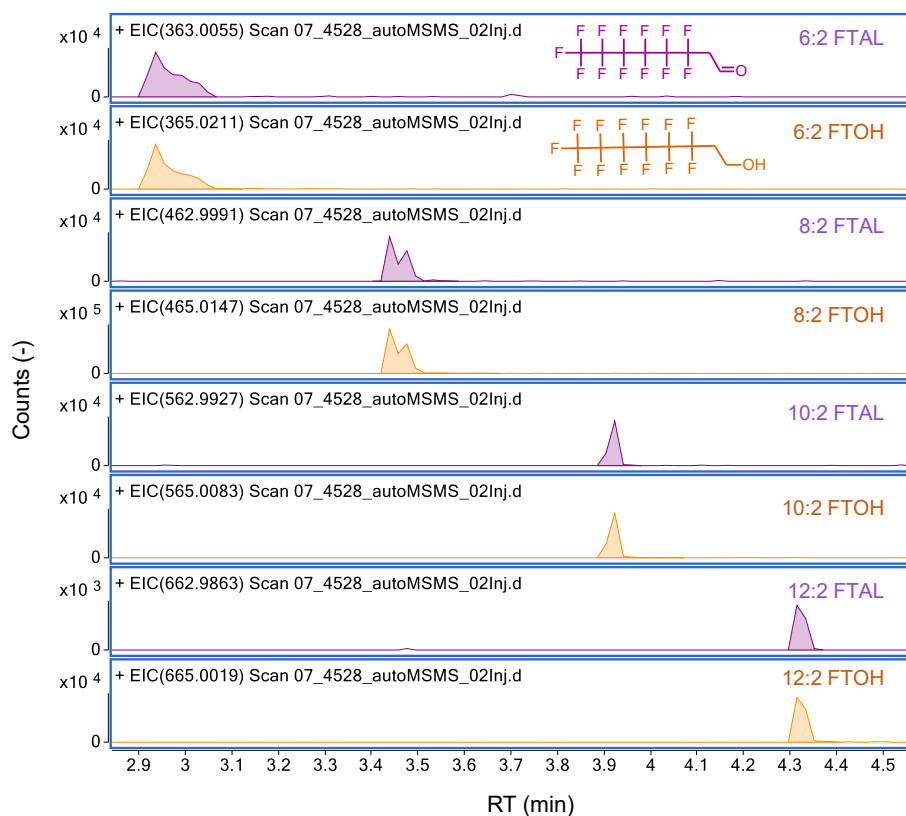


Figure S 20: EICs of FTOHs and FTALs measured by GC-APCI-QTOF in paper extract P2. Only 6:2 FTOH was verified with an authentic reference standard. Other compounds are identified based on their accurate mass and occurrence of homologues. Further evidence is provided by the level 1 identification of related diPAPs in paper P2 and their correlating chain-length distribution (e.g. Figure S13). Note that FTOHs up to C₁₈ were detected in low abundances.

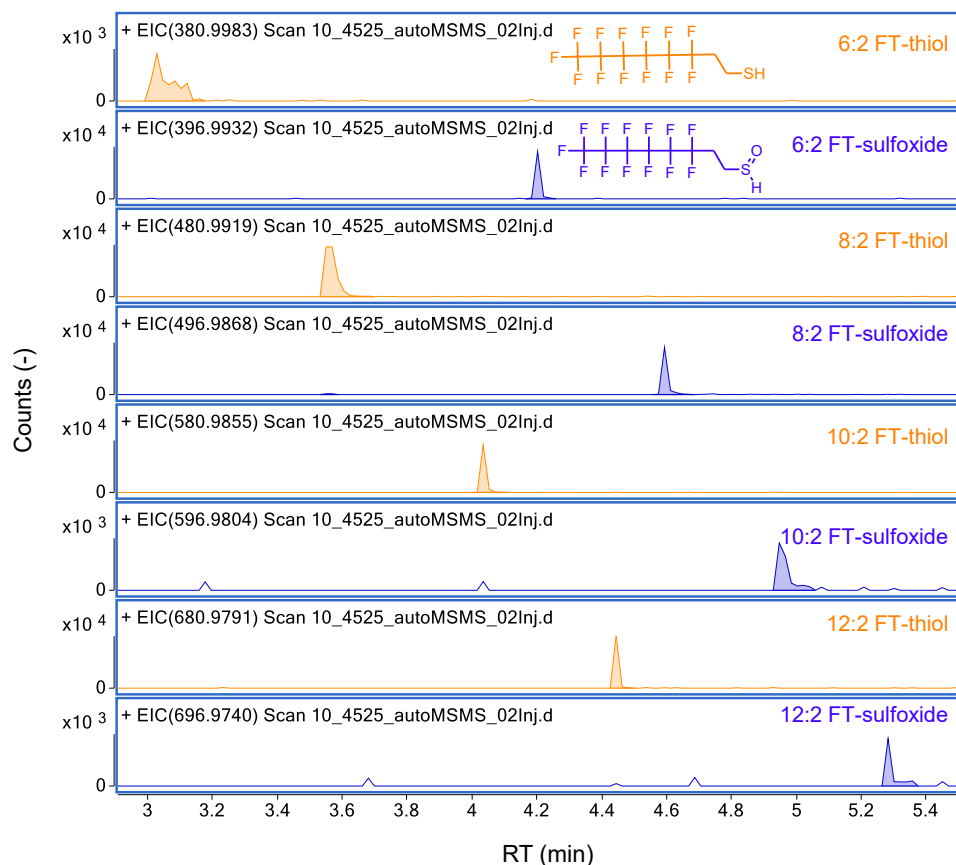


Figure S 21: EICs of FT-thiols and FT-sulfoxides measured by GC-APCI-QTOF in paper extract P1. Both classes are tentatively identified based on their accurate mass and occurrence of several homologues. Level 1 identification of related FTMAPs, other sulfur based PFAS provide, and their correlating chain length distribution provide further evidence (e.g. Figure S13).

References

1. Bugsel, B.; Bauer, R.; Herrmann, F.; Maier, M. E.; Zwiener, C., LC-HRMS screening of per- and polyfluorinated alkyl substances (PFAS) in impregnated paper samples and contaminated soils. *Anal Bioanal Chem* **2022**, *414*, (3), 1217-1225.
2. Zweigle, J.; Bugsel, B.; Zwiener, C., FindPFAS: Non-Target Screening for PFAS horizontal line Comprehensive Data Mining for MS2 Fragment Mass Differences. *Anal Chem* **2022**.
3. Portoles, T.; Mol, J. G.; Sancho, J. V.; Hernandez, F., Advantages of atmospheric pressure chemical ionization in gas chromatography tandem mass spectrometry: pyrethroid insecticides as a case study. *Anal Chem* **2012**, *84*, (22), 9802-10.
4. Rosch, A.; Beck, B.; Hollender, J.; Singer, H., Picogram per liter quantification of pyrethroid and organophosphate insecticides in surface waters: a result of large enrichment with liquid-liquid extraction and gas chromatography coupled to mass spectrometry using atmospheric pressure chemical ionization. *Anal Bioanal Chem* **2019**, *411*, (14), 3151-3164.
5. Zhang, J.; Nosaka, Y., Mechanism of the OH Radical Generation in Photocatalysis with TiO₂ of Different Crystalline Types. *The Journal of Physical Chemistry C* **2014**, *118*, (20), 10824-10832.
6. Hirakawa, T.; Yawata, K.; Nosaka, Y., Photocatalytic reactivity for O₂⁻ and OH radical formation in anatase and rutile TiO₂ suspension as the effect of H₂O₂ addition. *Applied Catalysis A: General* **2007**, *325*, (1), 105-111.
7. Page, S. E.; Arnold, W. A.; McNeill, K., Terephthalate as a probe for photochemically generated hydroxyl radical. *J Environ Monit* **2010**, *12*, (9), 1658-65.
8. Houtz, E. F.; Sedlak, D. L., Oxidative conversion as a means of detecting precursors to perfluoroalkyl acids in urban runoff. *Environ Sci Technol* **2012**, *46*, (17), 9342-9.
9. Janda, J.; Nodler, K.; Scheurer, M.; Happel, O.; Nurenberg, G.; Zwiener, C.; Lange, F. T., Closing the gap - inclusion of ultrashort-chain perfluoroalkyl carboxylic acids in the total oxidizable precursor (TOP) assay protocol. *Environ Sci Process Impacts* **2019**, *21*, (11), 1926-1935.
10. Charbonnet, J. A.; McDonough, C. A.; Xiao, F.; Schwichtenberg, T.; Cao, D.; Kaserzon, S.; Thomas, K. V.; Dewapriya, P.; Place, B. J.; Schymanski, E. L.; Field, J. A.; Helbling, D. E.; Higgins, C. P., Communicating Confidence of Per- and Polyfluoroalkyl Substance Identification via High-Resolution Mass Spectrometry. *Environ Sci Technol Lett* **2022**, *9*, (6), 473-481.

Appendix 7

Publication 7

Non-extractable PFAS in functional textiles – Characterization by complementary methods: oxidation, hydrolysis, and fluorine sum parameters

Jonathan Zweigle,⁺ Catharina Capitain,⁺ Fabian Simon,^{||} Philipp Roesch,[‡] Boris Bugsel,⁺ Christian
Zwiener,⁺

⁺Environmental Analytical Chemistry, Department of Geosciences, University of Tübingen,
Schnarrenbergstraße 94-96, 72076 Tübingen, Germany

^{||}Federal Institute for Materials Research and Testing (BAM), Division 1.1 – Inorganic Trace Analysis,
Richard-Willstätter-Straße 11, 12489 Berlin, Germany

[‡]Federal Institute for Materials Research and Testing (BAM), Division 4.3 - Contaminant Transfer and
Environmental Technologies, Unter den Eichen 87, 12205, Berlin, Germany

Published in: Environmental Science: Processes & Impacts, 25(8), 1298-1310.

DOI: 10.1039/D3EM00131H

Reprinted with permission from Environmental Science – Processes and Impacts: Zweigle, J., Capitain, C.,
Simon, F., Roesch, P., Bugsel, B., & Zwiener, C. (2023). Non-extractable PFAS in functional textiles -
characterization by complementary methods: oxidation, hydrolysis, and fluorine sum parameters. Environ
Sci Process Impacts, 25(8), 1298-1310. <https://doi.org/10.1039/d3em00131h>



Cite this: *Environ. Sci.: Processes
Impacts*, 2023, 25, 1298

Non-extractable PFAS in functional textiles – characterization by complementary methods: oxidation, hydrolysis, and fluorine sum parameters†

Jonathan Zweigle,^a Catharina Capitain,^a Fabian Simon,^b Philipp Roesch,^c
Boris Bugsel^a and Christian Zwiener^{a*}

Per- and polyfluoroalkyl substances (PFAS) are widely used for durable water-repellent finishing of different fabrics and textiles such as outdoor clothing, carpets, medical textiles and more. Existing PFAS extraction techniques followed by target analysis are often insufficient for detecting widely used side-chain fluorinated polymers (SFPs) that are barely or non-extractable. SFPs are typically copolymers consisting of a non-fluorinated backbone with perfluoroalkyl side-chains to obtain desired properties. We compared the accessible analytical information and performance of complementary techniques based on oxidation (dTOP and PhotoTOP assays), hydrolysis (THP assay), standard extraction, extractable organic fluorine (EOF), and total fluorine (TF) with five functional textiles and characterized 7 further textiles only by PhotoTOP oxidation. The results show that when applied directly to textile samples, dTOP and PhotoTOP oxidation and also hydrolysis (THP) are able to capture large fractions of TF in the form of perfluoroalkyl side-chains present in the textiles while methods relying on extracts (EOF, target and non-target analysis) yield much lower fractions of TF (e.g., factor ~25–50 lower). The conversion of large fractions of the measured TF into PFCAs or FTOHs from fluorinated side chains is in contrast to previous studies. Concentrations ranged from <LOQ to over ~1000 mg F kg⁻¹ after oxidation/hydrolysis and <LOQ to over 2000 mg F kg⁻¹ for TF, while EOF and target PFAS in extracts were detected at much lower concentrations (up to ~60 mg F kg⁻¹) (amount of fluorine is in the order: extraction ≪ EOF ≪ oxidation/hydrolysis ≅ TF). Perfluoroalkyl carboxylic acids (PFCAs) and fluorotelomer alcohols (FTOHs) from THP hydrolysis and PhotoTOP oxidation both represented chain-length distribution in the textiles showing that long-chain SFPs are still used in current textiles. Further advantages and disadvantages of the applied methods are discussed.

Received 5th April 2023
Accepted 12th July 2023

DOI: 10.1039/d3em00131h

rsc.li/espi

Environmental significance

In comparison to other per- and polyfluoroalkyl substances (PFAS), side-chain fluorinated polymers (SFPs) are a group of less studied PFAS that are widely used for textile coatings. While these polymers are potentially non-hazardous for humans during their use phase, they have been shown to emit perfluoroalkyl acids (PFAAs) through abrasion and sunlight exposure and eventually at the end of their life-cycle where they can act as a long-term source of persistent and mobile or bioaccumulative chemicals. Methods besides extraction are therefore of high relevance to capture perfluoroalkyl side-chains directly in products to be able to assess their potential contribution to volatile (fluorotelomer alcohols) and ionic PFAS (PFAAs) both indoors and in the environment.

Introduction

Per- and polyfluoroalkyl substances (PFAS) are a large and complex class of anthropogenic chemicals with countless applications in industry and consumer products.^{1–3} Due to their intrinsic properties that include for instance high stability and non-stick characteristics, currently a huge number of products and processes rely on their use.^{4,5} Those properties, however, also cause negative side-effects such as environmental persistence, adverse effects on human health and either high mobility in the case of short chain or bioaccumulation for long-chain PFAS.⁶ Furthermore, degradable PFAS eventually transform into persistent end-products such

^aEnvironmental Analytical Chemistry, Department of Geosciences, University of Tübingen, Schnarrenbergstraße 94–96, 72076 Tübingen, Germany. E-mail: christian.zwiener@uni-tuebingen.de

^bFederal Institute for Materials Research and Testing (BAM), Division 1.1 – Inorganic Trace Analysis, Richard-Willstätter-Straße 11, 12489 Berlin, Germany

^cFederal Institute for Materials Research and Testing (BAM), Division 4.3 – Contaminant Transfer and Environmental Technologies, Unter den Eichen 87, 12205, Berlin, Germany

† Electronic supplementary information (ESI) available. See DOI: <https://doi.org/10.1039/d3em00131h>

as perfluoroalkyl acids (PFAAs) which were used in the past but certain long-chain PFAAs (*e.g.*, PFOS and PFOA) are largely regulated globally.⁷ Due to the extensive use, PFAS were detected in all environmental media, including water,^{8,9} biota,^{10,11} air,^{12,13} indoor environments,¹⁴ and globally in rainwater.¹⁵

While monomeric target PFAS such as PFAAs, selected PFAA precursors and also volatile PFAS such as fluorotelomer alcohols (FTOHs) can be (partially) extracted from most matrices and are therefore more or less routinely analyzed by liquid- or gas chromatography coupled to mass spectrometry, polymeric PFAS cannot be directly detected by this technique since they are often not extractable or ionizable.^{16,17} Besides polymers such as Teflon (polytetrafluoroethylene, PTFE) which is considered to be rather safe with respect to direct PFAS exposure during its use (but not production), there are other PFAS copolymers that are prone to release PFAAs or FTOHs due to degradation processes which are therefore considered PFAS precursors.^{18–22} Those side-chain fluorinated copolymers (SFPs) are characterized by a hydrocarbon polymer backbone which is equipped with poly- or perfluoroalkyl side-chains (schematic representation in Fig. 1).²³ Due to covalent bonding to the non-fluorinated polymer they are more durable than monomers during use. Different materials such as textiles or textile fibers can be finished with different SFP formulations that are part of the group of durable water-repellent (DWR) coatings. These are based on a very wide range of different chemistries, both with or without fluorine.^{23,24} Fluorinated DWR coatings are used *e.g.*, in outdoor and medical textiles but also for carpets and many more diverse applications.^{23,24}

Since SFPs were shown to be PFAA precursors that lead to the release of different PFAS (volatile, mobile, or bioaccumulative depending on the chain length and functional group) either directly or *via* microplastic fibers, it is important to be able to quantify or at least estimate the amount and length of the perfluoroalkyl side-chains in finished products. Comprehensive methods that do not rely on extraction (of barely extractable SFPs), are typically sum parameters such as total fluorine which can be determined *via* different techniques such as particle-induced gamma-ray emission (PIGE) spectroscopy or by combustion ion-chromatography (CIC).^{25,26} Other approaches based on X-ray photoelectron spectroscopy (XPS) are able to quantify the atomic percentage of fluorine directly on product surfaces.¹⁶ While those methods are useful in a quantitative manner, they are associated with the loss of information on the identity of PFAS when used exclusively. Structural information such as chain-length distribution of an SFP within a product cannot be obtained. However, methods relying on oxidation such as the direct total oxidizable precursor (dTOP) assay, the recently developed PhotoTOP assay, and the total hydrolysable precursor (THP) assay can be used directly on products such as textiles.^{17,27–29} Target oxidation products (PFAAs or FTOHs) can be quantified with routine methods and information on chain-length distribution can be combined with results from fluorine sum parameters to characterize SFPs in a quantitative manner regarding their total or extractable fluorine content. Most studies concentrated the characterization of PFAA precursors in textiles only on extraction and further oxidation of extracts *via* the TOP assay and there is only a very limited application of those conversion methods directly to the coated textile

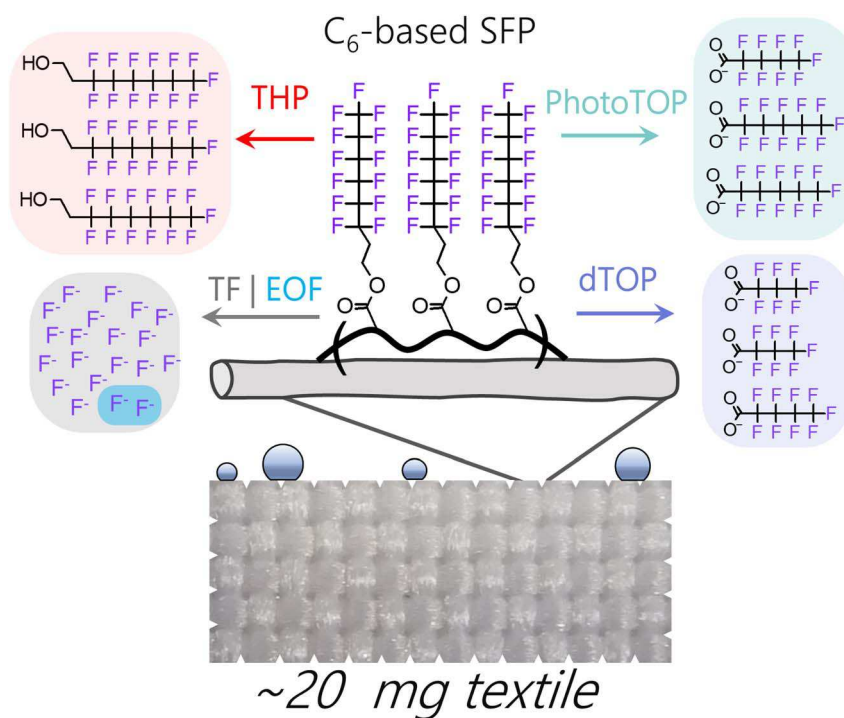


Fig. 1 Schematic illustration of a textile containing an acrylate C₆-based side-chain fluorinated polymer (SFP) and the respective end products of dTOP, PhotoTOP, and total hydrolysable precursor (THP) assay and EOF and TF analyses.

itself.^{17,18,28,29} Therefore, we used five functional textiles to investigate the advantages of direct chemical treatment *via* the dTOP, PhotoTOP, and THP for the characterization of SFPs in textiles and compared those results with those of methods relying on extraction [target and non-target analysis and extractable organic fluorine (EOF) analysis] and TF measurements. Our study aims to verify how techniques relying on oxidation and hydrolysis (directly applied on the textiles) perform in comparison to sum parameters such as EOF and TF and whether a quantitative conversion of fluorinated side chains (into PFCAs or FTOHs) is possible by comparing fluorine in C_nF_{2n+1} -chains of target analytes with TF. Of special importance is the highlighting of techniques that can be directly applied to the textiles (PhotoTOP, dTOP, THP, and TF) by comparison with methods relying on extraction (analysis of PFAS in extracts or EOF). To this end, we characterized seven further functional textiles by only extraction and direct PhotoTOP oxidation and discuss the occurrence and types of characterized SFPs.

Materials and methods

Chemicals and reagents

The origin and specifications of all used chemicals are given in the ESI (Section S1†).

Textile collection and prioritization using the contact angle θ

Different functional textile samples were ordered from two German textile online shops (stoff4you.de and efabrics.de), chosen based on their descriptions to be water repellent. When possible, colorless textiles were purchased to avoid potential interference with dyes. For contact angle measurements, photos of 20 μ L water and sunflower oil drops were taken on \sim 1 cm textile strips (both sides) using a Canon EOS 1200D digital single-lens reflex camera with a background light source (examples in Fig. S1†). Contact angles θ were determined with the contact angle plugin of ImageJ (<https://imagej.nih.gov/ij/index.html>) with at least five points using the manual point procedure. Clearly oil wetting textiles were excluded from analysis since they typically do not contain fluorinated DWR finishing. 12 final textiles were chosen due to their low water and/or oil contact angles including textiles with a higher contact angle for reference.

Textile extraction

To extract potential PFAS from the textiles, samples were cut into pieces of 4 cm² with pre-rinsed scissors (isopropanol), weighed in 15 mL centrifuge tubes and covered with 5 mL MeOH followed by sonication for 1 h. Afterwards, samples were placed on a horizontal shaker for \sim 21 h and sonicated for an additional hour. In the next step, 1 mL aliquots were taken (triplicate), centrifuged for 10 min @ 20 817 relative centrifugal forces (rcf) and 800 μ L of supernatant was transferred into HPLC vials and stored at 5 °C until analysis or further processing. An extraction blank was processed identically to consider background contamination during the extraction

process. For extraction recovery tests see section Quality control.

PhotoTOP oxidation

For the application of the previously developed PhotoTOP²⁸ (12 samples, selected extracts, and blank), 20 mg of thin textile strips (\sim 1 mm; pre-rinsed scissors) were weighed into 20 mL EPA screw (Pyrex) glass vials and combined with 20 mg TiO₂, 23 mL of pre-heated water (\sim 50 °C) and a magnetic stir bar. In the case of extract oxidation, 700 μ L extract was spiked onto TiO₂ and evaporated overnight. After thorough mixing and 5 min sonication, the vials were placed in a UVA Cube 400 [Hönle UV Technology; 1200 W lamp (SOL 1200 RF2); for setup details see Zweigle *et al.* 2022]²⁸ and irradiated for 5 h (selected textiles up to 10 h). For PFAS quantification and non-target screening, 100 μ L samples were taken and diluted with 900 μ L MeOH followed by centrifugation (30 min @ 20 817 rcf). Subsequently, 600 μ L of supernatant was transferred into HPLC vials for analysis.

Direct TOP (dTOP) oxidation assay

A modified direct TOP assay from Liagkouridis *et al.* 2021 was applied to four textiles, one textile extract, and a blank.¹⁷ Briefly, 20 mg of textile was placed in a 60 mL EPA glass screw vial (or 700 μ L extract) and 10 ng of isotopically labeled PFCA standard was spiked and the solvent was left to evaporate overnight. The next day, 30 mL of water, 0.48 g potassium persulfate, and 4.56 mmol NaOH were added, and the solution was vortexed and placed in a water bath at 85 °C for 6 h. Afterwards, the samples were allowed to cool to room temperature and the pH was adjusted to 6–8 with HCl. For sample clean-up, SPE cartridges (Chromabond HR-XAW, 3 mL, 200 mg, Macherey-Nagel) were conditioned with 6 mL MeOH with 0.1% NH₄OH, 3 mL MeOH, and 6 mL water and samples were passed through at a rate of approximately one drop per second using vacuum. The cartridges were then washed with 6 mL water and dried. After drying, PFCAs were eluted with 3 mL MeOH, followed by 6 mL MeOH with 0.1% NH₄OH. The eluates were evaporated until dryness under a gentle stream of N₂, reconstituted in 1 mL MeOH, vortexed thoroughly, sonicated for 5 min, and vortexed again. Subsequently, the samples were centrifuged for 10 min @ 20 817 rcf and the supernatant was transferred into HPLC vials for analysis. An additional SPE blank was processed in the same manner.

Total hydrolysable precursor (THP) assay

For the application of the THP assay²⁹ (five textiles, one extract, and a blank), 750 μ L of a 1 M NaOH solution (22.5/2.5 MeOH/water) and 30 mg small textile pieces (or 700 μ L extract) were combined in 1.5 mL glass vials, vortexed, and placed in an oven at 60 °C for 16 h. After cooling to room temperature, 300 μ L of the solution was transferred into 10 mL glass vials, where 900 μ L of a 1 : 1 mixture of methyl-*tert*-butylether (MTBE) and *n*-hexane was added, followed by 3 mL of water. After 30 min of shaking, separation of the organic phase from the aqueous phase was allowed. The lower water layer was removed and anhydrous Na₂SO₄ was added to remove excess water until the

organic solution became clear. 450 μL of the clear solution was transferred to plastic Eppendorf tubes together with 75 mg Na_2SO_4 and left to dry for 1 h with occasional shaking. Finally, all samples were centrifuged for 10 min @ 20 817 rcf and 200 μL of supernatant was transferred to a HPLC vial with a glass inlet for analysis with GC-QTOF-MS.

PFAS target and non-target screening (NTS)

PFAAs from PhotoTOP and dTOP oxidation experiments were quantified by HPLC-QqQ-MS/MS (1290 Infinity II HPLC System coupled to a 6490 Triple Quadrupole MS, Agilent Technologies). Separation was achieved by gradient elution (A: 95/5 water/MeOH + 2 mM NH_4Ac , B: 5/95 water/MeOH + 2 mM NH_4Ac) on a C_{18} column (Waters Acquity UPLC BEH C_{18} , 1.7 μm , 2.1×100 mm) at a flow rate of 0.4 mL min^{-1} at constant 60 $^\circ\text{C}$ (for details on gradient, ionization, and instrument parameters see Tables S1 and S2†). The ESI was operated in the negative mode and all PFAAs were quantified using two MRM mass transitions except for PFBA (Table S4†). The injection volume was 5 μL and quantification was performed with seven calibration standards (50 ng L^{-1} –10 $\mu\text{g L}^{-1}$) measured before and after each set of samples. MeOH blanks and quality controls (1 $\mu\text{g L}^{-1}$ calibration standard) were measured after every ~ 10 th sample to monitor the instrument drift. PFAAs in samples from dTOP experiments were corrected using isotopically labeled internal standards.

FTOHs were quantified ($<10:2$ FTOH) and semi-quantified ($\geq 10:2$ FTOH) with an Agilent 7890B GC (Agilent HP-5MS UI column, 30 m \times 0.25 mm, 0.25 μm film) coupled to an Agilent 6550 QTOF-MS *via* an atmospheric pressure chemical ionization (APCI) interface. A 9.7 min temperature program was applied, starting at 50 $^\circ\text{C}$ for 1 min and increasing at a rate of 30 $^\circ\text{C min}^{-1}$ to 250 $^\circ\text{C}$ which was held for 2 min. Helium was used as carrier gas at 1 mL min^{-1} and a constant water flow of 0.1 mL min^{-1} into the APCI source was achieved with the HPLC pump which keeps the humidity at a constant high level to increase ionization efficiency.^{30,31} The corona current was turned off before 2.5 min to prevent solvent ionization. The injection volume was 1 μL with pulsed splitless injection (instrument parameters in Table S3†). 6:2 and 8:2 FTOH were quantified with standards (10 $\mu\text{g L}^{-1}$ –10 mg L^{-1}) while concentrations of $n:2$ FTOHs ($n \geq 10$) were semi-quantified based on the response of 8:2 FTOH. Each sequence included a solvent blank and MS data were acquired at 10 spectra/s in a range from m/z 60–500.

GC- and HPLC-QTOF raw data from textile extracts, selected PhotoTOP samples, and THP extracts were further screened for unknown PFAS with a non-target screening approach as described previously (small suspect list, FindPFAS and KMD analysis).²⁸ Measurement and data analysis details are given in the ESI (Section S2†).

Extractable organic fluorine (EOF) analysis by HR-CS-GFMS

0.25 g textile samples (cut into pieces of 2 cm^2) were weighted in 15 mL polypropylene PP tubes in methodical triplicates. 5 mL of MeOH was added for extraction. Samples were incubated in an

ultrasonic bath for 1 h, followed by overnight (20 h) shaking in a vortex mixer at 500 rpm. After this, samples were again incubated in an ultrasonic bath for 1 h. Upon centrifugation (10 min, 3900 rpm), the supernatant was collected and directly analyzed by high resolution-continuum source-graphite furnace molecular absorption spectrometry (HR-CS-GFMS). A contrAA 800 HR-CS-GFMS system (Analytik Jena AG, Jena, Germany) and the software ASpect CS 2.2.2.0 (Analytik Jena AG, Jena, Germany) were utilized for EOF analysis. The method is based on the detection of GaF at 211.248 nm as described by Metzger *et al.* 2019 and Gehrenkemper and Simon *et al.* 2021.^{32,33} For external calibration, PFOA standards were used at the following concentrations: 0, 25, 50, 75, 100, and 125 $\mu\text{g F L}^{-1}$. Both samples and standards were measured in instrumental triplicate. The limits of detection and quantification were 3.4 $\mu\text{g F kg}^{-1}$ and 10.3 $\mu\text{g F kg}^{-1}$, respectively.³⁴

Total fluorine analysis by CIC

TF in textile samples was quantified *via* direct analysis using combustion ion chromatography (CIC). CIC combines a combustion and an absorption unit (AQF-2100H, GA-210, Mitsubishi Chemical Analytech, Tokyo, Japan) connected to ion chromatography (ICS Integrion, Thermo Fisher Scientific GmbH, Dreieich, Germany). Therefore, uniformly punched textile discs (~ 5 –10 mg) were weighed directly into pre-cured ceramic boats and subsequently analyzed by CIC in triplicates. In between, a cleaning step was performed, combusting a blank sample boat under the applied measurement conditions. Quantification of the samples was enabled using ten point calibration curves from 1 to 250 $\mu\text{g L}^{-1} \text{F}^{-1}$ for all TF measurements. Therefore, 200 μL of a freshly prepared aqueous NH_4F calibration solution was injected into clean ceramic boats and subsequently combusted. In order to maintain calibration precision, all calibration samples were combusted twice, yielding an average value for each calibration point. Details on the limits of quantification (LOQ) and detection (LOD), instrumentation, and measurement parameters are provided in the ESI (Section S2, Tables S5–S8,† for further details see also Gehrenkemper *et al.* 2021 and Roesch *et al.* 2021).^{33,35}

Quality control

To ensure reliable generation of data regarding the occurrence of SFPs in textiles, several quality control measures were included in the study. An extraction test with PFAAs was performed to ensure that these classes are quantitatively extracted from the textile by the applied extraction procedure (see ESI, Fig. S2†). Techniques such as the PhotoTOP and TOP assay were shown in the past to quantitatively yield PFCAs from precursor oxidation when applied without a matrix.^{28,36,37} However, in the presence of textile matrix, a quantitative conversion of SFPs to PFAAs cannot be easily calculated. For each technique (screening, PhotoTOP, dTOP, THP, EOF, and TF) always procedural blank experiments (no textile) were performed to account for general PFAS background as well as instrumental blanks and regular QC measurements were carried out.

The LOQ for HPLC-QqQ and HPLC-QTOF measurements was defined as a S/N ratio > 50 for signals at the second lowest calibration point (100 ng L⁻¹ for PFCAs and 10 µg L⁻¹ for FTOHs). LOQ were 1.2 µg F kg⁻¹ for extraction (PFAAs), 0.82 mg F kg⁻¹ for PhotoTOP, 0.36 mg F kg⁻¹ for dTOP, and 1 mg F kg⁻¹ for THP.

Results and discussion

Textile prioritization

Textiles coated with DWR formulations typically exhibit low contact angles with water, while in the case of fluorinated DWR coatings also oil and stain repellent properties are achieved which is further dependent on the textile surface roughness.^{38–40} Therefore, contact angles can be useful for prioritization to exclude textiles that are totally oil wetting. In total, 12 functional textiles (*e.g.*, an outdoor-, umbrella-, awning-, and sunbed fabric and shower curtain) were selected for deep investigation due to their low water and/or oil contact angles while two water repellent but oil wetting textiles were included as references (see Fig. 2, details on textiles in Table 1). Several textiles such as T07 and T12 showed highly different angles on both sides, which can be indicative of one-sided coating of the final textile with a DWR formulation or a multi-layered textile, like that used for fire-fighting gear,⁴¹ rather than directly coated textile fibers. This observation was consistent with the available textile

descriptions for T07 which stated that it contained a coating on one side. While for several textiles oil repellency was low, all textiles were water repellent at least on one side.

PFAS screening in textile extracts

Methanol extracts of the 12 textiles were screened for potential PFAS by HPLC-QTOF-MS. Except for concentrations of PFOA (~0.01 mg F kg⁻¹) and PFHxA (~0.005 mg F kg⁻¹) in T15, no further PFAS were detected (LOQ = 1.2 µg F kg⁻¹). Neither Kendrick mass defect (KMD) analysis, nor fragment mass differences in acquired MS/MS spectra were detected, providing the first evidence that these textiles do not contain significant concentrations of extractable PFAS, indicating (due to the observed contact angles) the presence of coatings with either non-fluorinated formulations, partially extractable residues or non-extractable polymeric PFAS such as SFPs.

Textile oxidation *via* PhotoTOP assay

To investigate potential non-extractable PFAS in textiles, first, the previously developed PhotoTOP was directly applied for 5 h to the 12 textile samples and 3 textile extracts (T05, T07, and T15).²⁸ Several textiles formed considerable concentrations of different PFCAs when oxidized directly (Fig. 3a and Table 1) ranging from C₄ (PFBA) up to C₁₂ (PFDoDA) and mainly either PFOA or PFHxA were the dominant oxidation products with different chain-length distributions and concentrations. No perfluoroalkyl sulfonic acids were detected. While T15 and T20 were dominated by PFHxA and low concentrations of PFHpA and PFPeA indicating a C₆-based SFP coating (C₆F₁₃-R), T03, T05, T07, T12, and T17 preferentially formed PFOA (C₈-based). Since the PhotoTOP was shown to conserve the chain lengths of precursors in the form of (*n* - 1) perfluorinated carbon atoms in the molecule (*e.g.*, PFOA from 8 : 2 FTOH),²⁸ at this point, the observed PFCA chain-length distribution is expected to roughly reflect the actual perfluoroalkyl side chains on the textiles. T03 and T17 seem to contain almost only C₈-chains (similar to T15 and T20 for C₆) whereas for T05 and T07 distributions from C₅-C₁₂ peaking at C₈ were observed. Only T25 differed from these two groups since only PFHpA was formed after oxidation.

Concentrations of the sum of PFCAs (ΣPFCAs) ranged from <LOQ for T10, T11, T19, and T23 up to 149 mg m⁻² for T15 or to 1601 mg kg⁻¹ (= 1067 mg F kg⁻¹) due to the fabric density, which corresponds to approximately 1% fluorine content in the textile (for details see Table 1). Regarding contact angles, textiles with oil wetting but water-repellent surfaces did not show detectable concentrations of PFCAs after direct oxidation with the PhotoTOP (see also Fig. S3†).

The typical chain length distributions of T05 and T07 can be indicative of fluorotelomer-based SFPs such as *e.g.*, (meth)acrylate polymers with attached FTOHs (chain length distribution from synthesis).^{42,43} However, perfluoroalkyl sulfonamido ethanol-based SFPs can also be composed of combinations of different perfluoroalkyl chains (C₃-C₁₂).²⁴ A distinction between these types, however, cannot be made on the basis of PFCAs from PhotoTOP oxidation only since sulfonamide-based

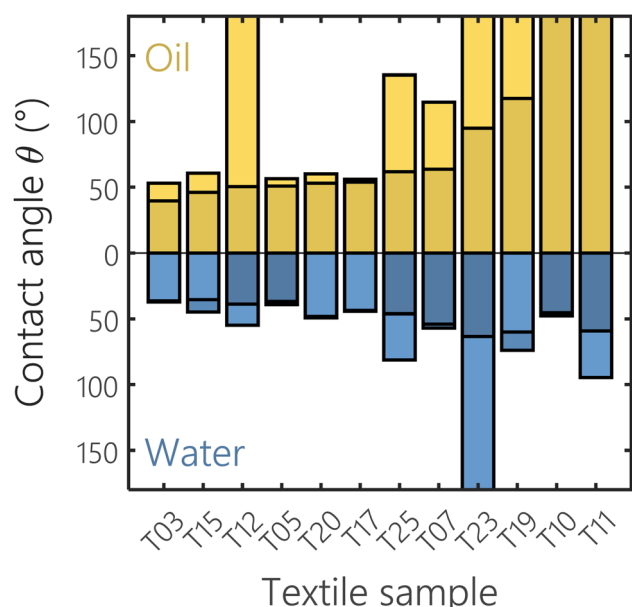


Fig. 2 Contact angles θ of sunflower oil (yellow) and water (blue) for the 12 functional textiles in order of increasing oil contact angle. For every textile, two overlaid bars are shown (light and dark color for the respective side) for the contact angles of both sides since for most textiles, no optical difference between both sides was observed. Note that strongly differing contact angles on both sides are indicative of the application of a DWR formulation to the final textile rather than fibers directly containing DRW formulations. For totally wetting textiles, θ was set to 180°. Contact angles vs. PFCAs formed after PhotoTOP oxidation are shown in Fig. S3†

Table 1 Summary of the results from different methods for the investigation of fluorine content and chain length distribution of side-chain fluorinated polymers (SFPs) as well as extractable PFAS residues in functional textile samples^a

Sample	Type	Available information	Density (kg m ⁻²)	PFAAs from extraction (mg F kg ⁻¹)	\sum PFCAS _{PhotoTOP} (mg F kg ⁻¹)	\sum PFCAS _{dTOP} (mg F kg ⁻¹)	\sum FTOHs _{THP} (mg F kg ⁻¹)	TF (mg F kg ⁻¹)	EOF (mg F kg ⁻¹)
T05	Awning fabric	OR, WR, Teflon coating, mildew resistant, 80% polyacrylic, 20% polyester	0.25	~0.01	164 ± 12	220.5	1440 ^b	579 ± 36	14 ± 1
T07	Imitation linen	WR, abrasion proof, weather resistant, 100% polyester, colourless polyurethane coating and WR coating	0.22	<LOQ	68 ± 7	—	402 ^b	179 ± 15	1 ± 0.2
T15	Outdoor fabric	Weather resistant, Teflon coating, 60% polyacrylic, 40% polyester, Oeko-Tex standard 100 certified	0.18	~0.005	540 ± 60	717.5	249 ^b	2061 ± 126	25 ± 4
T20	Shower curtain	WR, 100% polyester	0.08	<LOQ	1067 ± 191	570.3	406 ^b	2064 ± 34	64 ± 2
T10	Unknown fabric	WR	0.22	<LOQ	<LOQ	<LOQ	<LOQ	19.1 ^c ± 3	<LOQ
T03	Sunbed fabric	—	0.24	<LOQ	344 ± 30	—	—	—	—
T11	Unknown fabric	WR	0.22	<LOQ	<LOQ	—	—	—	—
T12	Unknown fabric	WR	0.29	<LOQ	12 ± 1	—	—	—	—
T17	Umbrella fabric	WR, stain resistant, UV resistant fabric, polyacrylic fabric, Teflon coating	0.20	<LOQ	87 ± 12	—	—	—	—
T19	Jersey fabric	Stain resistant, 81% cotton, 19% polyurethane, Oeko-Tex standard 100 certified	0.19	<LOQ	<LOQ	—	—	—	—
T23	Upholstery leatherette	(Salt)water proof, flame-, stain-, UV-, disinfectant-, blood-, urine resistant, 65% polyester, 35% polyurethane	0.63	<LOQ	<LOQ	—	—	—	—
T25	Cordura fabric	WR, abrasion resistant, 94% polyamide, 6% polyurethane	0.41	<LOQ	13 ± 3	—	—	—	—

^a Note that for the first five samples all techniques were used (except for dTOP in the case of T07), while for the other textiles only PhotoTOP investigations and extractions were performed. Oxidative (PhotoTOP (5 h) and dTOP (6 h)) and hydrolytic (THP (16 h)) methods were applied directly to the textiles. Data from extract oxidation are not shown in Table 1. Duplicates. Note that oxidation of selected MeOH textile extracts yielded slightly lower but similar fluorine concentrations (in the form of PFCAs) than EOF. Fluorine from FTOHs that exceed the TF measurements probably results from an overestimation of the semi-quantified FTOHs (>8:2). LOQ were 1.2 µg F kg⁻¹ for extraction (PFAAs), 0.82 mg F kg⁻¹ for PhotoTOP, 0.36 mg F kg⁻¹ for dTOP, 1 mg F kg⁻¹ for THP, 10.3 µg F kg⁻¹ for EOF, and 18 mg F kg⁻¹ for TF, respectively. Abbreviations: OR: oil repellent, WR: water repellent, “—”: not determined, and LOQ: limit of quantification. ^b FTOHs ≥ 10:2 were semi-quantified.

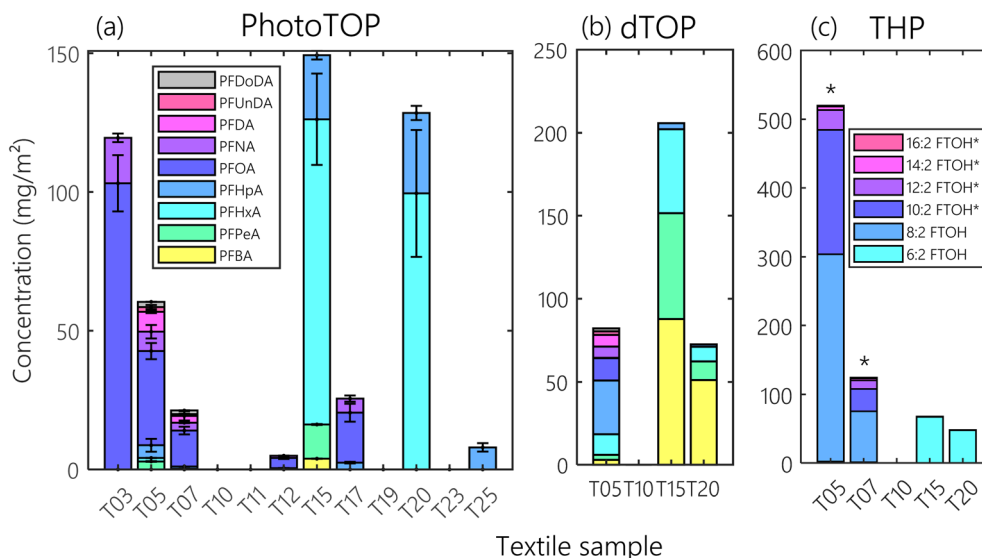


Fig. 3 Concentrations of PFCAs after 5 h of PhotoTOP oxidation (a) and 6 h of dTOP oxidation (b), as well as of FTOHs after 16 h of THP hydrolysis (c) for selected textiles. Error bars for PhotoTOP measurements correspond to duplicate sampling, and asterisks mark estimated concentrations of $n : 2$ FTOHs with $n \geq 10$. Note that in extracts of all textiles besides traces of PFCAs no other PFAS were detected by NTS.

precursors also form PFCAs but of one chain length (e.g., PFOA from the C_8 sulfonamide precursor).

To confirm the results from NTS that much lower concentrations of extractable PFAS were present in the textiles compared to direct oxidation (non-extractables), three extracts (T05, T07, and T15) were also oxidized. Oxidation of the extracts of T05 and T15 yielded 25–50 times smaller concentrations (mainly PFOA for T05 and PFHxA for T15) than direct oxidation and for T07 no PFCAs were detected after extract oxidation, which strengthens the observation of non-extractable SFPs.

Textile oxidation via dTOP assay

The dTOP assay was applied to four textiles (T05, T10, T15, and T20) and the extract of T07 (Fig. 3b). Similar to the PhotoTOP oxidation, for T15 the highest Σ PFCAs concentrations (205 mg m^{-2}) were formed after dTOP oxidation but were dominated by PFBA, PFPeA, and PFHxA, showing that stronger chain shortening of the perfluoroalkyl chain occurred compared to PhotoTOP oxidation which was also true for T20 (lower overall concentration). We did not include perfluoropropionic acid (PFPrA) and trifluoroacetic acid (TFA) in our analyses, but due to the dominance of PFBA, it is important to note that formation of PFPrA and TFA is not unlikely, especially in the case of the C_6 -based formulations. Formation of ultra-short chain PFCAs from TOP oxidation was observed in numerous studies and can be a considerable fraction of the Σ PFCAs.^{37,44–46} T05 showed both similar concentrations and chain-length patterns as the results of the PhotoTOP oxidation; however, PFCAs were shifted by one CF_2 -unit to shorter chains. After oxidation of the T07 extract only trace amounts of C_7 – C_{10} PFCAs were formed (Σ PFCAs = 0.13 mg m^{-2}), while in T10 no PFCAs were detected. Overall, similar results for PFCAs were observed, but shifted to short chain PFCAs compared to the PhotoTOP.

Textile hydrolysis via THP assay

Five textiles (T05, T07, T10, T15, and T20) and the T07 extract were exposed to hydrolysis via the THP assay, where FTOHs $<10 : 2$ were quantified with analytical reference standards or semi-quantified ($\geq 10 : 2$) based on the response of $8 : 2$ FTOH (Fig. 3c). The highest estimated concentrations were found after hydrolysis of T05 ($\sim 520 \text{ mg m}^{-2}$) composed of $6 : 2$ – $16 : 2$ FTOHs ($8 : 2$ FTOH was dominant) which exceeded concentrations determined by both dTOP and PhotoTOP assay (for mg F kg^{-1} comparison see Table 1). T07 showed a similar FTOH pattern but with a lower overall concentration ($\sim 124 \text{ mg m}^{-2}$). T15 and T20 formed almost exclusively $6 : 2$ FTOH with 68 and 48 mg m^{-2} , respectively. Only traces of $8 : 2$ – $12 : 2$ FTOH were found in the T07 extract ($\sim 2.3 \text{ mg m}^{-2}$), while in T10 no FTOH could be detected.

Since hydrolysis is a much more selective cleaving process for ester bonds and does not affect saturated hydrocarbon moieties in comparison to OH-radicals, the THP provides unchanged perfluoroalkyl chains (as FTOHs).²⁹ Therefore, the observation of mixed chain lengths for T05 and T07 and one distinct chain length (C_6 -based) for T15 and T20 gives valuable information on the true chain lengths of SFP precursors which is not unambiguously available for the oxidative techniques. Furthermore, it demonstrated that those textiles are all coated with telomer-based SFPs which supports previous findings from PhotoTOP and dTOP assays. Perfluoroalkyl side-chains in telomer-based SFPs are typically connected via an ester linkage to non-fluorinated polymer backbones which are e.g., acrylates, methacrylates, or polyurethane.^{23,47,48} We hypothesize that the strong differences in the case of some textiles (e.g., T15) between the yields from oxidation techniques (PhotoTOP and dTOP) and the THP potentially result from a selective hydrolysis which can be kinetically highly variable depending on the hydrolysable

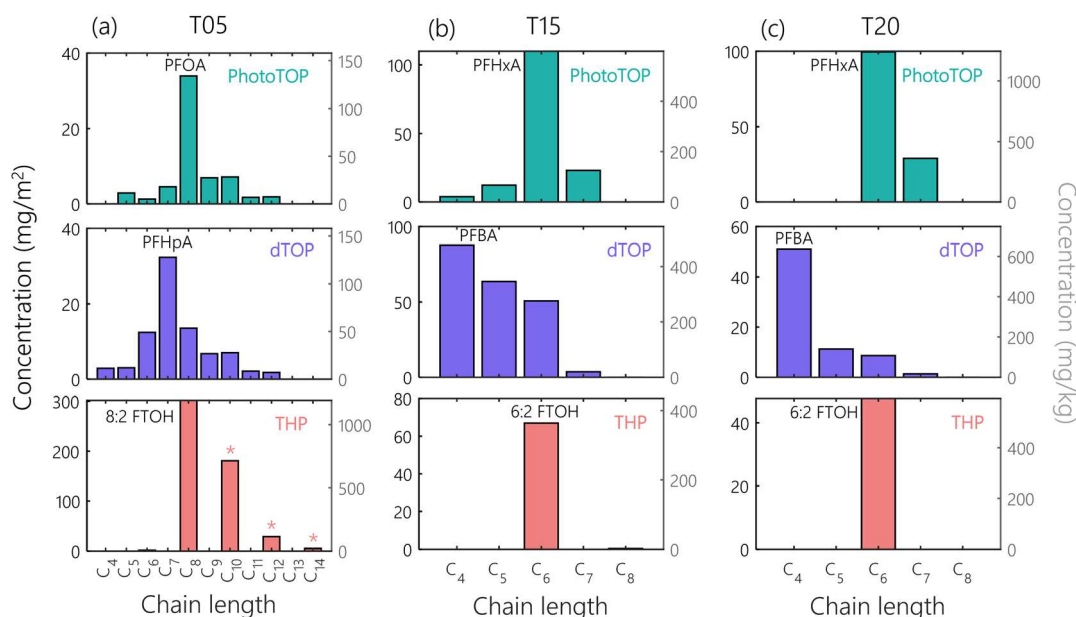


Fig. 4 Comparison of concentrations of PFCAs and FTOHs formed from application of PhotoTOP (green), dTOP (blue), and THP (red) to textiles T05, T15, and T20. Note that in the case of PFCAs, the total chain length (including carboxylic acid) is shown (e.g., PFOA = C₈) while for FTOHs the perfluoroalkyl chain length was used (e.g., 8 : 2 FTOH = C₆). In the case of hydrolysis by the THP assay no chain-shortening is expected. While the PhotoTOP was able to conserve the main perfluoroalkyl chain to ($n - 1$) PFCAs, the dTOP resulted in shorter chain PFCAs. Therefore, it is not unlikely that PFCAs shorter than PFBA were formed (PFPrA and TFA). Asterisks mark semi-quantified concentrations of $n : 2$ FTOHs with $n \geq 10$.

linkage compared to non-selective OH-radical processes during dTOP and PhotoTOP (see also Table 1).

Method comparison and correlation with TF and EOF

Concentrations of formed Σ PFCAs after PhotoTOP oxidation (<LOQ–149 mg m⁻²) were in a similar range to those formed after dTOP oxidation (<LOQ–205 mg m⁻²), while concentration estimates from hydrolysis (THP) slightly exceeded the concentrations of PFCAs which were produced during PhotoTOP and dTOP oxidation (<LOQ to ~520 mg m⁻²). All three methods were applied to the SFP containing textiles T05, T15, and T20 (Fig. 4). While for T05 the THP yielded the highest quantities of FTOHs, and T15 and T20 showed the highest values of PFCAs after dTOP and PhotoTOP oxidation, respectively. For textile T5, however, the concentrations of semi-quantified FTOHs after hydrolysis (THP) were almost 10-fold compared to the oxidative techniques, whereas ranges of T15 and T20 were similar (note that when comparing mass concentrations of for instance PFOA with 8 : 2 FTOH a difference of approximately 10% arises from their different molar masses (414 and 464 g mol⁻¹)). The observed differences could arise from the properties of the textile type which may affect the oxidation and hydrolysis processes. Especially the water-repellent character of a textile which is also dependent on the textile surface structure itself typically hinders water, hydroxide ions and OH-radicals from penetrating the material. Additionally, the fabric type presumably plays an important role. While cotton (cellulose) will be decomposed by both hydrolysis and oxidation, other synthetic materials are much more inert resulting in much lower oxidant consumption. The selectivity of hydrolysis (different chemical

linkages between e.g., FTOHs and the polymer backbone) compared to non-selective OH-radical processes could also explain high discrepancies between oxidation and hydrolysis. An effect of fabric type on the release of PFAAs during textile aging was shown previously.⁴⁹ Here, of course systematic errors in the semi-quantification of $\geq 10 : 2$ FTOHs could also play a major role.

The THP assay has the clear advantage of perfluoroalkyl chain length conservation. This is also partially provided by the PhotoTOP since telomer-based precursors mainly yield PFCAs with chain lengths of ($n - 1$) perfluorinated carbon atoms. For example, PFOA is formed from 8 : 2 FTOH. Perfluoroalkane sulfonyl fluoride (PASF)-based PFAS only yield PFCAs with one defined chain length from both the PhotoTOP and dTOP (e.g., PFOA from C₈ sulfonamide).²⁸ Therefore, the PhotoTOP offers more structural information than the dTOP (Fig. 4). Furthermore, with respect to sample preparation effort, both the THP and PhotoTOP do not need time consuming and partially discriminating SPE which yields highly different recoveries for PFAAs of different chain lengths depending on the used sorbent material. Potential losses from ultra-short chain PFCAs after dTOP oxidation should always be included in mass balance considerations if appropriate methods are available.³⁷

To bring the three methods in a quantitative context with complementary sum parameter approaches, the EOF and TF results were correlated with Σ PFCAs (Fig. 5, see also Table 1) and Σ FTOHs (Fig. S4†). Both dTOP and PhotoTOP assays correlated remarkably well with TF (R^2 of 0.96 and 0.82) and also EOF measurements (R^2 of 0.97 and 0.47) and yielded approximately half the amount of fluorine in the form of PFCAs

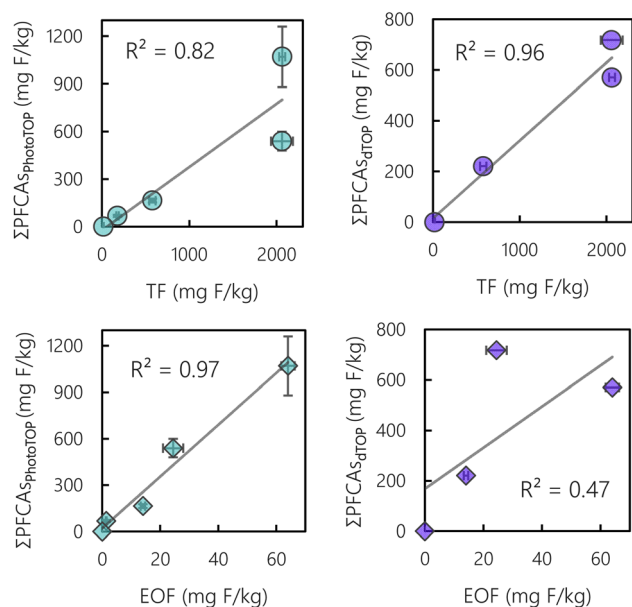


Fig. 5 Correlation of fluorine in Σ PFCA₅ after PhotoTOP and dTOP oxidation (mg F kg^{-1}) vs. fluorine from TF and EOF measurements. Compared with TF, an almost complete conversion ($\sim 50\%$) of SFPs to PFCA₅ was possible with the PhotoTOP and dTOP directly applied to the textiles. However, the measured EOF was rather low due to insufficient extraction of SFPs, which is also reflected by low concentrations of PFCA₅ in oxidized textile extracts. Note that for the PhotoTOP (5 h) and dTOP (6 h) the oxidation was not necessarily complete (Fig. S5 and S6†). Furthermore, due to stronger chain-shortening during dTOP oxidation the amount of fluorine is generally underestimated. Error bars from PhotoTOP measurements correspond to duplicate sampling (error calculated using Gaussian error propagation), while for EOF and TF they represent triplicate measurements.

compared to TF. Fluorine from PFCA₅ and FTOHs was converted on a molar basis to the mass of fluorine (see the ESI†). This is in contrast to the outcome by Liagkouridis *et al.* 2022 who applied the dTOP to different textiles and observed a strong inefficiency of dTOP oxidation in converting SFPs to PFCA₅ (dTOP yields were roughly 1% of the TF).¹⁷ In our case, however, up to 50% of the TF could be explained using conversion of perfluoroalkyl side-chains to PFCA₅ by oxidation. Since the concentrations of PFCA₅ still increased after 5 h for these textiles (correlation plots in Fig. 5 include the measured concentrations after 5 h of oxidation), a complete conversion (up to 100%) seems to be possible after approximately 10 h. This becomes more obvious in Fig. S5† where the concentration approximately doubled after 10 h which is then approximately 100% of TF. Reaching the final reaction yield can also be observed by decreasing PFCA₅ formation rates for selected textiles during longer PhotoTOP oxidation (Fig. S5†). Also, for the dTOP assay, oxidation times of 3 h and 6 h (T05 and T15) suggested that potentially even higher PFCA₅ concentrations could have been formed if oxidation times had been extended (Fig. S6†). It should be further noted that the amount of fluorine from Σ PFCA₅ after dTOP oxidation (and also PhotoTOP oxidation) is generally underestimated because the chain shortening

(*e.g.*, PFBA from a C₆-based SFP) leads to a loss of fluorine in the mass balance.

The EOF was lower by more than a factor of 30 compared to TF measurements which is in good agreement with the results after the oxidation of textile extracts where PFCA₅ were also 25–50 times lower than those after direct oxidation of the textiles. The EOF results are approximately a factor of 2 higher when compared to the textile extract after PhotoTOP oxidation. Here, the higher EOF fraction could originate from fluorinated non-polymeric residues that are non-oxidizable or form not detected oxidation products.

Discussion of SFPs in investigated textile samples

PFCA₅ release from SFPs was detected by PhotoTOP oxidation in eight of the 12 textiles ranging from 12 to over $1000 \text{ mg F kg}^{-1}$ textile or ~ 3 to over 97 mg F m^{-2} textile (up to $\sim 150 \text{ mg m}^{-2}$ PFCA₅ or $\sim 1600 \text{ mg kg}^{-1}$ PFCA₅; note: maximum concentrations correspond to different textiles due to different densities). The results were clearly confirmed by similar and complementary techniques (dTOP, THP, EOF, and TF, see Table 1 for details). Concentrations of PFAS in textiles from previous studies were in similar ranges but rather variable: extracts of school uniforms formed up to 308 mg kg^{-1} target PFAS after TOP assay and up to 3160 mg kg^{-1} 6 : 2 FTOH after hydrolysis.⁵⁰ Nikiforov measured 300 mg m^{-2} FTOHs after hydrolysis of polyester textiles,²⁹ Zhu and Kannan found 1296 mg m^{-2} of PFCA₅ in water repellent textiles after the TOP assay,⁵¹ and medical textiles investigated by Liagkouridis *et al.* ranged from 28 to 560 mg F m^{-2} .¹⁷ TF measurements by complementary techniques such as particle-induced gamma ray emission (PIGE) spectroscopy were also in similar ranges (*e.g.*, an umbrella fabric with 68 mg F m^{-2})^{52–54} Although PFOA, PFOS, and their precursors are (partially) regulated under the Stockholm Convention on persistent organic pollutants and many companies voluntarily phase out long-chain PFAS, several SFPs in current textiles (all textiles except for the unknown textiles which were bought in the years 2021 and 2022) still contain long-chain PFAS up to C₁₆ as for instance the awning fabric (T05).⁷ C₈-based SFPs are also found in the sunbed fabric (T03), imitation linen (T07), and umbrella fabric (T15), while others exclusively contain C₆F₁₃ moieties (Fig. 3). The observed distributions originate from typical telomer-based synthesis and are often observed, but can potentially also be attributed to impurities.^{24,42,43,47} The water-repellent jersey (T19) and outdoor fabric (T15) were both certified by the OekoTex Standard 100 which states that all components of the product have been tested for harmful substances and the product is therefore certified to be harmless to health. While T19 did not form PFCA₅ after oxidation, T15 yielded the highest PFCA₅ concentrations after oxidation compared to all textiles (Σ PFCA₅PhotoTOP 540 mg F kg^{-1} , 2061 mg F kg^{-1} TF) although it was stated to be coated with Teflon (polytetrafluoroethylene) which would not be oxidized to the observed PFCA₅ patterns. Besides an SFP-based DWR impregnation, Teflon can also be present in the textile, but not exclusively, since the PFCA₅ after PhotoTOP oxidation explain roughly one quarter of the TF (note that a longer

oxidation time would have likely increased the explainable fraction of the TF, Fig. S5†). Rodgers *et al.*⁵⁵ observed that among textiles described as water/stain resistant, PFAS concentrations were similar regardless of “green” labels (including nontoxic terms or green certification such as Greenguard Gold or Oeko-Tex 100) showing that labeling in general should be handled with care.⁵⁵ This is further highlighted by the fact that both awning (T5) and umbrella fabric (T17) were also described with Teflon coatings, but showed totally different chain-length distributions than T15 which shows that besides Teflon, SFPs are likely present. Significant amounts of PFCAs also formed for the imitation linen (T7), which was declared to have a polyurethane coating on one side and a colorless water-repellent coating on the other side, and also for the shower curtain (T20), which was labelled as water repellent without further information. The upholstery leatherette (T23) for the medical sector did not contain any PFAS after oxidation, despite its water/stain/UV/flame resistant properties.

Conclusions

SFPs are a class of rather barely investigated PFAA precursors due to the lack of reference standards and the general challenges of investigating PFAS in polymers. Nevertheless, polymers have recently gained increasing attention since they are often high production chemicals that are insufficiently characterized and labeled due to their complex composition.⁵⁶ Complementary methods to standard PFAS target analysis, such as oxidation (PhotoTOP and dTOP), hydrolysis (THP), or sum parameters (*e.g.*, TF), are essential to detect SFPs in textiles because their extraction is often insufficient and may lead to strong underestimation of the actual PFAS content. Even if oxidation/hydrolysis are not always applicable in a fully quantitative manner, they can still provide valuable information which is not accessible by target PFAS methods in extracts.

Although the extractable fraction is potentially an upper limit to which humans are exposed during the lifecycle of a textile and SFPs in textiles are probably non-hazardous during use (covalent bonds), numerous studies showed important concerns: volatile FTOHs can be emitted into indoor environments which can lead to direct exposure *via* air,⁵⁷ and both PFAAs and microplastic fibers form during use (*e.g.*, weathering, sunlight *etc.*) and washing which is of special concern for long-chain SFPs still in use.^{18,19,49,58} Furthermore, at the end of their lifecycle, SFPs can cause problems during disposal in landfills, incineration or in recycling streams. There, such polymers can act as a long-term source for PFAAs in soil and groundwater when they are slowly degraded.^{20,21,59–64} Similarly, microplastic fibers are transported with waste water to treatment plants where they also act as PFAA precursors which may emit persistent and mobile chemicals into the environment *via* water or sludge.^{19,65} Therefore, new techniques such as oxidation and hydrolysis are important to detect the real extent of complex SFPs in products and uncover their use and fate. In the future, polymers should be considered for stricter regulations or placed under the essential use concept since they currently contribute

to the emission of persistent, mobile and bioaccumulative substances.^{66,67}

Author contributions

JZ planned the study, supervised the experimental part and wrote the first draft of the manuscript. CC conducted the oxidation and hydrolysis experiments and was part of writing the first draft. FS performed EOF measurements and reviewed the manuscript. PR performed TF measurements and reviewed the manuscript. BB reviewed the manuscript. CZ supervised the study and reviewed the manuscript.

Conflicts of interest

The authors declare no competing financial interest.

Acknowledgements

The authors acknowledge DBU (Deutsche Bundesstiftung Umwelt) for the scholarship of JZ.

References

- 1 M. G. Evich, M. J. B. Davis, J. P. McCord, B. Acrey, J. A. Awkerman, D. R. U. Knappe, A. B. Lindstrom, T. F. Speth, C. Tebes-Stevens, M. J. Strynar, Z. Wang, E. J. Weber, W. M. Henderson and J. W. Washington, Per- and polyfluoroalkyl substances in the environment, *Science*, 2022, **375**, eabg9065.
- 2 J. Glüge, M. Scheringer, I. T. Cousins, J. C. DeWitt, G. Goldenman, D. Herzke, R. Lohmann, C. A. Ng, X. Trier and Z. Wang, An overview of the uses of per- and polyfluoroalkyl substances (PFAS), *Environ. Sci.: Processes Impacts*, 2020, **22**, 2345–2373.
- 3 Z. Wang, J. C. DeWitt, C. P. Higgins and I. T. Cousins, A Never-Ending Story of Per- and Polyfluoroalkyl Substances (PFASs)?, *Environ. Sci. Technol.*, 2017, **51**, 2508–2518.
- 4 E. Kissa, *Fluorinated Surfactants and Repellents*, CRC Press, 2001.
- 5 L. G. T. Gaines, Historical and current usage of per- and polyfluoroalkyl substances (PFAS): a literature review, *Am. J. Ind. Med.*, 2023, **66**, 353–378.
- 6 I. T. Cousins, J. C. DeWitt, J. Glüge, G. Goldenman, D. Herzke, R. Lohmann, C. A. Ng, M. Scheringer and Z. Wang, The high persistence of PFAS is sufficient for their management as a chemical class, *Environ. Sci.: Processes Impacts*, 2020, **22**, 2307–2312.
- 7 Stockholm Convention, *The New POPs under the Stockholm Convention*, <https://www.pops.int/TheConvention/ThePOPs/TheNewPOPs/tabid/2511/Default.aspx>, (accessed 21.03.2023).
- 8 F. Xiao, Emerging poly- and perfluoroalkyl substances in the aquatic environment: a review of current literature, *Water Res.*, 2017, **124**, 482–495.
- 9 H. A. Kaboré, S. Vo Duy, G. Munoz, L. Méité, M. Desrosiers, J. Liu, T. K. Sory and S. Sauvé, Worldwide drinking water

- occurrence and levels of newly-identified perfluoroalkyl and polyfluoroalkyl substances, *Sci. Total Environ.*, 2018, **616–617**, 1089–1100.
- 10 M. Mazzoni, A. Buffo, F. Cappelli, S. Pascariello, S. Polesello, S. Valsecchi, P. Volta and R. Bettinetti, Perfluoroalkyl acids in fish of Italian deep lakes: environmental and human risk assessment, *Sci. Total Environ.*, 2019, **653**, 351–358.
 - 11 K. Lee, J. J. Alava, P. Cottrell, L. Cottrell, R. Grace, I. Zysk and S. Raverty, Emerging Contaminants and New POPs (PFAS and HBCDD) in Endangered Southern Resident and Bigg's (Transient) Killer Whales (*Orcinus orca*): In Utero Maternal Transfer and Pollution Management Implications, *Environ. Sci. Technol.*, 2023, **57**, 360–374.
 - 12 K. Winkens, J. Koponen, J. Schuster, M. Shoeib, R. Vestergren, U. Berger, A. M. Karvonen, J. Pekkanen, H. Kiviranta and I. T. Cousins, Perfluoroalkyl acids and their precursors in indoor air sampled in children's bedrooms, *Environ. Pollut.*, 2017, **222**, 423–432.
 - 13 S. M. Hall, S. Patton, M. Petreas, S. Zhang, A. L. Phillips, K. Hoffman and H. M. Stapleton, Per- and Polyfluoroalkyl Substances in Dust Collected from Residential Homes and Fire Stations in North America, *Environ. Sci. Technol.*, 2020, **54**, 14558–14567.
 - 14 M. E. Morales-McDevitt, J. Becanova, A. Blum, T. A. Bruton, S. Vojta, M. Woodward and R. Lohmann, The Air that we Breathe: neutral and volatile PFAS in Indoor Air, *Environ. Sci. Technol. Lett.*, 2021, **8**, 897–902.
 - 15 I. T. Cousins, J. H. Johansson, M. E. Salter, B. Sha and M. Scheringer, Outside the Safe Operating Space of a New Planetary Boundary for Per- and Polyfluoroalkyl Substances (PFAS), *Environ. Sci. Technol.*, 2022, **56**, 11172–11179.
 - 16 A. K. Tokranov, N. Nishizawa, C. A. Amadei, J. E. Zenobio, H. M. Pickard, J. G. Allen, C. D. Vecitis and E. M. Sunderland, How Do We Measure Poly- and Perfluoroalkyl Substances (PFASs) at the Surface of Consumer Products?, *Environ. Sci. Technol. Lett.*, 2018, **6**, 38–43.
 - 17 I. Liagkouridis, R. Awad, S. Schellenberger, M. M. Plassmann, I. T. Cousins and J. P. Benskin, Combined Use of Total Fluorine and Oxidative Fingerprinting for Quantitative Determination of Side-Chain Fluorinated Polymers in Textiles, *Environ. Sci. Technol. Lett.*, 2021, **9**, 30–36.
 - 18 S. Schellenberger, I. Liagkouridis, R. Awad, S. Khan, M. Plassmann, G. Peters, J. P. Benskin and I. T. Cousins, An Outdoor Aging Study to Investigate the Release of Per-And Polyfluoroalkyl Substances (PFAS) from Functional Textiles, *Environ. Sci. Technol.*, 2022, **56**, 3471–3479.
 - 19 S. Schellenberger, C. Jonsson, P. Mellin, O. A. Levenstam, I. Liagkouridis, A. Ribbenstedt, A. C. Hanning, L. Schultes, M. M. Plassmann, C. Persson, I. T. Cousins and J. P. Benskin, Release of Side-Chain Fluorinated Polymer-Containing Microplastic Fibers from Functional Textiles During Washing and First Estimates of Perfluoroalkyl Acid Emissions, *Environ. Sci. Technol.*, 2019, **53**, 14329–14338.
 - 20 J. W. Washington, J. Ellington, T. M. Jenkins, J. J. Evans, H. Yoo and S. C. Hafner, Degradability of an acrylate-linked, fluorotelomer polymer in soil, *Environ. Sci. Technol.*, 2009, **43**, 6617–6623.
 - 21 J. W. Washington and T. M. Jenkins, Abiotic Hydrolysis of Fluorotelomer-Based Polymers as a Source of Perfluorocarboxylates at the Global Scale, *Environ. Sci. Technol.*, 2015, **49**, 14129–14135.
 - 22 J. W. Washington, K. Rankin, E. L. Libelo, D. G. Lynch and M. Cyterski, Determining global background soil PFAS loads and the fluorotelomer-based polymer degradation rates that can account for these loads, *Sci. Total Environ.*, 2019, **651**, 2444–2449.
 - 23 H. Holmquist, S. Schellenberger, I. van der Veen, G. M. Peters, P. E. Leonards and I. T. Cousins, Properties, performance and associated hazards of state-of-the-art durable water repellent (DWR) chemistry for textile finishing, *Environ. Int.*, 2016, **91**, 251–264.
 - 24 OECD, *Synthesis Report on Understanding Side-Chain Fluorinated Polymers and Their Life Cycle*, OECD Series on Risk Management, 2022.
 - 25 L. Schultes, G. F. Peaslee, J. D. Brockman, A. Majumdar, S. R. McGuinness, J. T. Wilkinson, O. Sandblom, R. A. Ngwenyama and J. P. Benskin, Total Fluorine Measurements in Food Packaging: How Do Current Methods Perform?, *Environ. Sci. Technol. Lett.*, 2019, **6**, 73–78.
 - 26 L. A. Schaidler, S. A. Balan, A. Blum, D. Q. Andrews, M. J. Strynar, M. E. Dickinson, D. M. Lunderberg, J. R. Lang and G. F. Peaslee, Fluorinated Compounds in U.S. Fast Food Packaging, *Environ. Sci. Technol. Lett.*, 2017, **4**, 105–111.
 - 27 B. Göckener, M. Eichhorn, R. Lammer, M. Kotthoff, J. Kowalczyk, J. Numata, H. Schafft, M. Lahrssen-Wiederholt and M. Bucking, Transfer of Per- and Polyfluoroalkyl Substances (PFAS) from Feed into the Eggs of Laying Hens. Part 1: Analytical Results Including a Modified Total Oxidizable Precursor Assay, *J. Agric. Food Chem.*, 2020, **68**, 12527–12538.
 - 28 J. Zweigle, B. Bugsel, C. Capitain and C. Zwiener, PhotoTOP: PFAS Precursor Characterization by UV/TiO₂ Photocatalysis, *Environ. Sci. Technol.*, 2022, **56**, 15728–15736.
 - 29 V. A. Nikiforov, Hydrolysis of FTOH precursors, a simple method to account for some of the unknown PFAS, *Chemosphere*, 2021, **276**, 130044.
 - 30 T. Portoles, J. G. Mol, J. V. Sancho and F. Hernandez, Advantages of atmospheric pressure chemical ionization in gas chromatography tandem mass spectrometry: pyrethroid insecticides as a case study, *Anal. Chem.*, 2012, **84**, 9802–9810.
 - 31 A. Rosch, B. Beck, J. Hollender and H. Singer, Picogram per liter quantification of pyrethroid and organophosphate insecticides in surface waters: a result of large enrichment with liquid-liquid extraction and gas chromatography coupled to mass spectrometry using atmospheric pressure chemical ionization, *Anal. Bioanal. Chem.*, 2019, **411**, 3151–3164.
 - 32 M. Metzger, P. Ley, M. Sturm and B. Meermann, Screening method for extractable organically bound fluorine (EOF) in

- river water samples by means of high-resolution-continuum source graphite furnace molecular absorption spectrometry (HR-CS GF MAS), *Anal. Bioanal. Chem.*, 2019, **411**, 4647–4660.
- 33 L. Gehrenkemper, F. Simon, P. Roesch, E. Fischer, M. von der Au, J. Pfeifer, A. Cossmer, P. Wittwer, C. Vogel, F. G. Simon and B. Meermann, Determination of organically bound fluorine sum parameters in river water samples-comparison of combustion ion chromatography (CIC) and high resolution-continuum source-graphite furnace molecular absorption spectrometry (HR-CS-GFMAS), *Anal. Bioanal. Chem.*, 2021, **413**, 103–115.
- 34 F. Simon, L. Gehrenkemper, M. V. Au, P. Wittwer, P. Roesch, J. Pfeifer, A. Cossmer and B. Meermann, A fast and simple PFAS extraction method utilizing HR-CS-GFMAS for soil samples, *Chemosphere*, 2022, 133922, DOI: [10.1016/j.chemosphere.2022.133922](https://doi.org/10.1016/j.chemosphere.2022.133922).
- 35 P. Roesch, C. Vogel, T. Huthwelker, P. Wittwer and F. G. Simon, Investigation of per- and polyfluoroalkyl substances (PFAS) in soils and sewage sludges by fluorine K-edge XANES spectroscopy and combustion ion chromatography, *Environ. Sci. Pollut. Res. Int.*, 2022, **29**, 26889–26899.
- 36 E. F. Houtz and D. L. Sedlak, Oxidative conversion as a means of detecting precursors to perfluoroalkyl acids in urban runoff, *Environ. Sci. Technol.*, 2012, **46**, 9342–9349.
- 37 J. Janda, K. Nodler, M. Scheurer, O. Happel, G. Nurenberg, C. Zwiener and F. T. Lange, Closing the gap - inclusion of ultrashort-chain perfluoroalkyl carboxylic acids in the total oxidizable precursor (TOP) assay protocol, *Environ. Sci.: Processes Impacts*, 2019, **21**, 1926–1935.
- 38 G. W. Curtzwiler, P. Silva, A. Hall, A. Ivey and K. Vorst, Significance of Perfluoroalkyl Substances (PFAS) in Food Packaging, *Integr. Environ. Assess. Manage.*, 2021, **17**, 7–12.
- 39 S. Schellenberger, P. J. Hill, O. Levenstam, P. Gillgard, I. T. Cousins, M. Taylor and R. S. Blackburn, Highly fluorinated chemicals in functional textiles can be replaced by re-evaluating liquid repellency and end-user requirements, *J. Cleaner Prod.*, 2019, **217**, 134–143.
- 40 S. Schellenberger, P. Gillgard, A. Stare, A. Hanning, O. Levenstam, S. Roos and I. T. Cousins, Facing the rain after the phase out: performance evaluation of alternative fluorinated and non-fluorinated durable water repellents for outdoor fabrics, *Chemosphere*, 2018, **193**, 675–684.
- 41 D. J. Muensterman, I. A. Titaley, G. F. Peaslee, L. D. Minc, L. Cahuas, A. E. Rodowa, Y. Horiuchi, S. Yamane, T. N. J. Fouquet, J. C. Kissel, C. C. Carignan and J. A. Field, Disposition of Fluorine on New Firefighter Turnout Gear, *Environ. Sci. Technol.*, 2022, **56**, 974–983.
- 42 W. A. Gebbink, S. Ullah, O. Sandblom and U. Berger, Polyfluoroalkyl phosphate esters and perfluoroalkyl carboxylic acids in target food samples and packaging—method development and screening, *Environ. Sci. Pollut. Res.*, 2013, **20**, 7949–7958.
- 43 G. Yuan, H. Peng, C. Huang and J. Hu, Ubiquitous Occurrence of Fluorotelomer Alcohols in Eco-Friendly Paper-Made Food-Contact Materials and Their Implication for Human Exposure, *Environ. Sci. Technol.*, 2016, **50**, 942–950.
- 44 J. Rupp, M. Guckert, U. Berger, W. Drost, A. Mader, K. Nodler, G. Nurenberg, J. Schulze, R. Sohlmann and T. Reemtsma, Comprehensive target analysis and TOP assay of per- and polyfluoroalkyl substances (PFAS) in wild boar livers indicate contamination hot-spots in the environment, *Sci. Total Environ.*, 2023, **871**, 162028.
- 45 F. T. Lange, R. Söhlmann, A. K. Seeger and H. Salowsky, *Aussagekraft der Anwendung des Total Oxidizable Precursor (TOP) Assays auf Bodenprobenextrakte und wässrige Eluate*, Mitt Umweltchem Ökotox, 2022.
- 46 M. Ateia, D. R. Chiang, M. Cashman and C. Acheson, Total Oxidizable Precursor (TOP) Assay? Best Practices, Capabilities and Limitations for PFAS Site Investigation and Remediation, *Environ. Sci. Technol. Lett.*, 2023, **10**(4), 292–301.
- 47 R. C. Buck, J. Franklin, U. Berger, J. M. Conder, I. T. Cousins, P. de Voogt, A. A. Jensen, K. Kannan, S. A. Mabury and S. P. van Leeuwen, Perfluoroalkyl and polyfluoroalkyl substances in the environment: terminology, classification, and origins, *Integr. Environ. Assess. Manage.*, 2011, **7**, 513–541.
- 48 C. Gremmel, T. Fromel and T. P. Knepper, Systematic determination of perfluoroalkyl and polyfluoroalkyl substances (PFASs) in outdoor jackets, *Chemosphere*, 2016, **160**, 173–180.
- 49 I. van der Veen, S. Schellenberger, A. C. Hanning, A. Stare, J. de Boer, J. M. Weiss and P. E. G. Leonards, Fate of Per- and Polyfluoroalkyl Substances from Durable Water-Repellent Clothing during Use, *Environ. Sci. Technol.*, 2022, **56**, 5886–5897.
- 50 C. Xia, M. L. Diamond, G. F. Peaslee, H. Peng, A. Blum, Z. Wang, A. Shalin, H. D. Whitehead, M. Green, H. Schwartz-Narbonne, D. Yang and M. Venier, Per- and Polyfluoroalkyl Substances in North American School Uniforms, *Environ. Sci. Technol.*, 2022, **56**, 13845–13857.
- 51 H. Zhu and K. Kannan, Total oxidizable precursor assay in the determination of perfluoroalkyl acids in textiles collected from the United States, *Environ. Pollut.*, 2020, **265**, 114940.
- 52 E. E. Ritter, M. E. Dickinson, J. P. Harron, D. M. Lunderberg, P. A. DeYoung, A. E. Robel, J. A. Field and G. F. Peaslee, PIGE as a screening tool for Per- and polyfluorinated substances in papers and textiles, *Nucl. Instrum. Methods Phys. Res., Sect. B*, 2017, **407**, 47–54.
- 53 G. F. Peaslee, J. T. Wilkinson, S. R. McGuinness, M. Tighe, N. Caterisano, S. Lee, A. Gonzales, M. Roddy, S. Mills and K. Mitchell, Another Pathway for Firefighter Exposure to Per- and Polyfluoroalkyl Substances: Firefighter Textiles, *Environ. Sci. Technol. Lett.*, 2020, **7**, 594–599.
- 54 A. E. Robel, K. Marshall, M. Dickinson, D. Lunderberg, C. M. Butt, G. F. Peaslee, H. M. Stapleton and J. A. Field, Closing the Mass Balance on Fluorine on Papers and Textiles, *Environ. Sci. Technol.*, 2017, **51**, 9022–9032.
- 55 K. M. Rodgers, C. H. Swartz, J. Occhialini, P. Bassignani, M. McCurdy and L. A. Schaidler, How Well Do Product

- Labels Indicate the Presence of PFAS in Consumer Items Used by Children and Adolescents?, *Environ. Sci. Technol.*, 2022, **56**, 6294–6304.
- 56 Z. Wang, H. Wiesinger and K. Groh, Time to Reveal Chemical Identities of Polymers and UVCBs, *Environ. Sci. Technol.*, 2021, **55**, 14473–14476.
- 57 A. S. Young, H. M. Pickard, E. M. Sunderland and J. G. Allen, Organic Fluorine as an Indicator of Per- and Polyfluoroalkyl Substances in Dust from Buildings with Healthier versus Conventional Materials, *Environ. Sci. Technol.*, 2022, **56**, 17090–17099.
- 58 I. van der Veen, A. C. Hanning, A. Stare, P. E. G. Leonards, J. de Boer and J. M. Weiss, The effect of weathering on per- and polyfluoroalkyl substances (PFASs) from durable water repellent (DWR) clothing, *Chemosphere*, 2020, **249**, 126100.
- 59 T. Stoiber, S. Evans and O. V. Naidenko, Disposal of products and materials containing per- and polyfluoroalkyl substances (PFAS): a cyclical problem, *Chemosphere*, 2020, **260**, 127659.
- 60 M. H. Russell, W. R. Berti, B. Szostek and R. C. Buck, Investigation of the biodegradation potential of a fluoroacrylate polymer product in aerobic soils, *Environ. Sci. Technol.*, 2008, **42**, 800–807.
- 61 J. W. Washington, T. M. Jenkins, K. Rankin and J. E. Naile, Decades-scale degradation of commercial, side-chain, fluorotelomer-based polymers in soils and water, *Environ. Sci. Technol.*, 2015, **49**, 915–923.
- 62 L. Li, J. Liu, J. Hu and F. Wania, Degradation of Fluorotelomer-Based Polymers Contributes to the Global Occurrence of Fluorotelomer Alcohol and Perfluoroalkyl Carboxylates: A Combined Dynamic Substance Flow and Environmental Fate Modeling Analysis, *Environ. Sci. Technol.*, 2017, **51**, 4461–4470.
- 63 R. Lohmann, I. T. Cousins, J. C. DeWitt, J. Glüge, G. Goldenman, D. Herzke, A. B. Lindstrom, M. F. Miller, C. A. Ng, S. Patton, M. Scheringer, X. Trier and Z. Wang, Are Fluoropolymers Really of Low Concern for Human and Environmental Health and Separate from Other PFAS?, *Environ. Sci. Technol.*, 2020, **54**, 12820–12828.
- 64 E. S. Coffin, D. M. Reeves and D. P. Cassidy, PFAS in municipal solid waste landfills: sources, leachate composition, chemical transformations, and future challenges, *Curr. Opin. Environ. Sci. Health*, 2023, **31**, 100418.
- 65 F. Fredriksson, U. Eriksson, A. Karrman and L. W. Y. Yeung, Per- and polyfluoroalkyl substances (PFAS) in sludge from wastewater treatment plants in Sweden – First findings of novel fluorinated copolymers in Europe including temporal analysis, *Sci. Total Environ.*, 2022, **846**, 157406.
- 66 I. T. Cousins, G. Goldenman, D. Herzke, R. Lohmann, M. Miller, C. A. Ng, S. Patton, M. Scheringer, X. Trier, L. Vierke, Z. Wang and J. C. DeWitt, The concept of essential use for determining when uses of PFASs can be phased out, *Environ. Sci.: Processes Impacts*, 2019, **21**, 1803–1815.
- 67 J. Glüge, R. London, I. T. Cousins, J. DeWitt, G. Goldenman, D. Herzke, R. Lohmann, M. Miller, C. A. Ng, S. Patton, X. Trier, Z. Wang and M. Scheringer, Information Requirements under the Essential-Use Concept: PFAS Case Studies, *Environ. Sci. Technol.*, 2022, **56**, 6232–6242.

Supporting Information

Non-extractable PFAS in functional textiles – Characterization by complementary methods: oxidation, hydrolysis, and fluorine sum parameters

Jonathan Zweigle,⁺ Catharina Capitain,⁺ Fabian Simon,^{||} Philipp Roesch,[‡] Boris Bugsel,
+ Christian Zwiener^{+,*}

⁺Environmental Analytical Chemistry, Department of Geosciences, University of Tübingen, Schnarrenbergstraße
94-96, 72076 Tübingen, Germany

^{||}Federal Institute for Materials Research and Testing (BAM), Division 1.1 – Inorganic Trace Analysis, Richard-
Willstätter-Straße 11, 12489 Berlin, Germany

[‡]Federal Institute for Materials Research and Testing (BAM), Division 4.3 - Contaminant Transfer and
Environmental Technologies, Unter den Eichen 87, 12205, Berlin, Germany

**Corresponding author*

Contents

S1 CHEMICALS AND REAGENTS	2
S2 INSTRUMENTAL ANALYSIS	2
Table S 1: Gradient elution used for HPLC-QTOF-MS and HPLC-QqQ-MS measurements.	2
Table S 2: Instrument and ESI source parameters used during HPLC-QqQ-MS/MS measurements.	2
Table S 3: Summary of APCI and QTOF parameters	3
Table S 4: MRM parameters for PFCAs measured by HPLC-QqQ-MS.	3
Non-target screening by HPLC-QTOF-MS and GC-QTOF-MS.	4
TF measurements by combustion ion chromatography	4
Conversion of fluorine from PFCAs and FTOHs to mass fluorine	5
Table S 5: Combustion parameters used for TF measurements.	6
Table S 6: Ion chromatography parameters.	6
Table S 7: TF boat program.	6
Table S 8: IC eluent gradient program.	6
S3 SUPPORTING FIGURES	7
Figure S 1: Examples of photos taken of water and sunflower oil droplets on textile surfaces to determine the contact angle.	7
Extraction recovery test	7
Figure S 2: Extraction recoveries for PFHpA, PFOA, and PFOS from spike experiments with two textiles.	7
Figure S 3: Concentration of Σ PFCAs after 5 h PhotoTOP oxidation in different textiles vs. water and sunflower oil contact angles. Three textiles were completely oil wetting and no PFCAs formed after PhotoTOP oxidation. Water repellency was observed for all textiles.	8
Figure S 4: Correlation of partially semi-quantified Σ FTOHs after the THP assay vs. TF and EOF.	8
Figure S 5: Normalized peak areas of main PFCAs formed from PhotoTOP oxidation of textile T05 and T15 over a time of 10 h.	8
Figure S 6: Concentration of PFCAs after 3 and 6 h of dTOP oxidation in textile T05 and T15 respectively.	9
REFERENCES	9

42 S1 Chemicals and reagents

43 LC/MS grade water, methanol (MeOH), ammonium acetate (NH₄Ac), and formic acid (FA)
44 were purchased from Thermo Fisher Scientific, as well as hydrochloric acid (32%). Sodium
45 hydroxide (NaOH), tert-butyl methyl ether (MTBE, ≥ 99.5%), and Titanium(IV)dioxide (TiO₂
46 anatase, powder, 99.8% trace metal basis) were ordered from Sigma-Aldrich. Hydrogen
47 peroxide solution (H₂O₂, ≥ 30%) was purchased from Fluka Analytical. Potassium persulfate
48 (≥ 99%) and ammonium hydroxide solution (25% NH₄OH) originated from Acros Organics.
49 Anhydrous Na₂SO₄ and n-hexane for gas chromatography were purchased from Merck.
50 PFCA reference standards (PFBA, PFPeA, PFHxA, PFHpA, PFOA, PFNA, PFDA, PFUnDA,
51 PFDoDA, PFTTrDA, PFTeDA, PFHxDA, and PFODA) and, a mass-labelled PFAS extraction
52 standard solution (MPFAC-C-ES) were ordered from Wellington Laboratories.

53 S2 Instrumental analysis

54 **Table S 1:** Gradient elution used for HPLC-QTOF-MS and HPLC-QqQ-MS measurements. Eluent A: 95/5
55 water/MeOH + 2 mM NH₄Ac, eluent B: 5/95 water/MeOH + 2mM NH₄Ac.

6550 QTOF-MS			6490 QqQ-MS		
Time (min)	A (%)	B (%)	Time (min)	A (%)	B (%)
0.0	85	15	0.0	60	40
2.0	30	70	1.0	40	60
5.0	10	90	3.5	0	100
10.0	0	100	6.0	0	100
15.0	0	100	6.1	60	40
15.1	85	15	8.0	60	40
22.0	85	15			

56

57 **Table S 2:** Instrument and ESI source parameters used during HPLC-QqQ-MS/MS measurements.

	6490 QqQ	6550 QTOF
Instrument parameters		
Gas Temp (°C)	150	150
Gas Flow (L/min)	16	16
Nebulizer pressure (psig)	45	35
Sheath gas temperature (°C)	380	380
Sheath gas flow (L/min)	12	12
Fragmentor voltage (V)	380	360
Ion source parameter (ESI)		
Capillary voltage (V)	3000	3000
Nozzle voltage (V)	0	300

58

59 **Table S 3:** Summary of APCI and QTOF parameters used during GC-QTOF-MS measurements.

APCI/QTOF Parameter	Value
Gas Temp (°C)	270
Drying gas (L/min)	11
Fragmentor voltage (V)	150
Capillary voltage (V)	1000
Corona current (µA)	1

60 **Table S 4:** MRM parameters for PFCAs measured by HPLC-QqQ-MS. Precursor and corresponding product ion
 61 with the respective collision energy (CE).

Compound	Precursor ion	Product ion	CE (eV)	Compound	Precursor ion	Product ion	CE (eV)
PFBA	212.9	168.8	5	H2PFDA	477	393	15
¹³ C ₄ -PFBA	217	172	5	H4PFUnA	491	367	25
PFPeA	262.9	68.8	45	H4PFUnA	491	387	15
PFPeA	262.9	219	5	PFOSA	498	78	40
¹³ C ₅ -PFPeA	268	70	45	L-PFOS	499	79.7	55
¹³ C ₅ -PFPeA	268	223	5	L-PFOS	499	99	50
L-PFBS	298.9	79.8	40	¹³ C ₈ -PFOS	507	80	50
L-PFBS	298.9	98.9	30	¹³ C ₈ -PFOS	507	99	55
¹³ C ₃ -PFBS	302	80	40	PFDA	512.9	268.9	15
¹³ C ₃ -PFBS	302	99	30	PFDA	512.9	468.8	10
PFHxA	312.9	119	25	¹³ C ₆ -PFDA	519	270	15
PFHxA	312.9	268.9	5	¹³ C ₆ -PFDA	519	474	15
¹³ C ₅ -PFHxA	318	120	25	L-PFNS	549	80	50
¹³ C ₅ -PFHxA	318	273	5	L-PFNS	549	99	50
L-PFPeS	349	80	25	PFUnA	563	519	5
L-PFPeS	349	99	30	PFUnA	563	269	15
PFHpA	362.8	168.7	15	¹³ C ₇ -PFUnA	570	270	15
PFHpA	362.8	318.8	5	¹³ C ₇ -PFUnA	570	525	5
¹³ C ₄ -PFHpA	367	169	15	L-PFDS	599	80	55
¹³ C ₄ -PFHpA	367	322	5	L-PFDS	599	99	55
L-PFHxS	398.8	79.9	45	PFDoA	613	369	15
L-PFHxS	398.8	98.9	45	PFDoA	613	569	10
¹³ C ₃ -PFHxS	402	80	45	¹³ C ₂ -PFDoA	615	369	15
¹³ C ₃ -PFHxS	402	99	45	¹³ C ₂ -PFDoA	615	570	10
PFOA	412.9	168.7	20	PFTTrDA	663	169	30
PFOA	412.9	368.7	5	PFTTrDA	663	619	10
¹³ C ₈ -PFOA	421	172	15	L-PFDoS	699	80	55
¹³ C ₈ -PFOA	421	376	5	L-PFDoS	699	99	50
H4PFOS	427	81	40	PFTeDA	713	169	25
H4PFOS	427	407	25	PFTeDA	713	669	10
L-PFHpS	449	80	50	¹³ C ₂ -PFTeDA	715	169	25
L-PFHpS	449	99	45	¹³ C ₂ -PFTeDA	715	670	10
PFNA	462.9	218.8	15	PFHxDA	813	169	45
PFNA	462.9	418.8	5	PFHxDA	813	769	10
¹³ C ₉ -PFNA	472	223	15	PFODA	913	169	40
¹³ C ₉ -PFNA	472	427	5	PFODA	913	869	15
H2PFDA	477	63	5				

62 **Non-target screening by HPLC-QTOF-MS and GC-QTOF-MS**

63 Textile extracts and selected PhotoTOP samples were analyzed by HPLC-QTOF-MS (1260
64 Infinity HPLC system, coupled to a 6550 QTOF mass spectrometer, Agilent Technologies).
65 A Poroshell 120 EC-C₁₈ column (2.7 μm, 2.1 × 100 mm) was used at a flow rate of 0.3 mL/min
66 (40 °C) with a 23 min gradient program (for details see Table S1). The ESI source was operated
67 in negative mode (details in Table S2). 5 μL sample was injected with a prior threefold needle
68 wash in isopropanol. Each measurement set included a MeOH and extraction blank. Data
69 acquisition (3 spectra/s) started after a 1 min waste line in the data-dependent acquisition mode
70 (ddMS², precursor selection threshold of 1000 counts and 0.5 min exclusion after 3 MS/MS
71 spectra) with a static exclusion list generated from blank injections. The *m/z* range in MS was
72 100 – 1700 and 70 – 1700 in MS/MS. MS/MS spectra were acquired by using a linear mass-

73 dependent collision energy of $CE(m/z) = \frac{3 m/z}{100} + 15 \text{ eV}$.

74 For peak finding, the MolecularFeatureExtraction algorithm of the Agilent Qualitative 10.0
75 Software was used, and Kendrick mass defect analysis was applied to CSV files to find
76 potential PFAS homologues as previously described.¹ FindPFAS was used to search all
77 MS/MS for fragment mass differences characteristic to PFAS (e.g., ΔCF₂, ΔC₂F₄, ΔHF).²
78 Furthermore, chromatograms of suspected PFAS were manually extracted to check for their
79 occurrence. The identical procedure was applied to the GC-QTOF-MS raw data.

80 **TF measurements by combustion ion chromatography**

81 For determination of the instrumental LOQ and LOD values, the standard protocol according
82 to DIN 32645 was followed. Therein, ten repeated measurements of twenty different blank
83 samples (empty sample boats) were conducted. Subsequently, the standard deviation (SD) was
84 calculated, divided by the slope of the calibration curve (1-250 μg/L F⁻) and multiplied times
85 3, resulting in the instrumental LOD value of 3 μg/L. Factor ten was used for the determination

86 of the instrumental LOQ (= 10 µg/L). All measured fluoride values per sample were above the
87 determined LOQ.

88 The CIC was controlled by the software Chromeleon 7.2.10 (Thermo Fisher Scientific GmbH,
89 Dreieich, Germany). The combustion unit consisted of an autosampler (ASC-270LS)
90 connected to the induction furnace (AQF-2100H) operating between 1000 and 1050 °C. Prior
91 to combustion, all ceramic boats were prebaked for at least 5 min at 1000 °C to avoid organic
92 contamination. All samples were hydro-pyrolyzed in the horizontal combustion furnace
93 operating at 1050 °C under a flow of O₂ (300 mL/min), Ar (150 mL/min) using sample specific
94 boat programs (Table S7). Combustion gases were absorbed in a freshly prepared 3 mM NH₃
95 absorption solution, added with an internal standard for monitoring the exact absorption
96 volume by ion chromatography. For TF measurements, the water supply level was set to “4”
97 and the medium absorption volume of the GA210 (~16 mL) was selected. A 5 µL aliquot was
98 injected into the ion chromatography using Dionex IonPac AG20 (2 × 50 mm) as guard column
99 and Dionex IonPac AS20 (2 × 250mm) as analytic column, both maintained at a constant
100 column temperature of 30 °C. Chromatographic separation was directed by an automated
101 KOH eluent generator, controlled by an optimized gradient program (5 mM to 50 mM) at a
102 constant flow rate of 0.25 mL/min (Table S8). Fluoride ions were sensed by a conductivity
103 detector using 50 mM H₂SO₄ as suppressor regenerant. For calculation of detected peak areas
104 and fluoride concentrations chromatography data system Chromeleon 7.2.10 (Thermo Fisher
105 Scientific) was used. After combustion of the samples and subsequent quantification of the
106 fluoride amount by IC, the collected raw data were transferred to an external computer for
107 more detailed evaluation in Origin 2020 (OriginLab Corporation).

108 **Conversion of fluorine from PFCAs and FTOHs to mass fluorine**

109 To convert PFCAs and FTOHs to mass of fluorine, the measured mass concentration (µg/L)
110 of each compound (e.g., PFPeA, PFHxA and PFHpA) was converted into moles of substance

111 per textile mass (e.g., $\mu\text{mol/kg}$). Then, by using the number of fluorine atoms, the mass of
 112 fluorine per mass of textile was calculated (e.g. mg/kg).

113 **Table S 5:** Combustion parameters used for TF measurements.

Combustion component	
Combustion device	AQF-2100H, AI Enviroscience, Mitsubishi Chemical Analytech Co., Ltd.
Operating temperature	1050 °C
Ar carrier gas flow	150 mL/min
Ar flow of water supply	100 mL/min
O ₂ flow	300 mL/min
Absorption solution/internal standard	3.0 mM NH ₃ solution + 2.2 mg/L MeSO ₃ H
Starting Absorption volume	8.5 ml (TF)
Final Absorption volume	16 (TF)
Sample amount	5-10 mg (TF)
Water supply level	4 (TF)

114

115 **Table S 6:** Ion chromatography parameters.

Ion chromatography component	
IC-device	ICS Integriion, Thermo Fisher Scientific
Detector	conductivity detector
Guard column	AG20 2x50mm guard column
Analytical column	Dionex IonPac AS20 2x250mm
Eluent	gradient KOH
Flow rate	0.25 mL/min
Run time	22 min
Column temperature	30 °C
Injection volume	5 μl (TF)
Suppressor regenerant	50 mM H ₂ SO ₄

116

117 **Table S 7:** TF boat program.

Pos	Time (s)	Pos	Time (s)	End Time (s)	Cool Time (s)	Home Time (s)	Ar Time (s)	O ₂ Time (s)
100	90	210	60	300	60	200	0	600

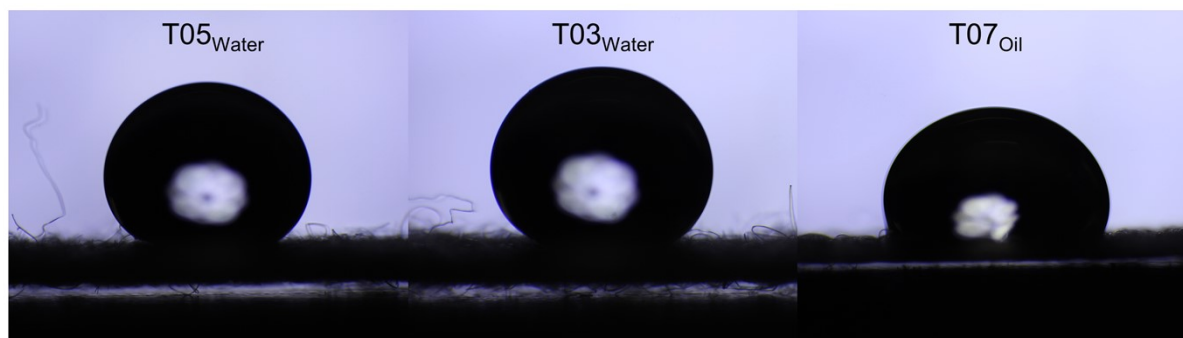
118

119 **Table S 8:** IC eluent gradient program.

Time (min)	Eluent concentration (mM)
0	Start, 1.0
0.1	1.0
0.2	2.0
1.0	2.0
10.0	5.0
10.5	5.0
11.0	80.0
14.0	80.0
14.5	1.0
22.0	stop run

120

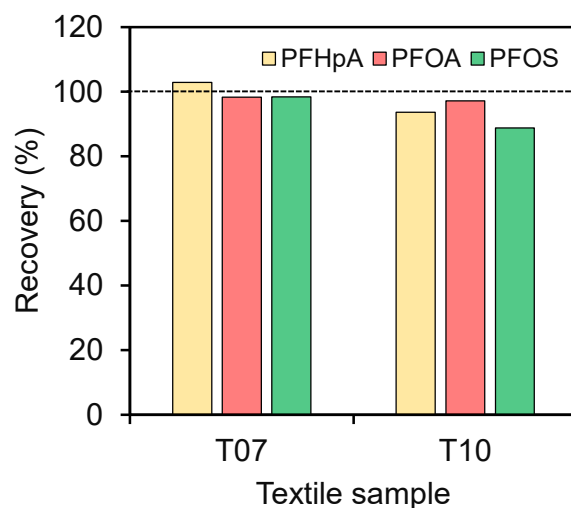
121 S3 Supporting figures



122
123 **Figure S 1:** Examples of photos taken of water and sunflower oil droplets on textile surfaces to determine the
124 contact angle.

125 Extraction recovery test

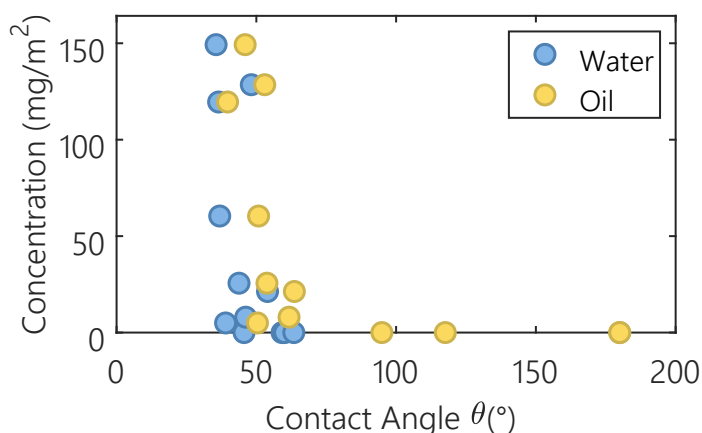
126 An extraction recovery test was performed to verify that the applied extraction technique
127 quantitatively extracts PFAAs from the textiles. Two 4 cm² textile pieces and a control without
128 textile (T07, T10) were spiked with a methanolic mixture of PFHpA, PFOA, and PFOS (50
129 ng each) and left until the MeOH was evaporated. Afterwards, those textiles were extracted
130 by our used extraction procedure (Figure S2) and measured by HPLC-QTOF-MS. The
131 recoveries ranged from 88% up to 102%.



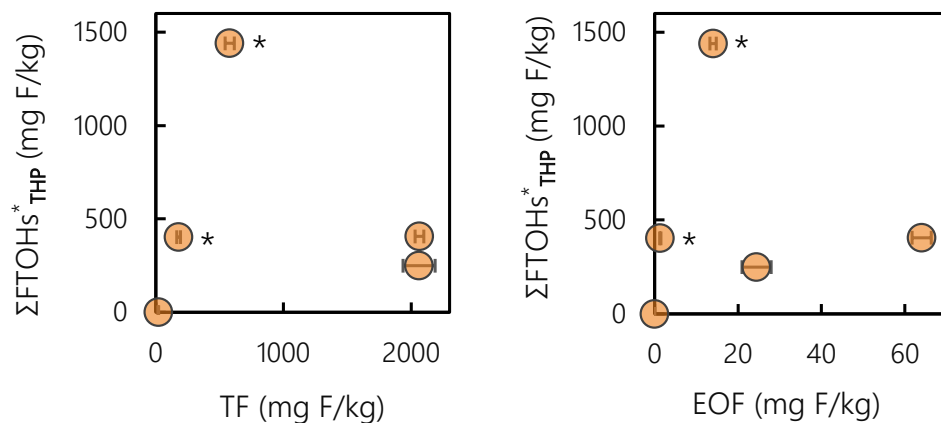
132

133 **Figure S 2:** Extraction recoveries for PFHpA, PFOA, and PFOS from spike experiments with two textiles.

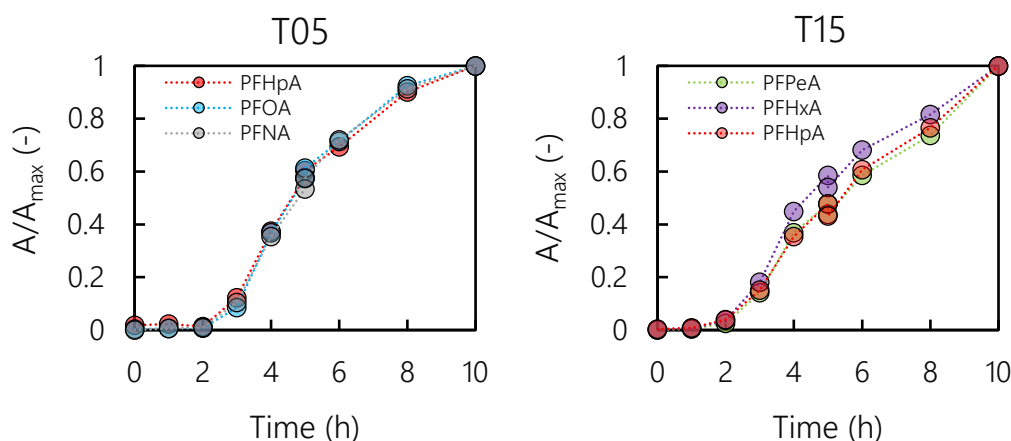
134



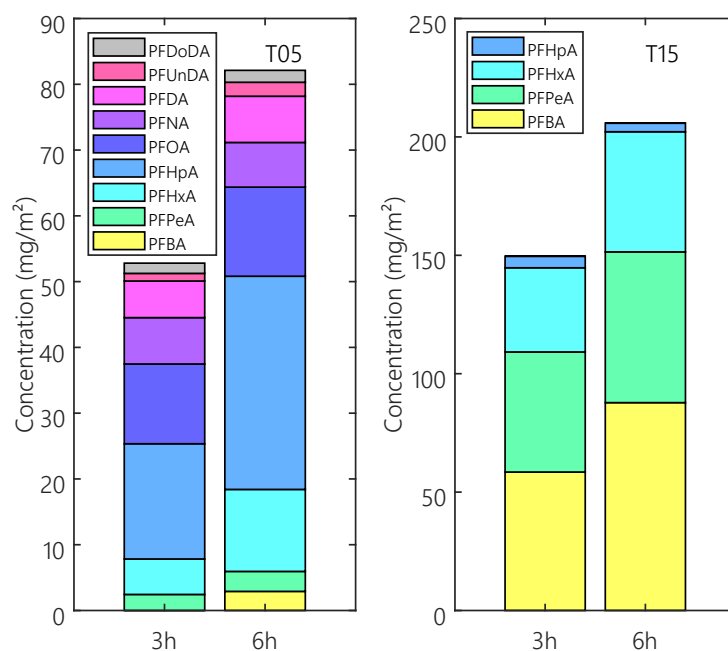
135
 136 **Figure S 3:** Concentration of ΣPFCAs after 5 h PhotoTOP oxidation in different textiles vs. water and sunflower
 137 oil contact angles. Three textiles were completely oil wetting and no PFCAs formed after PhotoTOP oxidation.
 138 Water repellency was observed for all textiles.
 139



140
 141 **Figure S 4:** Correlation of partially semi-quantified ΣFTOHs after the THP assay vs. TF and EOF. Data points
 142 marked with asterisks include estimated concentrations of n:2 FTOHs with $n \geq 10$. Here, probably an
 143 overestimation occurred because more fluorine from hydrolysis than from TF measurements is unlikely.



144
 145 **Figure S 5:** Normalized peak areas of main PFCAs formed from PhotoTOP oxidation of textile T05 and T15
 146 over a time of 10 h. Note that although the concentrations still increased after 5 h the formation rates decreased.
 147 The data in Table 1 represents concentrations after 5 h of oxidation. Data was acquired by HPLC-QTOF-MS.



148

149 **Figure S 6:** Concentration of PFCAs after 3 and 6 h of dTOP oxidation in textile T05 and T15 respectively.

150

151 **References**

- 152 1. J. Zweigle, B. Bugsel, C. Capitain and C. Zwiener, PhotoTOP: PFAS Precursor
 153 Characterization by UV/TiO(2) Photocatalysis, *Environ Sci Technol*, 2022, **56**, 15728-15736.
 154 2. J. Zweigle, B. Bugsel and C. Zwiener, FindPFAS: Non-Target Screening for PFAS -
 155 Comprehensive Data Mining for MS2 Fragment Mass Differences, *Anal Chem*, 2022, **94**,
 156 10788-10796.